

ALEXANDRE MANIÇOBA DA ROSA FERRAZ JARDIM

ENERGY AND CARBON FLUXES IN BRAZILIAN SEMI-ARID LANDSCAPES:
HOW THE ESTABLISHMENT OF CACTUS PLANTATIONS CAN MITIGATE THE
ADVANCE OF DESERTIFICATION

Recife
Pernambuco, Brazil
2023

ALEXANDRE MANIÇOBA DA ROSA FERRAZ JARDIM

ENERGY AND CARBON FLUXES IN BRAZILIAN SEMI-ARID LANDSCAPES:
HOW THE ESTABLISHMENT OF CACTUS PLANTATIONS CAN MITIGATE THE
ADVANCE OF DESERTIFICATION

Thesis submitted to the Agricultural Engineering
Graduate Program of the Federal Rural
University of Pernambuco in partial fulfillment of
the requirements for the degree of Doctor in
Agricultural Engineering.

Advisor: Prof. Dr. Thieres George Freire da Silva.
Co-Advisors: Prof. Dr. Luciana Sandra Bastos de
Souza, and Dr. José Edson Florentino de Morais.

Recife
Pernambuco, Brazil
2023

Dados Internacionais de Catalogação na Publicação
Universidade Federal Rural de Pernambuco
Sistema Integrado de Bibliotecas da UFRPE

J37e Jardim, Alexandre Maniçoba da Rosa Ferraz
Energy and carbon fluxes in Brazilian semi-arid landscapes: how the
establishment of cactus plantations can mitigate the advance of desertification /
Alexandre Maniçoba da Rosa Ferraz Jardim. – 2023.
358 f.: il.

Orientador: Thieres George Freire da Silva.
Coorientadora: Luciana Sandra Bastos de Souza
Coorientador: José Edson Florentino de Moraes
Inclui referências.

Tese (Doutorado em Engenharia Agrícola) – Universidade Federal Rural de
Pernambuco, Programa de Pós-Graduação em Engenharia Agrícola, Recife, 2023.

1. Flux partitioning. 2. Surface energy balance. 3. Cacti. 4. Caatinga. 5. Climate
change. I. Silva, Thieres George Freire da, orientador II. Título.

CDD 630

ALEXANDRE MANIÇOBA DA ROSA FERRAZ JARDIM

Energy and carbon fluxes in Brazilian semi-arid landscapes: how the establishment of cactus plantations can mitigate the advance of desertification

Thesis presented to the Federal Rural University of Pernambuco, as partial fulfillment of the requirements for the Graduate Program in Agricultural Engineering, to obtain the title of Doctor in Agricultural Engineering.

DEFENDED and APPROVED on January 25, 2023.

Examination Board

Prof. Dr. Luciana Sandra Bastos de Souza
Federal Rural University of Pernambuco | UFRPE
Academic Unit of Serra Talhada | UAST

Prof. Dr. Daniela de Carvalho Lopes
Federal University of São João del-Rei | UFSJ

Prof. Dr. Antonio José Steidle Neto
Federal University of São João del-Rei | UFSJ

Prof. Dr. Abelardo Antônio de Assunção Montenegro
Internal Examiner
Federal Rural University of Pernambuco | UFRPE

Prof. Dr. Thieres George Freire da Silva
Federal Rural University of Pernambuco | UFRPE
Academic Unit of Serra Talhada | UAST

*“To everything there is a season,
and a time for every purpose under heaven”.*

- Ecclesiastes 3:1.

*“If I have seen further than others,
it is by standing upon the shoulders of giants”.*

- Isaac Newton.

DEDICATION

I dedicate this thesis work to my loving parents, Iamí Maniçoba da Rosa Ferraz Jardim and Valdomiro Ferraz Jardim Filho (*in memoriam*), and my sister Camila. Everything I am today is because of you.

I also dedicate this thesis to God Almighty, the creator who gives us wisdom, knowledge and understanding, and all Scientists (science only real when shared).

$\int_{\heartsuit}^{\infty}$ My love for you all can never be quantified.

God bless you.

ACKNOWLEDGEMENTS

First and foremost, I would like to praise and thank God and Nossa Senhora Aparecida, for always being with me in every moment of my life, guiding and illuminating my path to good paths, always with faith and perseverance, not letting me fall into temptations. “[...] Those who sow with tears will reap with songs of joy. Those who go out weeping, carrying seed to sow, will return with songs of joy, carrying sheaves with them” (Psalm 126:5-6).

In addition to my efforts, the completion of this thesis largely depends on the encouragement and guidance of many others. I take this opportunity to express my gratitude to the people who contributed to the completion of this work.

Many thanks to my beloved and queen, my mother, Iamí Maniçoba da Rosa Ferraz Jardim, for all her unconditional love and affection. You always taught and encouraged me to be a person of principles, always keeping me in your prayers, advising and encouraging me in my studies and in my life. You are undoubtedly my greatest example of life and the great love of my life. Many times I heard our song: “[...] *Quem ama não esquece quem ama, o amor é assim, eu tenho esquecido de mim, mas dela eu nunca me esqueço* [...]”. To my beloved and wonderful father, Valdomiro Ferraz Jardim Filho (*in memoriam*), who always supported my studies and always rooted for me in all my achievements. This achievement is once again ours, and I know that in another spiritual plane that you inhabit, you are always looking at me and taking care of me, thank you for everything my guardian angel. I thank my beloved sister, Camila (Lilinha), for the encouragement and fraternal love throughout my life, especially in the most difficult times we spent together, life is hard my sister, but God is always merciful. Thanks for the calls and for making me smile when you didn't even know I was sad. I would like to thank my brother-in-law, Breno Leonardo, for all his support and encouragement. From the bottom of my heart, I don't have words to thank you enough for all the love and admiration I have for you ♡.

To my Advisor, Dr. Thieres George Freira da Silva, for the education, teachings, advice and guidance provided. During all these academic years of coexistence, he never discredited me, always lifting me up, preparing me for new academic battles, and, moreover, he always saw a potential (i.e., that even I didn't know) and believed that I would be able to

achieve my goals and dreams. You are synonymous with respect and gratitude, a great example that I carry within my ideals, without a doubt an admirable and kind professional, your perseverance was often “fuel” for my incentives and attitudes. Thank you also for treating me like a son. Without her guidance and constant feedback this PhD would not have been achievable.

My sincere thanks to my Co-Advisory Committee, Dr. Luciana Sandra Bastos de Souza, you were always present, attentive, patient and with excellent teachings, a true “mãezona”, always encouraging me to fly higher and higher. You are a being of light and love, thank you for caring and for treating me like a son. To Dr. José Edson Florentino de Morais, who always supported me with valuable academic, scientific and personal advice. Certainly, you are an admirable professional and of great simplicity, thank you very much for everything, “Mestre”.

Thanks to all my family members, for every vote of confidence, positive vibes and encouragement. I also apologize for my absence during many times.

My sincere thanks to the Freire family for being so special and kind. Elania (Nana), Helena (Lena) and Elaine (Cunha), I love you so much, thank you for welcoming me with so much love and care. All of you are undoubtedly extremely special to me (♡). God cover them with blessings and graces. Nana my beautiful companion, thank you so much for all your patience, sweet face, complicity and love. You sure make me a better human being.

To my friends and class members (2019.1) of the Graduate Program in Agricultural Engineering (PGEA), you were true companions and key players in this forging process. I emphasize my special thanks to Raliuson, Marcos, Anderson and George, for the days and nights of study, for the strength in moments of weakness, since, without you, my brothers, this journey would have been more “arduous and suffered”, and you managed to transform her in bright and pleasurable.

I also thank the inner core of the PGEA, especially our Coordinators, Dr. Ênio Farias de França e Silva and Dr. Mário Monteiro Rolim, you are excellent professionals and thank you very much for your efforts to maintain our Graduate Program with quality. During all these years you have always been attentive and kept your doors open at any time, regardless of the time of day, always concerned about our well-being and professional growth.

Many thanks also to Professors Dr. Luciana Souza, Dr. Daniela Lopes, Dr. Antonio Steidle Neto, and Dr. Abelardo Montenegro, for accepting the invitation to participate in my evaluation panel and for the essential scientific comments, helping to enrich our study.

I thank all the members of the Grupo de Agrometeorologia no Semiárido (GAS), more than a group, a Family, for the great moments together, for the heavy field activities with the “punishing” sun, but always with enthusiasm, a smile on the face and commitment, striving for quality and love for research. I have learned and have been learning a lot from each of you and I wish you all success in your professional and academic careers. My sincere thanks to the member of the group, Carlos André, for his help in field activities, companionship and tireless trips to the Serrinha experimental field. I would like to thank the Barros family, especially senhor Luiz and Dona Socorro, owners of the “Algodões farm”, an experimental site in Serrinha. Thank you so much for being so hospitable, cheerful and attentive. God bless each one of you.

To the Federal Rural University of Pernambuco (UFRPE), the Academic Unit of Serra Talhada (UAST) and the Postgraduate Program in Crop Protection (PGPV) for the institutional support in carrying out our research. I also thank the Portuguese Foundation for Science and Technology (FCT), through projects ASHMOB (CENTRO-01-0145-FEDER-029351), GOLis (PDR2020-101-030913, Partnership nr. 344/Initiative nr. 21), MUSSEFLOW (PTDC /BIA-EVL/29199/2017), MEDWATERICE (PRIMA/0006/2018), and through the strategic project UIDB/04292/2020 granted to MARE—Marine and Environmental Sciences Centre, University of Coimbra. I am especially grateful to Prof. Dr. João Pedroso de Lima for believing in my research and for the financial support I received through the University of Coimbra, Department of Civil Engineering. I would like to thank all my professors for the good classes and scientific and academic teachings. I would like to thank all the institution's technicians for their availability and promptness, as well as the guards, always caring for our safety.

To the Pernambuco Science and Technology Support Foundation - FACEPE (APQ-1159-1.07/14, APQ-0300-5.03/17, APQ-0639-5.01/21), to the National Council for Scientific and Technological Development - CNPq (421003 /2018-9, 309421/2018-7, 402622/2021-9, 309558/2021-2), the Brazilian Agricultural Research Corporation - Embrapa Semiárido (10.18.03.039.00.02.00) and the São Paulo Research Foundation - FAPESP

(2017/22269-2) for financial support and to FACEPE itself for granting the scholarship (IBPG-0216-5.03/19).

Finally, I thank everyone who contributed directly or indirectly to the realization of this dream, I also apologize to those who did not have their names mentioned on paper, but know that in memory and feelings they have my eternal gratitude. May the Almighty God continue to bless you all!

My sincere thanks to everyone!

SUMMARY

GENERAL ABSTRACT.....	18
GENERAL INTRODUCTION	19
References	21
CHAPTER 1	23
Understanding interactive processes: a review of CO ₂ flux, evapotranspiration, and energy partitioning under stressful conditions in dry forest and agricultural environments	23
Abstract.....	23
Introduction	24
Literature review.....	26
Energy and mass fluxes in dry forest environments.....	27
Methods of measuring fluxes in ecosystems	30
Sap flow method.....	31
Eddy covariance method	33
Remote sensing-based surface energy balance.....	36
Carbon allocation and partitioning in ecosystems.....	41
Factors controlling variation in carbon dioxide efflux from surface litter	43
Factors affecting respiration from soil, litter, and soil organic matter	46
Conclusions	48
References	49
Acknowledgements	69
CHAPTER 2.....	70
A systematic review of energy and mass fluxes, and biogeochemical processes in seasonally dry tropical forests and cactus ecosystems	70
Abstract.....	70
1. Introduction	70
2. Methodology.....	72
3. Literature review.....	73
3.1. Seasonally dry forest and cactus ecosystems in semi-arid regions	73
4. Land use and land cover changes on the dry diagonal	77

5. Energy and mass fluxes	78
6. Storage: interaction and stocks of biophysical elements in dry forest ecosystems	80
7. Nutrient cycling	82
8. Conclusion	83
Acknowledgements	84
References	84
CHAPTER 3	93
Spatiotemporal climatic analysis in Pernambuco State, Northeast Brazil.....	93
Abstract.....	93
1. Introduction	94
2. Material and methods	96
2.1 Study area and data used	96
2.2 Data analysis and statistical techniques used	98
2.3 Classification dataset for ENSO warm and cold episodes	101
3. Results and discussion	101
4. Conclusion	112
Acknowledgments	113
References	113
CHAPTER 4.....	126
Using remote sensing to quantify the joint effects of climate and land-use changes on the Caatinga biome	126
Abstract.....	126
1. Introduction	127
2. Materials and Methods	129
2.1. Study Area	129
2.2. Satellite Images and Weather Datasets.....	131
2.3. Vegetation Indices	133
2.4. Methodology for Estimating Evapotranspiration Using Satellite Images	134
2.4.1. Surface Albedo Adjustment.....	135
2.5. Determination of Surface-energy Partitioning	137
2.5.1. Calculation of Energy Fluxes (H and LE) and Evaporative Fraction.....	138

2.6. Estimate of ET _a Using SEBAL Method	139
2.7. Land Use and Land Cover Dynamics	140
2.8. Statistical Analyses.....	141
2.8.1. Goodness of Fit.....	142
3. Results and Discussion	142
3.1. Comparisons of Land Use and Land Cover (LULC)	142
3.2. Rainfall Variability in Land Cover Classes	146
3.3. Vegetation Cover Indices of the Municipality	147
3.4. Land Surface Temperature (LST) in the Studied Classes	150
3.5. Variations of the Actual Evapotranspiration (ET _a) of Land Use Classes.....	152
3.6. Statistical Relations Between the Variables Studied and Land Use.....	154
4. Conclusions	158
References	161
CHAPTER 5	176
Genotypic differences relative photochemical activity, inorganic and organic solutes and yield performance in clones of the forage cactus under semi-arid environment	176
Abstract.....	176
1 Introduction	177
2 Material and methods	178
2.1 Study area and species under evaluation	178
2.2 Measurement of chlorophyll fluorescence and accessory pigments	180
2.2.1 Chlorophyll fluorescence.....	180
2.2.2 Chlorophyll and carotenoid content	181
2.3 Measurement of carbohydrates.....	181
2.4 Levels of Sodium (Na ⁺) and potassium (K ⁺).....	182
2.5 Morphometry and dry matter accumulation	182
2.6 Statistical analysis	182
3 Results	183
3.1 Measurement of the parameters of chlorophyll fluorescence.....	183
3.2 Chlorophyll and carotenoid content of the cladodes	186
3.3 Carbohydrate content.....	186

3.4. Na ⁺ and K ⁺ concentration	187
3.5 Morphometry and dry matter accumulation	189
3.6 Association between variables with principal component analysis.....	189
4 Discussion.....	191
5 Conclusion.....	197
Acknowledgements	198
References	198
CHAPTER 6.....	207
To what extent are turbulent flux, the energy budget and water relations in the field compromised in <i>Nopalea cochenillifera</i> during the wet and dry seasons?	207
Abstract.....	207
1. Introduction	208
2. Materials and methods.....	210
2.1. Location and information of the experimental area.....	210
2.2. Measuring the meteorological variables.....	212
2.3. Surface energy balance method.....	213
2.3.1 Data selection criteria for the energy balance method	214
2.4. Resource use efficiency.....	216
2.4.1. Water efficiency	216
2.4.2. Radiation use efficiency	216
2.4.3. Nutrient use efficiency.....	217
2.5. Analysing growth, phenology, cutting time and yield.....	218
2.6. Measuring the plant water status	220
2.7. Indicators of water and environmental stress	220
2.8. Soil moisture.....	221
2.9. Statistical analysis	221
3. Results	222
3.1. Surface energy budget	222
3.2. NDVI signatures, environmental data and the impact of drought.....	228
3.3. Growth parameters, phenological characteristics, and cutting time	231
3.4. Water relations, Bowen ratio, biophysical efficiency, and yield.....	233

3.5. Interrelationships between environmental variables and plant responses	235
4. Discussion.....	237
4.1. Mean daytime patterns, seasonal variations in the energy fluxes, and evapotranspiration	237
4.2. Variations in the NDVI, seasonal environmental changes and soil moisture	240
4.3. Allometry, phenological phase, and cutting time	241
4.4. Water relations and biophysical parameters of cladodes.....	242
4.5. Principal component analysis (PCA).....	244
5. Conclusions	245
Acknowledgments	246
References	246
CHAPTER 7.....	258
Quantifying the energy budget, water use efficiency and photochemistry of two of the most cultivated cactus species in the world.....	258
Abstract.....	258
1. Introduction	259
2. Materials and methods.....	262
2.1. Description of the experimental sites	262
2.2. Measurements and instrumentation.....	265
2.3. Calculation of the surface energy balance and parameters.....	265
2.4. Criteria for selecting data for the energy balance method.....	266
2.5. Yield measurements	267
2.6. Allometry and measurements of plant growth	267
2.7. Plant water status: cladode water content, succulence, and water use efficiency	269
2.8. Indices of environmental and physiological stress	269
2.9. Data analysis.....	270
3. Results	271
3.1. Daytime variation in the energy fluxes	271
3.2. Seasonal and interannual characteristics of the energy fluxes	272
3.3. Changes in energy partitioning for surfaces with cacti	276
3.4. Changes in the vegetation, photochemical and pigment indices	277

3.5. Rates of plant growth, morphology, and physiology	279
3.6. Water relations, increase in annual biomass yield, and water use efficiency.....	281
3.7. Associations between variables	283
4. Discussion.....	285
4.1. Energy balance and partitioning	285
4.2. Temporal responses to rain of the NDVI, PRI and CI in the cactus canopy	288
4.3. Plant dynamics and growth rate.....	289
4.4. Plant water relations and biomass production	291
4.5. Explanatory power of the different combinations of variables	292
5. Conclusions	293
Acknowledgments	294
References	294
CHAPTER 8.....	307
Sink or carbon source? How the <i>Opuntia</i> cactus interacts in the use of carbon, nutrients and radiation in a semi-arid environment	307
Abstract.....	307
1. Introduction	308
2. Materials and methods.....	310
2.1. Study site description	310
2.2. Measurements of environmental variables	312
2.3. Flux measurements and data processing	313
2.4. Surface energy budget	314
2.5. Energy budget partitioning	315
2.5.1. Energy balance closure.....	315
2.6. Biomass yield and growth allometry	316
2.7. Resource use efficiencies.....	317
2.7.1. Water use efficiency	317
2.7.2. Radiation use efficiency and interception photosynthetically active radiation	317
2.7.3. Nutrient stocks and use efficiency.....	318
2.7.4. Carbon stock and efficiency	319
2.8. Statistical analysis	319

3. Results	320
3.1. Energy balance closing overview	320
3.2. Environmental conditions during the experimental period	321
3.3. Seasonal and temporal variation in the balance of carbon, energy and radiation	324
3.4. Characteristics of seasonal changes in radiation, energy, carbon and water fluxes	331
3.5. Flux partitioning	333
3.6. Yield and efficiency responses in the use of biophysical resources	334
3.7. Principal component analysis	336
4. Discussion.....	338
4.1. Energy balance closure and overview of site environmental conditions.....	338
4.2. Changes in the balance of carbon, energy, and radiation	340
4.3. Flux partitioning and efficiency in the use of biophysical resources in cactus cultivation	342
4.4. Relations between variables and environment	344
5. Conclusions	345
Acknowledgments	346
References	346

GENERAL ABSTRACT

Vegetated surfaces are considered important in controlling environmental degradation processes and improving water, carbon, and energy fluxes on the Earth's surface. Dry forests and cacti crops are common vegetation in arid and semi-arid environments. Therefore, Caatinga and cactus areas were investigated using techniques such as energy balance through meteorological tower data, eddy covariance, and satellite images emphasizing hyperspectral vegetation monitoring. In addition, data on cacti's physiological, photochemical, and morphometric responses in a semi-arid environment were explored. This study was divided into eight chapters emphasizing meteorological variations, energy, water, and carbon flux responses in Caatinga and cacti (*Opuntia* and *Nopalea*) in the Brazilian semi-arid region. The use of methods that integrate data from climate monitoring towers and remote sensing products helps to improve the accuracy of determining energy fluxes on a global scale. In dry forest areas, woody species can store large amounts of carbon (C) in their biomass above and below ground. The significant increase in agricultural areas resulted in the progressive reduction of the Caatinga biome. Furthermore, the phases of the El Niño-Southern Oscillation directly influenced the rainfall variability in the Pernambuco study. The values for the effective quantum yield of PSII and changes in photochemical quenching was higher in the 'Orelha de Elefante Mexicana' cactus clone. In cactus clones, there was a difference in non-photochemical quenching. In general, cactus cultivation showed significantly higher net radiation (R_n) during the wet season, being on average 14% higher than during the dry season and transitions. There was no difference in evapotranspiration during the wet or dry seasons, but there was a 40% reduction during the dry-wet transition. The H/R_n ratio showed a decreasing behavior from the dry to the wet season, with a reduction of 36.90% in *Nopalea* and 14.04% in *Opuntia*. The Normalized Difference Vegetation Index (NDVI) varied from 0.19 to 0.67 (*Nopalea*) and from 0.17 to 0.70 for *Opuntia*, similar to the Chlorophyll Index, which maintained the seasonality of the NDVI. Overall, spatial patterns for the Photochemical Reflectance Index were found from -0.01 to 0.14 for *Nopalea* and *Opuntia*. Under the same conditions, *Opuntia* showed the highest growth and net assimilation rates. The average water content of the cladode was 86.01% in *Nopalea* and 88.91% in *Opuntia*. Biomass and water use efficiency was higher in *Opuntia* (56.01 Mg ha⁻¹ and 7.54 kg m⁻³, respectively). These comparisons indicate greater sensitivity in *Nopalea* and more meaningful quantification of surface energy balance in *Opuntia*. The radiation use efficiency of the wet season was 81.48% higher than in the dry season. Clearly, these comparisons indicate that the cactus is a potential year-round carbon sink (net ecosystem CO₂ exchange [NEE]: -4,517 g C m⁻²; gross primary production [GPP]: 2,352 g C m⁻²). The results help us to understand that most of the R_n energy is used in the sensible heat flux (58% ratio).

Keywords: flux partitioning, surface energy balance, cacti, Caatinga, climate change, photosynthesis, desertification

GENERAL INTRODUCTION

With the large emissions of greenhouse gases and the influence of meteorological factors, the semi-arid regions of the planet are expected to become even drier (Bao et al., 2022; Dass et al., 2018). For decades, vegetation in a semi-arid climate has been experiencing interannual variability in the absorption of carbon dioxide (CO₂), a decrease in rainfall, and an increase in temperature, which has triggered serious environmental problems. In terrestrial ecosystems, grasslands cover approximately 30–40% of the land surface and forests approximately 30%; these environments are responsible for providing a carbon sequestration from the atmosphere of approximately 20% to 90% (Balasubramanian et al., 2020; Besnard et al., 2018). When the ecosystem is disturbed, there is a tendency for increased heterotrophic respiration due to the increase in above-ground biomass from litter, while gross primary production suffers problems due to reduced leaf area, thus increasing the net release of CO₂ into the atmosphere (Besnard et al., 2018). This type of imbalance can cause problems in the carbon balance on vegetated surfaces since the global net carbon balance is the difference between the gains and losses of this element. Basically, ecosystems assimilate carbon through photosynthesis and the same can be lost in the form of CO₂ through the respiration of organisms (autotrophs and heterotrophs) and volatilization of organic compounds (Viglizzo et al., 2019). C₄ photosynthesis and crassulacean acid metabolism (CAM) plants are responsible for covering important ecological niches in grasslands, tropical forests, and arid ecosystems, with 25% of terrestrial primary production represented by C₄ plants in grasslands, while CAM plants represent 50% of plant biomass in arid and semi-arid regions (Hartzell et al., 2018).

CAM photosynthesis is an ancient adaptation of the C₃ pathway, being more efficient due to the control of stomatal opening, commonly performed during the night. The resultant of this photosynthetic process provides water use efficiency three to six times higher compared to the photosynthetic species C₄ and C₃, respectively, and, consequently, a potential increase in the net absorption of CO₂ (Niechayev et al., 2019). Cacti of the genera *Opuntia* and *Nopalea*, holders of the CAM pathway, are important plants of the Cactaceae family, which stand out due to their survival in environments considered inhospitable for several agricultural species, presenting high efficiency in the use of water and carbon, and

adapting well to high temperatures and low water availability (Nobel, 1991; Nobel and Zutta, 2008; Winter and Smith, 2022). In addition, cacti are great producers of biomass and can be used in animal and human food.

Globally, climate change threatens to increase the frequency, duration and geographic distribution of droughts. In this way, the interest in expanding studies and techniques that help in the evaluation of the behavior of ecosystems is of great relevance. Monitoring the volume and spatialization of rainfall events, changes in the energy and carbon balance of vegetation, and understanding the morphophysiological behavior of plants can be a way to mitigate how environmental conditions influence the performance of species. Thus, techniques such as energy balance using meteorological tower data, eddy covariance, satellite images with emphasis on hyperspectral monitoring of vegetation, physiological and photochemical responses using chlorophyll fluorescence and morphometric data were used in this study to quantify responses of cactus vegetation and Caatinga in a semi-arid environment. This study was divided into eight chapters with an emphasis on meteorological variations, energy, water and carbon flux responses in the Caatinga, as well as in cacti (*Opuntia* and *Nopalea*) in the Brazilian semi-arid region.

References

- Balasubramanian, D., Zhou, W.J., Ji, H.L., Grace, J., Bai, X.L., Song, Q.H., Liu, Y.T., Sha, L.Q., Fei, X.H., Zhang, X., Zhao, J. Bin, Zhao, J.F., Tan, Z.H., Zhang, Y.P., 2020. Environmental and management controls of soil carbon storage in grasslands of southwestern China. *J. Environ. Manage.* 254, 109810. <https://doi.org/10.1016/J.JENVMAN.2019.109810>
- Bao, Y., Liu, T., Duan, L., Tong, X., Zhang, Y., Wang, G., Singh, V.P., 2022. Variations and controlling factors of carbon dioxide and methane fluxes in a meadow-rice ecosystem in a semi-arid region. *CATENA* 215, 106317. <https://doi.org/10.1016/J.CATENA.2022.106317>
- Besnard, S., Carvalhais, N., Arain, M.A., Black, A., De Bruin, S., Buchmann, N., Cescatti, A., Chen, J., Clevers, J.G.P.W., Desai, A.R., Gough, C.M., Havrankova, K., Herold, M., Hörtnagl, L., Jung, M., Knohl, A., Kruijt, B., Krupkova, L., Law, B.E., Lindroth, A., Noormets, A., Rouspard, O., Steinbrecher, R., Varlagin, A., Vincke, C., Reichstein, M., 2018. Quantifying the effect of forest age in annual net forest carbon balance. *Environ. Res. Lett.* 13, 124018. <https://doi.org/10.1088/1748-9326/AAEAEB>
- Dass, P., Houlton, B.Z., Wang, Y., Warlind, D., 2018. Grasslands may be more reliable carbon sinks than forests in California. *Environ. Res. Lett.* 13, 074027. <https://doi.org/10.1088/1748-9326/AACB39>
- Hartzell, S., Bartlett, M.S., Porporato, A., 2018. Unified representation of the C3, C4, and CAM photosynthetic pathways with the Photo3 model. *Ecol. Modell.* 384, 173–187. <https://doi.org/10.1016/J.ECOLMODEL.2018.06.012>
- Niechayev, N.A., Pereira, P.N., Cushman, J.C., 2019. Understanding trait diversity associated with crassulacean acid metabolism (CAM). *Curr. Opin. Plant Biol.* 49, 74–85. <https://doi.org/10.1016/J.PBI.2019.06.004>
- Nobel, P.S., 1991. Achievable productivities of certain CAM plants: basis for high values compared with C3 and C4 plants. *New Phytol.* 119, 183–205. <https://doi.org/10.1111/J.1469-8137.1991.TB01022.X>
- Nobel, P.S., Zutta, B.R., 2008. Temperature tolerances for stems and roots of two cultivated cacti, *Nopalea cochenillifera* and *Opuntia robusta*: Acclimation, light, and drought. *J. Arid Environ.* 72, 633–642. <https://doi.org/10.1016/J.JARIDENV.2007.08.005>

- Viglizzo, E.F., Ricard, M.F., Taboada, M.A., Vázquez-Amábile, G., 2019. Reassessing the role of grazing lands in carbon-balance estimations: Meta-analysis and review. *Sci. Total Environ.* 661, 531–542. <https://doi.org/10.1016/J.SCITOTENV.2019.01.130>
- Winter, K., Smith, J.A.C., 2022. CAM photosynthesis: the acid test. *New Phytol.* 233, 599–609. <https://doi.org/10.1111/NPH.17790>

CHAPTER 1

Understanding interactive processes: a review of CO₂ flux, evapotranspiration, and energy partitioning under stressful conditions in dry forest and agricultural environments

Abstract

Arid and semiarid environments are characterized by low water availability (e.g., in soil and atmosphere), high air temperature, and irregularity in the spatio-temporal distribution of rainfall. In addition to the economic and environmental consequences, drought also causes physiological damage to crops and compromises their survival in ecosystems. The removal of vegetation is responsible for altering the energy exchange of heat and water in natural ecosystems and agricultural areas. The fluxes of CO₂ are also changed, and environments with characteristics of sinks, which can be sources of CO₂ after anthropic disturbances. These changes can be measured through methods such as e.g., sap flow, eddy covariance, remote sensing, and energy balance. Despite the relevance of each method mentioned above, there are limitations in their applications that must be respected. Thus, this review aims to quantify the processes and changes of energy fluxes, CO₂, and their interactions with the surfaces of terrestrial ecosystems in dry environments. Studies report that the use of methods that integrate data from climate monitoring towers and remote sensing products helps to improve the accuracy of the determination of energy fluxes on a global scale, also helping to reduce the dissimilarity of results obtained individually. Through the collection of works in the literature, it is reported that several areas of the Brazilian Caatinga biome, which is a Seasonally Dry Tropical Forest have been suffering from changes in land use and land cover. Similar fluxes of sensible heat in areas with cacti and Caatinga can be observed in studies. On the other hand, one of the variables influenced mainly by air temperature is net radiation. In dry forest areas, woody species can store large amounts of carbon in their biomass above and below ground. The use of cacti can modify the local carbon budget when using tree crops together. Therefore, the study highlights the complexity and severity of land degradation and changes in CO₂, water, and energy fluxes in dry environments with areas of forest, grassland, and cacti. Vegetation energy balance is also a critical factor, as these simulations are helpful for use in forecasting weather or climate change. We also highlight the need for more studies

32 that address environmental conservation techniques and cactus in the conservation of
33 degraded areas.

34

35 **Keywords:** Eddy covariance, gross primary productivity, energy balance method, semiarid,
36 dry forest.

37

38 **Introduction**

39 The environments that have deficient climatic conditions, quite common to be seen
40 in arid and semiarid locations in the world, are under increasing pressure, mainly due to
41 climate change and anthropic factors. These areas are sensitive to climate vulnerabilities and
42 are also prone to drought and land degradation events, and, in addition, water scarcity is a
43 factor that significantly worsens the resilience of terrestrial ecosystems (Seidl et al., 2016;
44 Spinoni et al., 2021). The processes of environmental degradation cause serious problems in
45 the survival of plants and threaten food security. In addition, changes in land use/land cover
46 can promote invaluable losses in biodiversity and affect natural resources. The main
47 consequences of these disturbances mentioned above are the increase in the emission of
48 greenhouse gases and the biogeochemical and biogeophysical changes in the landscapes
49 (Ribeiro et al., 2016; Silva Junior et al., 2020; Guillen-Cruz et al., 2021; Jardim et al., 2022).

50 On a global scale, inappropriate land use and occupation practices in forest areas
51 resulted in a decrease of 420 million hectares between 1990 and 2020. In addition, forests
52 can store about 55% of environmental carbon due to species efficiency (Ahirwal et al., 2021),
53 and one-third of all anthropogenic carbon emissions are a consequence of land use and land
54 cover practices (Lai et al., 2016).

55 On the other hand, an important carbon sink in ecosystems is the soil (Rossel et al.,
56 2014), and according to Menezes et al. (2021), when it comes to dry tropical forest,
57 considering areas with dense Caatinga and sparse Caatinga (open vegetation) this carbon
58 stock can vary from 72 to 76%, respectively. Furthermore, with changes in land use/land
59 cover, the decrease or increase in agricultural and forest areas can impact available energy,
60 carbon dioxide (CO₂) flux, surface albedo, and evapotranspiration (Bright et al., 2017; Liu et
61 al., 2021b; Li et al., 2022). In addition to these factors, when there is a decrease in the leaf
62 area of landscapes, there is a reduction in evapotranspiration and latent heat flux, resulting in

63 greater energy for heating the air and soil (Bright et al., 2017), which becomes an
64 environment of stressful conditions.

65 The interaction of the land surface with the boundary layer of the atmosphere
66 promotes energy gain and loss changes and, consequently, regulates climates through
67 biogeochemical and biophysical processes. The presence of different types of surfaces found
68 in biomes and ecosystems can significantly change the energy budget and, e.g., impact the
69 dissipation of heat and water in these locations (Huang et al., 2018). Forest species are
70 responsible for transferring 60 to 80% of soil water to the atmosphere through
71 evapotranspiration (Schlesinger & Jasechko, 2014; Hu et al., 2018). In addition to
72 evapotranspiration, variables such as net radiation, CO₂, sensible, latent, and soil heat fluxes
73 are essential for understanding energy feedback in ecosystems. However, partitioning the
74 energy, water, and CO₂ budget on a space-time scale in ecosystems often becomes onerous
75 and with some uncertainties (Baldocchi, 2003; Valayamkunnath et al., 2019). Methods such
76 as e.g., sap flow, eddy covariance, remote sensing, and energy balance (Maltese et al., 2018;
77 Dhungel et al., 2021; Chandel et al., 2021) are fundamental for determining mass and energy
78 fluxes in these areas.

79 In Seasonally Dry Tropical Forests such as the Caatinga (exclusive Brazilian biome),
80 due to its richness of endemic, arboreal, shrubby, herbaceous, and cactus species, several
81 studies are concentrated in this biome with stressful climatic conditions and high water deficit
82 (Teixeira et al., 2008; Silva et al., 2017; Campos et al., 2019; Santos et al., 2020). Such
83 interest may also be related to the loss of biodiversity resulting from prolonged droughts over
84 the years and anthropic disturbances (Campos et al., 2019; de Jesus et al., 2022). According
85 to the results of these studies (e.g., Schulz et al., 2016; Araújo Filho et al., 2018; Pereira et
86 al., 2020; de Oliveira et al., 2021), even under severe drought conditions, the Caatinga biome
87 remains an important carbon sink; however, prolonged drought and drier soil conditions can
88 cause aridification and, thus, reduce net primary production (NPP) levels and decrease the
89 carbon assimilation of its vegetation. In addition, changes in the energy exchange of soil-
90 vegetation-atmosphere interactions can change turbulent heat flux and thermal energy in the
91 soil. For example, during the dry season, Silva et al. (2017), in the Caatinga area (northeastern
92 region of Brazil), observed average net radiation and latent heat flux of 19.6 MJ m⁻² day⁻¹
93 and 2.3 MJ m⁻² day⁻¹, respectively. However, in the vegetation of cactus (*Opuntia ficus-*

94 *indica*), in a semiarid region of Italy, Consoli et al. (2013a) reported net radiation of 19 MJ
95 $\text{m}^{-2} \text{day}^{-1}$, partitioned into sensible and latent heat fluxes ($9.3 \text{ MJ m}^{-2} \text{day}^{-1}$ and 6.2 MJ m^{-2}
96 day^{-1} , respectively). Therefore, detailed knowledge of the responses of vegetation mass and
97 energy fluxes in interaction with meteorological conditions and terrestrial ecosystems on a
98 seasonal and annual scale is necessary.

99 The different photosynthetic metabolism (e.g., C3, C4, and CAM—crassulacean acid
100 metabolism) present in Caatinga biome species can influence carbon capture, gas exchange,
101 and energy balance (Silva et al., 2017; Hartzell et al., 2018; de Oliveira et al., 2020). In a
102 semiarid environment, C4 plants are predominant in pastures, because tropical grasses
103 commonly have a C4 photosynthetic pathway—assisting in the survival and cycling of water
104 and nutrients; on the other hand, CAM plants are present in pasture and forest areas, thus
105 representing 6% of vascular plants worldwide (Morgan et al., 2011; Holtum et al., 2016;
106 Nichols et al., 2016; Hartzell et al., 2018). However, despite significant carbon sequestration
107 and water use efficiency, CAM plants in agriculture are still neglected (Hogewoning et al.,
108 2021).

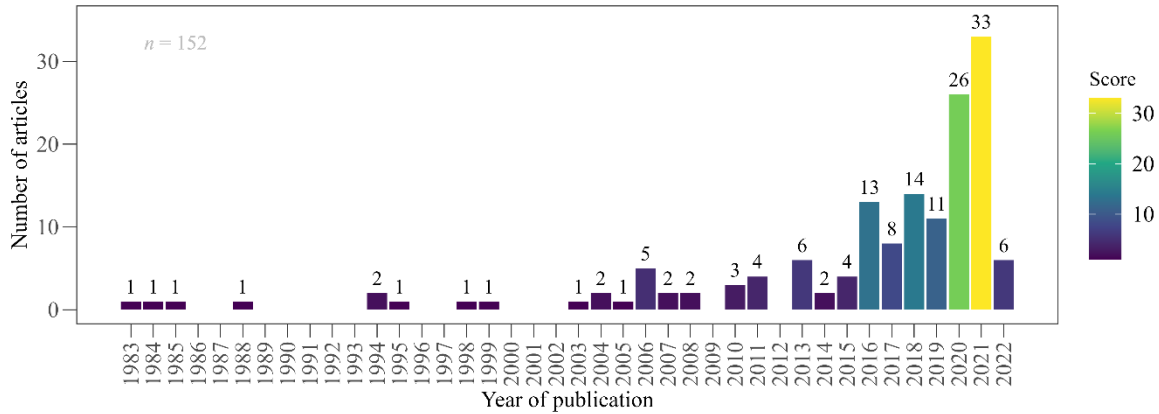
109 Thus, motivated by the existing gaps in the literature and anthropic influences on
110 energy and mass fluxes in deficient environments, we carried out this review work to
111 substantiate and quantify the energy balance in Caatinga and cactus areas in dry
112 environments. The objective of this review was to quantify the processes and changes of
113 energy fluxes, CO_2 , and their interactions with the surfaces of terrestrial ecosystems in dry
114 environments.

115

116 **Literature review**

117 In this review article, we compiled and synthesized 152 peer-reviewed articles
118 published from 1983 to 2022 (Fig. 1). Our literature selection criterion was through keyword
119 combinations for each section described in the review: (“forest” OR “dry forest”) AND
120 (“land-use” OR “pasture land-use”) AND (“litterfall” OR “litter”) AND (“climate” OR
121 “climate change”) AND (“flux” OR “flux density”) AND (“eddy covariance” OR “sonic
122 anemometer”) AND (“ CO_2 fluxes” OR “ CO_2 ”) AND (“CAM photosynthetic pathway” OR
123 “CAM pathway” OR “Crassulacean acid metabolism”) AND (“trees” OR “shrubs” OR
124 “grassland”) AND (“C4 plant”, “C3 plant” OR “CAM plant”) AND (“semiarid” OR

125 “semiarid landscape”) AND (“cacti” OR “cactus”), “agricultural systems”, “livestock”,
 126 “environmental modeling”, “transpiration”, “photosynthesis”, “respiration”,
 127 “evapotranspiration”, “sap flow”, “energy balance”, “carbon sink”, “carbon source”, AND
 128 “remote sensing”. In the present study, the literature search was performed using databases
 129 from Google Scholar, ScienceDirect, Web of Science, and Scopus.
 130



131
 132 **Fig. 1** Number of articles per year used in this study

133
 134 We then created the sections that we will discuss throughout this review. Here, we
 135 reviewed the broader set of literature to discuss Energy and mass fluxes in dry forest
 136 environments. The next section deals with Methods of measuring fluxes in ecosystems, while
 137 the last section reports on Carbon allocation and partitioning in ecosystems.

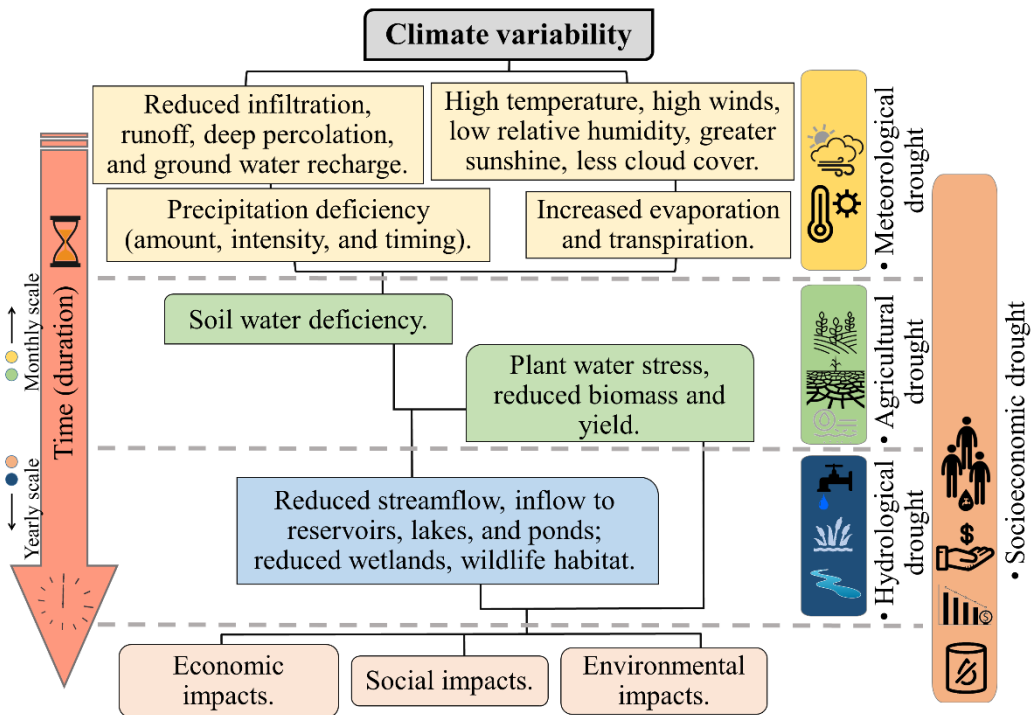
138
 139 **Energy and mass fluxes in dry forest environments**

140 The arid and semiarid climates regions are characterized by low water availability
 141 (e.g., in the soil and the atmosphere), high air temperature, and irregularity in the spatio-
 142 temporal distribution of rainfall. These mentioned factors are key elements for the
 143 understanding of climate change predicted for the coming decades (IPCC, 2021), and with
 144 the increase of the global population, the demand for food grows, and the exploitation of
 145 natural resources will be intensified, causing greater environmental damage. Furthermore, in
 146 agricultural and/or forest ecosystems, abiotic factors such as, for example, drought and heat
 147 are the main causes of death and deleterious damage to species, promoting a decrease in yield

148 and low photosynthetic performance, which leads to a reduction in food resources (Cook et
 149 al., 2016; Esquivel-Muelbert et al., 2017; Ray et al., 2019; Rocha et al., 2020).

150 As a result of the increase in the frequency of occurrence and magnitude of drought
 151 events in Brazil and the world, plant species have a high susceptibility to a decrease in leaf
 152 area and/or death of individuals, which compromises their assimilation and allocation of
 153 carbon (C) (Feldpausch et al., 2016; Rocha et al., 2020). In addition, the cumulative effects
 154 of drought also cause physiological damage to crops that compromise their survival in
 155 ecosystems (Feldpausch et al., 2016). Among natural phenomena with high complexity and
 156 damage capacity, drought is one of the most dangerous, characterized by long water deficit
 157 periods (Xu et al., 2019; Ding et al., 2021). Droughts can be subdivided into (i)
 158 meteorological drought; (ii) hydrological drought; (iii) agricultural drought; and (iv)
 159 socioeconomic drought (Yao et al., 2020; Ding et al., 2021) (Fig. 2).

160



161

162 **Fig. 2** Flowchart of the four types of drought and their main intrinsic relationships to social
 163 and environmental impacts

164

165 The damage from droughts becomes more aggravating, and this occurs mainly due to
166 lower availability and access to water, even when the years are not of climatic anomalies.
167 When there is a prolonged water shortage, a meteorological drought can become a
168 hydrological drought, consequently causing agricultural and socioeconomic damage to the
169 population (Xu et al., 2019; Guo et al., 2020; Noorisameleh et al., 2020). In low-latitude
170 forests with hostile climates (i.e., arid and semiarid), heat stress and drought cause changes
171 in atmospheric water demand, causing species to change their transpiration capacity (Liu et
172 al., 2013; Hu et al., 2018) and, consequently, changes in the net productivity of the ecosystem
173 (Cavaleri et al., 2015).

174 Particularly, species from forest ecosystems are responsible for transferring 60 to 80%
175 of the water from the soil to the atmosphere by evapotranspiration (Schlesinger & Jasechko,
176 2014; Hu et al., 2018); however, these quantities are smaller when reporting to areas of dry
177 forest—Caatinga. Low-latitude tropical forests play a key role in the planet's vegetation cover
178 rates (15% of the Earth's surface) and, in addition, contribute significantly to soil carbon
179 stocks and atmospheric carbon fluxes (Cavaleri et al., 2015). The mass and energy fluxes in
180 these environments undergo changes in the rainy and dry seasons, mainly controlled by
181 weather and vegetation conditions, respectively (Silva et al., 2017).

182 Places with arid and semiarid climates undergo changes both in the distribution and
183 in the amount of rainfall. In particular, these climates occur in different parts of the world
184 and have high water scarcity and economic losses (Mady et al., 2020). The Brazilian semiarid
185 region is characterized as one of the most populous semiarid areas worldwide (Lindoso et al.,
186 2018). In northeastern Brazil, a region that covers a large part of the Brazilian semiarid region
187 and, consequently, the Caatinga biome, there is significant rainfall variation in rainfall events
188 (500 to 2,000 mm year⁻¹). This is because the region suffers from meteorological phenomena,
189 e.g., El Niño-Southern Oscillation (ENSO), Sea Surface Temperature (SST) anomalies, and
190 Inter-Tropical Convergence Zone (ITCZ) (Nobre et al., 2006; Marengo & Bernasconi, 2015;
191 Marengo et al., 2020). In addition, it has a high air temperature, an aridity index of up to 0.5,
192 a risk of drought above 60%, and a high incidence of solar radiation, causing a decrease in
193 soil moisture, and increasing the possible levels of stress for the species (Nobre et al., 2006;
194 Marengo & Bernasconi, 2015; Marengo et al., 2020). The Caatinga biome has 6,053 species
195 in its flora (Jacob et al., 2020), of which 4,657 are angiosperms, and 913 are endemic

196 (Bonatelli et al., 2021). Its ecophysiology consists of xerophilous plants with different
197 growth habits and succulent and deciduous plants, which provides tolerance to environmental
198 stresses (Jacob et al., 2020; Bonatelli et al., 2021).

199 Furthermore, in areas of Caatinga (Brazilian Seasonally Dry Tropical Forest), the
200 relationship with the vegetation surface and the atmospheric conditions, e.g., in the rainy and
201 dry season, cause instability to close the surface energy balance. However, in this type of dry
202 forest, when partitioning the energy balance components in the rainy season, the results are
203 more satisfactory, and an excessive conversion of net radiation into sensible heat flux (H) is
204 common (Teixeira et al., 2008; Silva et al., 2017; Campos et al., 2019; Santos et al., 2020).

205 In rainy periods with low values of the vapor pressure deficit, the vegetation increases
206 its evapotranspiration due to the atmospheric gradient that helps in greater stomatal openings.
207 In this way, the meteorological conditions control the fluxes (Silva et al., 2017; Campos et
208 al., 2019), making the vegetation respond to water availability in the soil-atmosphere system
209 (Marques et al., 2020). In dry seasons, there is a leaf fall (i.e., caducifolia—leaf habit of
210 perennial or deciduous species) in most of the species that make up the Caatinga. This type
211 of adaptive mechanism helps in the resistance and resilience of the ecosystem, drastically
212 reducing gas exchange and water consumption (Silva et al., 2017; Santos et al., 2020;
213 Marques et al., 2020) since tropical forests are commonly exposed to long periods of water
214 deficit (Tan et al., 2019; Borges et al., 2020).

215

216 **Methods of measuring fluxes in ecosystems**

217 The vegetation removal and environmental disturbances are responsible for altering
218 heat and water's energy exchange in natural ecosystems and agricultural areas. For example,
219 anthropogenic actions have caused the massive removal of native forests, transforming them
220 mainly into agricultural cultivation areas. This type of practice alters the biophysical
221 exchanges with the atmosphere, making it necessary to measure the magnitude of these
222 changes to understand the process better (Antongiovanni et al., 2020). Among the various
223 methods of measuring and/or estimating mass and energy flows in the literature, the
224 following stand out: (1) sap flow, (2) eddy covariance, (3) remote sensing, and (4) energy
225 balance (Maltese et al., 2018; Dhungel et al., 2021; Chandel et al., 2021). All these methods

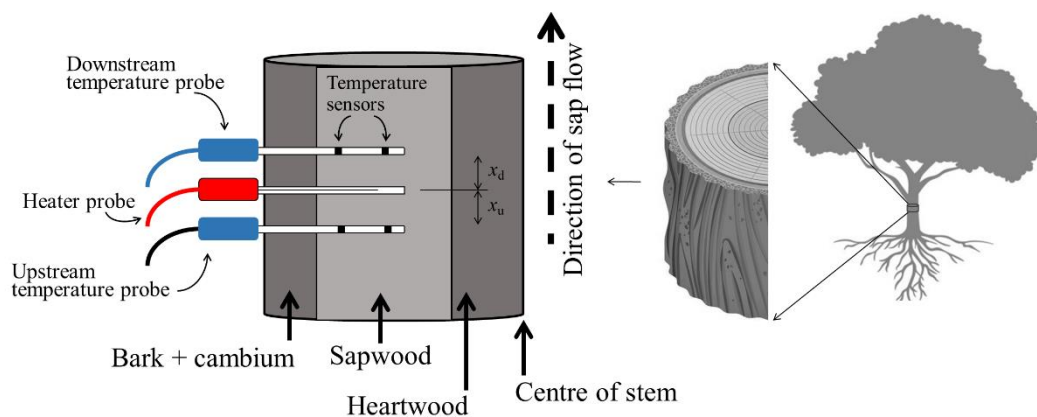
226 are essential for determining evapotranspiration (ET) from natural/artificial forest
227 ecosystems and irrigated/rainfed agricultural areas.

228

229 *Sap flow method*

230 Sap flow is a technique often used in conjunction with another method, e.g., eddy
231 covariance. The application of the sap flow method consists of measuring transpiration of the
232 species by thermal dissipation probes. For this, soil evaporation data must also be quantified
233 with mini-lysimeters and, thusly, the evapotranspiration of the system is determined. Probes
234 are inserted into the xylem in the trunk or stem region and quantify the sap velocity and heat
235 pulses. The probes are similar to needles, which are inserted in parallel into the trunk/stem
236 of trees at breast height (~1.30 m) or above the buttress roots (i.e., roots exposed above the
237 soil surface) (Fig. 3).

238



239

240 **Fig. 3** Diagram of the sap flow meters and heat-pulse probes implanted radially into a stem.
241 The upstream temperature sensor is installed at a distance x_u below the heater, and the
242 downstream sensor at a distance x_d above the heater

243

244 Despite being a usual method, some care should be taken, such as sensor calibration
245 for the studied species (Williams et al., 2004; Consoli & Papa, 2013; Fuchs et al., 2017; Link
246 et al., 2020). The tangential and axial distances of the sensors are crucial since they are
247 inserted in the equations for quantifying the flows. When opening a fissure in the trunk to
248 install the probe in the sapwood, one must avoid obstruction of the flow at the site and not
249 excessively damage the fibers (Barrett et al., 1995; Moore et al., 2010; Wullschleger et al.,

250 2011; Vandegehuchte & Steppe, 2013). According to Barrett et al. (1995), damage caused in
 251 the installation of the sensor alters the axial direction of the flow; and in the short and long
 252 term, these injuries can cause problems in the dissipation of heat flow in the wood (Moore et
 253 al., 2010; Wullschleger et al., 2011). This is also caused by disruption of xylem vessels,
 254 causing anatomical changes and negatively influencing physiological processes such as
 255 transpiration.

256 The sap flow has an intimate connection between the water and hydraulic
 257 relationships of plants with the atmosphere. This energy gradient promotes the transpiration
 258 flow of species and contributes to the hydrological cycle. About 45,000 km³ of water per
 259 year is transpired by terrestrial vegetation (Poyatos et al., 2021). Mathematically, the sap
 260 flow density can be determined by equations that relate heat and humidity in the sapwood
 261 region (Equations 1 and 2) (Granier, 1985; Vandegehuchte & Steppe, 2013). Thus, to
 262 consolidate the plant's water relationships, the daily water use per tree (kg day⁻¹) can be
 263 applied to understand water consumption by multiplying the sap flow density by the sapwood
 264 area (Kotowska et al., 2021).

265

$$266 \quad SFD = \frac{\rho_d}{\rho_s} + \left(MC + \frac{c_{dw}}{c_s} \right) \cdot V_h \quad (1)$$

$$267 \quad F_d = \alpha \cdot K^\zeta \quad (2)$$

268

269 where SFD and F_d are the sap flux densities (m³ m⁻² s⁻¹ and g m⁻² s⁻¹, respectively), ρ_d is the
 270 dry density of the sapwood (kg m⁻³), ρ_s is the density of the sap (assumed to be the density
 271 of water of 1,000 kg m⁻³), MC is the sapwood water content (i.e., considering the weight of
 272 water over dry weight of wood), c_{dw} is the specific heat capacity of the woody matrix (1,200
 273 J kg⁻¹ K⁻¹ at 20 °C), c_s is the specific heat capacity of the sap (using the water, 4186 J kg⁻¹
 274 K⁻¹ at 20 °C), V_h is the heat velocity (m s⁻¹), α and ζ are the coefficients dependent on the
 275 amount of heat applied proposed by Granier (1985), and K is the dimensionless sap flow
 276 index (i.e., $K = \frac{(\Delta T_o - \Delta T)}{\Delta T}$, where ΔT_o is the maximum temperature difference (°C) between the
 277 two sensor needles, when there is no sap flow or minimum sap flow, and ΔT is the
 278 temperature difference at a given time).

279

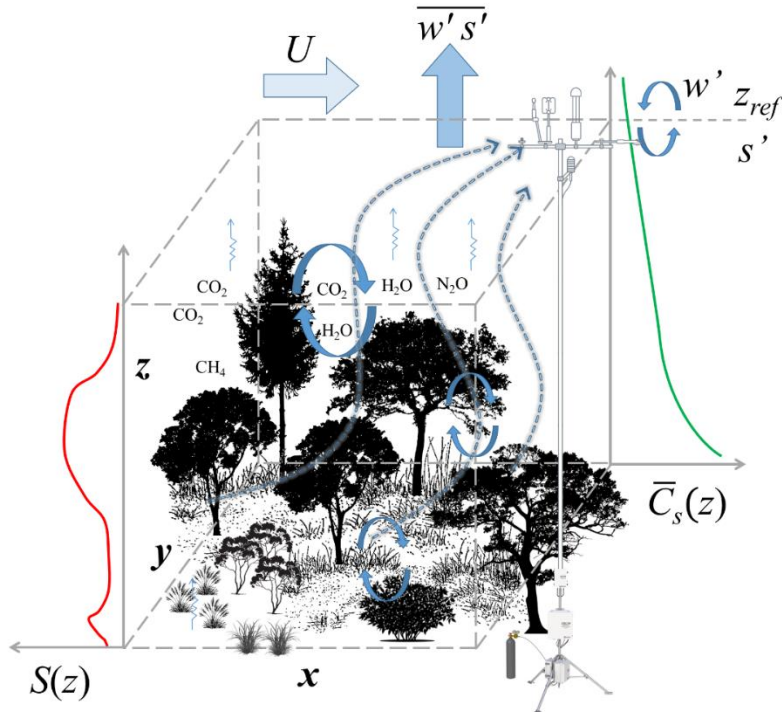
280 Particularities between sap flows were observed by Kotowska et al. (2021), where
281 species with higher hydraulic efficiency have significantly higher flow. In addition, medium-
282 sized plants in the same area had no direct effect on this efficiency, and the environment was
283 an expressive controller of the hydraulic gradient, with these characteristics being
284 differentiated in wet and dry forests. Goldsmith (2013) encourages that the analysis of this
285 variable and the observations in the soil-plant-atmosphere system should be correlated due
286 to the intrinsic relationships between them.

287

288 *Eddy covariance method*

289 Another widely used method, with several monitoring towers worldwide, is the eddy
290 covariance method, capable of directly measuring vertical turbulent flows from different
291 surfaces. This method quantifies the fluxes of energy and gases, e.g., methane (CH₄), nitrous
292 oxide (N₂O), carbon dioxide (CO₂), and water vapor, between the biosphere and the
293 atmosphere (Moffat et al., 2007; Rannik et al., 2016). At the canopy-atmosphere interface,
294 the sensor daily, on a daytime and night-time scale, quantifies the net exchange of CO₂ in the
295 ecosystem employing an infrared gas analyzer. Despite its expressive use in several
296 agricultural and forestry land areas, the method is criticized due to errors or uncertainty of
297 fluxes not fully accounted for within and below the sensor field, and horizontal advection,
298 which makes it difficult to interpret the fluxes (Baldocchi, 2003; Loescher et al., 2006; Xu et
299 al., 2018b; Levy et al., 2020) (Fig. 4).

300



301

302 **Fig. 4** Schematic view of a monitoring tower with eddy covariance. Local-scale
 303 measurements of flows are made directly in situ

304

305 In Fig. 4 the vertical turbulent flux of mass and energy is quantified at the reference
 306 height (z_{ref}), referring to all sources and sinks [$S(z)$] in the ecosystem of the study area (i.e.,
 307 range area represented by the grey dotted line), which can be calculated by integrating
 308 $\overline{w's'}(z_{ref}) = - \int_{z=0}^{z_{ref}} S_s(z)$, where $\overline{w's'}$ is the covariance between wind speed fluctuations and the
 309 corresponding perturbations in a scalar concentration. The correlated eddies of vertical wind
 310 speed (w') and scalar concentration (s') are responsible for transporting mass and energy
 311 vertically. $\overline{C}_s(z)$ is the schematic concentration profile of the area (Baldocchi, 2003; Loescher
 312 et al., 2006; Xu et al., 2018b; Levy et al., 2020).

313

314 As with any method of quantifying energy and mass fluxes, this one has pros and
 315 cons. Among the several existing advantages, the main ones are: it is not a destructive method
 316 (i.e., it does not cause disturbances in vegetation and soil), which thus demands a lower
 317 workload and can be used on large scales, in addition to being a method independent.
 318 However, when applied in places with unstable atmospheric conditions and uneven terrain,
 the readings have low accuracy and/or coherence (Billesbach, 2011; Yuan et al., 2019),

319 mainly due to absent advection fluxes and energy instability surface, which is considered a
320 disadvantage (Baldocchi et al., 1988), given that quantifying this flow is a difficult task, as it
321 requires having several towers in the same site (Xu et al., 2020; Matthews and Schume,
322 2022).

323 However, in the last two decades, the eddy covariance technique has still been one of
324 the most important in determining fluxes in arid, semiarid, and humid ecosystems. Studies
325 carried out in riparian cottonwood forests in Lethbridge, Alberta, Canada by Flanagan et al.
326 (2017) and Flanagan et al. (2021) have indicated that the energy budget of latent and sensible
327 heat fluxes was satisfactory and with good results. According to the authors, such flux
328 variations were driven by the availability of energy in the ecosystem and acted as CO₂ sinks
329 in the growing season. In this season, the energy consumed by plants for their physiological
330 activities increases; on the other hand, the net energy present in the environment decreases
331 (Xue et al., 2021).

332 Currently, some flux networks can be accessed to acquire energy budget data between
333 the biosphere and atmosphere, e.g., the National Observatory of Water and Carbon Dynamics
334 in the Caatinga Biome (NOWCDCB), AmeriFlux, FluxNet, CarboEuroFlux, FluxNet-
335 Canada, among others. The towers for monitoring the variables of turbulent fluxes of CO₂,
336 sensible heat, and latent heat, are equipped with an eddy covariance system. Installed in
337 towers above the surface, e.g., forest canopy and cropland, the basic equipment is an open-
338 path, infrared gas analyzer—IRGA (for quantification of CO₂ and water vapor) and three-
339 dimensional sonic anemometer (i.e., to quantify wind direction and speed), connected to a
340 datalogger (Niu et al., 2021). It is worth mentioning that installing other micrometeorological
341 sensors is of paramount importance for quantifying environmental variables. For example, in
342 Brazil, NOWCDCB has ensured monitoring in several areas of the Caatinga biome,
343 providing data on carbon stocks and fluxes from this ecosystem (e.g., Mendes et al., 2020,
344 2021; Menezes et al., 2021; Costa et al., 2022).

345 The absorption of energy by the surface in the layers close to the ground is one of the
346 factors responsible for generating the turbulent movements of the energy flux. The upward
347 and downward movement of air that forms inside and above the canopy carries particles with
348 different vertical speeds up and down in the form of eddies (Fig. 4). On a diurnal scale, CO₂
349 fluxes are represented by the net exchange of carbon from photosynthesis (i.e., consumption

350 of CO₂) and ecosystem respiration (i.e., the release of CO₂ to the environment). In respiration,
351 a process that occurs mostly at night, autotrophic (e.g., roots, stems, leaves) and heterotrophic
352 respiration (e.g., soil-dwelling microorganisms) predominate, occurring simultaneously.
353 Thus, knowing the concentration of CO₂ and the vertical velocity of the air parcels, we can
354 determine the vertical flux (Equation 3) (Burba and Anderson, 2010; Velasco & Roth, 2010).
355

$$356 \quad F = \overline{c' \cdot w'} = \frac{1}{n} \sum_{i=1}^n (w'_i \cdot c'_i) \quad (3)$$

357
358 where F is the turbulent vertical flux of CO₂, $\overline{c'}$ is the covariance between the instantaneous
359 deviations of the CO₂ concentration, $\overline{w'}$ is the covariance between the instantaneous
360 deviations from the vertical wind speed, and n is the number of samples during the averaging
361 time. For example, F is expressed in units of mass per area and time (g m⁻² s⁻¹) or equivalent
362 units, with mass being expressed in micromoles (μmol), grams of CO₂ (g), or grams of
363 carbon (g C), the area in m², ha or km², and the time in seconds, hours, days or years.
364

365 It is important to emphasize that the footprint (i.e., part of the surface that contains
366 the source and sinks elements that contribute to the vertical flux) of the constituent gases in
367 the atmosphere in which it is intended to be analyzed must contain a large and homogeneous
368 surface. According to Grimmond and Oke (1999), it can be 100 to 300 times the height of
369 the analyzed surface in urban areas (e.g., with buildings); in a forested area, Rebmann et al.
370 (2005) reported minimum requirements of 50 to 100 m roughness lengths. In an agricultural
371 field, Arriga et al. (2017) used a measurement height of 2.35 m above the canopy, whose
372 vegetation had a height of 1.0 m. This characteristic helps the dataset, not present
373 inconsistency problems, also known as noise (Velasco & Roth, 2010). Hence, other methods
374 can be applied to measure fluxes in ecosystems.

375

376 *Remote sensing-based surface energy balance*

377 On a space-time scale, remote sensing data are applied to quantify fluxes in forest and
378 agricultural areas. This tool, which in different spatial resolutions has open access to images
379 and is very useful for quantifying energy balance components; as well as their interactions

380 with water scarcity phenomena in the atmosphere and soil. The spectral monitoring of the
381 canopy and the unification of meteorological variables are essential data for model inputs
382 (Saleska et al., 2016; Liu et al., 2021a). Models such as SEBAL (Surface Energy Balance
383 Algorithm for Land), METRIC (Mapping EvapoTranspiration at high Resolution with
384 Internalized Calibration), and SEBS (Surface Energy Balance System) are the main
385 algorithms used in remote sensing to quantify energy fluxes (Allen et al., 2011; Wagle et al.,
386 2017; Mokhtari et al., 2021). With the images in hand, the principle consists of identifying
387 cold and hot pixels, and through interactive methods, the fluxes on the surface are determined
388 (Allen et al., 2011).

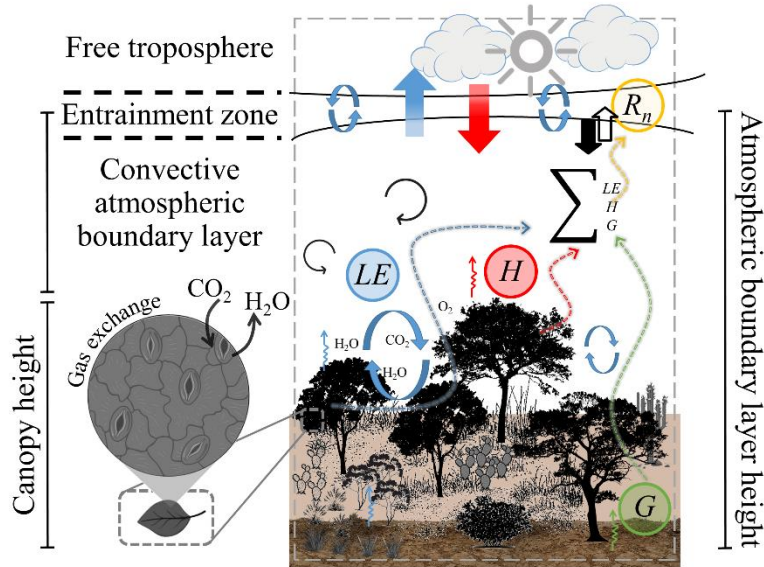
389 The application of remote sensing techniques in the determination of fluxes has been
390 gaining strength over the years due to the practicality and low cost of application. For the
391 determination of turbulent flows on the surface, the technique is based on the use of auxiliary
392 surface parameters (e.g., albedo, emissivity, relief, vegetation cover index, leaf area index,
393 land surface temperature, among others), as well as, latent heat fluxes, sensible heat, soil heat
394 flux and evapotranspiration can be determined (Shang et al., 2020; Nisa et al., 2021). Using
395 observational data from FLUXNET, Bodesheim et al. (2018) were able to quickly and
396 accurately determine the global latent heat flux through remote sensing. In addition, recent
397 studies have reported that the use of methods that integrate data from towers and remote
398 sensing products can help to improve the accuracy of energy flux determination on a global
399 scale and that they also help to reduce the dissimilarity of results obtained individually
400 (Bodesheim et al., 2018; Xu et al., 2018a; Shang et al., 2020).

401 In a study carried out by de Oliveira et al. (2022), using data from the Moderate
402 Resolution Imaging Spectroradiometer (MODIS), for the application of remote sensing,
403 together with data monitored by in situ flux towers over Caatinga areas, were fundamental
404 for the quantification of gross primary production (GPP). Also, according to the authors, the
405 MODIS products, i.e., GPP and ET, showed high accuracy (about 60%) on a vegetated
406 surface with Caatinga. Since this biome has intrinsic characteristics and endemic species,
407 monitoring the GPP helps to understand the behavior of CO₂ exchanges in this ecosystem
408 (Costa et al., 2022). Furthermore, carbon and water fluxes vary across most surfaces; for
409 example Costa et al. (2022) observed more intense seasonal changes in GPP in sites with
410 Caatinga and Pantanal than in Amazon and Cerrado (Brazilian Savanna). Due to this,

411 monitoring vegetation with high frequency and low cost in different parts of the world makes
412 MODIS a widely used sensor (MacBean et al., 2018). On the other hand, there are advantages
413 and disadvantages to MODIS. As a disadvantage, it has a large resolution, and, as an
414 advantage, it has daily periodicity and spectral sensitivity, which helps in the application of
415 energy balance, analysis of vegetation indices, and quantification of GPP (Wu et al., 2008;
416 MacBean et al., 2018; Yao et al., 2018).

417 The surface energy balance can be measured independently using sensors or
418 estimated using equations on an ecosystem scale. The energy components of this application
419 result in net radiation (R_n), from which the latent heat flux (LE), sensible heat flux (H), and
420 soil heat flux (G) are partitioned (Wagle et al., 2017; Mauder et al., 2020). However, the
421 instrumentation used to measure mainly the LE component is not always applicable or
422 accessible. Thus, this variable was quantified in several studies by the simplified energy
423 balance residue, i.e., $LE = R_n - G - H$ (Wagle et al., 2017; Chen and Liu, 2020; Mauder et
424 al., 2020; Castellví et al., 2020). In addition, there are other terms linked to energy
425 represented in the canopy and energy used in the process of photosynthesis, but no more than
426 2% in these types of ecosystems (Heilman et al., 1994; Allen et al., 1998). The LE is the
427 energy associated with water vaporization and evapotranspiration; R_n is the energy from the
428 atmosphere and the surface of the soil-canopy system (i.e., converted into thermal energy or
429 long-wave and short-wave heat); G is the soil heating energy, and H is the energy available
430 for heating the air. These parameters mentioned above are fundamental for the occurrence of
431 gas exchange in plants (Fig. 5).

432



433

434 **Fig. 5** Diurnal interactions between latent heat fluxes (LE), sensible heat (H), soil heat (G),
 435 and net radiation (R_n) in a Brazilian Seasonally Dry Tropical Forest (Caatinga). The dashed
 436 arrows in blue, red, and green colors are contributors to the energy balance. Note: in this
 437 flowchart, we do not show the influence of horizontal advection, which also affects the
 438 atmospheric boundary layer.

439

440 In the transfer of energy from surfaces, there are variations in heat fluxes according
 441 to vegetation, soil exposure, and local humidity (Faridatul et al., 2020). In areas with Caatinga
 442 and agriculture, net radiation presents lower results ($< 20\%$) when compared to areas of
 443 exposed soil, in which this variation ranges from 25 to 30%. On vegetated surfaces, energy
 444 transfer to the atmosphere during the day is slower, conserving it for a longer time (Lima et
 445 al., 2021). One of the variables that mostly contributes to air temperature variation is net
 446 radiation due to the energetic contribution of LE and H . According to Oliveira et al. (2006),
 447 values lower than $25 \text{ MJ m}^{-2} \text{ day}^{-1}$ of global solar radiation were observed at times with
 448 milder temperatures ($\sim 24 \text{ }^\circ\text{C}$), and $28.5 \text{ MJ m}^{-2} \text{ day}^{-1}$ when the temperature was higher
 449 (above $30 \text{ }^\circ\text{C}$), in the Caatinga area. In contrast, Silva et al. (2017) found R_n values in the
 450 Caatinga of $19.6 \text{ MJ m}^{-2} \text{ day}^{-1}$, soil heat flux ranging from 0.01 to $1.07 \text{ MJ m}^{-2} \text{ day}^{-1}$, and
 451 in the dry and rainy season, the average LE was $2.3 \text{ MJ m}^{-2} \text{ day}^{-1}$ and $4.8 \text{ MJ m}^{-2} \text{ day}^{-1}$,
 452 respectively.

453 Unfortunately, in areas with expressive vegetation of cactus species, this information
454 is still developing in the literature. Under arid conditions in the Atacama Desert, Kalthoff et
455 al. (2006) evaluated the heat fluxes of mixed areas, with the presence of irrigated agriculture
456 (e.g., viticulture), shrub, and cacti. Also, according to the authors, sensible heat throughout
457 the year was more prominent than latent heat, with sensible heat being the largest dominant
458 energy sink during the day. In the semiarid region, in *O. ficus-indica* cultivation (Consoli et
459 al., 2013a), they observed net radiation of $19 \text{ MJ m}^{-2} \text{ day}^{-1}$, part of which was destined for
460 H ($9.3 \text{ MJ m}^{-2} \text{ day}^{-1}$) and LE ($6.2 \text{ MJ m}^{-2} \text{ day}^{-1}$), corresponding to 49 and 33%, respectively.
461 Furthermore, Consoli et al. (2013b) reported that the heat flux in the soil during the cactus
462 growth period presented very low values, close to zero. Interestingly, this energetic partition
463 is similar to the Caatinga, perhaps due to resistance to water deficit and stomatal regulation.
464 In cacti, the sensible heat flux may also be higher due to atmospheric instability, causing
465 convection to become efficient and transfer more energy to this component (Consoli et al.,
466 2013b).

467 The variability of available energy is notorious, whether in Caatinga ecosystems or
468 with cacti. In Caatinga, greater expressiveness was reported throughout the year for sensible
469 heat flux (Teixeira et al., 2008; Borges et al., 2020), and in cactus, this similarity of flux
470 occurs in cactus—*Opuntia* (Consoli et al., 2013b), as well as in columnar cactus—*Carnegiea*
471 *gigantea* (Flanagan and Flanagan, 2018). Although, the sensible heat flux has greater
472 magnitudes in the rainy season; this caveat is also valid for the soil heat flux (Teixeira et al.,
473 2008; Consoli et al., 2013b; Flanagan and Flanagan, 2018).

474 Among the components of the simplified surface energy balance, the soil heat flux
475 (G) is an often neglected constituent (Heusinkveld et al., 2004). However, this variable is
476 closely related to plants and the atmosphere. Under arid climate conditions, Saito et al. (2006)
477 pointed out that the bare soil has its heat and water fluxes affected. In forest areas, the
478 variability of flows may be linked to soil characteristics, canopy density of species and root
479 biomass heterogeneity, factors that mainly alter the flux of carbon dioxide in the soil
480 (Kulmala et al., 2019; Palmroth et al., 2019). In addition, changes in land use and land cover
481 can modify the local hydrological dynamics, as well as influence ecosystem services.

482

483 **Carbon allocation and partitioning in ecosystems**

484 In vegetated areas, despite advances in monitoring and carbon partitioning of
 485 ecosystems, there are still uncertainties related to these processes. Carbon emission and/or
 486 capture have a significant relationship with the global carbon balance in terrestrial
 487 ecosystems. One of the most relevant variables in the carbon balance is the net ecosystem
 488 CO₂ exchange (NEE), which is simply determined through gross primary productivity (GPP)
 489 and ecosystem respiration (R_{eco}) (Table 1). The NEE can be quantified independently of the
 490 photosynthetic metabolism of the species (e.g., C3, C4, and CAM—crassulacean acid
 491 metabolism; see Fig. 6); however, each metabolism has its particularities. Furthermore, as it
 492 is a CO₂ balance, NEE must be measured on a day and night scale since there is a daytime
 493 CO₂ uptake from C3 and C4; however, in CAM, there is a predominance of nocturnal uptake
 494 of atmospheric CO₂. Thus, the GPP corresponds to photosynthesis (i.e., it is the amount of
 495 carbon absorbed by the vegetation), and the R_{eco} refers to the sum of carbon efflux from the
 496 respiration of autotrophic and heterotrophic organisms (Zanotelli et al., 2015; Campioli et
 497 al., 2016; Schimel & Schneider, 2019).

498

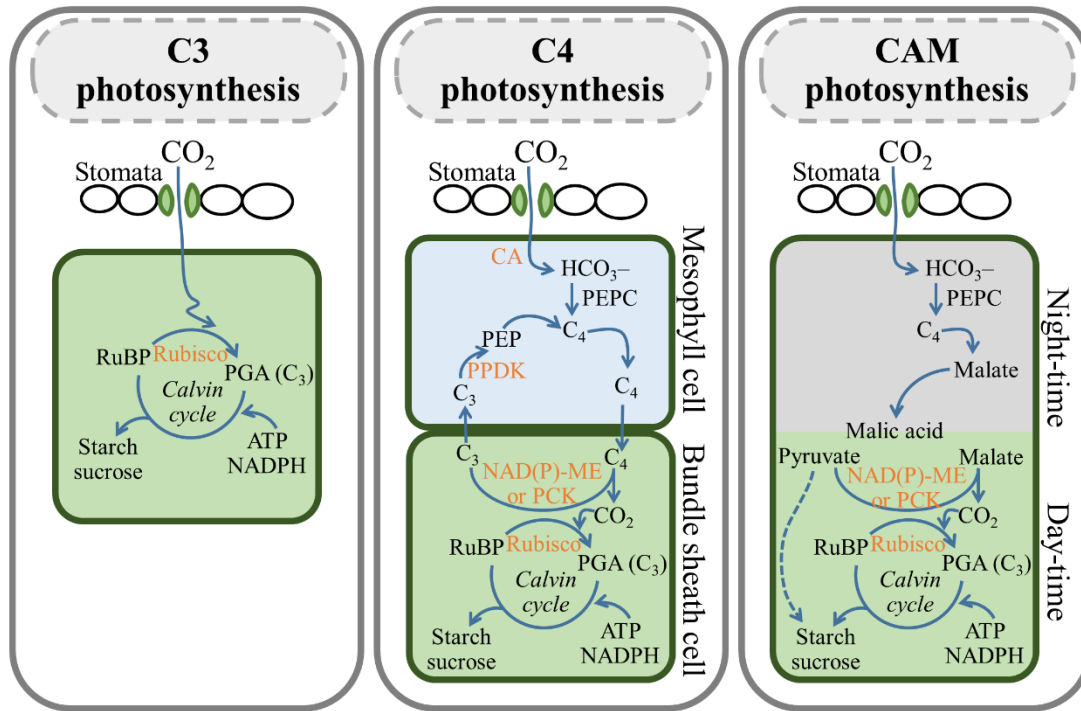
499 **Table 1** List of equations for estimating the carbon balance in ecosystems and relevant
 500 components

Equation	Source
$NEE = -GPP + R_{eco}$	(Schimel & Schneider, 2019)
$GPP = NPP + R_a$	(Campioli et al., 2016)
$R_{eco} = R_a + R_h$	(Campioli et al., 2016)
$NEP = GPP - R_{eco} = NPP - R_h$	(Campioli et al., 2016)
$NECB = NEP + OF - FH$	(Zanotelli et al., 2015)
$CUE = \frac{NPP}{GPP}$	(Zanotelli et al., 2015)

where NEE is the net ecosystem CO₂ exchange, GPP is the gross primary production, R_{eco} is the ecosystem respiration, NPP is the net primary production (quantified above- and belowground), R_a is the autotrophic respiration (quantified above- and belowground), R_h is the heterotrophic respiration from soil and coarse woody debris, NEP is the net

ecosystem production, *NECB* is the net ecosystem carbon balance, *OF* are the organic fertilizers, *FH* is the fruit harvest, and *CUE* is the carbon use efficiency.

501



502

503 **Fig. 6** Carbon pathway in the photosynthetic metabolism of C3, C4, and CAM plants
 504 (crassulacean acid metabolism)

505

506 The carbon assimilation carried out by the species is fundamental for determining the
 507 productivity of the crop or biome. With the plant's carbon budget, we can determine the net
 508 biome production (i.e., $NBP = -NEE - Yield - \epsilon$), where *Yield* is harvested crop yield, and
 509 ϵ is the carbon losses caused by disturbances, e.g., fires. Net biome production (NBP) results
 510 are positive and negative scale, indicating that the environment can be a carbon source or
 511 sink (Pecchioni et al., 2020; Zhou et al., 2021). In pasture areas under semiarid conditions,
 512 biotic and abiotic factors can compromise the carbon balance. For example, water deficit and
 513 air and soil temperature cause heat stress on plants and soil microorganisms, negatively
 514 altering the carbon exchange capacity of the ecosystem (Wang et al., 2019).

515 Major differences exist between the photosynthetic and transpiration rates of C3, C4,
 516 and CAM plants. CAM species have substantially higher efficiency in carbon assimilation

517 than species performing C3 or C4 photosynthesis. However, even with high carbon
518 utilization, CAM plants in agriculture are still neglected (Hogewoning et al., 2021). On the
519 other hand, cactus cultivation goes beyond the use of fruits and cladodes to feed humans and
520 animals. In environmental and economic matters, the stock of carbon in the soil has been an
521 efficient alternative (Bautista-Cruz et al., 2018), and it is worth noting that on average, 36.2%
522 of the cladode of *Opuntia* is composed of carbon, with one adult plant is capable of fixing
523 8.29 kg of CO₂ per year (Gomez-Casanovas et al., 2007). Considering 1 hectare of *Opuntia*
524 *ficus-indica*, carbon fixation can reach 63.25 kg day⁻¹ (Andreu-Coll et al., 2020). These
525 carbon fixation values may vary depending on environmental conditions, agricultural
526 practices, the number of cladodes per plant, and cultivation density. The carbon present in
527 the *Opuntia* structures can be used to produce substrate for bacteria that help in the
528 fermentation of biomass to produce biogas (Quiroz et al., 2021). Despite the high capture and
529 use of CO₂, cactus cultivation can be stimulated for agricultural areas as a carbon credit.
530 However, there are still uncertainties about the carbon balance in areas cultivated with these
531 plants.

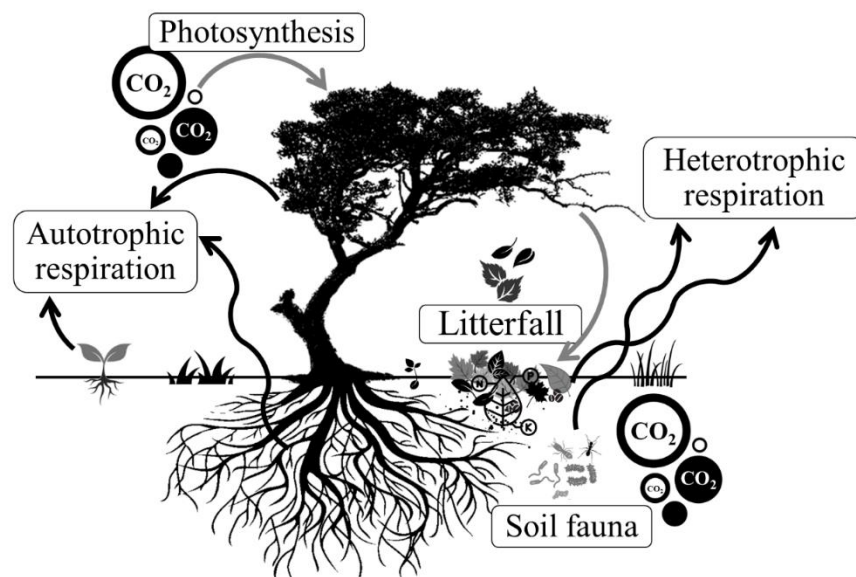
532

533 *Factors controlling variation in carbon dioxide efflux from surface litter*

534 In forested areas, woody species can store large amounts of carbon in their above-
535 and below-ground biomass. Therefore, the implementation of forests as a CO₂ sequester has
536 low costs between 10 USD to 68 USD t CO₂-eq (López-Pacheco et al., 2021). In the Caatinga
537 area under semiarid conditions, Silva et al. (2017) reported uptake of 2.82 t C ha⁻¹ year⁻¹,
538 and in pasture 3.62 t C ha⁻¹ year⁻¹. In pastures in the Cerrado, results of 842 g C m⁻² year⁻¹
539 were observed (Arruda et al., 2016), and according to Ferreira et al. (2020) in Caatinga, it is
540 4.63 g CO₂ m⁻² day⁻¹ (is equal to 461 g C m⁻² year⁻¹, for reference, 1 g C = 0.083 mol CO₂
541 = 3.664 g CO₂). The lowest values of CO₂ uptake generally occur in the dry season in the
542 Caatinga, this is due to the fall of leaves, a phenomenon that does not occur in pastures. On
543 the other hand, deciduous leaves do not occur in the cactus, giving the plant absorption of
544 CO₂ throughout the year, keeping the carbon stored efficiently.

545 In the interaction of the soil-plant system, one of the main contributors to the natural
546 return of carbon to the soil is litterfall. The litter material comes from the forest and crops
547 debris, which, in turn, are deposited on the soil and subsequently decomposed by soil-

548 dwelling microorganisms, jointly aided by environmental conditions (Fig. 7). In this way,
549 carbon is maintained in the soil, and plants benefit by supporting vegetative growth (Fang et
550 al., 2015; Riutta et al., 2021). However, the quantity and quality of these deposited materials
551 are crucial for the carbon balance. As reported by Fang et al. (2015), the greater the litterfall
552 inflows into forest areas, there is an increase in the loss of litter mass and constituted carbon.
553 This type of characteristic may be due to the accelerated decomposition of the material and
554 available nutrients, increasing soil respiration and, consequently, CO₂ emission.
555



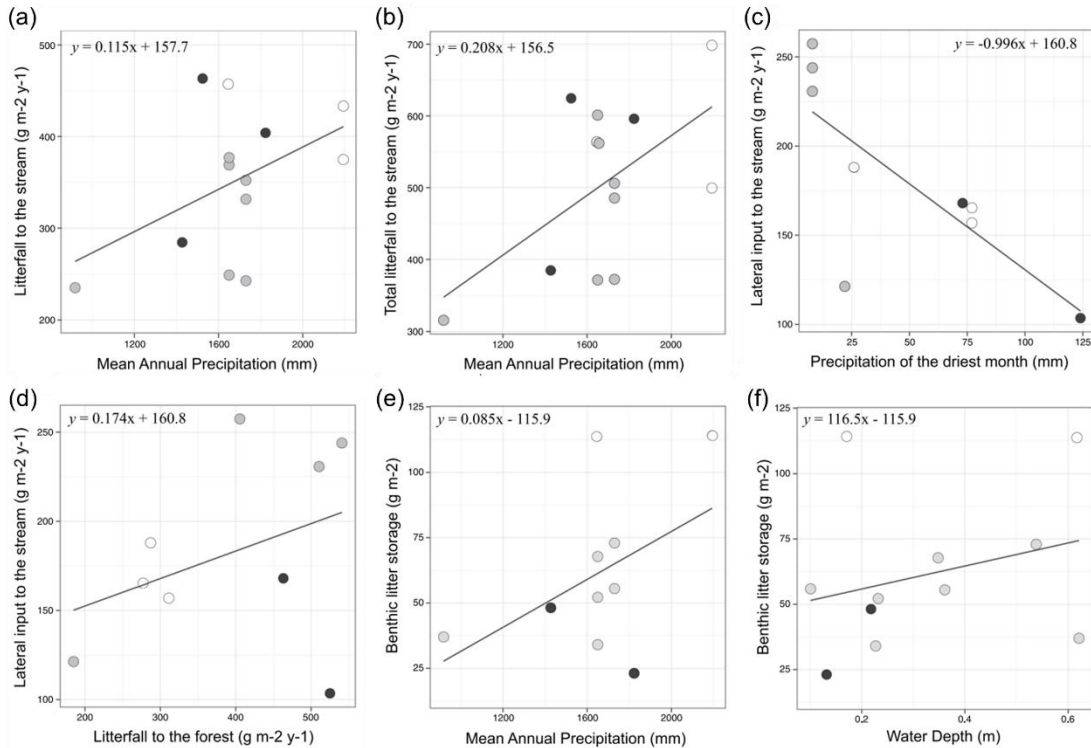
556
557 **Fig. 7** Conceptual diagram illustrating litter components and carbon dioxide (CO₂) emissions
558 through autotrophic and heterotrophic respiration in a forested area
559

560 Therefore, whether in planted or natural forest areas, the losses of litter mass and
561 carbon contained in it are differentiated. In addition, not only due to debris deposited in the
562 soil, but environmental conditions exert seasonality in the emission of CO₂ and respiratory
563 flux of the ecosystem. Fang et al. (2015) observed that in seasons with warm-wet conditions,
564 there were higher soil respiration rates when compared to cool-dry seasons. In areas with
565 cactus and legume agroforestry systems, variations in carbon content and soil respiration
566 were also observed (Camelo et al., 2021). Also, according to the authors, climatic conditions
567 influence these variables, and plants with CAM metabolism, despite the lower contribution
568 with canopy debris, help deposition plant material from the root system (De León-González

569 et al., 2018; Camelo et al., 2021). In addition, this root system in rainy periods helps rapidly
570 capture carbon and decreases CO₂ emission from soil respiration (De León-González et al.,
571 2018). Air temperature and soil moisture are variables that contribute to the carbon balance
572 in cactus areas, and, in addition, carbon and calcium from cladodes are fundamental in the
573 decomposition of cactus litterfall (Bilderback et al., 2021).

574 While there is much evidence in a forested landscape, for example, comparing
575 Atlantic forest, Amazon forest, and Cerrado savanna biomes, Tonin et al. (2017) observed
576 variations in litter inputs on a space-time scale as a function of rainfall and water depth
577 through regression model (Fig. 8). The findings highlighted an increase in litter storage with
578 annual precipitation and water depth. Moreover, temporal patterns of litterfall were
579 consistently different among biomes. Techniques such as cutting management in Caatinga
580 forest species can help in the deposition and decomposition rate of litter (Barreto-Garcia et
581 al., 2021; Matos et al., 2021). According to Barreto-Garcia et al. (2021), the use of clear
582 cutting and selective cutting by diameter in species of the Caatinga biome, in the short term,
583 negatively influences soil microbial activity because soil carbon suffers greater losses in the
584 form of CO₂. To help understand litter deposition, variables such as global solar radiation,
585 soil heat flux, precipitation, vapor pressure deficit, and Normalized Difference Vegetation
586 Index are factors that control the deposition of this material in the soil (Queiroz et al., 2019).
587 In addition, the maintenance of carbon in the litter soil is essential for the release of nutrients
588 such as nitrogen and thus will assist in the survival and maintenance of Caatinga species
589 (Queiroz et al., 2019; Menezes et al., 2021; Silva et al., 2021).

590



591

592 **Fig. 8** Relationships between litter inputs, benthic storage and their predictors in Atlantic
 593 forest (black circles), Amazon (white circles), and Cerrado streams (grey circles): (a) litterfall
 594 vs. mean annual precipitation; (b) total litterfall vs. mean annual precipitation; (c) lateral
 595 inputs vs. precipitation of the driest month; (d) lateral inputs vs. litterfall to the forest; (e)
 596 storage vs. mean annual precipitation; and (f) storage vs. water depth. More details can be
 597 found in Tonin et al. (2017)

598

599 *Factors affecting respiration from soil, litter, and soil organic matter*

600

One of the biggest drivers of carbon efflux in terrestrial ecosystems is soil respiration.
 601 This variable ranks at approximately 75 to 100 Pg C year⁻¹ on the terrestrial sphere and
 602 deserves significant attention as far as CO₂ emissions from fossil fuels (Riutta et al., 2021).
 603 In areas with buildings, the search for urban green landscapes is constant. Thus, in arid
 604 regions, the use of cacti, together with xerophilous tree and shrub species, contributes to the
 605 regulation of biogeochemical cycles, in addition to maintaining carbon for a longer time fixed
 606 in the soil (Guillen-Cruz et al., 2021). In areas of the Caatinga, carbon is not significantly
 607 released into the atmosphere in the wet season, and in the dry season, the vegetation can still
 608 act as a carbon sink, with low respiration rates (Mendes et al., 2020). Then also, according

609 to the authors, the respiration of the ecosystem in 2014 was higher and more significant ($p <$
610 0.01) than in 2015, both in the dry season and wet season (Table 2). However, these results
611 are low when compared to Amazon, Cerrado, and Atlantic forest due to low organic carbon
612 in relation to humid regions. Although the measurement of carbon dynamics in vegetated
613 areas is important information for society and the academic community, many uncertainties
614 are raised due to interactive processes and autotrophic and heterotrophic soil respiration
615 changes.

616

617 **Table 2** Seasonal variation and annual net ecosystem CO₂ exchange (NEE), gross primary
618 production (GPP), ecosystem respiration (R_{eco}) and ecosystem carbon-use efficiency
619 (NEP/GPP ratio) fin the study period. Source: (Mendes et al., 2020)

Year	Variable	Statistics	Dry-wet transition	Wet season	Wet-dry transition	Dry season	Annual
2014	NEE	Mean	-0.50 ± (0.05)	-0.70 ± (0.33)	-0.25 ± (0.04)	-0.26 ± (0.03)	-0.46 ± (0.03)
		Sum	-45.9	-84.0	-14.9	-24.2	-169.0
	GPP	Mean	-1.20 ± (0.08)	-1.68 ± (0.10)	-0.73 ± (0.06)	-0.64 ± (0.04)	-1.14 ± (0.06)
		Sum	-110.6	-200.8	-44.3	-59.0	-414.7
	R_{eco}	Mean	0.70 ± (0.04)	0.98 ± (0.04)	0.48 ± (0.03)	0.39 ± (0.01)	0.68 ± (0.03)
		Sum	64.7	117.0	29.4	34.7	246.0
NEP/GPP	Ratio	0.41	0.42	0.34	0.41	0.41	
2015	NEE	Mean	-0.28 ± (0.03)	-0.63 ± (0.07)	-0.30 ± (0.03)	-0.36 ± (0.01)	-0.40 ± (0.02)
		Sum	-17.9	-56.0	-27.1	-44.0	-145.0
	GPP	Mean	-0.79 ± (0.03)	-1.43 ± (0.08)	0.78 ± (0.04)	-0.71 ± (0.02)	-0.92 ± (0.04)
		Sum	-49.0	-127.0	72.0	-86.0	-334.0
	R_{eco}	Mean	0.51 ± (0.02)	0.80 ± (0.04)	0.49 ± (0.02)	0.34 ± (0.02)	0.52 ± (0.02)
		Sum	30.9	71.3	44.8	42.0	189.0
NEP/GPP	Ratio	0.36	0.44	0.38	0.51	0.43	

Bold values are significantly different between each season in 2014 and its correspondent season in 2015 at the 0.05 level ($p < 0.05$).
The results are given in the form mean ± standard deviation (g C m⁻² year⁻¹ or g C m⁻²).

620

621 Thus, as a way of decreasing the efflux of CO₂ in the ecosystem, the use of CAM
622 plants can modify the local carbon budget when tree crops are used together (Owen et al.,
623 2016). For Guevara-Escobar et al. (2021), cacti may not be highly expressive in decreasing
624 the nocturnal CO₂ source when exposed to other cultures of C3 and C4 metabolism.
625 However, it is known that cacti of the species *O. ficus-indica* under fields with a high density
626 of individuals have expressive nocturnal assimilation of CO₂. Nevertheless, when exposed to
627 extreme droughts, the net uptake of CO₂ shows an extreme reduction (Acevedo et al., 1983;

628 Nobel & Hartsock, 1984). Indeed, not only due to environmental and climatic circumstances,
629 but the age of the cladodes and the plant influence the preference for CO₂ uptake, as cladodes
630 with initial weeks of emergence can open their stomata during the daytime and capture CO₂
631 (Acevedo et al., 1983). In summary, *Opuntia*, when exposed to high CO₂, absence of water
632 stress, and favorable temperature (i.e., 25 °C during the day and 15 °C at night), significantly
633 increases the production of biomass, thickness, and the number of cladodes (Nobel & Israel,
634 1994; Neupane et al., 2021).

635

636 **Conclusions**

637 In the present study, we carried out a survey of studies focusing on carbon and energy
638 fluxes in terrestrial ecosystems. We emphasize that deforestation can cause serious problems
639 in the energy and carbon balance, and areas with Caatinga can suffer significant damage due
640 to the composition of species with different photosynthetic metabolism, considering that
641 plants with crassulacean acid metabolism (CAM) can work efficiently in low water vapor
642 and CO₂. However, more intense anthropic disturbances and the increase in aridity, predicted
643 by climate simulations, could significantly negatively affect large species. Thus,
644 understanding the energy balance of vegetation is also a critical factor, as these simulations
645 are helpful for use in weather forecasting or climate change prediction. In this context, due
646 to the findings in this review, future research may be encouraged on:

647 (1) Water use and carbon allocation above and below ground.

648 (2) Plant responses under extreme growing conditions, particularly to long periods of
649 drought.

650 (3) Climate simulations in cactus and Caatinga agricultural areas.

651

652 **Statements and Declarations**

653 All authors have read and understood the statement of policy of interests.

654

655 **Ethical Responsibilities of Authors**

656 The authors declare no competing interests.

657

658 **Data availability**

659 The datasets generated during and/or analyzed during the current study are available from
660 the corresponding author on reasonable request.

661

662 **References**

663 Acevedo, E., Badilla, I., & Nobel, P. S. (1983). Water Relations, Diurnal Acidity Changes,
664 and Productivity of a Cultivated Cactus, *Opuntia ficus-indica*. *Plant Physiology*, 72(3),
665 775–780. <https://doi.org/10.1104/PP.72.3.775>

666 Ahirwal, J., Kumari, S., Singh, A. K., Kumar, A., & Maiti, S. K. (2021). Changes in soil
667 properties and carbon fluxes following afforestation and agriculture in tropical forest.
668 *Ecological Indicators*, 123, 107354. <https://doi.org/10.1016/J.ECOLIND.2021.107354>

669 Allen, R. G., Pereira, L. S., Raes, D., & Smith, M. (1998). Crop evapotranspiration:
670 Guidelines for computing crop water requirements. In *Food and Agriculture*
671 *Organization of the United Nations* (Issue 56).
672 <http://www.fao.org/docrep/X0490E/x0490e00.htm#Contents>

673 Allen, R., Irmak, A., Trezza, R., Hendrickx, J. M. H., Bastiaanssen, W., & Kjaersgaard, J.
674 (2011). Satellite-based ET estimation in agriculture using SEBAL and METRIC.
675 *Hydrological Processes*, 25(26), 4011–4027. <https://doi.org/10.1002/HYP.8408>

676 Andreu-Coll, L., Cano-Lamadrid, M., Noguera-Artiaga, L., Lipan, L., Carbonell-Barrachina,
677 Á. A., Rocamora-Montiel, B., Legua, P., Hernández, F., & López-Lluch, D. (2020).
678 Economic estimation of cactus pear production and its feasibility in Spain. *Trends in*
679 *Food Science & Technology*, 103, 379–385.
680 <https://doi.org/10.1016/J.TIFS.2020.07.003>

681 Antongiovanni, M., Venticinque, E. M., Matsumoto, M., & Fonseca, C. R. (2020). Chronic
682 anthropogenic disturbance on Caatinga dry forest fragments. *Journal of Applied*
683 *Ecology*, 57(10), 2064–2074. <https://doi.org/10.1111/1365-2664.13686>

684 Araújo Filho, R. N. de, Freire, M. B. G. dos S., Wilcox, B. P., West, J. B., Freire, F. J., &
685 Marques, F. A. (2018). Recovery of carbon stocks in deforested caatinga dry forest soils
686 requires at least 60 years. *Forest Ecology and Management*, 407, 210–220.
687 <https://doi.org/10.1016/J.FORECO.2017.10.002>

688 Arriga, N., Rannik, Ü., Aubinet, M., Carrara, A., Vesala, T., & Papale, D. (2017).
689 Experimental validation of footprint models for eddy covariance CO₂ flux

690 measurements above grassland by means of natural and artificial tracers. *Agricultural*
691 *and Forest Meteorology*, 242, 75–84.
692 <https://doi.org/10.1016/J.AGRFORMET.2017.04.006>

693 Arruda, P. H. Z. de, Vourlitis, G. L., Santanna, F. B., Pinto Jr, O. B., Lobo, F. de A., &
694 Nogueira, J. D. S. (2016). Large net CO₂ loss from a grass-dominated tropical savanna
695 in south-central Brazil in response to seasonal and interannual drought. *Journal of*
696 *Geophysical Research: Biogeosciences*, 121(8), 2110–2124.
697 <https://doi.org/10.1002/2016JG003404>

698 Baldocchi, D. D. (2003). Assessing the eddy covariance technique for evaluating carbon
699 dioxide exchange rates of ecosystems: past, present and future. *Global Change Biology*,
700 9(4), 479–492. <https://doi.org/10.1046/J.1365-2486.2003.00629.X>

701 Baldocchi, D. D., Hicks, B. B., & Meyers, T. P. (1988). Measuring Biosphere-Atmosphere
702 Exchanges of Biologically Related Gases with Micrometeorological Methods. *Ecology*,
703 69(5), 1331–1340. <https://doi.org/10.2307/1941631>

704 Barreto-Garcia, P. A. B., Batista, S. G. M., Gama-Rodrigues, E. F. da, de Paula, A., & Batista,
705 W. C. A. (2021). Short-term effects of forest management on soil microbial biomass
706 and activity in caatinga dry forest, Brazil. *Forest Ecology and Management*, 481,
707 118790. <https://doi.org/10.1016/J.FORECO.2020.118790>

708 Barrett, D. J., Hatton, T. J., Ash, J. E., & Ball, M. C. (1995). Evaluation of the heat pulse
709 velocity technique for measurement of sap flow in rainforest and eucalypt forest species
710 of south-eastern Australia. *Plant, Cell & Environment*, 18(4), 463–469.
711 <https://doi.org/10.1111/J.1365-3040.1995.TB00381.X>

712 Bautista-Cruz, A., Leyva-Pablo, T., León-González, F. de, Zornoza, R., Martínez-Gallegos,
713 V., Fuentes-Ponce, M., & Rodríguez-Sánchez, L. (2018). Cultivation of *Opuntia ficus-*
714 *indica* under different soil management practices: A possible sustainable agricultural
715 system to promote soil carbon sequestration and increase soil microbial biomass and
716 activity. *Land Degradation & Development*, 29(1), 38–46.
717 <https://doi.org/10.1002/LDR.2834>

718 Bilderback, A. H., Torres, A. J., Vega, M., & Ball, B. A. (2021). The structural and nutrient
719 chemistry during early-stage decomposition and desiccation of cacti in the Sonoran
720 Desert. *Journal of Arid Environments*, 195, 104636.

721 <https://doi.org/10.1016/J.JARIDENV.2021.104636>

722 Billesbach, D. P. (2011). Estimating uncertainties in individual eddy covariance flux
723 measurements: A comparison of methods and a proposed new method. *Agricultural and*
724 *Forest Meteorology*, 151(3), 394–405.
725 <https://doi.org/10.1016/J.AGRFORMET.2010.12.001>

726 Bodesheim, P., Jung, M., Gans, F., Mahecha, M. D., & Reichstein, M. (2018). Upscaled
727 diurnal cycles of land-Atmosphere fluxes: A new global half-hourly data product. *Earth*
728 *System Science Data*, 10(3), 1327–1365. <https://doi.org/10.5194/ESSD-10-1327-2018>

729 Bonatelli, M. L., Lacerda-Júnior, G. V., dos Reis Junior, F. B., Fernandes-Júnior, P. I., Melo,
730 I. S., & Quecine, M. C. (2021). Beneficial Plant-Associated Microorganisms From
731 Semiarid Regions and Seasonally Dry Environments: A Review. *Frontiers in*
732 *Microbiology*, 11, 3331. <https://doi.org/10.3389/FMICB.2020.553223/BIBTEX>

733 Borges, C. K., dos Santos, C. A. C., Carneiro, R. G., da Silva, L. L., de Oliveira, G., Mariano,
734 D., Silva, M. T., da Silva, B. B., Bezerra, B. G., Perez-Marin, A. M., & Medeiros, S. de
735 S. (2020). Seasonal variation of surface radiation and energy balances over two
736 contrasting areas of the seasonally dry tropical forest (Caatinga) in the Brazilian semi-
737 arid. *Environmental Monitoring and Assessment*, 192(8), 1–18.
738 <https://doi.org/10.1007/s10661-020-08484-y>

739 Bright, R. M., Davin, E., O'Halloran, T., Pongratz, J., Zhao, K., & Cescatti, A. (2017). Local
740 temperature response to land cover and management change driven by non-radiative
741 processes. *Nature Climate Change*, 7(4). <https://doi.org/10.1038/nclimate3250>

742 Burba, G., & Anderson, D. (2010). *A Brief Practical Guide to Eddy Covariance Flux*
743 *Measurements: Principles and Workflow Examples for Scientific and Industrial*
744 *Applications* (LI-COR Biosciences (ed.); 1st ed., Vol. 1). www.licor.com

745 Camelo, D., Dubeux Jr, J. C. B., Santos, M. V. F. dos, Lira, M. A., Fracetto, G. G. M.,
746 Fracetto, F. J. C., Cunha, M. V. da, & Freitas, E. V. de. (2021). Soil Microbial Activity
747 and Biomass in Semiarid Agroforestry Systems Integrating Forage Cactus and Tree
748 Legumes. *Agronomy*, 11(8), 1558. <https://doi.org/10.3390/AGRONOMY11081558>

749 Campioli, M., Malhi, Y., Vicca, S., Luyssaert, S., Papale, D., Peñuelas, J., Reichstein, M.,
750 Migliavacca, M., Arain, M. A., & Janssens, I. A. (2016). Evaluating the convergence
751 between eddy-covariance and biometric methods for assessing carbon budgets of

752 forests. *Nature Communications*, 7(1), 13717. <https://doi.org/10.1038/ncomms13717>

753 Campos, S., Mendes, K. R., da Silva, L. L., Mutti, P. R., Medeiros, S. S., Amorim, L. B., dos
754 Santos, C. A. C., Perez-Marin, A. M., Ramos, T. M., Marques, T. V., Lucio, P. S., Costa,
755 G. B., Santos e Silva, C. M., & Bezerra, B. G. (2019). Closure and partitioning of the
756 energy balance in a preserved area of a Brazilian seasonally dry tropical forest.
757 *Agricultural and Forest Meteorology*, 271, 398–412.
758 <https://doi.org/10.1016/j.agrformet.2019.03.018>

759 Castellví, F., Suvočarev, K., Reba, M. L., & Runkle, B. R. K. (2020). A new free-convection
760 form to estimate sensible heat and latent heat fluxes for unstable cases. *Journal of*
761 *Hydrology*, 586, 124917. <https://doi.org/10.1016/J.JHYDROL.2020.124917>

762 Cavaleri, M. A., Reed, S. C., Smith, W. K., & Wood, T. E. (2015). Urgent need for warming
763 experiments in tropical forests. *Global Change Biology*, 21(6), 2111–2121.
764 <https://doi.org/10.1111/gcb.12860>

765 Chandel, A. K., Khot, L. R., Molaei, B., Peters, R. T., Stöckle, C. O., & Jacoby, P. W. (2021).
766 High-Resolution Spatiotemporal Water Use Mapping of Surface and Direct-Root-Zone
767 Drip-Irrigated Grapevines Using UAS-Based Thermal and Multispectral Remote
768 Sensing. *Remote Sensing*, 13(5), 954. <https://doi.org/10.3390/RS13050954>

769 Chen, J. M., & Liu, J. (2020). Evolution of evapotranspiration models using thermal and
770 shortwave remote sensing data. *Remote Sensing of Environment*, 237, 111594.
771 <https://doi.org/10.1016/J.RSE.2019.111594>

772 Consoli, S., Inglese, G., & Inglese, P. (2013a). Determination of Evapotranspiration and
773 Annual Biomass Productivity of a Cactus Pear [*Opuntia ficus-indica* L. (Mill.)] Orchard
774 in a Semiarid Environment. *Journal of Irrigation and Drainage Engineering*, 139(8),
775 680–690. [https://doi.org/10.1061/\(ASCE\)IR.1943-4774.0000589](https://doi.org/10.1061/(ASCE)IR.1943-4774.0000589)

776 Consoli, S., Inglese, P., & Inglese, G. (2013b). Determination of evapotranspiration and crop
777 coefficient of cactus pear (*Opuntia ficus-indica* Mill.) with an energy balance technique.
778 *Acta Horticulturae*, 995, 117–124.
779 <https://doi.org/10.17660/ACTAHORTIC.2013.995.14>

780 Consoli, S., & Papa, R. (2013). Corrected surface energy balance to measure and model the
781 evapotranspiration of irrigated orange orchards in semi-arid Mediterranean conditions.
782 *Irrigation Science*, 31(5), 1159–1171. <https://doi.org/10.1007/S00271-012-0395-4>

783 Cook, B. I., Anchukaitis, K. J., Touchan, R., Meko, D. M., & Cook, E. R. (2016).
784 Spatiotemporal drought variability in the mediterranean over the last 900 years. *Journal*
785 *of Geophysical Research*, *121*(5), 2060–2074. <https://doi.org/10.1002/2015JD023929>

786 Costa, G. B., Santos Silva, C. M., Mendes, K. R., M dos Santos, J. G., Neves, T. T. A. T.,
787 Silva, A. S., Rodrigues, T. R., Silva, J. B., Dalmagro, H. J., Mutti, P. R., Nunes, H. G.
788 G. C., Peres, L. V, Santana, R. A. S., Viana, L. B., Almeida, G. V, Bezerra, B. G.,
789 Marques, T. V, Ferreira, R. R., Oliveira, C. P., ... Andrade, M. U. G. (2022). WUE and
790 CO₂ Estimations by Eddy Covariance and Remote Sensing in Different Tropical
791 Biomes. *Remote Sensing*, *14*(14), 3241. <https://doi.org/10.3390/RS14143241>

792 de Jesus, J. B., de Oliveira, D. G., Araújo, W. S., da Cruz, L. S., & Kuplich, T. M. (2022).
793 Influence of anthropization on the floristic composition and phytosociology of the
794 Caatinga susceptible to desertification in the state of Sergipe, Brazil. *Tropical Ecology*,
795 *1*, 1–11. <https://doi.org/10.1007/S42965-021-00201-1/FIGURES/4>

796 De León-González, F., Fuentes-Ponce, M. H., Bautista-Cruz, A., Leyva-Pablo, T., Castillo-
797 Juárez, H., & Rodríguez-Sánchez, L. M. (2018). Cactus crop as an option to reduce soil
798 C–CO₂ emissions in soils with declining fertility. *Agronomy for Sustainable*
799 *Development*, *38*(8), 1–10. <https://doi.org/10.1007/S13593-017-0481-3>

800 de Oliveira, A. C. P., Nunes, A., Rodrigues, R. G., & Branquinho, C. (2020). The response
801 of plant functional traits to aridity in a tropical dry forest. *Science of The Total*
802 *Environment*, *747*, 141177. <https://doi.org/10.1016/J.SCITOTENV.2020.141177>

803 de Oliveira, M. L., dos Santos, C. A. C., de Oliveira, G., Perez-Marin, A. M., & Santos, C.
804 A. G. (2021). Effects of human-induced land degradation on water and carbon fluxes in
805 two different Brazilian dryland soil covers. *Science of The Total Environment*, *792*,
806 148458. <https://doi.org/10.1016/J.SCITOTENV.2021.148458>

807 de Oliveira, M. L., dos Santos, C. A. C., de Oliveira, G., Silva, M. T., da Silva, B. B., Cunha,
808 J. E. d. B. L., Ruhoff, A., & Santos, C. A. G. (2022). Remote sensing-based assessment
809 of land degradation and drought impacts over terrestrial ecosystems in Northeastern
810 Brazil. *Science of The Total Environment*, *835*, 155490.
811 <https://doi.org/10.1016/J.SCITOTENV.2022.155490>

812 Dhungel, R., Aiken, R., Evett, S. R., Colaizzi, P. D., Marek, G., Moorhead, J. E., Baumhardt,
813 R. L., Brauer, D., Kutikoff, S., & Lin, X. (2021). Energy Imbalance and

814 Evapotranspiration Hysteresis Under an Advective Environment: Evidence From
815 Lysimeter, Eddy Covariance, and Energy Balance Modeling. *Geophysical Research*
816 *Letters*, 48(1), e2020GL091203. <https://doi.org/10.1029/2020GL091203>

817 Ding, Y., Xu, J., Wang, X., Cai, H., Zhou, Z., Sun, Y., & Shi, H. (2021). Propagation of
818 meteorological to hydrological drought for different climate regions in China. *Journal*
819 *of Environmental Management*, 283, 111980.
820 <https://doi.org/10.1016/j.jenvman.2021.111980>

821 Esquivel-Muelbert, A., Baker, T. R., Dexter, K. G., Lewis, S. L., ter Steege, H., Lopez-
822 Gonzalez, G., Monteagudo Mendoza, A., Brienen, R., Feldpausch, T. R., Pitman, N.,
823 Alonso, A., van der Heijden, G., Peña-Claros, M., Ahuite, M., Alexiades, M., Álvarez
824 Dávila, E., Murakami, A. A., Arroyo, L., Aulestia, M., ... Phillips, O. L. (2017).
825 Seasonal drought limits tree species across the Neotropics. *Ecography*, 40(5), 618–629.
826 <https://doi.org/10.1111/ecog.01904>

827 Fang, X., Zhao, L., Zhou, G., Huang, W., & Liu, J. (2015). Increased litter input increases
828 litter decomposition and soil respiration but has minor effects on soil organic carbon in
829 subtropical forests. *Plant and Soil*, 392(1), 139–153. [https://doi.org/10.1007/S11104-](https://doi.org/10.1007/S11104-015-2450-4)
830 [015-2450-4](https://doi.org/10.1007/S11104-015-2450-4)

831 Faridatul, M. I., Wu, B., Zhu, X., & Wang, S. (2020). Improving remote sensing based
832 evapotranspiration modelling in a heterogeneous urban environment. *Journal of*
833 *Hydrology*, 581, 124405. <https://doi.org/10.1016/J.JHYDROL.2019.124405>

834 Feldpausch, T. R., Phillips, O. L., Brienen, R. J. W., Gloor, E., Lloyd, J., Lopez-Gonzalez,
835 G., Monteagudo-Mendoza, A., Malhi, Y., Alarcón, A., Álvarez Dávila, E., Alvarez-
836 Loayza, P., Andrade, A., Aragao, L. E. O. C., Arroyo, L., Aymard C., G. A., Baker, T.
837 R., Baraloto, C., Barroso, J., Bonal, D., ... Vos, V. A. (2016). Amazon forest response
838 to repeated droughts. *Global Biogeochemical Cycles*, 30(7), 964–982.
839 <https://doi.org/10.1002/2015GB005133>

840 Ferreira, R. R., Mutti, P., Mendes, K. R., Campos, S., Marques, T. V., Oliveira, C. P.,
841 Gonçalves, W., Mota, J., Difante, G., Urbano, S. A., Fernandes, L., Bezerra, B. G., &
842 Silva, C. M. S. E. (2020). An assessment of the MOD17A2 gross primary production
843 product in the Caatinga biome, Brazil. *International Journal of Remote Sensing*, 42(4),
844 1275–1291. <https://doi.org/10.1080/01431161.2020.1826063>

845 Flanagan, L. B., & Flanagan, J. E. M. (2018). Seasonal controls on ecosystem-scale CO₂ and
846 energy exchange in a Sonoran Desert characterized by the saguaro cactus (*Carnegiea*
847 *gigantea*). *Oecologia*, 187(4), 977–994. <https://doi.org/10.1007/S00442-018-4187-2>

848 Flanagan, L. B., Nikkel, D. J., Scherloski, L. M., Tkach, R. E., Smits, K. M., Selinger, L. B.,
849 & Rood, S. B. (2021). Multiple processes contribute to methane emission in a riparian
850 cottonwood forest ecosystem. *New Phytologist*, 229(4), 1970–1982.
851 <https://doi.org/10.1111/NPH.16977>

852 Flanagan, L. B., Orchard, T. E., Logie, G. S. J., Coburn, C. A., & Rood, S. B. (2017). Water
853 use in a riparian cottonwood ecosystem: Eddy covariance measurements and scaling
854 along a river corridor. *Agricultural and Forest Meteorology*, 232, 332–348.
855 <https://doi.org/10.1016/J.AGRFORMET.2016.08.024>

856 Fuchs, S., Leuschner, C., Link, R., Coners, H., & Schuldt, B. (2017). Calibration and
857 comparison of thermal dissipation, heat ratio and heat field deformation sap flow probes
858 for diffuse-porous trees. *Agricultural and Forest Meteorology*, 244–245, 151–161.
859 <https://doi.org/10.1016/J.AGRFORMET.2017.04.003>

860 Goldsmith, G. R. (2013). Changing directions: the atmosphere–plant–soil continuum. *New*
861 *Phytologist*, 199(1), 4–6. <https://doi.org/10.1111/NPH.12332>

862 Gomez-Casnovas, N., Blanc-Betes, E., Gonzalez-Meler, M. A., & Azcon-Bieto, J. (2007).
863 Changes in Respiratory Mitochondrial Machinery and Cytochrome and Alternative
864 Pathway Activities in Response to Energy Demand Underlie the Acclimation of
865 Respiration to Elevated CO₂ in the Invasive *Opuntia ficus-indica*. *Plant Physiology*,
866 145(1), 49–61. <https://doi.org/10.1104/PP.107.103911>

867 Granier, A. (1985). Une nouvelle méthode pour la mesure du flux de sève brute dans le tronc
868 des arbres. *Annals of Forest Science*, 42(2), 193–200.
869 <https://doi.org/10.1051/forest:19850204>

870 Grimmond, C. S. B., & Oke, T. R. (1999). Aerodynamic Properties of Urban Areas Derived
871 from Analysis of Surface Form. *Journal of Applied Meteorology and Climatology*,
872 38(9), 1262–1292. [https://doi.org/10.1175/1520-0450\(1999\)038<1262:APOUAD>2.0.CO;2](https://doi.org/10.1175/1520-0450(1999)038<1262:APOUAD>2.0.CO;2)

874 Guevara-Escobar, A., González-Sosa, E., Cervantes-Jimenez, M., Suzán-Azpiri, H.,
875 Queijeiro-Bolanos, M. E., Carrillo-Ángeles, I., & Cambron-Sandoval, V. H. (2021).

876 Machine learning estimates of eddy covariance carbon flux in a scrub in the Mexican
877 highland. *Biogeosciences*, 18(2), 367–392. <https://doi.org/10.5194/BG-18-367-2021>

878 Guillen-Cruz, G., Rodríguez-Sánchez, A. L., Fernández-Luqueño, F., & Flores-Rentería, D.
879 (2021). Influence of vegetation type on the ecosystem services provided by urban green
880 areas in an arid zone of northern Mexico. *Urban Forestry & Urban Greening*, 62,
881 127135. <https://doi.org/10.1016/J.UFUG.2021.127135>

882 Guo, Y., Huang, S., Huang, Q., Leng, G., Fang, W., Wang, L., & Wang, H. (2020).
883 Propagation thresholds of meteorological drought for triggering hydrological drought at
884 various levels. *Science of the Total Environment*, 712, 136502.
885 <https://doi.org/10.1016/j.scitotenv.2020.136502>

886 Hartzell, S., Bartlett, M. S., & Porporato, A. (2018). Unified representation of the C3, C4,
887 and CAM photosynthetic pathways with the Photo3 model. *Ecological Modelling*, 384,
888 173–187. <https://doi.org/10.1016/J.ECOLMODEL.2018.06.012>

889 Heilman, J. L., McInnes, K. J., Savage, M. J., Gesch, R. W., & Lascano, R. J. (1994). Soil
890 and canopy energy balances in a west Texas vineyard. *Agricultural and Forest
891 Meteorology*, 71(1–2), 99–114. [https://doi.org/10.1016/0168-1923\(94\)90102-3](https://doi.org/10.1016/0168-1923(94)90102-3)

892 Heusinkveld, B. G., Jacobs, A. F. G., Holtslag, A. A. M., & Berkowicz, S. M. (2004). Surface
893 energy balance closure in an arid region: role of soil heat flux. *Agricultural and Forest
894 Meteorology*, 122(1–2), 21–37. <https://doi.org/10.1016/J.AGRFORMET.2003.09.005>

895 Hogewoning, S. W., Boogaart, S. A. J. van den, Tongerlo, E. van, & Trouwborst, G. (2021).
896 CAM-physiology and carbon gain of the orchid *Phalaenopsis* in response to light
897 intensity, light integral and CO₂. *Plant, Cell & Environment*, 44(3), 762–774.
898 <https://doi.org/10.1111/PCE.13960>

899 Holtum, J. A. M., Hancock, L. P., Edwards, E. J., Crisp, M. D., Crayn, D. M., Sage, R., &
900 Winter, K. (2016). Australia lacks stem succulents but is it depauperate in plants with
901 crassulacean acid metabolism (CAM)? *Current Opinion in Plant Biology*, 31, 109–117.
902 <https://doi.org/10.1016/J.PBI.2016.03.018>

903 Hu, G., Liu, H., Shangguan, H., Wu, X., Xu, X., & Williams, M. (2018). The role of
904 heartwood water storage for sem-arid trees under drought. *Agricultural and Forest
905 Meteorology*, 256–257, 534–541. <https://doi.org/10.1016/j.agrformet.2018.04.007>

906 Huang, L., Zhai, J., Liu, J., & Sun, C. (2018). The moderating or amplifying biophysical

907 effects of afforestation on CO₂-induced cooling depend on the local background climate
908 regimes in China. *Agricultural and Forest Meteorology*, 260–261, 193–203.
909 <https://doi.org/10.1016/J.AGRFORMET.2018.05.020>

910 IPCC. (2021). *Climate Change 2021: The Physical Science Basis. Contribution of Working*
911 *Group I to the Sixth Assessment Report of the Intergovernmental Panel on Climate*
912 *Change*. (V. Masson-Delmotte, P. Zhai, A. Pirani, S. L. Connors, C. Péan, S. Berger, N.
913 Caud, Y. Chen, L. Goldfarb, M. I. Gomis, M. Huang, K. Leitzell, E. Lonnoy, J. B. R.
914 Matthews, T. K. Maycock, T. Waterfield, O. Yelekçi, R. Yu, & B. Zhou (eds.);
915 Cambridge). In Press.
916 [https://www.ipcc.ch/report/ar6/wg1/downloads/report/IPCC_AR6_WGI_Full_Report.](https://www.ipcc.ch/report/ar6/wg1/downloads/report/IPCC_AR6_WGI_Full_Report.pdf)
917 pdf

918 Jacob, M. C. M., Medeiros, M. F. A. de, & Albuquerque, U. P. (2020). Biodiverse food plants
919 in the semiarid region of Brazil have unknown potential: A systematic review. *Plos One*,
920 15(5), e0230936. <https://doi.org/10.1371/JOURNAL.PONE.0230936>

921 Jardim, A. M. R. F., Araújo Júnior, G. N., Silva, M. V., Santos, A., Silva, J. L. B., Pandorfi,
922 H., Oliveira-Júnior, J. F., Teixeira, A. H. C., Teodoro, P. E., de Lima, J. L. M. P., Silva
923 Junior, C. A., Souza, L. S. B., Silva, E. A., & Silva, T. G. F. (2022). Using Remote
924 Sensing to Quantify the Joint Effects of Climate and Land Use/Land Cover Changes on
925 the Caatinga Biome of Northeast Brazilian. *Remote Sensing*, 14(8), 1911.
926 <https://doi.org/10.3390/RS14081911>

927 Kalthoff, N., Fiebig-Wittmaack, M., Meißner, C., Kohler, M., Uriarte, M., Bischoff-Gauß,
928 I., & Gonzales, E. (2006). The energy balance, evapo-transpiration and nocturnal dew
929 deposition of an arid valley in the Andes. *Journal of Arid Environments*, 65(3), 420–
930 443. <https://doi.org/10.1016/J.JARIDENV.2005.08.013>

931 Kotowska, M. M., Link, R. M., Röhl, A., Hertel, D., Hölscher, D., Waite, P.-A., Moser, G.,
932 Tjoa, A., Leuschner, C., & Schuldt, B. (2021). Effects of Wood Hydraulic Properties on
933 Water Use and Productivity of Tropical Rainforest Trees. *Frontiers in Forests and*
934 *Global Change*, 3, 598759. <https://doi.org/10.3389/FFGC.2020.598759>

935 Kulmala, L., Pumpanen, J., Kolari, P., Dengel, S., Berninger, F., Köster, K., Matkala, L.,
936 Vanhatalo, A., Vesala, T., & Bäck, J. (2019). Inter- and intra-annual dynamics of
937 photosynthesis differ between forest floor vegetation and tree canopy in a subarctic

938 Scots pine stand. *Agricultural and Forest Meteorology*, 271, 1–11.
939 <https://doi.org/10.1016/J.AGRFORMET.2019.02.029>

940 Lai, L., Huang, X., Yang, H., Chuai, X., Zhang, M., Zhong, T., Chen, Z., Chen, Y., Wang,
941 X., & Thompson, J. R. (2016). Carbon emissions from land-use change and
942 management in China between 1990 and 2010. *Science Advances*, 2(11).
943 https://doi.org/10.1126/SCIADV.1601063/SUPPL_FILE/1601063_SM.PDF

944 Levy, P., Drewer, J., Jammet, M., Leeson, S., Friborg, T., Skiba, U., & Oijen, M. van. (2020).
945 Inference of spatial heterogeneity in surface fluxes from eddy covariance data: A case
946 study from a subarctic mire ecosystem. *Agricultural and Forest Meteorology*, 280,
947 107783. <https://doi.org/10.1016/J.AGRFORMET.2019.107783>

948 Li, Y., Liu, Y., Bohrer, G., Cai, Y., Wilson, A., Hu, T., Wang, Z., & Zhao, K. (2022). Impacts
949 of forest loss on local climate across the conterminous United States: Evidence from
950 satellite time-series observations. *Science of The Total Environment*, 802, 149651.
951 <https://doi.org/10.1016/J.SCITOTENV.2021.149651>

952 Lima, C. E. S. de, Costa, V. S. de O., Galvíncio, J. D., Silva, R. M. da, & Santos, C. A. G.
953 (2021). Assessment of automated evapotranspiration estimates obtained using the GP-
954 SEBAL algorithm for dry forest vegetation (Caatinga) and agricultural areas in the
955 Brazilian semiarid region. *Agricultural Water Management*, 250, 106863.
956 <https://doi.org/10.1016/J.AGWAT.2021.106863>

957 Lindoso, D. P., Eiró, F., Bursztyn, M., Rodrigues-Filho, S., & Nasuti, S. (2018). Harvesting
958 Water for Living with Drought: Insights from the Brazilian Human Coexistence with
959 Semi-Aridity Approach towards Achieving the Sustainable Development Goals.
960 *Sustainability*, 10(3), 622. <https://doi.org/10.3390/SU10030622>

961 Link, R. M., Fuchs, S., Arias Aguilar, D., Leuschner, C., Castillo Ugalde, M., Valverde
962 Otarola, J. C., & Schuldt, B. (2020). Tree height predicts the shape of radial sap flow
963 profiles of Costa-Rican tropical dry forest tree species. *Agricultural and Forest*
964 *Meteorology*, 287, 107913. <https://doi.org/10.1016/J.AGRFORMET.2020.107913>

965 Liu, H., Park Williams, A., Allen, C. D., Guo, D., Wu, X., Anenkhonov, O. A., Liang, E.,
966 Sandanov, D. V., Yin, Y., Qi, Z., & Badmaeva, N. K. (2013). Rapid warming accelerates
967 tree growth decline in semi-arid forests of Inner Asia. *Global Change Biology*, 19(8),
968 2500–2510. <https://doi.org/10.1111/gcb.12217>

969 Liu, L., Gong, F., Chen, X., Su, Y., Fan, L., Wu, S., Yang, X., Zhang, J., Yuan, W., Ciais,
970 P., & Zhou, C. (2021a). Bidirectional drought-related canopy dynamics across
971 pantropical forests: a satellite-based statistical analysis. *Remote Sensing in Ecology and*
972 *Conservation*, 1–20. <https://doi.org/10.1002/RSE2.229>

973 Liu, J., You, Y., Li, J., Sitch, S., Gu, X., Nabel, J. E. M. S., Lombardozzi, D., Luo, M., Feng,
974 X., Arneth, A., Jain, A. K., Friedlingstein, P., Tian, H., Poulter, B., & Kong, D. (2021b).
975 Response of global land evapotranspiration to climate change, elevated CO₂, and land
976 use change. *Agricultural and Forest Meteorology*, 311, 108663.
977 <https://doi.org/10.1016/J.AGRFORMET.2021.108663>

978 Loescher, H. W., Law, B. E., Mahrt, L., Hollinger, D. Y., Campbell, J., & Wofsy, S. C.
979 (2006). Uncertainties in, and interpretation of, carbon flux estimates using the eddy
980 covariance technique. *Journal of Geophysical Research: Atmospheres*, 111(D21), 21–
981 90. <https://doi.org/10.1029/2005JD006932>

982 López-Pacheco, I. Y., Rodas-Zuluaga, L. I., Fuentes-Tristan, S., Castillo-Zacarías, C., Sosa-
983 Hernández, J. E., Barceló, D., Iqbal, H. M. N., & Parra-Saldívar, R. (2021).
984 Phycocapture of CO₂ as an option to reduce greenhouse gases in cities: Carbon sinks in
985 urban spaces. *Journal of CO₂ Utilization*, 53, 101704.
986 <https://doi.org/10.1016/J.JCOU.2021.101704>

987 MacBean, N., Maignan, F., Bacour, C., Lewis, P., Peylin, P., Guanter, L., Köhler, P., Gómez-
988 Dans, J., & Disney, M. (2018). Strong constraint on modelled global carbon uptake
989 using solar-induced chlorophyll fluorescence data. *Scientific Reports*, 8(1), 1–12.
990 <https://doi.org/10.1038/s41598-018-20024-w>

991 Mady, B., Lehmann, P., Gorelick, S. M., & Or, D. (2020). Distribution of small seasonal
992 reservoirs in semi-arid regions and associated evaporative losses. *Environmental*
993 *Research Communications*, 2(6), 061002. <https://doi.org/10.1088/2515-7620/AB92AF>

994 Maltese, A., Awada, H., Capodici, F., Ciraolo, G., Loggia, G. La, & Rallo, G. (2018). On the
995 Use of the Eddy Covariance Latent Heat Flux and Sap Flow Transpiration for the
996 Validation of a Surface Energy Balance Model. *Remote Sensing*, 10(2), 195.
997 <https://doi.org/10.3390/RS10020195>

998 Marengo, J. A., & Bernasconi, M. (2015). Regional differences in aridity/drought conditions
999 over Northeast Brazil: present state and future projections. *Climatic Change*, 129(1–2),

1000 103–115. <https://doi.org/10.1007/S10584-014-1310-1/FIGURES/5>

1001 Marengo, J. A., Cunha, A. P. M. A., Nobre, C. A., Ribeiro Neto, G. G., Magalhaes, A. R.,
1002 Torres, R. R., Sampaio, G., Alexandre, F., Alves, L. M., Cuartas, L. A., Deusdará, K.
1003 R. L., & Álvaro, R. C. S. (2020). Assessing drought in the drylands of northeast Brazil
1004 under regional warming exceeding 4 °C. *Natural Hazards*, 103(2), 2589–2611.
1005 <https://doi.org/10.1007/S11069-020-04097-3/TABLES/3>

1006 Marques, T. V., Mendes, K., Mutti, P., Medeiros, S., Silva, L., Perez-Marin, A. M., Campos,
1007 S., Lúcio, P. S., Lima, K., dos Reis, J., Ramos, T. M., da Silva, D. F., Oliveira, C. P.,
1008 Costa, G. B., Antonino, A. C. D., Menezes, R. S. C., Santos e Silva, C. M., & Bezerra,
1009 B. (2020). Environmental and biophysical controls of evapotranspiration from
1010 Seasonally Dry Tropical Forests (*Caatinga*) in the Brazilian Semiarid. *Agricultural and*
1011 *Forest Meteorology*, 287, 107957. <https://doi.org/10.1016/j.agrformet.2020.107957>

1012 Matos, P. S., Barreto-Garcia, P. A. B., Gama-Rodrigues, E. F., de Paula, A., & de Oliveira,
1013 A. M. (2021). Short-term effects of forest management on litter decomposition in
1014 Caatinga dry forest. *Energy, Ecology and Environment*, 7(2), 130–141.
1015 <https://doi.org/10.1007/S40974-021-00231-4>

1016 Matthews, B., & Schume, H. (2022). Tall tower eddy covariance measurements of CO₂
1017 fluxes in Vienna, Austria. *Atmospheric Environment*, 274, 118941.
1018 <https://doi.org/10.1016/J.ATMOSENV.2022.118941>

1019 Mauder, M., Foken, T., & Cuxart, J. (2020). Surface-Energy-Balance Closure over Land: A
1020 Review. *Boundary-Layer Meteorology*, 177(2), 395–426.
1021 <https://doi.org/10.1007/S10546-020-00529-6>

1022 Mendes, K. R., Campos, S., da Silva, L. L., Mutti, P. R., Ferreira, R. R., Medeiros, S. S.,
1023 Perez-Marin, A. M., Marques, T. V., Ramos, T. M., de Lima Vieira, M. M., Oliveira,
1024 C. P., Gonçalves, W. A., Costa, G. B., Antonino, A. C. D., Menezes, R. S. C., Bezerra,
1025 B. G., & Santos e Silva, C. M. (2020). Seasonal variation in net ecosystem CO₂
1026 exchange of a Brazilian seasonally dry tropical forest. *Scientific Reports*, 10(1), 1–16.
1027 <https://doi.org/10.1038/s41598-020-66415-w>

1028 Mendes, K. R., Campos, S., Mutti, P. R., Ferreira, R. R., Ramos, T. M., Marques, T. V., Dos
1029 Reis, J. S., de Lima Vieira, M. M., Silva, A. C. N., Marques, A. M. S., da Silva, D. T.
1030 C., da Silva, D. F., Oliveira, C. P., Gonçalves, W. A., Costa, G. B., Pompelli, M. F.,

1031 Marengo, R. A., Antonino, A. C. D., Menezes, R. S. C., ... Santos E Silva, C. M. (2021).
1032 Assessment of SITE for CO₂ and Energy Fluxes Simulations in a Seasonally Dry
1033 Tropical Forest (Caatinga Ecosystem). *Forests*, 12(1), 86.
1034 <https://doi.org/10.3390/F12010086>

1035 Menezes, R. S. C., Sales, A. T., Primo, D. C., Albuquerque, E. R. G. M. de, Jesus, K. N. de,
1036 Pareyn, F. G. C., Santana, M. da S., Santos, U. J. dos, Martins, J. C. R., Althoff, T. D.,
1037 Nascimento, D. M. do, Gouveia, R. F., Fernandes, M. M., Loureiro, D. C., Araújo Filho,
1038 J. C. de, Giongo, V., Duda, G. P., Alves, B. J. R., Ivo, W. M. P. de M., ... Sampaio, E.
1039 V. de S. B. (2021). Soil and vegetation carbon stocks after land-use changes in a
1040 seasonally dry tropical forest. *Geoderma*, 390, 114943.
1041 <https://doi.org/10.1016/J.GEODERMA.2021.114943>

1042 Moffat, A. M., Papale, D., Reichstein, M., Hollinger, D. Y., Richardson, A. D., Barr, A. G.,
1043 Beckstein, C., Braswell, B. H., Churkina, G., Desai, A. R., Falge, E., Gove, J. H.,
1044 Heimann, M., Hui, D., Jarvis, A. J., Kattge, J., Noormets, A., & Stauch, V. J. (2007).
1045 Comprehensive comparison of gap-filling techniques for eddy covariance net carbon
1046 fluxes. *Agricultural and Forest Meteorology*, 147(3–4), 209–232.
1047 <https://doi.org/10.1016/J.AGRFORMET.2007.08.011>

1048 Mokhtari, A., Ahmadi, A., Daccache, A., & Drechsler, K. (2021). Actual Evapotranspiration
1049 from UAV Images: A Multi-Sensor Data Fusion Approach. *Remote Sensing*, 13(12),
1050 2315. <https://doi.org/10.3390/RS13122315>

1051 Moore, G. W., Bond, B. J., Jones, J. A., & Meinzer, F. C. (2010). Thermal-dissipation sap
1052 flow sensors may not yield consistent sap-flux estimates over multiple years. *Trees*,
1053 24(1), 165–174. <https://doi.org/10.1007/S00468-009-0390-4>

1054 Morgan, J. A., Lecain, D. R., Pendall, E., Blumenthal, D. M., Kimball, B. A., Carrillo, Y.,
1055 Williams, D. G., Heisler-White, J., Dijkstra, F. A., & West, M. (2011). C₄ grasses
1056 prosper as carbon dioxide eliminates desiccation in warmed semi-arid grassland.
1057 *Nature*, 476(7359), 202–205. <https://doi.org/10.1038/nature10274>

1058 Neupane, D., Mayer, J. A., Niechayev, N. A., Bishop, C. D., & Cushman, J. C. (2021). Five-
1059 year field trial of the biomass productivity and water input response of cactus pear
1060 (*Opuntia* spp.) as a bioenergy feedstock for arid lands. *GCB Bioenergy: Bioproducts for
1061 a Sustainable Bioeconomy*, 13(4), 719–741. <https://doi.org/10.1111/GCBB.12805>

1062 Nichols, K. L., Del Grosso, S. J., Derner, J. D., Follett, R. F., Archibeque, S. L., Stewart, C.
1063 E., & Paustian, K. H. (2016). Nitrous oxide and methane fluxes from cattle excrement
1064 on C3 pasture and C4-dominated shortgrass steppe. *Agriculture, Ecosystems &*
1065 *Environment*, 225, 104–115. <https://doi.org/10.1016/J.AGEE.2016.03.026>

1066 Nisa, Z., Khan, M. S., Govind, A., Marchetti, M., Lasserre, B., Magliulo, E., & Manco, A.
1067 (2021). Evaluation of SEBS, METRIC-EEFlux, and QWaterModel Actual
1068 Evapotranspiration for a Mediterranean Cropping System in Southern Italy. *Agronomy*,
1069 11(2), 345. <https://doi.org/10.3390/AGRONOMY11020345>

1070 Niu, Y., Li, Y., Wang, M., Wang, X., Chen, Y., & Duan, Y. (2021). Variations in seasonal
1071 and inter-annual carbon fluxes in a semi-arid sandy maize cropland ecosystem in
1072 China's Horqin Sandy Land. *Environmental Science and Pollution Research*, 1–18.
1073 <https://doi.org/10.1007/S11356-021-15751-Z>

1074 Nobel, P. S., & Hartsock, T. L. (1984). Physiological responses of *Opuntia ficus-indica* to
1075 growth temperature. *Physiologia Plantarum*, 60(1), 98–105.
1076 <https://doi.org/10.1111/J.1399-3054.1984.TB04257.X>

1077 Nobel, P. S., & Israel, A. A. (1994). Cladode development, environmental responses of CO₂
1078 uptake, and productivity for *Opuntia ficus-indica* under elevated CO₂. *Journal of*
1079 *Experimental Botany*, 45(3), 295–303. <https://doi.org/10.1093/JXB/45.3.295>

1080 Nobre, P., Marengo, J. A., Cavalcanti, I. F. A., Obregon, G., Barros, V., Camilloni, I.,
1081 Campos, N., & Ferreira, A. G. (2006). Seasonal-to-Decadal Predictability and
1082 Prediction of South American Climate. *Journal of Climate*, 19(23), 5988–6004.
1083 <https://doi.org/10.1175/JCLI3946.1>

1084 Noorisameleh, Z., Khaledi, S., Shakiba, A., Firouzabadi, P. Z., Gough, W. A., & Qader
1085 Mirza, M. M. (2020). Comparative evaluation of impacts of climate change and
1086 droughts on river flow vulnerability in Iran. *Water Science and Engineering*, 13(4), 265–
1087 274. <https://doi.org/10.1016/j.wse.2020.05.001>

1088 Oliveira, M. B. L., Santos, A. J. B., Manzi, A. O., Alvalá, R. C. S., Correia, M. F., & Moura,
1089 M. S. B. (2006). Trocas de energia e fluxo de carbono entre a vegetação de caatinga e
1090 atmosfera no Nordeste brasileiro. *Revista Brasileira de Meteorologia*, 21, 378–386.

1091 Owen, N. A., Choncubhair, Ó. N., Males, J., Laborde, J. I. del R., Rubio-Cortés, R., Griffiths,
1092 H., & Lanigan, G. (2016). Eddy covariance captures four-phase crassulacean acid

1093 metabolism (CAM) gas exchange signature in *Agave*. *Plant, Cell & Environment*, 39(2),
1094 295–309. <https://doi.org/10.1111/PCE.12610>

1095 Palmroth, S., Bach, L. H., Lindh, M., Kolari, P., Nordin, A., & Palmqvist, K. (2019).
1096 Nitrogen supply and other controls of carbon uptake of understory vegetation in a boreal
1097 *Picea abies* forest. *Agricultural and Forest Meteorology*, 276–277, 107620.
1098 <https://doi.org/10.1016/J.AGRFORMET.2019.107620>

1099 Pecchioni, G., Bosco, S., Volpi, I., Mantino, A., Dragoni, F., Giannini, V., Tozzini, C., Mele,
1100 M., & Ragolini, G. (2020). Carbon Budget of an Agroforestry System after Being
1101 Converted from a Poplar Short Rotation Coppice. *Agronomy*, 10(9), 1251.
1102 <https://doi.org/10.3390/AGRONOMY10091251>

1103 Pereira, M. P. S., Mendes, K. R., Justino, F., Couto, F., da Silva, A. S., da Silva, D. F., &
1104 Malhado, A. C. M. (2020). Brazilian Dry Forest (Caatinga) Response To Multiple
1105 ENSO: the role of Atlantic and Pacific Ocean. *Science of The Total Environment*, 705,
1106 135717. <https://doi.org/10.1016/J.SCITOTENV.2019.135717>

1107 Poyatos, R., Granda, V., Flo, V., Adams, M. A., Adorján, B., Aguadé, D., Aidar, M. P. M.,
1108 Allen, S., Alvarado-Barrientos, M. S., Anderson-Teixeira, K. J., Aparecido, L. M., Altaf
1109 Arain, M., Aranda, I., Asbjornsen, H., Baxter, R., Beamesderfer, E., Berry, Z. C.,
1110 Berveiller, D., Blakely, B., ... Martínez-Vilalta, J. (2021). Global transpiration data
1111 from sap flow measurements: The SAPFLUXNET database. *Earth System Science*
1112 *Data*, 13(6), 2607–2649. <https://doi.org/10.5194/ESSD-13-2607-2021>

1113 Queiroz, M. G. de, Silva, T. G. F. da, Zolnier, S., de Souza, C. A. A., de Souza, L. S. B.,
1114 Steidle Neto, A. J., de Araújo, G. G. L., & Ferreira, W. P. M. (2019). Seasonal patterns
1115 of deposition litterfall in a seasonal dry tropical forest. *Agricultural and Forest*
1116 *Meteorology*, 279, 107712. <https://doi.org/10.1016/J.AGRFORMET.2019.107712>

1117 Quiroz, M., Varnero, M. T., Cuevas, J. G., & Sierra, H. (2021). Cactus pear (*Opuntia ficus-*
1118 *indica*) in areas with limited rainfall for the production of biogas and biofertilizer.
1119 *Journal of Cleaner Production*, 289, 125839.
1120 <https://doi.org/10.1016/J.JCLEPRO.2021.125839>

1121 Rannik, Ü., Peltola, O., & Mammarella, I. (2016). Random uncertainties of flux
1122 measurements by the eddy covariance technique. *Atmospheric Measurement*
1123 *Techniques*, 9(10), 5163–5181. <https://doi.org/10.5194/AMT-9-5163-2016>

- 1124 Ray, D. K., West, P. C., Clark, M., Gerber, J. S., Prishchepov, A. V., & Chatterjee, S. (2019).
1125 Climate change has likely already affected global food production. *Plos One*, *14*(5),
1126 e0217148. <https://doi.org/10.1371/journal.pone.0217148>
- 1127 Rebmann, C., Göckede, M., Foken, T., Aubinet, M., Aurela, M., Berbigier, P., Bernhofer,
1128 C., Buchmann, N., Carrara, A., Cescatti, A., Ceulemans, R., Clement, R., Elbers, J. A.,
1129 Granier, A., Grünwald, T., Guyon, D., Havránková, K., Heinesch, B., Knohl, A., ...
1130 Yakir, D. (2005). Quality analysis applied on eddy covariance measurements at complex
1131 forest sites using footprint modelling. *Theoretical and Applied Climatology*, *80*(2), 121–
1132 141. <https://doi.org/10.1007/S00704-004-0095-Y>
- 1133 Ribeiro, K., Sousa-Neto, E. R. de, Carvalho, J. A. de, Sousa Lima, J. R. de, Menezes, R. S.
1134 C., Duarte-Neto, P. J., da Silva Guerra, G., & Ometto, J. P. H. B. (2016). Land cover
1135 changes and greenhouse gas emissions in two different soil covers in the Brazilian
1136 Caatinga. *Science of The Total Environment*, *571*, 1048–1057.
1137 <https://doi.org/10.1016/J.SCITOTENV.2016.07.095>
- 1138 Riutta, T., Kho, L. K., Teh, Y. A., Ewers, R., Majalap, N., & Malhi, Y. (2021). Major and
1139 persistent shifts in below-ground carbon dynamics and soil respiration following
1140 logging in tropical forests. *Global Change Biology*, *27*(10), 2225–2240.
1141 <https://doi.org/10.1111/GCB.15522>
- 1142 Rocha, S. J. S. S. da, Torres, C. M. M. E., Villanova, P. H., Schettini, B. L. S., Jacovine, L.
1143 A. G., Leite, H. G., Gelcer, E. M., Reis, L. P., Neves, K. M., Comini, I. B., & Silva, L.
1144 F. da. (2020). Drought effects on carbon dynamics of trees in a secondary Atlantic
1145 Forest. *Forest Ecology and Management*, *465*, 118097.
1146 <https://doi.org/10.1016/j.foreco.2020.118097>
- 1147 Rossel, R. A. V., Webster, R., Bui, E. N., & Baldock, J. A. (2014). Baseline map of organic
1148 carbon in Australian soil to support national carbon accounting and monitoring under
1149 climate change. *Global Change Biology*, *20*(9), 2953–2970.
1150 <https://doi.org/10.1111/GCB.12569>
- 1151 Saito, H., Šimůnek, J., & Mohanty, B. P. (2006). Numerical Analysis of Coupled Water,
1152 Vapor, and Heat Transport in the Vadose Zone. *Vadose Zone Journal*, *5*(2), 784–800.
1153 <https://doi.org/10.2136/VZJ2006.0007>
- 1154 Saleska, S. R., Wu, J., Guan, K., Araujo, A. C., Huete, A., Nobre, A. D., & Restrepo-Coupe,

1155 N. (2016). Dry-season greening of Amazon forests. *Nature*, 531(7594), E4–E5.
1156 <https://doi.org/10.1038/nature16457>

1157 Santos, C. A. C. dos, Mariano, D. A., Nascimento, F. das C. A. do, Fabiane, F. R., de Oliveira,
1158 G., Silva, M. T., da Silva, L. L., da Silva, B. B., Bezerra, B. G., Safa, B., Medeiros, S.
1159 de S., & Neale, C. M. U. (2020). Spatio-temporal patterns of energy exchange and
1160 evapotranspiration during an intense drought for drylands in Brazil. *International*
1161 *Journal of Applied Earth Observation and Geoinformation*, 85, 101982.
1162 <https://doi.org/10.1016/j.jag.2019.101982>

1163 Schimel, D., & Schneider, F. D. (2019). Flux towers in the sky: global ecology from space.
1164 *New Phytologist*, 224(2), 570–584. <https://doi.org/10.1111/NPH.15934>

1165 Schlesinger, W. H., & Jasechko, S. (2014). Transpiration in the global water cycle.
1166 *Agricultural and Forest Meteorology*, 189–190, 115–117.
1167 <https://doi.org/10.1016/j.agrformet.2014.01.011>

1168 Schulz, K., Voigt, K., Beusch, C., Almeida-Cortez, J. S., Kowarik, I., Walz, A., & Cierjacks,
1169 A. (2016). Grazing deteriorates the soil carbon stocks of Caatinga forest ecosystems in
1170 Brazil. *Forest Ecology and Management*, 367, 62–70.
1171 <https://doi.org/10.1016/J.FORECO.2016.02.011>

1172 Seidl, R., Spies, T. A., Peterson, D. L., Stephens, S. L., & Hicke, J. A. (2016). REVIEW:
1173 Searching for resilience: addressing the impacts of changing disturbance regimes on
1174 forest ecosystem services. *Journal of Applied Ecology*, 53(1), 120–129.
1175 <https://doi.org/10.1111/1365-2664.12511>

1176 Shang, K., Yao, Y., Li, Y., Yang, J., Jia, K., Zhang, X., Chen, X., Bei, X., & Guo, X. (2020).
1177 Fusion of Five Satellite-Derived Products Using Extremely Randomized Trees to
1178 Estimate Terrestrial Latent Heat Flux over Europe. *Remote Sensing*, 12(4), 687.
1179 <https://doi.org/10.3390/RS12040687>

1180 Silva, A. M. D. O., Freire, F. J., Barbosa, M. D., Ferreira, R. L. C., Freire, M. B. G. D. S., da
1181 Silva, M. I. O., Borges, C. H. A., & de Lima, D. R. M. (2021). Residence Time and
1182 Release of Carbon and Nitrogen from Litter in Caatinga. *Floresta e Ambiente*, 28(4), 1–
1183 11. <https://doi.org/10.1590/2179-8087-FLORAM-2021-0053>

1184 Silva, P. F. da, Lima, J. R. de S., Antonino, A. C. D., Souza, R., Souza, E. S. de, Silva, J. R.
1185 I., & Alves, E. M. (2017). Seasonal patterns of carbon dioxide, water and energy fluxes

1186 over the Caatinga and grassland in the semi-arid region of Brazil. *Journal of Arid*
1187 *Environments*, 147, 71–82. <https://doi.org/10.1016/J.JARIDENV.2017.09.003>

1188 Silva Junior, C. A. da, Teodoro, P. E., Delgado, R. C., Teodoro, L. P. R., Lima, M., de Andréa
1189 Pantaleão, A., Baio, F. H. R., de Azevedo, G. B., de Oliveira Sousa Azevedo, G. T.,
1190 Capristo-Silva, G. F., Arvor, D., & Facco, C. U. (2020). Persistent fire foci in all biomes
1191 undermine the Paris Agreement in Brazil. *Scientific Reports*, 10(1), 1–14.
1192 <https://doi.org/10.1038/s41598-020-72571-w>

1193 Spinoni, J., Barbosa, P., Cherlet, M., Forzieri, G., McCormick, N., Naumann, G., Vogt, J. V.,
1194 & Dosio, A. (2021). How will the progressive global increase of arid areas affect
1195 population and land-use in the 21st century? *Global and Planetary Change*, 205,
1196 103597. <https://doi.org/10.1016/J.GLOPLACHA.2021.103597>

1197 Tan, Z. H., Zhao, J. F., Wang, G. Z., Chen, M. P., Yang, L. Y., He, C. S., Restrepo-Coupe,
1198 N., Peng, S. S., Liu, X. Y., da Rocha, H. R., Kosugi, Y., Hirano, T., Saleska, S. R.,
1199 Goulden, M. L., Zeng, J., Ding, F. J., Gao, F., & Song, L. (2019). Surface conductance
1200 for evapotranspiration of tropical forests: Calculations, variations, and controls.
1201 *Agricultural and Forest Meteorology*, 275, 317–328.
1202 <https://doi.org/10.1016/j.agrformet.2019.06.006>

1203 Teixeira, A. H. de C., Bastiaanssen, W. G. M., Ahmad, M. D., Moura, M. S. B., & Bos, M.
1204 G. (2008). Analysis of energy fluxes and vegetation-atmosphere parameters in irrigated
1205 and natural ecosystems of semi-arid Brazil. *Journal of Hydrology*, 362(1–2), 110–127.
1206 <https://doi.org/10.1016/J.JHYDROL.2008.08.011>

1207 Tonin, A. M., Gonçalves, J. F., Bambi, P., Couceiro, S. R. M., Feitoza, L. A. M., Fontana, L.
1208 E., Hamada, N., Hepp, L. U., Lezan-Kowalczyk, V. G., Leite, G. F. M., Lemes-Silva,
1209 A. L., Lisboa, L. K., Loureiro, R. C., Martins, R. T., Medeiros, A. O., Morais, P. B.,
1210 Moretto, Y., Oliveria, P. C. A., Pereira, E. B., ... Boyero, L. (2017). Plant litter
1211 dynamics in the forest-stream interface: precipitation is a major control across tropical
1212 biomes. *Scientific Reports*, 7(1), 1–14. <https://doi.org/10.1038/s41598-017-10576-8>

1213 Valayamkunnath, P., Sridhar, V., Zhao, W., & Allen, R. G. (2019). A comprehensive analysis
1214 of interseasonal and interannual energy and water balance dynamics in semiarid
1215 shrubland and forest ecosystems. *Science of The Total Environment*, 651, 381–398.
1216 <https://doi.org/10.1016/J.SCITOTENV.2018.09.130>

- 1217 Vandegehuchte, M. W., & Steppe, K. (2013). Sap-flux density measurement methods:
1218 working principles and applicability. *Functional Plant Biology*, 40(3), 213–223.
1219 <https://doi.org/10.1071/FP12233>
- 1220 Velasco, E., & Roth, M. (2010). Cities as Net Sources of CO₂: Review of Atmospheric CO₂
1221 Exchange in Urban Environments Measured by Eddy Covariance Technique.
1222 *Geography Compass*, 4(9), 1238–1259. [https://doi.org/10.1111/J.1749-](https://doi.org/10.1111/J.1749-8198.2010.00384.X)
1223 [8198.2010.00384.X](https://doi.org/10.1111/J.1749-8198.2010.00384.X)
- 1224 Wagle, P., Bhattarai, N., Gowda, P. H., & Kakani, V. G. (2017). Performance of five surface
1225 energy balance models for estimating daily evapotranspiration in high biomass
1226 sorghum. *ISPRS Journal of Photogrammetry and Remote Sensing*, 128, 192–203.
1227 <https://doi.org/10.1016/J.ISPRSJPRS.2017.03.022>
- 1228 Wang, N., Quesada, B., Xia, L., Butterbach-Bahl, K., Goodale, C. L., & Kiese, R. (2019).
1229 Effects of climate warming on carbon fluxes in grasslands— A global meta-analysis.
1230 *Global Change Biology*, 25(5), 1839–1851. <https://doi.org/10.1111/GCB.14603>
- 1231 Williams, D. G., Cable, W., Hultine, K., Hoedjes, J. C. B., Yopez, E. A., Simonneaux, V.,
1232 Er-Raki, S., Boulet, G., De Bruin, H. A. R., Chehbouni, A., Hartogensis, O. K., &
1233 Timouk, F. (2004). Evapotranspiration components determined by stable isotope, sap
1234 flow and eddy covariance techniques. *Agricultural and Forest Meteorology*, 125(3–4),
1235 241–258. <https://doi.org/10.1016/J.AGRFORMET.2004.04.008>
- 1236 Wu, G., De Leeuw, J., Skidmore, A., Prins, H., & Liu, Y. (2008). Comparison of MODIS
1237 and Landsat TM5 images for mapping tempo–spatial dynamics of Secchi disk depths in
1238 Poyang Lake National Nature Reserve, China. *International Journal of Remote Sensing*,
1239 29(8), 2183–2198. <https://doi.org/10.1080/01431160701422254>
- 1240 Wullschleger, S. D., Childs, K. W., King, A. W., & Hanson, P. J. (2011). A model of heat
1241 transfer in sapwood and implications for sap flux density measurements using thermal
1242 dissipation probes. *Tree Physiology*, 31(6), 669–679.
1243 <https://doi.org/10.1093/TREEPHYS/TPR051>
- 1244 Xu, C., McDowell, N. G., Fisher, R. A., Wei, L., Sevanto, S., Christoffersen, B. O., Weng,
1245 E., & Middleton, R. S. (2019). Increasing impacts of extreme droughts on vegetation
1246 productivity under climate change. *Nature Climate Change*, 9(12), 948–953.
1247 <https://doi.org/10.1038/s41558-019-0630-6>

- 1248 Xu, K., Sühling, M., Metzger, S., Durden, D., & Desai, A. R. (2020). Can Data Mining Help
1249 Eddy Covariance See the Landscape? A Large-Eddy Simulation Study. *Boundary-Layer*
1250 *Meteorology*, 176(1), 85–103. [https://doi.org/10.1007/S10546-020-00513-](https://doi.org/10.1007/S10546-020-00513-0)
1251 [0/FIGURES/9](https://doi.org/10.1007/S10546-020-00513-0)
- 1252 Xu, T., Guo, Z., Liu, S., He, X., Meng, Y., Xu, Z., Xia, Y., Xiao, J., Zhang, Y., Ma, Y., &
1253 Song, L. (2018a). Evaluating Different Machine Learning Methods for Upscaling
1254 Evapotranspiration from Flux Towers to the Regional Scale. *Journal of Geophysical*
1255 *Research: Atmospheres*, 123(16), 8674–8690. <https://doi.org/10.1029/2018JD028447>
- 1256 Xu, K., Metzger, S., & Desai, A. R. (2018b). Surface-atmosphere exchange in a box: Space-
1257 time resolved storage and net vertical fluxes from tower-based eddy covariance.
1258 *Agricultural and Forest Meteorology*, 255, 81–91.
1259 <https://doi.org/10.1016/J.AGRFORMET.2017.10.011>
- 1260 Xue, L., Fu, F., Chen, X., Liu, Y., Han, Q., Liao, S., & Wei, Q. (2021). Analysis on water
1261 use efficiency of *Populus euphratica* forest ecosystem in arid area. *Theoretical and*
1262 *Applied Climatology*, 145(1), 717–730. <https://doi.org/10.1007/S00704-021-03636-7>
- 1263 Yao, F., Si, M., Li, W., & Wu, J. (2018). A multidimensional comparison between MODIS
1264 and VIIRS AOD in estimating ground-level PM_{2.5} concentrations over a heavily
1265 polluted region in China. *Science of The Total Environment*, 618, 819–828.
1266 <https://doi.org/10.1016/J.SCITOTENV.2017.08.209>
- 1267 Yao, N., Li, L., Feng, P., Feng, H., Li Liu, D., Liu, Y., Jiang, K., Hu, X., & Li, Y. (2020).
1268 Projections of drought characteristics in China based on a standardized precipitation and
1269 evapotranspiration index and multiple GCMs. *Science of the Total Environment*, 704,
1270 135245. <https://doi.org/10.1016/j.scitotenv.2019.135245>
- 1271 Yuan, J., Jose, S., Hu, Z., Pang, J., Hou, L., & Zhang, S. (2019). Biometric and Eddy
1272 Covariance Methods for Examining the Carbon Balance of a *Larix principis-rupprechtii*
1273 Forest in the Qinling Mountains, China. *Forests*, 9(2), 67.
1274 <https://doi.org/10.3390/F9020067>
- 1275 Zanutelli, D., Montagnani, L., Manca, G., Scandellari, F., & Tagliavini, M. (2015). Net
1276 ecosystem carbon balance of an apple orchard. *European Journal of Agronomy*, 63, 97–
1277 104. <https://doi.org/10.1016/J.EJA.2014.12.002>
- 1278 Zhou, W., Guan, K., Peng, B., Tang, J., Jin, Z., Jiang, C., Grant, R., & Mezbahuddin, S.

1279 (2021). Quantifying carbon budget, crop yields and their responses to environmental
1280 variability using the ecosys model for U.S. Midwestern agroecosystems. *Agricultural*
1281 *and Forest Meteorology*, 307, 108521.
1282 <https://doi.org/10.1016/J.AGRFORMET.2021.108521>

1283

1284 **Acknowledgements**

1285 The authors are thankful to the Research Support Foundation of the Pernambuco State
1286 (FACEPE, APQ-0215-5.01/10 and APQ-1159-1.07/14), the National Council for Scientific
1287 and Technological Development (CNPq) through the fellowship of the Research Productivity
1288 Program (PQ 309421/2018-7), and the Coordination for the Improvement of Higher
1289 Education Personnel (CAPES - Finance Code 001) for funding the research and study grants.
1290 We are also grateful to the Associate Editor, Ph.D. Jose Alexander Elvir for helpful
1291 comments, and two anonymous reviewers for their invaluable feedback on an earlier version
1292 of this paper.

1293

CHAPTER 2

A systematic review of energy and mass fluxes, and biogeochemical processes in seasonally dry tropical forests and cactus ecosystems

Abstract

Regions with arid and semi-arid climates are characterized by hostile climatic conditions of high water deficit in the soil-atmosphere system. Local landscapes with climates of low rainfall and relative humidity, and high air temperature, such as regions of sub-humid, semi-arid, and arid zones, cover approximately 45.4% of the entire land surface of the planet, to which the biomes with dry forests occupy a total area of 1079×10^4 km². Thus, this review aims to quantify the processes and changes in energy, water, and carbon fluxes, and their interactions with the surfaces of terrestrial ecosystems of Caatinga and cacti in semi-arid environments. Studies report that forests in arid and semi-arid environments show resilience to local diversity, prominent in the interrelationship of species, which favors the survival of individuals with changes in the ecological niche. One of the main modifications in land occupation and land use in dryland landscapes is the implementation of agriculture. Furthermore, carbon and energy fluxes in terrestrial ecosystems undergo significant changes with the removal of native vegetation. Therefore, the damage caused by deforestation can cause serious problems in the energy and carbon balance, compromising species' survival. Finally, we emphasize that CAM photosynthesis plants can be an alternative in places with high environmental degradation problems.

Keywords: carbon stocks, energy balance, deforestation, cacti, Caatinga

1. Introduction

The Earth's surface is composed of a diversity of landscapes and scenarios that cover the regions of the planet in their different edaphoclimatic conditions. Arid and semi-arid climate regions are characterized by hostile climatic conditions of high water deficit in the soil-atmosphere system, significantly affecting the fauna and flora populations that inhabit these locations (Huang et al. 2016). In a region of flora with shrubby and herbaceous

32 vegetation, climate change associated with land use influences natural processes, as well as
33 future perspectives related to species survival (Schulz et al. 2016; Silva et al. 2018, 2020;
34 Fischer 2018). With the growing demand for food, the disturbances caused in the soil-
35 vegetation-atmosphere system lead to losses in biodiversity and compromise fragile
36 landscapes in semi-arid regions (Althoff et al. 2018; Weiler et al. 2020). The Caatinga biome
37 is a typical Brazilian ecosystem that covers areas with high water deficits. The seasonally dry
38 tropical forest known as Caatinga is diverse and characterized by various endemic species of
39 fauna and flora (Althoff et al. 2018). Among the numerous families of plants that mostly
40 occur in this region, cacti (Cactaceae Juss.) are the species that stand out (Moura et al. 2016),
41 both from the point of view of tolerance and for their importance in local ecosystem services.

42 As a result of environmental degradation processes, which include pollution on both
43 the land and the atmosphere, deforestation, soil salinization, burning and greenhouse effect,
44 plant species are primarily threatened by environmental degradation processes in Brazilian
45 semi-arid conditions. In addition to disrupting the dynamics of plant species reproduction
46 and the survival of the biome, it has detrimental effects on local natural resources as well as
47 the population residing in these regions. Cactus (*Opuntia* spp. and *Nopalea* spp.) is one of
48 the most promising species for cultivation in arid and semi-arid regions and can also be used
49 in areas with the presence of environmental degradation (e.g., erosion and deforestation)
50 (Alary et al. 2007). In addition to climate and land use changes, poor management of
51 environmental resources contributes massively to the productive decline of these species,
52 altering the dynamics of vegetation, physical, chemical, and biological properties of soils, as
53 well as the fluxes of energy, carbon and of water in the soil-plant-atmosphere system (Moura
54 et al. 2016; Chazdon et al. 2016a; Nanni et al. 2019).

55 The need to maximize agricultural and livestock systems is one of the key points in
56 terms of exploration and land use change (Fernandes et al. 2020b). The fact that vegetated
57 surfaces assume the role of important sinks of carbon dioxide—CO₂ (Schulz et al. 2016), soil
58 exposure in hostile environments brings consequences such as the reduction of soil and air
59 moisture, in addition to increasing the sensible heat flux (Rotenberg and Yakir 2011; Brugger
60 et al. 2019). Soil moisture content is a vital bridge for plants as a source of water recharge
61 (Cheng et al. 2021), contributing to plant thermoregulation through transpiration. The water
62 stored by crops in their vegetative structures mitigates thermal and water stress, preventing

63 plants from excessively losing water to the atmosphere (Cheng et al. 2021). The native
64 species of the Caatinga, including cactus, are tolerant to water stress and high air
65 temperatures. However, although cactus plants do not have deciduous leaves (i.e., perennial
66 or deciduous foliar habits), like the tree and shrub species of this biome, they present other
67 alternatives, such as physiological and anatomical ones, for storing and balancing water in
68 the driest periods (Dória et al. 2016; Ricardo et al. 2018). These adaptive anatomical and
69 morphophysiological features are: crassulacean acid metabolism (CAM), aquiferous
70 parenchyma, leaves modified into spines, succulent cladode-shaped roots, and stems.

71 With the instability of the leaf area, in periods with the presence of vegetation, the
72 balance of energy and water present changes throughout the year between the dry and rainy
73 seasons. These changes modify the behavior of the energy balance, where the heat fluxes
74 when interacting with the environment's surface can be accounted for and distinguished
75 (Santos et al. 2020a). Methods for determining the energy balance, e.g., eddy covariance and
76 Bowen ratio, have the quantification of evapotranspiration as a product, in addition to being
77 well-known methods in the literature (Wagle et al. 2020; Longo et al. 2020; Ferreira et al.
78 2020). However, these methods are not commonly characterized and applied in
79 Caatinga/cactus areas. This energy available in the environment can be used in organic matter
80 decomposition processes (e.g., litter) (Queiroz et al. 2019), thus making nutrients available
81 to plants (Zhu et al. 2021).

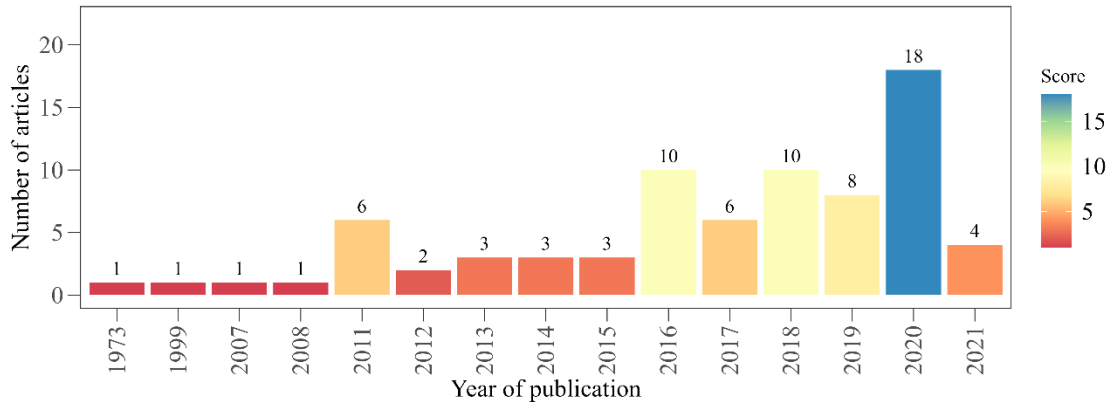
82 Therefore, with the differentiation of ecosystem surfaces and species of type C3, C4,
83 and CAM, we carried out a systematic review to investigate the patterns of energy-water-
84 carbon fluxes in ecosystems of cacti and Caatinga aiming at understanding the contributions
85 of the Caatinga with litter deposition, its nutrient stocks, and decomposition. For this, several
86 papers were accessed online and used according to their theme and relevance.

87

88 **2. Methodology**

89 First, we conducted a literature search from 1973 to 2021 for the construction of this
90 systematic review. Search results were limited to journal articles. In addition, search strings
91 were constructed using online databases sourced from Scopus, Web of Science, Google
92 Scholar, and Science Direct with keywords related to ecosystems, soil, dry land, dry forest,
93 C4 plant, C3 plant, CAM plant, environmental modeling, evapotranspiration, tree, cactus,

94 energy balance, eddy covariance, sonic anemometer, litterfall, litter, mineralization, carbon,
 95 water, Land-Use/Cover Change, LUCC, turbulent flows, climate change, arid and semi-arid.
 96 Boolean operators “AND” and “OR” were used to combine the keywords described above.
 97 Finally, we used 77 articles for the construction of this review article (Figure 1).
 98



99
 100 **Figure 1.** Distribution of selected publications by year.

101
 102 **3. Literature review**

103 *3.1. Seasonally dry forest and cactus ecosystems in semi-arid regions*

104 Landscapes in places with climates of low rainfall and relative humidity, and high air
 105 temperature (e.g., regions of sub-humid, semi-arid and arid zones) cover approximately
 106 45.4% of the entire land surface of the planet, to which the biomes with dry forests occupy a
 107 total area of 1079×10^4 km². Despite the hostile climate of these regions, they are densely
 108 populated, and these areas are facing the processes of climate change and land use, negatively
 109 compromising biodiversity and species habitat (Almeida et al. 2011; Práválie 2016; Bastin
 110 et al. 2017). It is estimated that by the end of the 21st century, climate change will cause the
 111 expansion of semi-arid lands to an extent equivalent to half the land surface of the globe
 112 (Huang et al. 2016).

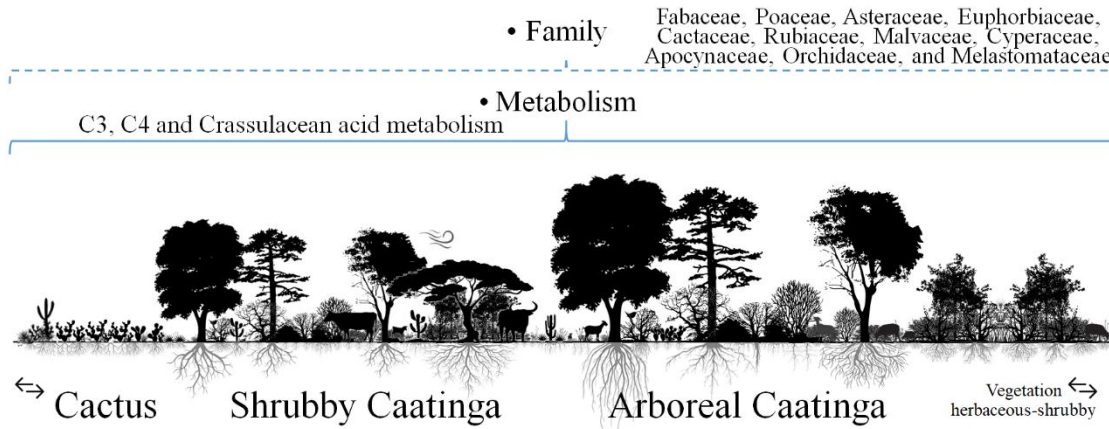
113 These environmental changes and anthropic influences provide a reduction in rainfall
 114 volumes and an increase in air temperature. Tropical vegetation landscapes have undergone
 115 drastic changes over the years in terms of their coverage due to fires and loss of biodiversity
 116 caused by the invasion of exotic species, and bad practices in land use, influencing the future
 117 perspectives of these areas (Schulz et al. 2016; Silva et al. 2018, 2020; Fischer 2018).

118 The main impacts on biodiversity loss in semi-arid regions of Brazil are related to
119 exacerbated disturbances in land use, prominent from the expansion of agricultural activities
120 (Bogoni et al. 2018; Weiler et al. 2020). These growing anthropic pressures are driven by the
121 high demand for food, the exploration and expansion of pasture areas to feed beef cattle, and
122 the constant extraction of wood. Thus, these actions lead to a reduction in the capacity for
123 regrowth and regeneration of natural species, compromising the resilience of the local
124 vegetation and, as a consequence, declining the vitality of the local biome (Althoff et al.
125 2018; Milliken et al. 2018). One of the biomes with high susceptibility to these impacts and
126 historically neglected is the Caatinga. This biome is composed of a dry tropical forest of high
127 expressiveness in the Northeast region of Brazil (Mariano et al. 2018; Fernandes et al. 2020a),
128 with an area of approximately 912 thousand km², comprising a high richness of flora and
129 fauna (Marinho et al. 2019; Ledru et al. 2020). However, despite the significant territorial
130 extension of this biome, about 45% of its total area is already deforested and compromised,
131 with only 7.8% protected by law (Pacheco et al. 2018).

132 In the Caatinga areas, plant species may vary in height and canopy characteristics
133 (i.e., canopy projection and leaf density), varying according to edaphoclimatic conditions,
134 mainly due to water availability in the soil. Some plants can reach 15 to 20 m in height, with
135 significant leaf density in the canopy and biomass. However, most plants in this complex
136 ecosystem are 5–10 m in height and have low soil cover, forming forest fragments with open
137 spaces similar to Savanna (Moura et al. 2016). In addition to tree and shrub species, the
138 Caatinga has plants that make up the herbaceous stratum and are dependent on the growth
139 dynamics of larger individuals, as well as soil moisture and climate conditions (Moura et al.
140 2016; Moraes et al. 2020).

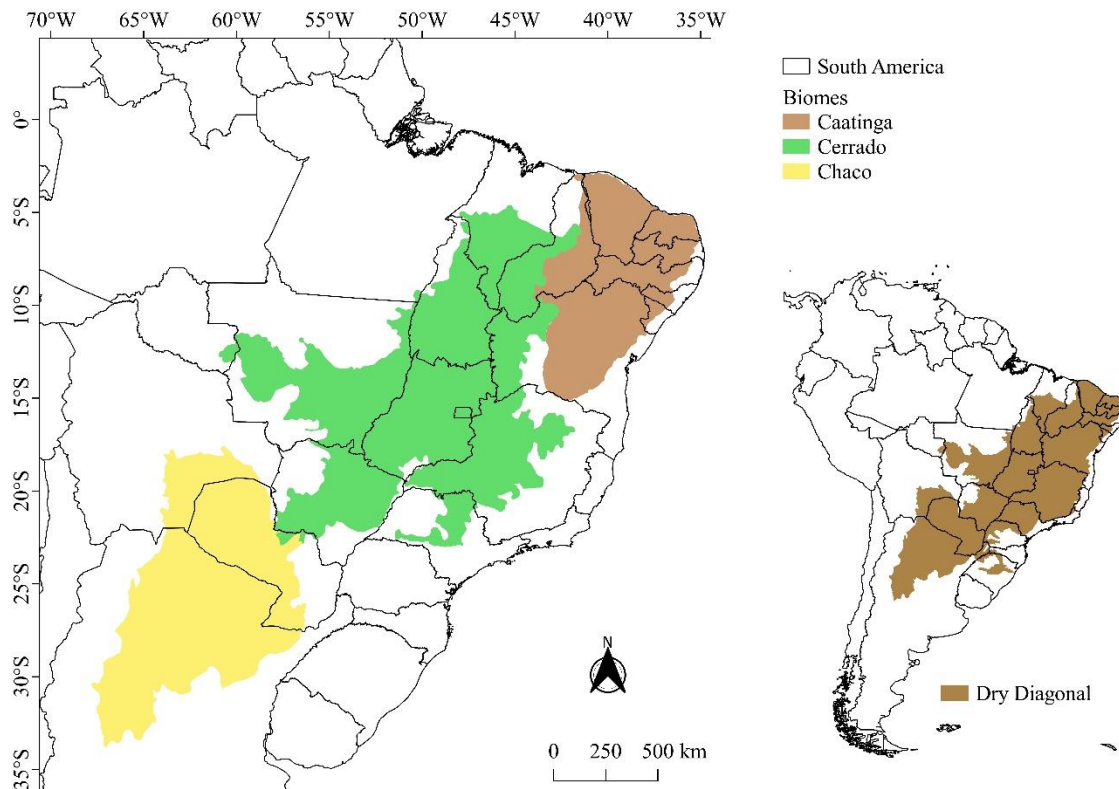
141 Furthermore, in the Caatinga, the herbaceous stratum is quite rich and diverse,
142 presenting several phylogenetic groups of species with high resilience and tolerance to
143 edaphoclimatic disturbances (Carrión et al. 2017). Among the individuals present in the
144 Caatinga, the species of the Cactaceae family are in great expression (Moura et al. 2016) due
145 to their adaptability, being one of the most diverse with 1480 species recognized in the
146 Neotropics (Goettsch et al. 2015). The cactus (*Opuntia* spp. and *Nopalea* spp.), despite being
147 an exotic species, is widely cultivated and widespread in arid and semi-arid environments for
148 forage production, living fences, composition in the diet of animals and humans, and

149 recovery of areas undergoing degradation processes (Carrión et al. 2017; Lemos et al. 2021).
 150 In addition to being a highly resilient and promising crop in dry lands, its agricultural
 151 cultivation and/or spontaneous growth in native vegetation of Caatinga forest can effectively
 152 contribute to improving soil carbon sequestration and ecosystem enrichment (Figure 2).
 153



154
 155 **Figure 2.** Scheme of the main plant families that make up the Caatinga biome. Note:
 156 Illustration with observations of canopy cover transitions, with tree, shrub and herbaceous
 157 species.

158
 159 The Caatinga, with distinct floristic vegetation because they are located in the region
 160 known as the dry diagonal (Figure 3), is marked by seasonal stresses arising from climatic
 161 factors (latitude, altitude, sea conditions, sea currents, vegetation, air masses, relief, and
 162 other) (Gomes et al. 2019b), and soil management. A significant part of this biome is in a
 163 fallow state for natural regeneration, due to extensive activities such as cattle raising and
 164 reduced soil fertility, leaving it exposed to weathering agents. These sites are considered
 165 environmental hotspot areas, these sites deserve attention due to vegetation changes (mainly
 166 deforestation and reforestation), global biogeoclimatic and ecological dynamics, and carbon
 167 fluxes (Chazdon et al. 2016b; Moura et al. 2016; Nanni et al. 2019).
 168



169

170 **Figure 3.** Geographic representation of dry diagonal distribution in South America. Note:
 171 The forests included in this ecosystem are Caatinga (seasonally dry tropical forest), Cerrado
 172 (Savanna) and Chaco biomes.

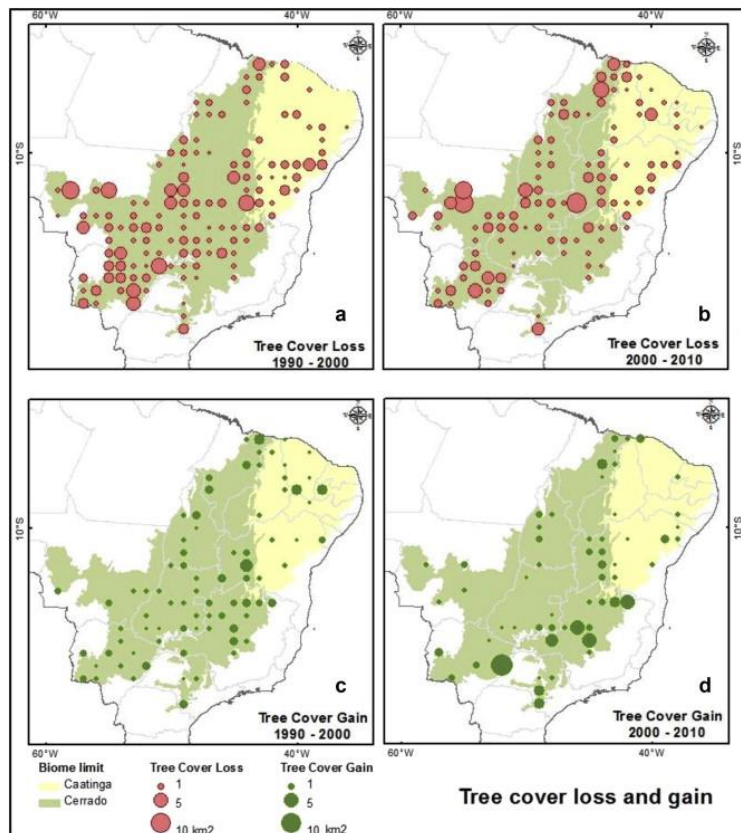
173

174 Although anthropic alterations, such as the removal of native vegetation through
 175 deforestation for the exploitation of agricultural crops, and together with climatic conditions
 176 result in significant environmental changes, this type of environment can compromise the
 177 dry seasonal forests inserted in these biomes (Figure 3). This type of environment does not
 178 only have xeromorphic species. Furthermore, its floristic composition is quite diversified,
 179 showing biogeographic affinities, which make up 11,392 species in the Cerrado (Savanna),
 180 4,322 species in the Caatinga (seasonally dry tropical forest), and 3,400 species in the Chaco
 181 (Forzza et al. 2012; Collevatti et al. 2020). All these ecosystems with dry, semi-arid, and arid
 182 climatic conditions have peculiarities in the composition of flora and fauna, which are altered
 183 by the problems of climate change and land use. Based on climate similarities, the Chaco
 184 differs from the Cerrado and the Caatinga due to winter frosts (Werneck 2011).

185

186 **4. Land use and land cover changes on the dry diagonal**

187 Forests in arid and semi-arid environments show resilience to local diversity,
188 prominent in the interrelationship of species, which favors the survival of individuals with
189 changes in the ecological niche (Filazzola and Lortie 2014). Vegetation resilience is linked
190 to the adaptive capacity of species and/or systems to resume their original functions after
191 suffering environmental disturbances (Holling 1973; Lin 2011; Anderson and Bollig 2016),
192 and when this is not achieved, stand failures and loss of diversity occur of the vegetation.
193 Due to the loss of biodiversity and adaptive inability, the transitions of the vegetation cover
194 of forested areas are often altered due to the intensification of agricultural activity, a factor
195 that still generates many uncertainties for the environment (Wilson et al. 2017), since, even
196 with the insertion of vegetation cover of crops on the soil, abrupt losses occur due to the
197 reduction in species diversity (Figure 4) (Beuchle et al. 2015; Chazdon et al. 2016a).
198



199
200 **Figure 4.** Gross tree cover loss and gain per sampling unit of the Caatinga and Cerrado
201 biomes during 1990–2010. (a) tree cover loss from 1990 to 2000, (b) tree cover loss from
202 2000 to 2010, (c) regrowth/afforestation from 1990 to 2000, and (d) afforestation from 2000

203 to 2010 (Beuchle et al. 2015).

204

205 Deforestation has been a common practice for hundreds of years (Pinheiro Junior et
206 al. 2019), and in recent decades the practice has been intensifying in tropical forests in dry
207 regions. Worldwide, Brazil is the second largest holder of gross losses of forested areas
208 (Hansen et al. 2013), and damage to these vegetation and biomes is caused by increases in
209 agricultural frontiers, driven by the exploitation of commodity crops, availability of labor
210 and favorable climatic conditions (Fehlenberg et al. 2017), causing substantial damage to
211 natural vegetation (Hansen et al. 2013). Approximately 28.6 million people depend on the
212 resources of these forests, and losses from deforestation ecosystem services' disruption cause
213 catastrophic global damage (Tabarelli et al. 2018).

214 Forested areas, when deforested, take decades to regenerate secondary forest
215 vegetation; however, this last type of vegetation does not present the same floristic diversity
216 as the original forest. With the changes in land use and land cover, in 2017 approximately 1
217 million hectares of forest were lost in Brazil. This was a key factor for the increase in the
218 emission of greenhouse gases into the atmosphere since the country is the seventh largest
219 emitter of carbon dioxide equivalent (Le Quéré et al. 2015; Fernandes et al. 2020b).

220 The balance in carbon (C) emission is fundamental for understanding anthropogenic
221 disturbances in ecosystems (Le Quéré et al. 2015). The emission of fossil fuels and changes
222 in land use contribute to the emission of 10 Pg C year⁻¹ (Poulter et al. 2014). One of the main
223 changes in the occupation and use of land in dryland landscapes is the implementation of
224 agriculture (Fernandes et al. 2020b). Because these sites play a significant role as CO₂ sinks,
225 modifications to these environments alter CO₂ fluxes in the soil-plant-atmosphere system
226 (Schulz et al. 2016).

227

228 **5. Energy and mass fluxes**

229 Agricultural and industrial activities emit the most greenhouse gases (carbon dioxide,
230 methane, and nitrous oxide) into the atmosphere. The agricultural sector is responsible for
231 approximately 10 to 12% of this emission, and due to this magnitude, Federal Law No.
232 12,187 of December 29, 2009, proposed incentives for low-carbon agriculture in Brazil
233 (Figueirêdo et al. 2013). The interaction of biotic factors and anthropogenic interventions can

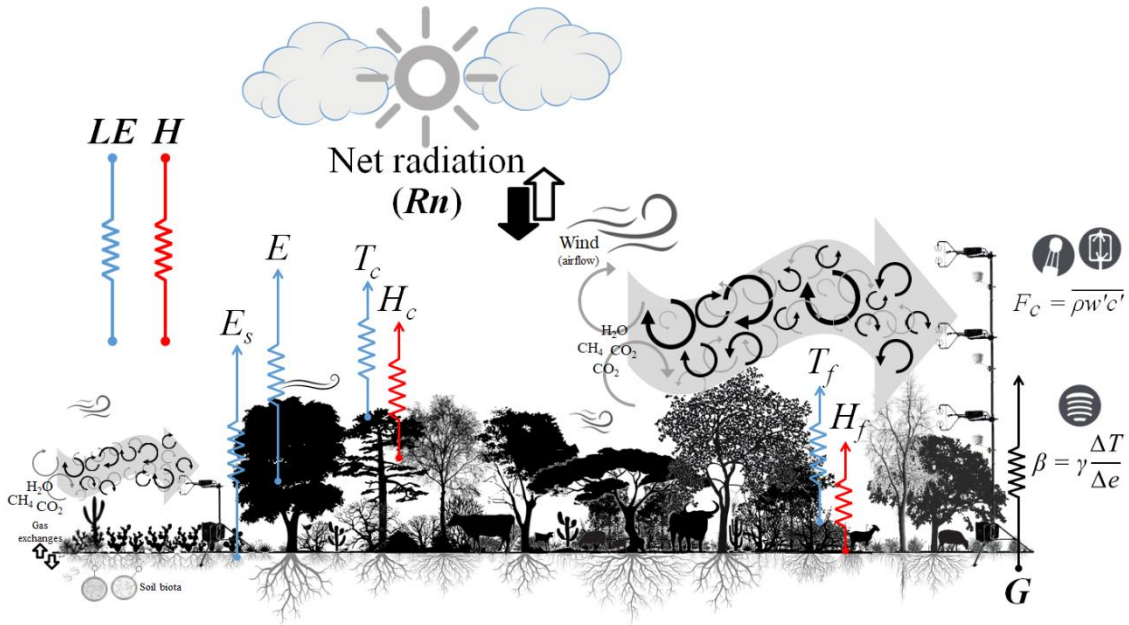
234 change the emission dynamics of these gases, mainly in the CO₂ flux in forest and agricultural
235 ecosystems. Because it is a constituent gas of the atmosphere and quite dynamic, its
236 production and concentration can change in time and space, whether in aquatic or terrestrial
237 ecosystems (Stets et al. 2017).

238 In vegetation of semi-arid environments, low soil cover, exposure to high-intensity
239 solar radiation, and low water availability alter the CO₂ flux and, consequently, contribute to
240 considerable effects on the sensible heat flux of the environment. These conditions affect
241 convective activities and decrease air humidity, making the environment more hostile
242 (Rotenberg and Yakir 2011; Brugger et al. 2019). The accumulation of energy in the canopy
243 makes the plant need to dissipate heat to the environment through transpiration (i.e., cooling
244 process). However, due to the low water availability in the root zone, such physiological
245 output becomes costly (Kröniger et al. 2018).

246 Shrubby vegetation generally has lower water requirements when compared to large
247 tree species. In semi-arid environments, surrounding shrubs play a crucial role in dissipating
248 sensible heat flux, transferring energy to overlying layers and, subsequently, to the
249 atmosphere (Rotenberg and Yakir 2011). Vegetation with adequate density in semi-arid
250 zones helps to maintain water bodies and soil moisture due to the interception of rain by the
251 canopy and retention by the roots, making water available to the species and helping to
252 dissipate energy by latent heat flux (Cheng et al. 2021).

253 The heat fluxes (latent— LE , sensible— H , and soil— G), which are partitioned into
254 net radiation (R_n), are elements of the energy balance and result from the interaction of energy
255 with surfaces that alter the local ET (Santos et al. 2020a). Quantifying energy exchange with
256 the environment can be performed using methods, such as eddy covariance and Bowen ratio
257 (Wagle et al. 2020; Longo et al. 2020; Ferreira et al. 2020). The process of water loss through
258 plant transpiration causes their stomata to open, transfer water to the atmosphere, and capture
259 CO₂ (Figure 5). In environments where water availability is restricted, like arid and semi-
260 arid regions, species have high water extraction efficiency through deep root systems,
261 seeking moisture where non-adapted species commonly cannot reach (Abdallah et al. 2020).
262 These characteristics are noticeable in Caatinga species due to adaptations and morphological
263 modifications.

264



265

266 **Figure 5.** Schematic view of the diurnal energy balance in an ecosystem. Net radiation (R_n)
 267 is balanced by sensible (H), latent (LE) heat fluxes, and soil heat flux (G). The constituents
 268 for LE are surface evaporation (E) and transpiration (T). The subscript letters c , f , and s are
 269 assigned to the canopy, forest floor and soil, respectively. Flow measurements can be made
 270 using the Bowen ratio (β) and eddy covariance methods, as represented in the diagram on the
 271 right.

272

273 The heat exchange and mass of dryland ecosystems are governed by water
 274 availability. When water is restricted, damage to the ecosystem's gross primary productivity
 275 is often more severe than ecosystem respiration, causing these sites to shift from sinks to
 276 carbon sources (Biederman et al. 2017; Nosoetto et al. 2020). Understanding these phenomena
 277 in sink-source dynamics helps understand carbon stocks in ecosystems (Nosoetto et al. 2020).
 278 Furthermore, in dry forest areas, like Caatinga, there is a multispecific floristic composition,
 279 which in conjunction with the different metabolisms (e.g., C3, C4 and CAM), drives
 280 biophysical resources and carbon use by plants (Oliveira et al. 2020).

281

282 **6. Storage: interaction and stocks of biophysical elements in dry forest ecosystems**

283

284

Soil is a reservoir of nutrients, ions, water and carbon. In addition, it is also the habitat
 of several microorganisms that play an essential role in the ecosystem. In the biosphere, the

285 soil is of fundamental importance in organic carbon stocks and is a significant sink of
286 atmospheric carbon dioxide (CO₂). However, the ability to store organic carbon in the soil is
287 governed by some factors, e.g., climatic conditions, soil type and local vegetation (Gomes et
288 al. 2019a). Despite the soil's carbon storage capacity, the soil respiration process releases
289 CO₂ into the environment, basically due to three factors: metabolism of microorganisms,
290 respiration of macro- and micro-fauna, and roots (Santos et al. 2020b).

291 The dry tropical forest has relevant storage of nutrients in the soil (e.g., carbon,
292 nitrogen, and phosphorus) when compared to those contained in the vegetation biomass
293 (Medorio-García et al. 2020). In tropical ecosystems, about 30 to 60% of carbon is stored in
294 the soil (Don et al. 2011), contributing to its fertility and decreasing erosion processes and
295 susceptibility to desertification (Farina et al. 2020).

296 About 471 Pg of C is stored in organic form in tropical forests (Pan et al. 2011).
297 However, when forests are cleared, the carbon that is stored in the soil layers, and above the
298 surface, like in plant biomass, is released into the atmosphere (Baccini et al. 2012). Although
299 semi-arid vegetation is not very dense, this type of environment makes a significant
300 contribution to carbon retention (Poulter et al. 2014). CO₂ plays several important roles in
301 plants, including the main substrate for photosynthesis and enhancing the carboxylation rate
302 when in favorable concentrations (Piao et al. 2019).

303 As semi-arid environments are deficient in water, the increase in CO₂ concentration
304 favors stomatal regulation, keeping plants with their stomata partially closed, that is reducing
305 excessive water loss. This implies an improvement in the efficiency of water use of the
306 species and the photosynthetic capacity (Keenan et al. 2013; Piao et al. 2019). Trees in these
307 environments, when subjected to water limitations, can outline three adaptive strategies, such
308 as (i) drought prevention; (ii) drought resistance capacity; and (iii) drought tolerance, all of
309 which are linked to physiological mechanisms (Chaturvedi et al. 2020). However, under these
310 conditions, nutrient absorption becomes reduced.

311 Plants benefit from the minerals and organic matter present in the soil, as well as their
312 characteristics, such as humidity, topography, and mineral constituents, that alter the
313 maintenance and fixation of carbon (Zong et al. 2021). This type of material can be
314 maintained with the deposition of Caatinga leaves in the soil, which provides nutrients such
315 as nitrogen, phosphorus, and potassium, and after mineralization, become indispensable for

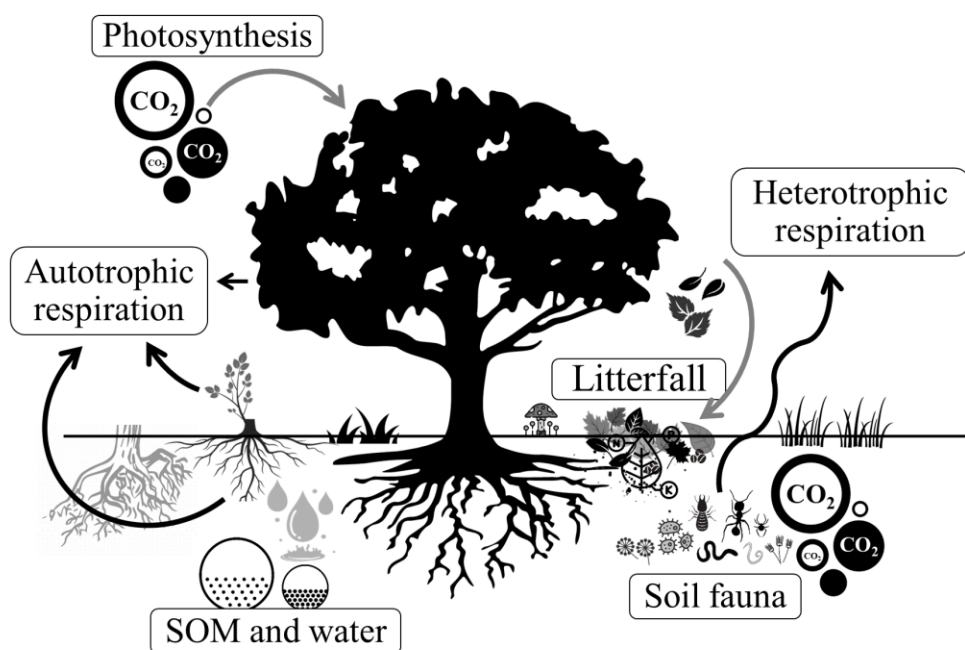
316 the development of plants.

317

318 **7. Nutrient cycling**

319 The climate is an abiotic component that contributes significantly to regulating the
320 biogeochemical activity of terrestrial ecosystems. Vegetation, in turn, is a biotic constituent
321 that plays a key role in the availability of finite resources for soils. An important nutrient
322 replenisher for the soil is the litter (Moura et al. 2016), which comes from constituent
323 materials of plants (i.e., branches, dry leaves, flowers, fruits, seeds) and, when decomposed,
324 releases nutrients and organic compounds, helping in the composition of soil organic matter,
325 as well as in maintaining the microbiota (Farina et al. 2020). In addition to the return of
326 nutrients to the soil, the soil is less exposed to incident solar radiation after the mineralization
327 of the biomass made available by the litter. Consequently, there is a sudden attenuation of
328 the thermal amplitudes (Figure 6). In areas of the Caatinga, the excessive elevation of soil
329 temperature alters the dynamics of nitrogen and oxygen, increasing soil anaerobiosis and,
330 therefore, increasing the emission of nitrous oxide (N_2O) in the atmosphere. However, even
331 with these observations, the Caatinga has low emissions of harmful gases compared to other
332 biomes (Ribeiro et al. 2016).

333



334

335 **Figure 6.** Schematic illustration of litter deposition in soil and its interaction with soil

336 organisms and plants. SOM is the soil organic matter.

337

338 The heterotrophic organisms active in the cycling of nutrients have as energy source
339 precursors the elements made available by the litter (Rai et al. 2016). This nutrient
340 availability in dry forests in semi-arid regions has an ecological footprint for maintaining
341 plant growth. The deposition of debris in the soil is not only a factor governed by climatic
342 conditions, but also by the characteristics of the canopy of plant species (Carrera et al. 2008;
343 Rai et al. 2016). The constituents and their quality, e.g., nitrogen content, C/N ratio, and
344 lignin percentage, influence the decomposition capacity of the material and, mainly, the
345 speed of decomposition (Jamaludheen and Kumar 1999).

346 The species with higher concentrations of nitrogen in the vegetative structures present
347 a more accelerated decomposition rate. In this way, the litter commonly presents a
348 decomposition listed in some phases, being, initially (i) a deposition phase, later there is (ii)
349 a faster release of nutrients and, the final phase, characterized by (iii) deceleration in the
350 release of compounds (Carrera et al. 2008). The seasonality of environmental conditions and
351 the low and/or high deposition of debris in the soil can change the rate of decomposition of
352 the material (Queiroz et al. 2019).

353 Several nutrients are found in litter, in addition to carbon, hydrogen, and oxygen, the
354 primary (N, P, and K) and secondary macro (Ca, Mg and S) and micronutrients (Fe, Cu, Zn,
355 Mn, Ni, B, Cl, and Mo). Macronutrients are part of essential molecules and are needed in
356 large amounts, having a structural function in plants, while micronutrients are needed in
357 smaller amounts and have a regulatory function. Thus, cycling processes favor the storage of
358 these nutrients, as well as their availability to plants in gross primary production through this
359 recycling (Carrera et al. 2008; Queiroz et al. 2019; Zhu et al. 2021). Costly nutrients such as
360 nitrogen, phosphorus, and potassium in forest ecosystems are made available to plants
361 through the litter in a high percentage of return, favoring the production of biomass and
362 helping in metabolic processes and tolerance to stress (biotic and abiotic) due to plants being
363 well nourished (Zhu et al. 2021).

364

365 **8. Conclusion**

366 This review reveals that carbon and energy fluxes in terrestrial ecosystems undergo

367 significant changes with the removal of native vegetation. The damage caused by
368 deforestation implies serious problems in the energy and carbon balance, compromising the
369 survival of species. Plants with CAM photosynthesis can be an alternative in places with high
370 environmental degradation problems. In addition, the use of these plants can be a tool to
371 make ecosystems more resilient due to the high efficiency in the use of water and CO₂. Due
372 to the importance of cactus and Caatinga ecosystems, future research is needed to understand
373 carbon deposition in the soil and species' survival.

374

375 **Acknowledgements**

376 The authors would like to express their deep gratitude to the Research Support
377 Foundation of the Pernambuco State (FACEPE, APQ-0215–5.01/10 and APQ-1159–
378 1.07/14), the National Council for Scientific and Technological Development (CNPq)
379 through the fellowship of the Research Productivity Program (PQ 309421/2018–7), and the
380 Coordination for the Improvement of Higher Education Personnel (CAPES, Finance Code
381 001) for funding the research and study grants.

382

383 **References**

- 384 Abdallah MAB, Durfee N, Mata-Gonzalez R, et al (2020) Water Use and Soil Moisture
385 Relationships on Western Juniper Trees at Different Growth Stages. *Water* 12:1596.
386 <https://doi.org/10.3390/W12061596>
- 387 Alary V, Nefzaoui A, Jemaa M Ben (2007) Promoting the adoption of natural resource
388 management technology in arid and semi-arid areas: Modelling the impact of spineless
389 cactus in alley cropping in Central Tunisia. *Agric Syst* 94:573–585.
390 <https://doi.org/10.1016/J.AGSY.2007.02.003>
- 391 Almeida ALS, Albuquerque UP, Castro CC (2011) Reproductive biology of *Spondias*
392 *tuberosa* Arruda (Anacardiaceae), an endemic fructiferous species of the caatinga (dry
393 forest), under different management conditions in northeastern Brazil. *J Arid Environ*
394 75:330–337. <https://doi.org/10.1016/J.JARIDENV.2010.11.003>
- 395 Althoff TD, Menezes RSC, Pinto A de S, et al (2018) Adaptation of the century model to
396 simulate C and N dynamics of Caatinga dry forest before and after deforestation. *Agric*
397 *Ecosyst Environ* 254:26–34. <https://doi.org/10.1016/J.AGEE.2017.11.016>

398 Anderson DM, Bollig M (2016) Resilience and collapse: histories, ecologies, conflicts and
399 identities in the Baringo-Bogoria basin, Kenya. *J East African Stud* 10:1–20.
400 <https://doi.org/10.1080/17531055.2016.1150240>

401 Baccini A, Goetz SJ, Walker WS, et al (2012) Estimated carbon dioxide emissions from
402 tropical deforestation improved by carbon-density maps. *Nat Clim Chang* 2:.
403 <https://doi.org/10.1038/nclimate1354>

404 Bastin JF, Berrahmouni N, Grainger A, et al (2017) The extent of forest in dryland biomes.
405 *Science* (80-) 356:635–638.
406 [https://doi.org/10.1126/SCIENCE.AAM6527/SUPPL_FILE/AAM6527_BASTIN_DA](https://doi.org/10.1126/SCIENCE.AAM6527/SUPPL_FILE/AAM6527_BASTIN_DATA)
407 [TABASE-S1.CSV.ZIP](https://doi.org/10.1126/SCIENCE.AAM6527/SUPPL_FILE/AAM6527_BASTIN_DATA/TABASE-S1.CSV.ZIP)

408 Beuchle R, Grecchi RC, Shimabukuro YE, et al (2015) Land cover changes in the Brazilian
409 Cerrado and Caatinga biomes from 1990 to 2010 based on a systematic remote sensing
410 sampling approach. *Appl Geogr* 58:116–127.
411 <https://doi.org/10.1016/J.APGEOG.2015.01.017>

412 Biederman JA, Scott RL, Bell TW, et al (2017) CO₂ exchange and evapotranspiration across
413 dryland ecosystems of southwestern North America. *Glob Chang Biol* 23:4204–4221.
414 <https://doi.org/10.1111/GCB.13686>

415 Bogoni JA, Pires JSR, Graipel ME, et al (2018) Wish you were here: How defaunated is the
416 Atlantic Forest biome of its medium- to large-bodied mammal fauna? *PLoS One*
417 13:e0204515. <https://doi.org/10.1371/journal.pone.0204515>

418 Brugger P, De Roo F, Kröniger K, et al (2019) Contrasting turbulent transport regimes
419 explain cooling effect in a semi-arid forest compared to surrounding shrubland. *Agric*
420 *For Meteorol* 269–270:19–27. <https://doi.org/10.1016/j.agrformet.2019.01.041>

421 Carrera AL, Bertiller MB, Larreguy C (2008) Leaf litterfall, fine-root production, and
422 decomposition in shrublands with different canopy structure induced by grazing in the
423 Patagonian Monte, Argentina. *Plant Soil* 311:39–50. [https://doi.org/10.1007/s11104-](https://doi.org/10.1007/s11104-008-9655-8)
424 [008-9655-8](https://doi.org/10.1007/s11104-008-9655-8)

425 Carrión JF, Gastauer M, Mota NM, Meira-Neto JAA (2017) Facilitation as a driver of plant
426 assemblages in Caatinga. *J Arid Environ* 142:50–58.
427 <https://doi.org/10.1016/j.jaridenv.2017.03.006>

428 Chaturvedi RK, Tripathi A, Raghubanshi AS, Singh JS (2020) Functional traits indicate a

429 continuum of tree drought strategies across a soil water availability gradient in a tropical
430 dry forest. For Ecol Manage 118740. <https://doi.org/10.1016/j.foreco.2020.118740>

431 Chazdon RL, Brancalion PHS, Laestadius L, et al (2016a) When is a forest a forest? Forest
432 concepts and definitions in the era of forest and landscape restoration. *Ambio* 45:538–
433 550. <https://doi.org/10.1007/s13280-016-0772-y>

434 Chazdon RL, Broadbent EN, Rozendaal DMA, et al (2016b) Carbon sequestration potential
435 of second-growth forest regeneration in the Latin American tropics. *Sci Adv*
436 2:e1501639. <https://doi.org/10.1126/sciadv.1501639>

437 Cheng Y, Zhan H, Yang W, et al (2021) An ecohydrological perspective of reconstructed
438 vegetation in the semi-arid region in drought seasons. *Agric Water Manag* 243:106488.
439 <https://doi.org/10.1016/j.agwat.2020.106488>

440 Collevatti RG, Lima NE, Vitorino LC (2020) The Diversification of Extant Angiosperms in
441 the South America Dry Diagonal. In: Rull V, Carnaval A (eds) *Neotropical*
442 *Diversification: Patterns and Processes*. Springer, Cham, pp 547–568

443 Don A, Schumacher J, Freibauer A (2011) Impact of tropical land-use change on soil organic
444 carbon stocks - a meta-analysis. *Glob Chang Biol* 17:1658–1670.
445 <https://doi.org/10.1111/j.1365-2486.2010.02336.x>

446 Dória LC, Podadera DS, Batalha MA, et al (2016) Do woody plants of the Caatinga show a
447 higher degree of xeromorphism than in the Cerrado? *Flora Morphol Distrib Funct Ecol*
448 *Plants* 224:244–251. <https://doi.org/10.1016/j.flora.2016.09.002>

449 Farina R, Sándor R, Abdalla M, et al (2020) Ensemble modelling, uncertainty and robust
450 predictions of organic carbon in long-term bare-fallow soils. *Glob Chang Biol* 15441.
451 <https://doi.org/10.1111/gcb.15441>

452 Fehlenberg V, Baumann M, Gasparri NI, et al (2017) The role of soybean production as an
453 underlying driver of deforestation in the South American Chaco. *Glob Environ Chang*
454 45:24–34. <https://doi.org/10.1016/j.gloenvcha.2017.05.001>

455 Fernandes MF, Cardoso D, de Queiroz LP (2020a) An updated plant checklist of the
456 Brazilian Caatinga seasonally dry forests and woodlands reveals high species richness
457 and endemism. *J Arid Environ* 174:104079.
458 <https://doi.org/10.1016/j.jaridenv.2019.104079>

459 Fernandes MM, Fernandes MR de M, Garcia JR, et al (2020b) Assessment of land use and

460 land cover changes and valuation of carbon stocks in the Sergipe semiarid region,
461 Brazil: 1992–2030. Land use policy 99:104795.
462 <https://doi.org/10.1016/j.landusepol.2020.104795>

463 Ferreira TR, Silva BBD, De Moura MSB, et al (2020) The use of remote sensing for reliable
464 estimation of net radiation and its components: a case study for contrasting land covers
465 in an agricultural hotspot of the Brazilian semiarid region. Agric For Meteorol
466 291:108052. <https://doi.org/10.1016/j.agrformet.2020.108052>

467 Figueirêdo MCB de, Kroeze C, Potting J, et al (2013) The carbon footprint of exported
468 Brazilian yellow melon. J Clean Prod 47:404–414.
469 <https://doi.org/10.1016/j.jclepro.2012.09.015>

470 Filazzola A, Lortie CJ (2014) A systematic review and conceptual framework for the
471 mechanistic pathways of nurse plants. Glob Ecol Biogeogr 23:1335–1345.
472 <https://doi.org/10.1111/geb.12202>

473 Fischer AP (2018) Forest landscapes as social-ecological systems and implications for
474 management. Landsc Urban Plan 177:138–147.
475 <https://doi.org/10.1016/j.landurbplan.2018.05.001>

476 Forzza RC, Baumgratz JFA, Bicudo CEM, et al (2012) New Brazilian Floristic List
477 Highlights Conservation Challenges. Bioscience 62:39–45.
478 <https://doi.org/10.1525/bio.2012.62.1.8>

479 Goettsch B, Hilton-Taylor C, Cruz-Piñón G, et al (2015) High proportion of cactus species
480 threatened with extinction. Nat Plants 1:1–7. <https://doi.org/10.1038/nplants.2015.142>

481 Gomes LC, Faria RM, de Souza E, et al (2019a) Modelling and mapping soil organic carbon
482 stocks in Brazil. Geoderma 340:337–350.
483 <https://doi.org/10.1016/j.geoderma.2019.01.007>

484 Gomes VGN, Valiente-Banuet A, Araujo AC (2019b) Reproductive phenology of cacti
485 species in the Brazilian Chaco. J Arid Environ 161:85–93.
486 <https://doi.org/10.1016/j.jaridenv.2018.11.001>

487 Hansen MC, Potapov P V., Moore R, et al (2013) High-resolution global maps of 21st-
488 century forest cover change. Science (80-) 342:850–853.
489 <https://doi.org/10.1126/science.1244693>

490 Holling CS (1973) Resilience and Stability of Ecological Systems. Annu Rev Ecol Syst 4:1–

491 23. <https://doi.org/10.1146/annurev.es.04.110173.000245>

492 Huang J, Yu H, Guan X, et al (2016) Accelerated dryland expansion under climate change.
493 *Nat Clim Chang* 6:166–171. <https://doi.org/10.1038/nclimate2837>

494 Jamaludheen V, Kumar BM (1999) Litter of multipurpose trees in Kerala, India: Variations
495 in the amount, quality, decay rates and release of nutrients. *For Ecol Manage* 115:1–11.
496 [https://doi.org/10.1016/S0378-1127\(98\)00439-3](https://doi.org/10.1016/S0378-1127(98)00439-3)

497 Keenan TF, Hollinger DY, Bohrer G, et al (2013) Increase in forest water-use efficiency as
498 atmospheric carbon dioxide concentrations rise. *Nature* 499:324–327.
499 <https://doi.org/10.1038/nature12291>

500 Kröniger K, De Roo F, Brugger P, et al (2018) Effect of Secondary Circulations on the
501 Surface–Atmosphere Exchange of Energy at an Isolated Semi-arid Forest. *Boundary-*
502 *Layer Meteorol* 169:209–232. <https://doi.org/10.1007/s10546-018-0370-6>

503 Le Quéré C, Moriarty R, Andrew RM, et al (2015) Global Carbon Budget 2015. *Earth Syst*
504 *Sci Data* 7:349–396. <https://doi.org/10.5194/ESSD-7-349-2015>

505 Ledru MP, Jeske-Pieruschka V, Bremond L, et al (2020) When archives are missing,
506 deciphering the effects of public policies and climate variability on the Brazilian semi-
507 arid region using sediment core studies. *Sci Total Environ* 723:137989.
508 <https://doi.org/10.1016/j.scitotenv.2020.137989>

509 Lemos M de, Ferreira-Neto M, Santos Fernandes C dos, et al (2021) The effect of domestic
510 sewage effluent and planting density on growth and yield of prickly pear cactus in the
511 semiarid region of Brazil. *J Arid Environ* 185:104372.
512 <https://doi.org/10.1016/j.jaridenv.2020.104372>

513 Lin BB (2011) Resilience in Agriculture through Crop Diversification: Adaptive
514 Management for Environmental Change. *Bioscience* 61:183–193.
515 <https://doi.org/10.1525/bio.2011.61.3.4>

516 Longo M, Saatchi S, Keller M, et al (2020) Impacts of Degradation on Water, Energy, and
517 Carbon Cycling of the Amazon Tropical Forests. *J Geophys Res Biogeosciences* 125:.
518 <https://doi.org/10.1029/2020JG005677>

519 Mariano DA, Santos CAC do., Wardlow BD, et al (2018) Use of remote sensing indicators
520 to assess effects of drought and human-induced land degradation on ecosystem health
521 in Northeastern Brazil. *Remote Sens Environ* 213:129–143.

522 <https://doi.org/10.1016/j.rse.2018.04.048>

523 Marinho F, Oehl F, da Silva IR, et al (2019) High diversity of arbuscular mycorrhizal fungi
524 in natural and anthropized sites of a Brazilian tropical dry forest (Caatinga). *Fungal Ecol*
525 40:82–91. <https://doi.org/10.1016/j.funeco.2018.11.014>

526 Medorio-García HP, Alarcón E, Flores-Esteves N, et al (2020) Soil carbon, nitrogen and
527 phosphorus dynamics in sugarcane plantations converted from tropical dry forest. *Appl*
528 *Soil Ecol* 154:103600. <https://doi.org/10.1016/j.apsoil.2020.103600>

529 Milliken W, Gasson P, Pareyn F, et al (2018) Impact of management regime and frequency
530 on the survival and productivity of four native tree species used for fuelwood and
531 charcoal in the caatinga of northeast Brazil. *Biomass and Bioenergy* 116:18–25.
532 <https://doi.org/10.1016/j.biombioe.2018.05.010>

533 Moraes CA de, Oliveira MAT de, Behling H (2020) Late Holocene climate dynamics and
534 human impact inferred from vegetation and fire history of the Caatinga, in Northeast
535 Brazil. *Rev Palaeobot Palynol* 282:104299.
536 <https://doi.org/10.1016/j.revpalbo.2020.104299>

537 Moura PM, Althoff TD, Oliveira RA, et al (2016) Carbon and nutrient fluxes through litterfall
538 at four succession stages of Caatinga dry forest in Northeastern Brazil. *Nutr Cycl*
539 *Agroecosystems* 105:25–38. <https://doi.org/10.1007/s10705-016-9771-4>

540 Nanni AS, Sloan S, Aide TM, et al (2019) The neotropical reforestation hotspots: A
541 biophysical and socioeconomic typology of contemporary forest expansion. *Glob*
542 *Environ Chang* 54:148–159. <https://doi.org/10.1016/j.gloenvcha.2018.12.001>

543 Nosetto MD, Luna Toledo E, Magliano PN, et al (2020) Contrasting CO₂ and water vapour
544 fluxes in dry forest and pasture sites of central Argentina. *Ecohydrology*.
545 <https://doi.org/10.1002/eco.2244>

546 Oliveira ACP de, Nunes A, Rodrigues RG, Branquinho C (2020) The response of plant
547 functional traits to aridity in a tropical dry forest. *Sci Total Environ* 747:141177.
548 <https://doi.org/10.1016/j.scitotenv.2020.141177>

549 Pacheco AA, Neves ACO, Fernandes GW (2018) Uneven conservation efforts compromise
550 Brazil to meet the Target 11 of Convention on Biological Diversity. *Perspect Ecol*
551 *Conserv* 16:43–48. <https://doi.org/10.1016/j.pecon.2017.12.001>

552 Pan Y, Birdsey RA, Fang J, et al (2011) A large and persistent carbon sink in the world's

553 forests. *Science* (80-) 333:988–993. <https://doi.org/10.1126/science.1201609>

554 Piao S, Wang X, Park T, et al (2019) Characteristics, drivers and feedbacks of global
555 greening. *Nat Rev Earth Environ* 1:14–27. <https://doi.org/10.1038/s43017-019-0001-x>

556 Pinheiro Junior CR, Pereira MG, de Souza O. Filho J, Beutler SJ (2019) Can topography
557 affect the restoration of soil properties after deforestation in a semiarid ecosystem? *J*
558 *Arid Environ* 162:45–52. <https://doi.org/10.1016/J.JARIDENV.2018.11.004>

559 Poulter B, Frank D, Ciais P, et al (2014) Contribution of semi-arid ecosystems to interannual
560 variability of the global carbon cycle. *Nature* 509:600–603.
561 <https://doi.org/10.1038/nature13376>

562 Právělie R (2016) Drylands extent and environmental issues. A global approach. *Earth-*
563 *Science Rev* 161:259–278. <https://doi.org/10.1016/J.EARSCIREV.2016.08.003>

564 Queiroz MG de, Silva TGF da, Zolnier S, et al (2019) Seasonal patterns of deposition litterfall
565 in a seasonal dry tropical forest. *Agric For Meteorol* 279:107712.
566 <https://doi.org/10.1016/J.AGRFORMET.2019.107712>

567 Rai A, Singh AK, Ghosal N, Singh N (2016) Understanding the effectiveness of litter from
568 tropical dry forests for the restoration of degraded lands. *Ecol Eng* 93:76–81.
569 <https://doi.org/10.1016/J.ECOLENG.2016.05.014>

570 Ribeiro K, Sousa-Neto ER de, Carvalho JA de, et al (2016) Land cover changes and
571 greenhouse gas emissions in two different soil covers in the Brazilian Caatinga. *Sci*
572 *Total Environ* 571:1048–1057. <https://doi.org/10.1016/J.SCITOTENV.2016.07.095>

573 Ricardo SDF, Coe HHG, Dias RR, et al (2018) Reference collection of plant phytoliths from
574 the Caatinga biome, Northeast Brazil. *Flora* 249:1–8.
575 <https://doi.org/10.1016/J.FLORA.2018.09.003>

576 Rotenberg E, Yakir D (2011) Distinct patterns of changes in surface energy budget associated
577 with forestation in the semiarid region. *Glob Chang Biol* 17:1536–1548.
578 <https://doi.org/10.1111/J.1365-2486.2010.02320.X>

579 Santos CAC dos, Mariano DA, das Chagas A. do Nascimento F, et al (2020a) Spatio-
580 temporal patterns of energy exchange and evapotranspiration during an intense drought
581 for drylands in Brazil. *Int J Appl Earth Obs Geoinf* 85:101982.
582 <https://doi.org/10.1016/J.JAG.2019.101982>

583 Santos ÉM da C, Araujo KD, Souza MA, et al (2020b) Relief and edaphoclimatic conditions

584 as influencing agents of CO₂ release in Alagoas Caatinga, Brazil. *Soil Res* 58:306–313.
585 <https://doi.org/10.1071/SR19156>

586 Schulz K, Voigt K, Beusch C, et al (2016) Grazing deteriorates the soil carbon stocks of
587 Caatinga forest ecosystems in Brazil. *For Ecol Manage* 367:62–70.
588 <https://doi.org/10.1016/J.FORECO.2016.02.011>

589 Silva JVC de L da, Hirschfeld MNC, Cares JE, Esteves AM (2020) Land use, soil properties
590 and climate variables influence the nematode communities in the Caatinga dry forest.
591 *Appl Soil Ecol* 150:103474. <https://doi.org/10.1016/J.APSOIL.2019.103474>

592 Silva UBT da, Delgado-Jaramillo M, Aguiar LM de S, Bernard E (2018) Species richness,
593 geographic distribution, pressures, and threats to bats in the Caatinga drylands of Brazil.
594 *Biol Conserv* 221:312–322. <https://doi.org/10.1016/J.BIOCON.2018.03.028>

595 Stets EG, Butman D, McDonald CP, et al (2017) Carbonate buffering and metabolic controls
596 on carbon dioxide in rivers. *Global Biogeochem Cycles* 31:663–677.
597 <https://doi.org/10.1002/2016GB005578>

598 Tabarelli M, Leal IR, Scarano FR, da Silva JMC (2018) *The future of the Caatinga*. Springer
599 International Publishing

600 Wagle P, Skaggs TH, Gowda PH, et al (2020) Flux variance similarity-based partitioning of
601 evapotranspiration over a rainfed alfalfa field using high frequency eddy covariance
602 data. *Agric For Meteorol* 285–286:107907.
603 <https://doi.org/10.1016/J.AGRFORMET.2020.107907>

604 Weiler A, Núñez K, Silla F (2020) Forest matters: Use of water reservoirs by mammal
605 communities in cattle ranch landscapes in the Paraguayan Dry Chaco. *Glob Ecol*
606 *Conserv* 23:e01103. <https://doi.org/10.1016/J.GECCO.2020.E01103>

607 Werneck FP (2011) The diversification of eastern South American open vegetation biomes:
608 Historical biogeography and perspectives. *Quat Sci Rev* 30:1630–1648.
609 <https://doi.org/10.1016/J.QUASCIREV.2011.03.009>

610 Wilson SJ, Schelhas J, Grau R, et al (2017) Forest ecosystem-service transitions: the
611 ecological dimensions of the forest transition. *Ecol Soc* 22:. [https://doi.org/10.5751/ES-](https://doi.org/10.5751/ES-09615-220438)
612 [09615-220438](https://doi.org/10.5751/ES-09615-220438)

613 Zhu X, Zou X, Lu E, et al (2021) Litterfall biomass and nutrient cycling in karst and nearby
614 non-karst forests in tropical China: A 10-year comparison. *Sci Total Environ*

615 758:143619. <https://doi.org/10.1016/J.SCITOTENV.2020.143619>
616 Zong M, Lin C, Li S, et al (2021) Tillage activates iron to prevent soil organic carbon loss
617 following forest conversion to cornfields in tropical acidic red soils. *Sci Total Environ*
618 761:143253. <https://doi.org/10.1016/J.SCITOTENV.2020.143253>
619

CHAPTER 3

Spatiotemporal climatic analysis in Pernambuco State, Northeast Brazil

Abstract

The main factors responsible for the greatest natural disasters are related to extreme weather events for which no country is really well-prepared, particularly in Latin America, and specifically in Brazil. This research was developed to determine the spatiotemporal climatic similarities of municipalities along a longitudinal gradient from the east to north-east of Pernambuco State, in northeastern Brazil, from 1993 to 2018, based on applied statistics. The daily meteorological database (rainfall, air temperature, humidity, pressure, wind and evaporation) registered at eight manual meteorological stations of the National Institute of Meteorology, with a historical period of 26 years. The meteorological data were subjected to descriptive statistics, the cluster analysis (CA), and the principal components analysis (PCA), to identify which components are most affected in the climatic patterns. This study also carried out investigations into the influence of the possible dynamic causes of the El Niño-Southern Oscillation (ENSO) phases on the rainfall patterns of the municipalities. The eigenvalues of the three PCAs > 1 . PC 1 and PC 2 showed a total variance of 59.50%. The variables rainfall and relative humidity presented a higher correlation with the municipalities of Recife and Triunfo (group G_1). The municipalities of Petrolândia, Cabrobó and Ouricuri were grouped according to the variables evaporation, air temperature and atmospheric pressure (group G_2). The CA was able to indicate the cluster of municipalities with similar climatic characteristics. The ENSO phases directly influence the variability of rainfall in both homogeneous groups identified in the study. Based on multivariate statistical analysis, it is possible to determine the meteorological seasonality between the different regions of the State of Pernambuco - northeastern Brazil. Such an analysis is important for the population in the eight municipalities, since it makes it possible to improve the productivity of economic activities, especially crop cultivation and livestock rearing.

Keywords: Meteorological variables, ENSO, Cluster Analysis, Principal Component Analysis, Vulnerability

32

33 **1. Introduction**

34 The main factors responsible for the greatest natural disasters in urban and rural areas
35 are climate extremes (droughts and floods), earthquakes, forest-fire, and some associated
36 with climate change. These events have become common in several regions of the globe (de
37 Lima et al., 2013; Pereira et al., 2018; Nogueira et al., 2020; Singh et al., 2020) and
38 particularly in the north-east of Brazil (Cavalcanti, 2012; Costa et al., 2020). Climatic
39 changes in several countries, occurring over decades, are negatively affecting human
40 development and activities, decreasing biodiversity and causing degradation of agricultural
41 land worldwide (Zarei et al., 2019; Rega et al., 2019; Singh et al., 2020).

42 Northeastern Brazil (NEB) is characterized by presenting distinct climatic conditions
43 throughout its territory, encompassing places with low and high spatiotemporal variability of
44 rainfall and a wide extent of semi-arid lands, which corroborates climate vulnerability
45 (Martins et al., 2019; Comin et al., 2020; Costa et al., 2021), and accentuates its high social
46 vulnerability, with emphasis on worse Human Development Indexes (HDI) - (Marengo et
47 al., 2018; Lyra et al., 2017; IBGE, 2019; Feindouno et al., 2020). Places with an arid and
48 semi-arid climate present a great challenge for the management of water resources, whether
49 in cities or agricultural areas (Sadeghi et al., 2016).

50 Multiple factors can cause spatiotemporal variations in meteorological variables (e.g.,
51 rainfall, air temperature, relative humidity, wind speed, and solar radiation), such as elements
52 linked to topography, the proximity of large water bodies, among others, thus compromising
53 the management of water resources (Raziei, 2018; Santos et al., 2020). This collection of
54 meteorological information and temporal variations is decisive—ideally for applying
55 statistical models and understanding climate risks in a region (de Lima and Lovejoy, 2015;
56 Comin et al., 2020; Diez-Sierra and del Jesus, 2020). Anthropogenic actions in the environment
57 have a significant effect on climate change by changing local weather conditions and so
58 compromising agriculture and the environment (Herath et al., 2018).

59 Agro-ecological zoning and the characterization of homoclimatic regions, based on
60 meteorological variables, have become necessary for planning actions aimed at economic,
61 social and environmental activities. Marumbwa et al. (2019) used the technique of grouping
62 meteorological data in arid and semi-arid environments and observed changes in the rainfall

63 events of the biomes, which allowed decisions to be taken on adapting to climate change and
64 alternatives for ecosystem conservation. In this context, the use of classical statistics makes
65 it possible to explain the relationship of up to two variables; however, the application of
66 multivariate statistics allows us to explain a set of two or more variables. Therefore, the use
67 of multivariate statistics associated with climatic data has grown over the years, to infer
68 clustering information based on its meteorological similarity (Saraçlı et al., 2013; Raziei,
69 2018; Silva et al., 2021).

70 The State of Pernambuco located in the East part of NEB (ENEB) exhibits great
71 spatial and temporal variability of the rainfall regime, due to the diversified geography of the
72 region and the proximity to the Atlantic ocean. In this context, the climate is characterized as
73 tropical-humid (coastal strip) and semi-arid as a result of the shape and morphology of the
74 state, and especially because of the active atmospheric systems (Silva et al., 2017; Jardim et
75 al., 2019; Leal et al., 2020; Comin et al., 2020; Silva et al., 2021). The region is influenced
76 by several meteorological systems that operate more precisely on the synoptic and sub-
77 synoptic scale; there are Frontal Systems (FS), Intertropical Convergence Zone (ITCZ), East
78 Waves Disturbances (EWD), Upper Tropospheric Cyclonic Vortices (UTCV), and South
79 Atlantic Subtropical High (SASH); in mesoscale are the Instability Lines (IL), Mesoscale
80 Convective Complexes (MCC), mesoscale circulation (sea-land and valley-mountain
81 breezes); and on a microscale are small convective cells, orographic circulation, these being
82 major factors in the modification of air mass flow on a vertical and horizontal scale (Molion
83 and Bernardo, 2002; Reboita et al., 2010, 2012; Lyra et al., 2014; Utida et al., 2019). In
84 addition, in the ENEB region, there are modes of climatic variability that interfere with
85 climatic variability and the dynamics of the region's biomes (Correia Filho et al., 2019), for
86 example, El Niño-Southern Oscillation (ENSO), Pacific Decadal Oscillation (PDO) and
87 Atlantic interhemispheric sea surface temperature gradient (AITG) - (Lyra et al., 2017;
88 Erfanian et al., 2017).

89 In recent years, several climatological studies have been carried out at ENEB with an
90 emphasis on climate variability (Moscati and Gan, 2007; Correia Filho et al., 2019), climate
91 projections (Utida et al., 2019; Marengo et al., 2020), among others. However, few studies
92 have characterized climatic similarity in the ENEB region (Marinho et al., 2020; Medeiros
93 et al., 2020). The objective of this paper was to determine the spatiotemporal climatic

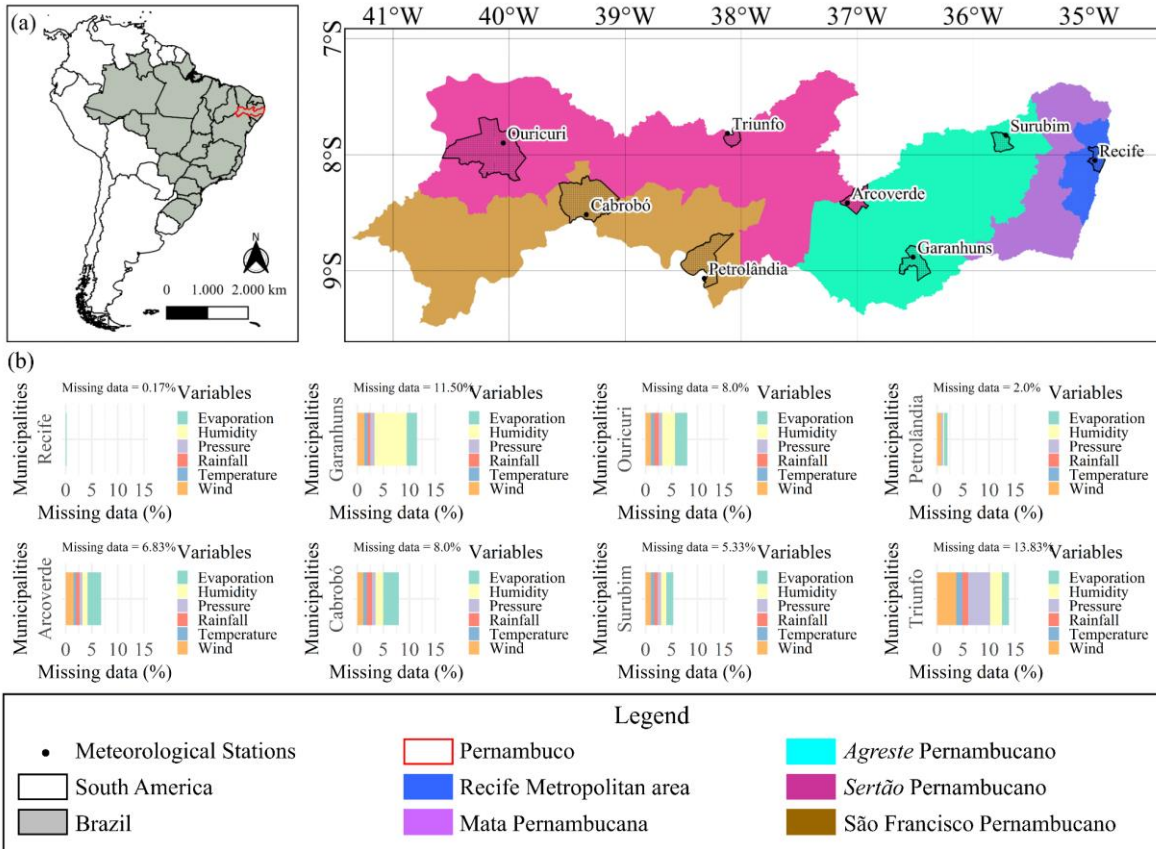
94 similarities of municipalities along a longitudinal gradient from the east to north-east of
95 Pernambuco State, Brazil, in the period 1993 to 2018.

96

97 **2. Material and methods**

98 *2.1 Study area and data used*

99 The study region comprises the Pernambuco State, with an area of 98,937 km², which
100 covers eight municipalities (Ouricuri, Cabrobó, Petrolândia, Triunfo, Arcoverde, Garanhuns,
101 Surubim and Recife), from the *Sertão* mesoregion to the *Zona da Mata* (Figure 1a). The
102 characteristic climates in the state's mesoregions, according to the Köppen classification are
103 “BSh” (semi-arid in low latitude and altitude), “As” (tropical with dry summer) and “Am”
104 (tropical monsoon) that influence a proportion of 61.4%, 32.7%, and 4.9% of their territory,
105 respectively (Alvares et al., 2013). The smaller coastal region (metropolitan area) with “Am”
106 climate, and the *Sertão* region and zone of transition of the state with “BSh” and “As” climate
107 (Medeiros et al., 2018) showing in those places, high seasonal and interannual variability of
108 rainfall (Rodrigues et al., 2020). According to the Brazilian Institute of Geography and
109 Statistics (IBGE), the total population of the eight studied municipalities is approximately
110 2,080,424 inhabitants (IBGE, 2019). The state presents a transition of vegetation starting
111 from the longitudinal axis from east to west, represented by ‘Atlantic Forest’ to ‘Seasonal
112 Dry Tropical Forest’ (known as *Caatinga*) - (Correia Filho et al., 2019; Queiroz et al., 2020a).
113



114

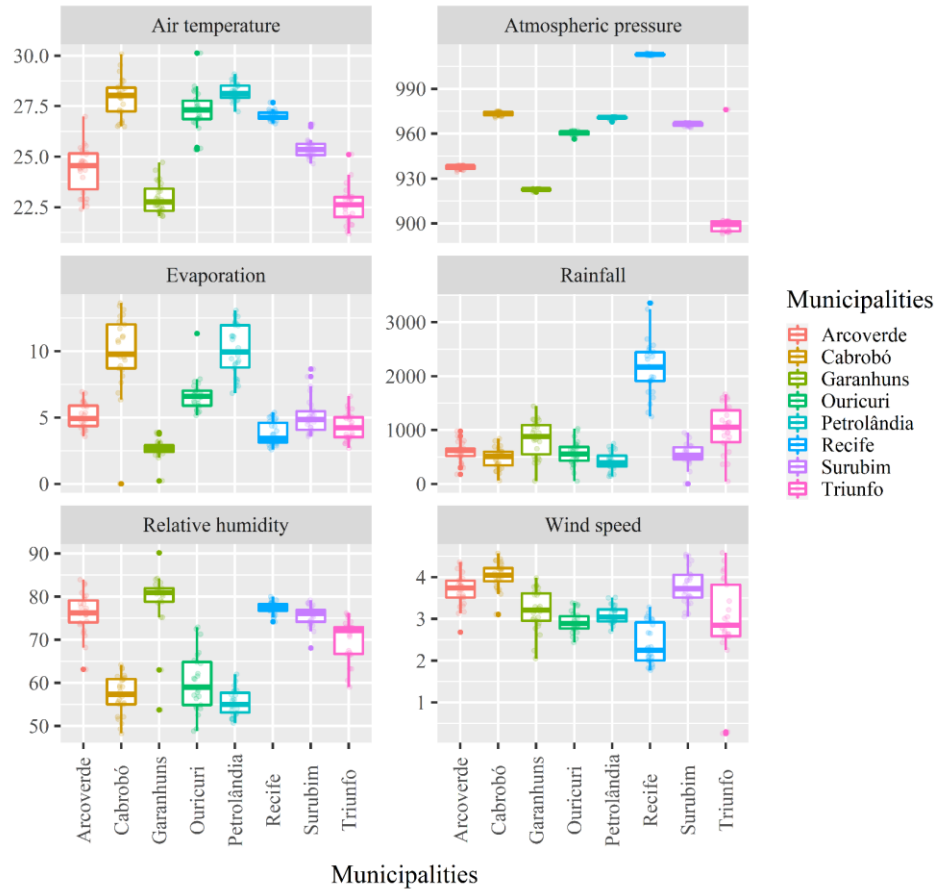
115 **Fig. 1.** The geographic location of the eight municipalities in the State of Pernambuco, Brazil
 116 (a); and (b) missing data from meteorological stations. Note: Variable not shown in the graph
 117 indicates contains no missing data in that municipality.

118

119 We first examined the database from eight conventional (manual) meteorological
 120 stations in a historical series of 26 years (1993 to 2018) of daily data, belonging to BDMEP
 121 (Meteorological Database for Teaching and Research), from the National Institute of
 122 Meteorology (INMET, 2019). With the data series, data consistency analysis was performed
 123 (average, data inference and identification of outliers), in spreadsheets, which considered the
 124 years with complete data, for better quality (minimum of missing data in the respective years)
 125 - (Figure 1b). We performed a boxplot analysis to identify outliers and statistical properties,
 126 i.e. three percentiles (median and interquartile range), and the minimum and maximum values
 127 (whisker, represented by the small vertical [upper-lower] lines of the standard boxplot)
 128 constituting the five-number summary of all meteorological parameters used in our study

129 (see Figure 2). This type of analysis of climatological consistency helps to flag suspicious
 130 values (Lima et al., 2021).

131



132

133 **Fig. 2.** Boxplots of yearly meteorological data sets (air temperature - °C year⁻¹, atmospheric
 134 pressure - hPa year⁻¹, evaporation - mm year⁻¹, rainfall - mm year⁻¹, relative humidity - %
 135 year⁻¹, and wind speed - m s⁻¹ year⁻¹) in the period 1993–2018 of the eight municipalities in
 136 the State of Pernambuco, Brazil. Note: Lines were used to indicate the boundaries of the
 137 adjusted boxplot.

138

139 *2.2 Data analysis and statistical techniques used*

140 The meteorological data of each municipality were subjected to descriptive statistics
 141 (boxplots), to identify the spatial distribution of these analyzed parameters. In the cluster
 142 analysis and principal component analysis, all the meteorological variables were
 143 standardized, since their measurement units differ from each other, trying to ensure that they

144 have the same score reliability (i.e., to eliminate the scale effect). After standardization,
 145 cluster analysis (CA) was performed by the dendrogram, using Ward's aggregation method
 146 and employed at Euclidean distance (Ward, 1963). In general, this method is regarded as very
 147 efficient when it comes to climate data and considers the squared Euclidean distance as a
 148 measure of dissimilarity or similarity to clustering (Wilks, 2011; Lima et al., 2021).

149 The similarities were attributed to the meteorological variables (rainfall - mm,
 150 average air temperature - °C, average relative humidity - %, evaporation - mm, average wind
 151 speed - m s⁻¹, and atmospheric pressure - hPa), by calculating the Euclidean distance (d_{ij}) and
 152 by the hierarchical method of Ward (indicated for analysis of climatic data and demonstrating
 153 more realistic results) between two objects (i and j), in which, the shorter their distance, the
 154 greater the quantitative similarity between individuals (Ward, 1963; Lyra et al., 2014), as
 155 described in Equations 1 and 2, respectively.

156

$$157 \quad d_{ij} = \sqrt{\sum_{k=1}^n (x_{ik} - x_{jk})^2} \quad (1)$$

158

159 where, d_{ij} is the Euclidean distance; x_{ik} and x_{jk} are the data observed at the meteorological
 160 stations of municipalities i and j , respectively.

161

$$162 \quad W = \left[\sum_{i=1}^n x_i^2 - \frac{1}{n} \left(\sum_{i=1}^n x_i \right)^2 \right] \quad (2)$$

163

164 where, W is the minimum intergroup variance by Ward's hierarchical method; n is the number
 165 of elements; x_i is the i -th member of the group.

166

167 Subsequently, principal component analysis (PCA) was used to identify which
 168 components are most affected by the climatic patterns of the municipalities. This method
 169 allows statistical parameters to reduce orthogonal and non-correlated variables, which
 170 explain most of the total variation (Xie et al., 2019; Jardim et al., 2021). When faced with a
 171 very large data set we apply this analysis to reduce its size, while minimizing any loss of

172 information, and expanding the interpretation of the variability data explained. In the
173 application of the analysis, diverse components are created; however, the first component
174 will be the most important, as it explains the highest percentage of the data variance, while
175 the later components created in the analysis represent a lower variation of the data. Moreover,
176 we also performed the Pearson correlation test for the six meteorological variables in the
177 eight municipalities, to observe the strongest associations between the variables, with a
178 significance level at $p\text{-value} \leq 0.05$.

179 The Kaiser criterion was used, considering eigenvalues (λ) above 1.0. Nevertheless,
180 when above 1.0 they generate components with a relevant amount of information contained
181 in the original data, discarding components with eigenvalues below 1.0 (Kaiser, 1960). In the
182 PCA, the eigenvalue corresponds to the variance of each principal component (PC),
183 therefore, it is an important measure to explain the variation of the data (Jolliffe, 1990).

184 We conducted the PCA following four fundamental steps to build the analysis. In the
185 first step, we perform the standardization of the dataset (i.e., the entire data to have zero mean
186 and unit standard deviation). The second step consisted of calculating the covariance matrix
187 to identify the possible correlation between the variables in the data set sampled in this study.
188 In the third step, we calculate the eigenvalues (Equation 3) and eigenvectors (Equation 4) for
189 the covariance matrix to thus determine the principal components of the data. Later, in the
190 fourth step, we constructed a characteristic vector matrix (A) containing the principal
191 components (PCs), which includes the eigenvalues selected greater than the unity ($\lambda > 1$).
192 The new data sets are formed by multiplying the matrix of the vector of transposed
193 characteristics (A^T) by the standardized data matrix (E). The principal component analysis is
194 a decomposition of an $m \times w$ matrix X , with m measurements performed and w variables
195 (Equation 5).

196

$$197 \quad |(C - \lambda \cdot I)| = 0 \quad (3)$$

198

$$199 \quad |(C - \lambda \cdot I)| \cdot v = 0 \quad (4)$$

200

$$201 \quad X = A^T \cdot E \quad (5)$$

202

203 where C is the covariance matrix; I is the identity matrix of the same dimension; v is the
204 eigenvector; A is the data matrix that contains the loadings (i.e., matrix $A \in \mathcal{R}^{w \times r}$); superscript
205 T denotes matrix transposition; E is the data matrix that contains the scores (i.e., matrix $E \in$
206 $\mathcal{R}^{m \times r}$); and r is the dimension of number independent columns in X and is bounded by the
207 minimum of m and w .

208

209 The entire data set was standardized to obtain a better physical interpretation of the
210 variables, and to maximize the correlation of the variables and components (Nehrani et al.,
211 2020). All analyses were performed using R software version 4.0.1 (R Core Team, 2020).

212

213 *2.3 Classification dataset for ENSO warm and cold episodes*

214 Information on climatic fluctuations in the occurrence of ENSO was obtained from
215 the database of the National Oceanic and Atmospheric Administration and Climate
216 Prediction Center - NOAA/CPC (NOAA/CPC, 2020). ENSO is a phenomenon that results
217 from the atmosphere-ocean interaction that affects the global climate (Patra et al., 2020). The
218 years of El Niño, La Niña, and neutral from 1993 to 2018, were based on a limit of ± 0.5 °C
219 of the sea surface temperature (SST) of the equatorial Pacific ocean and the Oceanic Niño
220 Index (ONI), with a minimum of five consecutive 3-month averages seasons overlapping in
221 the Niño 3.4 region (5° N– 5° S, 120° – 170° W, calculated based on the ERSST.v5 dataset) –
222 (Huang et al., 2016). Data used was found at the following website:
223 http://www.cpc.ncep.noaa.gov/products/analysis_monitoring/ensostuff/ensoyears.shtml.

224 We consider the major La Niña and El Niño phenomena regarding the occurrence of negative
225 and positive anomalies, respectively. Such anomalies are presented on the NOAA/CPC
226 online open-access platform, defined as the continuous average of three months and classified
227 as warm (red) and cold (blue) according to NOAA/CPC (2020). Thus, this type of
228 investigation of ENSO contributes to understanding rainfall variability in the NEB
229 (Ndehedehe et al., 2020; Medeiros and Oliveira, 2021).

230

231 **3. Results and discussion**

232 Table 1 shows the principal components of the meteorological variables with their
233 respective loadings, eigenvalues, the total variance of each component, and the accumulated

234 total variance. The eigenvalues for the first three PCs were greater than 1.0, and thus
 235 considered relevant according to the criterion of Kaiser (1960). However, only components
 236 1 (PC 1) and 2 (PC 2) were used for two-dimensional graphic projection, as they carry the
 237 highest rate of total variance for explaining the variables, about 59.50%.

238

239 **Table 1.** Summary of principal component analysis, consisting of loadings, eigenvalues and
 240 percentages (%) of the variance of meteorological variables of the eight municipalities in the
 241 State of Pernambuco.

Variables	PC 1	PC 2	PC 3
Rainfall	0.659	-0.566	0.087
Temperature	-0.747	-0.486	0.092
Humidity	0.581	0.038	0.644
Pressure	-0.306	-0.616	0.515
Wind	-0.309	0.627	0.617
Evaporation	-0.847	0.007	0.016
Eigenvalues	2.239	1.333	1.079
Variance (%)	37.30	22.20	18.00
Cumulative variance (%)	37.30	59.50	77.50

242 PC – is the principal component.

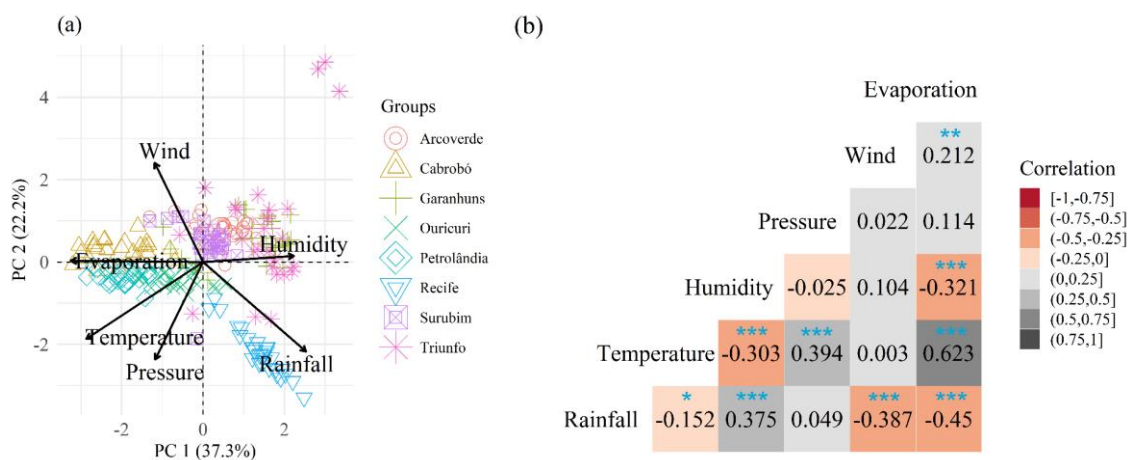
243

244 Similar results corroborate the present study (e.g., Darand and Daneshvar, 2014;
 245 Braga et al., 2012; Raziei, 2018). Darand and Daneshvar (2014), for example, analyzed a
 246 historical series of rainfall from 1951 to 2007, seeking to regionalize rainfall regimes in Iran,
 247 and obtained eigenvalues for the first three principal components above 1.0 and total variance
 248 of 70.98%, for the first two PCs. Raziei (2018) evaluated the monthly rainfall time series of
 249 155 meteorological stations distributed in Iran (1990 to 2014) and obtained a total variance
 250 of 70.70% for PC 1 and PC 2, agreeing with results obtained in this study. Braga et al. (2012)
 251 identified three PCs that explain 94.0% of the total monthly rainfall variance in Rio Grande
 252 do Norte, NEB. The studies by Farrokhi et al. (2020) and El Alaoui El Fels et al. (2020),
 253 using climatic data, also demonstrated the relevance of applying the principal component

254 analysis technique and highlighted a better understanding of the meteorological phenomena,
 255 as well as the high response of the total variance to explain the data by the components.

256 Figures 3a and 3b respectively show the principal components and Pearson's
 257 correlation matrix of the environmental variables for the eight studied municipalities. The
 258 variables of rainfall and relative air humidity presented greater relations with Recife and
 259 Triunfo, explained by PC 1 (37.30%) with loadings of 0.659 and 0.581, respectively,
 260 denoting a strong and positive relationship in this principal component for the variables
 261 mentioned above. Even though Recife is close to the coastal environment, and Triunfo is in
 262 the inland *Sertão*, the two municipalities have similar climatic conditions due to the
 263 orography and influence of oceanic air masses, causing thermal gradients and providing the
 264 greater expression of these variables. These two municipalities are the ones that have the
 265 largest record of annual rainfall and relative humidity (see Figure 2). To explore this question,
 266 we emphasize that there was a significant positive correlation between rainfall and humidity
 267 (see Figure 3b) with the value of 0.375 ($p < 0.001$).

268



269

270 **Fig. 3.** Principal component analysis, scores plot of the first two principal components (a),
 271 and Pearson correlation matrix (b) of the meteorological variables of the eight municipalities
 272 in Pernambuco State, Brazil. Note: *, **, and *** correlation is significant at the 0.05, 0.01
 273 and 0.001 level, respectively.

274

275 The geographical position is essential to determine the relationship between these two
 276 variables. The meteorological station of Recife receives large masses of humid air coming
 277 from the Atlantic ocean and therefore records high rainfall indexes; associated with this, the

278 ITCZ, EWD, trade winds, and the circulation of sea breezes act as the most important systems
279 in the rainfall on the coast of NEB (Reboita et al., 2012; Braga et al., 2012; Lyra et al., 2014;
280 Anjos and Lopes, 2019). High air humidity is common in Recife, to the point of causing
281 discomfort, very often in densely populated and urbanized areas (Souza Hacon et al., 2019).
282 In addition, it is important to mention that due to climatic and anthropogenic conditions, the
283 metropolitan region of Recife is affected by the urban heat island (UHI) phenomenon
284 (Monteiro et al., 2021), and it has been reported that the region's annual rainfall has a
285 tendency to increase (Nóbrega et al., 2015).

286 The Triunfo station is at an altitude of more than 1,000 m (see Figure 1), and the most
287 important static factor in determining climate is the relief, which acts as a natural barrier to
288 advancing air masses and so influences the distribution of air humidity and maintenance of
289 air temperature. Also, the microscale effects, such as orographic circulation and small
290 convective cells, provide higher levels of rainfall above 1,000 mm year⁻¹ (Molion and
291 Bernardo, 2002; Valadão et al., 2017). According to Slavich et al. (2014) and Sobral et al.
292 (2018) the presence of physiographic factors can influence climate characteristics and local
293 biodiversity, mainly rainfall and wind patterns.

294 The municipalities of Petrolândia, Cabrobó and Ouricuri are grouped according to the
295 variables evaporation, air temperature and atmospheric pressure, explained by PC 1 with
296 negative loadings of -0.847, -0.747, and -0.306, respectively. Inversely proportional to
297 evaporation, temperature and pressure were the variable relative humidity of the air, being
298 higher in the municipalities of Triunfo, Surubim, Arcoverde, Garanhuns and Recife. These
299 results are statistically elucidated in an underlying way through the principal component
300 analysis presented in Figure 3a. Studies by Arraes et al. (2016) also classified these
301 municipalities as places with high relative humidity, since evaporation is not too high,
302 confirming our studies.

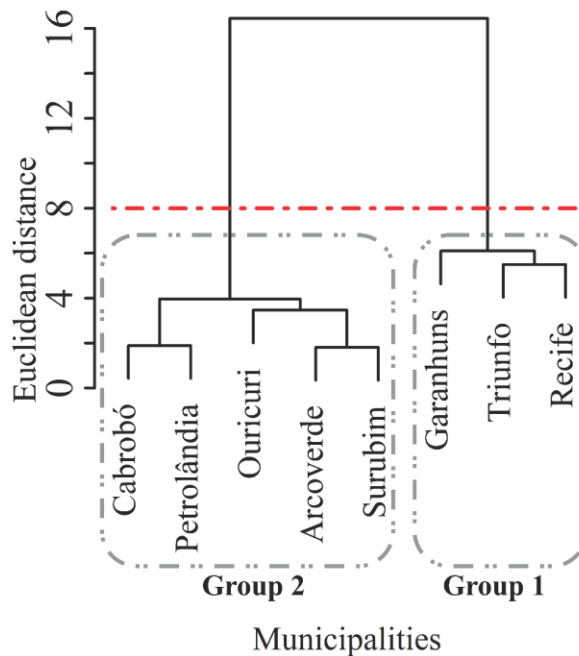
303 The wind speed variable was slightly related in the municipalities of Cabrobó,
304 Surubim and Arcoverde. Although Recife is on the coast, with higher rainfall, wind
305 conditions were not very relevant in the analysis. The municipality of Arcoverde receives air
306 masses from the ITCZ in the same way as Cabrobó; however, other mechanisms can directly
307 or indirectly alter the average behavior of local variables, like the eastern winds that transfer
308 moisture to the NEB (Comin et al., 2020).

309 In this context, it is possible that the SASH, an ever-present phenomenon on the NEB
310 coast (Lyra et al., 2014), can strengthen the southeast (SE) trade winds, together with the
311 local effects of a thermal gradient, which acts mainly to intensify or attenuate existing winds
312 (Moscati and Gan, 2007). The influence of the surface characteristics (e.g., relief, soil type,
313 soil cover and presence of water bodies) are equally determining factors for the dynamics of
314 meteorological variables processes. These situations can be noted in the studies developed
315 by Molion and Bernardo (2002) and Souza and Oyama (2017). These researchers verified
316 the connection between the trade winds and the sea breeze, which can penetrate up to 300
317 km inland from the coast. Silva et al. (2016) and Pimenta et al. (2019) confirm that the NEB
318 is notable for high wind speeds, mainly in the coastal region.

319 Atmospheric pressure, too, had little influence on the grouping of municipalities,
320 explained by PC 2 (22.20% and showed a strong negative loading of -0.616). However, it
321 was possible to observe (Figure 3a), that the municipality of Triunfo had the lowest values
322 of atmospheric pressure, due to its altitude, above 1,000 m (Figure 1). Thus, we find that
323 Triunfo has an inverse proportionality to atmospheric pressure (Figure 3a). According to
324 Sumesh et al. (2019), the topography of a locality has a great influence on the cloud system
325 and contributes to the amount and periodicity of rainfall in high places due to the overlapping
326 of hot and cold clouds, which favors the saturation of the atmosphere.

327 Figure 4 shows the dendrogram obtained by Ward's hierarchical method through the
328 Euclidean distance. The cut horizontal line of the Euclidean distance in the dendrogram was
329 considered to be half the greatest distance between the groups with homogeneous
330 characteristics, thus characterizing two large distinct groups.

331



332

333 **Fig. 4.** Dendrogram for the classification of the two groups (G_1 and G_2), formed by Ward's
 334 hierarchical method with the Euclidean distance of the meteorological variables for the eight
 335 municipalities in the State of Pernambuco, Brazil.

336

337 In group 1 (G_1), made up of the municipalities of Recife, Triunfo and Garanhuns
 338 (Figure 4) - (average Euclidean distance of 5.80), the smallest homogeneous group formed
 339 and distributed in the mesoregions *Agrreste*, Metropolitan and *Sertão* (see Figure 1), they were
 340 grouped by the similarity of the rainfall events, emphasizing the municipalities of Recife and
 341 Triunfo, which have normal climatic rainfall above $1,000 \text{ mm year}^{-1}$. Curiously, although
 342 Triunfo is located in the semi-arid region of the country, the region has a climate with rainfall
 343 ranging from 500 to 800 mm year^{-1} . Therefore, its altitude directly influences the annual
 344 rainfall volumes since it is at a higher altitude than the average compared to other
 345 municipalities from the semi-arid region (see Figure 2). The region is influenced by the ITCZ,
 346 which varies latitudinally, and in the period from February to May, when the position is
 347 further south ($\sim 4^\circ \text{S}$), it contributes to more intense rainfall events (Utida et al., 2019). This
 348 especially affects Recife, which is on the NEB coast and has rainfall above $1,500 \text{ mm year}^{-1}$
 349 (Oliveira et al., 2017). The significant influence on rainfall volumes at high altitude locations

350 was also reported by El Alaoui El Fels et al. (2020); however, the authors report an exception
351 due to the influence of the shelter effect, which may not accurately represent the overall
352 rainfall in their region compared to neighboring municipalities.

353 Group 2 (G₂), referring to the municipalities of Surubim, Arcoverde, Ouricuri,
354 Petrolândia and Cabrobó, the largest homogeneous group formed and distributed in the
355 mesoregions of *Agreste*, *Sertão* and São Francisco Pernambucano (Figure 1), shows
356 similarity regarding the climatic variables (evaporation, wind and air temperature), and the
357 Euclidean distances for these municipalities were also similar (Figure 4), with average
358 clustering of 2.78. Environmental factors can also influence the grouping of climatic
359 variables, for example from the interaction between vegetation cover and mesoscale
360 phenomena in the atmospheric circulation (Oliveira et al., 2017). The vegetation of the
361 *Caatinga* biome is related to the local rainfall index, which shows the seasonality of the
362 vegetation, with the municipalities in the semi-arid being characterized by this biome
363 (Ribeiro et al., 2016; Almeida et al., 2019; Correia Filho et al., 2019; Queiroz et al., 2020b).
364 Recently, Marengo et al. (2020) evaluated the projections of vegetative stress conditions from
365 the Vegetation Health Index (VHI) and indicated semi-desert and arid conditions that will
366 replace the *Caatinga* in 2100. This could seriously compromise food security and increase
367 social vulnerability in the NEB. Group 2 (G₂) regions are places with drier environments and
368 located in the central area of the Brazilian semi-arid region, due to the local topography,
369 under the influence of the Serra da Borborema (i.e. a topographic barrier against the
370 atmospheric flow), which deflects the trade winds and the sea breezes that arrive in these
371 regions, leaving the environment with a water deficit (Lyra et al., 2014).

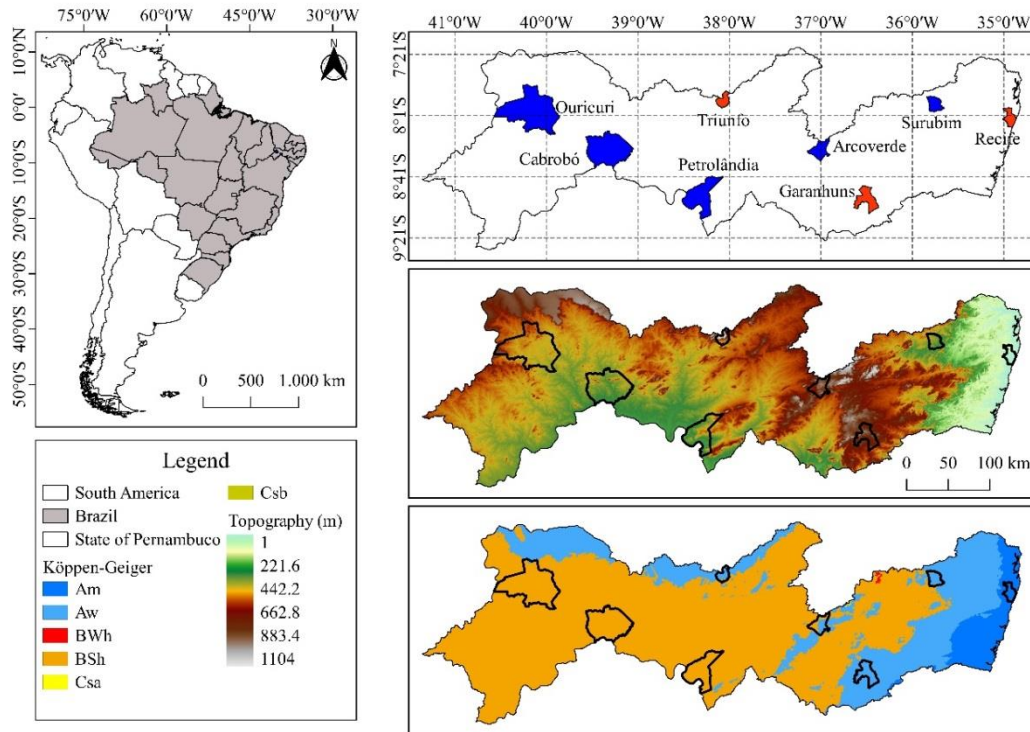
372 A study by Lima et al. (2019) observed variations in the rainfall and air temperature
373 for the NEB region. They indicated that this variability was due to atmospheric phenomena
374 that affect it, such as sea breezes, trade winds, ITCZ, UTCV and FS. It is known that the
375 ENSO climate variability coupled with the sea surface temperature (SST) anomalies interfere
376 with rainfall, air temperature and wind patterns in NEB (Molion and Bernardo, 2002; Braga
377 et al., 2012; Lyra et al., 2017).

378 The distances generated by groups G₁ and G₂ explain the spatiotemporal
379 characteristics of similarity or dissimilarity that each municipality has in its climatic

380 conditions (Saraçlı et al., 2013). This supports our understanding of the drier and wetter parts
381 of the country.

382 Based on the CA technique, the G₂ group was formed by the municipalities of
383 Cabrobó and Petrolândia (see Figures 4 and 5). According to the IBGE, both municipalities
384 showed agricultural diversity and high volume production of food through permanent and
385 non-permanent crops; for example, with a range of 14 crops (Cabrobó) and 16 crops
386 (Petrolândia) - (Andrade, 1975; Cierjacks et al., 2016; Hagel et al., 2019; IBGE, 2020). Such
387 diversification and increase production are due to the similar climatic characteristics, which
388 favor the development of a diversity of crops, and further encouraged by the municipalities
389 being located close to the São Francisco River. This ensures the production of irrigated crops
390 at different times of the year (Cierjacks et al., 2016; Santos et al., 2020; Teixeira et al., 2020).
391 Mostly in the semi-arid region, family farming predominates with the cultivation of beans,
392 maize, rice, and cassava. However, when not properly managed, it becomes more vulnerable
393 to the impact of climate variability due to the edaphoclimatic conditions of the region
394 (Rossato et al., 2017).

395



396

397 **Fig. 5.** Map of the clusters of municipalities (Group 1 (G_1): Recife, Triunfo and Garanhuns;
 398 and Group 2 (G_2): Surubim, Arcoverde, Ouricuri, Petrolândia and Cabrobó), topographic
 399 elevation and Köppen climate classification for the State of Pernambuco.

400

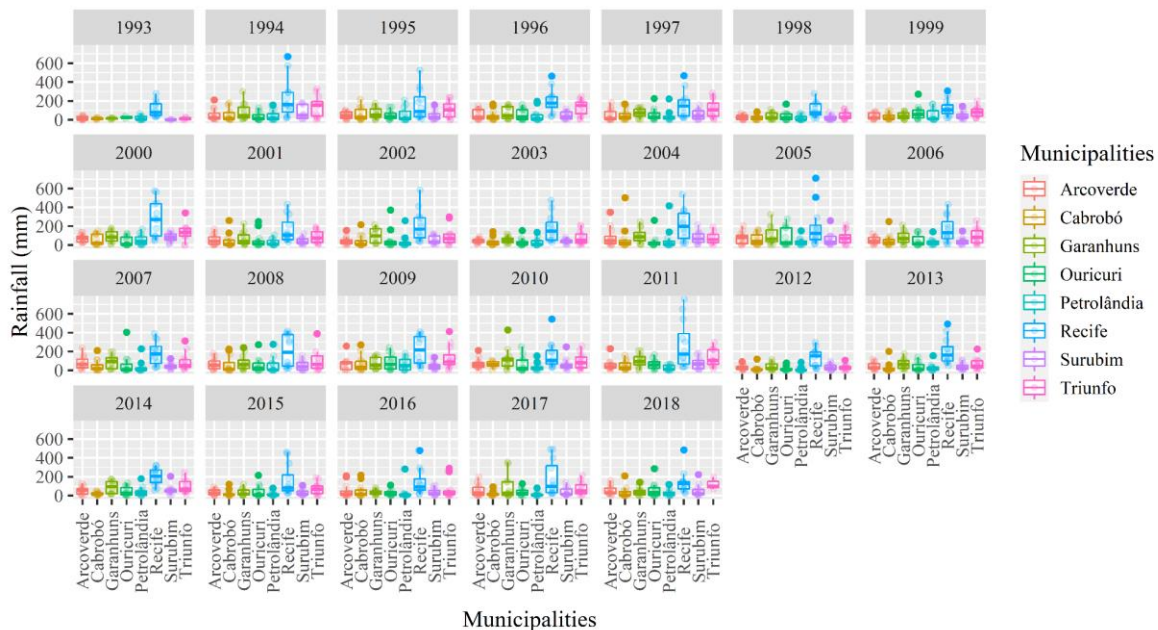
401 The municipalities of Cabrobó and Petrolândia stand out on the axis with the same
 402 climatic conditions according to the Köppen classification, categorized as “BSh” (Alvares et
 403 al., 2013). The municipalities of Triunfo, Garanhuns and Recife, comprise the G_1 group
 404 (Figures 4 and 5), regardless of altitude, the municipalities have similar climatic
 405 characteristics, being “Am” and “Aw”, according to the Köppen classification, like the results
 406 obtained previously by Medeiros et al. (2018), with the classification of three climatic regions
 407 in the State of Pernambuco. According to Souza et al. (2021), despite the climatic variations
 408 in Pernambuco, the performance of the ENSO phases and the variability of the AITG (Lyra
 409 et al., 2017) cause interruptions in the grain harvest and crop gathering across the state. The
 410 problems caused by the decrease in rainfall because of meteorological droughts hinder the
 411 development of crops, causing the agricultural drought (Rossato et al., 2017).

412

413 Afterwards, we examined the historical analysis of the meteorological data (Figure 2)
 to identify the influence of the ENSO phases. Figure 6 shows the study region’s annual

414 rainfall data, highlighting the most extreme ENSO phases (i.e., more intense/persistent in El
 415 Niño and La Niña phases). All the municipalities evaluated reported intra-annual variations
 416 in rainfall records. Such intra-annual variability is due to the ENSO phases (El Niño and La
 417 Niña), which cause droughts and rains throughout the state (Jong et al., 2016; Souza et al.,
 418 2018; Silva et al., 2019; Rodrigues et al., 2020), where the intra-annual variability is more
 419 accentuated in the rainfall in the municipalities that are near the coast (Rao et al., 1993;
 420 Rodrigues et al., 2020). However, in the inland, the variations are less accentuated but still
 421 existing, caused by meteorological systems and the ITCZ seasonal modulation (Lyra et al.,
 422 2014; Gomes and Lima, 2021).

423



424

425 **Fig. 6.** Boxplot of annual rainfall (mm) of the eight municipalities in the State of
 426 Pernambuco, Brazil, in the period 1993–2018. Note: We highlight the most extreme El Niño-
 427 Southern Oscillation phases (i.e., more intense/persistent in El Niño and La Niña phases) that
 428 occurred in the study period according to NOAA/CPC (2020).

429

430 Lower rainfall was recorded in 1993 under the influence of the ENSO-neutral phase
 431 (NOAA/CPC, 2020). Despite being an ENSO-neutral phase year, rainfall volumes were
 432 influenced by previous El Niño years (Cavalcanti, 2015). In 1997–1998, under what has been
 433 called the El Niño of the century, there was a significant decrease in rainfall for all

434 municipalities, with approximately 50% of the rainfall recorded in 1998, being below average
435 (see Figure 2), which was caused by a severe drought in the semi-arid region of NEB
436 (Marengo et al., 2013; Correia Filho et al., 2019). The drought events that occurred in this
437 region caused serious problems and threats to the local biome (i.e. *Caatinga*) - (Correia Filho
438 et al., 2019; Pereira et al., 2020) and thus compromised the quality of life of the inhabitants,
439 by causing collapses in subsistence agriculture – commonly practiced by farmers in the
440 region (Justino et al., 2013; Novaes et al., 2013; Pereira et al., 2020). Previous studies
441 reported the occurrence of La Niña in northeastern Brazil in 1998–1999 (Andreoli and
442 Kayano, 2006; Kayano et al., 2011), with a predominance of strong La Nina in 1999 (Kayano
443 and Capistrano, 2014). These findings are consistent with the results found in the present
444 study for changes in rainfall. In the 2002–2003 biennium, all the municipalities studied
445 except Recife were marked by the occurrence of drought caused by El Niño, and resulting in
446 economic losses (Marengo et al., 2013; Rossato et al., 2017).

447 The years 2004–2005 were marked by above average rainfall (Figure 6), of the
448 climatological normal of the municipalities, except Triunfo. This decrease in rainfall was
449 caused by microclimatic effects with the topography of the site bringing rain to neighboring
450 municipalities and blocking air masses at high altitudes. This phenomenon was also reported
451 by El Alaoui El Fels et al. (2020) in places at an altitude higher than 1,000 m above sea level
452 (asl). The main reasons are the geographical position of the study site together with the role
453 of ENSO in decreasing and/or increasing rainfall, and being influenced by AITG and other
454 micro and large-scale phenomena (Marengo and Espinoza, 2016; Lyra et al., 2017; Zanin
455 and Satyamurty, 2020; Fonsêca et al., 2020).

456 The rains that occurred in the 2014–2015 biennium showed significant decreases,
457 mainly in 2015, due to a super El Niño (Marengo et al., 2018; Correia Filho et al., 2019;
458 NOAA/CPC, 2020). Highlight for the municipality of Garanhuns with high rainfall recorded
459 in 2014 under the influence of the ENSO-neutral phase (NOAA/CPC, 2020). In the years
460 2012 to 2017, the entire NEB was affected by a prolonged extreme drought (Marengo et al.,
461 2017), caused by anomalies in the Pacific (Silva et al., 2019), leading to damage to natural,
462 economic and social resources (Costa et al., 2020). Such damage caused by ENSO, when it
463 comes to drought, give rise to changes in the SST of the Pacific and Atlantic oceans and thus
464 influence the productivity and carbon balance of vegetation in NEB (Pereira et al., 2020).

465 For NEB, in the five-year period 2011–2016 observations of extreme drought were reported
466 by Brito et al. (2018) and by Cunha et al. (2019), with critical periods from 2012 to 2017,
467 respectively. Indeed, 2012 is one of the years of greatest drought and impact for the Brazilian
468 semi-arid region (Paredes-Trejo and Barbosa, 2017; Marengo et al., 2017; Rossato et al.,
469 2017). The existence of contrasting changes in rainfall patterns in the region is a typical
470 feature of the climate in Brazil with the presence of ENSO (Grimm, 2011).

471 The decreases in rainy periods and rainfall over the years in the NEB region could put
472 the semi-arid areas of these locations at serious risk of desertification (Costa et al., 2020).
473 The damage caused by drought in Brazil between 1995 and 2014 was particularly
474 catastrophic in the NEB region, where 48% of the events occurred, and the State of
475 Pernambuco was the third most affected by natural disasters, which account for 16.2% of
476 damage caused throughout the region (Souza et al., 2021). However, the rains that occurred
477 in the 2017–2018 biennium were marked by a moderate ENSO phase (La Niña) -
478 (NOAA/CPC, 2020) which increased the rains (mainly in 2017) except for certain
479 municipalities, e.g., Ouricuri, Cabrobó and Petrolândia, these being municipalities that are
480 farthest from the coast (see Figure 6), which weakens the advances of air masses.

481

482 **4. Conclusion**

483 In this study we used multivariate statistical analysis to determine the meteorological
484 seasonality between the different regions of the State of Pernambuco, north-east Brazil. This
485 analysis is important for the population as it makes it possible to improve the productivity of
486 economic activities, especially crop production and livestock rearing. It should be noted that
487 atmospheric pressure, air temperature, evaporation and wind speed are positively associated
488 with the locations of Ouricuri, Petrolândia and Cabrobó. However, rain and relative humidity
489 were associated with a negative component, related to Recife, Garanhuns, Arcoverde and
490 Triunfo. It is worth mentioning that the physiographic factors and the main meteorological
491 systems are responsible for the associations identified in our study, which in turn can cause
492 extreme weather events and social vulnerability. The municipality of Triunfo stands out
493 because of physiographic factors that together with the occurrence of ENSO contribute to the
494 lowest rainfall records compared with surrounding municipalities that presented anomalies

495 in the rains. The ENSO phases directly influence the variability of rainfall in both
496 homogeneous groups identified in the study.

497 In general, the study is promising and still provides support for agricultural and
498 livestock planning, not only for the municipalities investigated but for the entire territory of
499 the State of Pernambuco. Future research with climatic data should be carried out to include
500 other regions of Brazil, and longer data series, to support public policies and the management
501 of municipalities regarding the mitigation of the impacts of future climate scenarios and
502 conditions.

503

504 **Acknowledgments**

505 The authors would like to thank the Research Support Foundation of the Pernambuco
506 State (FACEPE - APQ-0215-5.01/10 and FACEPE - APQ-1159-1.07/14), the National
507 Council for Scientific and Technological Development (CNPq) also funds Silva T.G.F.,
508 Pandorfi H., and Oliveira-Júnior J.F. through fellowship of the Research Productivity
509 Program (CNPq 309421/2018-7, 304060/2016-0, and 309681/2019-7), and the Coordination
510 for the Improvement of Higher Education Personnel (CAPES - Finance Code 001) for the
511 research and study grants. We also thank the Editor-in-Chief, and two anonymous reviewers
512 for their helpful comments and valuable suggestions to improve the quality of the paper.

513

514 **References**

- 515 Almeida, C.L., Carvalho, T.R.A., Araújo, J.C. (2019). Leaf area index of Caatinga biome
516 and its relationship with hydrological and spectral variables. *Agricultural and Forest*
517 *Meteorology*, 279, 107705. <https://doi.org/10.1016/j.agrformet.2019.107705>
- 518 Alvares, C.A., Stape, J.L., Sentelhas, P.C., Gonçalves, J.L.M., Sparovek, G. (2013).
519 Köppen's climate classification map for Brazil. *Meteorologische Zeitschrift*, 22, 711–
520 728. <https://doi.org/10.1127/0941-2948/2013/0507>
- 521 Andrade, M.C. (1975). The modernization of agriculture in Northeastern Brazil. *Conference*
522 *of Latin Americanist Geographers*, 4, 79–87.
523 <https://www.jstor.org/stable/25765514?seq=1>
- 524 Andreoli, R.V., Kayano, M.T. (2006). Tropical Pacific and South Atlantic effects on rainfall
525 variability over Northeast Brazil. *International Journal of Climatology*, 26(13), 1895-

526 1912. <https://doi.org/10.1002/joc.1341>

527 Anjos, M., Lopes, A. (2019). Sea breeze front identification on the northeastern coast of
528 Brazil and its implications for meteorological conditions in the Sergipe region.
529 *Theoretical and Applied Climatology*, 137(3–4), 2151–2165.
530 <https://doi.org/10.1007/s00704-018-2732-x>

531 Arraes, F.D.D., Lima Junior, J.C., Oliveira, J.B., Macêdo, K.G., Couras, Y.S., Oliveira, W.C.
532 (2016). Parametrização da equação de Hargreaves-Samani para o estado do Pernambuco
533 – Brasil. *Revista Brasileira de Agricultura Irrigada*, 10(1), 410–419.
534 <https://doi.org/10.7127/rbai.v10n100369>

535 Braga, C.C., Macedo, M.J.H., Siva, B.B., Braga, R.C. (2012). Aplicação dos componentes
536 principais na simulação e consistência de séries temporais. *Revista de Geografia*
537 *(Recife)*, 29(1), 113–125.

538 Brito, S.S.B., Cunha, A.P.M.A., Cunningham, C.C., Alvalá, R.C., Marengo, J.A., Carvalho,
539 M.A. (2018). Frequency, duration and severity of drought in the Semiarid Northeast
540 Brazil region. *International Journal of Climatology*, 38(2), 517–529.
541 <https://doi.org/10.1002/joc.5225>

542 Cavalcanti, I.F.A. (2012). Large scale and synoptic features associated with extreme
543 precipitation over South America: A review and case studies for the first decade of the
544 21st century. *Atmospheric Research*, 118, 27–40.
545 <https://doi.org/10.1016/j.atmosres.2012.06.012>

546 Cavalcanti, I.F.A. (2015). The influence of extratropical Atlantic Ocean region on wet and
547 dry years in North-Northeastern Brazil. *Frontiers in Environmental Science*, 3, 34.
548 <https://doi.org/10.3389/fenvs.2015.00034>

549 Cierjacks, A., Pommeranz, M., Schulz, K., Almeida-Cortez, J. (2016). Is crop yield related
550 to weed species diversity and biomass in coconut and banana fields of northeastern
551 Brazil? *Agriculture, Ecosystems and Environment*, 220, 175–183.
552 <https://doi.org/10.1016/j.agee.2016.01.006>

553 Comin, A.N., Justino, F., Pezzi, L., Gurjão, C.D.S., Shumacher, V., Fernández, A., Sutil,
554 U.A. (2020). Extreme rainfall event in the Northeast coast of Brazil: a numerical
555 sensitivity study. *Meteorology and Atmospheric Physics*, 1–22.
556 <https://doi.org/10.1007/s00703-020-00747-0>

557 Correia Filho, W.L.F., Oliveira-Júnior, J.F., Santiago, D.B., Terassi, P.M.B., Teodoro, P.E.,
558 Gois, G., Blanco, C.J.C., Souza, P.H.A., Costa, M.S., Gomes, H.B., Santos, P.J. (2019).
559 Rainfall variability in the Brazilian northeast biomes and their interactions with
560 meteorological systems and ENSO via CHELSA product. *Big Earth Data*, 3(4), 315–
561 337. <https://doi.org/10.1080/20964471.2019.1692298>

562 Costa, R.L., Baptista, G.M.M., Gomes, H.B., Silva, F.D.S., Rocha Júnior, R.L., Araújo
563 Salvador, M., Herdies, D.L. (2020). Analysis of climate extremes indices over northeast
564 Brazil from 1961 to 2014. *Weather and Climate Extremes*, 28, 100254.
565 <https://doi.org/10.1016/j.wace.2020.100254>

566 Costa, M.S., Oliveira-Júnior, J.F., Santos, P.J., Correia Filho, W.L.F., Gois, G., Blanco,
567 C.J.C., Teodoro, P.E., Silva Junior, C.A. da, Santiago, D.B., Souza, E.O., Jardim,
568 A.M.R.F. (2021). Rainfall extremes and drought in Northeast Brazil and its relationship
569 with El Niño–Southern Oscillation. *International Journal of Climatology*, 41, E2111–
570 E2135, <https://doi.org/10.1002/joc.6835>

571 Cunha, A.P.M.A., Zeri, M., Leal, K.D., Costa, L., Cuartas, L.A., Marengo, J.A., Tomasella,
572 J., Vieira, R.M., Barbosa, A.A., Cunningham, C., Cal Garcia, J.V., Broedel, E., Alvalá,
573 R., Ribeiro-Neto, G. (2019). Extreme drought events over Brazil from 2011 to 2019.
574 *Atmosphere*, 10(11), 642. <https://doi.org/10.3390/atmos10110642>

575 Darand, M., Daneshvar, M.R.M. (2014). Regionalization of Precipitation Regimes in Iran
576 Using Principal Component Analysis and Hierarchical Clustering Analysis.
577 *Environmental Processes*, 1(4), 517–532. <https://doi.org/10.1007/s40710-014-0039-1>

578 de Lima, M.I.P., Espírito Santo, F., Ramos, A.M., de Lima, J.L.M.P. (2013). Recent changes
579 in daily precipitation and surface air temperature extremes in mainland Portugal, in the
580 period 1941-2007. *Atmospheric Research*, 27: 195–
581 209, <http://dx.doi.org/10.1016/j.atmosres.2012.10.001>.

582 de Lima, M.I.P., Lovejoy, S. (2015). Macroweather precipitation variability up to global and
583 centennial scales. *Water Resources Research*, 51(12), 9490–
584 9513. <https://doi.org/10.1002/2015WR017455>.

585 Diez-Sierra, J., del Jesus, M. (2020). Long-term rainfall prediction using atmospheric
586 synoptic patterns in semi-arid climates with statistical and machine learning methods.
587 *Journal of Hydrology*, 586, 124789. <https://doi.org/10.1016/j.jhydrol.2020.124789>

588 El Alaoui El Fels, A., Saidi, M.E.M., Bouiji, A., Benrhanem, M. (2020). Rainfall
589 regionalization and variability of extreme precipitation using artificial neural networks:
590 a case study from western central Morocco. *Journal of Water and Climate Change*.
591 <https://doi.org/10.2166/wcc.2020.217>

592 Erfanian, A., Wang, G., Fomenko, L. (2017). Unprecedented drought over tropical South
593 America in 2016: Significantly under-predicted by tropical SST. *Scientific Reports*,
594 7(1). <https://doi.org/10.1038/s41598-017-05373-2>

595 Farrokhi, A., Farzin, S., Mousavi, S.F. (2020). A New Framework for Evaluation of Rainfall
596 Temporal Variability through Principal Component Analysis, Hybrid Adaptive Neuro-
597 Fuzzy Inference System, and Innovative Trend Analysis Methodology. *Water*
598 *Resources Management*, 34(10), 3363–3385. [https://doi.org/10.1007/s11269-020-](https://doi.org/10.1007/s11269-020-02618-0)
599 [02618-0](https://doi.org/10.1007/s11269-020-02618-0)

600 Feindouno, S., Guillaumont, P., Simonet, C. (2020). The Physical Vulnerability to Climate
601 Change Index: An Index to Be Used for International Policy. *Ecological Economics*,
602 176, 106752. <https://doi.org/10.1016/j.ecolecon.2020.106752>

603 Fonsêca, D.N., Corrêa, A.C.B., Cavalcanti Tavares, B.A., Lira, D.R., Barros, A.C.M.,
604 Mützenberg, D.S. (2020). Coupling of tectonic factors and precipitation variability as a
605 driver of Late Quaternary aggradation in Northeast Brazil. *Earth Surface Processes and*
606 *Landforms*, 45(14), 3525–3539. <https://doi.org/10.1002/esp.4982>

607 Gomes, R.S., Lima, K.C. (2021). Influence of the modes of climate variability in the Tropical
608 Pacific and Atlantic on accumulated rainfall and reservoir water volumes in the
609 Northeast Brazil. *International Journal of Climatology*,
610 <https://doi.org/10.1002/joc.7132>

611 Grimm, A.M. (2011). Interannual climate variability in South America: impacts on seasonal
612 precipitation, extreme events, and possible effects of climate change. *Stochastic*
613 *Environmental Research and Risk Assessment*, 25(4), 537–554.
614 <https://doi.org/10.1007/s00477-010-0420-1>

615 Hagel, H., Hoffmann, C., Irmão, J.F., Doluschitz, R. (2019). Socio-economic aspects of
616 irrigation agriculture as livelihood for rural families in Brazil’s semi-arid northeast.
617 *Journal of Agriculture and Rural Development in the Tropics and Subtropics*, 120(2),
618 157–169. <https://doi.org/10.17170/kobra-20191127814>

619 Herath, S.M., Sarukkalige, R., Nguyen, V.T.V. (2018). Evaluation of empirical relationships
620 between extreme rainfall and daily maximum temperature in Australia. *Journal of*
621 *Hydrology*, 556, 1171–1181. <https://doi.org/10.1016/j.jhydrol.2017.01.060>

622 Huang, B., L'Heureux, M., Hu, Z.Z., Zhang, H.M. (2016). Ranking the strongest ENSO
623 events while incorporating SST uncertainty. *Geophysical Research Letters*, 43(17),
624 9165-9172. <https://doi.org/10.1002/2016GL070888>

625 Instituto Brasileiro de Geografia e Estatística – IBGE. (2019). *Censo demográfico do Estado*
626 *de Pernambuco*, viewed 15 April 2020. <https://cidades.ibge.gov.br/brasil/pe/panorama>

627 Instituto Brasileiro de Geografia e Estatística – IBGE. (2020). *Produção Agrícola Municipal*,
628 viewed 20 September 2020. <https://sidra.ibge.gov.br/Tabela/1612>

629 Instituto Nacional de Meteorologia – INMET (2019). *Banco de Dados Meteorológicos para*
630 *Ensino e Pesquisa*, viewed 12 December 2020. <https://portal.inmet.gov.br/>

631 Jardim, A.M.R.F., Queiroz, M.G., Araújo Júnior, G.N., Silva, M.J., Silva, T.G.F. (2019).
632 Estudos climáticos do número de dias de precipitação pluvial para o município de Serra
633 Talhada-PE. *Revista Engenharia na Agricultura*, 27(4), 330–337.
634 <https://doi.org/10.13083/reveng.v27i4.875>

635 Jardim, A.M.R.F., Santos, H.R.B., Alves, H.K.M.N., Ferreira-Silva, S.L., Souza, L.S.B.,
636 Araújo Júnior, G.N., Souza, M.S., Araújo, G.G.L., Souza, C.A.A., Silva, T.G.F. (2021).
637 Genotypic differences relative photochemical activity, inorganic and organic solutes
638 and yield performance in clones of the forage cactus under semi-arid environment. *Plant*
639 *Physiology and Biochemistry*, 162, 421-430.
640 <https://doi.org/10.1016/j.plaphy.2021.03.011>

641 Jolliffe, I.T. (1990). Principal component analysis: A beginner's guide — I. Introduction and
642 application. *Weather*, 45(10), 375–382. [https://doi.org/10.1002/j.1477-](https://doi.org/10.1002/j.1477-8696.1990.tb05558.x)
643 [8696.1990.tb05558.x](https://doi.org/10.1002/j.1477-8696.1990.tb05558.x)

644 Jong, B.-T., Ting, M., Seager, R. (2016). El Niño's impact on California precipitation:
645 seasonality, regionality, and El Niño intensity. *Environmental Research Letters*, 11,
646 054021. <https://doi.org/10.1088/1748-9326/11/5/054021>

647 Justino, F., Oliveira, E.C., Rodrigues, R.Á., Gonçalves, P.H.L., Souza, P.J.O.P., Stordal, F.,
648 Marengo, J., Silva, T.G., Delgado, R.C., Lindemann, D.S., Costa, L.C. (2013). Mean
649 and Interannual Variability of Maize and Soybean in Brazil under Global Warming

650 Conditions. *American Journal of Climate Change*, 02(04), 237–253.
651 <https://doi.org/10.4236/ajcc.2013.24024>

652 Kaiser, H.F. (1960). The Application of Electronic Computers to Factor Analysis.
653 *Educational and Psychological Measurement*, 20(1), 141–151.
654 <https://doi.org/10.1177/001316446002000116>

655 Kayano, M.T., Capistrano, V.B. (2014). How the Atlantic multidecadal oscillation (AMO)
656 modifies the ENSO influence on the South American rainfall. *International Journal of*
657 *Climatology*, 34(1), 162-178. <https://doi.org/10.1002/joc.3674>

658 Kayano, M.T, Andreoli, R.V., Souza, R.A.F. (2011). Evolving anomalous SST patterns
659 leading to ENSO extremes: relations between the tropical Pacific and Atlantic Oceans
660 and the influence on the South American rainfall. *International Journal of Climatology*,
661 31(8), 1119-1134. <https://doi.org/10.1002/joc.2135>

662 Leal, A.L.C., Lauria, D.C., Ribeiro, F.C.A., Viglio, E.P., Franzen, M., Lima, E.A.M. (2020).
663 Spatial distributions of natural radionuclides in soils of the state of Pernambuco, Brazil:
664 Influence of bedrocks, soils types and climates. *Journal of Environmental Radioactivity*,
665 211, 106046. <https://doi.org/10.1016/j.jenvrad.2019.106046>

666 Lima, A.O., Lyra, G.B., Abreu, M.C., Oliveira-Júnior, J.F., Zeri, M., Cunha-Zeri, G. (2021).
667 Extreme rainfall events over Rio de Janeiro State, Brazil: Characterization using
668 probability distribution functions and clustering analysis. *Atmospheric Research*, 247,
669 105221. <https://doi.org/10.1016/j.atmosres.2020.105221>

670 Lima, F.J.L., Martins, F.R., Costa, R.S., Gonçalves, A.R., Santos, A.P.P., Pereira, E.B.
671 (2019). The seasonal variability and trends for the surface solar irradiation in
672 northeastern region of Brazil. *Sustainable Energy Technologies and Assessments*, 35,
673 335–346. <https://doi.org/10.1016/j.seta.2019.08.006>

674 Lyra, G.B., Oliveira-Júnior, J.F., Gois, G., Cunha-Zeri, G., Zeri, M. (2017). Rainfall
675 variability over Alagoas under the influences of SST anomalies. *Meteorology and*
676 *Atmospheric Physics*, 129(2), 157–171. <https://doi.org/10.1007/s00703-016-0461-1>

677 Lyra, G.B., Oliveira-Júnior, J.F., Zeri, M. (2014). Cluster analysis applied to the spatial and
678 temporal variability of monthly rainfall in Alagoas state, Northeast of Brazil.
679 *International Journal of Climatology*, 34(13), 3546–3558.
680 <https://doi.org/10.1002/joc.3926>

681 Marengo, J.A., Espinoza, J.C. (2016). Extreme seasonal droughts and floods in Amazonia:
682 causes, trends and impacts. *International Journal of Climatology*, 36(3), 1033–1050.
683 <https://doi.org/10.1002/joc.4420>

684 Marengo, J.A., Alves, L.M., Soares, W.R., Rodriguez, D.A., Camargo, H., Riveros, M.P.,
685 Pablo, A.D. (2013). Two contrasting severe seasonal extremes in tropical South
686 America in 2012: Flood in Amazonia and drought in Northeast Brazil. *Journal of*
687 *Climate*, 26(22), 9137–9154. <https://doi.org/10.1175/JCLI-D-12-00642.1>

688 Marengo, J.A., Cunha, A.P.M.A., Nobre, C.A., Ribeiro Neto, G.G., Magalhaes, A.R., Torres,
689 R.R., Sampaio, G., Alexandre, F., Alves, L.M., Cuartas, L.A., Deusdará, K.R.L., Álvala,
690 R.C.S. (2020). Assessing drought in the drylands of northeast Brazil under regional
691 warming exceeding 4 °C. *Natural Hazards*, 103(2), 2589–2611.
692 <https://doi.org/10.1007/s11069-020-04097-3>

693 Marengo, J.A., Torres, R.R., Alves, L.M. (2017). Drought in Northeast Brazil—past, present,
694 and future. *Theoretical and Applied Climatology*, 129(3–4), 1189–1200.
695 <https://doi.org/10.1007/s00704-016-1840-8>

696 Marengo, J.A., Alves, L.M., Alvala, R.C.S., Cunha, A.P., Brito, S., Moraes, O.L.L. (2018).
697 Climatic characteristics of the 2010-2016 drought in the semiarid northeast Brazil
698 region. *Anais da Academia Brasileira de Ciencias*, 90(2), 1973–1985.
699 <https://doi.org/10.1590/0001-3765201720170206>

700 Marinho, K.F.S., Andrade, L.M.B., Spyrides, M.H.C., Santos e Silva, C.M., Oliveira, C.P.,
701 Bezerra, B.G., Mutti, P.R. (2020). Climate Profiles in Brazilian Microregions.
702 *Atmosphere*, 11(11), 1217. <https://doi.org/10.3390/atmos11111217>

703 Martins, M.A., Tomasella, J., Dias, C.G. (2019). Maize yield under a changing climate in the
704 Brazilian Northeast: Impacts and adaptation. *Agricultural Water Management*, 216,
705 339–350. <https://doi.org/10.1016/j.agwat.2019.02.011>

706 Marumbwa, F.M., Cho, M.A., Chirwa, P.W. (2019). Analysis of spatio-temporal rainfall
707 trends across southern African biomes between 1981 and 2016. *Physics and Chemistry*
708 *of the Earth, Parts A/B/C*, 114, 102808. <https://doi.org/10.1016/j.pce.2019.10.004>

709 Medeiros, F.J., Oliveira, C.P., Torres, R.R. (2020). Climatic aspects and vertical structure
710 circulation associated with the severe drought in Northeast Brazil (2012–2016). *Climate*
711 *Dynamics*, 55(9–10), 2327–2341. <https://doi.org/10.1007/s00382-020-05385-1>

712 Medeiros, F.J., Oliveira, C.P. (2021). Dynamical Aspects of the Recent Strong El Niño
713 Events and Its Climate Impacts in Northeast Brazil. *Pure and Applied Geophysics*.
714 <https://doi.org/10.1007/s00024-021-02758-3>

715 Medeiros, R.M., Holanda, R.M., Viana, M.A., Silva, V.P. (2018). Climate classification in
716 Köppen model for the state of Pernambuco - Brazil. *Revista de Geografia (Recife)*,
717 35(3), 219–234. <http://www.revista.ufpe.br/revistageografia>

718 Molion, L.C.B., Bernardo, S.O. (2002). Uma revisão da dinâmica das chuvas no Nordeste
719 Brasileiro. *Revista Brasileira de Meteorologia*, 17(1), 1–10.

720 Monteiro, F.F., Gonçalves, W.A., Andrade, L.M.B., Villavicencio, L.M.M., Santos Silva,
721 C.M. (2021). Assessment of Urban Heat Islands in Brazil based on MODIS remote
722 sensing data. *Urban Climate*, 35, 100726. <https://doi.org/10.1016/j.uclim.2020.100726>

723 Moscati, M.C.L., Gan, M.A. (2007). Rainfall variability in the rainy season of semiarid zone
724 of northeast Brazil (NEB) and its relation to wind regime. *International Journal of*
725 *Climatology*, 27(4), 493–512. <https://doi.org/10.1002/joc.1408>

726 National Oceanic and Atmospheric Administration/Climate Prediction Center – NOAA/CPC
727 (2020). *Cold & Warm Episodes by Season*, viewed 28 December 2020.
728 http://www.cpc.ncep.noaa.gov/products/analysis_monitoring/ensostuff/ensoyears.shtml
729 1

730 Ndehedehe, C.E., Haile, G.G., Agutu, N.O., Ferreira, V.G., Getirana, A., Okwuashi, O.
731 (2020). Hydrological hotspots of climatic influence in Brazil: a two-step regularization
732 approach. *Atmospheric Research*, 246, 105116.
733 <https://doi.org/10.1016/j.atmosres.2020.105116>

734 Nehrani, S.H., Askari, M.S., Saadat, S., Delavar, M.A., Taheri, M., Holden, N.M. (2020).
735 Quantification of soil quality under semi-arid agriculture in the northwest of Iran.
736 *Ecological Indicators*, 108, 105770. <https://doi.org/10.1016/j.ecolind.2019.105770>

737 Nóbrega, R.S., Farias, R.F.L., Santos, C.A.C. (2015). Variabilidade temporal e espacial da
738 precipitação pluviométrica em Pernambuco através de índices de extremos climáticos.
739 *Revista Brasileira de Meteorologia*, 30(2), 171–180. <https://doi.org/10.1590/0102-778620130624>

740

741 Nogueira, M., Lima, D.C.A., Soares, P.M.M. (2020). An integrated approach to project the
742 future urban climate response: Changes to Lisbon’s urban heat island and temperature

743 extremes. *Urban Climate*, 34, 100683. <https://doi.org/10.1016/j.uclim.2020.100683>

744 Novaes, R.L.M., Felix, S., Souza, R.D.F. (2013). Save Caatinga from drought disaster.
745 *Nature*, 498(7453), 170. <https://doi.org/10.1038/498170a>

746 Oliveira, P.T., Santos e Silva, C.M., Lima, K.C. (2017). Climatology and trend analysis of
747 extreme precipitation in subregions of Northeast Brazil. *Theoretical and Applied*
748 *Climatology*, 130(1–2), 77–90. <https://doi.org/10.1007/s00704-016-1865-z>

749 Paredes-Trejo, F., Barbosa, H. (2017). Evaluation of the SMOS-derived soil water deficit
750 index as agricultural drought index in Northeast of Brazil. *Water*, 9(6), 377.
751 <https://doi.org/10.3390/w9060377>

752 Patra, A., Min, S., Seong, M. (2020). Climate Variability Impacts on Global Extreme Wave
753 Heights: Seasonal Assessment Using Satellite Data and ERA5 Reanalysis. *Journal of*
754 *Geophysical Research: Oceans*, 125(12), e2020JC016754.
755 <https://doi.org/10.1029/2020JC016754>

756 Pereira, M.P.S., Mendes, K.R., Justino, F., Couto, F., Silva, A.S., Silva, D.F., Malhado,
757 A.C.M. (2020). Brazilian Dry Forest (Caatinga) Response To Multiple ENSO: the role
758 of Atlantic and Pacific Ocean. *Science of the Total Environment*, 705, 135717.
759 <https://doi.org/10.1016/j.scitotenv.2019.135717>

760 Pereira, S., Ramos, A.M., Rebelo, L., Trigo, R.M., Zêzere, J.L. (2018). A centennial
761 catalogue of hydro-geomorphological events and their atmospheric forcing. *Advances*
762 *in Water Resources*, 122, 98–112. <https://doi.org/10.1016/j.advwatres.2018.10.001>

763 Pimenta, F.M., Silva, A.R., Assireu, A.T., Almeida, V.S., Saavedra, O.R. (2019). Brazil
764 Offshore Wind Resources and Atmospheric Surface Layer Stability. *Energies*, 12(21),
765 4195. <https://doi.org/10.3390/en12214195>

766 Queiroz, M.G., Silva, T.G.F., Zolnier, S., Souza, C.A.A., Souza, L.S.B., Araújo Júnior, G.N.,
767 Jardim, A.M.R.F., Moura, M.S.B. (2020a). Partitioning of rainfall in a seasonal dry
768 tropical forest. *Ecohydrology and Hydrobiology*, 20(2), 230–242.
769 <https://doi.org/10.1016/j.ecohyd.2020.02.001>

770 Queiroz, M.G., Silva, T.G.F., Zolnier, S., Jardim, A.M.R.F., Souza, C.A.A., Araújo Júnior,
771 G.N., Morais, J.E.F., Souza, L.S.B. (2020b). Spatial and temporal dynamics of soil
772 moisture for surfaces with a change in land use in the semi-arid region of Brazil. *Catena*,
773 188, 104457. <https://doi.org/10.1016/j.catena.2020.104457>

774 R Core Team. (2020). *R: A language and environment for statistical computing*. R
775 *Foundation for Statistical Computing*. Vienna, Austria. <https://www.r-project.org/>

776 Rao, V.B., De Lima, M.C., Franchito, S.H. (1993). Seasonal and interannual variations of
777 rainfall over eastern Northeast Brazil. *Journal of Climate*, 6(9), 1754–1763.
778 [https://doi.org/10.1175/1520-0442\(1993\)006<1754:SAIVOR>2.0.CO;2](https://doi.org/10.1175/1520-0442(1993)006<1754:SAIVOR>2.0.CO;2)

779 Raziei, T. (2018). A precipitation regionalization and regime for Iran based on multivariate
780 analysis. *Theoretical and Applied Climatology*, 131(3–4), 1429–1448.
781 <https://doi.org/10.1007/s00704-017-2065-1>

782 Reboita, M.S., Gan, M.A., Rocha, R.P., Ambrizzi, T. (2010). Regimes de precipitação na
783 América do Sul: uma revisão bibliográfica. *Revista Brasileira de Meteorologia*, 2, 185–
784 204. <https://doi.org/10.1590/S0102-77862010000200004>

785 Reboita, M.S., Krusche, N., Ambrizzi, T., Rocha, R.P. (2012). Entendendo o tempo e o clima
786 na América do Sul. *Terra e Didática*, 8(1), 34–50.
787 <https://doi.org/10.20396/td.v8i1.8637425>

788 Rega, C., Helming, J., Paracchini, M.L. (2019). Environmentalism and localism in
789 agricultural and land-use policies can maintain food production while supporting
790 biodiversity. Findings from simulations of contrasting scenarios in the EU. *Land Use*
791 *Policy*, 87, 103986. <https://doi.org/10.1016/j.landusepol.2019.05.005>

792 Ribeiro, K., Sousa-Neto, E.R., Junior Carvalho, J.A., Lima, J.R.S., Menezes, R.S.C., Duarte-
793 Neto, P.J., Guerra, G.S., Ometto, J.P.H.B. (2016). Land cover changes and greenhouse
794 gas emissions in two different soil covers in the Brazilian Caatinga. *Science of the Total*
795 *Environment*, 571, 1048–1057. <https://doi.org/10.1016/j.scitotenv.2016.07.095>

796 Rodrigues, D.T., Gonçalves, W.A., Spyrides, M.H.C., Santos e Silva, C.M., Souza, D.O.
797 (2020). Spatial distribution of the level of return of extreme precipitation events in
798 Northeast Brazil. *International Journal of Climatology*, 40(12), 1–16.
799 <https://doi.org/10.1002/joc.6507>

800 Rossato, L., Alvalá, R.C.S., Marengo, J.A., Zeri, M., Cunha, A.P.M.A., Pires, L.B.M.,
801 Barbosa, H.A. (2017). Impact of soil moisture on crop yields over Brazilian semiarid.
802 *Frontiers in Environmental Science*, 5(73). <https://doi.org/10.3389/fenvs.2017.00073>

803 Sadeghi, S.M.M., Attarod, P., Van Stan, J.T., Pypker, T.G. (2016). The importance of
804 considering rainfall partitioning in afforestation initiatives in semiarid climates: A

805 comparison of common planted tree species in Tehran, Iran. *Science of the Total*
806 *Environment*, 568, 845–855. <https://doi.org/10.1016/j.scitotenv.2016.06.048>

807 Santos, A., Oliveira Lopes, P.M., Silva, M.V., Jardim, A.M.R.F., Moura, G.B.A., Fernandes,
808 G.S.T., Silva, D.A.O., Silva, J.L.B., Rodrigues, J.A.M., Silva, E.A., Oliveira-Júnior, J.F.
809 (2020). Causes and consequences of seasonal changes in the water flow of the São
810 Francisco river in the semiarid of Brazil. *Environmental and Sustainability Indicators*,
811 8, 100084. <https://doi.org/10.1016/j.indic.2020.100084>

812 Santos, M.O., Stosic, T., Stosic, B.D. (2012). Long-term correlations in hourly wind speed
813 records in Pernambuco, Brazil. *Physica A: Statistical Mechanics and Its Applications*,
814 391(4), 1546–1552. <https://doi.org/10.1016/j.physa.2011.08.041>

815 Saraçlı, S., Doğan, N., Doğan, I. (2013). Comparison of hierarchical cluster analysis methods
816 by cophenetic correlation. *Journal of Inequalities and Applications*, 2013(1), 203.
817 <https://doi.org/10.1186/1029-242X-2013-203>

818 Silva, A.R., Pimenta, F.M., Assireu, A.T., Spyrides, M.H.C. (2016). Complementarity of
819 Brazils hydro and offshore wind power. *Renewable and Sustainable Energy Reviews*,
820 56, 413–427. <https://doi.org/10.1016/j.rser.2015.11.045>

821 Silva, A.R., Santos, T.S., Queiroz, D.É., Gusmão, M.O., Silva, T.G.F. (2017). Variações no
822 índice de anomalia de chuva no Semiárido. *Journal of Environmental Analysis and*
823 *Progress*, 2(4), 377–384. <https://doi.org/10.24221/jeap.2.4.2017.1420.377-384>

824 Silva, B.K.N., Amorim, A.C.B., Silva, C.M.S., Lucio, P.S., Barbosa, L.M. (2019). Rainfall-
825 related natural disasters in the Northeast of Brazil as a response to ocean-atmosphere
826 interaction. *Theoretical and Applied Climatology*, 138(3–4), 1821–1829.
827 <https://doi.org/10.1007/s00704-019-02930-9>

828 Silva, M.V., Pandorfi, H., Jardim, A.M.R.F., Oliveira-Junior, J.F., Divincula, J.S., Giongo,
829 P.R., Silva, T.G.F., Almeida, G.L.P., Moura, G.B.A., Lopes, P.M.O. (2021). Spatial
830 modeling of rainfall patterns and groundwater on the coast of northeastern Brazil. *Urban*
831 *Climate*, 35, 100911. <https://doi.org/10.1016/j.uclim.2021.100911>

832 Singh, C., Bazaz, A., Ley, D., Ford, J., Revi, A. (2020). Assessing the feasibility of climate
833 change adaptation options in the water sector: Examples from rural and urban
834 landscapes. *Water Security*, 11, 100071. <https://doi.org/10.1016/j.wasec.2020.100071>

835 Slavich, E., Warton, D.I., Ashcroft, M.B., Gollan, J.R., Ramp, D. (2014). Topoclimate versus

836 macroclimate: how does climate mapping methodology affect species distribution
837 models and climate change projections? *Diversity and Distributions*, 20(8), 952–963.
838 <https://doi.org/10.1111/ddi.12216>

839 Sobral, B.S., Oliveira Júnior, J.F., Gois, G., Terassi, P.M.B., Pereira, C.R. (2018). Regime
840 de Vento na Serra do Mar-Rio de Janeiro, Brasil. *Revista Brasileira de Meteorologia*,
841 33(3), 441–451. <https://doi.org/10.1590/0102-7786333004>

842 Souza Hacon, S., Oliveira, B.F.A., Silveira, I. (2019). A Review of the Health Sector Impacts
843 of 4 °C or more Temperature Rise. In C. Nobre, J. Marengo, & W. Soares (Eds.),
844 *Climate Change Risks in Brazil* (pp. 67–129) Springer International Publishing.
845 https://doi.org/10.1007/978-3-319-92881-4_4

846 Souza, A.G.S.S., Ribeiro Neto, A., Souza, L.L. (2021). Soil moisture-based index for
847 agricultural drought assessment: SMADI application in Pernambuco State-Brazil.
848 *Remote Sensing of Environment*, 252, 112124.
849 <https://doi.org/10.1016/j.rse.2020.112124>

850 Souza, D.C., Oyama, M.D. (2017). Breeze potential along the Brazilian northern and
851 northeastern coast. *Journal of Aerospace Technology and Management*, 9(3), 368–378.
852 <https://doi.org/10.5028/jatm.v9i3.787>

853 Souza, T.C.O., Delgado, R.C., Magistrali, I.C., Santos, G.L., Carvalho, D.C., Teodoro, P.E.,
854 Silva Júnior, C.A., Caúla, R.H. (2018). Spectral trend of vegetation with rainfall in
855 events of El Niño-Southern Oscillation for Atlantic Forest biome, Brazil. *Environmental*
856 *Monitoring and Assessment*, 190(11), 1–14. [https://doi.org/10.1007/s10661-018-7060-](https://doi.org/10.1007/s10661-018-7060-1)
857 1

858 Sumesh, R.K., Resmi, E.A., Unnikrishnan, C.K., Jash, D., Sreekanth, T.S., Mol Resmi, M.C.,
859 Rajeevan, K., Nita, S., Ramachandran, K.K. (2019). Microphysical aspects of tropical
860 rainfall during Bright Band events at mid and high-altitude regions over Southern
861 Western Ghats, India. *Atmospheric Research*, 227, 178–197.
862 <https://doi.org/10.1016/j.atmosres.2019.05.002>

863 Teixeira, A.H.C., Takemura, C.M., Leivas, J.F., Pacheco, E.P., Bayma-Silva, G., Garçon,
864 E.A.M. (2020). Water productivity monitoring by using geotechnological tools in
865 contrasting social and environmental conditions: Applications in the São Francisco
866 River basin, Brazil. *Remote Sensing Applications: Society and Environment*, 18,

867 100296. <https://doi.org/10.1016/j.rsase.2020.100296>

868 Utida, G., Cruz, F.W., Etourneau, J., Bouloubassi, I., Schefuß, E., Vuille, M., Novello, V.F.,
869 Prado, L.F., Sifeddine, A., Klein, V., Zular, A., Viana, J.C.C., Turcq, B. (2019). Tropical
870 South Atlantic influence on Northeastern Brazil precipitation and ITCZ displacement
871 during the past 2300 years. *Scientific Reports*, 9(1). [https://doi.org/10.1038/s41598-018-](https://doi.org/10.1038/s41598-018-38003-6)
872 38003-6

873 Valadão, C.E.A., Carvalho, L.M.V., Lucio, P.S., Chaves, R.R. (2017). Impacts of the
874 Madden-Julian oscillation on intraseasonal precipitation over Northeast Brazil.
875 *International Journal of Climatology*, 37(4), 1859–1884.
876 <https://doi.org/10.1002/joc.4818>

877 Ward, J.H.Jr. (1963). Hierarchical Grouping to Optimize an Objective Function. *Journal of*
878 *the American Statistical Association*, 58(301), 236–244.
879 <https://doi.org/10.2307/2282967>

880 Wilks, D.S. (2011). *Statistical Methods in the Atmospheric Sciences*, Third Edition,
881 International Geophysics Series, Academic Press, Amsterdam, Holanda.

882 Xie, H., Dong, J., Shen, Z., Chen, L., Lai, X., Qiu, J., Wei, G., Peng, Y., Chen, X. (2019).
883 Intra- and inter-event characteristics and controlling factors of agricultural nonpoint
884 source pollution under different types of rainfall-runoff events. *Catena*, 182, 104105.
885 <https://doi.org/10.1016/j.catena.2019.104105>

886 Zanin, P.R., Satyamurty, P. (2020). Hydrological processes interconnecting the two largest
887 watersheds of South America from multi-decadal to inter-annual time scales: A critical
888 review. *International Journal of Climatology*, 40(9), 4006–4038.
889 <https://doi.org/10.1002/joc.6442>

890 Zarei, A.R., Shabani, A., Mahmoudi, M.R. (2019). Comparison of the climate indices based
891 on the relationship between yield loss of rain-fed winter wheat and changes of climate
892 indices using GEE model. *Science of the Total Environment*, 661, 711–722.
893 <https://doi.org/10.1016/j.scitotenv.2019.01.204>

894

CHAPTER 4

Using remote sensing to quantify the joint effects of climate and land-use changes on the Caatinga biome

Abstract

Caatinga biome, located in the Brazilian semi-arid region, is the most populous semi-arid region in the world, causing intensification in land degradation and loss of biodiversity over time. The main objective of this paper is to determine and analyze the changes in land cover and use, over time, on the biophysical parameters in the Caatinga biome in the semi-arid region of Brazil using remote sensing. Landsat-8 images were used, along with the Surface Energy Balance Algorithm for Land (SEBAL) in the Google Earth Engine platform, from 2013 to 2019, through spatiotemporal modeling of vegetation indices, i.e., leaf area index (LAI) and vegetation cover (V_C). Moreover, land surface temperature (LST) and actual evapotranspiration (ET_a) in Petrolina, the semi-arid region of Brazil, was used. The principal component analysis was used to select descriptive variables and multiple regression analysis to predict ET_a . The results indicated significant effects of land use and land cover changes on energy balances over time. In 2013, 70.2% of the study area was composed of Caatinga, while the lowest percentages were identified in 2015 (67.8%) and 2017 (68.7%). Rainfall records in 2013 ranged from 270 to 480 mm, with values higher than 410 mm in 46.5% of the study area, concentrated in the northern part of the municipality. On the other hand, in 2017 the lowest annual rainfall values (from 200 to 340 mm) occurred. Low vegetation cover rate was observed by LAI and V_C values, with a range of 0 to 25% vegetation cover in 52.3% of the area, which exposes the effects of the dry season on vegetation. The highest LST was mainly found in urban areas and/or exposed soil. In 2013, 40.5% of the region's area had LST between 48.0 and 52.0 °C, raising ET_a rates ($\sim 4.7 \text{ mm day}^{-1}$). Our model has shown good outcomes in terms of accuracy and concordance (coefficient of determination = 0.98, root mean square error = 0.498, and Lin's concordance correlation coefficient = 0.907). The significant increase in agricultural areas has resulted in the progressive reduction of the Caatinga biome. Therefore, mitigation and sustainable planning is vital to decrease the impacts of anthropic actions.

32

33 **Keywords:** tropical dry forest; surface energy balance; Brazilian semi-arid; SEBAL; actual
34 evapotranspiration

35

36 **1. Introduction**

37 The Caatinga biome occupies a large portion of the Brazilian semi-arid region. It has
38 a high ecological diversity of plant species, and it is considered the largest in the world under
39 semi-arid conditions [1,2]. It occupies an area of 900,000 km², which corresponds to
40 approximately 70% of the northeast region of Brazil (NEB). However, only 7.5% of this
41 habitat is protected by law [3–5]. The municipality of Petrolina, PE, Brazil, is located in the
42 semi-arid region of the Caatinga biome. It is within the hydrographic basin of the São
43 Francisco river, which favors the development of irrigated agriculture in the region, mainly
44 fruit-growing (e.g., grapes and mangoes) [6–8], and it leads to positive socioeconomic
45 implications, but also increases conflicts regarding water use [2,9].

46 Caatinga is located in the world's most populated dry area, with more than 53 million
47 inhabitants and a population density close to 34 inhabitants per km². This biome has been
48 affected by environmental degradation and loss of biodiversity over the last decades, mainly
49 by the intensification of agriculture (e.g., rainfed and irrigated crops cultivation), urban
50 expansion, and the advance of pasture areas replacing the natural vegetation [10–12].
51 Expanding agricultural activities has led to the deforestation of native areas, soil disturbance,
52 changes in the hydrological cycle, and higher carbon emissions [13–15]. Together with
53 climate changes, such as reduced rainfall and intensified drought events, this makes the
54 Caatinga biome and the Brazilian ecosystem the most threatened and susceptible to
55 desertification. Furthermore, these changes have been increasingly compromising natural
56 resources and environmental sustainability [16–19] due to the changes in surface properties
57 and biophysical variables, such as vegetation cover (V_C), land surface temperature (LST),
58 and evapotranspiration (ET) [20–22]. ET is one of the main response parameters of vegetated
59 areas as a function of local water conditions, and it is also an important component of the
60 hydrological cycle [23,24].

61 Therefore, monitoring physical–water indicators of environmental change conditions,
62 such as the loss of biodiversity of biomes and land use and occupation, is vital in managing

63 scarce water resources. Furthermore, these indicators may be helpful in the planning of
64 agricultural activities, as well as in the management of dry areas and the sustainable use and
65 management of natural resources [17,25–30].

66 In this scenario, remote sensing has been used as a tool that presents fast and low
67 operational costs, being efficient in calculating the biophysical parameters used in the energy,
68 water, and vegetation balances (e.g., [31–33]). In recent years, remote sensing has also been
69 considered a good alternative for replacing expensive and difficult-to-obtain equipment used
70 in in situ studies [34]. Furthermore, the modeling used in these balances is performed with
71 the help of algorithms, which are essential techniques in the extraction of information from
72 satellite images on a regional and global scale [27,28,33,35]. It may have its efficiency
73 improved by the use of open-source cloud programming languages, e.g., Google Earth
74 Engine (GEE). In GEE, the user can effectively implement algorithms and process large data
75 volumes [36].

76 In this context, there are several surface energy balance models, such as Mapping
77 EvapoTranspiration at high Resolution with Internalized Calibration (METRIC), Surface
78 Energy Balance System (SEBS), Simple Algorithm for Evapotranspiration Retrieving
79 (SAFER), Atmosphere–Land Exchange Inverse (Alexi), and the Energy Balance Algorithm
80 for Land (SEBAL), based on remote sensing data. The approach is substantiated on
81 biophysical parameters, such as LST, albedo, Normalized Difference Vegetation Index
82 (NDVI), and emissivity, that are crucial for estimating ET [16,37–42]. The SEBAL algorithm
83 has been widely and successfully applied to various world ecosystems, including semi-arid
84 conditions in Brazil [43–46]. Moreover, this method seeks to eliminate the propagation of
85 errors in the partitioning of the energy balance and the need for atmospheric correction in the
86 estimate of surface temperature. These interactions allow the generation of the sensible heat
87 flux corrected for atmospheric stability and instability conditions [47–51]. NDVI is one of
88 the most widely used indices in the literature for vegetation cover analysis, environmental
89 degradation, and vegetation primary production resilience, and it also helps in monitoring
90 agricultural crops, forest ecosystems, and drought assessments [52–54]. With applications in
91 several countries, Bastiaanssen et al. [49] have obtained highly accurate results using the
92 SEBAL algorithm on different vegetated surfaces with forests, agricultural crops (irrigated
93 and rainfed), and even extreme landscapes, such as desert areas. Previous studies have shown

94 that the SEBAL can be used in Petrolina, PE, Brazil, for the algorithm has already been
95 calibrated and validated for the region in various ecosystems with good agreement between
96 orbital images and field measurements [44,55–58].

97 Based on the above, the main objective of this paper is to determine and analyze the
98 changes in land cover, land use, and occupation on biophysical parameters in the Caatinga
99 biome in the semi-arid region of Brazil. In the present study, the changes were assessed from
100 2013 to 2019 using Landsat imagery, and biophysical parameters (net radiation, energy
101 balance, LAI, V_c , ET_a , and LST) were estimated by utilizing remote sensing. Additionally,
102 the SEBAL model was applied to determine the surface energy balance in different
103 vegetation environments. After applying the model, the dataset provided by SEBAL allowed
104 us to determine the turbulent fluxes and actual evapotranspiration (ET_a) of the different land
105 use and land cover (LULC) types. Thus, through the SEBAL products, the spatiotemporal
106 variation patterns of ET_a in agricultural and forestry areas were evaluated.

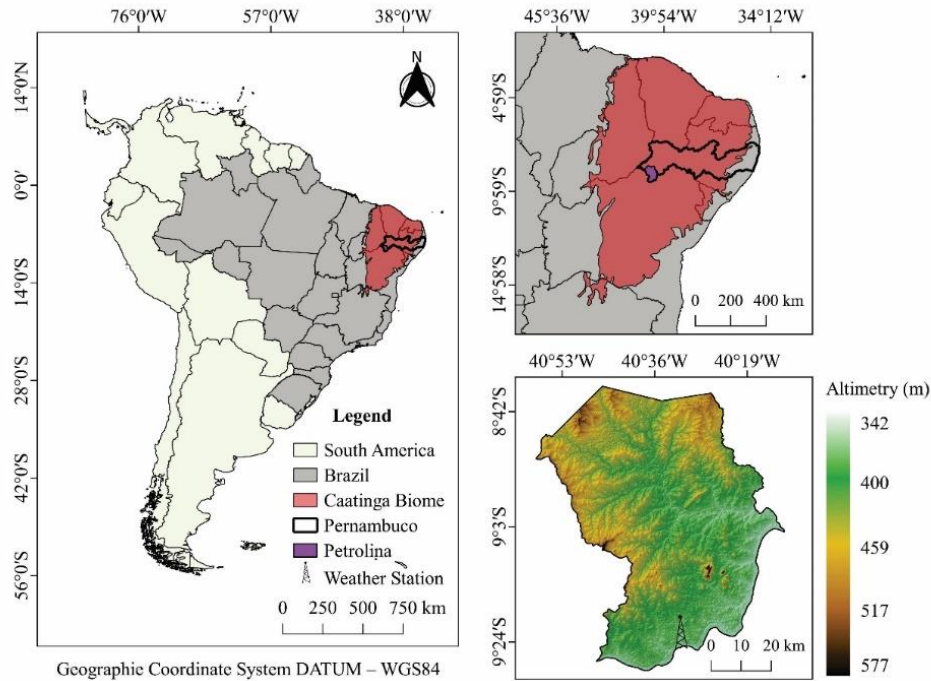
107

108 **2. Materials and Methods**

109 *2.1. Study Area*

110 The study was carried out in the municipality of Petrolina, located in the State of
111 Pernambuco, Brazil. The region comprises the domain of the Caatinga biome and it belongs
112 to the semi-arid region of the sub-mean of the São Francisco Valley. The town is considered
113 the largest fruit-growing center of the Brazilian semi-arid region due to the easy access to the
114 São Francisco river, which supplies the irrigated perimeters. The municipality comprises a
115 territorial area of 4561.870 km² (Figure 1), with an estimated population of 349,145
116 inhabitants [38].

117



118

119 **Figure 1.** Spatial location of the study area, municipality of Petrolina, Pernambuco,
 120 Northeast Brazil.

121

122 A characteristic of the Caatinga biome is the presence of different floristic mosaics,
 123 consisting of an area of tree and shrub vegetation, which presents its distribution conditioned
 124 to climatic and environmental variations, especially rainfall intensity and frequency [59], as
 125 well as geological configurations and soil properties [5]. The vegetation of this biome
 126 presents deciduous species adapted to water deficit conditions and with expressive biomass
 127 production in rainy seasons, resulting from the local climatic conditions [40,60]. The canopy
 128 cover of the species of the Caatinga biome presents discontinuous characteristics, making
 129 possible the soil exposure in dry periods, presence of herbaceous stratum, cactus species, and
 130 shrubs [23,60]. It is worth noting that this region presents an expressive modification of the
 131 native landscape (Caatinga) in areas of irrigated agricultural cultivation.

132 According to the Köppen–Geiger climate classification, the region’s climate is of the
 133 BSh type, characterized as semi-arid tropical, with an average air temperature of 26.4 °C,
 134 average relative humidity of 62%, and annual rainfall of 520 mm [61,62]. Rainfall pattern is
 135 irregular throughout the year, resulting from its geographical location and the Intertropical
 136 Convergence Zone (ITCZ) influence, with rainfall predominating from February to May

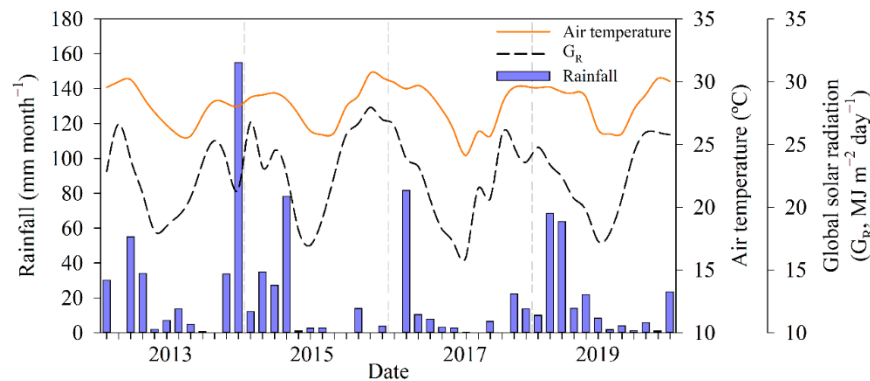
137 [10,63,64]. The predominant soils in the municipality are Typic Quartzipsamment, Ultisol
138 Plinthic, Arenosol, and Haplic Acrisol [65–67].

139

140 2.2. Satellite Images and Weather Datasets

141 Annual records of average air temperature ($^{\circ}\text{C}$), global radiation (MJ m^{-2}), relative
142 humidity (%), atmospheric pressure (kPa), wind speed (m s^{-1}), and rainfall (mm) were
143 obtained from the database of the National Institute of Meteorology [68] (Figure 2). The
144 average air temperature (T_a) ranged between 24.1 and 30.7 $^{\circ}\text{C}$, in which 2015 and 2019 were
145 the warmest years studied ($T_a > 28^{\circ}\text{C}$). Overall, November, December, January, February,
146 and March presented T_a values above 28 $^{\circ}\text{C}$ (Figure 2).

147



148

149 **Figure 2.** Monthly meteorological variations (rainfall, average air temperature, and global
150 solar radiation) of the municipality of Petrolina, Brazil, from 2013 to 2019.

151

152 The years 2013 (334.4 mm) and 2019 (221.6 mm) showed the highest rainfall rates.
153 Most of the rainfall recorded for Petrolina was concentrated from December to March (Figure
154 2). Such climatic conditions concerning the municipality were also reported in the literature
155 (e.g., [2,69]).

156

157 Rainfall data corresponding to the 30 days prior to the four imaging dates studied
158 used were obtained from the Climate Hazards Group InfraRed Precipitation with Station
159 (CHIRPS). CHIRPS are new precipitation products covering the coordinates 50° S–50° N
160 and 180° E–180° W, with 0.05° (± 5.3 km) spatial resolution and daily to seasonal, temporal
resolutions, available worldwide since 1981 [70]. CHIRPS data were extracted from the

161 Google Earth Engine platform (<https://earthengine.google.com/>, accessed on 20 August
 162 2021) using JavaScript programming language. Then, they were exported in spreadsheet
 163 format (*.xls), using the dataset since 1981 from the collection ee.ImageCollection (“UCSB-
 164 CHG/CHIRPS/DAILY”).

165 We used Operational Land Imager (OLI) Collection 1 Level 1 bands 2 (0.450–0.51
 166 μm), 3 (0.53–0.59 μm), and 4 (0.64–0.67 μm) in the visible spectrum, 5 (0.85–0.88 μm) in
 167 the near-infrared, and 6 (1.57–1.65 μm) and 7 (2.11–2.29 μm) in the shortwave infrared, all
 168 with a spatial resolution of 30 m, as well as band 10 from the Thermal Infrared Sensor (TIRS)
 169 with a 100 m spatial resolution. Besides this, we used four Landsat-8 OLI/TIRS images, path
 170 217 and row 66, corresponding to the years 2013, 2015, 2017, and 2019 (for the dates and
 171 times of the satellite overpass, see Table 1). The choice criteria adopted were the absence of
 172 clouds (<10%) and the images corresponding to the transition period between the dry and
 173 rainy seasons in the region under study, from the years of 2013 to 2019. This period presented
 174 severe and extreme drought events in the northeast [23,71]. All the images were obtained
 175 from the United States Geological Survey (USGS) platform (<https://earthexplorer.usgs.gov/>,
 176 accessed on 10 August 2021) and processed through the Land Surface Reflectance Code
 177 (LaSRC).

178
 179 **Table 1.** Date of the Landsat-8 satellite pass, followed by the Julian day (JD), Earth–Sun
 180 distance (dr, astronomical units—AU), local time of the equator pass (h, hour; min, minutes),
 181 zenith angle (θ , °), solar elevation angle (E, °), and sun azimuth angle (φ , °) for the
 182 municipality of Petrolina, Pernambuco, Brazil.

Acquisition Date	JD	dr	Local Time	θ	E	φ
5 October 2013	278	0.99	9 h 49 min a.m.	0.90	65.12	82.93
12 November 2015	316	0.99	9 h 48 min a.m.	0.90	64.85	113.46
16 October 2017	289	0.99	9 h 48 min a.m.	0.91	65.81	92.82
7 November 2019	311	0.99	9 h 48 min a.m.	0.90	65.41	110.36

183 Note: zenith angle (θ) = $\sin(E)$. Source: USGS/NASA [72].

184

185 2.3. *Vegetation Indices*

186 The Normalized Difference Vegetation Index (NDVI) was calculated to represent the
187 amount and quality of vegetation present on the surface, characterized as an indicator of wet
188 conditions, calculated using Equation (1).

189

$$\text{NDVI} = \frac{\rho_{\text{NIR}} - \rho_{\text{Red}}}{\rho_{\text{NIR}} + \rho_{\text{Red}}} \quad (1)$$

190

191 where ρ_{NIR} and ρ_{Red} are the reflectances measured in the near-infrared and red bands (i.e.,
192 Landsat-8 multispectral bands 5 and 4 of the OLI sensor), respectively, they range from -1
193 to $+1$. Values close to 1 on a positive scale correspond to high photosynthetic activity, and
194 when negative, generally correspond to water bodies.

195

196 Based on the NDVI, we calculated the vegetation cover (V_C) of the study area
197 (Equation (2)), according to Gao et al. [54].

198

$$V_C = \frac{\text{NDVI} - \text{NDVI}_S}{\text{NDVI}_V - \text{NDVI}_S} \cdot 100 \quad (2)$$

199

200 where V_C is the vegetation cover, NDVI_S is the minimum NDVI value from bare soil pixels
201 obtained in the study area, and NDVI_V is the maximum NDVI value found in vegetated areas,
202 i.e., from fully vegetated pixels. The NDVI_S and NDVI_V used to calculate V_C were obtained
203 from the domain of each NDVI image percentile map obtained from the NDVI histograms.

204

205 Soil-Adjusted Vegetation Index (SAVI) was calculated to observe the vegetation
206 cover of the area (Equation (3)).

207

$$\text{SAVI} = \frac{(1 + L) \cdot (\rho_{\text{NIR}} - \rho_{\text{Red}})}{(L + \rho_{\text{NIR}} + \rho_{\text{Red}})} \quad (3)$$

208

209 where L is the adjustment factor to the soil, which varies between 0 and 1 . The value 0 does
210 not reach change, and resembles the NDVI. In areas with low-density vegetation, the value

211 1 is assigned; for intermediate-density vegetation areas, the value of 0.5; and for areas with
212 high-density vegetation, the value 0.25 is assigned [73]. The adjustment factor of 0.5 was
213 adopted due to the study region indicating an intermediate vegetation coverage in most of the
214 year, with predominant vegetation of the Caatinga biome, in the Brazilian semi-arid region
215 [74–76].

216

217 To evaluate changes in vegetation biomass, the leaf area index (LAI, m² m⁻²) was
218 determined (Equation (4)), a fundamental biophysical variable for monitoring studies of
219 agricultural land and vegetation moisture conditions [50].

220

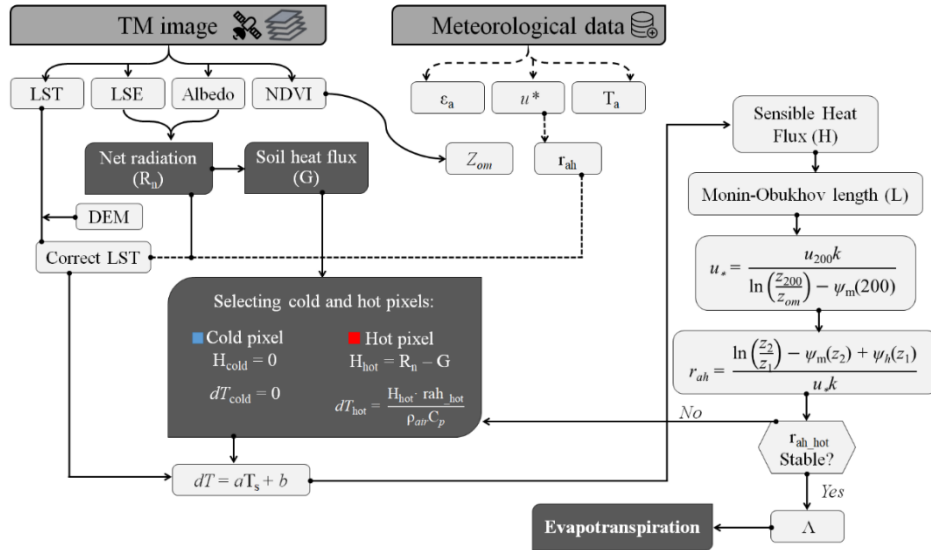
$$\text{LAI} = \frac{-\ln\left(\frac{0.69 - \text{SAVI}}{0.59}\right)}{0.91} \quad (4)$$

221

222 *2.4. Methodology for Estimating Evapotranspiration Using Satellite Images*

223 Evapotranspiration was estimated using the Energy Balance Algorithm for Land
224 (SEBAL). For this, routine meteorological data and spectral bands from the Landsat-8
225 satellite were used. The SEBAL algorithm was implemented using JavaScript code through
226 the Google Earth Engine (GEE) platform. The data were exported in spreadsheet format
227 (*.xls). SEBAL uses mathematical modeling and operations to calculate the surface energy
228 balance components and determine evapotranspiration. Thus, energy balance components are
229 computed pixel-by-pixel, as described in Figure 3. Here, we show that the algorithm has a
230 good performance and high accuracy, as well as being calibrated and validated with
231 simultaneous field and Landsat satellite measurements [47–49,55,58,60,77,78].

232



233

234 **Figure 3.** Flowchart of the SEBAL model for estimating evapotranspiration. Note: LST and
 235 LSE are the land surface temperature and land surface emissivity, respectively, NDVI is the
 236 Normalized Difference Vegetation Index, ϵ_a is the atmospheric emissivity, u^* is the friction
 237 velocity, T_a is the air temperature, R_n is the net radiation, G is the soil heat flux, z_{om} is the
 238 momentum roughness length, z_1 and z_2 are the two heights between the surface of the anchor
 239 pixels, r_{ah} is the near-surface aerodynamic resistance to heat transport, DEM is the digital
 240 elevation model, dT is the near-surface air temperature gradient, a and b are the calibration
 241 coefficients, LST or T_s is the land surface temperature, ρ_{air} is the air density, C_p is the specific
 242 heat of air, H is the sensible heat flux, ψ_m and ψ_h are the stability correction factors for
 243 momentum and sensible heat, respectively, k is the von Karman constant, u_{200} is the wind
 244 speed at the height of 200 m, and Λ is the evaporative fraction. These pre- and processing
 245 steps were performed inside Google Earth Engine (GEE) cloud platform. The acronyms and
 246 symbols used in this study are summarized in the Abbreviations section.

247

248 2.4.1. Surface Albedo Adjustment

249 The surface albedo (α_{sup}) corresponds to a measure of the reflectivity of the Earth's
 250 surface, for each pixel, with atmospheric correction obtained according to Equation (5)
 251 [50,79].

252

$$\alpha_{sup} = \frac{\alpha_{toa} - \alpha_{path}}{\tau_{sw}^2} \quad (5)$$

253

254 where α_{toa} is the albedo at the top of the atmosphere, that is, before atmospheric correction,
255 α_{path} is the atmospheric reflectance (set to 0.03, as used by Silva et al. [79]), and τ_{sw} is the
256 atmospheric transmissivity for clear sky conditions, according to Equation (6) [50,79]:

257

$$\tau_{sw} = 0.35 + 0.627 \cdot \exp \left[\frac{-0.00146 \cdot P_a}{K_t \cdot \cos(\theta)} - 0.075 \left(\frac{W}{\cos(\theta)} \right)^{0.4} \right] \quad (6)$$

258

259 where P_a is the atmospheric pressure (kPa), with dataset available freely in
260 <https://portal.inmet.gov.br/> (accessed on 10 August 2021), K_t is the turbidity coefficient of
261 the atmosphere ($K_t = 1.0$, for a clear sky day), according to Allen et al. [47] and Silva et al.
262 [79], θ is the solar zenith angle, and W is the precipitable water (mm), estimated from
263 Equation (7) [80].

264

$$W = 0.14 \cdot e_a \cdot P_a + 2.1 \quad (7)$$

265

266 where e_a is the actual atmospheric water vapor pressure (kPa), estimated from Equation (8).

267

$$e_a = \frac{HR \cdot e_s}{100} \quad (8)$$

268

269 where HR is the instantaneous relative humidity (%), and e_s is the water vapor saturation
270 pressure (kPa), estimated from Equation (9).

271

$$e_s = 0.6108 \cdot \exp \left(\frac{17.27 \cdot T_0}{237.3 + T_0} \right) \quad (9)$$

272

273 where T_0 is the instantaneous air temperature ($^{\circ}\text{C}$) at the moment of the satellite pass.

274

275 For obtaining α_{toa} , a linear combination of the spectral reflectance of the six reflective
276 OLI bands was performed according to Equation (10) [79]:

277

$$\alpha_{toa} = 0.300 r_2 + 0.277 r_3 + 0.233 r_4 + 0.143 r_5 + 0.036 r_6 + 0.001 r_7 \quad (10)$$

278

279 where $r_2, r_3, r_4, r_5, r_6,$ and r_7 are the surface spectral reflectances for bands 2, 3, 4, 5, 6, and 7
 280 of the Landsat-8 OLI, respectively.

281

282 We use Equation (11) to obtain each of the spectral reflectances.

283

$$r_b = \left(\frac{\text{Add}_b + \text{Mult}_b \cdot \text{DN}}{\cos(\theta) \cdot dr} \right) \quad (11)$$

284

285 where the terms Add_b and Mult_b belong to the radiometric rescaling group, specifically
 286 $\text{reflectance_add_band}$ (equal to -0.1) and $\text{reflectance_mult_band}$ (equal to 0.00002),
 287 respectively, presented in the metadata of each OLI—Landsat-8 image, DN is the digital
 288 number value corresponding to the pixel, θ is the solar zenith angle at the data acquisition
 289 time, and dr is the Earth–Sun distance in astronomical units.

290

291 *2.5. Determination of Surface-energy Partitioning*

292 Based on the surface energy balance components, the evaporative fraction was
 293 determined. Initially, the surface radiation balance or net radiation— R_n was calculated, which
 294 is distributed by the energy partitioning in front of the sensible heat fluxes— H , latent— LE ,
 295 and soil heat flux— G [47–50,60,77,78]. By performing this process, a linear relationship
 296 between the surface and air temperature gradient was considered to exist. From this
 297 relationship and the internal calibration process for extreme conditions such as temperature
 298 and humidity, it was established the need for obtaining the knowledge of the so-called
 299 “anchor pixels”, i.e., hot and cold pixels, which are indicative of zero and maximum
 300 evapotranspiration, respectively [47,48,60] (Figure 3).

301 The land surface temperature (LST) in K (Kelvin) was obtained using the spectral
 302 radiance in band 10 of the TIRS sensor and the emissivity in the nearest band— ϵ_{nb} by the
 303 modified Planck’s Law [81], as described in Equation (12).

304

$$LST = \frac{K_2}{\ln\left(\frac{\varepsilon_{nb} \cdot K_1}{L_{10}} + 1\right)} \quad (12)$$

305

306 where K_1 and K_2 are radiation constants specific for the Landsat-8 TIRS band 10, equaling
 307 $774.89 \text{ W m}^{-2} \text{ sr}^{-1} \mu\text{m}^{-1}$ and 1321.08 K , respectively, provided by NASA/USGS; and L_{10} is
 308 the radiance at the wavelength received by the sensors (band 10, the thermal band).

309

310 The ε_{nb} was calculated based on the LAI for each pixel according to Equation (13)
 311 [41].

312

$$\varepsilon_{nb} = 0.97 + 0.0033 \cdot LAI \quad (13)$$

313

314 Initially, the temperature variation and aerodynamic resistance to heat transport in all
 315 pixels of the study area (Petrolina, Pernambuco) were determined. The atmosphere was
 316 initially assumed to be in a neutral stability condition. For this study, the hot pixel was
 317 considered in the exposed soil plots (i.e., no vegetation cover and/or little vegetation and low
 318 moisture content), assuming LE equal to zero. The cold pixel was considered in grape orchard
 319 plots irrigated by micro-sprinklers, when H can be considered zero [47,48,60,77,78,82] (see
 320 Figure 3). Since turbulent effects affect atmospheric conditions and air resistance, the
 321 Monin–Obukhov similarity theory was applied and considered in the computation of H in all
 322 pixels of the study area. It is worth noting that the Monin–Obukhov length was used for
 323 corrections to the initial stable condition of the atmosphere [47–49,77,78].

324

325 2.5.1. Calculation of Energy Fluxes (H and LE) and Evaporative Fraction

326 The sensible heat flux (H) in SEBAL is calculated using an iterative procedure from
 327 the aerodynamic function (Equation (14)) [47–49,77,78].

328

$$H = \rho_{air} \cdot C_p \cdot \frac{(a + b \cdot LST)}{r_{ah}} \quad (14)$$

329

330 where ρ_{air} is the moist air density (kg m^{-3}), C_p is the air specific heat at constant pressure
 331 ($1004 \text{ J kg}^{-1} \text{ K}^{-1}$), a and b are calibration constants of the temperature difference between
 332 two heights (i.e., between the roughness length for heat transfer and the reference height,
 333 usually 0.1 and 2.0 m above the displacement plane), and r_{ah} is the near-surface aerodynamic
 334 resistance to heat transport (s m^{-1}). Fundamentally, the coefficients a and b are determined
 335 through an internal calibration for each satellite image by interactive processes. We consider
 336 extreme pixels of wet/cold and dry/hot spots. They were selected to develop a linear
 337 relationship between the aerodynamic temperature of the surface and the air temperature
 338 difference, and the LST.

339

340 By knowing the components of the surface energy balance, such as the net radiation
 341 (R_n , W m^{-2}), sensible heat flux (H , W m^{-2}), and soil heat flux (G , W m^{-2}), the latent heat flux
 342 (LE , W m^{-2}) was determined, both corresponding to the time of the satellite pass over the
 343 study area, according to Equation (15).

344

$$LE = R_n - H - G \quad (15)$$

345

346 Subsequently, we determined the evaporative fraction (Λ) according to Equation (16).

347

$$\Lambda = \left(\frac{LE}{R_n - G} \right) \quad (16)$$

348

349 2.6. Estimate of ET_a Using SEBAL Method

350 Finally, as a SEBAL product, we determine the actual evapotranspiration (ET_a , mm
 351 day^{-1}) [83] based on Equation (17) below, for each satellite image used. In this study, the
 352 implemented SEBAL model had already been extensively validated and calibrated under
 353 forests and agricultural land conditions [55,60,84].

354

$$ET_a = \left(\frac{\Lambda \cdot R_{n24} \cdot 86,400}{\lambda} \right) \quad (17)$$

355

356 where R_{n24} is the daily net radiation (W m^{-2}), 86,400 is a constant for daily timescale
357 conversion (i.e., converts from seconds to days), and λ is the latent heat of vaporization of
358 water (J kg^{-1}). Then, the latent heat of vaporization allows the ET_a expression in mm day^{-1} .
359 Hence, accurate estimation of R_{n24} (Equation (18)) was determined according to Bastiaanssen
360 et al. [49], and Lee and Kim [85]:

361

$$R_{n24} = \Lambda \cdot [(1 - \alpha_{sup}) \cdot R_n - a \cdot \tau_{sw}] \quad (18)$$

362

363 where a is a regression coefficient of the relationship between net longwave radiation and
364 atmospheric transmissivity on a daily scale, to which we assigned the value 143, as proposed
365 by Teixeira et al. [60]. The acronyms and symbols used in this study are summarized in the
366 Abbreviations section.

367

368 2.7. Land Use and Land Cover Dynamics

369 In the present study, we sought to evaluate the impacts of changes in land use and
370 land cover (LULC) under the biophysical variables in the municipality of Petrolina. Thus,
371 we performed the extraction of descriptive statistical parameters (i.e., minimum, maximum,
372 mean, median, and standard deviation) for the variables LAI, V_c , ET_a , LE , H , LST,
373 emissivity, and R_n in each class of LULC, from the maps available on the MapBiomass Brazil
374 platform [86]. This collection is highly reliable and it includes annual land use and land cover
375 (LULC) data for the period 1985–2019 and it prioritizes the following classes: (1) arboreal
376 Caatinga, (2) shrub Caatinga, (3) herbaceous Caatinga, (4) pasture, (5) agriculture, (6) mosaic
377 of agriculture and pasture, (7) urban area, and (8) water bodies with a spatial resolution of 30
378 meters [27,87].

379

380 The MapBiomass classification is a hierarchical system combining land use and land
381 cover. This classification is based on a pixel-by-pixel classification of Landsat images, where
382 we use the machine learning algorithm random forest. Thus, the LULC classes for 2013,
383 2015, 2017, and 2019 were converted from raster files to vector files. We use the
384 “polygonise” tool, which transforms classes into polygons with the help of QGIS 3.16
385 software [88]. After the new datasets were converted, the vector files were used to extract
385 the statistical parameters by using the “zonal statistics” tool of the QGIS 3.16 software [88].

386 This procedure provided a basis with greater data amplitude and greater coverage of the
387 region's surface under study, making it possible to compare the different land use and land
388 cover types. In addition, as a result of this process, four maps were generated, indicating the
389 land use and land cover changes.

390

391 2.8. Statistical Analyses

392 In this study, we applied a principal component analysis (PCA) on the biophysical
393 variables—e.g., LAI, V_C , ET_a , LE , H , LST, albedo, emissivity, and R_n —for 2013, 2015,
394 2017, and 2019. Principal component analysis was performed to reduce the large dataset and
395 convert the data series into sets of uncorrelated linear values without losing relevant
396 information [35,64]. PCA consists of computing the eigenvalues and eigenvectors of the
397 covariance matrix. Moreover, in the generation of PCA, diverse components are created, and
398 the first component is the most important, as it explains the highest percentage of the data
399 variance, while the later components created in the analysis represent a lower variation of the
400 data. Thus, the data were standardized, subtracting the minimum values from each value and
401 dividing by their interval in order to obtain the maximum amount of information extracted.
402 Only eigenvalues greater than 1.0 were taken into account, for they present expressive
403 information from the newly created dataset [89]. The generated loadings indicate the relative
404 importance of a given raw variable from the data sample in the principal component (PC)
405 [64]. Moreover, 400 random points were generated to compose the data of our regression
406 model. One hundred random points were generated across the study area (for variables LST,
407 H , and ET_a using SEBAL) for each assessment date [2] through the QGIS (e.g., using the
408 “random points inside polygon” and “point sampling” functions [88]).

409 Subsequently, we built a multiple linear regression model to determine ET_a
410 (predictand) in a simplified way. The selected variables were LST and H (predictors) due to
411 their strong correlation over the years with land use and land cover classes (results obtained
412 using PCA). This type of regression model assumes that there is a linear relationship between
413 the response variable y and the predictor variables (e.g., x_1, x_2, \dots, x_n); it may be described as
414 follows: $y = \beta_0 + \beta_1x_1 + \beta_2x_2 + \dots + \beta_nx_n + \varepsilon_{rr}$, wherein β_0 is the constant value, β_1, \dots, β_n are
415 regression coefficients, and ε_{rr} is the random error. The threshold for predictor variable
416 inclusion was $p < 0.05$.

417

418 2.8.1. Goodness of Fit

419 The model performance analysis was based on the root mean square error (RMSE,
420 the values close to zero reduce error and increase accuracy), the mean absolute error (MAE),
421 percent bias (PBIAS), Nash–Sutcliffe efficiency coefficient (NSE), Lin’s concordance
422 correlation coefficient (LCCC), Willmott’s index of agreement (d), which ranges from 0 to
423 1 (i.e., indicates no agreement at all and perfect agreement, respectively) [90–93], and
424 coefficient of determination (R^2 , i.e., indicates the model’s accuracy in the prediction of
425 response for a dataset) above 0.90. These metrics allowed us to evaluate the models’ quality
426 and enabled the extraction of relevant information in terms of applicability. Therefore, the
427 lower the PBIAS and RMSE values, the better the model prediction performance.
428 Furthermore, NSE is a reliable criterion for evaluating the model’s predictive ability. We also
429 used LCCC to measure precision and accuracy between predicted and measured values.
430 Moreover, it indicates the degree of agreement between two methods by measuring the
431 variation of their linear relationship from the 45-degree line through the origin. Thus, good
432 models have LCCC equal or close to 1 [91–93]. Additionally, we applied analysis of variance
433 (ANOVA) and the F -test ($p < 0.05$, Fisher’s F -test) to investigate the statistical significance
434 between ET_a values measured by the SEBAL algorithm and predicted by the model proposed
435 in this study. All statistical analyses were performed using the R software [94].

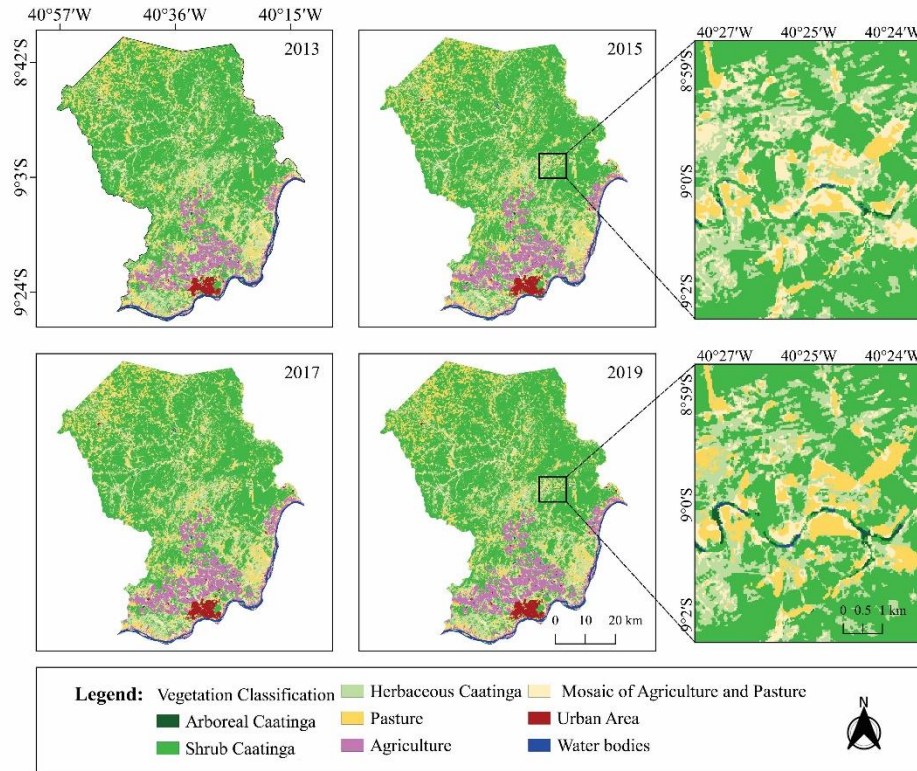
436

437 3. Results and Discussion

438 3.1. Comparisons of Land Use and Land Cover (LULC)

439 Based on the classification via the MapBiomias platform and on the Landsat-8
440 satellite, the thematic maps of land use and land cover for the years 2013, 2015, 2017, and
441 2019 were highlighted, with the main classes represented in Figure 4.

442



443

444 **Figure 4.** Thematic classification of cover and land use and occupation from MapBiomas
 445 between the years 2013 and 2019 for Petrolina, Pernambuco, Brazil.

446

447 The advances in exploration of agricultural areas for the municipality of Petrolina
 448 occurred mainly in areas nearby the São Francisco river, with a predominance of irrigated
 449 fruit farming. Moreover, the irrigated perimeters “Senador Nilo Coelho” and “Bebedouro”
 450 in these areas are located there, which, in the 1970s with the construction of the Sobradinho
 451 dam, boosted the exploitation and change in land use, impacting the Caatinga [37,95].

452 In 2013, 70.20% of the area (320,265.44 ha) of Petrolina was composed of Caatinga,
 453 being 51.60% shrub, 18.48% herbaceous, and the other 0.12% arboreal (see Figure 4 and
 454 Table 2).

455

456 **Table 2.** Annual quantification of land use and land cover conditions from 2013 to 2019 for
 457 the semi-arid region of Petrolina, Pernambuco, Brazil.

Classes	Annual Quantification of Land Use/Land Cover Types	
	(ha year ⁻¹)	

	2013	2015	2017	2019
Arboreal Caatinga	540.96	356.43	467.77	878.15
Shrub Caatinga	235,450.18	233,919.88	234,688.22	238,445.74
Herbaceous Caatinga	84,274.3	74,985.47	78,138.28	78,797.94
Pasture	53,346.49	55,356.09	60,156.62	60,176.26
Agriculture	31,919.62	34,209.91	35,678.87	36,718.13
Mosaic of Agriculture and Pasture	39,420.48	45,494.96	34,884.41	29,371.88
Urban area	4855.57	5496.18	5829.13	5825.78
Water bodies	6375.49	6364.17	6339.79	5969.21
Total	456,183.09	456,183.09	456,183.09	456,183.09

458 Source: Adapted from MapBiomass Brazil.

459

460 The lowest percentages of areas occupied by Caatinga vegetation were observed in
461 2015 (67.8%) and 2017 (68.7%), respectively. Compared to 2013, there was an average
462 reduction of 2%, equivalent to 9123.65 ha of native forest (Caatinga), while in 2019, the
463 reduction was only 0.45% (Table 2). It is important to emphasize that the reduction in
464 Caatinga refers to herbaceous native vegetation. Such phenomena are related to the increase
465 in areas of agriculture, pasture, and urban infrastructure, along with the occurrence of lower
466 rainfall rates recorded between 2015 and 2017. However, between 2013 and 2019, an
467 increase of 0.07 and 0.66% was observed in the native trees and shrubs vegetation areas,
468 respectively (Figure 4 and Table 2). Furthermore, the expansion of arboreal vegetation areas
469 occurred close to water bodies; on the other hand, the expansion of shrub vegetation occurred
470 to replace areas previously occupied by agricultural activities (3234.56 ha), mainly pasture
471 or in the ecological succession of areas of herbaceous vegetation (3679.17 ha)
472 (Supplementary Table S1 and Figure S1). Silva et al. [96] studied the spatial-temporal
473 evolution of agricultural activity in the Brazilian semi-arid region from 1998 to 2018, seeking
474 to investigate the resilience of the Caatinga biome during the dry season. The authors mention
475 that the expansion of the Caatinga biome occurred mainly with the reduction of agricultural
476 activity, which reinforces the results obtained in the present study.

477 In 2013, the areas occupied with pasture represented 11.7%, agriculture 7.0%, and
478 the mosaic of agriculture and pasture 8.64%, while areas with urban infrastructure and water
479 bodies presented an occupation of 1.06 and 1.40%, respectively (Figure 4 and Table 2). From
480 2013 to 2019, there was an increase in areas with agricultural activity in the region, while a
481 decrease in native herbaceous vegetation (Caatinga) was observed, which caused the
482 conversion of 10,972.34 ha of native herbaceous vegetation to areas of agricultural activity
483 (see Supplementary Table S1 and Figure S1). The types of LULC indicated the different
484 intensities of human activities in the area. Several authors have reported the occurrence of
485 severe drought events in NEB in the period between 2012 to 2016, in addition to the
486 intensification of anthropic activities in the study region [10,23,27,71,97,98]. Those factors
487 are responsible for significant changes in the phytosociology and floristic composition of the
488 biome [10,23,27,71,97,98].

489 Drought is costly to Brazil, for it causes strong impacts on agriculture and cattle
490 ranching. For example, the 2012–2013 drought resulted in economic losses of USD 1.5
491 billion for more than ten important crops in the region and USD 1.6 billion in cattle mortality
492 [99]. Furthermore, Marengo et al. [10] emphasize that among adverse natural climate
493 phenomena, drought is the factor that most affects society, as it impacts large territorial
494 extensions of NEB, with intensified and increasingly long-lasting events over the years.

495 The agricultural and cattle ranching activity were significant in 2015, 2017, and 2019
496 with 29.6, 28.7, and 27.7%, respectively. Among the agricultural activities, the class of
497 pastures (in this study, there is no detailed distinction between irrigated and non-irrigated
498 pasture areas) was responsible for the largest occupied area, with values of 55,356 ha in 2015;
499 60,156 ha in 2017, and 60,176 ha in 2019 (see Table 2). The expansion of pasture areas
500 resulted from the growing demand for food and for animal production, which favored
501 changes in land use and occupation and, consequently, it increased the deforestation rate of
502 the Caatinga biome [19]. Fleischer et al. [100] reported that the constant changes in land use
503 and land cover might cause a significant impact on the flux and carbon stock since they are
504 responsible for changing the sink capacity or carbon source of the ecosystem.

505 The agriculture class in 2015, 2017, and 2019 showed territorial occupation of 34,209,
506 35,678, and 36,718 ha, respectively, with an average increase of 0.80% (3616 ha) compared
507 to 2013 (Table 2). This growth was favored by the development of irrigated agriculture in

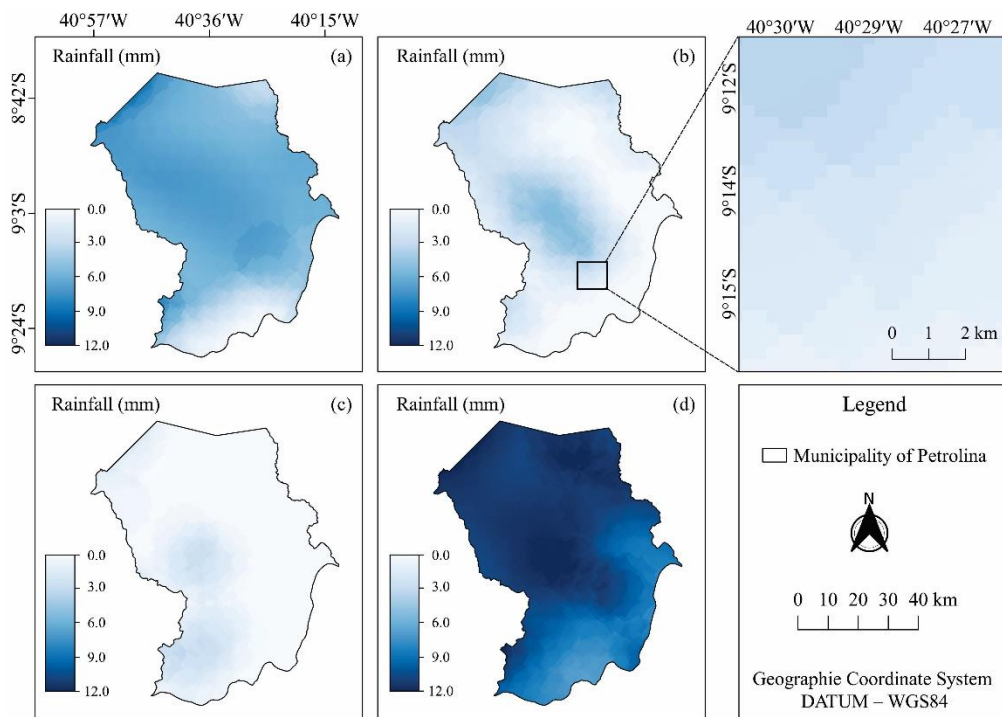
508 the region, due to the proximity of the São Francisco river's channel, maximizing mainly
509 fruit farming, e.g., grape and mango [6,7]. Most of the times, irrigated fields are inserted in
510 areas previously occupied by Caatinga, which results in changes in the physical, chemical,
511 and biological soil properties [6,65]. In addition, changes in greenhouse gas (GHG) emission
512 fluxes resulting from anthropogenic modifications on native vegetation are also reported in
513 the literature [19,100].

514

515 3.2. Rainfall Variability in Land Cover Classes

516 Analyzing the spatiotemporal rainfall dynamics in the region over the 30 days
517 preceding the passage of the Landsat-8 satellite on the four assessment dates (5 October 2013,
518 12 November 2015, 16 October 2017, and 7 November 2019) allowed us to observe the
519 variation in rainfall distribution and volume, whose average accumulated values were 5.63,
520 1.7, 0.59, and 10.4 mm, for the respective dates. Despite the low rainfall volume observed in
521 the region, some areas showed a tendency for higher rainfall occurrence, which may be
522 conditioned to the native vegetation and orographic effects of the region (Figure 5).

523



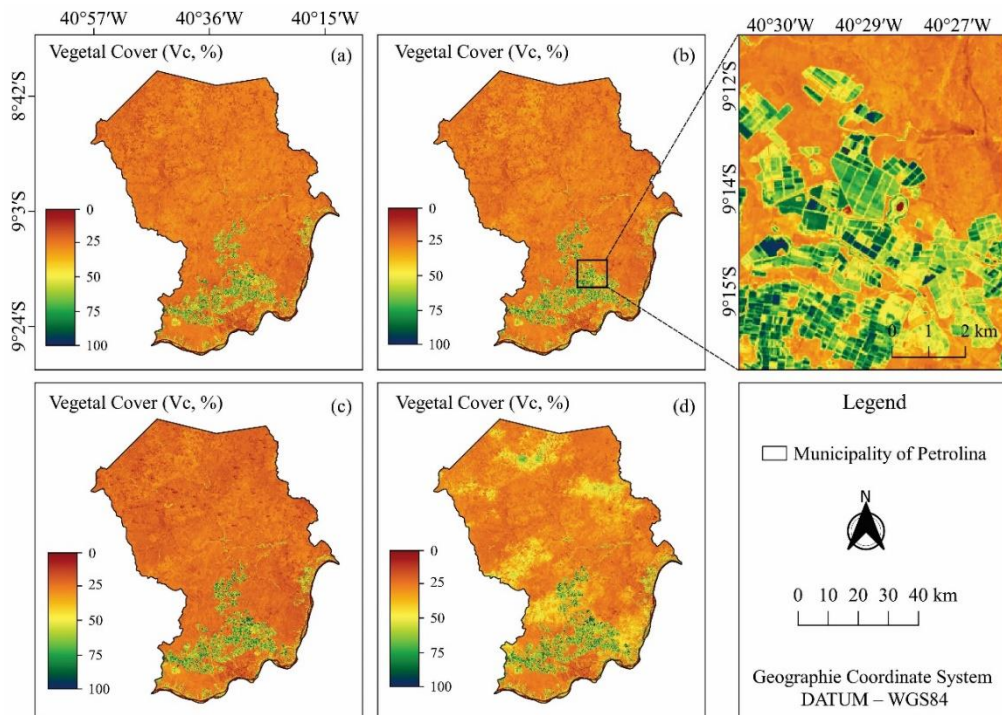
524

525 **Figure 5.** Spatiotemporal rainfall distribution (mm) for the CHIRPS satellite product in the
 526 municipality of Petrolina, Pernambuco, Brazil, in the 30-day period before the imaging dates
 527 5 October 2013 (a), 12 November 2015 (b), 16 October 2017 (c), and 7 November 2019 (d).
 528

529 Variations in rainfall distributions and volumes may have caused changes in
 530 vegetation cover, surface temperature, and evapotranspiration of the land portions observed
 531 in this study. Predominant vegetation of the Caatinga biome is quickly responsive to rainfall
 532 regimes, reducing foliage in the dry period (through deciduousness) and gaining biomass by
 533 the arrival of a new rainy period, which is considered a condition of defense and
 534 physiological adaptation of these highly efficient plants [101,102].
 535

536 3.3. Vegetation Cover Indices of the Municipality

537 Figure 6 shows the percent vegetation cover (V_C) in Petrolina. The first three imaging
 538 dates in the study showed that, on average, 52.26% of the territorial area of the region had 0
 539 to 25% vegetation cover (Figure 6a–c), revealing the direct effects of low rainfall volumes
 540 resulting from the dry season on native vegetation.
 541



542

543 **Figure 6.** Condition of the different types of vegetation cover in the Caatinga agroecosystem
544 in the municipality of Petrolina, Pernambuco, Brazil, on the imaging dates 5 October 2013
545 (a), 12 November 2015 (b), 16 October 2017 (c) and 7 November 2019 (d).

546

547 Under these conditions, variations in NDVI values are strongly linked to biomass
548 production [101]. In studies carried out in the Caatinga, Cunha et al. [22], Leivas et al. [21],
549 and Leivas et al. [103] reported that monitoring large-scale variations of water indicators and
550 vegetation status is of crucial importance to minimize the adverse effects of climate and land
551 use changes on mixed agroecosystems. Moreover, it can help in planning and decision-
552 making processes for rational use of natural resources to mitigate the effects and duration of
553 large-scale drought events.

554 The results reported here contribute to understanding water limitations and vegetation
555 behavior. Due to the proximity of the São Francisco river, which supplies the irrigation
556 systems, the areas of higher vegetation cover are found in the irrigated agriculture sites in the
557 southern part of the municipality and the few remaining fragments of arboreal Caatinga,
558 reaching average values of $58.71 \pm 22.18\%$ and $59.78 \pm 18.94\%$, respectively, throughout the
559 period under study (Figure 6). However, it can be observed that in areas dominated by
560 pasture, herbaceous, and shrub Caatinga, the mean values of V_C for the dates studied are
561 lower ($22.84 \pm 6.70\%$, $27.17 \pm 5.45\%$, and $24.56 \pm 4.74\%$, respectively) (see also Figure 4).
562 The advanced stage of pasture degradation and the intense grazing activity in natural areas
563 of Caatinga also impact the vegetation density and, hence, its spatiotemporal dynamics and
564 related surface variables such as NDVI, LST, albedo, and emissivity [2,71,104].

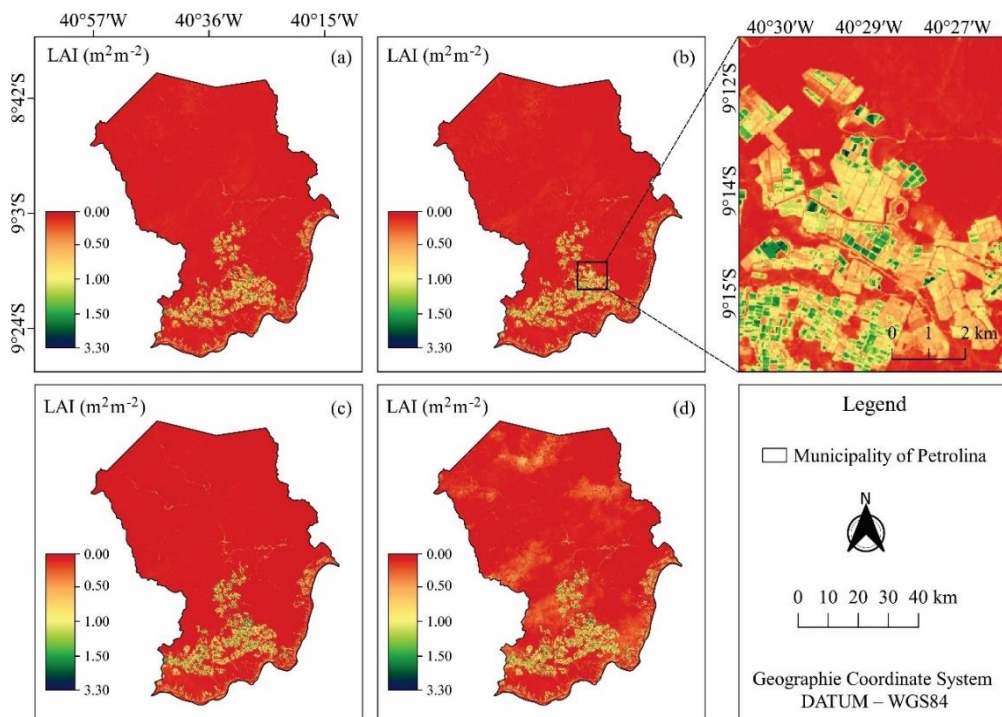
565 Santos et al. [102] emphasize that the arboreal vegetation is less susceptible to
566 climatic variations than shrub and herbaceous vegetation, leading to less drastic reductions
567 in V_C throughout the dry season. This characteristic is intrinsically linked to the adaptive
568 capacity of species, favoring them to withstand the stressful effects of abiotic factors [105].

569 It is essential to highlight that on 7 November 2019, there was an average increase of
570 46.81% of areas with V_C higher than 50% in the northern part of the municipality (Figure
571 6d), which indicates a response of vegetation to the behavior of rainfall in this period, since
572 this was the fraction of the polygon with the highest rainfall index during the 30 days prior
573 to this evaluation date (Figures 5 and 6). The interrelationship of vegetation with

574 meteorological variables plays a crucial role in the ability to slow the advance of aridity, loss
 575 of soil quality, and ecological diversity. In areas with consolidated vegetation, soil exposure
 576 to solar radiation becomes lower, causing the maintenance of soil moisture and consequently
 577 favoring the water availability in the environment for species. The intensification of anthropic
 578 activities can directly cause damage to native vegetation, such as soil and vegetation
 579 degradation; however, these changes can also influence climatic conditions and cause severe
 580 damage to ecosystem services.

581 During the studied dates, the LAI varied between 0.00 and 3.3 $\text{m}^2 \text{m}^{-2}$ (Figure 7).
 582 However, in 97% of the region under study, the LAI values were lower than 0.825 $\text{m}^2 \text{m}^{-2}$,
 583 for in periods with low water availability, the Caatinga usually presents low LAI [106]. The
 584 low LAI values can be justified not only by drought events but also by the characteristics of
 585 the soils, which, in general, are shallow and have low water storage capacity. In addition, it
 586 is worth noting that factors such as deforestation and intensive grazing activity in areas of
 587 native vegetation, as well as a high degree of degradation of pasture areas, historically, are
 588 common in this region, causing an imbalance of natural ecosystems [107,108].

589



590

591 **Figure 7.** Spatiotemporal distribution of leaf area index (LAI, $\text{m}^2 \text{m}^{-2}$) in the municipality of
592 Petrolina, Pernambuco, Brazil, on the imaging dates 5 October 2013 (a), 12 November 2015
593 (b), 16 October 2017 (c), and 7 November 2019 (d).

594

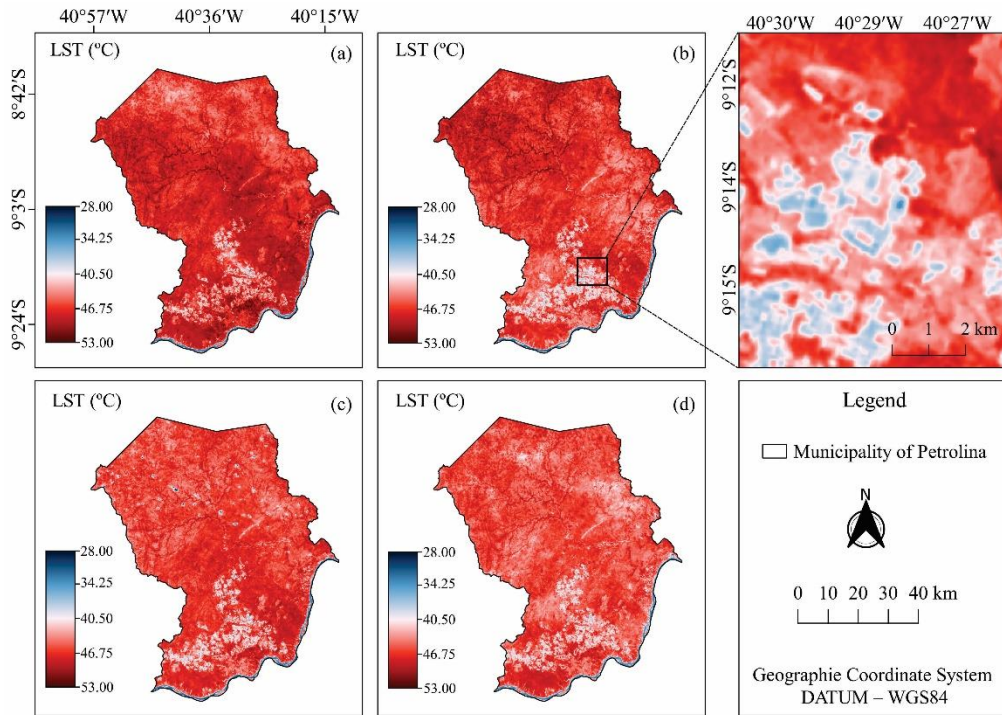
595 The highest heterogeneity in LAI values was seen on 7 November 2019 (0.24 ± 0.22
596 $\text{m}^2 \text{m}^{-2}$) (Figure 7d), increasing from the greater variability in the spatial distribution of
597 rainfall accumulation in the previous days. On the other hand, during the dates studied here,
598 the highest mean LAI values stood out only in areas of arboreal Caatinga ($0.58 \pm 0.45 \text{m}^2$
599 m^{-2}) and agriculture ($0.75 \pm 0.49 \text{m}^2 \text{m}^{-2}$), with the maximum values being associated with
600 irrigated agricultural areas, more specifically orchards, with increased biomass production.
601 However, in areas of pasture, urban infrastructure, and areas of arboreal and herbaceous
602 Caatinga, the LAI values were close to or equal to zero, making its variation more
603 homogeneous, that is, closer to the daily mean, with standard deviation (SD) ranging between
604 0.05 and $0.10 \text{m}^2 \text{m}^{-2}$ within the land cover classes (Figure 7).

605

606 *3.4. Land Surface Temperature (LST) in the Studied Classes*

607 In the present study, the minimum LST values were seen in areas of water bodies,
608 while the maximum LST values were seen in areas of exposed soils, located at points of
609 pasture and degraded Caatinga, urban infrastructure (asphalt, concrete, and gravel surfaces),
610 and agricultural areas undergoing soil preparation for cultivation (Figure 8). This result is
611 expected in bare soil locations under intense anthropic activity due to the transformation of
612 land use/land cover classes into non-evaporating surfaces. This makes the place's
613 temperature higher and reduces water availability in the soil, which causes serious problems
614 in agricultural crops. The computed LST map is shown in Figure 8.

615



616

617 **Figure 8.** Spatiotemporal distribution of the land surface temperature—LST (°C) in the
 618 municipality of Petrolina, Pernambuco, Brazil, on the imaging dates 5 October 2013 (a), 12
 619 November 2015 (b), 16 October 2017 (c) and 7 November 2019 (d).

620

621 Due to the replacement of primary vegetation with pastures, agricultural crops, and
 622 urban occupation, changes in land use can substantially affect the heat and mass exchange in
 623 the soil–plant–atmosphere system, propitiating the retention of a higher amount of heat by
 624 the Earth’s surface [2,52]. Land abandonment and excessive mechanical disturbance of the
 625 soil may also alter the heat exchange with the environment and cause lower thermal and
 626 radiant energy lag; thus, the land conversion had increased LST in the area of the non-
 627 evaporating surfaces.

628

629 It can be observed that the average LST values for the dates studied were higher in
 630 the areas dominated by pasture (47.69 ± 1.47 °C), herbaceous Caatinga (47.28 ± 1.27 °C),
 631 and shrub Caatinga (46.07 ± 1.44 °C), even higher than those observed in areas with urban
 632 infrastructure (45.80 ± 1.52 °C) (Figure 8). According to Zhao et al. [109,110], sites with
 633 different land cover types may have an LST increase gradient along the urban to rural profile.
 634 The high LST in the pasture, herbaceous, and shrub Caatinga areas is related to the lower
 percentage of ground covering by vegetation (see Figure 6), which results in drier exposed

635 soil, with higher albedos and lower evaporative cooling flux rates, a factor that increases
636 LST. Another related factor contributing to the high LST of pastures is that grasses have
637 shallower roots. Therefore, they can only access the water available in the superficial soil
638 layers, which depletes faster than in deeper layers [2]. Vegetation canopy can retain rainwater
639 and decrease groundwater recharge by altering evaporative flux and raising the land surface
640 temperature.

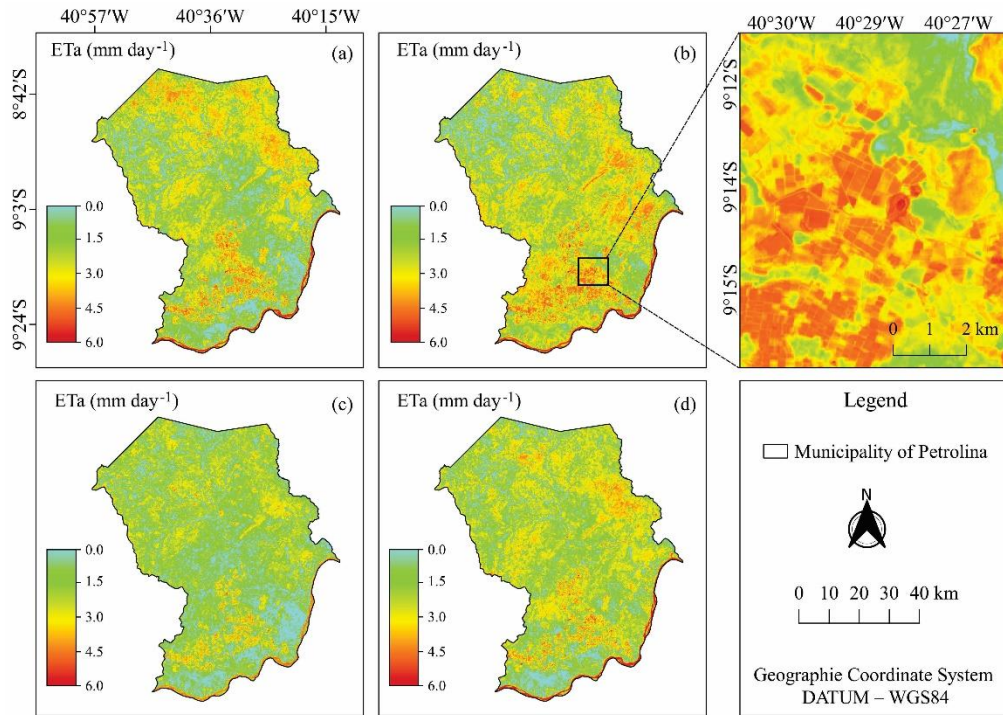
641 On the other hand, it is observed, in general, that in areas dominated by arboreal
642 Caatinga and agriculture, the average LST values are lower (38.99 ± 2.48 °C and $43.11 \pm$
643 2.30 °C, respectively) (Figure 8). The highest vegetation cover and the highest soil humidity
644 in the areas dominated by these classes favor LST reduction. However, they present the
645 greatest spatial variations of LST among all land use and land cover classes, according to the
646 standard deviation values (\pm SD). The main advantage of using LST data from satellite images
647 is the total surface coverage. In this way, each time series of pixels of the LST map can be
648 considered a “virtual weather station” [111].

649

650 *3.5. Variations of the Actual Evapotranspiration (ET_a) of Land Use Classes*

651 Rainfall regime directly influenced ET_a , so that on 16 October 2017 (Figure 9c), the
652 date with the lowest rainfall accumulation in the previous days, the lowest ET_a rates were
653 found, with an average value of 2.02 mm day^{-1} . On the other hand, on 7 November 2019
654 (Figure 9d), the period with the highest rainfall accumulation, average ET_a rates were 2.62
655 mm day^{-1} (Figure 9). According to Teixeira et al. [20], high evapotranspiration values in
656 Caatinga areas occur right after rains. Therefore, the previous rainfall raises soil water
657 availability and keeps native species with turgid structures and greener canopy.

658



659

660 **Figure 9.** Spatiotemporal distribution of actual evapotranspiration (ET_a , mm day^{-1}),
 661 calculated with Surface Energy Balance Algorithm for Land (SEBAL), in the municipality
 662 of Petrolina, Pernambuco, Brazil, on the imaging dates 5 October 2013 (a), 12 November
 663 2015 (b), 16 October 2017 (c), and 7 November 2019 (d).

664

665 The ET_a estimated by the SEBAL model showed variation both within and between
 666 land use and land cover classes. The lowest ET_a observations in all the evaluated dates were
 667 observed in the areas occupied by pasture and mosaic of agriculture and pasture classes, with
 668 average values of $0.70 \pm 0.73 \text{ mm day}^{-1}$ and $1.01 \pm 0.96 \text{ mm day}^{-1}$, respectively (Figure 9).
 669 These areas have dryland cultivation practices, which causes the lower water availability to
 670 affect the evapotranspiration rates; moreover, the heterogeneity of the areas causes sudden
 671 variations in ET_a .

672

673 On the other hand, due to the effect of the increase in air temperature and atmospheric
 674 demand verified throughout the dry season in Petrolina, combined with the presence of
 675 preserved riparian forests along stretches of water bodies and continuous irrigation in crops,
 676 higher mean ET_a values were observed in the arboreal Caatinga ($4.73 \pm 0.49 \text{ mm day}^{-1}$) and
 677 agriculture ($3.07 \pm 1.23 \text{ mm day}^{-1}$) classes. For presenting areas with irrigated and dry
 cultivation, the average values of this class become more variable. When there is a greater

678 contribution of moisture added to more dense vegetation, there is a favoring of the local
679 microclimate in the region [112,113], a phenomenon reported in areas of arboreal vegetation.

680 The shrub and herbaceous Caatinga classes showed greater heterogeneity indicated
681 by the largest standard deviations ($2.42 \pm 0.76 \text{ mm day}^{-1}$) and ($1.46 \pm 0.71 \text{ mm day}^{-1}$),
682 respectively, relative to the arboreal Caatinga class (Figure 9). Folhes et al. [114] reported
683 that the evapotranspiration values ($<2.0 \text{ mm day}^{-1}$) during the dry season for species of
684 herbaceous–shrubby Caatinga. In dry periods, the Caatinga vegetation uses the available
685 energy as sensible heat flux (H), limiting transpiration and photosynthesis, thus reducing
686 evapotranspiration values [20]. However, arboreal vegetation is able to compensate the high
687 vapor pressure deficit in the air, even in dry periods, when compared to shrub and herbaceous
688 vegetation, due to the deep root system keeping up with the water stored in the soil
689 [69,115,116].

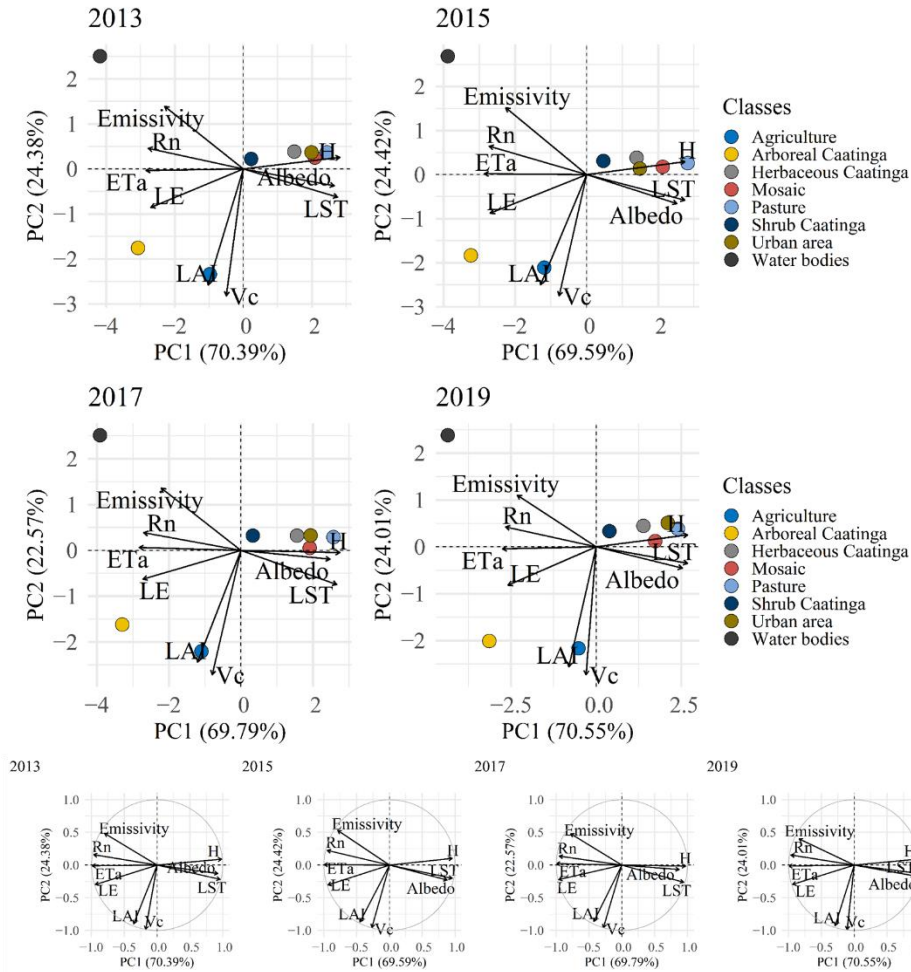
690 The arboreal and shrub species play a fundamental eco-hydrological role, maintaining
691 soil humidity and structuring its porosity, guaranteeing the maintenance of infiltration
692 capacity and favoring the survival of species [115].

693

694 *3.6. Statistical Relations Between the Variables Studied and Land Use*

695 In this study, we performed a PCA of the environmental variables in relation to land
696 use and land cover classes. Therefore, the first two components with eigenvalues greater than
697 1.0 were extracted separately for the years 2013, 2015, 2017, and 2019 (Figure 10). In 2013,
698 the two principal components explained 94.77% of the total variation, with 70.39% in the
699 principal component 1 (PC1) and 24.38% in the principal component 2 (PC2). On the other
700 hand, in 2015, 2017, and 2019, when added together, PC1 and PC2 represented 94.01, 92.34,
701 and 94.56% of the total variation, respectively (Figure 10). In addition, it can be seen that the
702 LULC class, with the least influence on components 1 and 2 in all years, is shrub Caatinga,
703 with average eigenvalues (0.31 and 0.37, respectively). In addition, the classes with the
704 greatest influence on PC1 with positive and negative eigenvalues are water bodies (2.69),
705 agriculture (-2.35), arboreal Caatinga (-1.92), pasture (0.34), mosaic (0.16), and urban area
706 (0.35). In PC2, the classes of LULC were water bodies (-4.36), mosaic (2.10), agriculture
707 (-1.0), and arboreal Caatinga (-3.40) (Figure 10).

708



709

710 **Figure 10.** Scores obtained by principal component analysis (PCA) of environmental
 711 variables and land use and land cover. PC1 and PC2 are the first and second dimensions of
 712 PCA data, respectively. The four inserted panels below the PCA scores plots refer to the
 713 loadings plots of the first two principal components from 2013 to 2019.

714

715 Through PCA, we observed that the ordering of variables in each principal component
 716 (PC) of the axes was influenced by the degree of vegetation cover and surface water status
 717 of the LULC classes (Figure 10). Thus, PC1 contributed more to the variability of the
 718 response of variables related to energy balance. Therefore, in PC2, the land use and land
 719 cover classes (i.e., pasture, mosaic, urban area, and herbaceous Caatinga) influenced the
 720 variables R_n , LE , ET_a , and emissivity with higher mean loadings (-0.95 , -0.94 , -0.99 , and
 721 -0.80 , respectively). On the other hand, they showed a high correlation with the variables H ,
 722 LST , and albedo. For these LULC classes, this may be related to the presence of bare soil

723 and thin vegetation covers that affect the regional microclimate and soil–plant–atmosphere
724 system fluxes, resulting in higher albedos, lower rates of evaporative cooling fluxes, and
725 highest LST [2,104].

726 On the other hand, PC2 contributed more to the variability of the responses of the
727 variables regarding the canopy interactions (LAI and V_C) due to the strong negative
728 correlation with cultivated land (i.e., agriculture class) (Figure 10). In all years, there was a
729 predominance for LE and LAI in areas with arboreal Caatinga and agriculture, with
730 agriculture presenting the highest V_C . Caatinga presents a strong relationship with LAI in
731 rainy periods due to the greater availability of water in the soil [117]. In the present study,
732 the samples were taken in the period with low rainfall, so the LAI was not expressive
733 compared to agricultural areas, which use irrigation and therefore increase the LAI. Thus, the
734 emissivity in the Caatinga vegetation is lower, for the emissivity of the soil is generally lower
735 than that of the leaves [2].

736 The results of the analysis of variance (ANOVA) and multiple regression analysis of
737 the established model are presented in Table 3. For the combination of two-variable models,
738 the two best pre-established parameters based on the PCA results were the variables LST and
739 H , used to build the regression model. In particular, these two variables are of great relevance
740 in transferring energy to the atmosphere. The ANOVA results also showed that the model
741 values are significant. Due to the observations, a joint analysis of the coefficient of
742 determination obtained ($R^2 = 0.98$) can be performed, emphasizing the P -value obtained from
743 our regression model, which was less than 0.001, thus indicating greater model accuracy and
744 reliability (Table 3). Notably, it can be seen that the model's F -value was 16,692.84, being
745 greater than the critical value of $F_{0.05} = 3.018$, which confirms the significance of the
746 proposed model. In addition, the variables used provided a high R^2 and LCCC, being essential
747 for the model's accuracy. Furthermore, the results showed that the multiple linear regression
748 model to determine ET_a achieved a coefficient of determination of 0.98, RMSE of 0.498,
749 MAE of 0.413, and d equal to 0.9620. It also resulted in PBIAS, NSE, and LCCC values
750 averaged between -13.32% , 0.826, and 0.907, respectively (Table 3). From the statistical
751 analysis, this model is described as $ET_a = 6.89 - 0.0527LST - 0.0120H$. Based on the RMSE,
752 LCCC, and d of this application, the use of the ET_a model, besides presenting a strong

753 correlation between the variables H and LST, as seen in Figure 10, expresses a biophysical
 754 model with enough efficiency and high agreement to determine ET_a .

755

756 **Table 3.** Analysis of variance (ANOVA) and regression coefficients results for the suggested
 757 model.

Source of Variation	df	SS	MS	F-Value	p-Value
Regression	2	464.41	232.21	16,692.84	<0.0001
LST	1	335.29	335.29	24,103.8	<0.0001
H	1	129.12	129.12	9281.9	<0.0001
Error	397	5.52	0.01		
Total	399	469.93			

Regression statistics				
Predictors in model	Regression coefficients			
	β_0	β_1	β_2	R^2
LST, H	6.89	-0.0527	-0.0120	0.98

Model	Statistical metrics					
	RMSE	MAE	PBIAS (%)	NSE	LCCC	d
	0.498	0.413	-13.32	0.826	0.907	0.9620

758 df: degrees of freedom, SS: sum of squares, MS: mean square, LST: land surface temperature,
 759 H : sensible heat flux, β_0 : intercept, β_1 and β_2 : estimated coefficient for the factor x , R^2 :
 760 coefficient of determination, RMSE: root mean square error, MAE: mean absolute error,
 761 PBIAS: percent bias, NSE: Nash–Sutcliffe efficiency coefficient, LCCC: Lin’s concordance
 762 correlation coefficient, and d : Willmott’s index of agreement. Based on F -test, at a
 763 probability of 0.05 ($p < 0.05$), significance of equation parameters for each response variable
 764 was determined.

765

766 The high d (0.9620) values for ET_a indicated that there was a good agreement between
 767 simulated and measured ET_a . In general, the ET_a model showed excellent agreement (LCCC
 768 > 0.9), high performance, and low RMSE (0.498) (Table 3). The PBIAS and MAE values for
 769 ET_a were between -13.32% and 0.413, confirming the close agreement. Consequently, this
 770 result describes the ability to simplify and accurately predict ET_a in deficit environments.

771 Applications of regression model analysis with environmental variables are common in the
772 literature in dry forests [117–119]. However, these implementations of variables in previous
773 studies may be challenging to acquire for specific locations, requiring more simplified
774 models. Our results also indicate the relationship between H and the LST of ecosystems to
775 determine ET_a , an important variable in the energy balances of environments worldwide.

776

777 **4. Conclusions**

778 In this study, we point out a significant tendency to increase the agricultural areas,
779 which results in the progressive decrease of the Brazilian Caatinga biome. The vegetation
780 cover is directly influenced by the soil–water regime; years of higher rainfall result in a lower
781 percentage of suppression of the native forest in the municipality of Petrolina, Pernambuco
782 (Brazil). The areas with pasture class presented hotspots due to degradative processes and
783 higher surface temperatures, influenced by the sensible heat flux. A gradual increase in LST
784 is observed in the municipality and it may cause future risks to forest areas.

785 The SEBAL algorithm used in a semi-arid environment is a helpful tool to determine
786 the energy and mass fluxes in different ecosystems. Notably, the Caatinga biome has
787 particularities in biophysical parameters, according to the land cover and soil exposure on
788 intra and inter-annual scales. The heterogeneity of the surface of the municipality of
789 Petrolina, as a function of land use and land cover patterns, alters the energy exchange with
790 the atmosphere. Our results also suggest a simplified and validated model for ET_a
791 determination in a semi-arid environment. The regression model could accurately predict the
792 spatial distribution of ET_a , with high R^2 and LCCC and low RMSE value.

793 Thus, it is possible to suggest that the implementation of agricultural activities in the
794 Petrolina should be carried out in a planned and sustainable way in order to mitigate the
795 impacts that anthropic action causes on the Caatinga, especially with the increased
796 vulnerability of this biome to the desertification process. However, further research is needed
797 to investigate the spatial variations of the types of crops covering the soil in the municipality,
798 as well as the dynamics of fires and their impacts on the diversity of the Caatinga biome.
799 Field surveys and the use of unmanned aerial systems (UAS) could provide more detailed
800 information at an intermediate and fine scale.

801

802 **Supplementary Materials:** The following are available online at
803 <https://www.mdpi.com/article/10.3390/rs14081911/s1>, Figure S1: Land use/land cover
804 changes in Petrolina between 2013 and 2019. Positive values indicate an expansion of the
805 respective land cover, negative values a contraction. The vertical axe is in million hectares
806 (Mha). Please see Supplementary Table S1 to access values of land use/land cover changes;
807 Table S1: Areas of expansion and contraction of land use/land cover changes in Petrolina
808 between 2013 and 2019. Positive values indicate an expansion of the respective land cover,
809 negative values a contraction. The values are in million hectares (Mha).

810

811 **Funding:** This research was funded by the Portuguese Foundation for Science and
812 Technology (FCT), through projects ASHMOB (CENTRO-01-0145-FEDER-029351),
813 GOLis (PDR2020-101-030913, Partnership nr. 344/Initiative nr. 21), MUSSEFLOW
814 (PTDC/BIA-EVL/29199/2017), MEDWATERICE (PRIMA/0006/2018), and through the
815 strategic project UIDB/04292/2020 granted to MARE—Marine and Environmental Sciences
816 Centre, University of Coimbra, Coimbra, Portugal.

817

818 **Institutional Review Board Statement:** Not applicable.

819

820 **Informed Consent Statement:** Not applicable.

821

822 **Data Availability Statement:** Landsat-8 image courtesy of the USGS/NASA
823 (<https://www.usgs.gov/core-science-systems/nli/landsat>, accessed on 10 August 2021);
824 MapBiomas data presented in this study are available at websites of Brazilian Annual Land
825 Use and Land Cover Mapping Project (<https://mapbiomas.org/en/project>, accessed on 20
826 August 2021); and the meteorological data presented in this study are available at the website
827 of the National Institute of Meteorology (<https://portal.inmet.gov.br/>, accessed on 10 August
828 2021).

829

830 **Acknowledgments:** The authors would like to thank the Research Support Foundation of the
831 Pernambuco State (FACEPE, Brazil—APQ-0215-5.01/10 and FACEPE - APQ-1159-
832 1.07/14), the National Council for Scientific and Technological Development (CNPq, Brazil)

833 and also funds through the fellowship of the Research Productivity Program (CNPq
 834 305286/2015-3, 304060/2016-0, 309681/2019-7, and 303767/2020-0), and the Coordination
 835 for the Improvement of Higher Education Personnel (CAPES, Brazil - Finance Code 001)
 836 for the research and study grants. The authors are also grateful for financial support from the
 837 Portuguese Foundation for Science and Technology (FCT), and the University of Coimbra,
 838 Portugal. In addition, we also would like to thank the anonymous reviewers for their
 839 insightful comments, of which significantly increased the value of this study.

840

841 **Conflicts of Interest:** The authors declare no conflicts of interest.

842

843 **Abbreviations**

844 Summary of all the symbols and acronyms used in this paper.

Item	Description
a and b	Are the calibration coefficients
C_p	Specific heat of air
d	Willmott's index of agreement
DEM	Digital elevation model
dT	Near-surface air temperature gradient
e_a	Actual atmospheric water vapor pressure
e_s	Water vapor saturation pressure
ET_a	Actual evapotranspiration
G	Soil heat flux
GEE	Google Earth Engine
H	Sensible heat flux
HR	Instantaneous relative humidity
k	von Karman constant
LAI	Leaf area index
LCCC	Lin's concordance correlation coefficient
LE	Latent heat flux
LSE	Land surface emissivity
LST	Land surface temperature

LULC	Land use and land cover
MAE	Mean absolute error
NDVI	Normalized Difference Vegetation Index
NSE	Nash-Sutcliffe efficiency coefficient
PBIAS	Percent bias
PCA	Principal component analysis
r_{ah}	Near-surface aerodynamic resistance to heat transport
RMSE	Root mean square error
R_n	Net radiation
R_{n24}	Daily net radiation
R^2	Coefficient of determination
SAVI	Soil-Adjusted Vegetation Index
T_0	Instantaneous air temperature
T_a	Air temperature
u^*	Friction velocity
u_{200}	Wind speed at the height of 200 m
V_C	Vegetation cover
W	Precipitable water
z_1 and z_2	Are the two heights between the surface of the anchor pixels
z_{om}	Momentum roughness length
α_{sup}	Surface albedo
ϵ_a	Atmospheric emissivity
Λ	Evaporative fraction
λ	Latent heat of vaporization of water
ρ_{air}	Air density
ψ_m and ψ_h	Stability correction factors for momentum and sensible heat, respectively

845

846 **References**

- 847 1. Arnan, X.; Leal, I.R.; Tabarelli, M.; Andrade, J.F.; Barros, M.F.; Câmara, T.; Jamelli,
848 D.; Knoechelmann, C.M.; Menezes, T.G.C.; Menezes, A.G.S.; et al. A framework for

- 849 deriving measures of chronic anthropogenic disturbance: Surrogate, direct, single and
850 multi-metric indices in Brazilian Caatinga. *Ecol. Indic.* **2018**, *94*, 274–282,
851 doi:10.1016/J.ECOLIND.2018.07.001.
- 852 2. Ferreira, T.R.; Silva, B.B.D.; De Moura, M.S.B.; Verhoef, A.; Nóbrega, R.L.B. The use
853 of remote sensing for reliable estimation of net radiation and its components: a case study
854 for contrasting land covers in an agricultural hotspot of the Brazilian semiarid region.
855 *Agric. For. Meteorol.* **2020**, *291*, 108052, doi:10.1016/J.AGRFORMET.2020.108052.
- 856 3. Moro, M.F.; Nic Lughadha, E.; de Araújo, F.S.; Martins, F.R. A Phytogeographical
857 Metaanalysis of the Semiarid Caatinga Domain in Brazil. *Bot. Rev.* **2016**, *82*, 91–148,
858 doi:10.1007/S12229-016-9164-Z.
- 859 4. Magalhães, K. do N.; Guarniz, W.A.S.; Sá, K.M.; Freire, A.B.; Monteiro, M.P.; Nojosa,
860 R.T.; Bieski, I.G.C.; Custódio, J.B.; Balogun, S.O.; Bandeira, M.A.M. Medicinal plants
861 of the Caatinga, northeastern Brazil: Ethnopharmacopeia (1980–1990) of the late
862 professor Francisco José de Abreu Matos. *J. Ethnopharmacol.* **2019**, *237*, 314–353,
863 doi:10.1016/J.JEP.2019.03.032.
- 864 5. Silva, É.E. de M. e.; Paixão, V.H.F.; Torquato, J.L.; Lunardi, D.G.; Lunardi, V. de O.
865 Fruiting phenology and consumption of zoochoric fruits by wild vertebrates in a
866 seasonally dry tropical forest in the Brazilian Caatinga. *Acta Oecologica* **2020**, *105*,
867 103553, doi:10.1016/J.ACTAO.2020.103553.
- 868 6. Santos, L.R. dos; Nascimento Lima, A.M.; Cunha, J.C.; Rodrigues, M.S.; Barros Soares,
869 E.M.; dos Santos, L.P.A.; Lopes da Silva, A.V.; Ferreira Fontes, M.P. Does irrigated
870 mango cultivation alter organic carbon stocks under fragile soils in semiarid climate?
871 *Sci. Hortic. (Amsterdam)*. **2019**, *255*, 121–127, doi:10.1016/J.SCIENTA.2019.05.015.
- 872 7. Leão, P.C. de S.; do Nascimento, J.H.B.; de Moraes, D.S.; de Souza, E.R. Yield
873 components of the new seedless table grape ‘BRS Ísis’ as affected by the rootstock under
874 semi-arid tropical conditions. *Sci. Hortic. (Amsterdam)*. **2020**, *263*, 109114,
875 doi:10.1016/J.SCIENTA.2019.109114.
- 876 8. Rallo, G.; Paço, T.A.; Paredes, P.; Puig-Sirera; Massai, R.; Provenzano, G.; Pereira, L.S.
877 Updated single and dual crop coefficients for tree and vine fruit crops. *Agric. Water*
878 *Manag.* **2021**, *250*, 106645, doi:10.1016/J.AGWAT.2020.106645.
- 879 9. Gomes, L.S.; Maia, A.G.; de Medeiros, J.D.F. Fuzzified hedging rules for a reservoir in

- 880 the Brazilian semiarid region. *Environ. Challenges* **2021**, *4*, 100125,
881 doi:10.1016/J.ENVC.2021.100125.
- 882 10. Marengo, J.A.; Torres, R.R.; Alves, L.M. Drought in Northeast Brazil—past, present,
883 and future. *Theor. Appl. Climatol.* **2017**, *129*, 1189–1200, doi:10.1007/S00704-016-
884 1840-8.
- 885 11. Martins, M.A.; Tomasella, J.; Rodriguez, D.A.; Alvalá, R.C.S.; Giarolla, A.; Garofolo,
886 L.L.; Júnior, J.L.S.; Paolicchi, L.T.L.C.; Pinto, G.L.N. Improving drought management
887 in the Brazilian semiarid through crop forecasting. *Agric. Syst.* **2018**, *160*, 21–30,
888 doi:10.1016/J.AGSY.2017.11.002.
- 889 12. Queiroz, M.G. de; Silva, T.G.F. da; Souza, C.A.A. de; Jardim, A.M. da R.F.; Araújo
890 Júnior, G. do N.; Souza, L.S.B.; Moura, M.S.B. Composition of Caatinga Species Under
891 Anthropic Disturbance and Its Correlation With Rainfall Partitioning. *Floresta e*
892 *Ambient.* **2021**, *28*, 20190044, doi:10.1590/2179-8087-FLORAM-2019-0044.
- 893 13. Barlow, J.; Lennox, G.D.; Ferreira, J.; Berenguer, E.; Lees, A.C.; Nally, R. Mac;
894 Thomson, J.R.; Ferraz, S.F. de B.; Louzada, J.; Oliveira, V.H.F.; et al. Anthropogenic
895 disturbance in tropical forests can double biodiversity loss from deforestation. *Nature*
896 **2016**, *535*, 144–147, doi:10.1038/nature18326.
- 897 14. Silva Junior, C.A. da; Teodoro, P.E.; Delgado, R.C.; Teodoro, L.P.R.; Lima, M.; de
898 Andréa Pantaleão, A.; Baio, F.H.R.; de Azevedo, G.B.; de Oliveira Sousa Azevedo,
899 G.T.; Capristo-Silva, G.F.; et al. Persistent fire foci in all biomes undermine the Paris
900 Agreement in Brazil. *Sci. Rep.* **2020**, *10*, 16246, doi:10.1038/s41598-020-72571-w.
- 901 15. Jardim, A.M. da R.F.; Silva, T.G.F. da; Souza, L.S.B. de; Araújo Júnior, G. do N.; Alves,
902 H.K.M.N.; Souza, M. de S.; Araújo, G.G.L. de; Moura, M.S.B. de Intercropping forage
903 cactus and sorghum in a semi-arid environment improves biological efficiency and
904 competitive ability through interspecific complementarity. *J. Arid Environ.* **2021**, *188*,
905 104464, doi:10.1016/J.JARIDENV.2021.104464.
- 906 16. Costa, M. da S.; Oliveira-Júnior, J.F. de; Santos, P.J. dos; Filho, W.L.F.C.; Gois, G. de;
907 Blanco, C.J.C.; Teodoro, P.E.; Junior, C.A. da S.; Santiago, D. de B.; Souza, E. de O.;
908 et al. Rainfall extremes and drought in Northeast Brazil and its relationship with El
909 Niño–Southern Oscillation. *Int. J. Climatol.* **2021**, *41*, E2111–E2135,
910 doi:10.1002/JOC.6835.

- 911 17. Tomasella, J.; Silva Pinto Vieira, R.M.; Barbosa, A.A.; Rodriguez, D.A.; de Oliveira
912 Santana, M.; Sestini, M.F. Desertification trends in the Northeast of Brazil over the
913 period 2000–2016. *Int. J. Appl. Earth Obs. Geoinf.* **2018**, *73*, 197–206,
914 doi:10.1016/J.JAG.2018.06.012.
- 915 18. Vieira, R.M.S.P.; Tomasella, J.; Alvalá, R.C.S.; Sestini, M.F.; Affonso, A.G.;
916 Rodriguez, D.A.; Barbosa, A.A.; Cunha, A.P.M.A.; Valles, G.F.; Crepani, E.; et al.
917 Identifying areas susceptible to desertification in the Brazilian northeast. *Solid Earth*
918 **2015**, *6*, 347–360, doi:10.5194/SE-6-347-2015.
- 919 19. Ribeiro, K.; Sousa-Neto, E.R. de; Carvalho, J.A. de; Sousa Lima, J.R. de; Menezes,
920 R.S.C.; Duarte-Neto, P.J.; da Silva Guerra, G.; Ometto, J.P.H.B. Land cover changes
921 and greenhouse gas emissions in two different soil covers in the Brazilian Caatinga. *Sci.*
922 *Total Environ.* **2016**, *571*, 1048–1057, doi:10.1016/J.SCITOTENV.2016.07.095.
- 923 20. Teixeira, A.H. de C.; Leivas, J.F.; Andrade, R.G.; Hernandez, F.B.T. Water productivity
924 assessments with Landsat 8 images in the Nilo Coelho irrigation scheme. *IRRIGA* **2015**,
925 *1*, 01–10, doi:10.15809/IRRIGA.2015V1N2P01.
- 926 21. Leivas, J.F.; Teixeira, A.H. de C.; Bayma-Silva, G.; Garçon, E.A.M.; Ronquim, C.C.
927 Water indicators based on SPOT 6 satellite images in irrigated area at the Paracatu River
928 Basin, Brazil. In Proceedings of the Remote Sensing for Agriculture, Ecosystems, and
929 Hydrology XIX, 104211I; International Society for Optics and Photonics: Bellingham,
930 WA, USA, 2017; Vol. 10421, p. 104211I.
- 931 22. Cunha, J.; Nóbrega, R.L.B.; Rufino, I.; Erasmi, S.; Galvão, C.; Valente, F. Surface
932 albedo as a proxy for land-cover clearing in seasonally dry forests: Evidence from the
933 Brazilian Caatinga. *Remote Sens. Environ.* **2020**, *238*, 111250,
934 doi:10.1016/J.RSE.2019.111250.
- 935 23. Barbosa, H.A.; Lakshmi Kumar, T. V.; Paredes, F.; Elliott, S.; Ayuga, J.G. Assessment
936 of Caatinga response to drought using Meteosat-SEVIRI Normalized Difference
937 Vegetation Index (2008–2016). *ISPRS J. Photogramm. Remote Sens.* **2019**, *148*, 235–
938 252, doi:10.1016/J.ISPRSJPRS.2018.12.014.
- 939 24. Queiroz, M.G.; Silva, T.G.F.; Zolnier, S.; Jardim, A.M. da R.F.; de Souza, C.A.A.;
940 Araújo Júnior, G. do N.; de Moraes, J.E.F.; de Souza, L.S.B. Spatial and temporal
941 dynamics of soil moisture for surfaces with a change in land use in the semi-arid region

- 942 of Brazil. *CATENA* **2020**, *188*, 104457, doi:10.1016/J.CATENA.2020.104457.
- 943 25. Fisher, J.B.; Melton, F.; Middleton, E.; Hain, C.; Anderson, M.; Allen, R.; McCabe,
944 M.F.; Hook, S.; Baldocchi, D.; Townsend, P.A.; et al. The future of evapotranspiration:
945 Global requirements for ecosystem functioning, carbon and climate feedbacks,
946 agricultural management, and water resources. *Water Resour. Res.* **2017**, *53*, 2618–2626,
947 doi:10.1002/2016WR020175.
- 948 26. Souza, R.; Hartzell, S.; Feng, X.; Dantas Antonino, A.C.; de Souza, E.S.; Menezes,
949 R.S.C.; Porporato, A. Optimal management of cattle grazing in a seasonally dry tropical
950 forest ecosystem under rainfall fluctuations. *J. Hydrol.* **2020**, *588*, 125102,
951 doi:10.1016/J.JHYDROL.2020.125102.
- 952 27. Fendrich, A.N.; Barretto, A.; de Faria, V.G.; de Bastiani, F.; Tenneson, K.; Guedes Pinto,
953 L.F.; Sparovek, G. Disclosing contrasting scenarios for future land cover in Brazil:
954 Results from a high-resolution spatiotemporal model. *Sci. Total Environ.* **2020**, *742*,
955 140477, doi:10.1016/J.SCITOTENV.2020.140477.
- 956 28. Lopes, V.C.; Parente, L.L.; Baumann, L.R.F.; Miziara, F.; Ferreira, L.G. Land-use
957 dynamics in a Brazilian agricultural frontier region, 1985-2017. *Land use policy* **2020**,
958 *97*, 104740, doi:10.1016/J.LANDUSEPOL.2020.104740.
- 959 29. Blondeel, H.; Landuyt, D.; Vangansbeke, P.; De Frenne, P.; Verheyen, K.; Perring, M.P.
960 The need for an understory decision support system for temperate deciduous forest
961 management. *For. Ecol. Manage.* **2021**, *480*, 118634,
962 doi:10.1016/J.FORECO.2020.118634.
- 963 30. Araujo, H.F.P. d.; Machado, C.C.C.; Pareyn, F.G.C.; Nascimento, N.F.F. d.; Araújo,
964 L.D.A.; Borges, L.A. d. A.P.; Santos, B.A.; Beirigo, R.M.; Vasconcellos, A.; Dias, B.
965 de O.; et al. A sustainable agricultural landscape model for tropical drylands. *Land use*
966 *policy* **2021**, *100*, 104913, doi:10.1016/J.LANDUSEPOL.2020.104913.
- 967 31. Liu, S.; Su, H.; Zhang, R.; Tian, J.; Chen, S.; Wang, W. Regional Estimation of Remotely
968 Sensed Evapotranspiration Using the Surface Energy Balance-Advection (SEB-A)
969 Method. *Remote Sens.* **2016**, *8*, 644, doi:10.3390/RS8080644.
- 970 32. Mutti, P.R.; da Silva, L.L.; Medeiros, S. de S.; Dubreuil, V.; Mendes, K.R.; Marques, T.
971 V.; Lúcio, P.S.; Santos e Silva, C.M.; Bezerra, B.G. Basin scale rainfall-
972 evapotranspiration dynamics in a tropical semiarid environment during dry and wet

- 973 years. *Int. J. Appl. Earth Obs. Geoinf.* **2019**, 75, 29–43, doi:10.1016/J.JAG.2018.10.007.
- 974 33. Teixeira, A.H. de C.; de Miranda, F.R.; Leivas, J.F.; Pacheco, E.P.; Garçon, E.A.M.
975 Water productivity assessments for dwarf coconut by using Landsat 8 images and
976 agrometeorological data. *ISPRS J. Photogramm. Remote Sens.* **2019**, 155, 150–158,
977 doi:10.1016/J.ISPRSJPRS.2019.07.006.
- 978 34. Moreira, E.B.M.; Nóbrega, R.S.; Silva, B.B. da; Ribeiro, E.P. Estimativa da
979 evapotranspiração em área urbana através de imagens digitais TM - Landsat 5. *Geosul*
980 **2019**, 34, 559–585, doi:10.5007/1982-5153.2019V34N72P559.
- 981 35. Silva, M.V. da; Pandorfi, H.; Almeida, G.L.P. de; Lima, R.P. de; Santos, A. dos; Jardim,
982 A.M. da R.F.; Rolim, M.M.; Silva, J.L.B. da; Batista, P.H.D.; Silva, R.A.B. da; et al.
983 Spatio-temporal monitoring of soil and plant indicators under forage cactus cultivation
984 by geoprocessing in Brazilian semi-arid region. *J. South Am. Earth Sci.* **2021**, 107,
985 103155, doi:10.1016/J.JSAMES.2021.103155.
- 986 36. Mhawej, M.; Faour, G. Open-source Google Earth Engine 30-m evapotranspiration rates
987 retrieval: The SEBALIGEE system. *Environ. Model. Softw.* **2020**, 133, 104845,
988 doi:10.1016/J.ENVSOFT.2020.104845.
- 989 37. Cabral Júnior, J.B.; Silva, C.M.S. e; de Almeida, H.A.; Bezerra, B.G.; Spyrides, M.H.C.
990 Detecting linear trend of reference evapotranspiration in irrigated farming areas in
991 Brazil's semiarid region. *Theor. Appl. Climatol.* **2019**, 138, 215–225,
992 doi:10.1007/S00704-019-02816-W.
- 993 38. IBGE Instituto Brasileiro de Geografia e Estatística Available online:
994 <https://cidades.ibge.gov.br/brasil/pe/petrolina/panorama> (accessed on Aug 29, 2021).
- 995 39. NASA Giovanni. National Aeronautics and Space Administration Available online:
996 <https://giovanni.gsfc.nasa.gov/giovanni/> (accessed on Aug 29, 2021).
- 997 40. Santos, C.A.G.; Silva, R.M. da; Silva, A.M.; Brasil Neto, R.M. Estimation of
998 evapotranspiration for different land covers in a Brazilian semi-arid region: A case study
999 of the Brígida River basin, Brazil. *J. South Am. Earth Sci.* **2017**, 74, 54–66,
1000 doi:10.1016/J.JSAMES.2017.01.002.
- 1001 41. Tasumi, M. Progress in Operational Estimation of Regional Evapotranspiration Using
1002 Satellite Imagery, University of Idaho: Moscow, ID, USA, 2003.
- 1003 42. Moletto-Lobos, I.; Mattar, C.; Barichivich, J. Performance of Satellite-Based

- 1004 Evapotranspiration Models in Temperate Pastures of Southern Chile. *Water* **2020**, *12*,
1005 3587, doi:10.3390/W12123587.
- 1006 43. Consoli, S.; Milani, M.; Cirelli, G.; Barbagallo, S.; Marzo, A.; Vanella, D.; Toscano, A.
1007 Energy and water balance of a treatment wetland under mediterranean climatic
1008 conditions. *Ecol. Eng.* **2018**, *116*, 52–60, doi:10.1016/j.ecoleng.2018.02.029.
- 1009 44. Liu, J.; You, Y.; Li, J.; Sitch, S.; Gu, X.; Nabel, J.E.M.S.; Lombardozzi, D.; Luo, M.;
1010 Feng, X.; Arneeth, A.; et al. Response of global land evapotranspiration to climate change,
1011 elevated CO₂, and land use change. *Agric. For. Meteorol.* **2021**, *311*, 108663,
1012 doi:10.1016/J.AGRFORMET.2021.108663.
- 1013 45. Hartzell, S.; Bartlett, M.S.; Porporato, A. Unified representation of the C3, C4, and CAM
1014 photosynthetic pathways with the Photo3 model. *Ecol. Modell.* **2018**, *384*, 173–187,
1015 doi:10.1016/J.ECOLMODEL.2018.06.012.
- 1016 46. Laipelt, L.; Ruhoff, A.L.; Fleischmann, A.S.; Bloedow Kayser, R.H.; Kich, E. de M.;
1017 Rocha, H.R. da; Usher Neale, C.M. Assessment of an Automated Calibration of the
1018 SEBAL Algorithm to Estimate Dry-Season Surface-Energy Partitioning in a Forest–
1019 Savanna Transition in Brazil. *Remote Sens.* **2020**, *12*, 1108, doi:10.3390/RS12071108.
- 1020 47. Allen, R.; Waters, R.; Bastiaanssen, W.; Tasumi, M.; Trezza, R. *SEBAL (Surface Energy*
1021 *Balance Algorithms for Land)—Idaho Implementation, Advanced Training and Users*
1022 *Manual, Version 1.0*; Idaho Department of Water Resources: Idaho, USA, 2002;
- 1023 48. Bastiaanssen, W.G.M. SEBAL- based sensible and latent heat fluxes in the irrigated
1024 Gediz Basin, Turkey. *J. Hydrol.* **2000**, *229*, 87–100, doi:10.1016/S0022-
1025 1694(99)00202-4.
- 1026 49. Bastiaanssen, W.G.M.; Noordman, E.J.M.; Pelgrum, H.; Davids, G.; Thoreson, B.P.;
1027 Allen, R.G. SEBAL Model with Remotely Sensed Data to Improve Water-Resources
1028 Management under Actual Field Conditions. *J. Irrig. Drain. Eng.* **2005**, *131*, 85–93,
1029 doi:10.1061/(ASCE)0733-9437(2005)131:1(85).
- 1030 50. Allen, R.G.; Tasumi, M.; Trezza, R. Satellite-Based Energy Balance for Mapping
1031 Evapotranspiration with Internalized Calibration (METRIC)—Model. *J. Irrig. Drain.*
1032 *Eng.* **2007**, *133*, 380–394, doi:10.1061/(asce)0733-9437(2007)133:4(380).
- 1033 51. Cheng, M.; Jiao, X.; Li, B.; Yu, X.; Shao, M.; Jin, X. Long time series of daily
1034 evapotranspiration in China based on the SEBAL model and multisource images and

- 1035 validation. *Earth Syst. Sci. Data* **2021**, *13*, 3995–4017, doi:10.5194/ESSD-13-3995-
1036 2021.
- 1037 52. Correia Filho, W.L.F.; Santiago, D. de B.; Oliveira-Júnior, J.F. de; Silva Junior, C.A. da
1038 Impact of urban decadal advance on land use and land cover and surface temperature in
1039 the city of Maceió, Brazil. *Land use policy* **2019**, *87*, 104026,
1040 doi:10.1016/J.LANDUSEPOL.2019.104026.
- 1041 53. Rouse, J.W.; Haas, R.H.; Schell, J.A.; Deering, D.W.; Harlan, J.C. Monitoring the
1042 Vernal Advancement and Retrogradation (Greenwave Effect) of Natural Vegetation.
1043 *NASA/GSFCT Type III Final Rep.* **1974**, 1–390.
- 1044 54. Gao, Q.; Li, Y.; Wan, Y.; Lin, E.; Xiong, W.; Jiangcun, W.; Wang, B.; Li, W. Grassland
1045 degradation in Northern Tibet based on remote sensing data. *J. Geogr. Sci.* **2006**, *16*,
1046 165–173, doi:10.1007/S11442-006-0204-1.
- 1047 55. Teixeira, A.H.C.; Bastiaanssen, W.G.M.; Ahmad, M.D.; Bos, M.G. Reviewing SEBAL
1048 input parameters for assessing evapotranspiration and water productivity for the Low-
1049 Middle São Francisco River basin, Brazil: Part B: Application to the regional scale.
1050 *Agric. For. Meteorol.* **2009**, *149*, 477–490, doi:10.1016/J.AGRFORMET.2008.09.014.
- 1051 56. Bright, R.M.; Davin, E.; O’Halloran, T.; Pongratz, J.; Zhao, K.; Cescatti, A. Local
1052 temperature response to land cover and management change driven by non-radiative
1053 processes. *Nat. Clim. Chang.* **2017**, *7*, doi:10.1038/nclimate3250.
- 1054 57. Bastiaanssen, W.G.M.; Pelgrum, H.; Soppe, R.W.O.; Thoreson, B.P.; Allen, R.G.;
1055 Teixeira, A.H.C. Thermal-infrared technology for local and regional scale irrigation
1056 analyses in horticultural systems. *Acta Hortic.* **2008**, *792*, 33–46,
1057 doi:10.17660/ACTAHORTIC.2008.792.2.
- 1058 58. Teixeira, A.H.C.; Bastiaanssen, W.G.M.; Moura, M.S.B.; Soares, J.M.; Ahmad, M.D.;
1059 Bos, M.G. Energy and water balance measurements for water productivity analysis in
1060 irrigated mango trees, Northeast Brazil. *Agric. For. Meteorol.* **2008**, *148*, 1524–1537,
1061 doi:10.1016/J.AGRFORMET.2008.05.004.
- 1062 59. Correia Filho, W.L.F.; Oliveira-Júnior, J.F. De; Santiago, D.D.B.; Terassi, P.M.D.B.;
1063 Teodoro, P.E.; Gois, G. De; Blanco, C.J.C.; Souza, P.H.D.A.; Costa, M. da S.; Gomes,
1064 H.B.; et al. Rainfall variability in the Brazilian northeast biomes and their interactions
1065 with meteorological systems and ENSO via CHELSA product. *Big Earth Data* **2019**, *3*,

- 1066 315–337, doi:10.1080/20964471.2019.1692298.
- 1067 60. Teixeira, A.H. d. C.; Bastiaanssen, W.G.M.; Ahmad, M.D.; Bos, M.G. Reviewing
1068 SEBAL input parameters for assessing evapotranspiration and water productivity for the
1069 Low-Middle São Francisco River basin, Brazil: Part A: Calibration and validation.
1070 *Agric. For. Meteorol.* **2009**, *149*, 462–476, doi:10.1016/J.AGRFORMET.2008.09.016.
- 1071 61. Alvares, C.A.; Stape, J.L.; Sentelhas, P.C.; de Moraes Gonçalves, J.L.; Sparovek, G.
1072 Köppen’s climate classification map for Brazil. *Meteorol. Zeitschrift* **2013**, *22*, 711–728,
1073 doi:10.1127/0941-2948/2013/0507.
- 1074 62. Beck, H.E.; Zimmermann, N.E.; McVicar, T.R.; Vergopolan, N.; Berg, A.; Wood, E.F.
1075 Present and future Köppen-Geiger climate classification maps at 1-km resolution. *Sci.*
1076 *Data* **2018**, *5*, 180214, doi:10.1038/sdata.2018.214.
- 1077 63. Oliveira, P.T.; Santos e Silva, C.M.; Lima, K.C. Climatology and trend analysis of
1078 extreme precipitation in subregions of Northeast Brazil. *Theor. Appl. Climatol.* **2017**,
1079 *130*, 77–90, doi:10.1007/S00704-016-1865-Z.
- 1080 64. Jardim, A.M. da R.F.; Silva, M.V. da; Silva, A.R.; Santos, A. dos; Pandorfi, H.; Oliveira-
1081 Júnior, J.F. de; de Lima, J.L.M.P.; Souza, L.S.B. de; Araújo Júnior, G. do N.; Lopes,
1082 P.M.O.; et al. Spatiotemporal climatic analysis in Pernambuco State, Northeast Brazil.
1083 *J. Atmos. Solar-Terrestrial Phys.* **2021**, *223*, 105733,
1084 doi:10.1016/J.JASTP.2021.105733.
- 1085 65. Preston, W.; Nascimento, C.W.A. do; Agra Bezerra da Silva, Y.J.; Silva, D.J.; Alves
1086 Ferreira, H. Soil fertility changes in vineyards of a semiarid region in Brazil. *J. Soil Sci.*
1087 *Plant Nutr.* **2017**, *17*, 672–685, doi:10.4067/S0718-95162017000300010.
- 1088 66. Menezes, K.M.S.; Silva, D.K.A.; Gouveia, G.V.; da Costa, M.M.; Queiroz, M.A.A.;
1089 Yano-Melo, A.M. Shading and intercropping with buffelgrass pasture affect soil
1090 biological properties in the Brazilian semi-arid region. *CATENA* **2019**, *175*, 236–250,
1091 doi:10.1016/J.CATENA.2018.12.021.
- 1092 67. Giongo, V.; Coleman, K.; da Silva Santana, M.; Salviano, A.M.; Olszveski, N.; Silva,
1093 D.J.; Cunha, T.J.F.; Parente, A.; Whitmore, A.P.; Richter, G.M. Optimizing
1094 multifunctional agroecosystems in irrigated dryland agriculture to restore soil carbon –
1095 Experiments and modelling. *Sci. Total Environ.* **2020**, *725*, 138072,
1096 doi:10.1016/J.SCITOTENV.2020.138072.

- 1097 68. INMET Instituto Nacional de Meteorologia Available online:
1098 <https://portal.inmet.gov.br/> (accessed on Aug 29, 2021).
- 1099 69. Borges, C.K.; dos Santos, C.A.C.; Carneiro, R.G.; da Silva, L.L.; de Oliveira, G.;
1100 Mariano, D.; Silva, M.T.; da Silva, B.B.; Bezerra, B.G.; Perez-Marin, A.M.; et al.
1101 Seasonal variation of surface radiation and energy balances over two contrasting areas
1102 of the seasonally dry tropical forest (Caatinga) in the Brazilian semi-arid. *Environ.*
1103 *Monit. Assess.* **2020**, *192*, 524, doi:10.1007/S10661-020-08484-Y.
- 1104 70. Funk, C.C.; Peterson, P.J.; Landsfeld, M.F.; Pedreros, D.H.; Verdin, J.P.; Rowland, J.D.;
1105 Romero, B.E.; Husak, G.J.; Michaelsen, J.C.; Verdin, A.P. *A Quasi-Global Precipitation*
1106 *Time Series for Drought Monitoring*; U.S. Geological Survey Data Series: USGS: Menlo
1107 Park, CA, USA, 2014; Vol. 832;.
- 1108 71. Marengo, J.A.; Aalves, L.M.; Alvala, R.C.; Cunha, A.P.; Brito, S.; Moraes, O.L.L.
1109 Climatic characteristics of the 2010-2016 drought in the semiarid Northeast Brazil
1110 region. *An. Acad. Bras. Cienc.* **2018**, *90*, 1973–1985, doi:10.1590/0001-
1111 3765201720170206.
- 1112 72. USGS (United States Geological Survey) Landsat Missions Timeline Available online:
1113 <https://landsat.usgs.gov/landsat-missions-timeline> (accessed on Aug 29, 2021).
- 1114 73. Huete, A.R. A soil-adjusted vegetation index (SAVI). *Remote Sens. Environ.* **1988**, *25*,
1115 295–309, doi:10.1016/0034-4257(88)90106-X.
- 1116 74. Silva, J.L.B. da; Moura, G.B. de A.; Silva, Ê.F. de F. e; Lopes, P.M.O.; Silva, T.T.F. da;
1117 Lins, F.A.C.; Silva, D.A. de O.; Ortiz, P.F.S. Spatial-temporal dynamics of the Caatinga
1118 vegetation cover by remote sensing in municipality of the Brazilian semi-arid. *Rev. Bras.*
1119 *Ciências Agrárias* **2019**, *14*, 1–10, doi:10.5039/AGRARIA.V14I4A7128.
- 1120 75. Rodrigues, J.A. de M.; Lopes, P.M.O.; Silva, J.L.B. da; Araújo, H.L.; Silva, M.V. da;
1121 Santos, A. dos; Batista, P.H.D.; Moura, G.B. de A. Spatial-temporal dynamics of
1122 Caatinga vegetation cover by remote sensing in the Brazilian semiarid region. *DYNA*
1123 **2020**, *87*, 109–117, doi:10.15446/DYNA.V87N215.87851.
- 1124 76. Batista, P.H.D.; Almeida, G.L.P. de; Silva, J.L.B. da; Pandorfi, H.; Silva, M.V. da; Silva,
1125 R.A.B. da; Melo, M.V.N. de; Lins, F.A.C.; Cordeiro Junior, J.J.F. Short-term grazing
1126 and its impacts on soil and pasture degradation. *DYNA* **2020**, *87*, 123–128,
1127 doi:10.15446/DYNA.V87N213.81853.

- 1128 77. Bastiaanssen, W.G.M.; Pelgrum, H.; Wang, J.; Ma, Y.; Moreno, J.F.; Roerink, G.J.; Van
1129 Der Wal, T. A remote sensing surface energy balance algorithm for land (SEBAL).: Part
1130 2: Validation. *J. Hydrol.* **1998**, *212–213*, 213–229, doi:10.1016/S0022-1694(98)00254-
1131 6.
- 1132 78. Bastiaanssen, W.G.M.; Menenti, M.; Feddes, R.A.; Holtslag, A.A.M. A remote sensing
1133 surface energy balance algorithm for land (SEBAL). 1. Formulation. *J. Hydrol.* **1998**,
1134 *212–213*, 198–212, doi:10.1016/S0022-1694(98)00253-4.
- 1135 79. Silva, B.B. da; Braga, A.C.; Braga, C.C.; Oliveira, L.M.M. de; Montenegro, S.M.G.L.;
1136 Barbosa, B. Procedures for calculation of the albedo with OLI-Landsat 8 images:
1137 Application to the Brazilian semi-arid. *Rev. Bras. Eng. Agrícola e Ambient.* **2016**, *20*, 3–
1138 8, doi:10.1590/1807-1929/AGRIAMBI.V20N1P3-8.
- 1139 80. Garrison, J.D.; Adler, G.P. Estimation of precipitable water over the United States for
1140 application to the division of solar radiation into its direct and diffuse components. *Sol.*
1141 *Energy* **1990**, *44*, 225–241, doi:10.1016/0038-092X(90)90151-2.
- 1142 81. Markham, B.L.; Barker, J.L. Landsat MSS and TM post-calibration dynamic ranges,
1143 exoatmospheric reflectances and at-satellite temperatures. *Landsat Tech. Notes* **1986**, *1*,
1144 3–8.
- 1145 82. Tang, R.; Li, Z.L.; Chen, K.S.; Jia, Y.; Li, C.; Sun, X. Spatial-scale effect on the SEBAL
1146 model for evapotranspiration estimation using remote sensing data. *Agric. For.*
1147 *Meteorol.* **2013**, *174–175*, 28–42, doi:10.1016/J.AGRFORMET.2013.01.008.
- 1148 83. Chang, Y.; Ding, Y.; Zhao, Q.; Zhang, S. Remote estimation of terrestrial
1149 evapotranspiration by Landsat 5 TM and the SEBAL model in cold and high-altitude
1150 regions: a case study of the upper reach of the Shule River Basin, China. *Hydrol.*
1151 *Process.* **2017**, *31*, 514–524, doi:10.1002/HYP.10854.
- 1152 84. Teixeira, A.H. d. C.; Bastiaanssen, W.G.M.; Ahmad, M.D.; Moura, M.S.B.; Bos, M.G.
1153 Analysis of energy fluxes and vegetation-atmosphere parameters in irrigated and natural
1154 ecosystems of semi-arid Brazil. *J. Hydrol.* **2008**, *362*, 110–127,
1155 doi:10.1016/J.JHYDROL.2008.08.011.
- 1156 85. Lee, Y.; Kim, S. The Modified SEBAL for Mapping Daily Spatial Evapotranspiration
1157 of South Korea Using Three Flux Towers and Terra MODIS Data. *Remote Sens.* **2016**,
1158 *8*, 983, doi:10.3390/RS8120983.

- 1159 86. MapBiomas Brasil Plataforma de Mapas e Dados Available online:
1160 <https://mapbiomas.org/> (accessed on Aug 29, 2021).
- 1161 87. Pérez-Hoyos, A.; Rembold, F.; Kerdiles, H.; Gallego, J. Comparison of Global Land
1162 Cover Datasets for Cropland Monitoring. *Remote Sens.* **2017**, *9*, 1118,
1163 doi:10.3390/RS9111118.
- 1164 88. QGIS Development Team. QGIS Geographic Information System. Open Source
1165 Geospatial Foundation Project 2021.
- 1166 89. Kaiser, H.F. The application of electronic computers to factor analysis. *Educ. Psychol.*
1167 *Meas.* **1960**, *20*, 141–151, doi:10.1177/001316446002000116.
- 1168 90. Holtum, J.A.M.; Hancock, L.P.; Edwards, E.J.; Crisp, M.D.; Crayn, D.M.; Sage, R.;
1169 Winter, K. Australia lacks stem succulents but is it depauperate in plants with
1170 crassulacean acid metabolism (CAM)? *Curr. Opin. Plant Biol.* **2016**, *31*, 109–117,
1171 doi:10.1016/J.PBI.2016.03.018.
- 1172 91. Zhao, D.; Li, N.; Zare, E.; Wang, J.; Triantafilis, J. Mapping cation exchange capacity
1173 using a quasi-3d joint inversion of EM38 and EM31 data. *Soil Tillage Res.* **2020**, *200*,
1174 104618, doi:10.1016/J.STILL.2020.104618.
- 1175 92. Lin, L.I.-K. A Concordance Correlation Coefficient to Evaluate Reproducibility.
1176 *Biometrics* **1989**, *45*, 268, doi:10.2307/2532051.
- 1177 93. Zhao, D.; Arshad, M.; Wang, J.; Triantafilis, J. Soil exchangeable cations estimation
1178 using Vis-NIR spectroscopy in different depths: Effects of multiple calibration models
1179 and spiking. *Comput. Electron. Agric.* **2021**, *182*, 105990,
1180 doi:10.1016/J.COMPAG.2021.105990.
- 1181 94. R Core Team R: The R Project for Statistical Computing Available online:
1182 <https://www.r-project.org/> (accessed on Aug 29, 2021).
- 1183 95. Correia, M.F.; da Silva Dias, M.A.F.; da Silva Aragão, M.R. Soil occupation and
1184 atmospheric variations over Sobradinho Lake area. Part two: a regional modeling study.
1185 *Meteorol. Atmos. Phys.* **2006**, *94*, 115–128, doi:10.1007/S00703-005-0174-3.
- 1186 96. Silva, M.V. da; Pandorfi, H.; Lopes, P.M.O.; Silva, J.L.B. da; de Almeida, G.L.P.; Silva,
1187 D.A. de O.; Santos, A. dos; Rodrigues, J.A. de M.; Batista, P.H.D.; Jardim, A.M. da R.F.
1188 Pilot monitoring of caatinga spatial-temporal dynamics through the action of agriculture
1189 and livestock in the brazilian semiarid. *Remote Sens. Appl. Soc. Environ.* **2020**, *19*,

- 1190 100353, doi:10.1016/J.RSASE.2020.100353.
- 1191 97. Gutiérrez, A.P.A.; Engle, N.L.; De Nys, E.; Molejón, C.; Martins, E.S. Drought
1192 preparedness in Brazil. *Weather Clim. Extrem.* **2014**, *3*, 95–106,
1193 doi:10.1016/J.WACE.2013.12.001.
- 1194 98. Ferreira, P.S.M.; Lopes, S. de F.; Trovão, D.M. de B.M. Patterns of species richness and
1195 abundance among cactus communities receiving different rainfall levels in the semiarid
1196 region of Brazil. *Acta Bot. Brasilica* **2016**, *30*, 569–576, doi:10.1590/0102-
1197 33062016ABB0084.
- 1198 99. Cunha, A.P.M.; Alvalá, R.C.; Nobre, C.A.; Carvalho, M.A. Monitoring vegetative
1199 drought dynamics in the Brazilian semiarid region. *Agric. For. Meteorol.* **2015**, *214–*
1200 *215*, 494–505, doi:10.1016/J.AGRFORMET.2015.09.010.
- 1201 100. Fleischer, E.; Khashimov, I.; Hölzel, N.; Klemm, O. Carbon exchange fluxes over
1202 peatlands in Western Siberia: Possible feedback between land-use change and climate
1203 change. *Sci. Total Environ.* **2016**, *545–546*, 424–433,
1204 doi:10.1016/J.SCITOTENV.2015.12.073.
- 1205 101. Silva Filho, R. da; Vasconcelos, R.S.; Galvão, C. de O.; Rufino, I.A.A.; Cunha, J.E.
1206 de B.L. Representação matemática do comportamento intra-anual do NDVI no Bioma
1207 Caatinga. *Ciência Florest.* **2020**, *30*, 473–488, doi:10.5902/1980509837279.
- 1208 102. Santos, A. dos; Oliveira Lopes, P.M.; Silva, M.V. da; Jardim, A.M. da R.F.; Barbosa
1209 de Albuquerque Moura, G.; Siqueira Tavares Fernandes, G.; Oliveira Silva, D.A. de;
1210 Bezerra da Silva, J.L.; de Moraes Rodrigues, J.A.; Araújo Silva, E.; et al. Causes and
1211 consequences of seasonal changes in the water flow of the São Francisco river in the
1212 semiarid of Brazil. *Environ. Sustain. Indic.* **2020**, *8*, 100084,
1213 doi:10.1016/J.INDIC.2020.100084.
- 1214 103. Leivas, J.F.; Andrade, R.G.; Victoria, D. de C.; Torresan, F.E.; Bolfe, E.L.
1215 Monitoramento da seca 2011/2012 no Nordeste brasileiro a partir do satélite SPOT-
1216 Vegetation e TRMM. *Rev. Eng. na Agric.* **2014**, *22*, 211–221,
1217 doi:10.13083/reveng.v22i3.454.
- 1218 104. Silveira, H.L.F.; Galvão, L.S.; Sanches, I.D.A.; LastNamede Sá, I.B.; Taura, T.A.
1219 Use of MSI/Sentinel-2 and airborne LiDAR data for mapping vegetation and studying
1220 the relationships with soil attributes in the Brazilian semi-arid region. *Int. J. Appl. Earth*

- 1221 *Obs. Geoinf.* **2018**, 73, 179–190, doi:10.1016/J.JAG.2018.06.016.
- 1222 105. Jardim, A.M. da R.F.; Santos, H.R.B.; Alves, H.K.M.N.; Ferreira-Silva, S.L.; Souza,
1223 L.S.B. de; Araújo Júnior, G. do N.; Souza, M. de S.; Araújo, G.G.L. de; Souza, C.A.A.
1224 de; Silva, T.G.F. da Genotypic differences relative photochemical activity, inorganic and
1225 organic solutes and yield performance in clones of the forage cactus under semi-arid
1226 environment. *Plant Physiol. Biochem.* **2021**, 162, 421–430,
1227 doi:10.1016/J.PLAPHY.2021.03.011.
- 1228 106. Miranda, R. de Q.; Nóbrega, R.L.B.; Moura, M.S.B. de; Raghavan, S.; Galvíncio,
1229 J.D. Realistic and simplified models of plant and leaf area indices for a seasonally dry
1230 tropical forest. *Int. J. Appl. Earth Obs. Geoinf.* **2020**, 85, 101992,
1231 doi:10.1016/J.JAG.2019.101992.
- 1232 107. Almeida, C.L.; de Carvalho, T.R.A.; de Araújo, J.C. Leaf area index of Caatinga
1233 biome and its relationship with hydrological and spectral variables. *Agric. For.*
1234 *Meteorol.* **2019**, 279, 107705, doi:10.1016/J.AGRFORMET.2019.107705.
- 1235 108. Pinheiro, E.A.R.; Metselaar, K.; Lier, Q. de J. van; Araújo, J.C. de Importance of soil-
1236 water to the Caatinga biome, Brazil. *Ecohydrology* **2016**, 9, 1313–1327,
1237 doi:10.1002/ECO.1728.
- 1238 109. Zhao, Z.; Sharifi, A.; Dong, X.; Shen, L.; He, B.J. Spatial Variability and Temporal
1239 Heterogeneity of Surface Urban Heat Island Patterns and the Suitability of Local Climate
1240 Zones for Land Surface Temperature Characterization. *Remote Sens.* **2021**, 13, 4338,
1241 doi:10.3390/RS13214338.
- 1242 110. Zhao, Z.Q.; He, B.J.; Li, L.G.; Wang, H.B.; Darko, A. Profile and concentric zonal
1243 analysis of relationships between land use/land cover and land surface temperature: Case
1244 study of Shenyang, China. *Energy Build.* **2017**, 155, 282–295,
1245 doi:10.1016/J.ENBUILD.2017.09.046.
- 1246 111. Feizizadeh, B.; Blaschke, T.; Nazmfar, H.; Akbari, E.; Kohbanani, H.R. Monitoring
1247 land surface temperature relationship to land use/land cover from satellite imagery in
1248 Maraqeh County, Iran. *J. Environ. Plan. Manag.* **2013**, 56, 1290–1315,
1249 doi:10.1080/09640568.2012.717888.
- 1250 112. Arraes, F.D.D.; Andrade, E.M.; Silva, D.A. Dinâmica do balanço de energia sobre o
1251 açude Orós e suas adjacências. *Rev. Caatinga* **2012**, 25, 119–127.

- 1252 113. Bezerra, J.M.; Moura, G.B. de A.; Silva, B.B. da; Lopes, P.M.O.; Silva, Ê.F. de F. e
1253 Parâmetros biofísicos obtidos por sensoriamento remoto em região semiárida do estado
1254 do Rio Grande do Norte, Brasil. *Rev. Bras. Eng. Agrícola e Ambient.* **2014**, *18*, 73–84,
1255 doi:10.1590/S1415-43662014000100010.
- 1256 114. Folhes, M.T.; Rennó, C.D.; Soares, J. V. Remote sensing for irrigation water
1257 management in the semi-arid Northeast of Brazil. *Agric. Water Manag.* **2009**, *96*, 1398–
1258 1408, doi:10.1016/J.AGWAT.2009.04.021.
- 1259 115. Eldridge, D.J.; Wang, L.; Ruiz-Colmenero, M. Shrub encroachment alters the spatial
1260 patterns of infiltration. *Ecohydrology* **2015**, *8*, 83–93, doi:10.1002/ECO.1490.
- 1261 116. Geissler, K.; Hahn, C.; Joubert, D.; Blaum, N. Functional responses of the herbaceous
1262 plant community explain ecohydrological impacts of savanna shrub encroachment.
1263 *Perspect. Plant Ecol. Evol. Syst.* **2019**, *39*, 125458, doi:10.1016/J.PPEES.2019.125458.
- 1264 117. Marques, T. V.; Mendes, K.; Mutti, P.; Medeiros, S.; Silva, L.; Perez-Marin, A.M.;
1265 Campos, S.; Lúcio, P.S.; Lima, K.; dos Reis, J.; et al. Environmental and biophysical
1266 controls of evapotranspiration from Seasonally Dry Tropical Forests (Caatinga) in the
1267 Brazilian Semiarid. *Agric. For. Meteorol.* **2020**, *287*, 107957,
1268 doi:10.1016/J.AGRFORMET.2020.107957.
- 1269 118. Santos, C.A.C.; Mariano, D.A.; das Chagas A. do Nascimento, F.; Fabiane, F.R.; de
1270 Oliveira, G.; Silva, M.T.; da Silva, L.L.; da Silva, B.B.; Bezerra, B.G.; Safa, B.; et al.
1271 Spatio-temporal patterns of energy exchange and evapotranspiration during an intense
1272 drought for drylands in Brazil. *Int. J. Appl. Earth Obs. Geoinf.* **2020**, *85*, 101982,
1273 doi:10.1016/J.JAG.2019.101982.
- 1274 119. Lima, C.E.S. de; Costa, V.S. de O.; Galvíncio, J.D.; Silva, R.M. da; Santos, C.A.G.
1275 Assessment of automated evapotranspiration estimates obtained using the GP-SEBAL
1276 algorithm for dry forest vegetation (Caatinga) and agricultural areas in the Brazilian
1277 semiarid region. *Agric. Water Manag.* **2021**, *250*, 106863,
1278 doi:10.1016/J.AGWAT.2021.106863.
- 1279

CHAPTER 5

Genotypic differences relative photochemical activity, inorganic and organic solutes and yield performance in clones of the forage cactus under semi-arid environment

Abstract

Plants with the crassulacean acid metabolism commonly present good adaptation to arid and semi-arid environments, but it highly depends on the type of species. In this study, chlorophyll fluorescence, the concentration of inorganic and organic solutes and the productive performance were evaluated along with their relationships in different clones of the genera *Opuntia* and *Nopalea*. The experiment was conducted from 2016 to 2018. Four clones of genus *Opuntia* were evaluated: ‘Orelha de Elefante Mexicana’ (OEM), ‘Orelha de Elefante Africana’ (OEA), V19 and F8; and two clones of genus *Nopalea*: ‘IPA Sertânia’ and ‘Miúda’. The experiment was arranged in a randomised block design, with six treatments and three replications. The following parameters were measured when harvesting: initial, maximum and variable fluorescence; the quantum yield of PSII (Fv/Fm); light-induction curves of the photochemical parameters ($\Delta F/F_m'$, qP, NPQ and ETR); the chlorophyll and carotenoid content; carbohydrates; the sodium (Na⁺) and potassium (K⁺) content; morphometry; and dry matter accumulation. The values for the effective quantum yield of PSII ($\Delta F/F_m'$) and the alterations in photochemical quenching were higher in the OEM clone ($P < 0.05$). There was a difference between clones for non-photochemical quenching, with the F8 clone having the highest values. The Fv/Fm was 0.87 for the OEM. ‘IPA Sertânia’ obtained the greatest Chl *a/b*, and the highest values for carbohydrate concentration were found in the OEA clone. The OEM clone showed the greatest accumulation of K⁺, in addition to a higher cladode area index and greater dry matter accumulation. The results of this study show the high physiological tolerance of the forage cactus to a semi-arid environment, which varies according to the clone.

Keywords: *Opuntia*, *Nopalea*, Chlorophyll, Carbohydrates, Agronomic characteristics.

31 **1 Introduction**

32 The changes occurring in terrestrial systems for decades have promoted changes in
33 climate that offer a challenge to the agricultural sector for food production. These variations
34 in climate can cause the extinction and/or compromise the survival of species from different
35 ecosystems (Aragón-Gastélum et al., 2014). Abiotic factors, e.g. drought, salinity, solar
36 radiation and extreme temperature, limit the growth of various crops and cause physiological
37 damage by overpowering photosynthetic capacity (Al-Turki et al., 2014; Lima et al., 2018).

38 As such, a key factor in food security is the choice of species that have a high capacity
39 for adaptation to extreme climates and for survival in places where other species find
40 difficulty (Cabrera et al., 2016). In arid and semi-arid environments, particularly in the semi-
41 arid region of Brazil, the forage cactus (*Opuntia* spp. and *Nopalea* spp.) is used to produce
42 cladodes for animal feed in areas of high temperature and low water regime (Lina and Eloisa,
43 2018; Rocchetti et al., 2018), where, despite these climate conditions, the forage cactus
44 retains the nutritional constituents and productive capacity that are important for the herds
45 (Meza-Herrera et al., 2019; Jardim et al., 2021).

46 In general, plant response to environmental stress can be identified by measuring
47 changes in chemistry and production. Among the parameters of photochemical efficiency,
48 chlorophyll-*a* fluorescence, the maximum quantum yield of photosystem II (Fv/Fm) and
49 electron transport (ETR) are considered particularly robust and extremely reliable tools
50 (Bussotti et al., 2020; Ojeda-Pérez et al., 2017; Oliveira et al., 2020). Cacti show high
51 concentrations of chlorophyll and photoprotective pigments, contributing to their
52 development (Bussotti et al., 2020; Cabrera et al., 2016) and maximising their photosynthetic
53 activity (Drezner, 2020; Ojeda-Pérez et al., 2017). However, despite this marked efficiency,
54 excessive light can cause damage to the photosystem (He et al., 2019; Oliveira et al., 2020).

55 Plants with the crassulacean acid metabolism (CAM), e.g. cacti, usually have an
56 excellent response to high thermal amplitudes, but this is highly dependent on the type of
57 species and the growth environment, which may have different effects on the photosystem
58 (Ojeda-Pérez et al., 2017; Walker et al., 2011; Nobel et al., 1986; Chetti and Nobel, 1988;
59 Nobel and De la Barrera, 2003). Al-Turki et al. (2014) state that *Euphorbia fractiflexa*,
60 despite being a CAM species; shows a reduction in the maximum quantum yield of the

61 photosystem II (Fv/Fm) in areas of high temperature, as a result of stomatal closure, which
62 helps in the photoprotection of the photosystem II (PSII) by dissipating energy.

63 In clones of *Opuntia*, this tolerance is more marked than in other CAM species
64 (Ojeda-Pérez et al., 2017). In addition to elevated tolerance to abiotic stresses, cacti also
65 presents a high water-use efficiency—which is estimated by the amount of CO₂ fixed
66 compared to the volume of transpired water. It is estimated to be about three and six times
67 higher than C4 and C3 plants, respectively (Silva-Ortega et al., 2008; Borland et al., 2009;
68 Borland et al., 2015; Cushman et al., 2015). This characteristic present in CAM plants is
69 favourable for their survival, and for its higher dry matter yield under adverse conditions
70 compared to other species, mainly presented in arid and semi-arid regions (Borland et al.,
71 2009; Cushman et al., 2015). However, it is not clear which biochemical or productive
72 parameters are most relevant when evaluating the photochemical efficiency of forage cacti
73 in agricultural areas of semi-arid environments.

74 This study tested the hypothesis that maintaining the photochemical efficiency of
75 forage cactus clones under semi-arid stressful conditions could favour the yield performance.
76 Thus, parameters of chlorophyll fluorescence, concentration of inorganic and organic solutes
77 and productive performance were evaluated together with their relationships in different
78 fully-grown clones of genera *Opuntia* and *Nopalea* in a semi-arid environment.

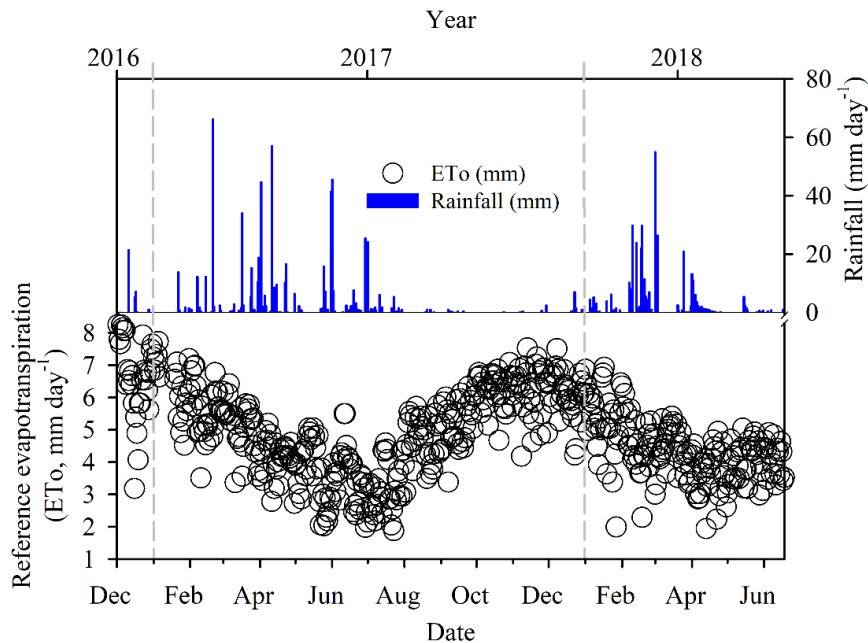
79

80 **2 Material and methods**

81 *2.1 Study area and species under evaluation*

82 The experiment was conducted from 2016 to 2018 at the Serra Talhada Academic
83 Unit of the Federal Rural University of Pernambuco, located in the municipality of Serra
84 Talhada, Pernambuco, Brazil (7°59' S, 38°15' W at 431 m a.s.l.). According to the Köppen
85 climate classification, the region has a semi-arid climate, type BSwH' (dry and hot with a
86 rainy season in the summer) (Alvares et al., 2013). The average rainfall is 642.1 mm year⁻¹,
87 with an average air temperature of 24.8 °C, relative humidity of 62.5% and atmospheric
88 demand greater than 1,800 mm year⁻¹ (Silva et al., 2015). During the experimental period,
89 the environmental conditions were monitored by an automatic weather station of the National
90 Institute of Meteorology, located 45 m away from the experimental field (Figure 1). The

91 reference evapotranspiration (ET_o) was calculated as per Penman-Monteith (Allen et al.,
 92 1998).
 93



94 **Figure 1.** Weather conditions in the municipality of Serra Talhada, Pernambuco, during the
 95 experimental period from 2016 to 2018.

96

97 The soil of the experimental area, of flat relief, was classified as a typical eutrophic
 98 Haplic Cambisol, with the following physical and chemical attributes measured at a depth of
 99 0.0–0.20 m: $\text{pH}_{(\text{water})} = 5.95$, electrical conductivity of the soil saturation extract = 0.32 dS
 100 m^{-1} , $\text{P}_{(\text{Mehlich-1})} = 168.96 \text{ mg dm}^{-3}$, $\text{K}^+ = 13.8 \text{ cmol}_c \text{ dm}^{-3}$, $\text{Na}^+ = 1.09 \text{ cmol}_c \text{ dm}^{-3}$; $\text{Ca}^{2+} = 3.45$
 101 $\text{cmol}_c \text{ dm}^{-3}$, $\text{Mg}^{2+} = 1.90 \text{ cmol}_c \text{ dm}^{-3}$, $\text{H+Al} = 0.6 \text{ cmol}_c \text{ dm}^{-3}$, sum of bases = 20.25 cmol_c
 102 dm^{-3} , cation exchange capacity = 20.85 $\text{cmol}_c \text{ dm}^{-3}$, base saturation = 97.15%; organic matter
 103 = 7.93 g kg^{-1} , organic carbon = 4.6 g kg^{-1} ; bulk density of 1.45 g cm^{-3} , sand = 828.6 g kg^{-1} ,
 104 silt = 148.25 g kg^{-1} , and clay = 23.15 g kg^{-1} . Before planting, the soil was prepared
 105 mechanically (ploughing and harrowing) and a total of 32.7 kg ha^{-1} NPK chemical fertiliser
 106 was applied (Jardim et al., 2020).

107 The forage cactus clones were planted in December 2016, inserting the basal cladodes
 108 up to 50% in the soil, in single rows, at a spacing of $1.2 \times 0.2 \text{ m}$, equal to a density of 41,667
 109 plants ha^{-1} . Four clones of genus *Opuntia* were used: ‘Orelha de Elefante Mexicana’ (OEM)

110 (*O. stricta* (Haw.) Haw.), ‘Orelha de Elefante Africana’ (OEA) (*O. undulata* Griffiths), V19
111 (*O. larreyi* F.A.C. Weber ex Coult.) and F8 (*O. atropes* Rose), and two clones of genus
112 *Nopalea*: ‘IPA Sertânia’ (IPA) (*N. cochenillifera* (L.) Salm-Dyck) and ‘Miúda’ (MIU) (*N.*
113 *cochenillifera* (L.) Salm-Dyck), all tolerant to the cochineal insect [*Dactylopius opuntiae*
114 (Cockerell, 1896)]. The experiment was arranged in a randomised block design, with six
115 treatments and three replications, where the treatments corresponded to the forage cactus
116 clones. Each plot comprised three rows of 15 plants of each clone, giving a total of 45 plants
117 per plot, distributed over an area of 3.60×3.0 m (10.8 m²).

118 Irrigation was carried out three times a week using a drip system with a uniformity
119 coefficient of 93% and a flow rate of 1.25 L h⁻¹ (working pressure: 100 kPa). The micro
120 drippers were spaced 0.4 m apart, providing water replacement based on 120% of the crop
121 evapotranspiration (ET_c) using the crop coefficient (K_c = 0.52) of the forage cactus (Queiroz
122 et al., 2016). The irrigation water had an electrical conductivity of 1.62 dS m⁻¹, and was
123 classified as C3, i.e. of high salinity (Richards, 1954), pH = 6.84, Na⁺ = 168.66 mg L⁻¹ and
124 K⁺ = 28.17 mg L⁻¹. The control of spontaneous plants and the cropping treatments included
125 manual weeding.

126

127 2.2 Measurement of chlorophyll fluorescence and accessory pigments

128 2.2.1 Chlorophyll fluorescence

129 Chlorophyll *a* (Chl *a*) fluorescence was measured 516 days after planting, between
130 09:00 and 12:00 h, using a portable pulse-modulated fluorometer (Mini-PAM II, Heinz Walz,
131 Effeltrich, Germany), in intermediate cladodes after a period of 50 min pre-adaptation to the
132 dark with the aid of support clips placed around the cladode. After the period of dark
133 adaptation, they were exposed to one flash at a photosynthetic photon flux density of 1600
134 $\mu\text{mol m}^{-2} \text{s}^{-1}$, giving the PSII parameters of initial (F_o), maximum (F_m) and variable
135 fluorescence (F_v), and maximum quantum yield (F_v/F_m).

136 For the rapid light-response curve, the cladodes were also adapted to the dark for a
137 period of 50 min and to photosynthetic photon flux densities (PPFD) of 0, 25, 45, 65, 90,
138 125, 190, 285, 420, 630, 820, 1150, 1500 $\mu\text{mol photons m}^{-2} \text{s}^{-1}$ at intervals of 20 s between
139 each PPFD, thereby obtaining the following parameters: the effective quantum yield of

140 photosystem II ($\Delta F/F_m'$), the photochemical quenching coefficient (qP), non-photochemical
141 quenching coefficient (NPQ), and the relative electron transport rate (ETR).

142

143 2.2.2 Chlorophyll and carotenoid content

144 Fresh cladodes harvested in the field were then identified and taken to the laboratory.
145 Two cross sections of approximately 2.0 cm thick each were performed in the centre of the
146 cladode. Samples were weighed on electronic balance for the chlorophyll analysis, as
147 described in more detail later. This also allowed the identification and the distribution of
148 epidermis structural tissues, i.e. upper epidermis—adaxial, lower epidermis—abaxial, and
149 also parenchymal cells (e.g. chlorenchyma and hydrenchyma in all-cell); which are
150 abundantly present on cladodes (in the inner part and including the cuticle layer) of cacti and
151 leaves of succulent plants, according to Scalisi et al. (2016) and Griffiths and Males (2017).
152 The chlorophyll (Chl) was extracted from a 0.2 g fresh weight (FW), removed from the
153 cladode, in contact with 5 mL 80% (v/v) acetone. The threaded test tubes were taken to a
154 refrigerated environment from 48 to 72 h, after that the levels of chlorophyll and carotenoids
155 (g kg^{-1}) were measured at absorbances of from 470 to 664 nm, and calculated using the
156 equations: Chlorophyll *a* (Chl *a*) = $[(12.21 \cdot A_{663}) - (2.81 \cdot A_{646})]$; Chlorophyll *b* (Chl *b*) =
157 $[(20.13 \cdot A_{646}) - (5.03 \cdot A_{663})]$; total Chlorophyll (total Chl) = $[(\text{Chl } a) + (\text{Chl } b)]$ and
158 Carotenoids (Car_{x+c}) = $[(1000 \cdot A_{470}) - (3.27 \cdot \text{Chl } a) - (104 \cdot \text{Chl } b)]/229$ (Lichtenthaler
159 and Wellburn, 1983).

160

161 2.3 Measurement of carbohydrates

162 In order to determine the total soluble carbohydrates, samples of 0.375 g of fresh
163 weight (FW) were collected from the central part of the cladodes (procedures for cross
164 section and tissue identification of fresh cladodes are described in detail according to the
165 section 2.2.2). The samples were then macerated in liquid nitrogen and homogenised with
166 1.5 mL of a 0.1 M potassium phosphate buffer solution (pH 7.0). The homogenate was then
167 centrifuged (Hettich, Mikro 220 R, DJB Labcare Ltd., Newport Pagnell, UK) at 12000 *g* for
168 15 minutes at 4 °C; the supernatant was then collected. The total soluble carbohydrates were
169 determined by the phenol-sulphuric acid method (Dubois et al., 1956), using D-(+)-glucose

170 (Sigma-Aldrich) as the standard. Absorbance readings were taken at 490 nm, and the results
171 expressed in $\mu\text{mol g}^{-1}$ FW.

172

173 *2.4 Levels of Sodium (Na^+) and potassium (K^+)*

174 The contents of Na^+ and K^+ were measured by flame photometry, as described by
175 Rodrigues et al. (2013). After oven-drying to determine the dry weight (DW), the cladode
176 tissue was ground in a Wiley knife-mill to obtain the flour, samples (20 mg) of which were
177 then submitted to extraction by incubating in test tubes with threaded caps containing 15 mL
178 ultra-pure water, and boiling in a water bath at 100 °C for 1 h. The extracts were filtered and
179 used for reading the Na^+ and K^+ in a flame photometer (Micronal, B462, São Paulo, Brazil).
180 The Na^+ and K^+ contents were estimated based on an NaCl and KCl standard curve
181 respectively (0 to 1000 μM), with the results expressed in $\mu\text{mol g}^{-1}$ DW.

182

183 *2.5 Morphometry and dry matter accumulation*

184 At the end of the clone cycle, morphometric variables of the cladodes (length, width
185 and perimeter) were measured with the aid of a tape (Jardim et al., 2020). These
186 measurements were used to calculate the cladode area index (CAI, $\text{m}^2 \text{m}^{-2}$) (Pinheiro et al.,
187 2015; Silva et al., 2014). The fresh weight of the plants (FW) was obtained using an electronic
188 balance. The complete working experimental plot was weighed, and the yield expressed in
189 kg plant^{-1} . The material was then placed in a forced air circulation oven at 55 °C to constant
190 weight to determine the dry matter (DM) of the forage cactus clones, expressed in kg DM
191 plant^{-1} .

192

193 *2.6 Statistical analysis*

194 The Shapiro-Wilk test for normality and Bartlett's test of homogeneity were applied
195 to the data and later to the analysis of variance (ANOVA). To determine possible differences
196 among the photochemical parameters (i.e., $\Delta\text{F}/\text{F}_m'$, qP, NPQ and ETR) of the clones
197 responding to photosynthetic photon flux densities, a ANOVA ($P < 0.05$) test was used. The
198 data were expressed by the mean and standard deviation for each treatment ($n = 3$). When
199 differences were detected by ANOVA, the mean values were compared by the Scott-Knott
200 test at a level of 0.05 probability ($P < 0.05$). The principal component analysis (PCA) was

201 carried out to detect the associations and correlations between the measured variables, and to
202 identify the most important factors in the productive performance of the six clones. Once the
203 data set was standardised to eliminate the influence of dimensions, and the principal
204 components were selected based on those with eigenvalues (λ) greater than 1.0 (Kaiser,
205 1960). All the analyses were carried out with the aid of the R software (R Core Team, 2020).

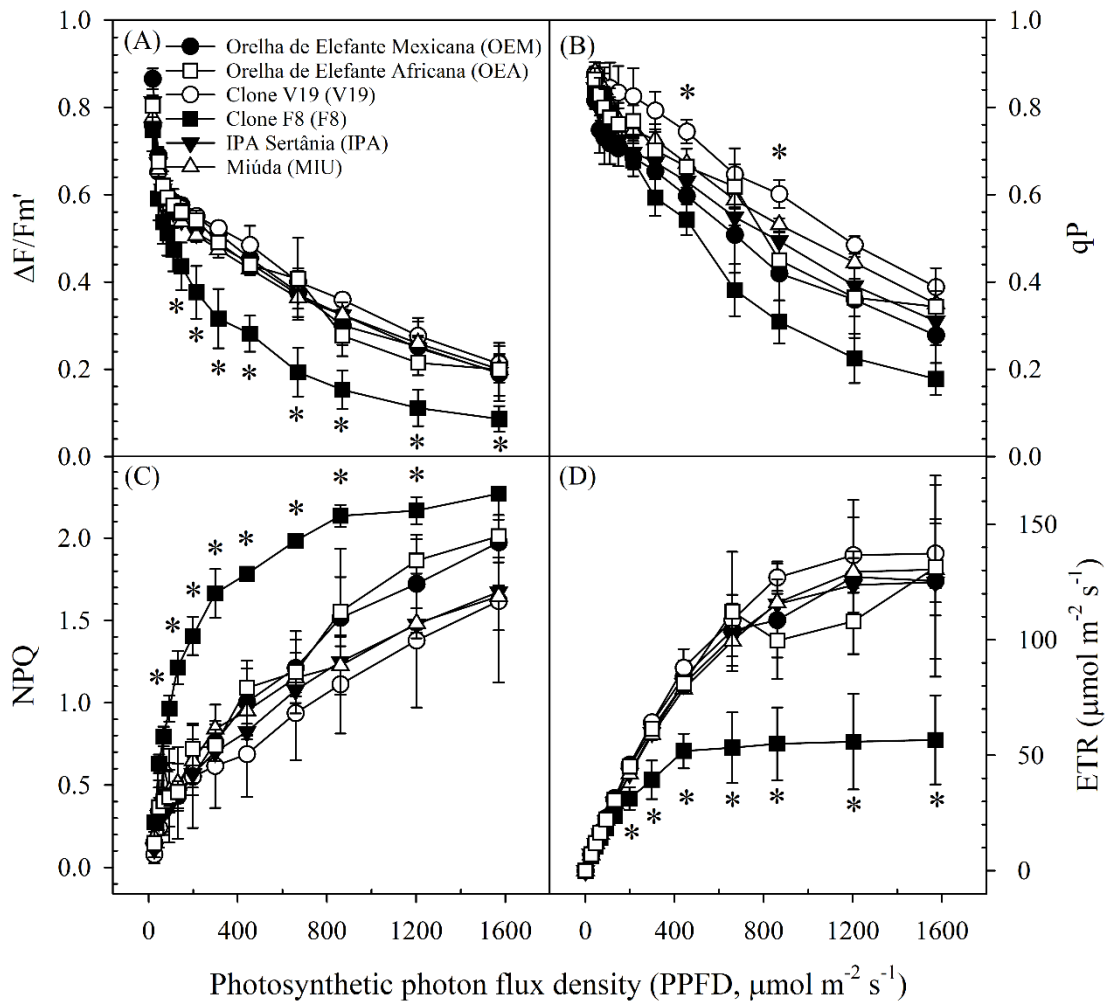
206

207 **3 Results**

208 *3.1 Measurement of the parameters of chlorophyll fluorescence*

209 Values for the effective quantum yield of photosystem II ($\Delta F/F_m'$) were higher at the
210 beginning of the analysis. All the clones have also been shown a decrease of $\Delta F/F_m'$ as the
211 photosynthetic photon flux density (PPFD) increased. At 1600 PPFD, the F8 clone displayed
212 less quantum efficiency ($P < 0.05$), approximately 43% of the mean $\Delta F/F_m'$ of the other
213 clones (Figure 2A). As shown in Figure 2A, clearly the greatest changes in $\Delta F/F_m'$ were
214 noticeable at 200 PPFD.

215



216 **Figure 2.** Induction curve of photochemical parameters in response to photosynthetic photon
 217 flux density (PPFD) in forage cactus clones irrigated with saline water in the semi-arid region
 218 of Brazil. (A) effective quantum yield of photosystem II ($\Delta F/F_m'$), (B) photochemical
 219 quenching (qP), (C) non-photochemical quenching (NPQ), and (D) relative electron transport
 220 rate (ETR, $\mu\text{mol m}^{-2} \text{s}^{-1}$) subjected to maximum light fluorescence. Data are presented as
 221 mean \pm standard deviation ($n = 3$). (*) Asterisks indicate significant differences among cacti
 222 at each value of PPFD ($P < 0.05$; ANOVA test). Data obtained between 09:00 and 12:00 h
 223 from different cladodes under steady state conditions, i.e. constant light intensity.

224

225 The trend for the changes in photochemical quenching (qP) (Figure 2B) were similar
 226 to the results for $\Delta F/F_m'$, with lower magnitudes at the higher PPFD, and differences between
 227 clones ($P < 0.05$). However, these variations were more marked from $600 \mu\text{mol m}^{-2} \text{s}^{-1}$,

228 demonstrating the stress suffered by the clones with the increase in light density. The ‘Orelha
 229 de Elefante Mexicana’, ‘Orelha de Elefante Africana’, V19, ‘IPA Sertânia’ and ‘Miúda’
 230 clones showed the greatest activity at the reaction centre, with F8 being 53% lower than the
 231 other clones, but displaying no significant difference ($P > 0.05$).

232 There was a significant difference between clones for non-photochemical quenching
 233 (NPQ) (Figure 2C) from the application of $100 \mu\text{mol m}^{-2} \text{s}^{-1}$ PPFD. Clone F8 had the highest
 234 NPQ values, indicating excessive heat dissipation in photosystem II due to the abiotic stress
 235 of the environment. Despite being a clone of genus *Opuntia*, F8 shows inferior performance
 236 to the other clones of the same genus ($P < 0.05$). The ‘Orelha de Elefante Mexicana’ and
 237 ‘Orelha de Elefante Africana’ clones showed similar NPQ values ($P > 0.05$), presumably, for
 238 they both have the same nuclear genome, as well as they are species included in the same
 239 genus i.e. *Opuntia*.

240 The relative electron transport rate (ETR) was different between clones from a PPFD
 241 of $200 \mu\text{mol m}^{-2} \text{s}^{-1}$ (Figure 2D). Above $400 \mu\text{mol m}^{-2} \text{s}^{-1}$, a significant difference was only
 242 found in clone F8 ($P < 0.05$), which at $1600 \mu\text{mol m}^{-2} \text{s}^{-1}$ reached a 44% reduction in ETR
 243 compared to the other clones ($P < 0.05$).

244 There was no effect from genus on the darkness-dependent parameters for initial
 245 fluorescence (F_o) ($P < 0.05$). However, for maximum fluorescence (F_m) and variable
 246 fluorescence (F_v), the F8 and V19 clones were less efficient, around 24% and 30%
 247 respectively in relation to the other clones (Table 1). Values for the maximum quantum yield
 248 of photosystem II (F_v/F_m) were higher in the ‘Orelha de Elefante Mexicana’ clone ($P <$
 249 0.05), at 0.87. On the other hand, clones V19, F8 and ‘Miúda’ showed 12% less efficiency
 250 than the ‘Orelha de Elefante Mexicana’ clone (Table 1).

251

252 **Table 1.** The photochemical parameters of initial (F_o), maximum (F_m) and variable (F_v)
 253 fluorescence, and maximum quantum yield of photosystem II (F_v/F_m) in forage cactus clones
 254 in a semi-arid environment.

Clones	F_o	F_m	F_v	F_v/F_m
‘Orelha de Elefante Mexicana’	293.33a	2180.67a	1887.33a	0.87a
‘Orelha de Elefante Africana’	368.00a	1866.33a	1498.33a	0.80b
V19	336.67a	1396.33b	1059.67b	0.76c

F8	410.00a	1661.00b	1251.00b	0.75c
‘IPA Sertânia’	391.67a	2093.00a	1701.33a	0.81b
‘Miúda’	428.00a	1909.00a	1481.00a	0.78c

Mean values followed by the same letters in a column do not differ statistically by Scott-Knott, at a level of 0.05 ($P < 0.05$).

255

256 3.2 Chlorophyll and carotenoid content of the cladodes

257 The photosynthetic and photoprotective pigments of the clones showed differences in
 258 relation to the genera of the cacti (Table 2). The concentrations of chlorophyll *a* (Chl *a*),
 259 chlorophyll *b* (Chl *b*) and total chlorophyll (total Chl) were higher in the ‘Orelha de Elefante
 260 Mexicana’ and V19 clones. The Chl *a/b* ratio also displayed differences between clones
 261 (Table 2). The ‘IPA Sertânia’ clone had the highest Chl *a/b* ratio ($P < 0.05$), 32% greater than
 262 the ‘Orelha de Elefante Africana’ and F8, and 51% greater than the ‘Orelha de Elefante
 263 Mexicana’, V19 and ‘Miúda’. There was no significant difference in the carotenoid
 264 concentration (Car_{x+c}) of the clones.

265

266 **Table 2.** Chlorophyll content (Chl *a*, Chl *b* and total Chl), the Chl *a/b* ratio and carotenoid
 267 content (Car_{x+c}) ($g\ kg^{-1}$) in forage cactus clones in a semi-arid environment.

Clones	Chl <i>a</i>	Chl <i>b</i>	Total Chl	Chl <i>a/b</i>	Car_{x+c}
‘Orelha de Elefante Mexicana’	0.0563a	0.0177a	0.0740a	3.3063c	0.0237a
‘Orelha de Elefante Africana’	0.0399b	0.0104b	0.0503b	3.8501b	0.0191a
V19	0.0498a	0.0216a	0.0715a	2.3092c	0.0183a
F8	0.0381b	0.0086b	0.0467b	4.1647b	0.0188a
‘IPA Sertânia’	0.0422b	0.0073b	0.0495b	5.8642a	0.0186a
‘Miúda’	0.0384b	0.0132b	0.0516b	2.9759c	0.0178a

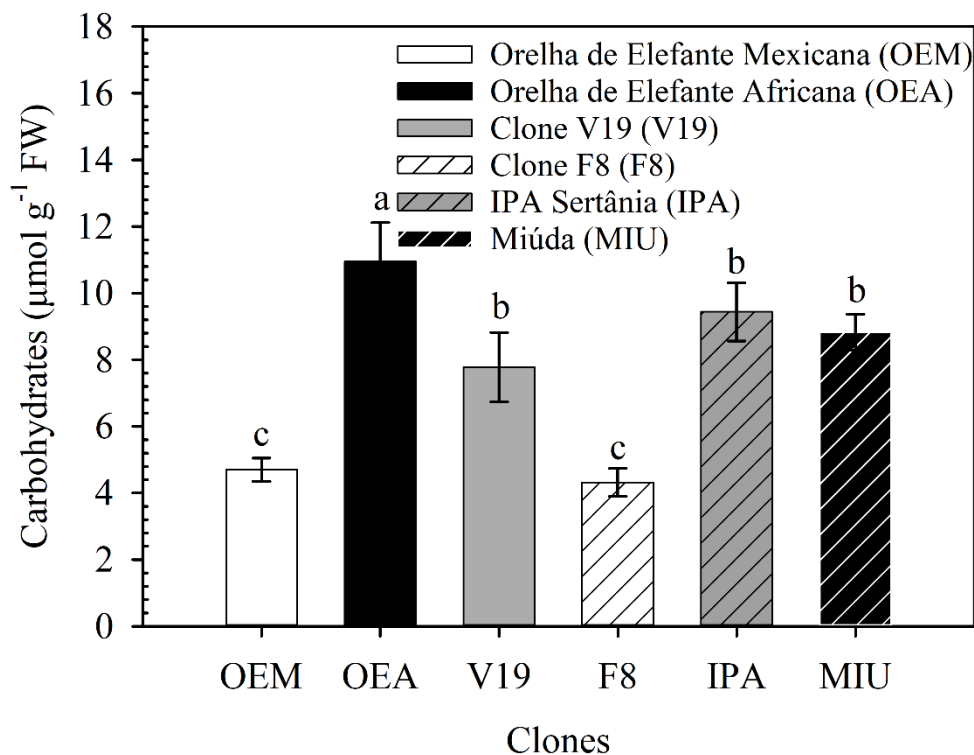
268 Mean values followed by the same letters in a column do not differ statistically by Scott-
 269 Knott, at a level of 0.05 ($P < 0.05$).

270

271 3.3 Carbohydrate content

272 There was a significant difference in carbohydrate concentration between clones, with
 273 the highest values found in the ‘Orelha de Elefante Africana’ clone (Figure 3), on average,

274 59% greater than in the ‘Orelha de Elefante Mexicana’ and F8 clones with the lowest
 275 concentration of carbohydrates.
 276



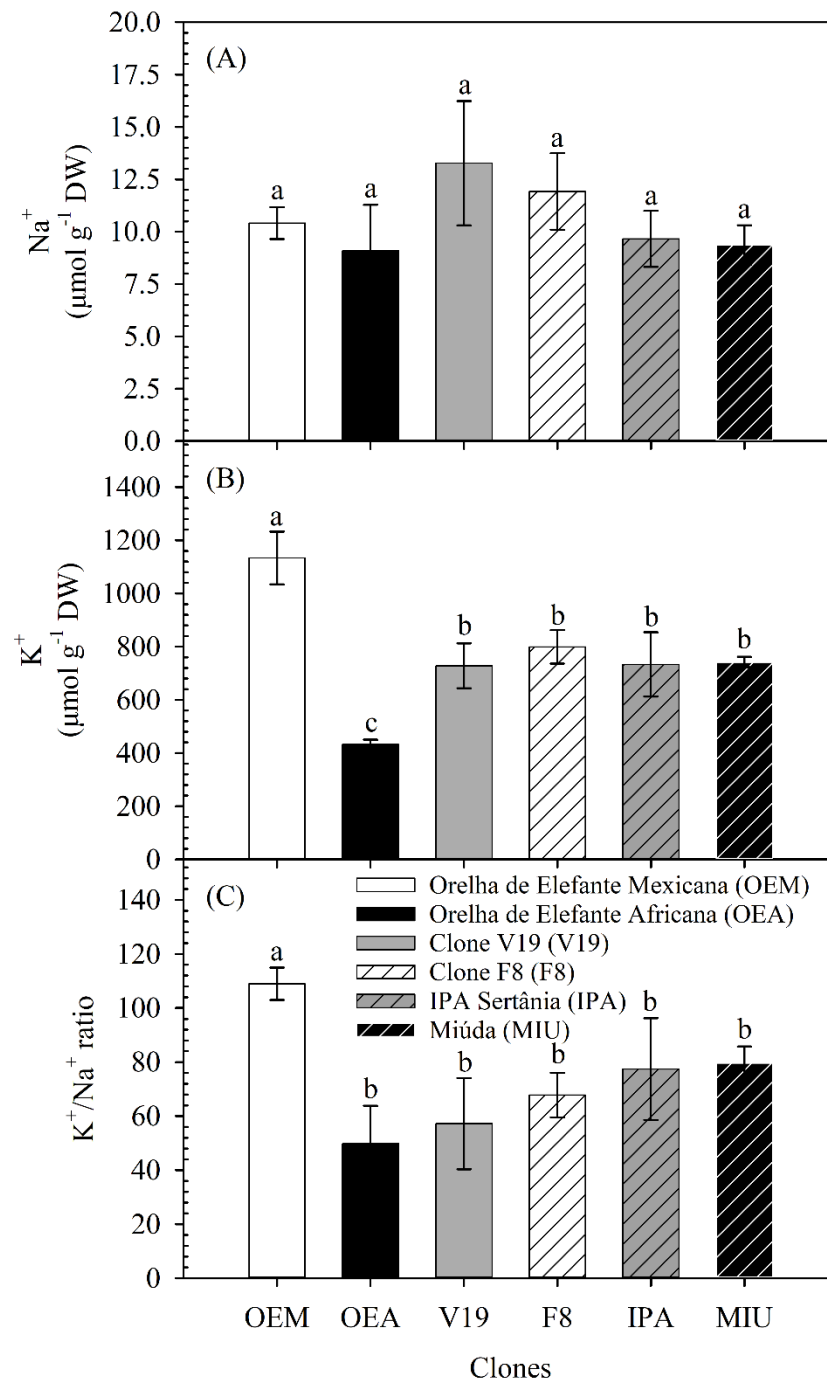
277 **Figure 3.** Total soluble carbohydrates in the cladodes of forage cactus clones irrigated with
 278 saline water in the semi-arid region of Brazil. Data are presented as mean ± standard
 279 deviation ($n = 3$). Mean values followed by the same letter do not differ statistically by Scott-
 280 Knott test at a level of 0.05 ($P < 0.05$).

281

282 3.4. Na^+ and K^+ concentration

283 The clones, regardless of genus, showed no difference ($P > 0.05$) in the sodium (Na^+)
 284 content of the cladode tissue (Figure 4A). Whereas the concentrations of potassium (K^+)
 285 displayed high values and a significant difference ($P < 0.05$) (Figure 4B). The ‘Orelha de
 286 Elefante Mexicana’ clone had the greatest accumulation of K^+ , being on average 66% higher
 287 than the V19, F8, ‘IPA Sertânia’ and ‘Miúda’ clones. The lowest concentrations of K^+ were
 288 seen in the ‘Orelha de Elefante Africana’ clone ($P < 0.05$), of $432.09 \mu\text{mol g}^{-1} \text{ DW}$, 62%
 289 lower than in the ‘Orelha de Elefante Mexicana’. Due to the significant variations in Na^+ and

290 K^+ content, the K^+/Na^+ ratio in the cladodes was much higher in the ‘Orelha de Elefante
 291 Mexicana’ in relation to the other clones ($P < 0.05$) (Figure 4C). On average, Na^+ and K^+
 292 levels in the ‘Orelha de Elefante Mexicana’ forage cactus were 39% higher than in the other
 293 clones.
 294



295 **Figure 4.** Na⁺ and K⁺ content, and the K⁺/Na⁺ ratio (A, B and C, respectively) in the cladodes
 296 of forage cactus clones irrigated with saline water in the semi-arid region of Brazil. Data are
 297 presented as mean ± standard deviation (*n* = 3). Mean values followed by the same letter do
 298 not differ statistically by Scott-Knott test at a level of 0.05 (*P* < 0.05).

299

300 3.5 Morphometry and dry matter accumulation

301 The morphometric and yield characteristics of the six clones are shown in Table 3.
 302 There was a significant difference for both the cladode area index (CAI) and cladode yield
 303 between the cacti (*P* < 0.05). The ‘Orelha de Elefante Mexicana’ and ‘Orelha de Elefante
 304 Africana’ clones had the greatest CAI, achieving 90% more than the F8 and ‘IPA Sertânia’
 305 clones. For dry matter accumulation, the ‘Orelha de Elefante Mexicana’ was 34% more
 306 productive than V19, ‘IPA Sertânia’ or ‘Miúda’, with a yield that was 54% greater than the
 307 F8 and ‘Orelha de Elefante Africana’ clones.

308

309 **Table 3.** Morphometry and dry matter production in forage cactus clones.

Clones	CAI (m ² m ⁻²)	Yield (kg DM plant ⁻¹)
‘Orelha de Elefante Mexicana’	0.9163a	0.5530a
‘Orelha de Elefante Africana’	1.0759a	0.2830c
V19	0.3163b	0.3794b
F8	0.1062c	0.2241c
‘IPA Sertânia’	0.0996c	0.3415b
‘Miúda’	0.3037b	0.3777b

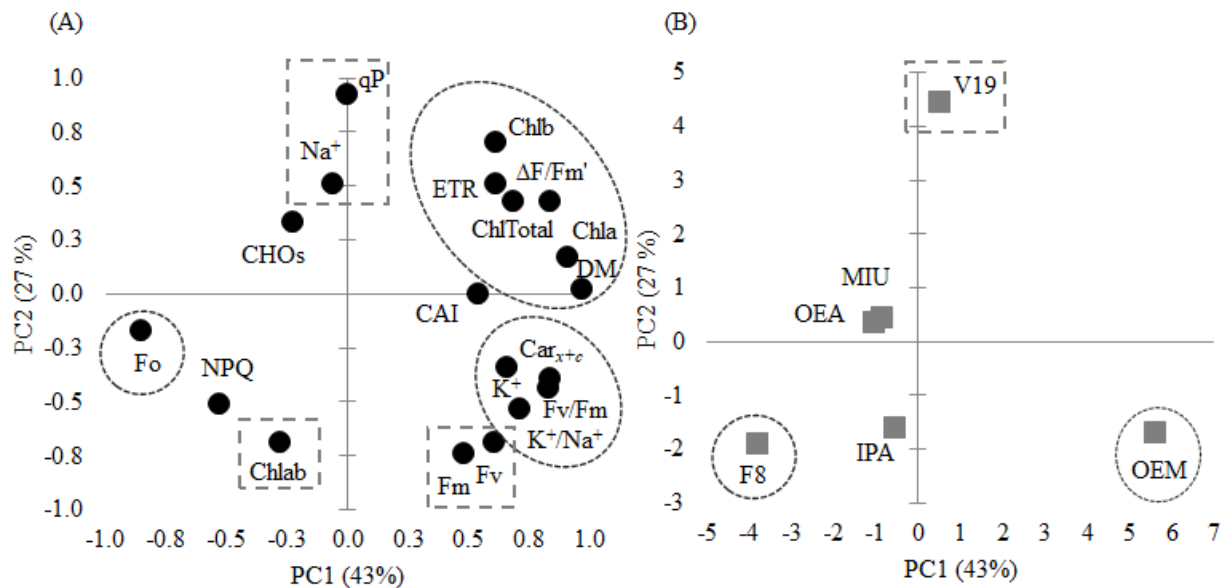
310 Mean values followed by the same letters in a column do not differ statistically by Scott-
 311 Knott, at a level of 0.05 (*P* < 0.05).

312

313 3.6 Association between variables with principal component analysis

314 In Figure 5, the principal component analysis between the variables under analysis
 315 showed that two principal components (PC) were enough to explain 70% of the total variation
 316 of the data. PC1 explained 43%, showing a negative correlation between dry matter (DM)
 317 production and initial fluorescence (Fo), and a positive correlation with the maximum
 318 quantum yield of photosystem II (Fv/Fm), effective quantum yield of photosystem II

319 ($\Delta F/Fm'$), relative electron transport rate (ETR), chlorophyll content (Chl *a*, Chl *b*, and total
 320 Chl), carotenoids (Car_{x+c}), K^+ content, and the K^+/Na^+ ratio (Figure 5A). The positive weights
 321 of this component had a greater association with the 'Orelha de Elefante Mexicana' and were
 322 inversely related to F8 (Figure 5B), indicating that, respectively, these variables explain the
 323 best and worst productive performance of these clones. PC2 explained 27% of the total
 324 variation in data, with a negative correlation with Chl *a/b*, Fv and Fm, and a positive
 325 correlation with the Na^+ content and photochemical quenching (qP). V19 showed a positive
 326 association with the Na^+ content and qP, and a negative association with Chl *a/b*, Fv and Fm
 327 (Figure 5A and B).
 328



329 **Figure 5.** Principal component analysis (PCA) between the photochemical parameters initial
 330 (F_o), maximum (F_m) and variable (F_v) fluorescence; the maximum quantum yield of
 331 photosystem II (F_v/F_m); effective quantum yield of photosystem II ($\Delta F/Fm'$); photochemical
 332 quenching (qP); non-photochemical quenching (NPQ); relative electron transport rate (ETR,
 333 $\mu\text{mol m}^{-2} \text{s}^{-1}$); chlorophyll content (Chl *a*, Chl *b* and total Chl) and the Chl *a/b* ratio;
 334 carotenoids (Car_{x+c}); total soluble carbohydrate content (CHO_s); Na^+ and K^+ content, and the
 335 K^+/Na^+ ratio; cladode area index (CAI); and dry matter (DM) production in forage cactus
 336 clones grown in a semi-arid environment. Note: PC - principal component; circles and
 337 rectangles show parameter groupings. The (A) panel shows the loadings for each factor, and

338 the (B) panel shows the distribution of forage cactus clones scores in the PCA in the
339 ordination. See section 2.1 for abbreviations of clone's names.

340

341 **4 Discussion**

342 Stressful environmental factors, e.g. drought, excessive solar radiation and
343 temperature, are responsible for changes in energy transfer in different species. As an
344 alternative to the harmful effects, the mechanisms of photoacclimation, whether
345 morphological or physiological, are activated so that there is no damage to the photosynthetic
346 system of species, especially to photosystem II (PSII) (He et al., 2019). The greatest changes
347 in $\Delta F/F_m'$, with sharper reductions as seen in the present results, confirm that tensions from
348 environmental factors express as stress in the plants, thereby dissipating more energy
349 (Makonya et al., 2019). The value of qP shows the portion of photosynthetic electrons
350 transferred after the pigment in the antenna of the reaction centre absorbs radiated light,
351 reflecting the opening of the photosystem II reaction centre. This dissipated energy shows
352 the ability of the plant to release more electrons from the PSII quinone receptor, resulting in
353 greater ATP and NADPH consumption. Generally, losses that occur in the photochemical
354 activity of the species are correlated with a reduction in stomatal conductance, restricting the
355 flow of CO₂ in the cells. In cactaceous species, e.g. *Opuntia streptacantha*, Ojeda-Pérez et
356 al. (2017) report up to 50% impairment of photochemical parameters and a reduction in the
357 consumption of malic acid when the plants are exposed to extreme temperatures (4 °C and
358 40 °C). The inhibition of $\Delta F/F_m'$ and qP (see Figure 2) support degradation of the
359 chlorophylls, promoting abnormality in photosynthetic capacity (Zhang and Liu, 2018).

360 The high fluorescence values for non-photochemical quenching (NPQ) reflect the
361 photoprotective action of the plants, which increases continuously during exposure to high
362 light density, favouring oxidative protection over the singlet oxygen generated in the
363 chlorophyll. In hostile environments, an increase in NPQ is an alternative for energy
364 dissipation linked to the xanthophyll cycle; although cacti show excellent adaptation to these
365 ecosystems, especially genus *Opuntia* to the large thermal amplitudes of day and night, they
366 compromise energy efficiency and CO₂ fixation (Ojeda-Pérez et al., 2017), as seen in the
367 present results (Figure 2C). In PSII, NPQ limits the excessive transport of electrons in the
368 region of photosystem I (PSI) via linear electron flow.

369 Despite their photochemical efficiency being compromised, cacti are able to maintain
370 photosynthetic activity. Cacti have specialised anatomical and physiological structures (e.g.
371 storage tissues, fast-growing roots, controlled transpiration and nocturnal CO₂ uptake), which
372 are crucial for survival and longevity in environments unfavourable to maintaining the water
373 status (Lina and Eloisa, 2018). Such photochemical changes in cacti of the genera under study
374 and among other species in environments under environmental stress have also been reported
375 in the literature. Water and temperature restrictions inhibit CO₂ uptake, closing the stomata
376 and reducing the thickness of the leaf structures (Aragón-Gastélum et al., 2014; Ojeda-Pérez
377 et al., 2017).

378 In succulent species of families Cactaceae and Agavaceae, low levels of ETR and
379 high levels of NPQ have been reported as factors of species plasticity in arid and semi-arid
380 environments that contribute to a tolerance of adverse factors, despite a reduction in
381 photosynthetic performance. ETR is involved in the transport of electrons to PSII, and NPQ
382 is involved in dissipating stressful levels of energy (Aragón-Gastélum et al., 2020, 2014).
383 For Aragón-Gastélum et al. (2014), the high temperatures also resulted in significant costly
384 changes in the electron transport rate in cacti.

385 Parameters of chlorophyll fluorescence, i.e. Fo, Fm, Fv and Fv/Fm, are commonly
386 used as indicators of plant sensitivity. For example, under normal conditions, Fv/Fm ranges
387 between 0.80 and 0.83 (Maxwell and Johnson, 2000); values of less than 0.80 indicate the
388 presence of stress to the plant (Aragón-Gastélum et al., 2014). Interestingly, two *Opuntia*
389 clones (V19 and F8) and one *Nopalea* clone ('Miúda') were the most affected. These
390 photochemical changes between the species *Nopalea cochenillifera* (Adams et al., 1989) and
391 *Opuntia basilaris* were investigated by Adams et al. (1987), who found significant changes
392 in solar-energy dissipation, corroborating the present results. However, these changes can be
393 found in species with another type of metabolism, i.e. in genotypes of *Cicer arietinum* (L.),
394 type C3, as reported by Makonya et al. (2019).

395 Despite being considered plants adapted to stressful conditions, changes in
396 photoinhibition can be seen in CAM (crassulacean acid metabolism) plants (see Table 1), as
397 well as in optional CAM species (i.e. C4/CAM metabolism), which, despite showing
398 metabolic plasticity, present reductions in photochemical yield when submitted to water
399 restrictions and high light intensity. These not-so-marked losses are caused by

400 photoprotective pigments, i.e. anthocyanins, which help to protect the photosynthetic
401 apparatus (Li et al., 2015). Working with *Opuntia streptacantha*, Ojeda-Pérez et al. (2017)
402 reported F_o and F_v/F_m similar to the present study; however, from the 10th day of exposure
403 to temperatures of 40 °C, the value for F_o was greater than 400, indicating a decline in
404 photosynthetic efficiency.

405 Cactus cladodes are rich in photosynthetic and photoprotective pigments, such as
406 chlorophylls and carotenoids, respectively, but also pigments such as betaxanthin and
407 betalains. These phenolic compounds contribute to the antioxidant capacity of the plants and
408 the production of protective enzymes (Kharrat et al., 2018). In cacti, due to the high presence
409 of chlorophylls in the region of the chloroplast, the production and regeneration of NADPH
410 remains efficient, even when subjected to high temperatures, favouring the photosynthetic
411 capacity and protecting from oxidative damage (Hara et al., 1997). Antioxidant functions in
412 the cactus can vary between *Opuntia* and *Nopalea* and within each species (Alves et al.,
413 2017).

414 Chl *a*, Chl *b*, total Chl and the Chl *a/b* ratio varied between clones; this did not occur
415 with the carotenoids (Table 2). These results are similar to those reported by Falcão et al.
416 (2013), in which the ‘Orelha de Elefante Mexicana’ displayed higher levels of Chl *a* than did
417 clone F8, while there was no difference in Chl *b* or the carotenoids ($P > 0.05$). Furthermore,
418 according to those authors, the levels of photosynthetic pigments in the cladodes may vary
419 according to the time of year. In *Nopalea cochenillifera* submitted to treatments with doses
420 of chromium, Adki et al. (2013) noted that, compared to the control treatment, the total
421 chlorophyll content was maintained in the plant tissue. Analysing seven clones of *Nopalea*
422 and *Opuntia*, Alves et al. (2017) found differences in the photoprotective pigments and
423 antioxidant capacity; however, during periods of greater water availability, clone V19
424 displayed lower concentrations of antioxidant compounds.

425 The Chl *a/b* ratio is positively related to the ability of the plants to intercept light
426 (Chen et al., 2019), with the marked green of the cladodes being the particular result of Chl
427 *a* (Cabrera et al., 2016), which is mainly responsible for the photochemical reaction, even
428 when the cladodes are undergoing post-harvest processing. The concentrations of Chl *a*, Chl
429 *b* and total Chl are high, and degradation occurs gradually throughout the storage process due
430 to enzyme activity (Guevara et al., 2003). It is worth noting that the chlorophyll content of

431 both the vegetative and reproductive structures is reduced during the ripening process
432 (Walker et al., 2011). Cayupán et al. (2011) reported changes in the colour of the pulp and
433 peel of the plant material, mainly due to changes in the Chl *a*, Chl *b* and total Chl content,
434 and the levels of pigments such as betalains, with the Chl *b* concentration being generally
435 more marked, which is different to the present study employing cladodes.

436 In clones of *Opuntia*, the high concentration of Chl *a* and total Chl promote an
437 improvement in PEPC (phosphoenolpyruvate carboxylase) activity, helping to fix CO₂ and
438 favouring the production of soluble sugars, which are not used exclusively for biomass
439 production, but to maintain the metabolic requirements of the plants (Falcão et al., 2013). In
440 this type of plant, because it uses CAM, the PEPC enzyme plays a key role in photosynthetic
441 metabolism, at high concentrations catalysing oxaloacetate and producing metabolic energy
442 (Walker et al., 2011). Above all, this metabolic energy is more efficient when the cladodes
443 are able to intercept photosynthetically active radiation, aiding in the production of a
444 substrate for photosynthesis; an efficiency that can be compromised even in sunny
445 environments due to the overlap between cladodes and to the plant architecture resulting in
446 photoinhibition (Drezner, 2020).

447 Carbohydrates are constituents found in most foods. In cacti the main carbohydrates
448 are sugars i.e. glucose and fruits (De Santiago et al., 2018). Clones of genus *Nopalea* have
449 higher concentrations of carbohydrates than do clones of genus *Opuntia*. However, in the
450 present study, some clones showed a high concentration of carbohydrates (Figure 3).
451 Carbohydrates in significant concentrations can be found in cactus species (Krümpel et al.,
452 2020), where they act as precursors of secondary metabolites (Falcão et al., 2013). *Nopalea*
453 clones have higher levels of non-fibrous carbohydrates, which is important for lamb diets,
454 aiding food intake, energy gain and digestive processes in the rumen (Cardoso et al., 2019).
455 Diaz-Vela et al. (2013) reported high levels of carbohydrates and antioxidant agent in
456 *Opuntia* clones.

457 Plant species tend to accumulate low-molecular-weight carbohydrates in order to
458 survive under hostile conditions. These compounds play a fundamental role in reducing
459 osmotic potential, helping to maintain the water status of the cells and reducing the
460 production of reactive oxygen species (Ahanger and Agarwal, 2017). Due to the
461 photochemical efficiency of the *Opuntia* clones (e.g., ‘Orelha de Elefante Mexicana’, IPA-

462 20 and F8), enzyme capacity and the regeneration of Rubisco (Ribulose-1,5-bisphosphate
463 carboxylase/oxygenase) are factors that favour the synthesis of secondary compounds and
464 the production of carbohydrates; these are more marked in the ‘Orelha de Elefante Mexicana’
465 among the three clones mentioned above, and aid resistance to abiotic agents (Falcão et al.,
466 2013).

467 Among the essential nutrients, potassium has a crucial regulatory function in the
468 metabolic process of plants, as an aid to the water absorption capacity and in controlling
469 stomatal opening and closing, promoting defence mechanisms against stress (Chakraborty et
470 al., 2016). Despite not being considered an essential nutrient for most plants, Na⁺ at low
471 concentrations has an osmotic function in the vacuole, since in agricultural areas with low
472 K⁺ availability, cation exchange occurs due to the affinity of the substrate during molecular
473 synthesis (White, 2013). Among the minerals present in the forage cactus, K⁺ is considered
474 to have the highest concentration (Dick et al., 2020; Galizzi et al., 2004). At high levels in
475 the plant, it helps in the firmness of its constituent parts, aiding in the formation of protein
476 compounds and favouring photosynthesis (Galizzi et al., 2004). Dick et al. (2020) also found
477 high concentrations of K⁺ compared to Na⁺ in cladodes of *Opuntia*, with levels of K⁺ four
478 times higher than those of Na⁺, characterising it as the most abundant mineral in the forage
479 cactus. These higher concentrations of K⁺ and negligible levels of Na⁺ were also highlighted
480 by Méndez et al. (2015) in *Opuntia* clones (*O. dillenii* and *O. ficus-indica*). The present
481 results corroborate earlier studies, and emphasise the affinity of forage cactus clones to the
482 mineral K⁺ (Figure 4).

483 The differences seen in Na⁺ and K⁺ content between clones showed that the ‘Orelha
484 de Elefante Mexicana’ had the highest K⁺/Na⁺ ratio (Figure 4C). These results demonstrate
485 its greater capacity for reducing Na⁺ accumulation in the cladodes as well as its greater
486 efficiency in K⁺ uptake, which could be attenuate the toxic effects of Na⁺ excess in the tissue
487 favouring cell ionic homeostasis. From the higher K⁺ amount relative to Na⁺ content
488 presented in the tissues in all clones here evaluated (see Figure 4B and A, respectively)
489 resulting in an elevated K⁺/Na⁺ ratio, the results suggest a relatively higher selectivity for K⁺
490 over Na⁺ in this genotype. The K⁺ content in the plant cell cytosol is estimated to be relatively
491 higher than the Na⁺ content, leading to an elevated K⁺/Na⁺ ratio, which is necessary to the
492 cell physiological functions (Wang et al., 2020).

493 Environment disturbances that affect the K^+/Na^+ ratio may change the cell ionic
494 balance and affect several biochemical and physiological processes key to plant growth and
495 yield. The results found in this study, showed that clones presented elevated K^+ uptake along
496 with an adequate allocation of this ion in the cladodes. And it is a characteristic that
497 contributes to resistance to water deficit under semi-arid areas. It is also an important
498 physiological characteristic even for the xerophytes succulents species, in which the increase
499 in Na^+ content relative to K^+ also may change cell ionic homeostasis (Wang et al., 2004;
500 Tang et al., 2015; Pan et al., 2016; Cui et al., 2019; Wang et al., 2020). This feature affords
501 the clone greater adaptability. It is evident that there is a high concentration of K^+ in the
502 tissues of the forage cactus (Figure 4B) influenced by the availability of the nutrient in the
503 soil and by the time of year, favouring the production of proteins when assimilated (Krümpel
504 et al., 2020).

505 In the present study, despite the low electrical conductivity of the soil saturation
506 extract, the cumulative effect of the salts found in the irrigation water may promote an
507 increase in the Na^+ of the soil-plant system. In a clone of *Nopalea cochenillifera*, the
508 highlighted presence of sodium in the soil caused changes in the morphometric
509 characteristics and a reduction in plant yield, especially in young cladodes, indicating a lower
510 tolerance to excess salt compared to others clones in this study (Freire et al., 2018).
511 Interestingly, *Opuntia* clones are less sensitive when grown in environments that have a
512 higher concentration of salts in the soil (Bañuelos et al., 2012).

513 Results indicate that supply of salts found in the plant tissue together with the
514 environmental conditions caused intrinsic changes in the morphology and yield of the cacti
515 (Table 3). Plant morphology undergoes changes when faced with exposure to established
516 conditions; the cactus is characteristic for its tortuous canopy structure, which results in
517 changes in light interception in order to overcome the conditions of stress and guarantee
518 survival (Adli et al., 2019; Pinheiro et al., 2015). It is reported in the literature that the ‘Orelha
519 de Elefante Mexicana’ has significant forage yield as well as being morphologically superior,
520 since the position of the cladodes makes the plant more efficient in using photoassimilates,
521 promoting more advantageous performance (Silva et al., 2015). Adli et al. (2019) found that
522 in clones of *Opuntia ficus-indica* under arid and semi-arid conditions, the environment has a
523 strong effect on the morphometric variables of the cacti, e.g. the width and length of the

524 cladodes, influencing the cladode area index. Silva et al. (2014) reported different CAI values
525 to the present results in clones of *Opuntia* and *Nopalea*, but a similar mean biomass yield
526 (Silva et al., 2015).

527 The cladode area index (CAI) is a yield indicator obtained from ratio between the
528 cladode area and the cultivated area by each plant, and it represents a morphometric feature
529 commonly used as yield indicator to forage cactus (Dubeux Jr. et al., 2006; Silva et al., 2014;
530 Pinheiro et al., 2015). In this study both forage cactus clones ‘Orelha de Elefante Mexicana’
531 and ‘Orelha de Elefante Africana’ presented similar elevated CAI, but ‘Orelha de Elefante
532 Africana’ showed yield relatively lower to dry matter. This apparent discrepancy observed
533 may be justified, at least in part, by the differences between the number and size of cladode,
534 which are intrinsic characteristic of each clone and/or species (Han and Felker, 1997; Dubeux
535 Jr. et al., 2006). In fact, the clone ‘Orelha de Elefante Africana’ presented a lower number of
536 cladode, but its cladode had relatively bigger size when compared to ‘Orelha de Elefante
537 Mexicana’. Thus, its yield did not present a direct relation with the CAI and this index can
538 not be used as the main yield marker for this clone.

539 Additionally, it was found that this performance is closely associated with the
540 maximum quantum yield of photosystem II (F_v/F_m), the effective quantum yield of
541 photosystem II ($\Delta F/F_m'$), the relative electron transport rate (ETR), the chlorophyll content
542 (Chl *a*, Chl *b*, and total Chl), carotenoids (Car_{x+c}), K^+ content, and the K^+/Na^+ ratio of the
543 clone that affords it greater dry matter accumulation (Figure 5).

544

545 **5 Conclusion**

546 The present study shows clear evidence that the stress of the environmental conditions
547 had a greater impact on the F8, V19 and ‘Miúda’ clones, reducing electron use efficiency in
548 carbon fixation, causing damage to PSII, and high energy dissipation. The low chlorophyll
549 and carbohydrate content is involved in the poor photochemical performance of the plants.
550 In addition, the ‘Orelha de Elefante Mexicana’ was superior in several photochemical
551 parameters, osmotic adjustment, CAI and biomass yield. The unprecedented evidence
552 provided by this study reports the high physiological tolerance of forage cactus species, as
553 an aid in dealing with the potential effects of semi-arid environments and selecting the
554 economically most important species of cactus for agricultural production systems. Further

555 studies are therefore essential to clarify the underlying photochemical mechanisms of the
556 forage cactus in different environments and at different points on the canopy, whether under
557 abiotic stress or not.

558

559 **Acknowledgements**

560 The authors would like to thank the Research Support Foundation of the State of
561 Pernambuco (FACEPE - APQ-0215-5.01/10 and FACEPE - APQ-1159-1.07/14) and the
562 National Council for Scientific and Technological Development (CNPq - 475279/2010-7,
563 476372/2012-7, 305286/2015-3, and 309421/2018-7) for their financial support. The authors
564 would also like to thank the Research Support Foundation of the State of Pernambuco and
565 Coordination for the Improvement of Higher Education Personnel (CAPES - Finance Code
566 001) for the research and study grants. We also thank anonymous reviewers for their useful
567 comments and suggestions.

568

569 **References**

- 570 Adams, W.W., Díaz, M., Winter, K., 1989. Diurnal changes in photochemical efficiency, the
571 reduction state of Q, radiationless energy dissipation, and non-photochemical
572 fluorescence quenching in cacti exposed to natural sunlight in northern Venezuela.
573 *Oecologia* 80, 553–561. <https://doi.org/10.1007/BF00380081>
- 574 Adams, W.W., Smith, S.D., Osmond, C.B., 1987. Photoinhibition of the CAM succulent
575 *Opuntia basilaris* growing in Death Valley: evidence from 77K fluorescence and
576 quantum yield. *Oecologia* 71, 221–228. <https://doi.org/10.1007/BF00377287>
- 577 Adki, V.S., Jadhav, J.P., Bapat, V.A., 2013. *Nopalea cochenillifera*, a potential chromium
578 (VI) hyperaccumulator plant. *Environ. Sci. Pollut. Res.* 20, 1173–1180.
579 <https://doi.org/10.1007/s11356-012-1125-4>
- 580 Adli, B., Touati, M., Yabrir, B., Bakria, T., Bezini, E., Boutekrabt, A., 2019. Morphological
581 characterization of some naturalized accessions of *Opuntia ficus-indica* (L.) Mill. in the
582 Algerian steppe regions. *South African J. Bot.* 124, 211–217.
583 <https://doi.org/10.1016/j.sajb.2019.04.017>
- 584 Ahanger, M.A., Agarwal, R.M., 2017. Potassium up-regulates antioxidant metabolism and
585 alleviates growth inhibition under water and osmotic stress in wheat (*Triticum aestivum*

586 L). Protoplasma 254, 1471–1486. <https://doi.org/10.1007/s00709-016-1037-0>

587 Al-Turki, T.A., Masrahi, Y.S., Sayed, O.H., 2014. Photosynthetic adaptation of *Euphorbia*
588 *fractiflexa* (Euphorbiaceae) and survival in arid regions of the Arabian Peninsula. J.
589 Plant Interact. 9, 107–111. <https://doi.org/10.1080/17429145.2013.774442>

590 Allen, R.G., Pereira, L.S., Raes, D., Smith, M., 1998. Crop evapotranspiration: Guidelines
591 for computing crop water requirements, Food and Agriculture Organization of the
592 United Nations. Rome.

593 Alvares, C.A., Stape, J.L., Sentelhas, P.C., Gonçalves, J.L.M., Sparovek, G., 2013. Köppen's
594 climate classification map for Brazil. Meteorol. Zeitschrift 22, 711–728.
595 <https://doi.org/10.1127/0941-2948/2013/0507>

596 Alves, F.A.L., Andrade, A.P., Bruno, R. de L.A., Silva, M.G. de V., Souza, M. de F.V.,
597 Santos, D.C., 2017. Seasonal variability of phenolic compounds and antioxidant activity
598 in prickly pear cladodes of *Opuntia* and *Nopalea* genres. Food Sci. Technol. 37, 536–
599 543. <https://doi.org/10.1590/1678-457x.19316>

600 Aragón-Gastélum, J.L., Flores, J., Yáñez-Espinosa, L., Badano, E., Ramírez-Tobías, H.M.,
601 Rodas-Ortíz, J.P., González-Salvatierra, C., 2014. Induced climate change impairs
602 photosynthetic performance in *Echinocactus platyacanthus*, an especially protected
603 Mexican cactus species. Flora Morphol. Distrib. Funct. Ecol. Plants 209, 499–503.
604 <https://doi.org/10.1016/j.flora.2014.06.002>

605 Aragón-Gastélum, J.L., Ramírez-Benítez, J.E., González-Durán, E., González-Salvatierra,
606 C., Ramírez-Tobías, H.M., Flores, J., Gutiérrez-Alcántara, E.J., Méndez-Guzmán, E.,
607 Jarquín-Gálvez, R., 2020. Photochemical activity in early-developmental phases of
608 *Agave angustifolia* subsp. *tequilana* under induced global warming: Implications to
609 temperature stress and tolerance. Flora Morphol. Distrib. Funct. Ecol. Plants 263,
610 151535. <https://doi.org/10.1016/j.flora.2019.151535>

611 Bañuelos, G.S., Stushnoff, C., Walse, S.S., Zuber, T., Yang, S.I., Pickering, I.J., Freeman,
612 J.L., 2012. Biofortified, selenium enriched, fruit and cladode from three *Opuntia* Cactus
613 pear cultivars grown on agricultural drainage sediment for use in nutraceutical foods.
614 Food Chem. 135, 9–16. <https://doi.org/10.1016/j.foodchem.2012.04.021>

615 Bussotti, F., Gerosa, G., Digrado, A., Pollastrini, M., 2020. Selection of chlorophyll
616 fluorescence parameters as indicators of photosynthetic efficiency in large scale plant

617 ecological studies. Ecol. Indic. 108, 105686.
618 <https://doi.org/10.1016/j.ecolind.2019.105686>

619 Borland, A.M., Griffiths, H., Hartwell, J., Smith, J.A.C., 2009. Exploiting the potential of
620 plants with crassulacean acid metabolism for bioenergy production on marginal lands.
621 J. Exp. Bot. 60, 2879–2896. <https://doi.org/10.1093/jxb/erp118>

622 Borland, A.M., Wullschleger, S.D., Weston, D.J., Hartwell, J., Tuskan, G.A., Yang, X.,
623 Cushman, J.C., 2015. Climate-resilient agroforestry: physiological responses to climate
624 change and engineering of crassulacean acid metabolism (CAM) as a mitigation
625 strategy. Plant, Cell & Environ. 38, 1833–1849. <https://doi.org/10.1111/pce.12479>

626 Cabrera, L.P., Reyes, T.F., Delgado, A.P., Ornela, R.E., Caro, D.A.P., De Posada, E.,
627 Arronte, M., 2016. Removal of *Opuntia* thorns by pulsed laser ablation: Bromatological
628 and microbiological analysis. J. Food Eng. 169, 38–43.
629 <https://doi.org/10.1016/j.jfoodeng.2015.08.019>

630 Cardoso, D.B., Carvalho, F.F.R. de, Medeiros, G.R. de, Guim, A., Cabral, A.M.D., Vêras,
631 R.M.L., Santos, K.C. dos, Dantas, L.C.N., Nascimento, A.G. de O., 2019. Levels of
632 inclusion of spineless cactus (*Nopalea cochenillifera* Salm Dyck) in the diet of lambs.
633 Anim. Feed Sci. Technol. 247, 23–31. <https://doi.org/10.1016/j.anifeedsci.2018.10.016>

634 Cayupán, Y.S.C., Ochoa, M.J., Nazareno, M.A., 2011. Health-promoting substances and
635 antioxidant properties of *Opuntia sp.* fruits. Changes in bioactive-compound contents
636 during ripening process. Food Chem. 126, 514–519.
637 <https://doi.org/10.1016/j.foodchem.2010.11.033>

638 Chakraborty, K., Bhaduri, D., Meena, H.N., Kalariya, K., 2016. External potassium (K⁺)
639 application improves salinity tolerance by promoting Na⁺-exclusion, K⁺-accumulation
640 and osmotic adjustment in contrasting peanut cultivars. Plant Physiol. Biochem. 103,
641 143–153. <https://doi.org/10.1016/j.plaphy.2016.02.039>

642 Chen, H., Li, Q.P., Zeng, Y.L., Deng, F., Ren, W.J., 2019. Effect of different shading
643 materials on grain yield and quality of rice. Sci. Rep. 9, 1–9.
644 <https://doi.org/10.1038/s41598-019-46437-9>

645 Chetti, M.B., Nobel, P.S., 1988. Recovery of photosynthetic reactions after high-temperature
646 treatments of a heat-tolerant cactus. Photosynthesis Res. 18, 277–286.
647 <https://doi.org/10.1007/BF00034832>

648 Cui, Y.N., Xia, Z.R., Ma, Q., Wang, W.Y., Chai, W.W., Wang, S. M., 2019. The synergistic
649 effects of sodium and potassium on the xerophyte *Apocynum venetum* in response to
650 drought stress. *Plant Physiol. Biochem.* 135, 489–498.
651 <https://doi.org/10.1016/j.plaphy.2018.11.011>

652 Cushman, J.C., Davis, S.C., Yang, X., Borland, A.M., 2015. Development and use of
653 bioenergy feedstocks for semi-arid and arid lands. *J. Exp. Bot.* 66, 4177–4193.
654 <https://doi.org/10.1093/jxb/erv087>

655 De Santiago, E., Domínguez-Fernández, M., Cid, C., De Peña, M.P., 2018. Impact of cooking
656 process on nutritional composition and antioxidants of cactus cladodes (*Opuntia ficus-*
657 *indica*). *Food Chem.* 240, 1055–1062. <https://doi.org/10.1016/j.foodchem.2017.08.039>

658 Diaz-Vela, J., Totosa, A., Cruz-Guerrero, A.E., de Lourdes Pérez-Chabela, M., 2013. *In*
659 *vitro* evaluation of the fermentation of added-value agroindustrial by-products: cactus
660 pear (*Opuntia ficus-indica* L.) peel and pineapple (*Ananas comosus*) peel as functional
661 ingredients. *Int. J. Food Sci. Technol.* 48, 1460–1467. <https://doi.org/10.1111/ijfs.12113>

662 Dick, M., Limberger, C., Thys, R.C.S., Rios, A.O., Flôres, S.H., 2020. Mucilage and cladode
663 flour from cactus (*Opuntia monacantha*) as alternative ingredients in gluten-free
664 crackers. *Food Chem.* 314, 126178. <https://doi.org/10.1016/j.foodchem.2020.126178>

665 Drezner, T.D., 2020. The importance of microenvironment: *Opuntia* plant growth, form and
666 the response to sunlight. *J. Arid Environ.* 178, 104144.
667 <https://doi.org/10.1016/j.jaridenv.2020.104144>

668 Dubeux Jr., J.C.B., Santos, M.V.F., Lira, M.A., Santos, D.C., Farias, I., Lima, L.E., Ferreira,
669 R.L.C., 2006. Productivity of *Opuntia ficus-indica* (L.) Miller under different N and P
670 fertilization and plant population in north-east Brazil. *J. Arid Environ.* 67, 357–372.
671 <https://doi.org/10.1016/j.jaridenv.2006.02.015>

672 Dubois, M., Gilles, K.A., Hamilton, J.K., Rebers, P.A., Smith, F., 1956. Colorimetric method
673 for determination of sugars and related substances. *Anal. Chem.*, 28, 350–356.

674 Falcão, H.M., Oliveira, M.T., Mergulhão, A.C., Silva, M. V., Santos, M.G., 2013.
675 Ecophysiological performance of three *Opuntia ficus-indica* cultivars exposed to
676 carmine cochineal under field conditions. *Sci. Hortic. (Amsterdam)*. 150, 419–424.
677 <https://doi.org/10.1016/j.scienta.2012.11.021>

678 Freire, J.L., Santos, M.V.F., Dubeux Júnior, J.C.B., Bezerra Neto, E., Lira, M.A., Cunha, M.

679 V., Santos, D.C., Amorim, S.O., Mello, A.C.L., 2018. Growth of cactus pear cv. Miúda
680 under different salinity levels and irrigation frequency. An. Acad. Bras. Cienc. 90,
681 3893–3900. <https://doi.org/10.1590/0001-3765201820171033>

682 Galizzi, F.A., Felker, P., González, C., Gardiner, D., 2004. Correlations between soil and
683 cladode nutrient concentrations and fruit yield and quality in cactus pears, *Opuntia ficus*
684 *indica* in a traditional farm setting in Argentina. J. Arid Environ. 59, 115–132.
685 <https://doi.org/10.1016/j.jaridenv.2004.01.015>

686 Griffiths, H., Males, J., 2017. Succulent plants. Curr. Biol. 27, 853–909.
687 <https://doi.org/10.1016/j.cub.2017.03.021>

688 Guevara, J.C., Yahia, E.M., Brito de la Fuente, E., Biserka, S.P., 2003. Effects of elevated
689 concentrations of CO₂ in modified atmosphere packaging on the quality of prickly pear
690 cactus stems (*Opuntia* spp.). Postharvest Biol. Technol. 29, 167–176.
691 [https://doi.org/10.1016/S0925-5214\(03\)00021-8](https://doi.org/10.1016/S0925-5214(03)00021-8)

692 Han, H., Felker, P., 1997. Field validation of water-use efficiency of the CAM plant *Opuntia*
693 *ellisiana* in south Texas. J. Arid Environ. 36, 133–148.
694 <https://doi.org/10.1006/jare.1996.0202>

695 Hara, M., Ohkawa, H., Narato, M., Shirai, M., Asada, Y., Karube, I., Miyake, J., 1997.
696 Regeneration of NADPH by cactus chloroplasts: Coupling reaction with P450
697 monooxygenase. J. Ferment. Bioeng. 84, 324–329. [https://doi.org/10.1016/S0922-](https://doi.org/10.1016/S0922-338X(97)89252-5)
698 [338X\(97\)89252-5](https://doi.org/10.1016/S0922-338X(97)89252-5)

699 He, L., Chen, J.M., Liu, J., Zheng, T., Wang, R., Joiner, J., Chou, S., Chen, B., Liu, Y., Liu,
700 R., Rogers, C., 2019. Diverse photosynthetic capacity of global ecosystems mapped by
701 satellite chlorophyll fluorescence measurements. Remote Sens. Environ. 232, 111344.
702 <https://doi.org/10.1016/j.rse.2019.111344>

703 Jardim, A.M.R.F., Silva, T.G.F., Souza, L.S.B., Souza, M.S., Morais, J.E.F., Araújo Júnior,
704 G.N., 2020. Multivariate analysis in the morpho-yield evaluation of forage cactus
705 intercropped with sorghum. Rev. Bras. Eng. Agrícola e Ambient. 24, 756–761.
706 <https://doi.org/10.1590/1807-1929/agriambi.v24n11p756-761>

707 Jardim, A.M.R.F., Silva, T.G.F., Souza, L.S.B., Araújo Júnior, G.N., Alves, H.K.M.N.,
708 Souza, M.S., Araujo, G.G.L., Moura, M.S.B., 2021. Intercropping forage cactus and
709 sorghum in a semi-arid environment improves biological efficiency and competitive

710 ability through interspecific complementarity. *J. Arid Environ.* 188, 104464.
711 <https://doi.org/10.1016/j.jaridenv.2021.104464>

712 Kaiser, H.F., 1960. The Application of Electronic Computers to Factor Analysis. *Educ.*
713 *Psychol. Meas.* 20, 141–151. <https://doi.org/10.1177/001316446002000116>

714 Kharrat, N., Salem, H., Mrabet, A., Aloui, F., Triki, S., Fendri, A., Gargouri, Y., 2018.
715 Synergistic effect of polysaccharides, betalain pigment and phenolic compounds of red
716 prickly pear (*Opuntia stricta*) in the stabilization of salami. *Int. J. Biol. Macromol.* 111,
717 561–568. <https://doi.org/10.1016/j.ijbiomac.2018.01.025>

718 Krümpel, J., George, T., Gasston, B., Francis, G., Lemmer, A., 2020. Suitability of *Opuntia*
719 *ficus-indica* (L) Mill. and *Euphorbia tirucalli* L. as energy crops for anaerobic digestion.
720 *J. Arid Environ.* 174, 104047. <https://doi.org/10.1016/j.jaridenv.2019.104047>

721 Li, Y.C., Lin, T.C., Martin, C.E., 2015. Leaf anthocyanin, photosynthetic light-use
722 efficiency, and ecophysiology of the South African succulent *Anacampseros rufescens*
723 (Anacampserotaceae). *South African J. Bot.* 99, 122–128.
724 <https://doi.org/10.1016/j.sajb.2015.04.001>

725 Lichtenthaler, H.K., Wellburn, A.R., 1983. Determinations of total carotenoids and
726 chlorophylls *a* and *b* of leaf extracts in different solvents. *Biochem. Soc. Trans.* 11, 591–
727 592. <https://doi.org/10.1042/bst0110591>

728 Lima, C.S., Ferreira-Silva, S.L., Carvalho, F.E.L., Lima Neto, M.C., Aragão, R.M., Silva,
729 E.N., Sousa, R.M.J., Silveira, J.A.G., 2018. Antioxidant protection and PSII regulation
730 mitigate photo-oxidative stress induced by drought followed by high light in cashew
731 plants. *Environ. Exp. Bot.* 149, 59–69. <https://doi.org/10.1016/j.envexpbot.2018.02.001>

732 Lina, A., Eloisa, L., 2018. How do young cacti (seeds and seedlings) from tropical xeric
733 environments cope with extended drought periods? *J. Arid Environ.* 154, 1–7.
734 <https://doi.org/10.1016/j.jaridenv.2018.03.009>

735 Makonya, G.M., Ogola, J.B.O., Muthama Muasya, A., Crespo, O., Maseko, S., Valentine,
736 A.J., Ottosen, C.O., Rosenqvist, E., Chimphango, S.B.M., 2019. Chlorophyll
737 fluorescence and carbohydrate concentration as field selection traits for heat tolerant
738 chickpea genotypes. *Plant Physiol. Biochem.* 141, 172–182.
739 <https://doi.org/10.1016/j.plaphy.2019.05.031>

740 Maxwell, K., Johnson, G.N., 2000. Chlorophyll fluorescence—a practical guide. *J. Exp. Bot.*

741 51, 659–668. <https://doi.org/10.1093/jexbot/51.345.659>

742 Méndez, L.P., Flores, F.T., Martín, J.D., Rodríguez Rodríguez, E.M., Díaz Romero, C., 2015.

743 Physicochemical characterization of cactus pads from *Opuntia dillenii* and *Opuntia*

744 *ficus indica*. Food Chem. 188, 393–398.

745 <https://doi.org/10.1016/J.FOODCHEM.2015.05.011>

746 Meza-Herrera, C.A., Santamaría-Estrada, C.E., Flores-Hernández, A., Cano-Villegas, O., la

747 Peña, C.G. De, Macias-Cruz, U., Calderón-Leyva, G., Ángel-García, O., Mellado, M.,

748 Carrillo-Moreno, D., Véliz-Deras, F.G., 2019. The *Opuntia effect* upon the out-of-

749 season embryo implantation rate in goats: Corpus luteal number, corpus luteal diameter

750 and serum progesterone concentrations. Livest. Sci. 228, 201–206.

751 <https://doi.org/10.1016/j.livsci.2019.09.002>

752 Nobel, P.S., Geller, G.N., Kee, S.C., Zimmerman, A.D., 1986. Temperatures and thermal

753 tolerances for cacti exposed to high temperatures near the soil surface. Plant, Cell &

754 Environ. 9, 279–287. <https://doi.org/10.1111/1365-3040.ep11611688>

755 Nobel, P.S., De la Barrera, E., 2003. Tolerances and acclimation to low and high

756 temperatures for cladodes, fruits and roots of a widely cultivated cactus, *Opuntia ficus-*

757 *indica*. New Phytol. 157, 271–279. <https://doi.org/10.1046/j.1469-8137.2003.00675.x>

758 Ojeda-Pérez, Z.Z., Jiménez-Bremont, J.F., Delgado-Sánchez, P., 2017. Continuous high and

759 low temperature induced a decrease of photosynthetic activity and changes in the diurnal

760 fluctuations of organic acids in *Opuntia streptacantha*. PLoS One 12, 1–18.

761 <https://doi.org/10.1371/journal.pone.0186540>

762 Oliveira, M.M.T., Shuhua, L., Kumbha, D.S., Zurgil, U., Raveh, E., Tel-Zur, N., 2020.

763 Performance of *Hylocereus* (Cactaceae) species and interspecific hybrids under high-

764 temperature stress. Plant Physiol. Biochem. 153, 30–39.

765 <https://doi.org/10.1016/j.plaphy.2020.04.044>

766 Pan, Y.Q., Guo, H., Wang, S.M., Zhao, B., Zhang, J.L., Ma, Q., Yin, H.J., Bao, A.K., 2016.

767 The Photosynthesis, Na⁺/K⁺ Homeostasis and Osmotic Adjustment of *Atriplex*

768 *canescens* in Response to Salinity. Front. Plant Sci. 7, 848.

769 <https://doi.org/10.3389/fpls.2016.00848>

770 Pinheiro, K.M., Silva, T.G.F., Diniz, W.J. da S., Carvalho, H.F. de S., Moura, M.S.B., 2015.

771 Indirect methods for determining the area index of forage cactus cladodes. Pesqui.

772 Agropecu. Trop. 45, 163–171. <https://doi.org/10.1590/1983-40632015v4530617>

773 Queiroz, M.G., Silva, T.G.F., Zolnier, S., Silva, S.M.S., Souza, C.A.A., Carvalho, H.F.S.,
774 2016. Relações hídrico-econômicas da palma forrageira cultivada em ambiente
775 Semiárido. Irriga Edição Esp, 141–154.
776 <https://doi.org/10.15809/irriga.2016v1n01p141-154>

777 R Core Team, 2020. R: A language and environment for statistical computing. R Foundation
778 for Statistical Computing.

779 Richards, L.A., 1954. Diagnosis and improvement of saline and alkali soils. Agricultural
780 hand book 60. U.S. Dept. of Agriculture, Washington, D.C.

781 Rocchetti, G., Pellizzoni, M., Montesano, D., Lucini, L., 2018. Italian *Opuntia ficus-indica*
782 Cladodes as Rich Source of Bioactive Compounds with Health-Promoting Properties.
783 Foods 7, 24. <https://doi.org/10.3390/foods7020024>

784 Rodrigues, C.R.F., Silva, E.N., Ferreira-Silva, S.L., Voigt, E.L., Viégas, R.A., Silveira,
785 J.A.G., 2013. High K⁺ supply avoids Na⁺ toxicity and improves photosynthesis by
786 allowing favorable K⁺: Na⁺ ratios through the inhibition of Na⁺ uptake and transport
787 to the shoots of *Jatropha curcas* plants. J. Plant Nutr. Soil Sci. 176, 157–164.
788 <https://doi.org/10.1002/jpln.201200230>

789 Scalisi, A., Morandi, B., Inglese, P., Lo Bianco, R., 2016. Cladode growth dynamics in
790 *Opuntia ficus-indica* under drought. Environ. Exp. Bot. 122, 158–167.
791 <http://dx.doi.org/10.1016/j.envexpbot.2015.10.003>

792 Silva, T.G.F., Araújo Primo, J.T., Morais, J.E.F., Diniz, W.J.S., Souza, C.A.A., Silva, M.C.,
793 2015. Crescimento e produtividade de clones de palma forrageira no semiárido e
794 relações com variáveis meteorológicas. Rev. Caatinga 28, 10–18.

795 Silva, T.G.F., Miranda, K.R., Santos, D.C., Queiroz, M.G., Silva, M.C., Cruz Neto, J.F.,
796 Araújo, J.E.M., 2014. Área do cladódio de clones de palma forrageira: modelagem,
797 análise e aplicabilidade. Rev. Bras. Ciências Agrárias 9, 633–641.
798 <https://doi.org/10.5039/agraria.v9i4a4553>

799 Silva-Ortega, C.O., Ochoa-Alfaro, A.E., Reyes-Agüero, J.A., Aguado-Santacruz, G.A.,
800 Jiménez-Bremont, J.F., 2008. Salt stress increases the expression of p5cs gene and
801 induces proline accumulation in cactus pear. Plant Physiol. Biochem. 46, 82–92.
802 <https://doi.org/10.1016/j.plaphy.2007.10.011>

803 Tang, X.L., Mu, X.M., Shao, H.B., Wang, H.Y., Brestic, M., 2015. Global plant-responding
804 mechanisms to salt stress: physiological and molecular levels and implications in
805 biotechnology. Crit. Rev. Biotechnol. 35, 425–437.
806 <https://doi.org/10.3109/07388551.2014.889080>

807 Walker, R.P., Famiani, F., Baldicchi, A., Cruz-Castillo, J.G., Inglese, P., 2011. Changes in
808 enzymes involved in photosynthesis and other metabolic processes in the fruit of
809 *Opuntia ficus-indica* during growth and ripening. Sci. Hortic. (Amsterdam). 128, 213–
810 219. <https://doi.org/10.1016/j.scienta.2011.01.017>

811 Wang, S., Wan, C., Wang, Y., Chen, H., Zhou, Z., Fu, H., Sosebee, R.E., 2004. The
812 characteristics of Na⁺, K⁺ and free proline distribution in several drought-resistant plants
813 of the Alxa Desert, China. J. Arid Environ. 56, 525–539. [https://doi.org/10.1016/S0140-](https://doi.org/10.1016/S0140-1963(03)00063-6)
814 [1963\(03\)00063-6](https://doi.org/10.1016/S0140-1963(03)00063-6)

815 Wang, X., Zhao, J., Fang, Q., Chang, X., Sun, M., Li, W., Li, Y., 2020. GmAKT1 is involved
816 in K⁺ uptake and Na⁺/K⁺ homeostasis in *Arabidopsis* and soybean plants. Plant Sci.
817 110736. <https://doi.org/10.1016/j.plantsci.2020.110736>

818 White, P.J., 2013. Improving potassium acquisition and utilisation by crop plants. J. Plant
819 Nutr. Soil Sci. 176, 305–316. <https://doi.org/10.1002/jpln.201200121>

820 Zhang, Y., Liu, G.J., 2018. Effects of cesium accumulation on chlorophyll content and
821 fluorescence of *Brassica juncea* L. J. Environ. Radioact. 195, 26–32.
822 <https://doi.org/10.1016/j.jenvrad.2018.09.017>

823

CHAPTER 6

To what extent are turbulent flux, the energy budget and water relations in the field compromised in *Nopalea cochenillifera* during the wet and dry seasons?

Abstract

The *in-situ* quantification of turbulent flux and evapotranspiration (ET) is necessary to monitor crop performance in stressful environments. However, little is known about the seasonal variability of these surface fluxes in cacti, where understanding is still in the early stages. In the present study, we investigate the interannual and seasonal behaviour of components of the surface energy balance (SEB), environmental conditions, morphophysiological parameters and water relations in a crop of *Nopalea cochenillifera* in the semi-arid region of Brazil. Data were collected from a micrometeorological tower between 2015 and 2017. The ET, and flux partitioning into net radiation (R_n), latent heat flux (LE), sensible heat flux (H), and soil heat flux (G) were obtained by means of the SEB, using the Bowen ratio. The performance of the cactus and its response to environmental factors were evaluated using growth rates, phenophases, biomass yield, water relations, the Normalised Difference Vegetation Index (NDVI) and the Evaporative Stress Index (ESI). Generally, R_n was significantly higher during the wet season, being on average 14% higher than during the dry season and transitions. LE was not significant between the wet season ($2.87 \text{ MJ m}^{-2} \text{ day}^{-1}$) or the dry season ($2.41 \text{ MJ m}^{-2} \text{ day}^{-1}$); during the wet-dry transition season, LE is reduced by 25% due to the cactus. During the dry-wet transition season in particular, H was 13% higher than during the other seasons. We observed a large decline in G (203%) during the wet season. At the same time, there was no difference in ET during the wet or dry seasons, however, there was a 40% reduction during the dry-wet transition. The wet seasons and wet-dry transition showed the lowest ESI values (a mean of 0.41 and 0.56, respectively). The mean NDVI was 0.23, cladode water content > 89%, and biomass 12.47 Mg ha^{-1} . These findings indicate high rates of growth, high biomass and a high cladode water content, and explain the response of the cactus regarding energy partitioning and ET.

Keywords: Energy redistribution; Semi-arid; Microclimate conditions; Cactus

32

33 **1. Introduction**

34 The cactus, *Nopalea cochenillifera* (L.) Salm-Dyck, is an important plant used in
35 animal diets in semi-arid environments, particularly in the driest areas of north-eastern Brazil
36 and around the world. This species of family Cactaceae is known worldwide for its tolerance
37 to abiotic stress, and is able to survive in places with low annual rainfall (250–450 mm)
38 (Jardim et al., 2021a; Kumar et al., 2022; Winter and Smith, 2022). Plants that exhibit
39 crassulacean acid metabolism (CAM) are more resistant, and have greater water use
40 efficiency (WUE) compared to plants with a C3 or C4 photosynthetic pathway, which are
41 normally less tolerant to high heat and severe drought (Hartzell et al., 2021; Ho et al., 2019;
42 Nobel, 1991; Scalisi et al., 2016). *N. cochenillifera* is composed of vegetative structures
43 called cladodes—modified succulent stems, which offer the animals a high concentration of
44 non-fibrous carbohydrates (~54.3%) and high total nutrient digestibility, in such a way that
45 they are considered a great source of energy. In addition, they are rich in water (~900 g kg⁻¹
46 dry matter) and minerals (especially, Ca²⁺, K⁺ and P). On the other hand, cladodes have low
47 levels of dry-matter, crude protein (~5.4%), neutral detergent fibre (~24.8%), and acid
48 detergent fibre (Dubeux Jr. et al., 2021; Pessoa et al., 2020; Rocha Filho et al., 2021).

49 Due to their high productive performance, several studies have been carried out with
50 cacti (*Opuntia* spp. and *Nopalea* spp.) in a semi-arid environment, adopting management
51 practices or evaluating the water deficit on the growth and productivity of the crop (e.g.,
52 Araújo Júnior et al., 2021; Campos et al., 2021; Jardim et al., 2021a; Kumar et al., 2022;
53 Scalisi et al., 2016). However, few studies have been developed to evaluate the plant-
54 environment interaction using the energy balance method, some with *Opuntia* spp. (Consoli
55 et al., 2013; Gibbs and Patten, 1970) and some with other species and ecosystems that include
56 Cactaceae (Flanagan and Flanagan, 2018; Guevara-Escobar et al., 2021; Lewis et al., 1977).
57 Consoli et al. (2013), under a semi-arid climate in Sicily (Italy), evaluated ecophysiological
58 variables and energy balance in an irrigated crop of *O. ficus-indica*, where they reported the
59 importance of applying a method that detected changes in plant transpiration on a daily scale
60 under wet and dry conditions. Pierini et al. (2014) reported that the heat flux is high in
61 vegetation that includes species of cactus (*O. spinosior* and *O. engelmannii*) in Tucson in the
62 Sonoran Desert (Arizona).

63 In terrestrial ecosystems, energy and water exchange plays a fundamental role in
64 hydrological control, climate phenomena and species survival. To quantify the land-
65 atmosphere fluxes, and understand this partition, the surface energy balance (SEB) predicts
66 variations in turbulent fluxes and evapotranspiration (ET) from interaction of the soil-
67 vegetation-atmosphere system (Alves et al., 2022; Anderson and Vivoni, 2016; Kuiyue
68 Zhang et al., 2022). In addition to being considered a fairly robust and valid method under
69 semi-arid conditions, it can be applied to different vegetated surfaces (e.g., areas of forest
70 and agricultural crops), and areas with small footprints (i.e., different fetch-to-height ratios)
71 (Awada et al., 2021; Guevara-Escobar et al., 2021; Hicks et al., 2020). Among the methods
72 used to determine turbulent flux, the Bowen ratio indirectly quantifies the latent heat flux
73 (LE) using net radiation (R_n), soil heat flux (G) and the air temperature and humidity gradients
74 (Bowen, 1926; Hu et al., 2014). In addition to being a low-cost method compared to the eddy
75 covariance and weighing lysimeter methods, the Bowen ratio method uses simple sensors,
76 and is preferred in ET studies in agricultural ecosystems (Hicks et al., 2020; Pokhariyal and
77 Patel, 2021; Pozníková et al., 2018).

78 On a global scale, part of the water from ecosystems is returned to the atmosphere by
79 the ET (Chen et al., 2022). Basically, two processes are involved in ET: evaporation—the
80 phenomenon concerning the change in the liquid phase from water to vapour; and
81 transpiration—the process of transferring water via the plant structures (e.g., stomata) to the
82 atmosphere in the form of water vapour. The sum of these two physical phenomena, i.e.,
83 evapotranspiration, consumes more than half of the solar energy, with approximately 60% of
84 the precipitation being transferred to the atmosphere by the LE (Allen et al., 1998; Awada et
85 al., 2021; Cheng et al., 2021; Cheng et al., 2022).

86 ET is perhaps one of the most studied variables in arid and semi-arid environments,
87 helping to explain the response of the vegetation to water availability. However, in dry
88 landscapes, the available energy is high, and when the ET decreases due to water availability,
89 there is an increase in the sensible heat flux (H) (Anderson and Vivoni, 2016; Awada et al.,
90 2021; Chen et al., 2022; Cheng et al., 2022). Within this context, these factors can trigger
91 conditions of stress for some plant species, and when added to the excessive heat flux and
92 high energy may become more hostile.

93 In the field, hydrological conditions (i.e., wet and dry seasons) can cause changes in
94 the energy fluxes and ET on different scales. In addition, the vegetation can modify the
95 release of energy in response to its growth and phenology (Awada et al., 2021; Hermance et
96 al., 2015; Lewis et al., 1977). In this respect, using such information as vegetation indices
97 (e.g., cladode area index, and Normalised Difference Vegetation Index) and growth indices
98 (e.g., growth rate and phenophases) can be fundamental in understanding plant feedback to
99 growing conditions.

100 Finally, although there are studies on monitoring mass and energy fluxes in dry forests
101 and grasslands in a semi-arid environment (Alves et al., 2022; Marques et al., 2020; Shao et
102 al., 2017; Silva et al., 2017; Yue et al., 2019), as far as we know, there are no studies that
103 report information on growth stages, ecophysiology or surface energy balance in *N.*
104 *cochenillifera*. Therefore, our hypothesis is that (i) even under adverse stress conditions, the
105 performance of the cactus for energy flux and evapotranspiration remains good; and (ii) its
106 growth, water relations, and water and nutrient use efficiency are maintained throughout each
107 season. Furthermore, we believe that our results will provide new insights into CAM plants
108 and their exchange of energy with the ecosystem. The aim of this study is to evaluate the
109 interannual and seasonal behaviour of components of the surface energy balance (SEB),
110 environmental conditions, morphophysiological parameters and water relations, during the
111 wet and dry seasons in a crop of *N. cochenillifera* in the semi-arid region of Brazil. To achieve
112 this aim, we quantified the heat fluxes, partitioned the net radiation, and determined growth
113 rates, plant phenophases and cladode succulence.

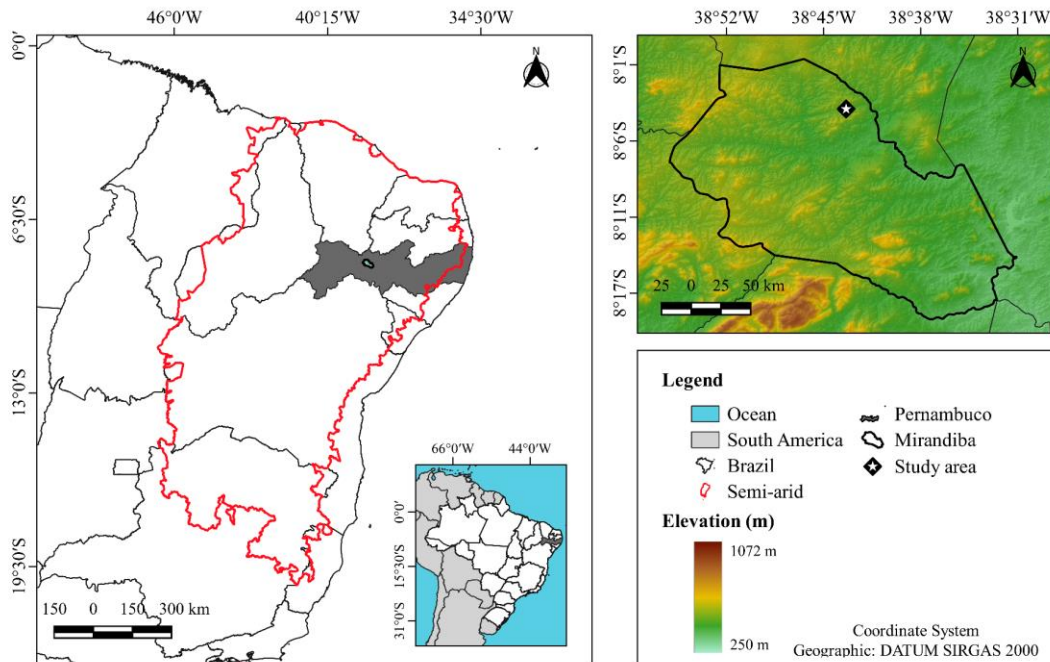
114

115 **2. Materials and methods**

116 *2.1. Location and information of the experimental area*

117 The experiment was conducted in a study area located in the district of Mirandiba, in
118 the state of Pernambuco, Brazil (8°3.73' S, 38°43.69' W, altitude 490 m) under the conditions
119 of a water deficit (Figure 1). According to the Köppen classification, the climate in the region
120 is classified as semi-arid, type BSh (i.e., dry and hot with a rainy season in the summer)
121 (Alvares et al., 2013; Beck et al., 2018). Rainfall predominates from January to June, with an
122 annual average of 431.8 mm, average air temperature of 25.2°C, relative humidity of 64.6%,
123 and a high atmospheric demand that can reach 1,600 mm year⁻¹. The environment is

124 characterised by high luminosity, irregular spatiotemporal distribution of the rainfall, and the
125 occurrence of periodic droughts.
126



127
128 Figure 1. Geographic location of the study area in the district of Mirandiba, Pernambuco,
129 Brazil.

130
131 Based on the beginning and end of the rainfall regime, we considered four seasons
132 (wet, wet-dry transition, dry, and dry-wet transition) for each year under study from 2015 to
133 2017. If the sum of rainfall values in the 30 days preceding or following the day under
134 analysis is less than 20 mm, and there have been less than five rainy days, it is considered a
135 dry season. However, if in the same time interval, rainfall values greater than 20 mm are
136 recorded on five or more days, the season is considered wet. A transition season is determined
137 when none of these criteria apply. If this happens after a dry season, it is said to be a dry-wet
138 transition season, and when it occurs after a wet season, it is considered a wet-dry transition
139 season (Leite-Filho et al., 2019; Salack et al., 2016). For example, using this approach the
140 wet season included 21 February 2015 to 23 July 2015, 7 January 2016 to 1 February 2016,

141 and 21 February 2017 to 1 July 2017; the wet-dry transition included 24 July 2015 to 21
142 August 2015, and 2 February 2016 to 26 July 2016; the dry season included 22 August 2015
143 to 7 December 2015, and 27 July 2016 to 17 November 2016; and the dry-wet transition, 8
144 December 2015 to 6 January 2016, and 18 November 2016 to 20 February 2017.

145 The soil in the experimental area was classified as a Chromic Luvisol (Soil Survey
146 Staff, 2014), comprising 54% sand, 21% silt and 25% clay. Soil samples were collected at
147 depths of 0–0.20 m, with a bulk density of 1.45 g cm^{-3} (measured by the cutting-ring
148 sampling method), soil organic carbon content of 10.1 g kg^{-1} , field capacity of $0.26 \text{ cm}^3 \text{ cm}^{-3}$,
149 soil pH of 6.1 (measured at a soil to water ratio of 1:2.5 using an ion pH meter), and terrain
150 slope between 3% to 5%.

151 The experiment was conducted from April 2015 to April 2017 over a total area of 1.8
152 ha, using the cactus, *Nopalea cochenillifera* (L.) Salm-Dyck, a species tolerant to
153 *Dactylopius opuntiae* Cockerell (Hemiptera: Dactylopiidae). The crop was planted in
154 January 2015. After the initial soil preparation (i.e., ploughing, harrowing and furrowing),
155 the cladodes were planted, leaving 50% of their height in the soil. The plants were arranged
156 in single crop rows with the cladodes aligned bilaterally (i.e., parallel to each other), at a
157 spacing of $2.0 \times 0.50 \text{ m}$ ($10,000 \text{ plants ha}^{-1}$). Cropping treatments (i.e., hand weeding, and
158 the application of herbicide and insecticide) were carried out whenever necessary to avoid
159 competition with spontaneous plants and promote full growth of the crop. The cactus was
160 grown under rainfed conditions throughout the evaluation cycle.

161

162 2.2. Measuring the meteorological variables

163 A 3-metre micrometeorological tower was installed in the centre of the experimental
164 area. Net radiation (R_n) data were measured using a closed-cell thermopile sensor (NR-Lite,
165 Kipp & Zonen, Delft, Netherlands), in addition to two net radiometers (SP-230, Apogee
166 Instruments, Logan, Utah, USA). The two radiometer sensors were installed 2.8 m above the
167 canopy, one to quantify the incident radiation and the other for radiation reflected by the
168 canopy (i.e., with the sensors facing up and down). The soil heat flux (G) was measured at a
169 depth of 0.05 m from the surface using a heat flux plate (HFT3, REBS, Hukseflux, Delft,
170 Netherlands) buried close to the crop row. Air temperature (T_a) and relative humidity (RH)
171 were determined using two aspiration psychrometers—creating a vertical profile 0.5 and 1.5

172 m above the surface of the soil. Wind speed and direction were measured using a Wind Sentry
173 model 03002 anemometer (R. M. Young Company, Traverse City, Michigan, USA). Rainfall
174 data were quantified using an automatic rain gauge (CS700-L, Hydrological Services Rain
175 Gauge, Liverpool, Australia) installed 3 m above the canopy, and the photosynthetically
176 active radiation (PAR) was measured using a quantum sensor (LI -190SB, LI-COR, Inc.,
177 Lincoln, Nebraska, USA). In addition, due to the size of the area and the location and height
178 of the meteorological instruments, a suitable search to height ratio (100:1) was determined
179 as per a methodology proposed by Heilman et al. (1989).

180 The data were collected every 60 seconds by data logger (CR10X, Campbell
181 Scientific Inc., North Logan, Utah, USA) with a storage interval of 10 minutes.
182 Measurements were collected continuously both day and night. However, the flux data used
183 in applying the Bowen ratio-energy balance (BREB) method were considered on a daytime
184 scale only. This is because at night, when the temperature/humidity gradients are small,
185 erroneous flux data may be quantified. Each dataset is referred to in terms of local time
186 (GMT-3).

187

188 2.3. Surface energy balance method

189 We used the surface energy balance (SEB) method, which is based on the law of
190 conservation of energy (Equation 1).

191

$$192 \quad R_n - G = LE + H \quad (1)$$

193

194 where R_n is the net radiation (W m^{-2}), G is the soil heat flux (W m^{-2}), LE is the latent heat
195 flux (W m^{-2}), and H is the sensible heat flux (W m^{-2}).

196

197 The turbulent flux components, i.e., sensible heat and latent heat fluxes were
198 determined based on the Bowen ratio (β) (Equation 2). The Bowen ratio method is widely
199 used to partition energy flux components in relation to the total available energy ($R_n - G$).
200 We can therefore estimate this ratio by quantifying the temperature gradient and vapour
201 pressure above the canopy (Bowen, 1926). In the present study, we did not assume similarity
202 of equality between the turbulent transfer coefficients of the sensible heat (K_h) or of the water

203 vapour (K_w) (Gavilán and Berengena, 2007). Therefore, latent heat flux (LE) and sensible
 204 heat flux (H) were estimated by combining the available energy balance and Bowen ratio
 205 (Equations 3 and 4, respectively).

206

$$207 \quad \beta = \frac{H}{LE} = \left(\frac{P_a \times c_p}{\lambda \times \varepsilon} \times \frac{\Delta T}{\Delta e} \times \frac{K_h}{K_w} \right) \quad (2)$$

$$208 \quad LE = \frac{R_n - G}{1 + \beta} \quad (3)$$

$$209 \quad H = \frac{\beta}{1 + \beta} \times (R_n - G) \quad (4)$$

210

211 where β is the Bowen ratio (dimensionless), P_a is the atmospheric pressure (kPa), c_p is the
 212 specific heat capacity of the air (1004.67 J kg⁻¹ °C⁻¹), λ is the latent heat of vaporisation
 213 (2.454 MJ kg⁻¹ at 20°C), ε is the ratio of the molecular weights of the air and water vapour
 214 (0.622), ΔT is the difference in air temperature between the two heights (°C), Δe is the
 215 difference in vapour pressure between the two heights (kPa), K_h is the eddy diffusivity for
 216 heat (m² s⁻¹), and K_w is the eddy diffusivity for water vapour (m² s⁻¹). Quality control was
 217 carried out on the calculated LE as per Perez et al. (1999).

218

219 Furthermore, in the present study, to calculate the energy balance closure, we ignored
 220 the energy from metabolic activities and heat storage in the plant tissue and in the canopy, as
 221 well as horizontal advection. This condition can be applied when the surface is uniform,
 222 keeping in mind that the vertical gradient that comprises the meteorological elements is far
 223 greater than the horizontal gradient. As such, these terms are ignored in building Equation 1
 224 (Hu et al., 2014; Pokhariyal and Patel, 2021).

225

226 *2.3.1 Data selection criteria for the energy balance method*

227 In the present study, for the acceptance and/or rejection criteria of the data collected
 228 by the Bowen ratio-energy balance (BREB) method, we used the approach proposed by Perez
 229 et al. (1999), which parameterises the criteria for using variables to compile the method
 230 (Table 1); this is because the Bowen ratio depends on measuring the temperature and vapour
 231 pressure gradients. That said, the presence of abnormal data occurs when the available-

232 energy heat flux ($R_n - G$) is very small. In this way, faults may occur in applying the energy
 233 balance by the Bowen ratio (β) and later trigger several errors, e.g., when (1) the sensor
 234 resolution is inadequate to solve the gradient in ΔT and Δe ; (2) stable atmospheric conditions,
 235 e.g., at dawn and dusk, return β values close to -1 , resulting in evapotranspiration tending to
 236 infinity, which is inconsistent; and (3) the conditions change abruptly, causing measurement
 237 errors (Table 2) (Hu et al., 2014; Ortega-Farias et al., 1996; Perez et al., 1999; Unland et al.,
 238 1996).

239

240 Table 1. Consistency criteria for data generated by the Bowen ratio method under non-
 241 advective conditions.

Available energy [†]	Vapour pressure gradient	Bowen ratio	Heat flux
$R_n - G > 0$	$\Delta e > 0$	$\beta > -1$	$LE > 0$ and $H \leq 0$ for $-1 < \beta \leq 0$ or $H > 0$ for $\beta > 0$
	$\Delta e < 0$	$\beta < -1$	$LE < 0$ and $H > 0$
$R_n - G < 0$	$\Delta e > 0$	$\beta > -1$	$LE > 0$ and $H < 0$
	$\Delta e < 0$	$\beta < -1$	$LE < 0$ and $H \geq 0$ for $-1 < \beta \leq 0$ or $H < 0$ for $\beta > 0$

242 [†] data considered satisfactory as described by Perez et al. (1999).

243 R_n is the net radiation, G is the soil heat flux, Δe is the difference in vapour pressure between
 244 the two measurement heights, β is the Bowen ratio, LE is the latent heat flux, and H is the
 245 sensible heat flux.

246

247 Table 2. Summary of error types when faults occur using the Bowen ratio-energy balance
 248 method.

Type of error	Applied conditions
A	$R_n - G > 0$, $\Delta e > 0$ and $\beta < -1 + \varepsilon $
B	$R_n - G > 0$, $\Delta e < 0$ and $\beta > -1 - \varepsilon $
C	$R_n - G < 0$, $\Delta e > 0$ and $\beta > -1 - \varepsilon $
D	$R_n - G < 0$, $\Delta e < 0$ and $\beta < -1 + \varepsilon $

249 *E*

Referring to a rapid change in temperature
and vapour pressure.

250 β is the Bowen ratio, and ε is the error interval that defines the threshold for excluding values
251 of the Bowen ratio close to -1 (Perez et al., 1999).

252 2.4. Resource use efficiency

253 2.4.1. Water efficiency

254 The actual evapotranspiration component (ET, mm day⁻¹) was calculated as described
255 in Equation 5 (Mulovhedzi et al., 2020). To help understand the aboveground dry biomass
256 yield in relation to the volume of water consumed, we calculated the water use efficiency
257 (WUE, kg m⁻³) of the crop (Equation 6) (Kai Zhang et al., 2022).

258

$$259 \quad ET = 86,400 \times \frac{LE}{\lambda \times \rho_w} \quad (5)$$

$$260 \quad WUE = \frac{Y}{ET} \quad (6)$$

261

262 where 86,400 is the time unit conversion factor (i.e., converting from seconds to days), *LE* is
263 the latent heat flux measured over 24 h (W m⁻²), ρ_w is the density of water (kg m⁻³), *Y* is the
264 dry matter yield (kg ha⁻¹), and ET is the total amount of seasonal evapotranspiration (m³
265 ha⁻¹).

266

267 2.4.2. Radiation use efficiency

268 The radiation use efficiency (RUE) of the cactus was calculated to describe the light-
269 absorption dynamics of the crop (Equation 7). To achieve this, we used the ratio between the
270 total aboveground dry weight of the plant and the radiation intercepted throughout the
271 growing season (Raza et al., 2019).

272

$$273 \quad RUE = \frac{Y}{I_0 \times fPAR} \quad (7)$$

274

275 where RUE is the radiation use efficiency (g MJ^{-1}), I_0 is the amount of daily incident
276 photosynthetically active radiation (PAR) above the canopy (MJ m^{-2}), and $f\text{PAR}$ is the
277 fraction of intercepted photosynthetically active radiation.

278

279 The intercepted photosynthetically active radiation was estimated monthly using the
280 AccuPAR LP-80 ceptometer (Decagon Devices, Logan, Utah, USA), manually calibrated
281 prior to taking the readings. To maintain consistent measurement conditions and avoid the
282 influence of the angle of the sun's rays, readings were taken under clear skies between 11:00
283 and 13:00, recording the incident radiation above and below the canopy. Three simultaneous
284 readings were taken below the canopy (with the sensor rod positioned parallel and
285 perpendicular to the crop rows) and one above, on four similar plants in the experimental
286 area. We then calculated $f\text{PAR}$ using Equation 8, and the light extinction coefficient (k) based
287 on the Beer–Lambert law (Equation 9). As the cactus has cladodes instead of leaves, we
288 calculated k considering the cladode area index (CAI).

289

$$290 \quad f\text{PAR} = \left(1 - \frac{I_t}{I_0}\right) \quad (8)$$

$$291 \quad f\text{PAR} = 1 - e^{(-k \times \text{CAI})} \quad (9)$$

292

293 where I_t is the PAR measured at the bottom of the canopy, and CAI is the cladode area index,
294 determined according to Pinheiro et al. (2014).

295

296 2.4.3. Nutrient use efficiency

297 After cutting (aboveground biomass), the cladodes were weighed on an electronic
298 scale to quantify the fresh biomass (g FM plant^{-1}) and then dried in a forced air circulation
299 oven at 55°C to constant weight, i.e., dry matter per plant (g DM plant^{-1}). The dried cladode
300 samples were then ground using a Model 4 Wiley mill (Thomas Scientific) with a 1 mm
301 sieve. The mineral-element concentration in the plant tissue was then determined:
302 phosphorus (P, mg kg^{-1}) using the vanadate-molybdate method with readings by UV-visible
303 spectrophotometry at 430 nm (Du Toit et al., 2018); potassium (K^+ , mg kg^{-1}) and sodium
304 (Na^+ , mg kg^{-1}) by flame photometry (Rodrigues et al., 2013); and Calcium (Ca^{2+} , mg kg^{-1})

305 and magnesium (Mg^{2+} , mg kg^{-1}) by atomic absorption spectrophotometry (Loupassaki et al.,
306 2007). Finally, nutrient use efficiency (NUE, mg m^{-3}) was calculated as per Equation 10.

307

$$308 \quad \text{NUE} = \frac{Y \times Nu}{\text{ET}} \quad (10)$$

309

310 where Nu is the concentration of the nutrient in the analysed sample of plant tissue (mg kg^{-1}).
311 To improve understanding of nutrient uptake by the plants, we adapted Equation 10 (Zhang
312 et al., 2020), making it a function of crop evapotranspiration. This adaptation affords more
313 clarity in explaining the nutrient uptake capacity of the plant from the soil solution, together
314 with the water consumption lost through evapotranspiration.

315

316 *2.5. Analysing growth, phenology, cutting time and yield*

317 Morphometric data were collected monthly and samples of plant biomass were taken
318 at 60-day intervals. Four plants were measured for each analysis in each evaluation period.
319 Height was evaluated considering the vertical distance from the ground to the apex of the
320 canopy, and width, considering the average of two measurements from the edge of the
321 canopy. The length (CL, cm), width (CW, cm) and perimeter (CP, cm) of the cladodes were
322 measured, and the number of cladodes (NC, units) determined by counting the cladodes in
323 order of appearance on the plant (i.e., first-order, second-order, third-order, and so on). The
324 total number of cladodes was determined summing the cladodes by order.

325 The cladode area (CA) was determined from the morphometric data as per the
326 equation proposed by Silva et al. (2014) (Equation 11). We then quantified the cladode area
327 index (CAI) using the equation proposed by Pinheiro et al. (2014) (Equation 12). In addition,
328 from the dry mass yield and cladode measurements, we calculated the morphophysiological
329 indices and phenology using a sigmoidal model with three parameters (Equation 13) and
330 accumulated degree-days (Equation 14) (Arnold, 1959; Jardim et al., 2021c).

331

$$332 \quad \text{CA} = 1.6691 \times \left(\frac{1 - e^{(-0.0243 \times \text{CP})}}{-0.0243} \right) \quad (11)$$

$$333 \quad CAI = \left[\frac{\sum_{i=1}^n (CA)}{n} \right] / \frac{10,000}{(S1 \times S2)} \quad (12)$$

$$334 \quad y = \frac{a}{1 + e^{\left(-\frac{x-x_0}{b}\right)}} \quad (13)$$

$$335 \quad ADD = \sum_{j=1}^n \left[\frac{(T_{max} + T_{min})}{2} - Tb \right] \quad (14)$$

336

337 where i is the observation number, n is the total number of observations, 10,000 is the
 338 conversion factor from cm^2 to m^2 , and $S1 \times S2$ is the spacing between the rows and plants
 339 (1.0×0.2 m), respectively.

340

341 The following parameters were used in the morphophysiological and phenological
 342 analysis: y is the response variable (e.g., cladode dry matter, cladode area index, and the
 343 number of cladodes); a is the maximum value for the growth rate (i.e., the distance between
 344 the two asymptotes); x is the accumulated degree-days; x_0 is the number of degree-days
 345 necessary for the plant to express 50% of the maximum growth rate (i.e., the inflection point
 346 of the curve); and b is the number of degree-days necessary to the start of growth; ADD is
 347 the accumulated degree-days ($^{\circ}\text{Cday}$); j is the daily time step; n is the total number of days;
 348 T_{max} is the daily maximum air temperature ($^{\circ}\text{C}$); T_{min} is the daily minimum air temperature
 349 ($^{\circ}\text{C}$); Tb is the lower base temperature ($^{\circ}\text{C}$). Tb is the minimum temperature at which cactus
 350 cladodes grow (22°C). If the daily average temperature drops below 22°C , the ADD becomes
 351 negative. Negative ADD values were set to zero.

352 The growth indices were then quantified: absolute growth rate (AGR, Mg ha^{-1}
 353 $^{\circ}\text{Cday}^{-1}$); relative growth rate (RGR, $\text{Mg Mg}^{-1} ^{\circ}\text{Cday}^{-1}$); net assimilation rate (NAR, Mg ha^{-1}
 354 $^{\circ}\text{Cday}^{-1}$); specific cladode area (SCA, $\text{Mg}^{-1} ^{\circ}\text{Cday}^{-1}$); and cladode emission rate (CER, units
 355 $^{\circ}\text{Cday}^{-1}$) based on earlier studies (Jardim et al., 2021c). The cladode emission rate is a very
 356 important variable in phenological analysis, as it is used to obtain the phenological phases of
 357 the crop (Amorim et al., 2017; Jardim et al., 2021c). We determined the cutting time as when
 358 the absolute growth rate reached 25% of the maximum peak (Jardim et al., 2021c).

359

360 2.6. *Measuring the plant water status*

361 The cladode water content (CWC, %) was calculated from the fresh matter weight
362 (FM) and dry matter weight (DM) of the samples (Equation 15) and from the cladode
363 succulence (CS, g cm⁻²) (Equation 16) (Corrado et al., 2020; Ho et al., 2019).

364

365
$$\text{CWC} = \left(\frac{\text{FM} - \text{DM}}{\text{FM}} \right) \times 100 \quad (15)$$

366
$$\text{CS} = \left(\frac{\text{FM} - \text{DM}}{\text{CA}} \right) \quad (16)$$

367

368 2.7. *Indicators of water and environmental stress*

369 In this study, we examined the Normalised Difference Vegetation Index (NDVI) and
370 the Evaporative Stress Index (ESI) for seasonal and interannual variations. The association
371 between the NDVI and ESI allows the health status of plants to be understood in response to
372 the intensity of hydrological drought (Anghileri et al., 2022; Wolf et al., 2016). The NDVI
373 was derived using images from the Landsat-8 Operational Land Imager (OLI) and Landsat-
374 7 Enhanced Thematic Mapper (ETM+), available on the United States Geological Survey
375 (USGS) website at 30 m resolution for the red (0.64–0.67 μm) and near-infrared (0.85–0.88
376 μm) bands (Jardim et al., 2022; Právělie et al., 2022). Landsat images acquired from April
377 2015 to April 2017 were then processed using the Google Earth Engine (GEE) platform.
378 With the GEE Application Programming Interface (API) we implemented code written in
379 JavaScript to quantify the NDVI (Jardim et al., 2022). In addition, a pixel-quality attribute
380 mask was applied to the images to mask clouds, cloud shadow and water using the CFMask
381 algorithm, with the values expressed as surface reflectance (Foga et al., 2017; Hurni et al.,
382 2019). The NDVI can take dimensionless values ranging from -1 to +1, being positive when
383 the crops show photosynthetic activity, and generally referring to bodies of water when
384 negative. On the other hand, low positive NDVI values are characteristic of stressed
385 vegetation or vegetation with a small leaf area.

386 Although the ESI can be quantified via remote sensing, we used field data to quantify
387 it as per Equation 17 (Anderson et al., 2007). The ESI generally ranges from 0 to 1, and is
388 linked to the evaporative demand of both the surface and the atmosphere. When the ESI is
389 close to 1, it indicates water stress in the ecosystem; when it approaches 0, it indicates the

390 absence of water stress (Wolf et al., 2016; Yue et al., 2019). In addition, the reference
391 evapotranspiration (ET_0) was estimated using the FAO-56 Penman-Monteith method, and
392 then multiplied by the crop coefficient (K_c) to obtain the potential crop evapotranspiration
393 (PET_c) (Allen et al., 1998).

394

$$395 \quad ESI = 1 - \frac{ET}{PET_c} \quad (17)$$

396

397 2.8. Soil moisture

398 We considered the soil water balance method proposed by Thornthwaite–Mather to
399 determine the available water fraction (AWF) over time (Bielski et al., 2018; Lyra et al.,
400 2016; Pardo et al., 2020; Thornthwaite and Mather, 1955). This fraction expresses the total
401 available water that a crop can extract without undergoing water stress (Bielski et al., 2018;
402 Pardo et al., 2020). Daily soil and micrometeorological data from the tower located in the
403 experimental area were used. The available water capacity of the soil and a respective root-
404 system depth of 75 cm and 60 mm were considered as per Aparecido et al. (2021) and
405 Almagbile et al. (2019).

406

407 2.9. Statistical analysis

408 In the first step, we applied nonlinear sigmoid functions for the morphophysiological
409 indices and cutting time, adopting the significance of the F-test ($P < 0.05$) and the coefficient
410 of determination ($R^2 > 0.85$) as the criterion for choosing the model. Data on the NDVI, ET_0 ,
411 ESI, available water fraction and rainfall were submitted to descriptive statistics and
412 expressed as the mean and standard deviation. In the next step, the time-scale data of the
413 energy balance components (R_n , LE , H , and G), ET , and VPD for the four seasons under
414 study (i.e., wet season, dry season, wet-dry transition and dry-wet transition) were submitted
415 to one-way analysis of variance (ANOVA) by F-test ($P < 0.05$). The mean values were
416 compared by Tukey's HSD (honestly significant difference) test for multiple comparisons
417 ($P < 0.05$). Data on the cladode water content and environmental conditions were evaluated
418 using boxplots showing the median, interquartile range and 1.5 times the interquartile range.

419 Finally, the interrelationships between the plant parameters and environmental
420 conditions were tested using principal component analysis (PCA). We applied PCA to the
421 mean value of the environmental variables (R_n , LE , H , G , VPD, ESI, NDVI and ET_0) and
422 plants variables (ET, NUE, WUE, AGR, RGR, NAR, SCA, CWC, CS, RUE and yield). The
423 response variables were standardised using the z-transform (mean = 0, standard deviation =
424 1), subtracting from the mean value and then dividing by the standard deviation. This is due
425 to the different magnitudes and units of the variables under study, and makes them directly
426 comparable. Significant principal components were selected according to the Kaiser
427 criterion, considering only eigenvalues greater than 1.0 (Jardim et al., 2021a, 2022; M. V. da
428 Silva et al., 2021). The analysis was carried out using the R software (R Core Team, 2022).

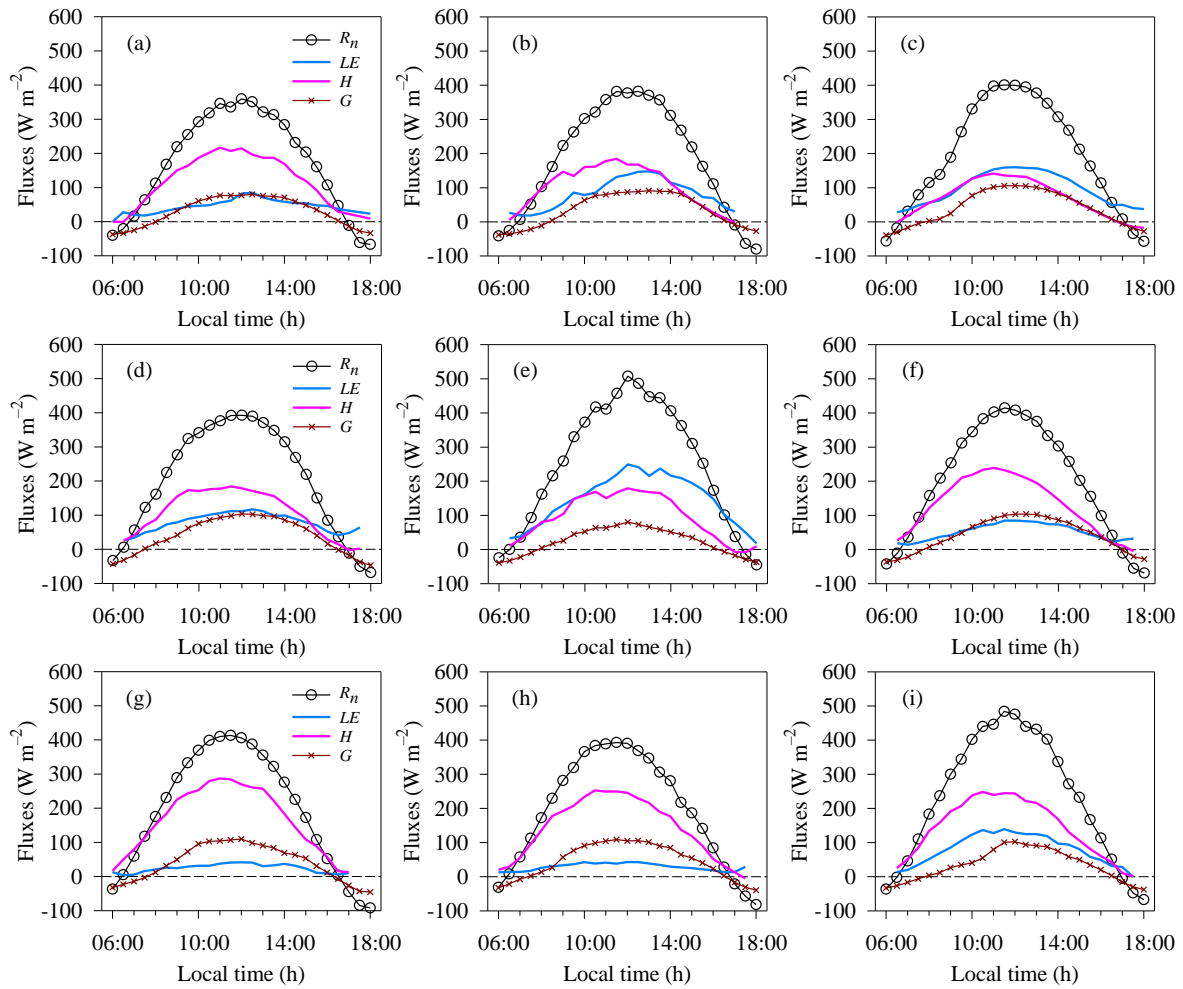
429

430 **3. Results**

431 *3.1. Surface energy budget*

432 Figure 2 shows daytime values for the hourly variation in the energy balance fluxes
433 during the experimental period, with the components evaluated during the wet and dry
434 seasons and their transitions (i.e., wet-dry and dry-wet seasons). During the wet season, the
435 lowest daily values for net radiation (R_n) were seen in 2015 (Figure 2a), and the maximum
436 in 2016 (Figure 2e), with mean values of 172.21 and 247.92 $W\ m^{-2}$, respectively. Among the
437 energy fluxes, most of the R_n came from the sensible heat flux (H), with the exception of
438 2015, which showed a mean value of 95.49 $W\ m^{-2}$. In 2017, the highest value was seen for
439 H (143.58 $W\ m^{-2}$), whereas 2015 and 2016 saw the lowest and highest values for latent heat
440 flux (LE), respectively, with a mean value of 47.62 and 145.38 $W\ m^{-2}$. During the wet season,
441 the soil heat flux (G) was greater in 2017, showing a mean value of 32.13 $W\ m^{-2}$, with a
442 gradual increase throughout the day and maximum values around noon (11:00 to 14:00 local
443 time). On the other hand, we found lower values for G during 2016, with a mean of 23.33 W
444 m^{-2} . As shown in Figures 2b and 2f (wet-dry transition), R_n was 12% lower than during the
445 wet season. There was a considerable variation in LE between 2015 and 2016, with mean
446 values of 80.88 and 51.32 $W\ m^{-2}$, respectively. This seasonal pattern was responsible for
447 smaller turbulent fluxes; furthermore, there was an increase in G (34%) compared to the
448 previous season.

449



450

451 Figure 2. Hourly daytime mean energy flux over the area of cactus for different periods: wet
 452 season (a, e, and i), wet-dry transition (b and f), dry season (c and g), and dry-wet transition
 453 (d and h). Here R_n is the net radiation, LE is the latent heat flux, H is the sensible heat flux,
 454 and G is the soil heat flux, all calculated in $W m^{-2}$. Note: panels (a), (b) and (c) show the
 455 seasons for 2015; (d), (e), (f) and (g) for 2016; and (h) and (i) for 2017.

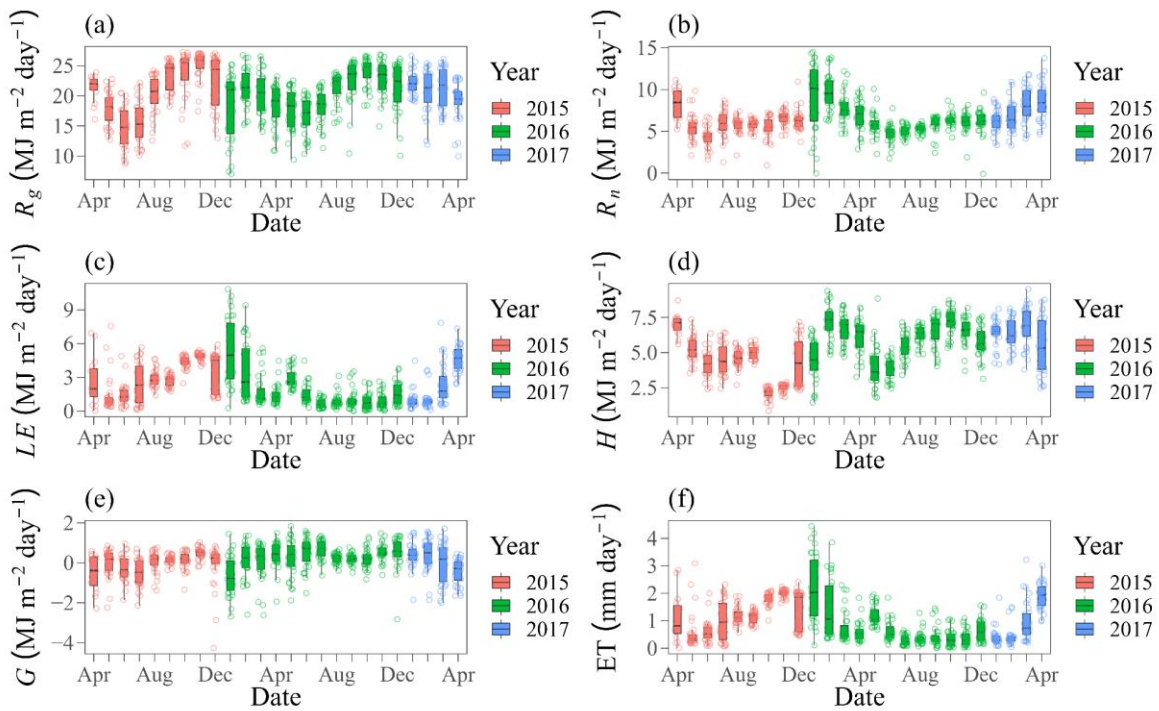
456

457 The values for R_n obtained throughout the day during the dry season in 2015 and 2016
 458 (Figure 2c and 2g) were very similar, with mean values of 191.83 and $194.02 W m^{-2}$,
 459 respectively. These results for the energy budget are similar to the wet-dry transition season,
 460 and different to those seen during the wet season. Specifically, G showed a significant
 461 increase (42%) compared to the wet season. For the turbulent fluxes, LE was 41% greater
 462 than H during the dry season in 2015. On the other hand, H showed contrasting behaviour in

463 2016 due to atmospheric conditions, being 141% higher than in 2015. Even so, the total
464 turbulent flux was similar for the two years mentioned above, with a mean value of 176 .87
465 W m^{-2} . In general, the turbulent fluxes exhibited opposite trends over time, and was the
466 component with the greatest contribution to the energy budget. Figures 2d and 2h show the
467 daily fluxes during the dry-wet transition season for 2016 and 2017. The result for R_n in 2016
468 was 3.79% higher than in 2017, and comparing the two transition seasons, the value for R_n
469 during the dry-wet transition season is higher than during the wet-dry transition (4%). There
470 was a large temporal variation in G during the study period. During the dry-wet transition
471 season especially, G was approximately 18% higher than during the other seasons. Despite
472 making a significant contribution to the energy balance, our results for H were approximately
473 2% (wet season), 6% (wet-dry transition) and 7% (dry season) higher during the dry-wet
474 transition season. Furthermore, for the same season, which includes a dry phase, there was a
475 reduction in LE (26%) compared to the other seasons. Based on this, it is clear that most of
476 the available net surface energy contributed to the sensible heat flux.

477 On a temporal scale, changes can clearly be seen in the energy budget throughout
478 each year (Figure 3). The mean values for global solar radiation (R_g) decrease significantly
479 from May to July, being 22% lower in relation to the other years (Figure 3a). We also saw a
480 greater range in December 2015 (median 24.38 $\text{MJ m}^{-2} \text{day}^{-1}$, interquartile range 18.47 to
481 25.92) and January 2016 (median 21 $\text{MJ m}^{-2} \text{day}^{-1}$, interquartile range 13.72 to 22.33). In
482 2015, 2016 and 2017 the mean values for R_g were 20.45, 20.27, and 20.84 $\text{MJ m}^{-2} \text{day}^{-1}$,
483 respectively, despite an intermonthly variation (median 20.96 $\text{MJ m}^{-2} \text{day}^{-1}$, interquartile
484 range 17.75 to 23.73). Figure 3b shows the variation in R_n throughout the experiment. In
485 April 2015, January and February 2016, and from March to April 2017, the values for R_n
486 were higher, with a mean of 8.82 $\text{MJ m}^{-2} \text{day}^{-1}$. However, the mean R_n for the three years
487 was 6.52 $\text{MJ m}^{-2} \text{day}^{-1}$ (median 6.15, interquartile range 5.27 to 7.21), with a reduction of
488 26% compared to the months with the higher values shown above. As a result of cloudiness,
489 R_n had the lowest values in June, with a mean of 4.51 $\text{MJ m}^{-2} \text{day}^{-1}$.

490



491

492 Figure 3. Time series for the energy budget in an area of cactus from 2015 to 2017. R_g is the
 493 global solar radiation (a), R_n is the net radiation (b), LE is the latent heat flux (c), H is the
 494 sensible heat flux (d), G is the soil heat flux (e), and ET is the evapotranspiration (f). The
 495 boxplots show the median; horizontal bars represent the 25th, 50th, and 75th percentiles;
 496 whiskers (lower and upper) represent the $1.5\times$ interquartile ranges. Corresponding data are
 497 represented by circles.

498

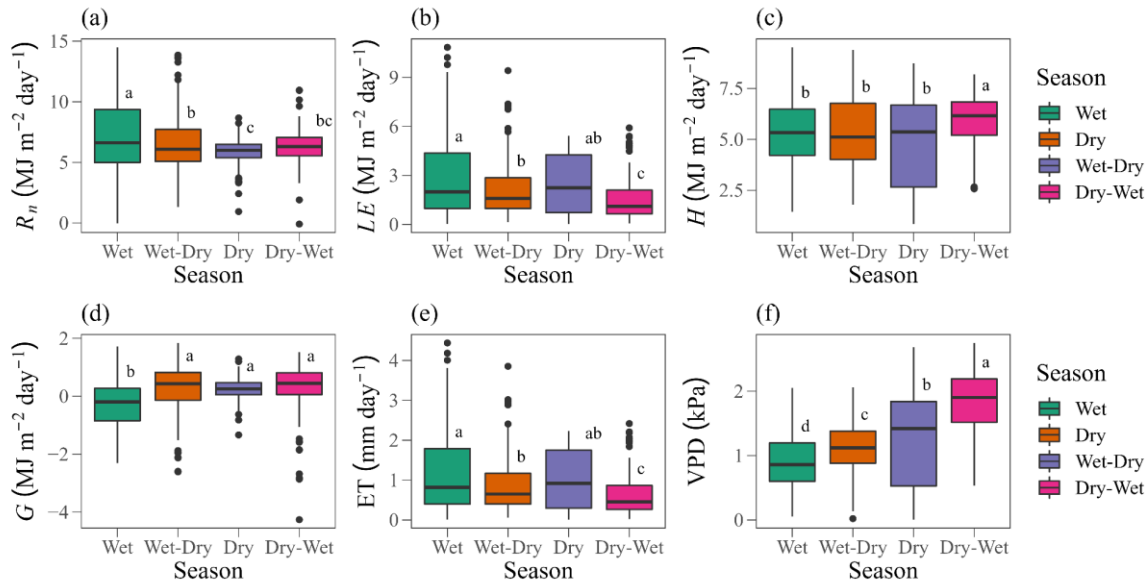
499 Figures 3c and 3d show the turbulent fluxes in the energy balance, with a mean value
 500 for LE of $2.32 \text{ MJ m}^{-2} \text{ day}^{-1}$, and maximum and minimum values of 5.41 and 0.70 MJ m^{-2}
 501 day^{-1} , respectively, in January (median $4.97 \text{ MJ m}^{-2} \text{ day}^{-1}$, interquartile range 2.88 to 7.83)
 502 and July (median $0.56 \text{ MJ m}^{-2} \text{ day}^{-1}$, interquartile range 0.31 to 0.98), both in 2016. After
 503 the occurrence of high LE values from January to April 2016, there was a significant value
 504 ($2.92 \text{ MJ m}^{-2} \text{ day}^{-1}$) in May 2016 due to the rainfall events (Figure 5i). Obvious inversion of
 505 the turbulent fluxes can be seen from the values for LE in relation to H (Figures 3c and 3d).
 506 Although the values for LE are relatively high, energy consumption is synchronous with that
 507 of H . During 2015–2017, H showed a mean value of $5.39 \text{ MJ m}^{-2} \text{ day}^{-1}$. Interestingly, the
 508 minimum values of H , with a mean of $2.11 \text{ MJ m}^{-2} \text{ day}^{-1}$ (median $2.21 \text{ MJ m}^{-2} \text{ day}^{-1}$,
 509 interquartile range 1.93 to 2.35) and maximum values, with a mean of $7.21 \text{ MJ m}^{-2} \text{ day}^{-1}$

510 (median $7.24 \text{ MJ m}^{-2} \text{ day}^{-1}$, interquartile range 6.80 to 7.86) occurred in October 2015 and
511 2016, respectively, and due to the influence of the rainfall, resulted in a difference of 71%.
512 Furthermore, H gradually increased in value from July to September 2015 and July to
513 October 2016, with mean values during this period of 4.70 and $6.37 \text{ MJ m}^{-2} \text{ day}^{-1}$,
514 respectively.

515 Figures 3e and 3f show the behaviour of G and of the evapotranspiration (ET). For G ,
516 the values were more negative during 2015 (April to July, and December) as well as in
517 January 2016, and April 2017. As shown, the minimum values (median $-0.77 \text{ MJ m}^{-2} \text{ day}^{-1}$,
518 interquartile range -1.37 to 0.10) and maximum values (median $0.71 \text{ MJ m}^{-2} \text{ day}^{-1}$,
519 interquartile range 0.36 to 1.07) ranged, on average, from -0.65 to $0.67 \text{ MJ m}^{-2} \text{ day}^{-1}$,
520 respectively. We found high values for ET when G and H were low. Despite the interannual
521 variability, the range of values for ET agree with the turbulent heat fluxes, ranging from 0.29
522 to 2.22 mm day^{-1} (median $0.23 \text{ MJ m}^{-2} \text{ day}^{-1}$, interquartile range 0.13 to 0.40 ; and median
523 $2.03 \text{ MJ m}^{-2} \text{ day}^{-1}$, interquartile range 1.18 to 3.21 , respectively), with a mean of 0.95 mm
524 day^{-1} during the period under study.

525 In Figure 4 and Table 3, we present a detailed seasonal boxplot analysis of the energy
526 budget, heat exchange capacity and water vapour in the cactus during the four seasons (wet,
527 wet-dry, dry, and dry-wet), together with the energy partition ratios. For R_n , the values were
528 significantly higher during the wet season (Tukey's HSD test, $P < 0.05$; median 6.61 MJ m^{-2}
529 day^{-1} , interquartile range 4.99 to 9.37), being on average 14% higher than during the other
530 seasons (Figure 4a). Despite showing similar mean values for R_n , during the dry season, the
531 energy was 7% lower than during the dry-wet transition season. For LE (Figure 4b), there
532 was no significant difference ($P > 0.05$) between the wet and dry seasons, with mean values
533 of 2.87 and $2.41 \text{ MJ m}^{-2} \text{ day}^{-1}$, respectively. On the other hand, there was a 25% reduction
534 ($P < 0.05$) in LE with the arrival of the wet-dry transition season. Notably, the lowest and
535 highest values for LE and H were seen during the dry-wet transition season, 1.57 and 5.89
536 $\text{MJ m}^{-2} \text{ day}^{-1}$, respectively. These effects were even greater for H (Figure 4c), with
537 significantly higher values ($P < 0.05$) during the dry-wet transition season (median = 6.16
538 $\text{MJ m}^{-2} \text{ day}^{-1}$, interquartile range 5.20 to 6.84). In general, during the dry-wet transition
539 season, H was 13% greater than during the other seasons, showing that in the cactus under a
540 semi-arid environment most of the R_n is destined for this process (Figure 4c). Verifying the

541 energy partitions (Table 3), the H/R_n ratio was generally responsible for the highest power
 542 consumption (58%). The LE/R_n ratio varied between 17% and 30%, with a total mean value
 543 of 24% over all the seasons. In addition, the G/R_n ratio reached an average of 17%, with the
 544 smallest partition (13%) during the wet season (Table 3).
 545



546
 547 Figure 4. Boxplot of seasonal variations in energy and water exchange in an area of cactus.
 548 R_n is the net radiation (a), LE is the latent heat flux (b), H is the sensible heat flux (c), G is
 549 the soil heat flux (d), ET is the evapotranspiration (e), and VPD is the vapour pressure deficit
 550 (f). The boxplots show the median; horizontal bars represent the 25th, 50th, and 75th
 551 percentiles; whiskers (lower and upper) represent the $1.5\times$ interquartile ranges; dots represent
 552 outliers. Significance was calculated using one-way analysis of variance (ANOVA) with
 553 Tukey's honestly significant difference (HSD) post hoc test. Different letters above each box
 554 indicate significant differences ($P < 0.05$).
 555

556 Table 3. Energy budget component partitioning during the wet, wet-dry, dry, and dry-wet
 557 seasons in an area of cactus.

Season	Partition ratio (%)		
	LE/R_n	H/R_n	G/R_n
Wet	30	57	13
Wet-dry	23	58	19

Dry	26	55	19
Dry-wet	17	64	19
Mean ratio	24	58	17

R_n is the net radiation; LE is the latent heat flux; H is the sensible heat flux; G is the soil heat flux.

558

559 The lowest values for G (Figure 4d) were seen during the wet season (-0.28 to 0.28
560 $\text{MJ m}^{-2} \text{day}^{-1}$), with a marked reduction of 203% in relation to the other seasons. The sharp
561 decrease in G and the G/R_n ratio during the wet season (Table 3) is clearly due to the high
562 volumes of rainfall and soil moisture (Figure 5) during this period. Similar to the behaviour
563 of LE , there was no significant difference in ET values during the wet or dry seasons (Figure
564 4e). This confirms the hypothesis that ET is maintained during the dry season and decreases
565 during the dry-wet transition season (median $0.46 \text{ MJ m}^{-2} \text{day}^{-1}$, interquartile range 0.26 to
566 0.86). We saw reductions of 40.31% and 26.68% during the dry-wet transition when
567 comparing the wet and dry seasons and the wet-dry transition season, respectively ($P < 0.05$).

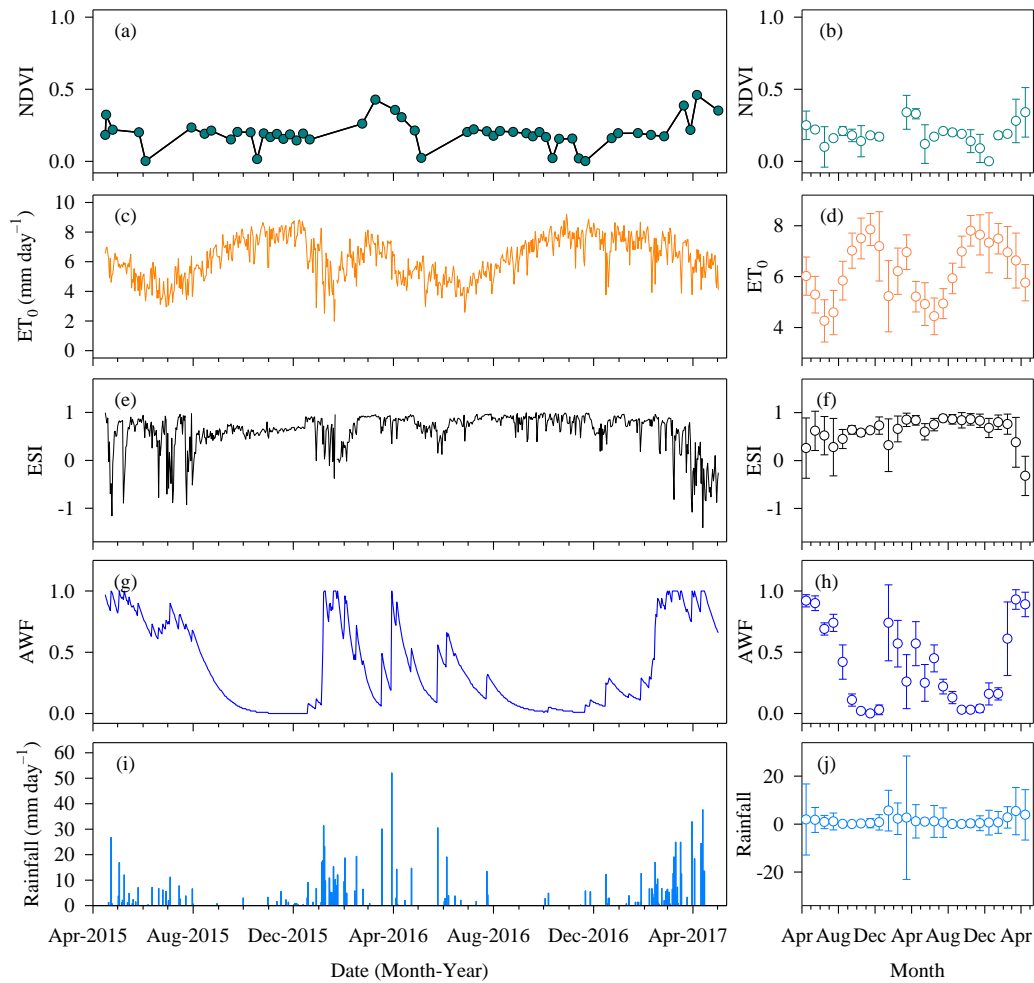
568 There was a clear significant seasonal variation in the vapour pressure deficit (VPD)
569 (Figure 4f), with a mean of 1.82 kPa during the dry-wet transition season, being 45% and
570 97% higher during the dry season (median 1.42 kPa , interquartile range 0.53 to 1.84) and wet
571 season (median 0.86 kPa , interquartile range 0.60 to 1.20), respectively. Furthermore, there
572 was a significant difference ($P < 0.05$) when comparing the VPD of the transition seasons,
573 where the VPD of the wet-dry season was 38% lower than that of dry-wet season (median
574 1.12 and 1.90 kPa , interquartile ranges 0.88 to 1.38 and 1.52 to 2.19 , respectively).

575

576 3.2. NDVI signatures, environmental data and the impact of drought

577 We selected a time series for the Normalised Difference Vegetation Index (NDVI),
578 reference evapotranspiration (ET_0), Evaporative Stress Index (ESI), available water fraction
579 (AWF) and rainfall during the experimental period (Figure 5). There was no NDVI saturation
580 during any of the cactus growing seasons (Figures 5a and 5b). The highest NDVI values were
581 seen during the wet season, with a mean of 0.23 . Every year, the mean value of the wet-dry,
582 dry, and dry-wet seasons (transitions) were, respectively, 9%, 26%, and 39% lower than
583 during the wet season. In addition, it should be noted that the NDVI decreased more

584 significantly (17%) during the change from the dry season to the dry-wet transition season
585 (Figure 5b). Despite oscillations in the NDVI trajectory in the area, the final periods of the
586 cycle show greater consistency, with a rise in the index. Variations in the NDVI are
587 influenced by the canopy cover, cladode morphometry (see Figure 6) and environmental
588 conditions (Figure 5c and 5e). As shown in Figure 5c and 5d, the mean values for ET_0 ranged
589 from 4.26 (± 0.83) to 7.85 (± 0.63) mm day^{-1} (mean \pm standard deviation), both variations
590 occurring in 2015. Variations, both intermonthly and throughout the year, can also be seen
591 in the ET_0 , with lower values between May and July, mainly due to the lower incidence of
592 solar radiation and the lower air temperature (Figure 5c). During the present study, the ET_0
593 was, on average, 6.24 mm day^{-1} , with emphasis on the dry season (6.87 mm day^{-1}) and the
594 dry-wet transition season (6.78 mm day^{-1}). On the other hand, we found lower values during
595 the wet and wet-dry seasons, of 5.79 and 5.33 mm day^{-1} , respectively. Although high ET_0
596 values can be found for approximately 48% of the experimental period, the values remained
597 below 6.24 mm day^{-1} .
598



599

600 Figure 5. Temporal evolution of the Normalised Difference Vegetation Index [NDVI] (a),
 601 reference evapotranspiration [ET_0] (c), Evaporative Stress Index [ESI] (e), available water
 602 fraction [AWF] (g), and rainfall (i) for an area cultivated with cactus. The five panels (b),
 603 (d), (f), (h), and (j) show monthly results over each year for NDVI, ET_0 , ESI, AWF and
 604 rainfall during the experimental period, respectively. Data with error bars represent the mean
 605 \pm SD (standard deviation).

606

607 The monthly mean ESI ranged from -0.32 to 0.88 (Figure 5f). We saw negative ESI
 608 values (Figure 5e and 5f) due to the concentrated rainfall events, favouring greater soil
 609 moisture (Figure 5g and 5i). The wet season and the wet-dry transition season had the lowest
 610 ESI values, with a mean of 0.41 and 0.56 , respectively. On the other hand, 2016 saw an
 611 exception in the behaviour of the ESI during the wet-dry transition season, with mean values

612 greater than 0.7. During the dry season, the index was 35% higher than during the other
613 seasons, reaching 78% compared to the wet season. This clearly confirms that the most
614 stressful conditions occur during the dry season, which in turn has a high atmospheric
615 demand. The variations in AWF largely occurred together with those of the above-mentioned
616 variables (Figure 5g); in addition, the greatest mean value (0.77) was seen during the wet
617 season. The monthly variation in AWF in the soil ranged from 0.002 to 0.931, and notably,
618 these variations showed more critical values during the dry season, with a mean of 0.12 and
619 0.09 during 2015 and 2016, respectively. However, even with a water scarcity during the
620 wet-dry and dry-wet transition seasons, the AWF was 0.48 and 0.31, respectively, being
621 289% greater compared to the dry season. Although the four seasons under study differ when
622 compared to each other, there was a similar trend in their behaviour for the same season in
623 each of the different years (Figure 5h).

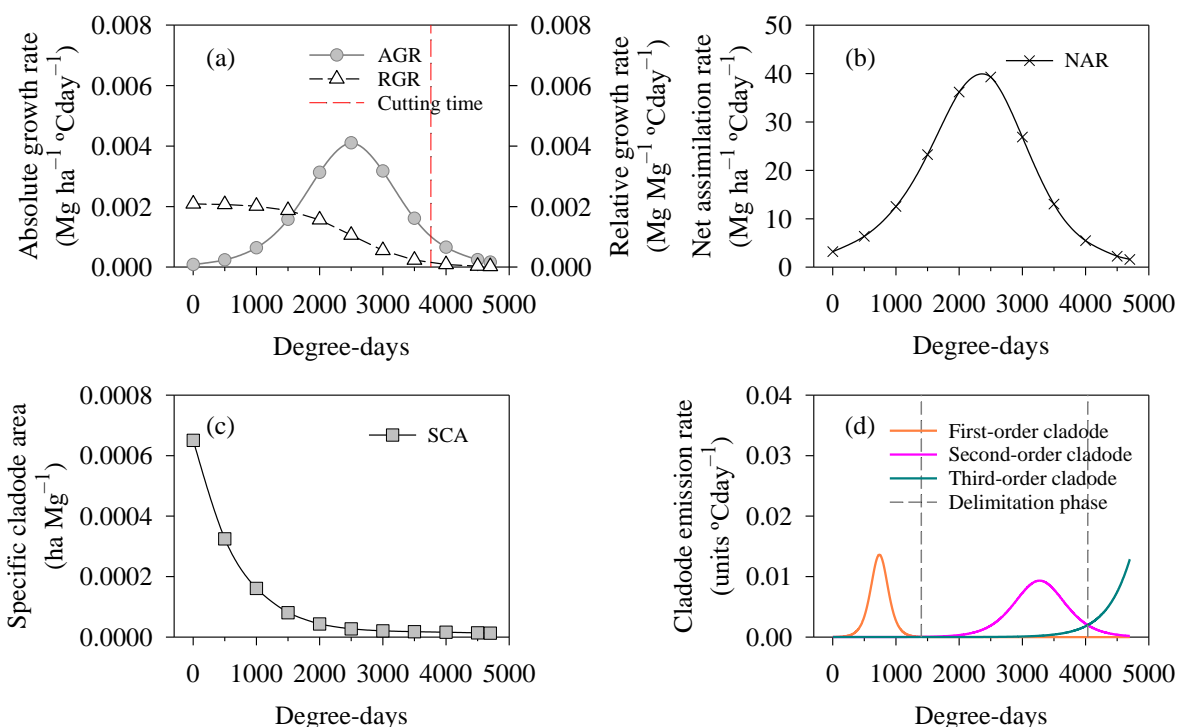
624 We found a clear variation in rainfall events during the experimental period (Figure
625 5i and 5j). The values for 2015, 2016 and 2017 were 183.31 (± 17.53), 477.13 (± 49.19) and
626 382.78 (± 61.71) mm year⁻¹, respectively, a total of 1043.22 mm (347.74 ± 150.01 mm
627 year⁻¹). In 2016, the period with the greatest accumulation of rain, more than 50% of the rain
628 was concentrated from January to February (wet season). In addition, it should be noted that
629 in March of the same year the rainfall events were less homogenous, resulting in higher
630 values for the standard deviation. In general, the months from August to November show an
631 extreme water deficit, with the monthly rainfall varying from 0 to 11.44 mm (Figure 5j).

632

633 *3.3. Growth parameters, phenological characteristics, and cutting time*

634 The curves of the morphophysiological parameters, phenophases, and cutting time of
635 the cactus are shown in Figure 6. Analysing the absolute growth rate (AGR), we found that
636 the cactus used more than 53% of the thermal time to reach the maximum AGR (0.0041 Mg
637 ha⁻¹ °Cday⁻¹) at 2500 °Cday. Based on the AGR, the ideal cutting time of the plants was at
638 3760 °Cday, although the species was harvested at 4700 °Cday (Figure 6a). Notably, the
639 relative growth rate (RGR) was higher during the initial growth period, and gradually
640 decreased until it reached minimum values. The maximum RGR value of the cactus was
641 0.0021 Mg Mg⁻¹ °Cday⁻¹. Again, both growth rates (i.e., AGR and RGR) showed a
642 significant fall in biomass accumulation upon reaching the cutting time. When analysing the

643 net assimilation rate (NAR), our results showed a mean NAR of $17.76 \text{ Mg ha}^{-1} \text{ }^\circ\text{Cday}^{-1}$, with
 644 a variation of 1.60 to $40.22 \text{ Mg ha}^{-1} \text{ }^\circ\text{Cday}^{-1}$. Although the NAR was higher at $2500 \text{ }^\circ\text{Cday}$,
 645 there was a 50% reduction in the photosynthetic capacity of the cactus by the end of the cycle
 646 ($4700 \text{ }^\circ\text{Cday}$) compared to the initial growth period (Figure 6b).
 647



648
 649 Figure 6. Absolute growth rate—AGR and relative growth rate—RGR (a), net assimilation
 650 rate—NAR (b), specific cladode area—SCA (c), and cladode emission rate (d) in *N.*
 651 *cochenillifera* (L.) Salm-Dyck under a semi-arid environment.

652

653 Figures 6c and 6d show the performance of the specific cladode area (SCA) and
 654 cladode emission rate. The SCA values were higher at the start, and decreased significantly
 655 over time, as was also seen with the RGR. The maximum SCA reached by the cactus was
 656 $0.00065 \text{ ha Mg}^{-1}$; furthermore, when the plants reached the thermal sum of $1500 \text{ }^\circ\text{Cday}$, there
 657 was a mean reduction of $0.00002 \text{ ha Mg}^{-1}$ in SCA over time. Our results show that the cactus
 658 had three cladode phenophases (Figure 6d). The first-order cladodes reached the highest
 659 emission rate during these phenophases, with a mean of $0.0136 \text{ units } ^\circ\text{Cday}$. There was a
 660 reduction of 32% and 5% in phenophases two and three, respectively, relative to the first

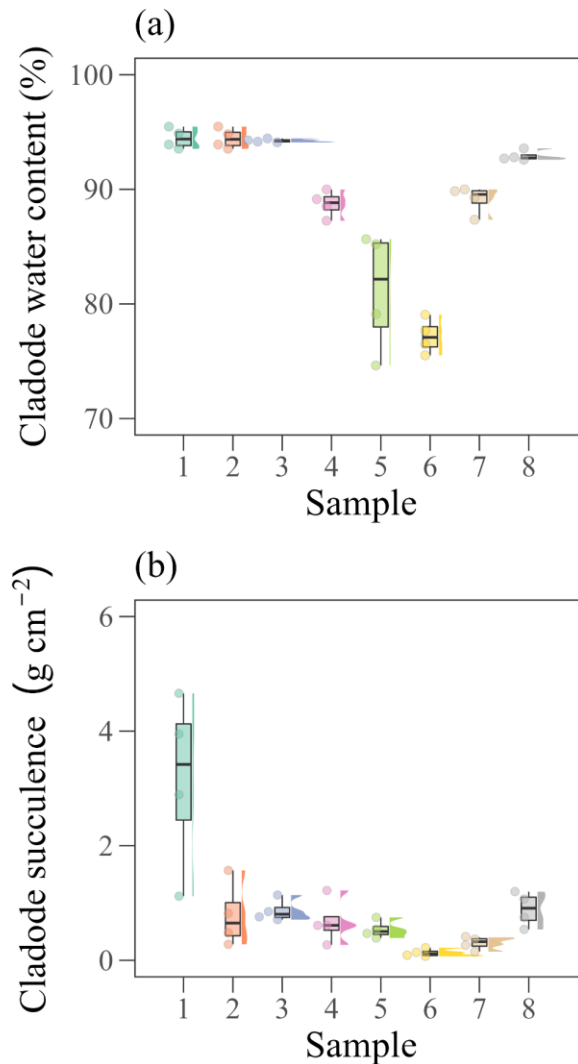
661 phenophase. Interestingly, we also found a prolongation of phenophase two, with an
662 accumulated thermal time of 2632 °Cday, while the first phenophase (1402 accumulated
663 °Cday) and third phenophase (666 °Cday, with the lowest cumulative value) were shorter.
664 We did not completely analyse the third phenophase, as the experiment had already been
665 harvested before the phenophase ended.

666

667 *3.4. Water relations, Bowen ratio, biophysical efficiency, and yield*

668 We found significant variation in the water relations of the cladodes throughout the
669 experimental period (Figure 7). The cladode water content (CWC) had a mean value of
670 89.03%, varying from 77% to 95%, with interquartile ranges of 76% to 78% and 94% to
671 95%, respectively (Figure 7a). We also found a more-expressive gradual loss of cladode
672 turgidity between samples four and six, and later, rehydration of the cladodes. Samples five
673 and six included October to December 2016, with low rainfall and low soil moisture (see
674 Figure 5). Although the lower water availability caused significant dehydration, the cladodes
675 rehydrated at the end of the cycle, with an increase of 20% in the CWC. From the second
676 sample onwards, the plants showed a similar variation in cladode succulence to that of the
677 CWC (Figure 7b). On the other hand, due to the high turgidity and smaller cladode area,
678 succulence was generally greater in the first sample (3.16 g cm^{-2}). The mean value for
679 cladode succulence was 0.92 g cm^{-2} , ranging from 0.07 to 4.66 g cm^{-2} . The magnitude of the
680 changes in water relations, whether increasing or decreasing, paralleled the levels of water
681 availability and cladode development.

682



683

684 Figure 7. Cladode water content (a) and cladode succulence (b) in *N. cochenillifera* (L.)
 685 Salm-Dyck over time (2015 to 2017) under a semi-arid environment. The boxplots show the
 686 median; horizontal bars represent the 25th, 50th, and 75th percentiles; whiskers (lower and
 687 upper) represent the 1.5× interquartile ranges.

688

689 Table 4 shows our results for the efficiency of the biophysical parameters, the Bowen
 690 ratio and biomass yield in the cactus at the end of the experimental period. The high radiation
 691 use efficiency (RUE) of the cactus can clearly be seen, with a mean value of 3.95 g MJ⁻¹,
 692 which favoured the process of photosynthesis, and consequently, significant biomass
 693 conversion, with a mean of 12.47 Mg ha⁻¹ dry matter. In addition, a value of 1.75 kg m⁻³ was
 694 found for water use efficiency (WUE). Considering the information provided by the surface

695 energy distribution between the turbulent fluxes, our results point to a mean Bowen ratio (β)
 696 of 3.53 (Table 4).

697

698 Table 4. Summary of the efficiency of the biophysical parameters, Bowen ratio and yield in
 699 the cactus at the end of the experimental period.

Variable	Mean value	Standard deviation
β (dimensionless)	3.53	± 2.45
Yield (Mg ha^{-1})	12.47	± 2.20
RUE (g MJ^{-1})	3.95	± 0.70
WUE (kg m^{-3})	1.75	± 0.31
NUE _[Calcium] (mg m^{-3})	29.03	± 1.14
NUE _[Magnesium] (mg m^{-3})	12.44	± 2.25
NUE _[Phosphorus] (mg m^{-3})	62.13	± 11.71
NUE _[Potassium] (mg m^{-3})	50.88	± 5.50
NUE _[Sodium] (mg m^{-3})	0.22	± 0.02

RUE is the radiation use efficiency; β is the annual Bowen ratio based on annual energy budgets; WUE is the water use efficiency; NUE is the nutrient use efficiency; Yield is the yield of aboveground dry biomass.

700

701 According to our results, the cactus showed greater efficiency in the use of
 702 phosphorus and potassium, with mean values of 62.13 and 50.88 mg m^{-3} , respectively (Table
 703 4). Calcium use efficiency was 133% higher than that of magnesium. Clearly, the cactus is
 704 highly efficient in using the above nutrients, while sodium use efficiency was low (0.22 mg
 705 m^{-3}), which indicates greater selectivity of the absorption channels for K^+ in relation to Na^+ .

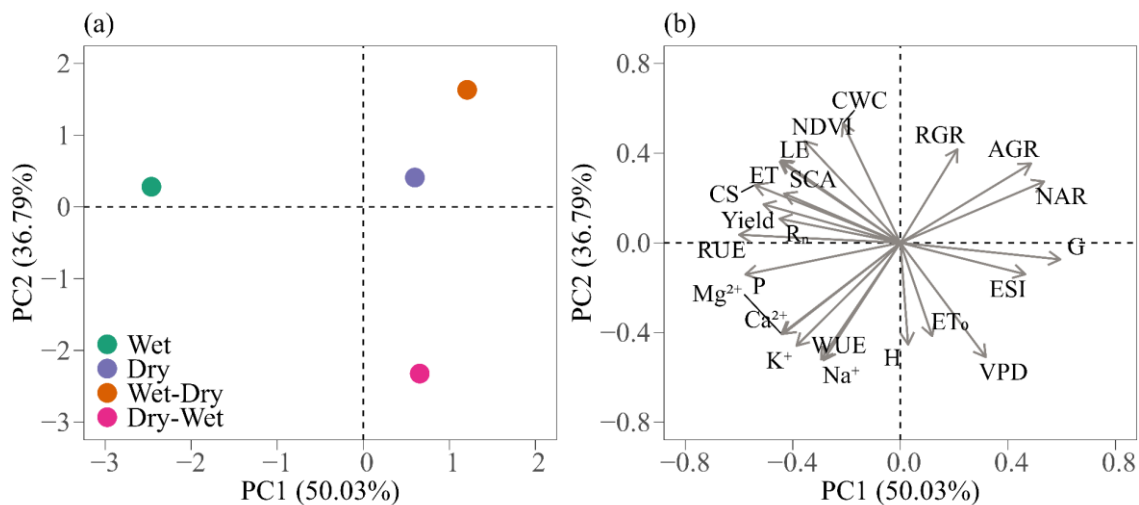
706

707 3.5. Interrelationships between environmental variables and plant responses

708 The interrelationship between the environmental variables and the plant variables can
 709 be explained using principal component analysis (PCA) (Figure 8). Our results show that the
 710 first two principal components were responsible for 86.82% of the total variance, with a
 711 strong relationship between the environmental and plant variables during the growing
 712 seasons. Despite presenting an eigenvalue greater than 1, the third principal component was

713 not shown due to the lack of any information relevant to the present study. On the other hand,
 714 with eigenvalues also greater than 1, the first principal component (PC1) contributed with
 715 50.03%, while the second principal component (PC2) contributed with 36.79% of the total
 716 variance. The PCA revealed the clear separation of the growing seasons along the two
 717 dimensions of the principal component (Figure 8a). The wet and dry seasons, and the wet-
 718 dry transition season presented the greatest contribution to PC1, with scores of -2.46 , 0.60
 719 and 1.21 , respectively. For PC2, the two transition seasons contributed the most, with scores
 720 of -2.32 (dry-wet) and 1.63 (wet-dry). In addition to the higher PC1 scores, there is an
 721 obvious difference between the groups of environmental and plant variables.

722



723

724 Figure 8. Principal component analysis (PCA) ordered biplot of environmental and plant
 725 factors. Score plot (a) and loading plot (b) of the first two principal components (PC) during
 726 the wet and dry seasons and transition periods. P (phosphorus), Mg²⁺ (magnesium), Ca²⁺
 727 (calcium), K⁺ (potassium), and Na⁺ (sodium) refer to the efficiency of use of each nutrient.
 728 The following abbreviations are used: net radiation (R_n), latent heat flux (LE), sensible heat
 729 flux (H), soil heat flux (G), evapotranspiration (ET), vapour pressure deficit (VPD),
 730 Evaporative Stress Index (ESI), Normalised Difference Vegetation Index ($NDVI$), water use
 731 efficiency (WUE), reference evapotranspiration (ET_0), absolute growth rate (AGR), relative
 732 growth rate (RGR), net assimilation rate (NAR), specific cladode area (SCA), cladode water
 733 content (CWC), cladode succulence (CS), radiation use efficiency (RUE), and biomass yield
 734 (Yield).

735

736 The variables G , NAR, AGR, ESI, VPD, RGR, ET_0 and H are positively correlated
737 with PC1, with loadings varying from 0.59 to 0.03 (Figure 8b). On the other hand, the
738 remaining variables (i.e., CWC, Na^+ , WUE, NDVI, K^+ , SCA, Ca^{2+} , Mg^{2+} , LE , ET , R_n , Yield,
739 CS, P, and RUE) showed a negative correlation with PC1, with loadings ranging from -0.21
740 to -0.60 . The dry season and wet-dry transition showed the highest correlation (most-
741 positive) with G (0.59), NAR (0.53), AGR (0.49) and RGR (0.21); the first three with the
742 greatest PC1 loadings. The results clearly show that for the above-mentioned seasons, the
743 cactus shows lower nutrient and water use efficiency (i.e., most-negative PC scores). In
744 particular, the group of variables showing a high correlation with the atmospheric conditions
745 (i.e., H , ET_0 , VPD and ESI) did so during the dry-wet transition season. In addition, the wet
746 season showed a positive correlation with the largest grouping of biophysical and plant
747 variables (Figure 8b).

748 All the variables grouped together during the wet season (e.g., CWC, NDVI, LE , ET ,
749 CS, SCA, Yield, R_n and RUE) had the highest (most-positive) contribution to the total
750 explained variance for PC2 (36.79%). The variables with the highest loading during the wet
751 season were CWC (0.53) and NDVI (0.45). In addition, during the wet season, the cactus
752 shows greater biomass yield, LE and ET than during the other seasons under study. Finally,
753 the correlation between the variables and the wet season shows that the cactus has a greater
754 SCA, CS and RUE, which explains the greater NDVI and biomass yield loadings.

755

756 **4. Discussion**

757 *4.1. Mean daytime patterns, seasonal variations in the energy fluxes, and evapotranspiration*

758 In semi-arid areas with a vegetated surface, the energy balance undergoes changes in
759 the soil-atmosphere system (Chen et al., 2022). The hourly energy partition showed the most-
760 sensitive variations, with changes in the fluxes during the morning and afternoon (Figure 2).
761 On the other hand, on a daily scale, the behaviour was similar, but of different magnitudes
762 over the years, as well as during the wet to dry and transition seasons (Figure 3). These more
763 marked variations in turbulent flux and soil heat flux were also seen by Shao et al. (2017),
764 and require greater attention when there is excessive heating of the environment, since this
765 can compromise photosynthetic efficiency. Evaporation and transpiration can reduce the heat
766 stored in the soil and in the plant, however, the cactus being a CAM plant, transpiration is

767 almost zero during the day (Hartzell et al., 2021; Nobel, 1991; Winter and Smith, 2022),
768 resulting in a smaller contribution to the LE .

769 Latent heat flux and sensible heat flux are the main variables in net energy
770 consumption, with H prominent in the energy budget of a surface cultivated with cactus. In
771 some cases, LE is less significant, an indication of environmental water limitations. Most of
772 the time, daytime fluxes show a downward concave shape, with minimum values occurring
773 at dawn and dusk (Awada et al., 2021; Nassar et al., 2021). It is possible that the proximity
774 of turbulent fluxes in the morning (before 10:00) during some wet and dry seasons may have
775 been due to the increased atmospheric demand and soil moisture that favour
776 evapotranspiration. CAM plants have the ability to cool the soil overnight (Cao et al., 2019),
777 and although their metabolism is generally nocturnal, we believe that this thermal reduction
778 lasted until the early hours of the morning (Guevara-Escobar et al., 2021). In this case,
779 evaporation from the soil may have resulted in greater change in the turbulent fluxes (Kuiyue
780 Zhang et al., 2022). Unlike forest species, cacti do not store intercepted water in the canopy,
781 but in the parenchymatic tissue. Such plants are able to carry out hydraulic redistribution of
782 the water in the soil, making it available in the surface layers. In this way, the evaporated
783 water may come mostly from the soil (Montesinos-Navarro et al., 2019; Novoa et al., 2021).

784 Based on the above analyses, we found similarities in the R_n curves (Figure 2).
785 However, it is clear that R_n was significantly higher during the wet season due to the greater
786 absorption of thermal and radiant energy by the humid atmosphere (Figure 4), contributing
787 to the LE (Alves et al., 2022; Silva et al., 2017). Using the surface energy balance with the
788 cactus *O. ficus-indica* (L.) Mill., Consoli et al. (2013) also found a higher R_n ($\sim 13 \text{ MJ m}^{-2}$
789 day^{-1}) in a semi-arid environment. The turbulent fluxes and soil heat flux showed marked
790 variations on an hourly scale and during the seasons under study (Figures 2 and 3). G was
791 clearly more expressive during the afternoon, mainly due to the accumulation of energy
792 throughout the morning, and with the greater soil moisture and radiation, there is an increase
793 in the thermal conductivity of the soil (Chen et al., 2022). In addition, the lower values for G
794 may be associated with the biophysical and growth parameters of the plants (Wang et al.,
795 2020). To substantiate this further, the cactus showed a high growth rate and high NDVI even
796 when there was a reduction in soil moisture, resulting in reduced radiation input due to the
797 greater soil cover. Although the cactus does not present a denser, more-uniform canopy, the

798 cladodes remain on the plant throughout the cycle, which may cause variations in energy
799 exchange due to the spaces between them. With greater results than those reported in the
800 present study, Flanagan and Flanagan (2018) found a mean value of $2 \text{ MJ m}^{-2} \text{ day}^{-1}$ for G in
801 an area of saguaro cactus (*Carnegiea gigantea*). Furthermore, the authors point out that the
802 greatest net energy dissipation was via surface heating and the sensible heat flux. Under semi-
803 arid conditions and vegetation consisting of the cacti *O. spinosior* and *O. engelmannii*, Pierini
804 et al. (2014) also found higher values for the sensible heat flux compared to the latent heat
805 flux.

806 Indeed, meteorological conditions have a strong relationship with the variables of the
807 surface energy balance (Figure 3 and Table 3). We saw a similar strong consistency in global
808 solar radiation (R_g), with seasonal trends consistent with the climate in the region (Lima et
809 al., 2019; T. G. F. da Silva et al., 2021). Areas of low latitude and dry climate in particular
810 have a lower LE and greater H (Jung et al., 2019). This is because the incidence of solar
811 radiation is high, and due to the low water availability, the latent heat flux is lower resulting
812 in limitations on evapotranspiration. The energy balance partition patterns were consistent
813 with the other environmental variables. For example, when the sensible heat energy was low,
814 the cactus increased evapotranspiration, behaving as an important energy sink (Figure 3).
815 Other studies point to variations in turbulent fluxes in areas of Cactaceae, and the effects of
816 changes in the energy balance due to water availability (e.g., Consoli et al., 2013; Flanagan
817 and Flanagan, 2018; Gibbs and Patten, 1970; Lewis et al., 1977).

818 The vapour pressure deficit (VPD) is closely related to ET (Dhungel et al., 2021).
819 Even under deficit conditions, more specifically during the dry season, the cactus maintained
820 ET on a significant scale. Interestingly, even during extremely critical periods (e.g., during
821 the dry season and dry-wet transition), the cactus can keep water lost to the atmosphere well
822 below that seen in species with C3 and C4 metabolism. For these plants, maintaining
823 transpiration during critical periods has important benefits, such as the removal of excessive
824 heat from the cladodes and the maintenance of net photosynthesis (Gibbs and Patten, 1970).
825 This supports our hypothesis that the cactus manages to maintain satisfactory ET. Under
826 rainfed conditions, as in the present study, the mean was 0.95 mm day^{-1} during the
827 experimental period, with a value of 1.18 mm day^{-1} during the wet season, 0.99 mm day^{-1}
828 during the dry season, 0.88 mm day^{-1} during the wet-dry transition, and 0.65 mm day^{-1}

829 during the dry-wet transition (Figure 4). In contrast, studies by Consoli et al. (2013),
830 Goldstein et al. (1991), and Lima et al. (2018), evaluating species of cactus (*Opuntia* spp.)
831 under irrigated conditions, found values for ET greater than 2 mm day⁻¹. Under rainfed
832 conditions, Han and Felker (1997) found a mean daily value of 1.44 mm in *O. ellisiana*.
833 While in a semi-arid ecosystem with cactus (*O. engelmannii*) and shrubs, Anderson and
834 Vivoni (2016) found approximate ET values ranging from 0 to 3.5 mm day⁻¹.

835

836 4.2. Variations in the NDVI, seasonal environmental changes and soil moisture

837 Vegetation and terrestrial ecosystems have intrinsic characteristics regarding
838 environmental conditions, and consequently different spectral responses. To evaluate plant
839 behaviour, the Normalised Difference Vegetation Index (NDVI) is a very promising method,
840 and widely used in arid and semi-arid ecosystems. This is because information in the near-
841 infrared spectrum has a direct relationship with the photosynthetic rate of the vegetation, and
842 helps in estimating biomass accumulation (Hermance et al., 2015). For the cactus, we found
843 an NDVI with a mean value of 0.19 throughout the experimental period (Figure 5). In
844 addition, there are reports of a low NDVI and low vegetation indices in areas of cacti (Ouko
845 et al., 2020). Similarly, M. V. da Silva et al. (2021) found vegetation indices ranging from
846 0.1 to 0.5 in areas cultivated with *O. stricta* and *N. cochenillifera* in the Agreste region of
847 Pernambuco, Brazil. The quick response of the NDVI for cacti, even under low water
848 availability, may be related to the roots that remain in the surface layers of the soil absorbing
849 rainwater and water vapour from the air (Ouko et al., 2020), thereby maintaining both growth
850 and photosynthesis, even if at a reduced rate. Furthermore, if the high atmospheric demand
851 is combined with water availability in the soil, plant evapotranspiration will be high.
852 Variations in atmospheric demand are generally caused by water availability and the time of
853 year. With a mean of 6.24 mm day⁻¹ (Figure 5c), the results for reference evapotranspiration
854 (ET₀) were consistent with the environmental conditions and the rainfall events that occurred.
855 The ET₀ in semi-arid regions of Brazil is high due to the high incidence of radiation and low
856 rainfall volumes, and can vary on average from 6 mm day⁻¹ in areas of cactus to more than
857 8 mm day⁻¹ in a seasonally dry forest (Caatinga) (Jardim et al., 2021b; Marques et al., 2020).

858 In the case of environments with high atmospheric demand and low soil moisture, the
859 Evaporative Stress Index (ESI) can identify problems in plant performance (Anderson et al.,

2007). Although the ESI presented values close to one during the present study, with this value classified as a stressor for the crop (Anderson et al., 2007), the cactus maintained its active development. The resistance to hostile climate and environmental factors is overcome due to the anatomical and morphophysiological characteristics of the plant (Gibbs and Patten, 1970; Han and Felker, 1997; Jardim et al., 2021a; Lima et al., 2018). On the other hand, when the periods of drought are more severe and prolonged, the yield, growth, and biochemical and physiological parameters of the cactus may be impaired (Jardim et al., 2021a; Scalisi et al., 2016; Ventura-Aguilar et al., 2017). In addition, characteristics of the root system, parenchymal tissue and stomatal control allow the cactus to take advantage of the soil moisture and show good performance even when water availability is low (Scalisi et al., 2016). The mean value of the rainfall was 347.74 mm year⁻¹, within the values for plant survival (Campos et al., 2021; Kumar et al., 2022).

872

873 4.3. Allometry, phenological phase, and cutting time

874 One characteristic of plants is to present differing adaptations, phenotypic plasticity
875 and behaviour in terms of growth rate. Earlier studies (e.g., Amorim et al., 2017; Araújo
876 Júnior et al., 2021; Jardim et al., 2021c; Souza et al., 2022) also reported similarities in the
877 growth curves of the cactus; however, compared to genus *Opuntia*, genus *Nopalea* does not
878 show very high rates of growth. When evaluating growth rates (i.e., absolute growth rate—
879 AGR and relative growth rate—RGR) in *N. cochenillifera* under rainfed conditions in a semi-
880 arid environment, Araújo Júnior et al. (2021) found a lower AGR (< 0.004 Mg ha⁻¹ °Cday⁻¹)
881 and higher RGR (> 0.002 Mg Mg⁻¹ °Cday⁻¹) compared to our results (Figure 6). The AGR
882 helps explain the ratio of dry matter accumulation in the crop, while the RGR shows the
883 relative increase in dry matter per unit of time (Jardim et al., 2021c). Generally, a reduction
884 in both of the above rates can clearly be seen throughout the cycle. This is because, as plants
885 grow, they consume photoassimilates, causing a natural reduction in these rates (Amorim et
886 al., 2017; Araújo Júnior et al., 2021; Jardim et al., 2021c; Souza et al., 2022). The ideal
887 cutting time favours a more promising crop, with better use of photoassimilates and better
888 biomass accumulation (Jardim et al., 2021c). Other studies point out that the cactus shows
889 variations in harvest time depending on the agronomic management and/or environmental

890 conditions (Amorim et al., 2017; Araújo Júnior et al., 2021; Jardim et al., 2021c; Souza et
891 al., 2022).

892 Our results showed high values for the cactus in terms of photosynthetic capacity, a
893 ratio predicted by the net assimilation rate (NAR). From our findings, the crop presented
894 significant net photosynthesis, with little influence from self-shading of the cladodes due to
895 the smaller specific cladode area (SCA), favouring a high NAR (Figures 6b and 6c). For
896 Scalisi et al. (2016), morphometric variables such as cladode area help us understand the
897 growth behaviour of plants. The number of cladodes is also a fundamental variable for
898 understanding the phenology of the cactus. In the present study, the cactus presented up to
899 the third phase, i.e., the successive emission of third-order cladodes (Figure 6d). This agrees
900 with other studies on cactus subjected to a semi-arid environment (Araújo Júnior et al., 2021;
901 Jardim et al., 2021c). These findings also confirm the hypothesis that plants continue to
902 develop, increasing their growth rate under different environmental conditions. On the other
903 hand, it is possible that, despite the plants having reached the third phase, the phases were
904 prolonged due to the low water availability.

905

906 *4.4. Water relations and biophysical parameters of cladodes*

907 Anatomically, the cactus has the capacity to store water in various structures, such as
908 parenchyma and hydrenchyma cells (Jardim et al., 2021a; Scalisi et al., 2016). Our results
909 showed that both the cladode water content and cladode succulence presented significant
910 variations (Figure 7). During dry periods, samples five and six showed greater water loss;
911 plants from sample six in particular lost more water due to the long period of drought (Scalisi
912 et al., 2016). In addition, when plants lose water to the environment, they reduce their cladode
913 area, resulting in a loss of cell turgor and succulence (Figure 7b) (Montesinos-Navarro et al.,
914 2019; Nobel, 1991; Scalisi et al., 2016). Even with a significant loss of cladode water content,
915 succulent plants are able to store water more efficiently than plants with a C3 or C4
916 photosynthetic pathway, favouring species survival and the metabolic pathways (Nobel,
917 1991; Ventura-Aguilar et al., 2017). While the cladodes are still young and have a smaller
918 area than mature cladodes, cladode succulence may be greater, since the area is reduced and
919 the water content is high, as seen in the first batch of samples (Figure 7b). These results
920 corroborate those of Scalisi et al. (2016), who found variations of approximately 45% to 85%

921 in cladode water content. When the number of cladodes increases, their water content may
922 decrease due to competition for water by the cladodes. Other studies point to variations of
923 60% to 95% in the cladode water content, influenced by soil moisture (Bilderback et al.,
924 2021; Melero-Meraz et al., 2022). Such variations in turgor may occur due to the drought
925 tolerance of the plant, since the cactus is able to maintain turgor pressure for months
926 (Goldstein et al., 1991; Nobel, 1991).

927 When plants are highly efficient in using biophysical resources, the probability of
928 achieving better yields is high (Jardim et al., 2021b). The results shown here generally
929 underline the high efficiency of the cactus in using radiation, water and nutrients (see Table
930 3). One of the factors to help in radiation use efficiency (RUE) is the canopy architecture,
931 which favours the interception of photosynthetically active radiation (PAR) and the capture
932 of CO₂, to be later converted into biomass (Cortazar et al., 1985; Flanagan and Flanagan,
933 2018; Nobel, 1991). The relationship between RUE, water use efficiency (WUE), and
934 nutrient use efficiency (NUE) is true, since the plants showed high dry biomass yield. The
935 study by Han and Felker (1997) reports the high WUE of *O. ellisiana* (1 kg of dry matter per
936 162 kg of water), however such results are still in the early stages for *N. cochenillifera* under
937 rainfed conditions. Our findings of 1.75 kg m⁻³ are higher than those reported by Mbava et
938 al. (2020) for C3 and C4 species, e.g., wheat (1.18 kg m⁻³), sorghum (1.48 kg m⁻³), maize
939 (1.47 kg m⁻³) and cotton (0.22 kg m⁻³).

940 As seen in earlier studies with the cactus (Du Toit et al., 2018; Nedjimi, 2021; Saraiva
941 et al., 2021), we found that the plants showed greater efficiency and accumulation for such
942 nutrients as P, K⁺, Ca²⁺, Mg²⁺ and Na⁺ (Table 4), in order of use efficiency. Nedjimi (2021)
943 and Saraiva et al. (2021), respectively evaluating *Opuntia* and *Nopalea*, also found greater
944 concentrations of P and K⁺ in the cladodes. They concluded that cacti have higher
945 concentrations of the above nutrients, favouring the nutritional value for human/animal
946 consumption. In addition, the high concentration of such nutrients as K⁺ can help improve
947 performance against abiotic factors, such as environmental changes, salinity and heat (Jardim
948 et al., 2021a). The high Bowen ratio was due to the greater heat flux (Table 4), conditions
949 characteristic of a deficient climate (Alves et al., 2022), and which can be damaging to crops.
950 High values can also be seen for the *H/LE* ratio in an arid ecosystem of cactus (Flanagan and
951 Flanagan, 2018). The Bowen ratio can change depending on the meteorological variables,

952 soil conditions and vegetation, in which case, adapted plants tend to suffer less. Despite the
953 semi-arid conditions to which the plants were exposed, the cactus showed a high yield of dry
954 biomass (mean of 12.47 Mg ha⁻¹). In this respect, our data are superior to those found by
955 Jardim et al. (2021a, 2021b), where the cactus was harvested at a younger age in a semi-arid
956 environment.

957

958 4.5. Principal component analysis (PCA)

959 For the purposes of this study, we applied PCA to the variables that were most
960 influenced by the wet and dry seasons and their transitions (Figure 8). The analysis allowed
961 a reduction in the data set, transforming the data into a series of interrelated variables without
962 losing the principal characteristics of the data. Several variables were correlated with the
963 growing seasons, and the first two principal components (PC) explained 86.82% of the total
964 variance, which was distributed over the 23 variables of the PC1 and PC2 coordinates. The
965 formed groups are clearly correlated based on water availability and the environmental
966 conditions. This is because, in addition to the microclimate caused by the rainfall, according
967 to Campos et al. (2021), the cactus responds to different levels of soil water availability.
968 Jardim et al. (2021a) used the PCA method to understand which environmental and plant
969 variables have greater interaction with different cactus genotypes (*Opuntia* spp. and *Nopalea*
970 spp.) irrigated with saline water in the semi-arid region of Brazil. Furthermore, according to
971 the authors, this type of analysis helps in understanding how plants behave in the face of
972 environmental stressors.

973 Previous studies showed the grouping of cladode and plant variables (Jardim et al.,
974 2021a; Kumar et al., 2022), where correlated variables of the same sign explain, for example,
975 the greater yield of the plants. It is interesting to see water use efficiency grouped with
976 nutrient use efficiency, since these variables were inversely related to the growth rates, which
977 explains their lesser accumulation during the wet-dry transition and dry season. Recently,
978 several studies have identified variations in the energy budget during wet and dry seasons
979 (Alves et al., 2022; Chen et al., 2022; Dhungel et al., 2021; Jardim et al., 2022). Plant
980 evapotranspiration may be limited by the available energy, water and evaporative demand;
981 thus, as the plants increased evapotranspiration, the heat stress index and evaporative demand
982 were reduced. The information presented here implies a clear effect from the wet and dry

983 seasons on energy balance, turbulent fluxes, and plant responses, due to grouping of the
984 variables and the contribution of each component.

985

986 **5. Conclusions**

987 In this study, we used data from a micrometeorological tower, remote sensing, and
988 morphometric and water variables of cactus plants during the wet to dry seasons of 2015–
989 2017. We analysed the seasonal and interannual variation in the components of the surface
990 energy balance, and performance of the cactus in a semi-arid environment. Our results lead
991 to the following conclusions: the energy budget showed seasonality, with the latent heat flux
992 (LE) and sensible heat flux (H) compromised more strongly during the dry-wet transition
993 season, 1.57 and $5.89 \text{ MJ m}^{-2} \text{ day}^{-1}$, respectively. The values for the H/R_n ratio on a seasonal
994 scale were always higher than those of the LE/R_n ratio during each of the four seasons. In
995 general, during the wet and dry seasons, cactus vegetation maintains high evapotranspiration
996 (1.08 mm day^{-1}). The dry season showed the lowest net radiation ($5.89 \text{ MJ m}^{-2} \text{ day}^{-1}$). The
997 soil heat flux (G) was strongly dependent on the rainfall and the end of the wet season; there
998 is no difference in soil heat transfer over the seasons. The seasonal fluctuations in the NDVI
999 and growth rates confirm the influence of the wet and dry seasons, however, the cactus plants
1000 maintained their growth even during the most critical periods. When there is moisture in the
1001 soil and a low vapour pressure deficit, more energy is consumed for LE , resulting in greater
1002 evapotranspiration; while there is a water restriction, more energy is attributed to G and H ,
1003 also increasing the Bowen ratio and Evaporative Stress Index. We found that energy
1004 distribution is greater, and preferably converted into sensible heat. The study also
1005 demonstrated how principal component analysis can help and be effectively used to
1006 understand the way plants respond to environmental factors, and which variables of the
1007 energy balance are correlated with plant growth.

1008 Our results can be a particularly valuable baseline for studies on cacti in semi-arid
1009 ecosystems, where we believe this to be a pioneering study, with application of the surface
1010 energy balance and flux partitioning to *Nopalea cochenillifera* (L.) Salm-Dyck. Finally, these
1011 findings may also be useful for decision makers in environmental management, the
1012 rehabilitation of degraded lands, and climate change, targeting CAM plants as an alternative
1013 way of reducing heat fluxes, and for their tolerance to low water availability. In future studies,

1014 it would be interesting to quantify CO₂ fluxes in the soil and in the environment in wetlands
1015 and drylands cultivated with cactus.

1016

1017 **Acknowledgments**

1018 The authors wish to thank the Research Support Foundation of the State of
1019 Pernambuco (FACEPE - APQ-0215-5.01/10 and FACEPE - APQ-1159-1.07/14) and the
1020 National Council for Scientific and Technological Development (CNPq - 152251/2018-9)
1021 for their financial support. Further thanks go to the Research Support Foundation of the State
1022 of Pernambuco and the Coordination for the Improvement of Higher Education Personnel
1023 (CAPES - Finance Code 001) for the research and study grants.

1024

1025 **References**

1026 Allen, R.G., Pereira, L.S., Raes, D., Smith, M., 1998. Crop Evapotranspiration: Guidelines
1027 for Computing Crop Water Requirements. FAO Irrigation and Drainage Paper 56,
1028 Rome.

1029 Almagbile, A., Zeitoun, M., Hazaymeh, K., Sammour, H.A., Sababha, N., 2019. Statistical
1030 analysis of estimated and observed soil moisture in sub-humid climate in north-western
1031 Jordan. *Environ. Monit. Assess.* 191, 1–21. [https://doi.org/10.1007/S10661-019-7230-](https://doi.org/10.1007/S10661-019-7230-9)
1032 [9/FIGURES/18](https://doi.org/10.1007/S10661-019-7230-9)

1033 Alvares, C.A., Stape, J.L., Sentelhas, P.C., Gonçalves, J.L. de M., Sparovek, G., 2013.
1034 Köppen's climate classification map for Brazil. *Meteorol. Zeitschrift* 22, 711–728.
1035 <https://doi.org/10.1127/0941-2948/2013/0507>

1036 Alves, J.D.N., Ribeiro, A., Rody, Y.P., Loos, R.A., 2022. Energy balance and surface
1037 decoupling factor of a pasture in the Brazilian Cerrado. *Agric. For. Meteorol.* 319,
1038 108912. <https://doi.org/10.1016/J.AGRFORMET.2022.108912>

1039 Amorim, D.M., Silva, T.G.F. da, Pereira, P. de C., Souza, L.S.B. de, Minuzzi, R.B., 2017.
1040 Phenophases and cutting time of forage cactus under irrigation and cropping systems.
1041 *Pesqui. Agropecuária Trop.* 47, 62–71. [https://doi.org/10.1590/1983-](https://doi.org/10.1590/1983-40632016V4742746)
1042 [40632016V4742746](https://doi.org/10.1590/1983-40632016V4742746)

1043 Anderson, C.A., Vivoni, E.R., 2016. Impact of land surface states within the flux footprint
1044 on daytime land-atmosphere coupling in two semiarid ecosystems of the Southwestern

1045 U.S. Water Resour. Res. 52, 4785–4800. <https://doi.org/10.1002/2015WR018016>

1046 Anderson, M.C., Norman, J.M., Mecikalski, J.R., Otkin, J.A., Kustas, W.P., 2007. A
1047 climatological study of evapotranspiration and moisture stress across the continental
1048 United States based on thermal remote sensing: 2. Surface moisture climatology. J.
1049 Geophys. Res. Atmos. 112. <https://doi.org/10.1029/2006JD007507>

1050 Anghileri, D., Bozzini, V., Molnar, P., Sheffield, J., 2022. Comparison of hydrological and
1051 vegetation remote sensing datasets as proxies for rainfed maize yield in Malawi. Agric.
1052 Water Manag. 262, 107375. <https://doi.org/10.1016/J.AGWAT.2021.107375>

1053 Aparecido, L.E. de O., Lorençone, J.A., Lorençone, P.A., de Meneses, K.C., Moraes, J.R. da
1054 S.C. de, 2021. Climate risk to peanut cultivation in Brazil across different planting
1055 seasons. J. Sci. Food Agric. 101, 5002–5015. <https://doi.org/10.1002/JSFA.11145>

1056 Araújo Júnior, G. do N., Silva, T.G.F. da, Souza, L.S.B. de, Araújo, G.G.L. de, Moura,
1057 M.S.B. de, Alves, C.P., Salvador, K.R. da S., Souza, C.A.A. de, Montenegro, A.A. de
1058 A., Silva, M.J. da, 2021. Phenophases, morphophysiological indices and cutting time in
1059 clones of the forage cacti under controlled water regimes in a semiarid environment. J.
1060 Arid Environ. 190, 104510. <https://doi.org/10.1016/J.JARIDENV.2021.104510>

1061 Arnold, C.Y., 1959. The determination and significance of the base temperature in a linear
1062 heat unit system. J. Am. Soc. Hortic. Sci. 74, 430–445.

1063 Awada, H., Di Prima, S., Sirca, C., Giadrossich, F., Marras, S., Spano, D., Pirastru, M., 2021.
1064 Daily Actual Evapotranspiration Estimation in a Mediterranean Ecosystem from
1065 Landsat Observations Using SEBAL Approach. Forests 12, 189.
1066 <https://doi.org/10.3390/F12020189>

1067 Beck, H.E., Zimmermann, N.E., McVicar, T.R., Vergopolan, N., Berg, A., Wood, E.F., 2018.
1068 Present and future Köppen-Geiger climate classification maps at 1-km resolution. Sci.
1069 Data 5, 180214. <https://doi.org/10.1038/sdata.2018.214>

1070 Bielski, C.H., Twidwell, D., Fuhlendorf, S.D., Wonkka, C.L., Allred, B.W., Ochsner, T.E.,
1071 Krueger, E.S., Carlson, J.D., Engle, D.M., 2018. Pyric herbivory, scales of
1072 heterogeneity and drought. Funct. Ecol. 32, 1599–1608. <https://doi.org/10.1111/1365-2435.13083/SUPPINFO>

1074 Bilderback, A.H., Torres, A.J., Vega, M., Ball, B.A., 2021. The structural and nutrient
1075 chemistry during early-stage decomposition and desiccation of cacti in the Sonoran

1076 Desert. J. Arid Environ. 195, 104636.
 1077 <https://doi.org/10.1016/J.JARIDENV.2021.104636>

1078 Bowen, I.S., 1926. The Ratio of Heat Losses by Conduction and by Evaporation from any
 1079 Water Surface. *Phys. Rev.* 27, 779. <https://doi.org/10.1103/PhysRev.27.779>

1080 Campos, A.R.F., Silva, A.J.P. da, de Jong van Lier, Q., Nascimento, F.A.L. do, Fernandes,
 1081 R.D.M., Almeida, J.N. de, Paz, V.P. da S., 2021. Yield and morphology of forage cactus
 1082 cultivars under drip irrigation management based on soil water matric potential
 1083 thresholds. *J. Arid Environ.* 193, 104564.
 1084 <https://doi.org/10.1016/J.JARIDENV.2021.104564>

1085 Cao, J.J., Hu, S., Dong, Q., Liu, L.J., Wang, Z.L., 2019. Green roof cooling contributed by
 1086 plant species with different photosynthetic strategies. *Energy Build.* 195, 45–50.
 1087 <https://doi.org/10.1016/J.ENBUILD.2019.04.046>

1088 Chen, Jingyan, Dong, G., Chen, Jiquan, Jiang, S., Qu, L., Legesse, T.G., Zhao, F., Tong, Q.,
 1089 Shao, C., Han, X., 2022. Energy balance and partitioning over grasslands on the
 1090 Mongolian Plateau. *Ecol. Indic.* 135, 108560.
 1091 <https://doi.org/10.1016/J.ECOLIND.2022.108560>

1092 Cheng, M., Shi, L., Jiao, X., Nie, C., Liu, S., Yu, X., Bai, Y., Liu, Yadong, Liu, Yuan, Song,
 1093 N., Jin, X., 2022. Up-scaling the latent heat flux from instantaneous to daily-scale: A
 1094 comparison of three methods. *J. Hydrol. Reg. Stud.* 40, 101057.
 1095 <https://doi.org/10.1016/J.EJRH.2022.101057>

1096 Consoli, S., Inglese, G., Inglese, P., 2013. Determination of Evapotranspiration and Annual
 1097 Biomass Productivity of a Cactus Pear [*Opuntia ficus-indica* L. (Mill.)] Orchard in a
 1098 Semiarid Environment. *J. Irrig. Drain. Eng.* 139, 680–690.
 1099 [https://doi.org/10.1061/\(ASCE\)IR.1943-4774.0000589](https://doi.org/10.1061/(ASCE)IR.1943-4774.0000589)

1100 Corrado, G., Chiaiese, P., Lucini, L., Miras-Moreno, B., Colla, G., Roupael, Y., 2020.
 1101 Successive Harvests Affect Yield, Quality and Metabolic Profile of Sweet Basil
 1102 (*Ocimum basilicum* L.). *Agronomy* 10, 830.
 1103 <https://doi.org/10.3390/AGRONOMY10060830>

1104 Cortazar, V.G. de, Acevedo, E., Nobel, P.S., 1985. Modeling of par interception and
 1105 productivity by *Opuntia ficus-indica*. *Agric. For. Meteorol.* 34, 145–162.
 1106 [https://doi.org/10.1016/0168-1923\(85\)90015-2](https://doi.org/10.1016/0168-1923(85)90015-2)

1107 Dhungel, R., Aiken, R., Evett, S.R., Colaizzi, P.D., Marek, G., Moorhead, J.E., Baumhardt,
1108 R.L., Brauer, D., Kutikoff, S., Lin, X., 2021. Energy Imbalance and Evapotranspiration
1109 Hysteresis Under an Advective Environment: Evidence From Lysimeter, Eddy
1110 Covariance, and Energy Balance Modeling. *Geophys. Res. Lett.* 48, e2020GL091203.
1111 <https://doi.org/10.1029/2020GL091203>

1112 Du Toit, A., De Wit, M., Hugo, A., 2018. Cultivar and Harvest Month Influence the Nutrient
1113 Content of *Opuntia* spp. Cactus Pear Cladode Mucilage Extracts. *Molecules* 23, 916.
1114 <https://doi.org/10.3390/MOLECULES23040916>

1115 Dubeux Jr., J.C.B., Santos, M.V.F. dos, Cunha, M.V. da, Santos, D.C. dos, Souza, R.T. de
1116 A., Mello, A.C.L. de, Souza, T.C. de, 2021. Cactus (*Opuntia* and *Nopalea*) nutritive
1117 value: A review. *Anim. Feed Sci. Technol.* 275, 114890.
1118 <https://doi.org/10.1016/J.ANIFEEDSCI.2021.114890>

1119 Flanagan, L.B., Flanagan, J.E.M., 2018. Seasonal controls on ecosystem-scale CO₂ and
1120 energy exchange in a Sonoran Desert characterized by the saguaro cactus (*Carnegiea*
1121 *gigantea*). *Oecologia* 187, 977–994. [https://doi.org/10.1007/S00442-018-4187-](https://doi.org/10.1007/S00442-018-4187-2)
1122 [2/FIGURES/10](https://doi.org/10.1007/S00442-018-4187-2)

1123 Foga, S., Scaramuzza, P.L., Guo, S., Zhu, Z., Dilley, R.D., Beckmann, T., Schmidt, G.L.,
1124 Dwyer, J.L., Joseph Hughes, M., Laue, B., 2017. Cloud detection algorithm comparison
1125 and validation for operational Landsat data products. *Remote Sens. Environ.* 194, 379–
1126 390. <https://doi.org/10.1016/J.RSE.2017.03.026>

1127 Gavilán, P., Berengena, J., 2007. Accuracy of the Bowen ratio-energy balance method for
1128 measuring latent heat flux in a semiarid advective environment. *Irrig. Sci.* 25, 127–140.
1129 <https://doi.org/10.1007/S00271-006-0040-1>

1130 Gibbs, J.G., Patten, D.T., 1970. Plant temperatures and heat flux in a Sonoran Desert
1131 ecosystem. *Oecologia* 5, 165–184. <https://doi.org/10.1007/BF00344882>

1132 Goldstein, G., Ortega, J.K.E., Nerd, A., Nobel, P.S., 1991. Diel Patterns of Water Potential
1133 Components for the Crassulacean Acid Metabolism Plant *Opuntia ficus-indica* when
1134 Well-Watered or Droughted. *Plant Physiol.* 95, 274–280.
1135 <https://doi.org/10.1104/PP.95.1.274>

1136 Guevara-Escobar, A., González-Sosa, E., Cervantes-Jimenez, M., Suzán-Azpíri, H.,
1137 Queijeiro-Bolanos, M.E., Carrillo-Ángeles, I., Cambron-Sandoval, V.H., 2021.

1138 Machine learning estimates of eddy covariance carbon flux in a scrub in the Mexican
1139 highland. *Biogeosciences* 18, 367–392. <https://doi.org/10.5194/BG-18-367-2021>

1140 Han, H., Felker, P., 1997. Field validation of water-use efficiency of the CAM plant *Opuntia*
1141 *ellisiana* in south Texas. *J. Arid Environ.* 36, 133–148.
1142 <https://doi.org/10.1006/JARE.1996.0202>

1143 Hartzell, S., Bartlett, M.S., Inglese, P., Consoli, S., Yin, J., Porporato, A., 2021. Modelling
1144 nonlinear dynamics of Crassulacean acid metabolism productivity and water use for
1145 global predictions. *Plant. Cell Environ.* 44, 34–48. <https://doi.org/10.1111/PCE.13918>

1146 Heilman, J.L., Brittin, C.L., Neale, C.M.U., 1989. Fetch requirements for bowen ratio
1147 measurements of latent and sensible heat fluxes. *Agric. For. Meteorol.* 44, 261–273.
1148 [https://doi.org/10.1016/0168-1923\(89\)90021-X](https://doi.org/10.1016/0168-1923(89)90021-X)

1149 Hermance, J.F., Augustine, D.J., Derner, J.D., 2015. Quantifying characteristic growth
1150 dynamics in a semi-arid grassland ecosystem by predicting short-term NDVI phenology
1151 from daily rainfall: a simple four parameter coupled-reservoir model. *Int. J. Remote*
1152 *Sens.* 36, 5637–5663. <https://doi.org/10.1080/01431161.2015.1103916>

1153 Hicks, B.B., Eash, N.S., O’Dell, D.L., Oetting, J.N., 2020. Augmented Bowen Ratio Analysis
1154 –I: Site Adequacy, Fetch and Heat Storage (ABRA). *Agric. For. Meteorol.* 290, 108035.
1155 <https://doi.org/10.1016/J.AGRFORMET.2020.108035>

1156 Ho, C.L., Chiang, J.M., Lin, T.C., Martin, C.E., 2019. First report of C4/CAM-cycling
1157 photosynthetic pathway in a succulent grass, *Spinifex littoreus* (Brum. f.) Merr., in
1158 coastal regions of Taiwan. *Flora* 254, 194–202.
1159 <https://doi.org/10.1016/J.FLORA.2018.08.005>

1160 Hu, S., Zhao, C., Li, J., Wang, F., Chen, Y., 2014. Discussion and reassessment of the method
1161 used for accepting or rejecting data observed by a Bowen ratio system. *Hydrol. Process.*
1162 28, 4506–4510. <https://doi.org/10.1002/HYP.9962>

1163 Hurni, K., Van Den Hoek, J., Fox, J., 2019. Assessing the spatial, spectral, and temporal
1164 consistency of topographically corrected Landsat time series composites across the
1165 mountainous forests of Nepal. *Remote Sens. Environ.* 231, 111225.
1166 <https://doi.org/10.1016/J.RSE.2019.111225>

1167 Jardim, A.M. da R.F., Santos, H.R.B., Alves, H.K.M.N., Ferreira-Silva, S.L., Souza, L.S.B.
1168 de, Araújo Júnior, G. do N., Souza, M. de S., Araújo, G.G.L. de, Souza, C.A.A. de,

1169 Silva, T.G.F. da, 2021a. Genotypic differences relative photochemical activity,
1170 inorganic and organic solutes and yield performance in clones of the forage cactus under
1171 semi-arid environment. *Plant Physiol. Biochem.* 162, 421–430.
1172 <https://doi.org/10.1016/J.PLAPHY.2021.03.011>

1173 Jardim, A.M. da R.F., Silva, T.G.F. da, Souza, L.S.B. de, Araújo Júnior, G. do N., Alves,
1174 H.K.M.N., Souza, M. de S., Araújo, G.G.L. de, Moura, M.S.B. de, 2021b. Intercropping
1175 forage cactus and sorghum in a semi-arid environment improves biological efficiency
1176 and competitive ability through interspecific complementarity. *J. Arid Environ.* 188,
1177 104464. <https://doi.org/10.1016/J.JARIDENV.2021.104464>

1178 Jardim, A.M. da R.F., Souza, L.S.B. de, Alves, C.P., Araújo, J.F.N. de, Souza, C.A.A. de,
1179 Pinheiro, A.G., Araújo, G.G.L. de, Campos, F.S., Tabosa, J.N., Silva, T.G.F. da, 2021c.
1180 Intercropping forage cactus with sorghum affects the morphophysiology and phenology
1181 of forage cactus. *African J. Range Forage Sci.* 1–12.
1182 <https://doi.org/10.2989/10220119.2021.1949749>

1183 Jardim, A.M.R.F., Araújo Júnior, G.N., Silva, M.V., Santos, A., Silva, J.L.B., Pandorfi, H.,
1184 Oliveira-Júnior, J.F., Teixeira, A.H.C., Teodoro, P.E., de Lima, J.L.M.P., Silva Junior,
1185 C.A., Souza, L.S.B., Silva, E.A., Silva, T.G.F., 2022. Using Remote Sensing to Quantify
1186 the Joint Effects of Climate and Land Use/Land Cover Changes on the Caatinga Biome
1187 of Northeast Brazilian. *Remote Sens.* 14, 1911. <https://doi.org/10.3390/RS14081911>

1188 Jung, M., Koirala, S., Weber, U., Ichii, K., Gans, F., Camps-Valls, G., Papale, D., Schwalm,
1189 C., Tramontana, G., Reichstein, M., 2019. The FLUXCOM ensemble of global land-
1190 atmosphere energy fluxes. *Sci. Data* 6, 1–14. [https://doi.org/10.1038/s41597-019-0076-](https://doi.org/10.1038/s41597-019-0076-8)
1191 8

1192 Kumar, S., Palsaniya, D.R., Kumar, T.K., Misra, A.K., Ahmad, S., Rai, A.K., Sarker, A.,
1193 Louhaichi, M., Hassan, S., Liguori, G., Ghosh, P.K., Govindasamy, P., Mahawer, S.K.,
1194 Bhargavi, H.A., 2022. Survival, morphological variability, and performance of *Opuntia*
1195 *ficus-indica* in a semi-arid region of India. *Arch. Agron. Soil Sci.* 1–18.
1196 <https://doi.org/10.1080/03650340.2022.2031998>

1197 Leite-Filho, A.T., de Sousa Pontes, V.Y., Costa, M.H., 2019. Effects of Deforestation on the
1198 Onset of the Rainy Season and the Duration of Dry Spells in Southern Amazonia. *J.*
1199 *Geophys. Res. Atmos.* 124, 5268–5281. <https://doi.org/10.1029/2018JD029537>

1200 Lewis, D.A., Nobel, P.S., Boyd, P.L., 1977. Thermal Energy Exchange Model and Water
1201 Loss of a Barrel Cactus, *Ferocactus acanthodes*. *Plant Physiol.* 60, 609–616.
1202 <https://doi.org/10.1104/PP.60.4.609>

1203 Lima, F.J.L. de, Martins, F.R., Costa, R.S., Gonçalves, A.R., dos Santos, A.P.P., Pereira,
1204 E.B., 2019. The seasonal variability and trends for the surface solar irradiation in
1205 northeastern region of Brazil. *Sustain. Energy Technol. Assessments* 35, 335–346.
1206 <https://doi.org/10.1016/J.SETA.2019.08.006>

1207 Lima, L.R., Silva, T.G.F., Jardim, A.M.R.F., Souza, C.A.A., Queiroz, M.G., Tabosa, J.N.,
1208 2018. Growth, water use and efficiency of forage cactus sorghum intercropping under
1209 different water depths. *Rev. Bras. Eng. Agrícola e Ambient.* 22, 113–118.
1210 <https://doi.org/10.1590/1807-1929/AGRIAMBI.V22N2P113-118>

1211 Loupassaki, M.H., Chartzoulakis, K.S., Digalaki, N.B., Androulakis, I.I., 2007. Effects of
1212 salt stress on concentration of nitrogen, phosphorus, potassium, calcium, magnesium,
1213 and sodium in leaves, shoots, and roots of six olive cultivars. *J. Plant Nutr.* 25, 2457–
1214 2482. <https://doi.org/10.1081/PLN-120014707>

1215 Lyra, Gustavo Bastos, de Souza, J.L., da Silva, E.C., Lyra, Guilherme Bastos, Teodoro, I.,
1216 Ferreira-Júnior, R.A., de Souza, R.C., 2016. Soil water stress co-efficient for estimating
1217 actual evapotranspiration of maize in northeastern Brazil. *Meteorol. Appl.* 23, 26–34.
1218 <https://doi.org/10.1002/MET.1516>

1219 Marques, T. V., Mendes, K., Mutti, P., Medeiros, S., Silva, L., Perez-Marin, A.M., Campos,
1220 S., Lúcio, P.S., Lima, K., dos Reis, J., Ramos, T.M., da Silva, D.F., Oliveira, C.P., Costa,
1221 G.B., Antonino, A.C.D., Menezes, R.S.C., Santos e Silva, C.M., Bezerra, B., 2020.
1222 Environmental and biophysical controls of evapotranspiration from Seasonally Dry
1223 Tropical Forests (Caatinga) in the Brazilian Semiarid. *Agric. For. Meteorol.* 287,
1224 107957. <https://doi.org/10.1016/J.AGRFORMET.2020.107957>

1225 Mbava, N., Mutema, M., Zengeni, R., Shimelis, H., Chaplot, V., 2020. Factors affecting crop
1226 water use efficiency: A worldwide meta-analysis. *Agric. Water Manag.* 228, 105878.
1227 <https://doi.org/10.1016/J.AGWAT.2019.105878>

1228 Melero-Meraz, V., Zegbe, J.A., Herrera, M.D., Guzmán-Maldonado, S.H., Medina-García,
1229 G., Sánchez-Toledano, B.I., Cruz-Bravo, R.K., Servín-Palestina, M., 2022. On-Farm
1230 Supplemental Irrigation of “Roja Lisa” Cactus Pear: Pre- and Postharvest Effects.

1231 Horticulturae 8, 483. <https://doi.org/10.3390/HORTICULTURAE8060483>

1232 Montesinos-Navarro, A., Verdú, M., Querejeta, J.I., Valiente-Banuet, A., 2019. Nurse shrubs
1233 can receive water stored in the parenchyma of their facilitated columnar cacti. J. Arid
1234 Environ. 165, 10–15. <https://doi.org/10.1016/J.JARIDENV.2019.04.011>

1235 Mulovhedzi, N.E., Araya, N.A., Mengistu, M.G., Fessehazion, M.K., du Plooy, C.P., Araya,
1236 H.T., van der Laan, M., 2020. Estimating evapotranspiration and determining crop
1237 coefficients of irrigated sweet potato (*Ipomoea batatas*) grown in a semi-arid climate.
1238 Agric. Water Manag. 233, 106099. <https://doi.org/10.1016/J.AGWAT.2020.106099>

1239 Nassar, A., Torres-rua, A., Kustas, W., Alfieri, J., Hipps, L., Prueger, J., Nieto, H., Alsina,
1240 M.M., White, W., McKee, L., Coopmans, C., Sanchez, L., Dokoozlian, N., 2021.
1241 Assessing Daily Evapotranspiration Methodologies from One-Time-of-Day sUAS and
1242 EC Information in the GRAPEX Project. Remote Sens. 13, 2887.
1243 <https://doi.org/10.3390/RS13152887>

1244 Nedjimi, B., 2021. Determination of Some Major and Trace Elements in Cladodes of Barbary
1245 fig (*Opuntia ficus-indica* Mill.) by X-ray Fluorescence Spectrometry. Biol. Trace Elem.
1246 Res. 199, 4353–4359. <https://doi.org/10.1007/S12011-020-02555-4/TABLES/5>

1247 Nobel, P.S., 1991. Achievable productivities of certain CAM plants: basis for high values
1248 compared with C3 and C4 plants. New Phytol. 119, 183–205.
1249 <https://doi.org/10.1111/J.1469-8137.1991.TB01022.X>

1250 Novoa, A., Foxcroft, L.C., Keet, J.H., Pyšek, P., Le Roux, J.J., 2021. The invasive cactus
1251 *Opuntia stricta* creates fertility islands in African savannas and benefits from those
1252 created by native trees. Sci. Rep. 11, 1–13. [https://doi.org/10.1038/s41598-021-99857-](https://doi.org/10.1038/s41598-021-99857-x)
1253 x

1254 Ortega-Farias, S.O., Cuenca, R.H., Ek, M., 1996. Daytime variation of sensible heat flux
1255 estimated by the bulk aerodynamic method over a grass canopy. Agric. For. Meteorol.
1256 81, 131–143. [https://doi.org/10.1016/0168-1923\(95\)02278-3](https://doi.org/10.1016/0168-1923(95)02278-3)

1257 Ouko, E., Omondi, S., Mugo, R., Wahome, A., Kasera, K., Nkurunziza, E., Kiema, J., Flores,
1258 A., Adams, E.C., Kuraru, S., Wambua, M., 2020. Modeling Invasive Plant Species in
1259 Kenya’s Northern Rangelands. Front. Environ. Sci. 8, 69.
1260 <https://doi.org/10.3389/FENVS.2020.00069/BIBTEX>

1261 Pardo, J.J., Martínez-Romero, A., Lélis, B.C., Tarjuelo, J.M., Domínguez, A., 2020. Effect

1262 of the optimized regulated deficit irrigation methodology on water use in barley under
1263 semiarid conditions. *Agric. Water Manag.* 228, 105925.
1264 <https://doi.org/10.1016/J.AGWAT.2019.105925>

1265 Perez, P.J., Castellvi, F., Ibañez, M., Rosell, J.I., 1999. Assessment of reliability of Bowen
1266 ratio method for partitioning fluxes. *Agric. For. Meteorol.* 97, 141–150.
1267 [https://doi.org/10.1016/S0168-1923\(99\)00080-5](https://doi.org/10.1016/S0168-1923(99)00080-5)

1268 Pessoa, D.V., Pereira de Andrade, A., Magalhães, A.L.R., Teodoro, A.L., Cordeiro dos
1269 Santos, D., Araújo, G.G.L. de, Medeiros, A.N. de, Nascimento, D.B. do, Valença, R. de
1270 L., Cardoso, D.B., 2020. Forage nutritional differences within the genus *Opuntia*. *J.*
1271 *Arid Environ.* 181, 104243. <https://doi.org/10.1016/J.JARIDENV.2020.104243>

1272 Pierini, N.A., Vivoni, E.R., Robles-Morua, A., Scott, R.L., Nearing, M.A., 2014. Using
1273 observations and a distributed hydrologic model to explore runoff thresholds linked with
1274 mesquite encroachment in the Sonoran Desert. *Water Resour. Res.* 50, 8191–8215.
1275 <https://doi.org/10.1002/2014WR015781>

1276 Pinheiro, K.M., Silva, T.G.F., Carvalho, H.F. de S., Santos, J.E.O., Morais, J.E.F., Zolnier,
1277 S., Santos, D.C. dos, 2014. Correlações do índice de área do cladódio com
1278 características morfogênicas e produtivas da palma forrageira. *Pesqui. Agropecuária*
1279 *Bras.* 49, 939–947. <https://doi.org/10.1590/S0100-204X2014001200004>

1280 Pokhariyal, S., Patel, N., 2021. Evaluation of variation in radiative and turbulent fluxes over
1281 winter wheat ecosystem along Indo-Gangetic region. *Arab. J. Geosci.* 14, 1–11.
1282 <https://doi.org/10.1007/S12517-021-08320-8/FIGURES/7>

1283 Pozníková, G., Fischer, M., van Kesteren, B., Orság, M., Hlavinka, P., Žalud, Z., Trnka, M.,
1284 2018. Quantifying turbulent energy fluxes and evapotranspiration in agricultural field
1285 conditions: A comparison of micrometeorological methods. *Agric. Water Manag.* 209,
1286 249–263. <https://doi.org/10.1016/J.AGWAT.2018.07.041>

1287 Prăvălie, R., Sîrodoev, I., Nita, I.A., Patriche, C., Dumitraşcu, M., Roşca, B., Tişcovschi, A.,
1288 Bandoc, G., Săvulescu, I., Mănoiu, V., Birsan, M.V., 2022. NDVI-based ecological
1289 dynamics of forest vegetation and its relationship to climate change in Romania during
1290 1987–2018. *Ecol. Indic.* 136, 108629.
1291 <https://doi.org/10.1016/J.ECOLIND.2022.108629>

1292 R Core Team, 2022. R: The R Project for Statistical Computing.

- 1293 Raza, M.A., Feng, L.Y., van der Werf, W., Cai, G.R., Khalid, M.H. Bin, Iqbal, N., Hassan,
1294 M.J., Meraj, T.A., Naeem, M., Khan, I., Rehman, S. ur, Ansar, M., Ahmed, M., Yang,
1295 F., Yang, W., 2019. Narrow-wide-row planting pattern increases the radiation use
1296 efficiency and seed yield of intercrop species in relay-intercropping system. Food
1297 Energy Secur. 8, e170. <https://doi.org/10.1002/FES3.170>
- 1298 Rocha Filho, R.R., Santos, D.C., Vêras, A.S.C., Siqueira, M.C.B., Monteiro, C.C.F., Mora-
1299 Luna, R.E., Farias, L.R., Santos, V.L.F., Chagas, J.C., Ferreira, M.A., 2021. Miúda
1300 (*Nopalea cochenillifera* (L.) Salm-Dyck) — The Best Forage Cactus Genotype for
1301 Feeding Lactating Dairy Cows in Semiarid Regions. Animals 11, 1774.
1302 <https://doi.org/10.3390/ANI11061774>
- 1303 Rodrigues, C.R.F., Silva, E.N., Ferreira-Silva, S.L., Voigt, E.L., Viégas, R.A., Silveira,
1304 J.A.G., 2013. High K⁺ supply avoids Na⁺ toxicity and improves photosynthesis by
1305 allowing favorable K⁺ : Na⁺ ratios through the inhibition of Na⁺ uptake and transport to
1306 the shoots of *Jatropha curcas* plants. J. Plant Nutr. Soil Sci. 176, 157–164.
1307 <https://doi.org/10.1002/JPLN.201200230>
- 1308 Salack, S., Klein, C., Giannini, A., Sarr, B., Worou, O.N., Belko, N., Bliefernicht, J.,
1309 Kunstman, H., 2016. Global warming induced hybrid rainy seasons in the Sahel.
1310 Environ. Res. Lett. 11, 104008. <https://doi.org/10.1088/1748-9326/11/10/104008>
- 1311 Saraiva, F.M., Dubeux, J.C.B., da Cunha, M.V., Menezes, R.S.C., Dos Santos, M.V.F.,
1312 Camelo, D., Ferraz, I., 2021. Manure Source and Cropping System Affect Nutrient
1313 Uptake by Cactus (*Nopalea cochenillifera* Salm Dyck). Agronomy 11, 1512.
1314 <https://doi.org/10.3390/AGRONOMY11081512>
- 1315 Scalisi, A., Morandi, B., Inglese, P., Lo Bianco, R., 2016. Cladode growth dynamics in
1316 *Opuntia ficus-indica* under drought. Environ. Exp. Bot. 122, 158–167.
1317 <https://doi.org/10.1016/J.ENVEXPBOT.2015.10.003>
- 1318 Shao, C., Chen, J., Li, L., Dong, G., Han, J., Abraha, M., John, R., 2017. Grazing effects on
1319 surface energy fluxes in a desert steppe on the Mongolian Plateau. Ecol. Appl. 27, 485–
1320 502. <https://doi.org/10.1002/EAP.1459>
- 1321 Silva, M.V. da, Pandorfi, H., Almeida, G.L.P. de, Lima, R.P. de, Santos, A. dos, Jardim,
1322 A.M. da R.F., Rolim, M.M., Silva, J.L.B. da, Batista, P.H.D., Silva, R.A.B. da, Lopes,
1323 P.M.O., Silva, D.C. da, 2021. Spatio-temporal monitoring of soil and plant indicators

1324 under forage cactus cultivation by geoprocessing in Brazilian semi-arid region. *J. South*
1325 *Am. Earth Sci.* 107, 103155. <https://doi.org/10.1016/J.JSAMES.2021.103155>

1326 Silva, P.F. da, Lima, J.R. de S., Antonino, A.C.D., Souza, R., de Souza, E.S., Silva, J.R.I.,
1327 Alves, E.M., 2017. Seasonal patterns of carbon dioxide, water and energy fluxes over
1328 the Caatinga and grassland in the semi-arid region of Brazil. *J. Arid Environ.* 147, 71–
1329 82. <https://doi.org/10.1016/J.JARIDENV.2017.09.003>

1330 Silva, T.G.F. da, de Queiroz, M.G., Zolnier, S., de Souza, L.S.B., de Souza, C.A.A., de
1331 Moura, M.S.B., de Araújo, G.G.L., Steidle Neto, A.J., dos Santos, T.S., de Melo, A.L.,
1332 da Cruz Neto, J.F., da Silva, M.J., Alves, H.K.M.N., 2021. Soil properties and
1333 microclimate of two predominant landscapes in the Brazilian semiarid region:
1334 Comparison between a seasonally dry tropical forest and a deforested area. *Soil Tillage*
1335 *Res.* 207, 104852. <https://doi.org/10.1016/J.STILL.2020.104852>

1336 Silva, T.G.F., Miranda, K.R., Santos, D.C., Queiroz, M.G., Silva, M.C., Cruz Neto, J.F.,
1337 Araújo, J.E.M., 2014. Área do cladódio de clones de palma forrageira: modelagem,
1338 análise e aplicabilidade. *Rev. Bras. Ciências Agrárias* 9, 626–632.
1339 <https://doi.org/10.5039/AGRARIA.V9I4A4553>

1340 Soil Survey Staff, 2014. *Keys to Soil Taxonomy*, 12th ed. USDA-Natural Resources
1341 Conservation Service, Washington, DC.

1342 Souza, M. de S., Silva, T.G.F. da, Souza, L.S.B. de, Alves, H.K.M.N., Leite, R.M.C., Souza,
1343 C.A.A. de, Araújo, G.G.L.D., Campos, F.S., Silva, M.J.D., Souza, P.J.D.O.P., 2022.
1344 Growth, phenology and harvesting time of cactus-millet intercropping system under
1345 biotic mulching. *Arch. Agron. Soil Sci.* 68, 764–778.
1346 <https://doi.org/10.1080/03650340.2020.1852553>

1347 Thornthwaite, C.W., Mather, J.R., 1955. *The water balance*. Laboratory of Climatology,
1348 Centerton, New Jersey.

1349 Unland, H.E., Houser, P.R., Shuttleworth, W.J., Yang, Z.L., 1996. Surface flux measurement
1350 and modeling at a semi-arid Sonoran Desert site. *Agric. For. Meteorol.* 82, 119–153.
1351 [https://doi.org/10.1016/0168-1923\(96\)02330-1](https://doi.org/10.1016/0168-1923(96)02330-1)

1352 Ventura-Aguilar, R.I., Bosquez-Molina, E., Bautista-Baños, S., Rivera-Cabrera, F., 2017.
1353 Cactus stem (*Opuntia ficus-indica* Mill): anatomy, physiology and chemical
1354 composition with emphasis on its biofunctional properties. *J. Sci. Food Agric.* 97, 5065–

1355 5073. <https://doi.org/10.1002/JSFA.8493>

1356 Wang, M., Wu, J., Lafleur, P., 2020. Comparison of energy fluxes between an undisturbed
1357 bog and an adjacent abandoned peatland pasture. *Agric. For. Meteorol.* 291, 108086.
1358 <https://doi.org/10.1016/J.AGRFORMET.2020.108086>

1359 Winter, K., Smith, J.A.C., 2022. CAM photosynthesis: the acid test. *New Phytol.* 233, 599–
1360 609. <https://doi.org/10.1111/NPH.17790>

1361 Wolf, S., Keenan, T.F., Fisher, J.B., Baldocchi, D.D., Desai, A.R., Richardson, A.D., Scott,
1362 R.L., Law, B.E., Litvak, M.E., Brunsell, N.A., Peters, W., van der Laan-Luijkx, I.T.,
1363 2016. Warm spring reduced carbon cycle impact of the 2012 US summer drought. *Proc.*
1364 *Natl. Acad. Sci. U. S. A.* 113, 5880–5885.
1365 https://doi.org/10.1073/PNAS.1519620113/SUPPL_FILE/PNAS.1519620113.SAPP.P
1366 DF

1367 Yue, P., Zhang, Q., Zhang, L., Li, H., Yang, Y., Zeng, J., Wang, S., 2019. Long-term
1368 variations in energy partitioning and evapotranspiration in a semiarid grassland in the
1369 Loess Plateau of China. *Agric. For. Meteorol.* 278, 107671.
1370 <https://doi.org/10.1016/J.AGRFORMET.2019.107671>

1371 Zhang, Kuiyue, Liu, D., Liu, H., Lei, H., Guo, F., Xie, S., Meng, X., Huang, Q., 2022. Energy
1372 flux observation in a shrub ecosystem of a gully region of the Chinese Loess Plateau.
1373 *Ecohydrol. Hydrobiol.* 22, 323–336. <https://doi.org/10.1016/J.ECOHYD.2021.10.001>

1374 Zhang, Kai, Wang, X., Li, Y., Zhao, J., Yang, Y., Zang, H., Zeng, Z., 2022. Peanut residue
1375 incorporation benefits crop yield, nitrogen yield, and water use efficiency of summer
1376 peanut – winter wheat systems. *F. Crop. Res.* 279, 108463.
1377 <https://doi.org/10.1016/J.FCR.2022.108463>

1378 Zhang, Q., Song, Y., Wu, Z., Yan, X., Gunina, A., Kuzyakov, Y., Xiong, Z., 2020. Effects
1379 of six-year biochar amendment on soil aggregation, crop growth, and nitrogen and
1380 phosphorus use efficiencies in a rice-wheat rotation. *J. Clean. Prod.* 242, 118435.
1381 <https://doi.org/10.1016/J.JCLEPRO.2019.118435>

1382

CHAPTER 7

Quantifying the energy budget, water use efficiency and photochemistry of two of the most cultivated cactus species in the world

Abstract

Linking knowledge of energy fluxes and evapotranspiration (ET) in cacti is useful for understanding plant growth. However, there is little quantitative understanding of the latent (LE) and sensible (H) heat fluxes in drylands of cactus. We therefore investigated the feedback from plants of *Nopalea* and *Opuntia* on an interannual and seasonal scale, of the surface energy balance (SEB) components, morphophysiological parameters, biomass, water relations and photochemical relationships during the wet and dry seasons of 2018–2021 in the semi-arid region of Brazil. To analyse the data, four periods were selected (dry season, wet season, and dry-wet and wet-dry transitions). Our results showed that the LE (105.26 W m^{-2}) of *Opuntia* was 77.02% greater than that of *Nopalea*. In all seasons, H was the SEB component with the highest energy consumption in the two cacti, with LE the second most affected. Under *Nopalea*, the soil heat flux increased at the surface (111.65%) during the wet and dry seasons (a mean of $1.61 \text{ MJ m}^{-2} \text{ day}^{-1}$). The mean ET of *Nopalea* and *Opuntia* was 1.71 and 1.96 mm day^{-1} , respectively. The H/R_n ratio showed decreasing behaviour from the dry to the wet season, with a reduction of 36.90% in *Nopalea* and 14.04% in *Opuntia*. The NDVI ranged from 0.19 to 0.67 (*Nopalea*), and 0.17 to 0.70 for *Opuntia*, similar to the Chlorophyll Index, which maintained the seasonality of the NDVI. Overall, we found spatial patterns for the Photochemical Reflectance Index of -0.01 to 0.14 for *Nopalea* and *Opuntia*. Under the same conditions, *Opuntia* showed a higher growth rate and net assimilation rate. The mean cladode water content was 86.01% in *Nopalea* and 88.91% in *Opuntia*. Biomass and water use efficiency were greater in *Opuntia* (56.01 Mg ha^{-1} and 7.54 kg m^{-3} , respectively). We also found that these comparisons indicate greater sensitivity in *Nopalea*, and more-significant quantification of the SEB in *Opuntia*.

Keywords: Latent heat flux; Energy partitioning; Semi-arid; CAM plants

32 **1. Introduction**

33 It is believed that climate change over many decades will have a negative impact on
34 the performance of many poorly adapted plant species. Around 41% of the earth's surface is
35 covered by drylands and 30% covered by pasture, an ecosystem that is of great importance
36 for global energy exchange in the land-vegetation-atmosphere system (Kumar et al., 2021;
37 Tai et al., 2021; Yao et al., 2020; Yue et al., 2018). However, not all plants that make up
38 these ecosystems have adapted; among vascular species, approximately 6% have developed
39 crassulacean acid metabolism (CAM), this photosynthetic pathway being well-adapted to the
40 most hostile of climate conditions (Borland et al., 2011; Nobel and De La Barrera, 2003;
41 Nobel and Zutta, 2008; Winter and Smith, 2022). The CAM pathway is an enhancement of
42 C3 photosynthesis, an evolutionary result of 20–30 million years (Hartzell et al., 2018;
43 Winter and Smith, 2022). Family Cactaceae Juss. includes an example of xerophytic species
44 considered models of the CAM photosynthetic pathway, such as the cacti of genera *Nopalea*
45 and *Opuntia*, specialists in assimilating carbon dioxide (CO₂) at night, thereby promoting a
46 significant improvement in water use efficiency—WUE (Borland et al., 2011; Jardim et al.,
47 2021a; Nobel, 1991; Winter and Smith, 2022). CAM plants typically have a higher WUE
48 than do C3 and C4 pathway plants, up to six and three times greater, respectively (Jardim et
49 al., 2021a; Winter and Smith, 2022). In response to the high WUE, the cactus has a water
50 demand of approximately 20% of the total demand of traditional crops (Neupane et al., 2021).

51 The cactus (*Nopalea cochenillifera* and *Opuntia stricta*) is commonly planted in arid
52 and semi-arid environments of low water availability (250–450 mm year⁻¹) and high
53 temperatures, which are generally unfavourable conditions for cultivating various C3 and C4
54 species (Kumar et al., 2022; Nobel, 1991; Winter and Smith, 2022). Countries such as
55 Mexico and Brazil lead the world in areas planted with cactus, with approximately three
56 million hectares and nine hundred thousand hectares, respectively (Ciriminna et al., 2019).
57 The cactus is an important forage, food, and medicinal crop, and can be consumed by humans
58 and animals (Acharya et al., 2019; Tenorio-Escandón et al., 2022). In addition to its powerful
59 metabolic pathway, its anatomical adaptations, such as a modified succulent stem—known
60 as cladode (flattened stem), spiny body, developed vacuole, impermeable epidermis,
61 mucilaginous cells, and prominent root system make this crop adept at tolerating
62 environments under abiotic stress (Santos-Díaz and Camarena-Rangel, 2019; Scalisi et al.,

63 2016; Tenorio-Escandón et al., 2022). According to Nobel and De La Barrera (2003), cacti
64 (*Nopalea* and *Opuntia*) can survive in regions with a high thermal amplitude (-6°C to 65°C)
65 and high vapour pressure deficit (VPD), although the excess light and heat can cause
66 problems in dissipating photochemical energy (Adams et al., 1989; Jardim et al., 2021a). Part
67 of the downward global solar radiation interacts with the plant canopy and with the soil,
68 promoting changes in the energy balance and evapotranspiration (Alves et al., 2022; Chen et
69 al., 2022; Dhungel et al., 2021). One way of understanding the response of plants to imposed
70 environmental conditions is by quantifying turbulent fluxes, growth and photochemical
71 parameters.

72 So far, there have been few studies quantifying turbulent fluxes by means of the
73 surface energy balance (SEB) in ecosystems with cacti (Flanagan and Flanagan, 2018;
74 Guevara-Escobar et al., 2021; Lewis et al., 1977) - only some with *Opuntia* (Consoli et al.,
75 2013a, 2013b; Unland et al., 1996) and none with *Nopalea*. The SEB is a promising method
76 for quantifying energy exchanges originating from the net radiation (R_n) and partitioned into
77 elements for heating the water, air and soil (Campos et al., 2019; Chen et al., 2022; Irmak
78 and Kukal, 2022). In addition to being a fairly robust method, it can be applied in various
79 ecosystems, from arid to humid (Jung et al., 2019; Unland et al., 1996; Yue et al., 2018). For
80 example, Consoli et al. (2013a) observed changes in the latent heat flux (LE) and sensible
81 heat flux (H) in irrigated *O. ficus-indica* in relation to the time of year and the physiological
82 state of the plants, in a cultivated area in western Sicily in the semi-arid region of Italy.
83 Furthermore, according to the authors, during the growth period of the cactus, SEB
84 evapotranspiration was fairly accurate when compared with microlysimeters. In terms of
85 water and energy fluxes, Pierini et al. (2014) reported higher values for H compared to LE in
86 an ecosystem with *O. spinisior* and *O. engelmannii* in the Sonoran Desert. Consoli et al.
87 (2013b) also used the SEB to determine evapotranspiration, where they found a high WUE
88 in plants of *O. ficus-indica* under the Mediterranean climate of Italy.

89 In agricultural ecosystems, the interaction between the biogeochemical cycle and the
90 vegetation is fundamental for understanding energy partitioning and the way changes occur
91 in the distribution of turbulent fluxes (i.e., LE and H) and the soil heat flux (G) on the surface
92 (Alves et al., 2022; Bezerra et al., 2022; Chen et al., 2022; Dhungel et al., 2021). These
93 elements, together with climate and environmental factors, can cause changes in

94 evapotranspiration (ET) during the plant growing season. Overall, ET is a variable of great
95 importance in the hydrologic cycle, comprising the physical processes of evaporation and
96 transpiration that transfer a mass of water and energy to the atmosphere (Chen et al., 2022;
97 Irmak and Kukal, 2022). Generally, this variable can be accurately determined by weighing-
98 lysimeter and eddy covariance techniques, despite being high-cost methods of determining
99 flux (Dhungel et al., 2021; Jung et al., 2019; Pokhariyal and Patel, 2021). Here, we highlight
100 the Bowen ratio-energy balance method, which quantifies the energy equivalent of ET, i.e.,
101 the latent heat flux using the R_n , air temperature, humidity and G , employing accurate sensors
102 at a lower cost (Bowen, 1926; Ortega-Farias et al., 1996; Yue et al., 2018). These
103 measurements are valuable for understanding the water status of plants and, consequently,
104 their levels of climate adaptation.

105 Integrating micrometeorological variables, such as vegetation indices (e.g.,
106 Normalised Difference Vegetation Index), physiological responses (e.g., Chlorophyll Index;
107 Photochemical Reflectance Index), and growth rates can help as early indicators of plant
108 response to abiotic stress (Jardim et al., 2021b; Perez-Priego et al., 2015; Sanchez et al.,
109 2022), since these variables can serve as indicators of biomass production, the photosynthetic
110 pigment pool and growth performance. Therefore, our hypothesis is that (i) cactus species
111 can maintain their performance for energy fluxes, ecophysiological fluxes and
112 evapotranspiration fluxes even under conditions of stress. Although the hypothesis tested
113 here may be true, we believe that (ii) *O. stricta* presents better adaptation and, consequently,
114 higher yield, and spectral, photochemical and hydric responses compared to *N.*
115 *cochenillifera*.

116 Based on the above, the aim of this study was to compare the feedback from cactus
117 plants (*Nopalea* and *Opuntia*) on an interannual and seasonal scale, of surface energy balance
118 components, morphophysiological parameters, biomass yield, water relations and
119 photochemical relationships during the wet and dry seasons in a semi-arid environment. To
120 achieve this goal, we quantified the heat fluxes, partitioned the net radiation, and calculated
121 growth rates, plant spectral responses, and cladode succulence. The arguments presented here
122 are based on four years observing surface fluxes, and six years analysing the growth of cacti.
123 This is also the first study to measure energy fluxes in *Nopalea* and *Opuntia*.

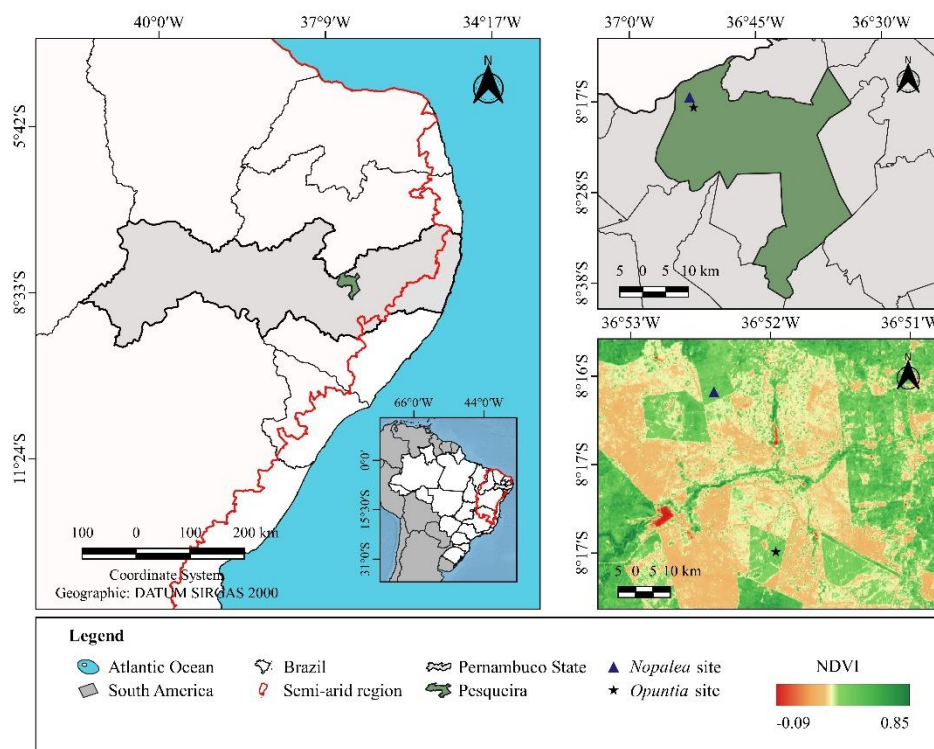
124

125 **2. Materials and methods**

126 *2.1. Description of the experimental sites*

127 We used experimental data from two micrometeorological towers located on the
128 'Várzea Alegre' farm (8°17' S, 36°53' W, at an altitude of 792 m above sea level), in the district
129 of Pesqueira in Pernambuco, Brazil (Figure 1). According to Köppen, the climate is classified
130 as hot semi-arid (BShw) (Beck et al., 2018) with irregular rainfall from January to July. The
131 mean annual rainfall and air temperature are 607 mm and 26°C, respectively. The soil texture
132 is a sandy loam, comprising 71% sand, 22% silt, and 7% clay at a depth of 0–0.40 m at the
133 site cultivated with *Nopalea cochenillifera* (L.) Salm-Dyck, while the site cultivated with
134 *Opuntia stricta* (Haw.) Haw. was of loamy sand (74% sand, 24% silt, and 3% clay), also at
135 a depth of 0–0.40 m. Table 1 shows the physical and chemical data of the soil from the
136 experimental sites.

137



138

139 Figure 1. Geographic location of the two study sites cultivated with *Nopalea* and *Opuntia* in
140 the district of Pesqueira, Pernambuco, Brazil.

141

142 Table 1. Physical and chemical properties of the soil at the experimental sites.

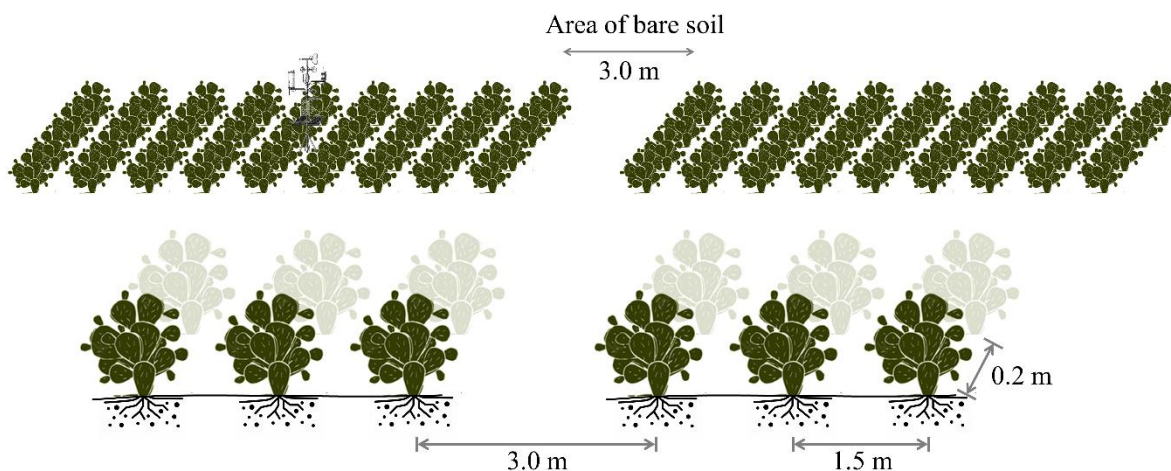
Description	Site	Site
<i>Physical attributes</i> (0–0.40 m)		
	<i>Nopalea cochenillifera</i>	<i>Opuntia stricta</i>
Sand (g kg ⁻¹)	714.88	738.20
Silt (g kg ⁻¹)	216.86	235.64
Clay (g kg ⁻¹)	68.26	26.16
Bulk density (g cm ⁻³)	1.66	1.64
Total porosity (%)	34.57	35.51
Soil texture	Sandy loam	Loamy sand
<i>Chemical attributes</i> (0.0–0.40 m)		
	<i>Nopalea cochenillifera</i>	<i>Opuntia stricta</i>
EC _e (dS m ⁻¹)	0.70	0.66
pH	5.13	5.40
P (mg dm ⁻³)	25.03	53.50
K ⁺ (cmol _c dm ⁻³)	0.26	0.21
Na ⁺ (cmol _c dm ⁻³)	0.09	0.11
Ca ²⁺ (cmol _c dm ⁻³)	4.43	4.38
Mg ²⁺ (cmol _c dm ⁻³)	1.09	1.25
H+Al (cmol _c dm ⁻³)	2.75	2.15
CEC (cmol _c dm ⁻³)	8.60	8.10
Base saturation (%)	63.83	72.90

EC_e is the electrical conductivity of the saturated soil paste extract; pH in H₂O at a ratio of 1:2.5 v/v; CEC is the cation exchange capacity.

143

144 The experiment was conducted from January 2015 to December 2021 with the cacti
 145 *Nopalea cochenillifera* (hereafter called *Nopalea*) and *Opuntia stricta* (hereafter called
 146 *Opuntia*), both species resistant to the carmine mealybug [*Dactylopius opuntiae* (Cockerell);
 147 Hemiptera: Dactylopiidae]. The soil was initially prepared by ploughing, harrowing and
 148 furrowing. The cladodes were then planted in January 2015, inserting 50% of their height
 149 into the soil. The two experimental sites comprised a planted area of approximately 27 ha of
 150 *Nopalea* and 36 ha of *Opuntia* (Figure 1). The linear distance between the sites was 2.4 km.
 151 All the plants were arranged in single rows, at a spacing of 1.5 × 0.2 m. For every nine rows

152 of cactus (i.e., plant rows with no bare areas) there was an uncultivated area of 3 m (i.e., areas
 153 of bare soil), this was repeated until reaching a total density of 27,273 plants ha⁻¹ (Figure 2).
 154 The cropping treatments included manual weeding, with herbicide and insecticide applied as
 155 necessary to avoid competition with weeds and promote full growth of the crop. Throughout
 156 the experimental period, the cacti were grown under rainfed conditions. All field
 157 management practices were the same at both sites.
 158



159
 160 Figure 2. Schematic diagram showing the planting patterns for *Nopalea* and *Opuntia*.
 161 Distances between rows and plants (1.5 × 0.2 m) are indicated. There was a distance of 3.0
 162 m between nine rows of cacti.

163
 164 In this study, to investigate the effects of rainfall availability on the vegetation, we
 165 evaluated the hydrological periods in four seasons (wet, wet-dry transition, dry, and dry-wet
 166 transition) from 2018 to 2021 (Table 2), based on the start and end of the rainfall (Leite-Filho
 167 et al., 2019; Salack et al., 2016).

168
 169 Table 2. Delimiting dates for the seasons based on the start and end of the rainfall, from 2018
 170 to 2021.

Dry season		Dry-wet transition		Wet season		Wet-dry transition	
Start date	End date	Start date	End date	Start date	End date	Start date	End date
01/01/2018	20/01/2018	21/01/2018	20/02/2018	21/02/2018	27/05/2018	28/05/2018	01/07/2018
02/07/2018	08/01/2019	09/01/2019	15/02/2019	16/02/2019	02/08/2019	03/08/2019	14/09/2019
15/09/2019	23/12/2019	24/12/2019	02/02/2020	03/02/2020	06/07/2020	07/07/2020	30/08/2020
31/08/2020	27/09/2020	28/09/2020	14/03/2021	15/03/2021	10/05/2021	11/05/2021	06/09/2021

171

172 *2.2. Measurements and instrumentation*

173 Meteorological measurements were obtained from January 2018 to December 2021,
174 from two towers, 3 m in height, installed in the centre of each experimental area, above the
175 cactus canopy. Each tower comprised the same type of sensors for measuring flux. To
176 measure the net radiation (R_n), closed-cell thermopile-type sensors were used (NR-Lite, Kipp
177 & Zonen, Delft, Netherlands). The two radiometric balance sensors were installed 2.8 m
178 above the canopy. The soil heat flux (G) was quantified using heat flux plates (HFT3, REBS,
179 Hukseflux, Delft, Netherlands) buried close to the rows of cactus at a depth of 0.05 m. Air
180 temperature and relative humidity were determined with the aid of two thermo-hygrometers
181 (HMP155A, Campbell Scientific, Logan, Utah, USA), creating a vertical profile of 0.5 and
182 1.5 m above the surface of the plant canopy. Rainfall data were quantified using an automatic
183 rain gauge (AeroCone, Rain Collect, Hayward, CA, USA), installed 3 m above the canopy.
184 In this study, a fetch to height ratio of more than 100:1 was obtained, an acceptable value
185 when measuring the Bowen ratio (Heilman et al., 1989). The dataset was recorded every 60
186 seconds (CR1000, Campbell Scientific Inc., Logan, Utah, USA), with a storage interval of
187 10 minutes. Measurements were collected continuously throughout the day and night.

188

189 *2.3. Calculation of the surface energy balance and parameters*

190 In this study we used the simplified version of the surface energy balance method.
191 This method is based primarily on the principle of conservation of energy (Equation 1).
192 According to Bowen (1926), the Bowen ratio (β) (Equation 2) can be calculated using the
193 sensible heat flux (H) to latent heat flux (LE) ratio. This ratio is closely linked to the vertical
194 gradients of air temperature and humidity; we therefore assume similarity of equality
195 between the turbulent transfer coefficients of sensible heat and water vapour suggested by
196 Gavilán and Berengena (2007). LE and H were estimated by combining the available energy
197 from the energy balance and the Bowen ratio (Equations 3 and 4). The flux data used in
198 applying the Bowen ratio-energy balance (BREB) method were considered on a daytime
199 scale, from sunrise to sunset only. This is because during the night and before sunrise, when
200 the temperature/humidity gradients are small, they can cause the quantification of erroneous

201 data and inconsistent fluxes (e.g., with β generally close to -1 or tending to infinity). Each
 202 dataset is referred to in local time (i.e., GMT-3).

203

$$204 \quad R_n - G = LE + H \quad (1)$$

$$205 \quad \beta = \frac{H}{LE} = \left(\frac{P_a \cdot c_p}{\lambda \cdot \varepsilon} \cdot \frac{\Delta T}{\Delta e} \cdot \frac{K_h}{K_w} \right) \quad (2)$$

$$206 \quad LE = \frac{R_n - G}{1 + \beta} \quad (3)$$

$$207 \quad H = \frac{\beta}{1 + \beta} \cdot (R_n - G) \quad (4)$$

208

209 where R_n is the net radiation (W m^{-2}); G is the soil heat flux (W m^{-2}); LE is the latent heat
 210 flux (W m^{-2}); H is the sensible heat flux (W m^{-2}); β is the Bowen ratio (dimensionless); P_a
 211 is the atmospheric pressure (kPa); c_p is the specific heat capacity of air ($1004.67 \text{ J kg}^{-1} \text{ }^\circ\text{C}^{-1}$);
 212 λ is the latent heat of vaporisation (2.454 MJ kg^{-1} at 20°C); ε is the ratio of the molecular
 213 weights of the air and water vapour (0.622); ΔT is the air temperature difference between two
 214 heights ($^\circ\text{C}$); Δe is the vapour pressure difference between two heights (kPa); K_h is the eddy
 215 diffusivity of heat ($\text{m}^2 \text{ s}^{-1}$); K_w is the eddy diffusivity of water vapour ($\text{m}^2 \text{ s}^{-1}$).

216

217 The energy from metabolic activities, heat storage in the plant tissue and canopy, and
 218 horizontal advection, were considered insignificant. As such, these energy components were
 219 not included in our energy balance algorithm (Equation 1) (Hu et al., 2014; Pokhariyal and
 220 Patel, 2021). After determining LE (W m^{-2}), we converted this variable into
 221 evapotranspiration (ET), dividing the LE by the latent heat of vaporisation of water in J kg^{-1} .
 222 In this way, the hourly values of ET are integrated, giving the daily values in mm day^{-1}
 223 (Mulovhedzi et al., 2020).

224

225 2.4. Criteria for selecting data for the energy balance method

226 For the acceptance and/or rejection criteria of the data collected by the BREB method,
 227 we used the approach proposed by Perez et al. (1999), which parameterises the criteria for
 228 using variables in composing the method. This is because the Bowen ratio depends on
 229 measuring temperature and vapour pressure gradients. That said, abnormal data is seen when

230 the available-energy heat flux is very small ($R_n - G$), or negative ($R_n - G < 0$). In this way,
231 errors can occur in applying the energy balance using the Bowen ratio (β), later triggering
232 physical inconsistency in the data. Here, we summarise some of the information that results
233 in errors in the results of the Bowen ratio method: (1) when the sensor resolution is inadequate
234 to resolve the gradient in ΔT and Δe ; (2) stable atmospheric conditions, e.g., at dawn and
235 dusk, cause β values close to -1, resulting in evapotranspiration tending to infinity, which is
236 clearly inconsistent; and (3) when conditions change abruptly, they induce measurement
237 errors (Hu et al., 2014; Ortega-Farias et al., 1996; Perez et al., 1999; Unland et al., 1996).

238

239 *2.5. Yield measurements*

240 Biomass yield was determined annually, considering the weight of four randomly
241 chosen representative plants from each site. The biomass above the basal cladode (a
242 vegetative structure planted directly in the soil) was fully harvested and weighed on an
243 electronic balance to quantify the fresh matter (g FM plant⁻¹), and then dried in a forced air
244 circulation oven at 55°C to constant weight. We determined the dry matter weight per plant
245 (g DM plant⁻¹), and the annual increase in productivity of the cacti (Mg ha⁻¹) was then
246 estimated, considering a final density of 27,273 plants ha⁻¹.

247

248 *2.6. Allometry and measurements of plant growth*

249 Every three months we collected morphometric and biomass data of the plants.
250 During the evaluations, four plants from each site were measured to comprise the
251 morphometric data, and another four plants were collected to analysis the biomass over time.
252 For each plant, we quantified morphometric variables of the cladodes and of the plant. The
253 length, width and perimeter of the cladodes were measured, and the number of cladodes
254 determined by order of appearance on the plant (i.e., first order, second order, third order and
255 so on); the total number of cladodes was then determined. To measure plant height, we
256 considered the vertical distance from the ground to the apex of the canopy; plant width was
257 measured as two widths of the top of the canopy. The collected samples were then used to
258 quantify the morphophysiological indices of the cacti. Using the morphometric data, the
259 cladode area—CA (Equation 5) and cladode area index—CAI (Equation 6) were determined
260 (Pinheiro et al., 2014; Silva et al., 2014). In addition, from the dry matter yield and cladode

261 parameters, we calculated the morphophysiological indices of the cacti using a three-
 262 parameter sigmoid model (Equation 7) (Jardim et al., 2021b).

263

$$264 \quad CA = \begin{cases} 1.6691 \cdot \left[\frac{1 - e^{(-0.0243 \cdot CP)}}{-0.0243} \right] & \text{for } Nopalea \\ 0.7086 \cdot \left[\frac{1 - e^{(-0.000045765 \cdot CL \cdot CW)}}{0.000045765} \right] & \text{for } Opuntia \end{cases} \quad (5)$$

$$265 \quad CAI = \left[\frac{\sum_{i=1}^n (CA)}{\frac{10,000}{(S1 \cdot S2)}} \right] \quad (6)$$

$$266 \quad y = \frac{a}{1 + e^{\left(-\frac{x-x_0}{b}\right)}} \quad (7)$$

267

268 where CP is the cladode perimeter (cm); CL is the cladode length (cm); CW is the cladode
 269 width (cm); i is the observation number; n is the total number of observations; 10,000 is the
 270 conversion factor from cm^2 to m^2 ; $S1 \times S2$ is the spacing between the rows and plants of each
 271 cactus (i.e., 1.5×0.2 m), respectively. The parameters for the morphophysiological analysis
 272 were: y - the response variable (e.g., cladode dry matter, cladode area index, and number of
 273 cladodes); a - the maximum value for the rate (i.e., the distance between the two asymptotes
 274); x - the accumulated days; x_0 - the number of days necessary for the plant to express 50%
 275 of the maximum rate (i.e., the inflection point of the curve), and b - the number of days
 276 necessary for the start of the rate.

277

278 We then quantified the absolute growth rate—AGR ($\text{Mg ha}^{-1} \text{ day}^{-1}$), relative growth
 279 rate—RGR ($\text{Mg Mg}^{-1} \text{ day}^{-1}$), net assimilation rate—NAR ($\text{Mg ha}^{-1} \text{ day}^{-1}$), and specific
 280 cladode area—SCA ($\text{Mg}^{-1} \text{ day}^{-1}$) (Jardim et al., 2021b; Khapte et al., 2022). The AGR
 281 represents the increase in dry biomass per unit of time, and the RGR the increase in dry
 282 biomass adjusted by the accumulated biomass per unit of time. NAR represents the dry mass
 283 produced per cladode area per unit of time; this variable is commonly used to represent the
 284 net photosynthetic rate of the plants. The SCA represents the cladode area used in
 285 photosynthesis (Jardim et al., 2021b). All the growth rates were calculated during the
 286 experimental period, from 2015 to 2021.

287

288 2.7. Plant water status: cladode water content, succulence, and water use efficiency

289 The water status of the plants was measured using biomass data and morphometric
290 variables. To this end, the cladode water content (CWC) and cladode succulence (CS) were
291 calculated for the two cacti. The cladodes were removed from the plants and immediately
292 weighed to quantify the fresh weight. They were then identified and left to dry in an oven at
293 55°C to constant weight. We calculated the cladode water content (%) from the fresh matter
294 (FM) and dry matter (DM) weight of the samples (Equation 8). Cladode succulence (g cm⁻²)
295 was determined by subtracting the dry from the fresh weight of the samples and dividing by
296 the cladode area—CA (Equation 9) (Corrado et al., 2020; Ho et al., 2019).

297

$$298 \quad \text{CWC} = \left(\frac{\text{FM} - \text{DM}}{\text{FM}} \right) \cdot 100 \quad (8)$$

$$299 \quad \text{CS} = \left(\frac{\text{FM} - \text{DM}}{\text{CA}} \right) \quad (9)$$

300

301 The water use efficiency (WUE) was calculated using the ratio between the annual
302 biomass yield of the crop and the evapotranspiration (Equation 10) (Kai Zhang et al., 2022).

303

$$304 \quad \text{WUE} = \frac{\text{DMY}}{\text{ET}} \quad (10)$$

305

306 where DMY is the annual dry matter yield (kg ha⁻¹); ET is the total annual evapotranspiration
307 (m³ ha⁻¹).

308

309 2.8. Indices of environmental and physiological stress

310 To assist in understanding the plant responses to environmental stress, we used
311 spectral reflectance indices, e.g., the Normalised Difference Vegetation Index (NDVI),
312 Photochemical Reflectance Index (PRI) and the Chlorophyll Index (CI), with discussions and
313 mathematical formalisms provided by Gitelson and Merzlyak (1994); Perez-Priego et al.
314 (2015) and Sanchez et al. (2022). These indices were calculated using images from the
315 Sentinel-2 MultiSpectral Instrument (MSI), which offers different spatial resolutions (i.e.,

316 10, 20, and 60 m) available from the United States Geological Survey (USGS,
317 <https://www.usgs.gov/>). Here, we use reflectances of 800 and 670 nm for the NDVI, 531 and
318 570 nm for the PRI, and 750 and 705 nm for the CI (Gitelson and Merzlyak, 1994; Perez-
319 Priego et al., 2015; Sanchez et al., 2022). The images were acquired from 16 January 2018
320 to 31 December 2021 under <10% cloud cover. All the image processing and calculations
321 were carried out using the Google Earth Engine (GEE) platform. In addition, we applied a
322 pixel quality attribute mask to the images, masking clouds, cloud shadow and water, using
323 the CFMask algorithm (Foga et al., 2017; Hurni et al., 2019).

324

325 2.9. Data analysis

326 We used the cladode area index and dry matter data to determine the growth rates of
327 the plants using nonlinear sigmoid models. The models were evaluated and chosen based on
328 significance ($P < 0.05$; using the F-test), and a coefficient of determination greater than 0.85.
329 To test the difference between the energy balance components, i.e., R_n , LE , H , and G , as well
330 as ET, and VPD during the four seasons under study (i.e., wet season, dry season, wet-dry
331 and dry-wet transitions) in the two species of cactus, we used Student's t-test and set a
332 significance of $P < 0.01$. We also included box and whisker plots, showing the median,
333 interquartile range and 1.5 times the interquartile range for the data related to cladode water
334 content, succulence, energy balance, ET and VPD. To examine the interrelationships
335 between the plant parameters and environmental conditions, principal component analysis
336 (PCA) was applied. This type of analysis is used to reduce variables or a large dataset using
337 orthogonal transformation, generating linearly uncorrelated variables (Lamichhane et al.,
338 2021). In this way, we constructed a PCA of twenty variables (R_n , LE , H , G , LE/R_n , H/R_n ,
339 G/R_n , VPD, NDVI, PRI, CI, ET, DMY, WUE, CWC, CS, AGR, RGR, NAR and SCA). In
340 addition, it should be noted that before carrying out the analysis, each response variable was
341 standardised using the z-transform, with zero mean and unit standard deviation. Finally, the
342 significant principal components were selected based on the Kaiser criterion, considering
343 only eigenvalues greater than 1.0 (Jardim et al., 2021a; Kaiser, 1960; Lamichhane et al.,
344 2021). The data were processed and analysed using the R software (R Core Team, 2022).

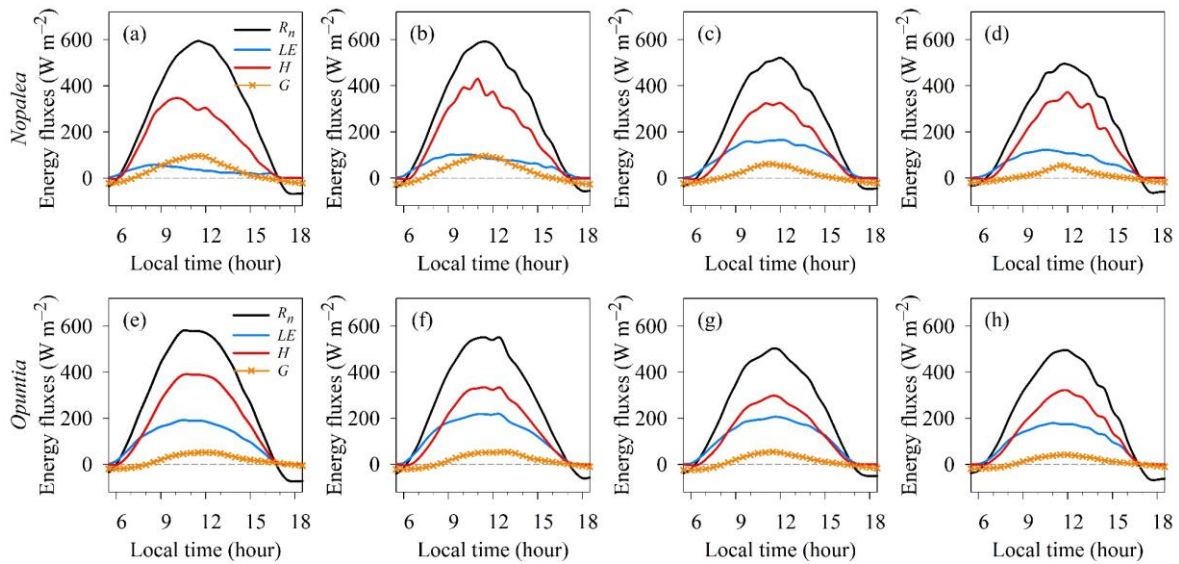
345

346 3. Results

347 3.1. Daytime variation in the energy fluxes

348 Figure 3 shows the daytime surface energy balance for the four seasons (dry season,
349 dry-wet transition, wet season, and wet-dry transition) from January 2018 to December 2021
350 on an hourly scale. The sites cultivated with *Nopalea* (Figure 3a–d) and *Opuntia* (Figure 3e–
351 h) had respective mean values of 249.19 and 245.60 W m⁻² for net radiation (R_n). The mean
352 latent heat flux (LE) for *Opuntia* was 105.26 W m⁻², 77.02% higher than at the site cultivated
353 with *Nopalea*. During the dry-wet transition season, *Opuntia* had the highest LE (117.36 W
354 m⁻²), ranging from 0.34 to 217.87 W m⁻², with a peak from 10:30 to 12:30 local time (Figure
355 3f). For *Nopalea*, the highest LE (90.53 W m⁻²) was seen during the wet season, varying
356 throughout the day from 1.21 to 165.22 W m⁻², with a peak from 09:30 to 12:30 (Figure 3c).
357 The sensible heat flux (H) was the most contrasting variable at both sites, with the highest
358 energy consumption in each season. In *Opuntia*, the greatest value for H was seen during the
359 dry season, with a mean of 183.33 W m⁻² (Figure 3e), 2.03% higher than in *Nopalea*, which
360 occurred during the dry-wet transition season (Figure 3b). In both of the cactus crops, the soil
361 heat flux (G) was greater during the dry season (Figure 3a and 3e), with 28.45 W m⁻² in
362 *Nopalea* and 16.65 W m⁻² in *Opuntia*. During the dry season, greater values for G in *Nopalea*
363 were clearly seen at dawn, with peaks between 11:00 and 12:30 in both cacti. Interestingly,
364 the lowest values for G were seen during the wet-dry transition season, with a mean of 8.25
365 W m⁻² (*Nopalea*) and 10.21 W m⁻² (*Opuntia*). Furthermore, during the same wet-dry
366 transition season, the R_n of the sites cultivated with *Opuntia* (218.75 W m⁻²) and *Nopalea*
367 (216.56 W m⁻²) were the lowest for the entire study period.

368



369

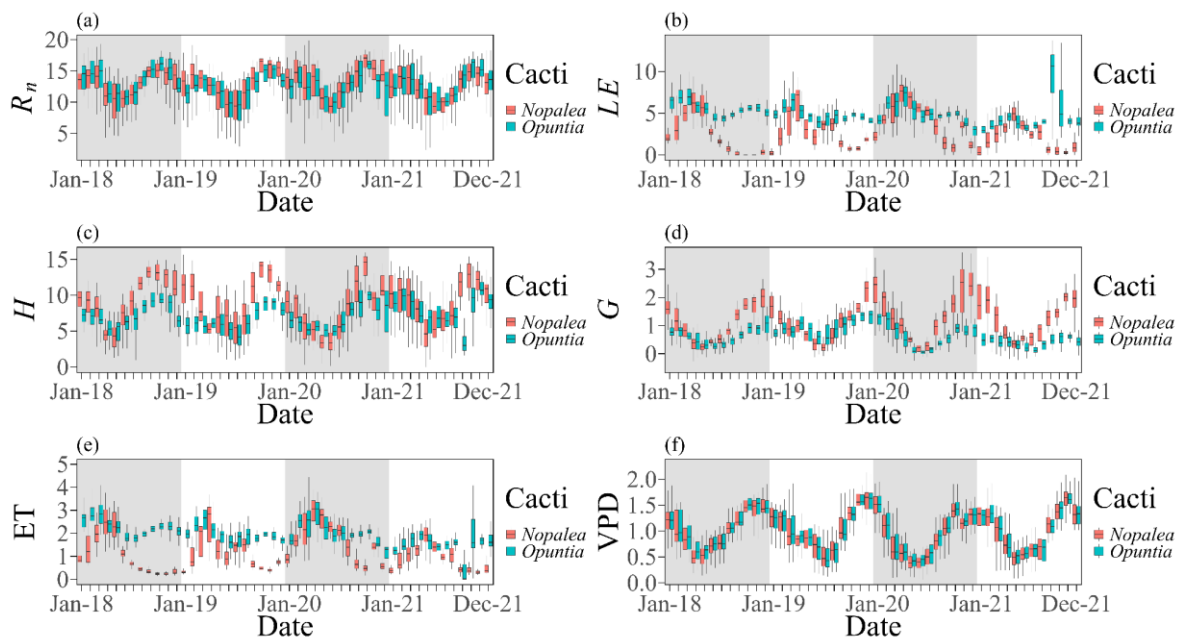
370 Figure 3. Mean daytime evolution of the surface energy balance components (net radiation—
 371 R_n , latent heat flux— LE , sensible heat flux— H , and soil heat flux— G) between the two
 372 experimental sites, with *Nopalea* (a–d) and *Opuntia* (e–h). The measurements were taken
 373 during the dry season (a and e), dry-wet transition season (b and f), wet season (c and g), and
 374 wet-dry transition season (d and h), from 2018 to 2021.

375

376 3.2. Seasonal and interannual characteristics of the energy fluxes

377 Our results for temporal variation in energy and water flux for two agroecosystems
 378 of *Nopalea* and *Opuntia* cacti are shown in Figure 4. On average, the values of R_n during the
 379 months under evaluation varied between 12.76 and 12.64 MJ m⁻² day⁻¹ for *Nopalea*
 380 (interquartile range 11.54 to 14.07) and *Opuntia* (interquartile range 11.85 to 13.76),
 381 respectively. At both sites, the lowest and highest values of R_n occurred in June and October,
 382 respectively (Figure 4a). In general, R_n patterns remained quite stable throughout the period
 383 under evaluation (2018–2021). There were clearly significant variations in LE between the
 384 sites cultivated with *Nopalea* and *Opuntia* (Figure 4b); for *Nopalea*, we found minimum and
 385 maximum mean values for LE ranging from 0.62 to 5.71 MJ m⁻² day⁻¹, with an overall mean
 386 value of 2.76 MJ m⁻² day⁻¹ (interquartile range 1.24 to 3.77), while LE for *Opuntia* was
 387 79.72% greater than for *Nopalea* during the evaluated period. Our results show a seasonal
 388 variation in LE , with higher values from January to June, and falling off from July to
 389 December. On the other hand, we clearly saw greater resistance in *Opuntia*, maintaining the

390 *LE* during periods of greater deficiency. For example, whereas *Nopalea* experienced a
 391 significant reduction in *LE* when the vapour pressure deficit (VPD) was high (~1.22 kPa),
 392 *Opuntia* maintained a stabilised *LE*, with less significant reductions. With the exception of
 393 November 2020, *Nopalea* had the lowest value for *LE* from September to November (0.69
 394 MJ m⁻² day⁻¹), while during the same period the value for *Opuntia* was higher (5.37 MJ m⁻²
 395 day⁻¹). As a result, *H* had a mean value of 8.84 MJ m⁻² day⁻¹ (interquartile range 6.36 to 10.86)
 396 in *Nopalea*, with a mean of 7.04 MJ m⁻² day⁻¹ (interquartile range 6.01 to 7.53) in *Opuntia*
 397 throughout the period (Figure 4c). In both cacti, the range of results for *H* was broader, and
 398 the results higher, between September and December.
 399



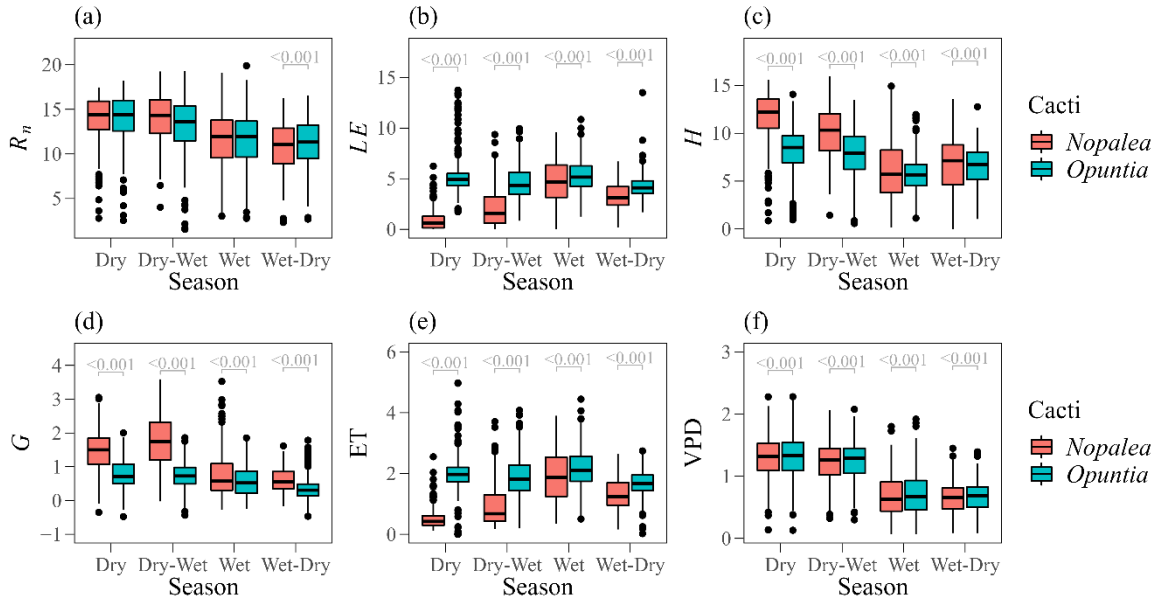
400
 401 Figure 4. Temporal variation in energy flux (i.e., net radiation— R_n (a), latent heat flux— LE
 402 (b), sensible heat flux— H (c), and soil heat flux— G (d), expressed in MJ m⁻² day⁻¹) and water
 403 (i.e., evapotranspiration— ET (e) and vapour pressure deficit— VPD (f), expressed in mm
 404 day⁻¹ and kPa, respectively) in two species of cactus from 2018 to 2021. The boxplots denote
 405 the median, 25th, 50th, and 75th percentiles, the whiskers indicate 1.5 times the interquartile
 406 range. The shaded areas represent year boundaries.

407
 408 Corresponding to the turbulent fluxes from the vegetated surfaces, Figure 4d shows
 409 the variations in G for the cacti. Notably, we found higher values for G in *Nopalea*, ranging

410 from 0.36 to 2.08 MJ m⁻² day⁻¹, with a mean of 1.16 MJ m⁻² day⁻¹. The results showed
411 differing patterns between surfaces, with *Nopalea* 81.85% greater than *Opuntia*. The highest
412 values, and the most-pronounced variation in *G* occurred from October to February: 1.78 MJ
413 m⁻² day⁻¹ in *Nopalea* and 0.86 MJ m⁻² day⁻¹ in *Opuntia*. In addition, on average, when
414 compared to the other months under analysis, a reduction can be seen for *G* between April
415 and August, of 66.10% in *Nopalea* and, to a lesser extent in *Opuntia* (48.04%) (Figure 4d),
416 the results being consistent with the location and time of year. The results for
417 evapotranspiration (ET) also showed significant variations over the years at sites with
418 *Nopalea* and *Opuntia* (Figure 4e). Both cacti kept the ET synchronous with the VPD (Figure
419 4f) and turbulent fluxes (i.e., *LE* and *H*). Under these conditions, the ET ranged from 0.43 to
420 2.30 mm day⁻¹ in *Nopalea* (mean 1.71 mm day⁻¹, interquartile range 0.61 to 1.53), and 1.65
421 to 2.46 mm day⁻¹ in *Opuntia* (mean 1.96 mm day⁻¹, interquartile range 1.71 to 2.13). Although
422 the VPD at both sites is similar, we found a strange variation in ET for *Nopalea* in relation
423 to *Opuntia*, with a mean reduction of 40.06% when comparing water lost to the atmosphere.
424 Similarly, during the last four months of each year (2018-2021), the decline in ET in *Nopalea*,
425 in relation to the overall mean ET, was more marked (53.42%), in contrast to *Opuntia*
426 (7.33%). The sharpest decline in ET occurred predominantly in October and December in
427 *Nopalea* and *Opuntia*, respectively.

428 Figure 5 shows the energy balance components, ET and VPD, during the dry season,
429 dry-wet transition, wet season, and wet-dry transition. Only during the wet-dry transition
430 season was there any highly significant difference in *R_n* between the two species of cactus (*P*
431 < 0.001) (Figure 5a). We also found the mean value of *R_n* to be 3.05% higher for *Opuntia*
432 during the wet-dry transition (median 11.33 MJ m⁻² day⁻¹, interquartile range 9.47 to 13.20)
433 compared to *Nopalea* for the same period. The *LE* was significantly higher in *Opuntia* during
434 the dry season (513.39%), with an interquartile range of 4.30 to 5.51 MJ m⁻² day⁻¹ (Figure
435 5b). During each of the seasons under evaluation, there was a significant difference in *LE*, *H*,
436 *G*, ET and VPD between the cacti. The lowest values for *LE* in *Nopalea* were during the dry
437 season (0.85 MJ m⁻² day⁻¹), whereas for *Opuntia* it was during the wet-dry transition season
438 (4.22 MJ m⁻² day⁻¹). Our results further show that, on average, during the wet season, the
439 difference in *LE* between *Opuntia* and *Nopalea* was relatively low (0.55 MJ m⁻² day⁻¹).

440



441

442 Figure 5. Boxplot showing energy flux components and water exchange in two species of
 443 cactus (*Nopalea cochenillifera* and *Opuntia stricta*) during the wet and dry seasons, and the
 444 dry-wet and wet-dry transition seasons. The P value was calculated using Student's t-test
 445 ($P < 0.01$). R_n is the net radiation in $\text{MJ m}^{-2} \text{day}^{-1}$ (a), LE is the latent heat flux in $\text{MJ m}^{-2} \text{day}^{-1}$
 446 (b), H is the sensible heat flux in $\text{MJ m}^{-2} \text{day}^{-1}$ (c), G is the soil heat flux in $\text{MJ m}^{-2} \text{day}^{-1}$
 447 (d), ET is the evapotranspiration in mm day^{-1} (e), and VPD is the vapour pressure deficit in
 448 kPa (f). The boxplots denote the median, 25th, 50th, and 75th percentiles, the whiskers
 449 indicate 1.5 times the interquartile range and individually plotted outliers.

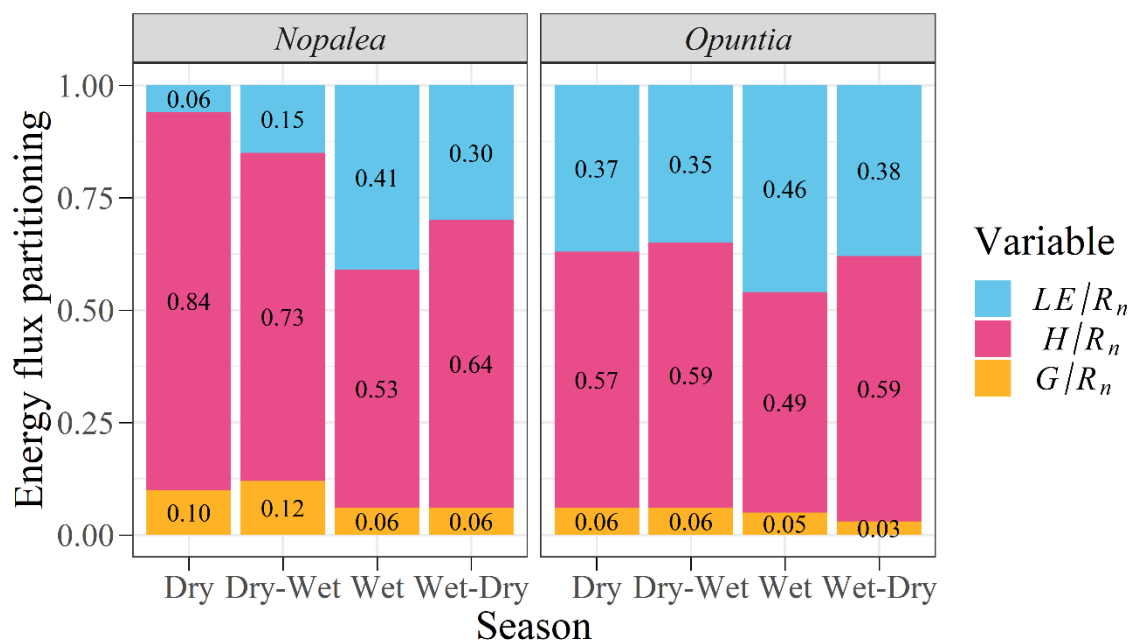
450

451 During the dry season and the dry-wet transition, H was higher and more significant
 452 in *Nopalea*, respectively 44.75% and 29.10% higher than in *Opuntia* for the same seasons
 453 (Figure 5c). This resulted in similar behaviour between the surfaces for the other fluxes, with
 454 G in *Nopalea* 139.03% higher than *Opuntia* during the dry-wet transition season, followed
 455 by 85.84% higher during the dry season ($P < 0.001$, Figure 5d). Although the sites generally
 456 have similar weather conditions, there were also differences between the surfaces for ET and
 457 VPD (Figure 5e–f). For *Nopalea*, the ET ranged from 0.49 to 1.92 mm day^{-1} , in contrast,
 458 *Opuntia* maintained ET at its most stable throughout the four seasons, ranging from 1.67 to
 459 2.17 mm day^{-1} .

460

461 3.3. Changes in energy partitioning for surfaces with cacti

462 Figure 6 shows the seasonal changes in energy partitioning during the four seasons
 463 for both cacti. Despite the similarity of energy inputs previously shown by R_n (Figure 5a),
 464 interaction with the two vegetated surfaces significantly alters energy partitioning (Figure 6).
 465 The H/R_n ratio in the area of *Nopalea* was the highest in each season (a mean of 0.69), 22.32%
 466 higher than the mean H/R_n ratio in *Opuntia*. Although the mean value of H/R_n is lower in
 467 *Opuntia* (18.25%), it is obvious that H was the main consumer of R_n in both areas of cacti,
 468 heating the air. We observed decreasing behaviour in H/R_n from the dry to the wet season,
 469 with a partition ratio 36.90% lower in *Nopalea* and 14.04% in *Opuntia*. During the same
 470 seasons, i.e., wet and dry, the LE/R_n ratio was highly variable in *Nopalea*, and at both sites
 471 LE was inversely proportional to the seasonal variations in H . The G/R_n ratio was equal to
 472 0.10 and 0.12 in *Nopalea* during the dry and dry-wet transition seasons, however, during the
 473 dry season and dry-wet transition, *Opuntia* was, respectively, 40% and 50% lower.
 474

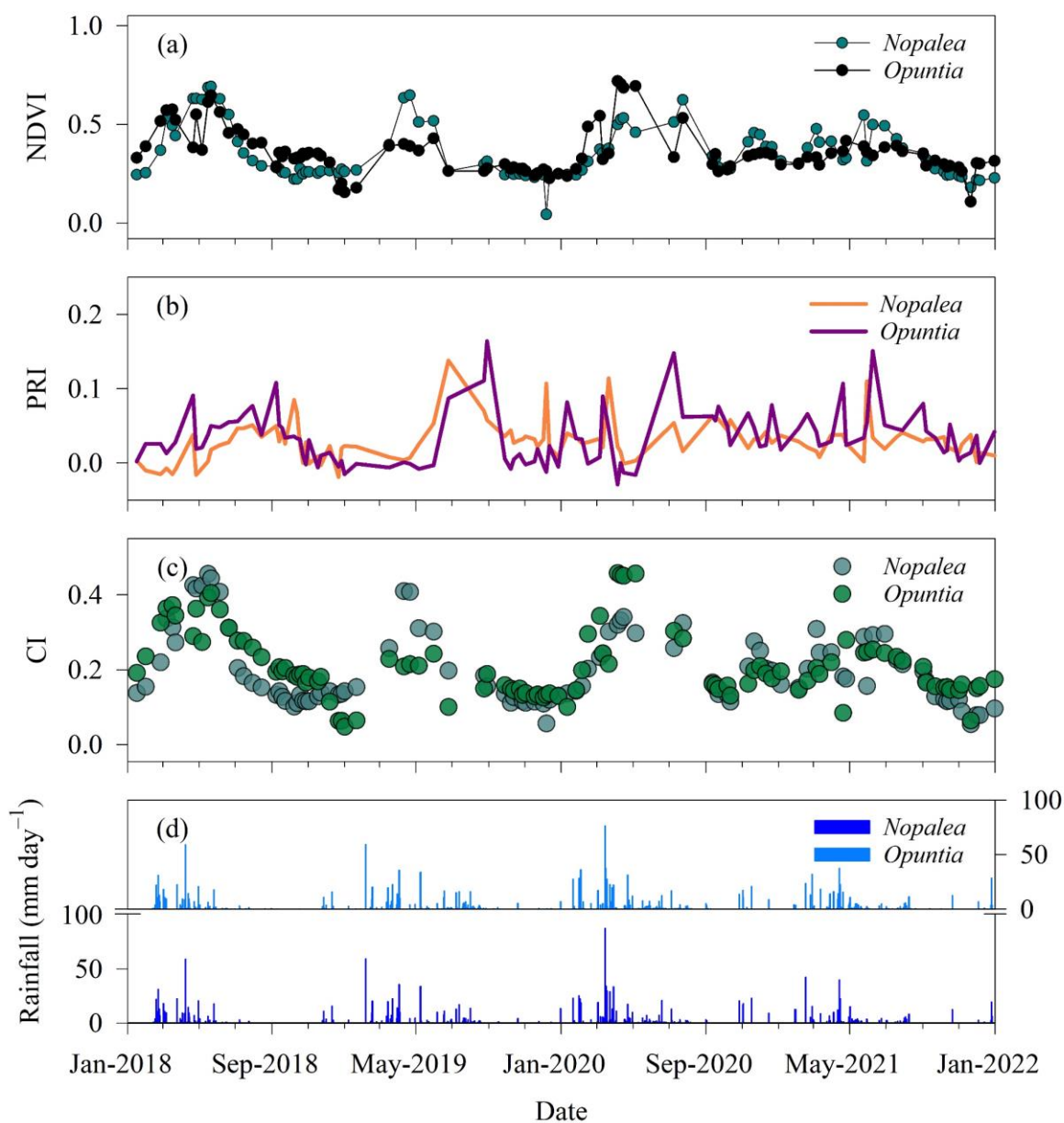


475
 476 Figure 6. Surface energy partitioning in two agroecosystems with cacti (*Nopalea*
 477 *cochenillifera* and *Opuntia stricta*).
 478

479 3.4. Changes in the vegetation, photochemical and pigment indices

480 Variations in the Normalised Difference Vegetation Index (NDVI), Photochemical
481 Reflectance Index (PRI), Chlorophyll Index (CI) and rainfall for the sites cultivated with
482 *Nopalea* and *Opuntia* are shown in Figure 7. The results show that the NDVI for *Nopalea*
483 ranged from 0.19 to 0.67 (mean \pm standard deviation: 0.36 ± 0.13), only slightly different to
484 *Opuntia*, with values between 0.17 and 0.70 (a mean of 0.37 ± 0.11) (Figure 7a). Furthermore,
485 we found that during the wet season the results for the NDVI were higher in both species.
486 This was also true for the CI (Figure 7c). The best results for NDVI and CI were clearly
487 between April and May, with a mean of 0.52 and 0.33, respectively, for *Nopalea*, whereas,
488 for *Opuntia*, during the months in question, the respective values were 5.34% and 5.60%
489 lower. We also found that between April and May the PRI showed a lower photochemical
490 response, with a mean of 0.02 for both cacti (Figure 7b).

491



492
 493 Figure 7. Normalised Difference Vegetation Index—NDVI (a), Photochemical Reflectance
 494 Index—PRI (b), Chlorophyll Index—CI (c), and rainfall (d) in two areas of cactus (*Nopalea*
 495 *cochenillifera* and *Opuntia stricta*), from January 2018 to December 2021.

496
 497 The photosynthetic responses of the plants under environmental conditions resulted
 498 in values for the PRI that ranged from -0.01 to 0.14 over the time series under evaluation. A
 499 joint assessment of the relationships between the NDVI, PRI, CI and rainfall, showed an
 500 increase in the PRI when water availability was low (Figure 7d). In particular, when the

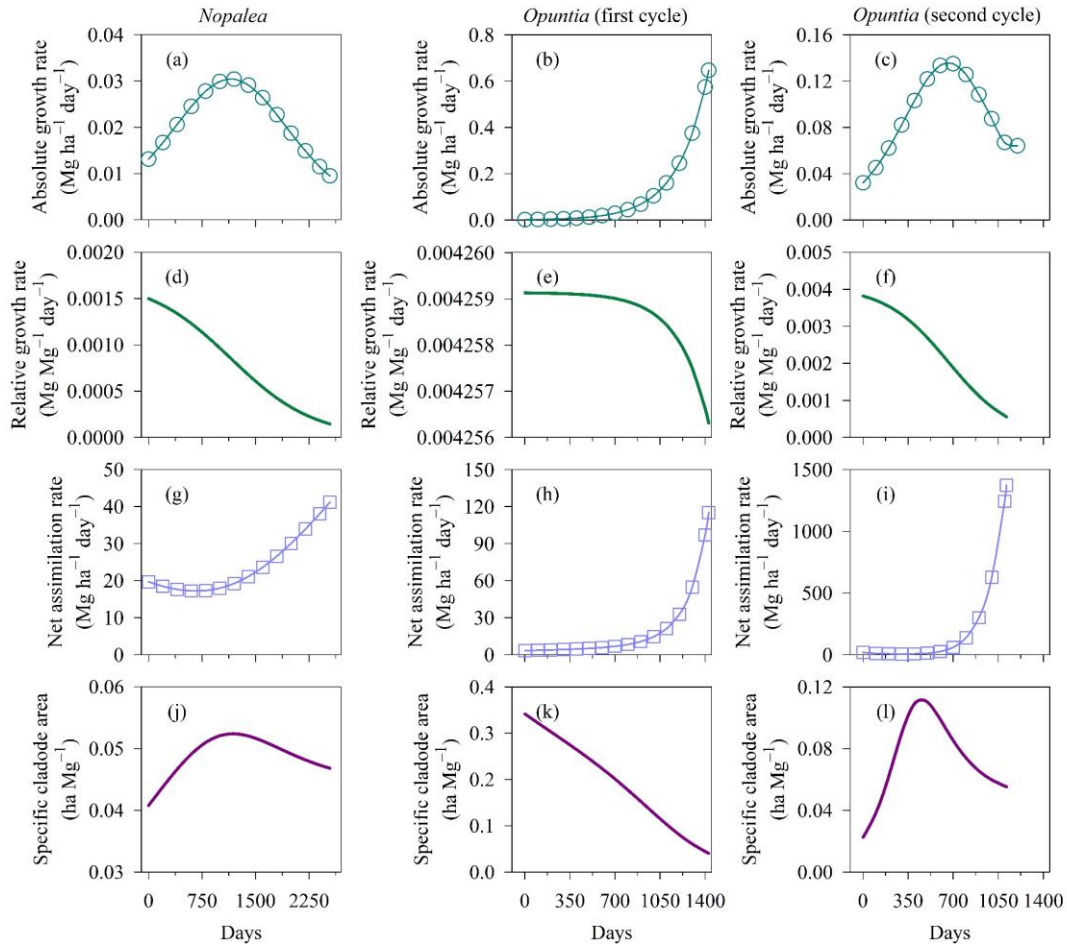
501 NDVI and CI were drastically reduced by the plants, the values of the PRI were higher. These
502 clear changes in the vegetation indices relative to the photosynthetic indices help clarify the
503 photochemical efficiency and pigment pools of the plants. In addition, when the PRI showed
504 no sudden variations relative to the NDVI or CI (November 2018 to May 2019 and November
505 2020 to May 2021), the cacti presented a reduced photosynthetic response despite a lack of
506 stress conditions. The temporal pattern of the rainfall was very similar at both sites: *Nopalea*
507 (mean 454.50 mm year⁻¹, total 1818.0 mm) and *Opuntia* (mean 472.48 mm year⁻¹, total
508 1889.90 mm), with 2020 the wettest year (Figure 7d). It is important to note that a brief 3.95%
509 greater difference in water availability in the area of *Opuntia* may have been one of the causes
510 of the changes in the PRI, CI and NDVI at the end of the experiment in 2021.

511

512 3.5. Rates of plant growth, morphology, and physiology

513 Figure 8 shows the seasonal variation in absolute growth rate (AGR), relative growth
514 rate (RGR), net assimilation rate (NAR), and specific cladode area (SCA) for the two species
515 under study. We measured morphometric variables in both cacti from 2015 to 2021 to assess
516 plant growth performance. During this period, one cycle of *Nopalea* and two cycles of
517 *Opuntia* were evaluated. For the latter, the first cycle was harvested on 12 December 2018
518 (day of year [DOY] 1428), and the second cycle on 31 December 2021 (DOY 1115). The
519 *Nopalea* was harvested on the same date, but 2543 days after planting. The absolute growth
520 rate curves for *Nopalea* in the first cycle (Figure 8a), and *Opuntia* in the second cycle (Figure
521 8c), were very similar, however, the performance of the AGR in *Opuntia* averaged 0.10 Mg
522 ha⁻¹ day⁻¹ (a peak of 0.14 Mg ha⁻¹ day⁻¹), with 0.02 Mg ha⁻¹ day⁻¹ (a peak of 0.03 Mg ha⁻¹ day⁻¹)
523 in *Nopalea*. When examining the AGR in *Opuntia* in more detail during the first cycle, we
524 found far higher values compared to *Nopalea* (379.61%). Similarly, the AGR in *Opuntia*
525 during the first cycle was 11.25% higher compared to the second cycle.

526



527

528 Figure 8. Seasonal changes in absolute growth rate (a–c), relative growth rate (d–f), net
 529 assimilation rate (g–i), and specific cladode area (j–l) in two species of cactus (*Nopalea*
 530 *cochenillifera* and *Opuntia stricta*) measured over a period of seven years (2015 to 2021).

531

532 In the present study, the results of the relative growth rate (RGR) ranged from 0.001
 533 to 0.0043 Mg Mg⁻¹ day⁻¹ for *Opuntia*, with lower values for *Nopalea*, ranging from 0.0001
 534 to 0.0015 Mg Mg⁻¹ day⁻¹ (Figure 8d–f). In addition, the RGR was notably higher during the
 535 initial growth period in both species, gradually falling until reaching minimum values.
 536 During the first cycle of *Opuntia*, we clearly saw a prolongation of the high values for RGR,
 537 which started to fall in October 2017 (DOY 1000) (Figure 8e). Overall, the RGR during the
 538 first *Opuntia* cycle was higher than during the second cycle, as well as higher than that of
 539 *Nopalea*, with a value greater than 0.004 Mg Mg⁻¹ day⁻¹. Similarly, the high values for AGR
 540 in *Opuntia* produced an expressive response in the NAR, with a mean of 17.60 Mg ha⁻¹ day⁻¹
 541 during the first cycle, and 175.15 Mg ha⁻¹ day⁻¹ during the second cycle (Figure 8h–i);

542 whereas for *Nopalea*, the mean value for NAR was 23.57 Mg ha⁻¹ day⁻¹ (Figure 8g). Our
543 results for NAR therefore show that species *Nopalea*, despite a high NAR throughout the
544 cycle, did not show greater photosynthetic capacity than *Opuntia*.

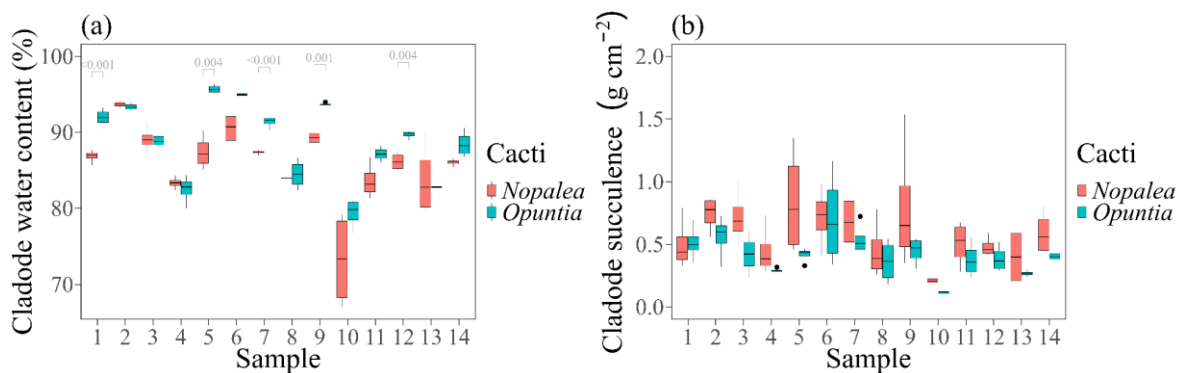
545 To further explore the contributions of environmental factors to the variation in plant
546 growth rates, we analysed the behaviour of the SCA (Figure 8j–l). During the first cycle,
547 *Opuntia* exhibited a mean SCA of 0.19 ha Mg⁻¹, ranging from 0.04 to 0.34 ha Mg⁻¹. These
548 results afforded a percentage superiority for the SCA in *Opuntia*; when compared to *Nopalea*
549 and to *Opuntia* in the second cycle the values were, respectively, 292.53% and 154.92%
550 higher. Despite the high values of the SCA in *Opuntia* during the first cycle, there was a
551 strong, almost linear reduction over time (Figure 8k). During the single cycle of *Nopalea* and
552 the second cycle of *Opuntia*, there was a peak in the SCA (humped curve) following the start
553 of evaluations; results observed around DOY 1175 and 450, respectively.

554

555 3.6. Water relations, increase in annual biomass yield, and water use efficiency

556 Figure 9 shows the cladode water content and cladode succulence for the two species
557 of cactus. There was a significant difference in the cladode water content during the sampling
558 periods (Figure 9a). We found more-pronounced dehydration in samples 4, 8, 10 and 13, with
559 a mean of 81.09% and 82.30% for *Nopalea* and *Opuntia*, respectively. In addition, the
560 cladode water content ranged from 73.24% to 93.69%, with a mean of 86.01% in *Nopalea*,
561 and, in contrast, a mean of 88.91% in *Opuntia*, reaching values between 79.43% and 95.71%.
562 Our results show a similar albeit not significant trend for cladode succulence in *Nopalea* and
563 *Opuntia* (Figure 9b). The minimum and maximum values obtained in both species ranged
564 from 0.22 to 0.84 g cm⁻² in *Nopalea* and 0.11 to 0.70 g cm⁻² in *Opuntia*. In fact, regardless of
565 the sampling period, cladode succulence in *Nopalea* was on average 40.03% greater than in
566 *Opuntia*. Although both have succulent cladodes, the high value for cladode succulence in
567 *Nopalea* was probably due to the smaller cladode area promoting greater succulence.

568



569

570 Figure 9. Variation in cladode water content (a) and cladode succulence (b) in two species of cactus
 571 (*Nopalea cochenillifera* and *Opuntia stricta*) from 2018 to 2021 in a semi-arid
 572 environment. The boxplots denote the median, 25th, 50th, and 75th percentiles, the whiskers
 573 indicate 1.5 times the interquartile range and individually plotted outliers. Student's t-test was
 574 used to examine the difference between the two species for each sampling period ($P < 0.01$).
 575

576

577 Both species of cactus showed variations in dry matter yield—DMY and water use
 578 efficiency—WUE over time (Table 3). For each year under evaluation, the mean annual
 579 increase in DMY in *Nopalea* was 0.32 Mg ha^{-1} , reaching a maximum value in 2018 (0.55 Mg
 580 ha^{-1}), since with the final samples in 2021 the increase in biomass yield was reduced by
 581 78.02%. On the other hand, the mean increase in DMY in *Opuntia* was 56.01 Mg ha^{-1} ,
 582 ranging from 23.39 to $118.03 \text{ Mg ha}^{-1}$ during the years under evaluation (2018–2021). These
 583 high biomass yields in *Opuntia* clearly follow the highest WUE presented by the species.
 584 Our results show a mean WUE of 7.54 kg m^{-3} for *Opuntia*, with significantly lower values
 585 found in *Nopalea*, a mean of 0.08 kg m^{-3} . For the final sampling period, WUE in *Nopalea*
 586 was 99.43% lower than *Opuntia* for the same year. This shows that, over time, both species
 587 have variations in water use capacity and biomass conversion. Here it should be noted that
 588 *Nopalea* showed greater sensitivity to environmental conditions due to poorer performance
 589 compared to *Opuntia* (Table 3).

589

590 Table 3. Increase in annual biomass yield, and water use efficiency in two species of cactus
 591 (*Nopalea cochenillifera* and *Opuntia stricta*), during 2018–2021.

Variable	Cacti	Year			
		2018	2019	2020	2021

DMY (Mg ha ⁻¹)	<i>Nopalea</i>	0.55	0.39	0.23	0.12
	<i>Opuntia</i>	118.03	23.39	45.97	36.66
WUE (kg m ⁻³)	<i>Nopalea</i>	0.14	0.10	0.04	0.04
	<i>Opuntia</i>	14.31	3.28	6.18	6.39

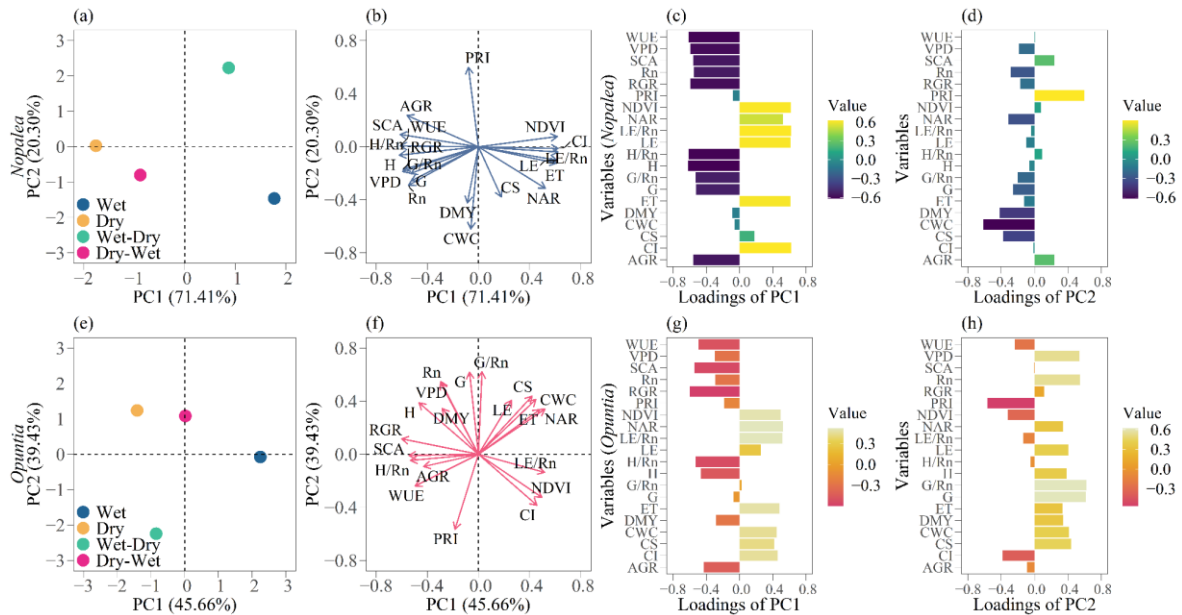
DMY is the dry matter yield and WUE is the water use efficiency.

592

593 3.7. Associations between variables

594 To examine patterns or trends in the sampled data, we applied principal component
595 analysis (PCA) for the two species of cactus (Figure 10). We used the first two principal
596 components (PC1 and PC2) to explain the total variance of the data. This criterion was
597 chosen, as the principal components present eigenvalues greater than 1 (Kaiser, 1960). Figure
598 10a shows the scores of PC1 (71.41%) and PC2 (20.30%) for *Nopalea*, responsible for
599 explaining 91.71% of the total accumulated variation. There was a clear difference between
600 the wet season (with respective PC1 and PC2 scores of 1.76 and -1.46), the dry season (with
601 respective PC1 and PC2 scores of -1.75 and 0.03), the wet-dry transition (with respective
602 PC1 and PC2 scores of 0.86 and 2.22) and the wet-dry transition (with PC1 and PC2 scores
603 of -0.87 and -0.79), in relation to the plant and environmental variables. In fact, in PC1, the
604 plant growth variables, such as SCA, AGR, RGR and WUE presented higher negative
605 loadings (-0.56, -0.56, -0.59 and -0.61, respectively) during the dry season and dry-wet
606 transition (Figure 10b–c). This may indicate that the species has less growth during wetter
607 periods. In contrast, the variables NAR, NDVI and CI showed positive grouping during the
608 wet season (Figure 10b), with strong positive loadings in PC1, and values of 0.52, 0.62 and
609 0.62, respectively (Figure 10c). Furthermore, ET, *LE* and the *LE/R_n* ratio presented loadings
610 greater than 0.6 during the same season in the above PC. We found high loadings, ranging
611 from -0.52 to -0.62 for *G*, *H*, VPD, *R_n*, *H/R_n* and *G/R_n* during the seasons with less water
612 availability and in PC1. For *Nopalea*, the most significant variables in PC2 were CWC (-
613 0.62) and PRI (0.60) (Figure 10d).

614



615

616 Figure 10. Key dimensions of the multivariate space of the cactus species (*Nopalea* and
 617 *Opuntia*) associated with the seasons, and environmental and plant variables. Biplots with
 618 scores from the principal component analysis—PCA (a and e), and loadings of the first two
 619 principal components (b and f). The bar graphs with loadings (c–d and g–h) show the
 620 contribution for each principal component. Variables: water use efficiency (WUE), vapour
 621 pressure deficit (VPD), specific cladode area (SCA), net radiation (R_n), relative growth rate
 622 (RGR), Photochemical Reflectance Index (PRI), Normalised Difference Vegetation Index
 623 (NDVI), net assimilation rate (NAR), latent heat flux (LE), sensible heat flux (H), soil heat
 624 flux (G), evapotranspiration (ET), dry matter yield (DMY), cladode water content (CWC),
 625 cladode succulence (CS), Chlorophyll Index (CI), and absolute growth rate (AGR).

626

627 The PCA results for *Opuntia* are shown in Figure 10e–h, where the first two
 628 components contributed with 85.09% of the total variance. PC1 separated the wet season
 629 from the other seasons, thereby contributing with 45.66% of the total variance. On the other
 630 hand, PC2 explained 39.43%, and was represented by the dry season and dry-wet transition
 631 (Figure 10e). The variables NAR (0.52), LE/R_n (0.52), NDVI (0.50), ET (0.48), CI (0.46),
 632 CWC (0.45) and CS (0.42) had the highest positive loadings in PC1 (Figure 10f–g). SCA and
 633 RGR had the highest contributions with negative loadings (-0.54 and -0.60, respectively) in
 634 PC1. We clearly saw higher NDVI and CI loadings when H and VPD were lower (Figure
 635 10f). During the dry season and dry-wet transition, both more strongly inserted in PC2 (scores

636 of 1.23 and 1.08, respectively), the most positively significant variables were G/R_n , G , R_n and
637 VPD, with respective loadings of 0.62, 0.62, 0.55 and 0.54. Here, we found that both *Nopalea*
638 and *Opuntia* showed similar groupings during the wet season, but with different loadings and
639 contributions.

640

641 **4. Discussion**

642 *4.1. Energy balance and partitioning*

643 The analyses presented here show that vegetation type can easily promote changes in
644 the surface energy fluxes (i.e., turbulent, radiation and ground heat), on a daily and seasonal
645 scale. We found that species of family Cactaceae, i.e., *Nopalea cochenillifera* and *Opuntia*
646 *stricta*, afford marked changes in the turbulent energy fluxes and available energy, even
647 under similar environmental conditions (Figures 3 and 4). In the present study, on an hourly
648 daytime scale, R_n and H were the most prominent variables for the two surfaces (Figure 3).
649 Over the year, these variations may even be similar (Rahman et al., 2019), but generally
650 undergo changes in magnitude and value over the course of each season due to energy
651 availability and the response of the vegetation (Bezerra et al., 2022; Rahman et al., 2019;
652 Souza et al., 2021). In addition, this type of behaviour is well supported by research in semi-
653 arid environments (Souza et al., 2021), being due to deficiencies and low water availability.
654 The sensible heat flux and net radiation gradually increase between 09:00 and 15:00, with
655 considerably higher peaks at noon in response to the greater absorption of surface energy
656 (Bezerra et al., 2022).

657 During the dry season, the combined effect of a high R_n and high H , together with a
658 low LE are conditions that can lead to a water deficit (Rahman et al., 2019). This is because
659 during the dry season, R_n is mainly converted into sensible heat flux (Kuiyue Zhang et al.,
660 2022). G also showed behaviour typically linked to the seasons and to humidity (e.g., rainfall
661 and VPD), considering that the thermal conditions of the soil are greater during the day due
662 to insolation, and can vary with the water availability, VPD, and physical characteristics of
663 the soil. Loss of energy contained in the soil surface can also occur due to the rainfall, which
664 partially helps to absorb this energy (Yang et al., 2022). In general, all hourly flux
665 components of the energy balance showed parabolic behaviour, synchronous with changes
666 in the R_n (Figure 3).

667 We found that during the early hours of the day (06:00–08:00) the plants, in response
668 to the environmental conditions, showed a high LE over the course of each season, with
669 maximum values between the hours of 11:00 and 13:00, being more marked during the wet
670 season and slightly lower during the dry season (Figure 3). During the dry season, even with
671 low water availability, the LE was positive around dawn in the areas of cactus, attesting to
672 the high gas exchange activity of these plants (Guevara-Escobar et al., 2021). Due to the
673 crassulacean acid metabolism (CAM) of the plants, they ideally open their stomata at night
674 and/or even during the day if the VPD is low; this phenomenon is seen during CAM phase
675 II, for carboxylation via ribulose-1,5-bisphosphate carboxylase-oxygenase (RuBisCO)
676 (Andrade and Nobel, 1997; Heyduk, 2022; Nobel, 1991; Winter and Smith, 2022). We
677 believe that this was one of the reasons for the higher LE during this period of the day.
678 According to Kuiyue Zhang et al. (2022), LE may be closely linked to plant transpiration,
679 which, as the rainfall increases, can rise rapidly due to evaporation, transpiration and the
680 energy contained in the exchange of water vapour (Ma et al., 2022). In the present study, H
681 was higher on an hourly scale during each season in both species of cactus. It is to be expected
682 that in areas cultivated with cacti in a semi-arid environment most of the radiant energy would
683 be lost as H , and when it rained, the plants would respond after a few days with an increase
684 in transpiration (Unland et al., 1996).

685 The seasonal variation in R_n was fairly consistent over the years, with lower values
686 in the middle of the year, and higher values at the beginning and end of the year. This
687 behaviour is typical of semi-arid environments at low latitudes (close to the equator), and
688 shows no marked variations. In addition, a high H and low LE occur at these locations due
689 to the atmospheric deficit (Jung et al., 2019). From the middle of each year, when the radiant
690 and surface fluxes were greater, *Opuntia* maintained evapotranspiration and LE high
691 compared to *Nopalea*, even with the high VPD of both surfaces (Figure 4). This confirms the
692 hypothesis of adaptability to hostile environments for *Opuntia* as opposed to *Nopalea*. CAM
693 plants in particular, as is the case of these cacti, are specialists in maintaining transpiration
694 under conditions of extreme drought without the loss of turgor pressure (Andrade and Nobel,
695 1997; Heyduk, 2022; Nobel, 1991; Winter and Smith, 2022). Furthermore, the large plant
696 vacuole can comprise up to 90% of the cell volume, store water apoplastically in the mucilage
697 and, as a result, increase photosynthetic and transpiration efficiency (Nobel et al., 1992), both

698 more expressive in *Opuntia* (Goldstein and Nobel, 1994). Cacti of genus *Opuntia* are tolerant
699 to variations in temperature (-6°C to 65°C) (Nobel and De La Barrera, 2003; Ojeda-Pérez et
700 al., 2017; Zutta et al., 2011), and have a high photochemical yield and chlorophyll content,
701 which helps their adaptive performance (Arias-Moreno et al., 2017; Jardim et al., 2021a).

702 The soil-vegetation-atmosphere interaction altered both radiant and convective heat
703 transfer at the soil surface. CAM plants are able to cool the soil (Cao et al., 2019; Soares,
704 2018), with *O. ficus-indica* having the ability to reduce the soil surface heat flux by 50%
705 (Soares, 2018). In ecosystems with Cactaceae, Flanagan and Flanagan (2018) found a daily
706 mean for G of around $2 \text{ MJ m}^{-2} \text{ day}^{-1}$, varying according to the rainfall pulses; our findings
707 were consistent with this study. Another important factor is the canopy architecture, which
708 possibly favoured a lower incidence of radiation on the surface in the area of *Opuntia*, since
709 each species has a different canopy architecture (Consoli et al., 2013b). During the growth
710 phase, *O. ficus-indica* (L.) Mill. G may present low values, or even values close to zero,
711 where any increase may be influenced by the high values of H (Consoli et al., 2013b).

712 During the wet and dry seasons, variations in R_n are closely linked to such factors as
713 the hydrological season, vegetation and contributions from turbulent fluxes. LE can also be
714 quite responsive to rainfall events during the dry season (Mendes et al., 2021), and, as these
715 are non-native species, there may be a reduction in R_n and LE/R_n (Alves et al., 2022). Another
716 factor is the reduced cloud cover, which may increase R_n during the dry season (Malhi et al.,
717 2002). Consoli et al. (2013a), evaluating the cactus *O. ficus-indica* (L.) Mill. in a semi-arid
718 environment in western Sicily, Italy, found a mean value for R_n of $\sim 13 \text{ MJ m}^{-2} \text{ day}^{-1}$,
719 consistent with our findings of $12.57 \text{ MJ m}^{-2} \text{ day}^{-1}$ over the four seasons (Figure 5). In seasons
720 with a high moisture deficit, such as the dry season, much of the energy ($\sim 70\%$) of the R_n is
721 converted into H (Campos et al., 2019; Costa et al., 2022). Pierini et al. (2014), in a study
722 with *O. spinisior* and *O. engelmannii*, found greater values for the sensible heat flux
723 compared to the latent heat flux. Thus, for dry-climate vegetation exposed to periods of
724 humidity the conversion of R_n into LE and H can be very similar (Campos et al., 2019); on
725 the other hand, when partitioned, their contributions differ according to the component and
726 the season. In the present study, the H/R_n ratio during the wet and dry seasons was slightly
727 similar for *Opuntia* (0.57 and 0.49, respectively), and for *Nopalea*, albeit with greater
728 variation (0.84 and 0.53, respectively) (Figure 6). The LE partitioning fluxes in *Nopalea* were

729 far lower, and this may indicate greater sensitivity to a lack of rain and, consequently, lower
730 water availability in the soil. Together with a high VPD and high H , plants can trigger
731 physiological controls that reduce stomatal conductance in the leaves and canopy, lowering
732 the LE and LE/R_n ratio (Yue et al., 2019). This is clearly noticeable in the daily ET, with a
733 mean of 1.71 mm day^{-1} in *Nopalea*, and 1.16 mm day^{-1} in *Opuntia*, reinforcing the findings
734 of Han and Felker (1997) with *O. ellisiana* under rainfed conditions (1.44 mm day^{-1}). When
735 irrigated, other species of genus *Opuntia* presented an ET greater than 2 mm day^{-1} (Consoli
736 et al., 2013a; Goldstein et al., 1991; Lima et al., 2018).

737

738 4.2. Temporal responses to rain of the NDVI, PRI and CI in the cactus canopy

739 We evaluated spectral indices of the cactus vegetation in response to the
740 environmental conditions in order to understand the yield performance and health of the
741 plants, using the NDVI and CI, and, by means of the PRI, their photosynthetic characteristics.
742 In general, the results showed, similar behaviour for the NDVI, ranging from 0.17 to 0.70 for
743 the cacti, with *Opuntia* being slightly higher (Figure 7). Silva et al. (2021) documented
744 spectral responses of the vegetation of between 0.1 and 0.5 in areas of *N. cochenillifera* and
745 *O. stricta*, in the Agreste region of Pernambuco, Brazil. These findings confirm the high
746 levels of chlorophyll, as well as the photochemical efficiency of the plants, and are consistent
747 with the results of Hartfield et al. (2022) and Jardim et al. (2021a). In addition, the NDVI can
748 help in understanding biomass performance and can also be an indicator of stress in the crops
749 (Gerhards et al., 2019). Because of this, we strengthened our investigational analysis of plant
750 stress, applying further indices related to the relevant photosynthetic pigments (e.g.,
751 chlorophylls and carotenoids) and the PRI. For Panigada et al. (2014), the PRI has a marked
752 ability for identifying water stress in the aerial part of plants. This is because the PRI is linked
753 to photosynthetic processes, and its sensitivity in identifying xanthophyll pigments reflects
754 photochemical stress in the plants due to increased heat dissipation (Norton et al., 2022;
755 Panigada et al., 2014). As such, the plants, by means of the xanthophyll cycle, increase their
756 spectral emissions and energy dissipation so as not to cause oxidative damage (Gamon et al.,
757 1997). Despite varying results for the PRI, the consistent responses, and its importance,
758 studies reporting its application in the cactus are scarce.

759 In the present study, the plants were clearly exposed to intense solar radiation due to
760 the semi-arid conditions of the region, with no effect from any interspecific shading other
761 than possible self-shading. Solar radiation can help in the production of starch and the growth
762 of cladodes, with the starch helping osmoregulation and photosynthetic activity (Horibe et
763 al., 2016). In fact, we found that both species stimulated NDVI and CI responses to rainfall.
764 This is because variations in the water potential of the tissues alter chlorophyll synthesis, and
765 change the daily net uptake of CO₂ (Dubeux Jr. et al., 2021). As such, the increase in
766 chlorophyll is advantageous for photosynthetic activity, and if water is available, the plants
767 find favourable conditions for development. Even under low water availability, the root
768 system of the cactus is efficient, with the rapid absorption of water influencing the response
769 of the vegetation indices (Ouko et al., 2020).

770

771 4.3. *Plant dynamics and growth rate*

772 Environmental conditions are important factors in the adaptive process of plants, and
773 can cause changes in the morphological and physiological characteristics of both species. As
774 the species are highly adaptable to conditions of stress, the cactus presents physiological
775 plasticity and a slow relative growth rate—RGR (Luo and Nobel, 1993; Martínez-Berdeja
776 and Valverde, 2008). In the present work, we found marked characteristics for the growth
777 rates of both species under study. As previously described by Jardim et al. (2021b) and
778 Araújo Júnior et al. (2021), both *Nopalea* and *Opuntia* generally showed a high growth rate,
779 but with different patterns of development (Figure 8). Various studies have shown this type
780 of behaviour in *Opuntia* [e.g., Araújo Júnior et al. (2021), Jardim et al. (2021b), Scalisi et al.
781 (2016), and Silva et al. (2014)], where the higher AGR and RGR, are probably related to the
782 high use of photoassimilates and to leaf expansion, represented by the NAR and SCA. In
783 *Nopalea*, the low values of the net assimilation rate and specific cladode area may serve as
784 an indication that photosynthesis is limiting plant growth. Another possible explanation is
785 that high resistance to desiccation and water stress in *Opuntia* compared to other species,
786 favours its development (Tapia et al., 2019). In addition, we do not rule out the benefits of
787 the extra 71.90 mm of rain in the area cultivated with *Opuntia*, which may have favoured
788 performance. For example, Han and Felker (1997) reported improvements in the
789 development and yield of the cacti after rainfall, with an increase in the photosynthetic area

790 (analogous to the cladode area index). For Hassan et al. (2020), such factors as light, soil
791 characteristics, temperature and the dry weight of the basal cladodes are essential for growth
792 in the cactus. This finding confirms our second hypothesis that *Opuntia* enjoys better
793 performance and successful growth parameters.

794 Among plant growth rates, it should be noted that both the absolute and relative
795 growth rate are indices that help in understanding the efficiency of dry biomass production.
796 That said, the high efficiency was fundamental to the productive performance of the cacti.
797 The results found by Araújo Júnior et al. (2021) show a higher AGR for *O. stricta* (0.0058
798 Mg ha⁻¹ °Cday⁻¹) compared to clones of *N. cochenillifera*, with a mean of 0.0048 Mg ha⁻¹
799 °Cday⁻¹ ('Miúda') and 0.0021 Mg ha⁻¹ °Cday⁻¹ ('IPA Sertânia') conducted under rainfed
800 conditions. Furthermore, according to the authors, the RGR was also higher at the start of the
801 experimental period, with *O. stricta* showing better results (0.0087 Mg Mg⁻¹ °Cday⁻¹) than
802 the *Nopalea* clones, which confirms our findings. Using a ground cover of straw, Souza et
803 al. (2022) found an AGR of 0.038 Mg ha⁻¹ °Cday⁻¹ and AGR of 0.0065 Mg Mg⁻¹ °Cday⁻¹ in
804 *O. stricta*. On the other hand, in contrast to the studies presented above, our results are
805 superior for AGR, but inferior to those reported for RGR. One possible explanation for the
806 poorer performance of the RGR may be linked to the high AGR and the increased demand
807 for assimilates by the vegetative structures. A high AGR and SCA can cause cladode shading,
808 thereby reducing the RGR (Jardim et al., 2021b; Silva et al., 2014; Souza et al., 2022).

809 The superior performance of the NAR may be related to a better use of the luminous
810 energy by *Opuntia*. This tactic is related to the rapid growth of the species, where two cycles
811 of *Opuntia* were superior in development to that of the single cycle of *Nopalea* (all evaluated
812 during the same chronological period). The high SCA of the *Opuntia* cactus in both cycles
813 may be a way of the plants better allocating photoassimilates, thereby expressing more-
814 significant growth rates. It is possible that self-shading caused greater problems in the growth
815 rates of *Nopalea* (Jardim et al., 2021b). For Izaguirre-Mayoral and Marys (1996), among
816 species with a CAM pathway, *N. cochenillifera* is not tolerant to shading, and this can cause
817 problems in absorbing CO₂. This characteristic was also seen in *O. ficus-indica* (Luo and
818 Nobel, 1993), but in this study we found a lower performance in *Nopalea*. Plants with
819 significant tolerance to stress have low relative growth rates and short stature (Luo and Nobel,
820 1993). For example, species of *Nopalea* are morphologically taller, while those of *Opuntia*

821 have smaller individuals (Nobel and Zutta, 2008); this may be a strong key indication of
822 tolerance in the present study.

823

824 4.4. Plant water relations and biomass production

825 A significant water content was found in the cladodes of both species, especially
826 *Opuntia*, with a mean value of 88.91% (\pm 5.07%). This particular trait was not so expressive
827 as to cause any significant difference in cladode succulence (Figure 9b), probably due to the
828 functional anatomical characteristics of CAM plants, which are able to store large volumes
829 of water in their cells (Borland et al., 2011; Hassan et al., 2020; Nobel, 1991; Nobel et al.,
830 1992; Winter and Smith, 2022). Furthermore, high succulence may be a key feature for
831 maximising biomass production when plants are under a water restriction, helping to
832 maximise the night-time absorption of CO₂ (Borland et al., 2011). This response may explain
833 the expressiveness of the plants of *Opuntia* in relation to those of *Nopalea*. Observations
834 concerning the high cladode water content were also reported by Scalisi et al. (2016) (45%
835 to 85%) and Melero-Meraz et al. (2022) (60% to 95%). One important explanation for the
836 variation in cladode water content is related to the availability of water in the soil (Melero-
837 Meraz et al., 2022; Scalisi et al., 2016), given that our plants did not undergo long months of
838 drought (see Figure 7d).

839 Consistent with earlier literature (Consoli et al., 2013b; Han and Felker, 1997; Lima
840 et al., 2018; Snyman, 2013), the cactus plants showed high WUE, with *Opuntia* higher (7.54
841 kg m⁻³) compared to *Nopalea* (0.08 kg m⁻³) throughout the experiment (Table 3). During the
842 dry season, WUE increased in both species, being greater than 8 kg m⁻³ in *Opuntia* and greater
843 than 0.1 kg m⁻³ in *Nopalea*. Generally, CAM plants have an exceptionally high WUE, around
844 three and six times higher than C4 and C3 plants, respectively (Jardim et al., 2021a; Snyman,
845 2013; Winter and Smith, 2022). In addition, genus *Opuntia* is known for its greater tolerance
846 than other CAM species, which are ideal for arid regions due to their enhanced conversion
847 of water into biomass (Han and Felker, 1997; Ojeda-Pérez et al., 2017). Such characteristics
848 as high WUE and aboveground biomass yield were noticeable in our study. Actually, these
849 results are not enough to report that *Nopalea* plants are more sensitive, but they demonstrate
850 the superiority of *Opuntia* in this environment. A respective WUE of 7.66 and 7.87 kg m⁻³
851 for *O. robusta* and *O. ficus-indica* were found by Snyman (2013) in Bloemfontein, in the

852 semi-arid region of South Africa. Although the results for WUE found by Snyman (2013) in
853 species of *Opuntia* are similar to those of the present study, the aboveground dry biomass
854 yield was lower, even with the plants receiving 521.75 mm of annual rainfall. Under optimal
855 conditions, dry matter production in C3, C4 and CAM species would be similar; on the other
856 hand, under the deficient conditions of arid and semi-arid climates, CAM plants present
857 greater biomass production (Snyman, 2013).

858

859 4.5. Explanatory power of the different combinations of variables

860 We used principal component analysis (PCA) to aid joint interpretation of the intrinsic
861 information of the data. Figure 10 shows distinct associations between the environmental
862 variables and variables of *Opuntia* and *Nopalea* during the dry season, dry-wet transition
863 season, wet season and wet-dry transition season. This type of PCA presentation using biplots
864 is very useful in a structure that includes large data matrices (Figure 10). For the first two
865 principal components, the plants of *Nopalea* and *Opuntia* retain high total variance for the
866 data, with 91.71% and 85.09%, respectively. During the wet season, variables such as WUE,
867 AGR and RGR are less expressive, showing that both cacti have less growth and reduce their
868 WUE. On the other hand, even with the poorly expressed variables mentioned above, the
869 plants showed no signs of stress, since the PRI was low (i.e., low loading in PC1), and NDVI
870 and CI were high (i.e., high loadings in PC1). This is because the vectors are in the same
871 direction, showing the strong correlation of the variables with each other, albeit conflicting
872 with the season. The cacti show satisfactory growth responses with the increased water
873 availability (Campos et al., 2021; Lima et al., 2018; Scalisi et al., 2016), however, their
874 growth may vary as shown here. In fact, there were improvements in the photosynthetic
875 efficiency of the plants, since the NAR, NDVI and CI were high. As they are CAM plants,
876 the available rainfall improves the microclimate conditions, resulting in an increase in CO₂
877 efflux (Campos et al., 2021; Nobel, 1991; Winter and Smith, 2022). Due to the high NAR
878 and low PRI, the high water content of the cladodes shown in our results may have favoured
879 cell turgor and improved photosynthetic activity (Winter and Smith, 2022).

880 Spatial projection of the first principal component highlighted for the variables
881 (vectors) energy balance and VPD, show that both environments, whether cultivated with
882 *Nopalea* or *Opuntia*, presented better-correlated R_n , H , G , VPD, H/R_n and G/R_n , and grouped

883 the most deficient seasons (i.e., dry season and dry-wet transition). According to Alves et al.
884 (2022), this is due to greater energy availability in the environment, which causes abundant
885 air and soil heating. As expected, the other variables of the energy balance (LE and LE/R_n)
886 and ET remained more correlated with the wet seasons due to the increase in water
887 availability in the system. Changes in energy availability and turbulent fluxes over the course
888 of each season have also been reported by various studies (Alves et al., 2022; Chen et al.,
889 2022; Dhungel et al., 2021; Jardim et al., 2022). Therefore, during seasons of greater water
890 availability, the variables better explain the health of the vegetation, chlorophyll,
891 photosynthetic performance and exchange of water vapour to the atmosphere, while the
892 growth variables have a greater correlation with the thermal conditions and the lower
893 availability of water.

894

895 **5. Conclusions**

896 Our analyses provide the first observational evidence of turbulent fluxes and surface
897 energy partitioning in two simultaneous cultivations of *Nopalea* and *Opuntia* cacti in a semi-
898 arid environment. In this study, we show interactive processes of energy and water vapour
899 exchange between the plants and the environment during the wet and dry seasons. The results
900 for the succulent species studied here, underline that, despite the CAM, their behaviour
901 during heat exchange and evapotranspiration differs over the course of each season. Further
902 analysis revealed that the latent (LE) and sensible (H) heat fluxes have marked seasonality,
903 with the low LE in *Nopalea* occurring during the dry season ($0.85 \text{ MJ m}^{-2} \text{ day}^{-1}$), while for
904 *Opuntia*, during the wet-dry transition season ($4.22 \text{ MJ m}^{-2} \text{ day}^{-1}$). During each season, the
905 LE and evapotranspiration (ET) were higher in *Opuntia*. In general, *Nopalea* provides greater
906 H and soil heat flux (G), even under humid conditions. In both cacti, H showed the highest
907 consumption of net radiation (R_n), with *Nopalea* having the highest H/R_n ratio and the lowest
908 LE/R_n ratio (mean 0.23) during each season. Furthermore, the vegetation showed different
909 responses for the spectral, photochemical, chlorophyll and water use efficiency indices,
910 which explains the better yield of *Opuntia* and the greater sensitivity of *Nopalea*. Similarly,
911 the growth rates and biomass of the cacti were different, with *Opuntia* obtaining the greatest
912 increments and adaptive plasticity.

913 Our findings offer new insights, and are fundamental to understanding how
914 biophysical factors influence CAM plants, further demonstrating that their adaptive abilities
915 can change even in individuals of the same family. In conclusion, this study can serve as a
916 valuable baseline for research with cacti in deficient environments. In particular, the findings
917 may also be useful in environmental management and the rehabilitation of degraded areas.
918 One important next step is to assess the potential CO₂ sink of these species for application in
919 agriculture, ecology and hydrology.

920

921 **Acknowledgments**

922 The authors wish to thank the Research Support Foundation of the State of
923 Pernambuco (FACEPE – APQ-476372/2012-7 and FACEPE - APQ-1159-1.07/14) and the
924 National Council for Scientific and Technological Development (CNPq - 421003/2018-9,
925 309421/2018-7, 402622/2021-9, 309558/2021-2) for their financial support. Further thanks
926 go to the Research Support Foundation of the State of Pernambuco and the Coordination for
927 the Improvement of Higher Education Personnel (CAPES - Finance Code 001) for the
928 research and study grants.

929

930 **References**

- 931 Acharya, P., Biradar, C., Louhaichi, M., Ghosh, S., Hassan, S., Moyo, H., Sarker, A., 2019.
932 Finding a Suitable Niche for Cultivating Cactus Pear (*Opuntia ficus-indica*) as an
933 Integrated Crop in Resilient Dryland Agroecosystems of India. Sustainability 11, 5897.
934 <https://doi.org/10.3390/SU11215897>
- 935 Adams, W.W., Díaz, M., Winter, K., 1989. Diurnal changes in photochemical efficiency, the
936 reduction state of Q, radiationless energy dissipation, and non-photochemical
937 fluorescence quenching in cacti exposed to natural sunlight in northern Venezuela.
938 Oecologia 80, 553–561. <https://doi.org/10.1007/BF00380081>
- 939 Alves, J.D.N., Ribeiro, A., Rody, Y.P., Loos, R.A., 2022. Energy balance and surface
940 decoupling factor of a pasture in the Brazilian Cerrado. Agric. For. Meteorol. 319,
941 108912. <https://doi.org/10.1016/J.AGRFORMET.2022.108912>
- 942 Andrade, J.L., Nobel, P.S., 1997. Microhabitats and Water Relations of Epiphytic Cacti and
943 Ferns in a Lowland Neotropical Forest1. Biotropica 29, 261–270.

944 <https://doi.org/10.1111/J.1744-7429.1997.TB00427.X>

945 Araújo Júnior, G. do N., Silva, T.G.F. da, Souza, L.S.B. de, Araújo, G.G.L. de, Moura,
946 M.S.B. de, Alves, C.P., Salvador, K.R. da S., Souza, C.A.A. de, Montenegro, A.A. de
947 A., Silva, M.J. da, 2021. Phenophases, morphophysiological indices and cutting time in
948 clones of the forage cacti under controlled water regimes in a semiarid environment. *J.*
949 *Arid Environ.* 190, 104510. <https://doi.org/10.1016/J.JARIDENV.2021.104510>

950 Arias-Moreno, D.M., Jiménez-Bremont, J.F., Maruri-López, I., Delgado-Sánchez, P., 2017.
951 Effects of catalase on chloroplast arrangement in *Opuntia streptacantha* chlorenchyma
952 cells under salt stress. *Sci. Rep.* 7, 1–14. <https://doi.org/10.1038/s41598-017-08744-x>

953 Beck, H.E., Zimmermann, N.E., McVicar, T.R., Vergopolan, N., Berg, A., Wood, E.F., 2018.
954 Present and future Köppen-Geiger climate classification maps at 1-km resolution. *Sci.*
955 *Data* 5, 180214. <https://doi.org/10.1038/sdata.2018.214>

956 Bezerra, B.G., Santos e Silva, C.M., Mendes, K.R., Mutti, P.R., Fernandes, L.S., Marques,
957 T. V., Câmara e Silva, C.L., Campos, S., de Lima Vieira, M.M., Urbano, S.A., Difante,
958 G. dos S., Ferreira, R.R., da Silva, D.T.C., Costa, G.B., Oliveira, P.E.S., de Oliveira,
959 C.P., Gonçalves, W.A., Lucio, P.S., 2022. CO₂ exchanges and evapotranspiration of a
960 grazed pasture under tropical climate conditions. *Agric. For. Meteorol.* 323, 109088.
961 <https://doi.org/10.1016/J.AGRFORMET.2022.109088>

962 Borland, A.M., Barrera Zambrano, V.A., Ceusters, J., Shorrocks, K., 2011. The
963 photosynthetic plasticity of crassulacean acid metabolism: an evolutionary innovation
964 for sustainable productivity in a changing world. *New Phytol.* 191, 619–633.
965 <https://doi.org/10.1111/J.1469-8137.2011.03781.X>

966 Bowen, I.S., 1926. The Ratio of Heat Losses by Conduction and by Evaporation from any
967 Water Surface. *Phys. Rev.* 27, 779. <https://doi.org/10.1103/PhysRev.27.779>

968 Campos, A.R.F., Silva, A.J.P. da, de Jong van Lier, Q., Nascimento, F.A.L. do, Fernandes,
969 R.D.M., Almeida, J.N. de, Paz, V.P. da S., 2021. Yield and morphology of forage cactus
970 cultivars under drip irrigation management based on soil water matric potential
971 thresholds. *J. Arid Environ.* 193, 104564.
972 <https://doi.org/10.1016/J.JARIDENV.2021.104564>

973 Campos, S., Mendes, K.R., da Silva, L.L., Mutti, P.R., Medeiros, S.S., Amorim, L.B., dos
974 Santos, C.A.C., Perez-Marin, A.M., Ramos, T.M., Marques, T. V., Lucio, P.S., Costa,

975 G.B., Santos e Silva, C.M., Bezerra, B.G., 2019. Closure and partitioning of the energy
976 balance in a preserved area of a Brazilian seasonally dry tropical forest. *Agric. For.*
977 *Meteorol.* 271, 398–412. <https://doi.org/10.1016/j.agrformet.2019.03.018>

978 Cao, J.J., Hu, S., Dong, Q., Liu, L.J., Wang, Z.L., 2019. Green roof cooling contributed by
979 plant species with different photosynthetic strategies. *Energy Build.* 195, 45–50.
980 <https://doi.org/10.1016/J.ENBUILD.2019.04.046>

981 Chen, Jingyan, Dong, G., Chen, Jiquan, Jiang, S., Qu, L., Legesse, T.G., Zhao, F., Tong, Q.,
982 Shao, C., Han, X., 2022. Energy balance and partitioning over grasslands on the
983 Mongolian Plateau. *Ecol. Indic.* 135, 108560.
984 <https://doi.org/10.1016/J.ECOLIND.2022.108560>

985 Ciriminna, R., Chavarría-Hernández, N., Rodríguez-Hernández, A.I., Pagliaro, M., 2019.
986 Toward unfolding the bioeconomy of nopal (*Opuntia* spp.). *Biofuels, Bioprod.*
987 *Biorefining* 13, 1417–1427. <https://doi.org/10.1002/BBB.2018>

988 Consoli, S., Inglese, G., Inglese, P., 2013a. Determination of Evapotranspiration and Annual
989 Biomass Productivity of a Cactus Pear [*Opuntia ficus-indica* L. (Mill.)] Orchard in a
990 Semiarid Environment. *J. Irrig. Drain. Eng.* 139, 680–690.
991 [https://doi.org/10.1061/\(ASCE\)IR.1943-4774.0000589](https://doi.org/10.1061/(ASCE)IR.1943-4774.0000589)

992 Consoli, S., Inglese, P., Inglese, G., 2013b. Determination of evapotranspiration and crop
993 coefficient of cactus pear (*Opuntia ficus-indica* Mill.) with an energy balance technique.
994 *Acta Hortic.* 995, 117–124. <https://doi.org/10.17660/ACTAHORTIC.2013.995.14>

995 Corrado, G., Chiaiese, P., Lucini, L., Miras-Moreno, B., Colla, G., Roupael, Y., 2020.
996 Successive Harvests Affect Yield, Quality and Metabolic Profile of Sweet Basil
997 (*Ocimum basilicum* L.). *Agronomy* 10, 830.
998 <https://doi.org/10.3390/AGRONOMY10060830>

999 Costa, G.B., Mendes, K.R., Viana, L.B., Almeida, G.V., Mutti, P.R., Silva, C.M.S., Bezerra,
1000 B.G., Marques, T.V., Ferreira, R.R., Oliveira, C.P., Gonçalves, W.A., Oliveira, P.E.,
1001 Campos, S., Andrade, M.U.G., Antonino, A.C.D., Menezes, R.S.C., 2022. Seasonal
1002 Ecosystem Productivity in a Seasonally Dry Tropical Forest (Caatinga) Using Flux
1003 Tower Measurements and Remote Sensing Data. *Remote Sens.* 14, 3955.
1004 <https://doi.org/10.3390/RS14163955>

1005 Dhungel, R., Aiken, R., Evett, S.R., Colaizzi, P.D., Marek, G., Moorhead, J.E., Baumhardt,

1006 R.L., Brauer, D., Kutikoff, S., Lin, X., 2021. Energy Imbalance and Evapotranspiration
1007 Hysteresis Under an Advective Environment: Evidence From Lysimeter, Eddy
1008 Covariance, and Energy Balance Modeling. *Geophys. Res. Lett.* 48, e2020GL091203.
1009 <https://doi.org/10.1029/2020GL091203>

1010 Dubeux Jr., J.C.B., Santos, M.V.F. dos, Cunha, M.V. da, Santos, D.C. dos, Souza, R.T. de
1011 A., Mello, A.C.L. de, Souza, T.C. de, 2021. Cactus (*Opuntia* and *Nopalea*) nutritive
1012 value: A review. *Anim. Feed Sci. Technol.* 275, 114890.
1013 <https://doi.org/10.1016/J.ANIFEEDSCI.2021.114890>

1014 Flanagan, L.B., Flanagan, J.E.M., 2018. Seasonal controls on ecosystem-scale CO₂ and
1015 energy exchange in a Sonoran Desert characterized by the saguaro cactus (*Carnegiea*
1016 *gigantea*). *Oecologia* 187, 977–994. [https://doi.org/10.1007/S00442-018-4187-](https://doi.org/10.1007/S00442-018-4187-2)
1017 [2/FIGURES/10](https://doi.org/10.1007/S00442-018-4187-2)

1018 Foga, S., Scaramuzza, P.L., Guo, S., Zhu, Z., Dilley, R.D., Beckmann, T., Schmidt, G.L.,
1019 Dwyer, J.L., Joseph Hughes, M., Laue, B., 2017. Cloud detection algorithm comparison
1020 and validation for operational Landsat data products. *Remote Sens. Environ.* 194, 379–
1021 390. <https://doi.org/10.1016/J.RSE.2017.03.026>

1022 Gamon, J.A., Serrano, L., Surfus, J.S., 1997. The photochemical reflectance index: an optical
1023 indicator of photosynthetic radiation use efficiency across species, functional types, and
1024 nutrient levels. *Oecologia* 112, 492–501. <https://doi.org/10.1007/S004420050337>

1025 Gavilán, P., Berengena, J., 2007. Accuracy of the Bowen ratio-energy balance method for
1026 measuring latent heat flux in a semiarid advective environment. *Irrig. Sci.* 25, 127–140.
1027 <https://doi.org/10.1007/S00271-006-0040-1>

1028 Gerhards, M., Schlerf, M., Mallick, K., Udelhoven, T., 2019. Challenges and Future
1029 Perspectives of Multi-/Hyperspectral Thermal Infrared Remote Sensing for Crop Water-
1030 Stress Detection: A Review. *Remote Sens.* 11, 1240.
1031 <https://doi.org/10.3390/RS11101240>

1032 Gitelson, A., Merzlyak, M.N., 1994. Spectral Reflectance Changes Associated with Autumn
1033 Senescence of *Aesculus hippocastanum* L. and *Acer platanoides* L. Leaves. Spectral
1034 Features and Relation to Chlorophyll Estimation. *J. Plant Physiol.* 143, 286–292.
1035 [https://doi.org/10.1016/S0176-1617\(11\)81633-0](https://doi.org/10.1016/S0176-1617(11)81633-0)

1036 Goldstein, G., Nobel, P.S., 1994. Water Relations and Low-Temperature Acclimation for

1037 Cactus Species Varying in Freezing Tolerance. *Plant Physiol.* 104, 675–681.
1038 <https://doi.org/10.1104/PP.104.2.675>

1039 Goldstein, G., Ortega, J.K.E., Nerd, A., Nobel, P.S., 1991. Diel Patterns of Water Potential
1040 Components for the Crassulacean Acid Metabolism Plant *Opuntia ficus-indica* when
1041 Well-Watered or Droughted. *Plant Physiol.* 95, 274–280.
1042 <https://doi.org/10.1104/PP.95.1.274>

1043 Guevara-Escobar, A., González-Sosa, E., Cervantes-Jimenez, M., Suzán-Azpiri, H.,
1044 Queijeiro-Bolanos, M.E., Carrillo-Ángeles, I., Cambron-Sandoval, V.H., 2021.
1045 Machine learning estimates of eddy covariance carbon flux in a scrub in the Mexican
1046 highland. *Biogeosciences* 18, 367–392. <https://doi.org/10.5194/BG-18-367-2021>

1047 Han, H., Felker, P., 1997. Field validation of water-use efficiency of the CAM plant *Opuntia*
1048 *ellisiana* in south Texas. *J. Arid Environ.* 36, 133–148.
1049 <https://doi.org/10.1006/JARE.1996.0202>

1050 Hartfield, K, Gillan, J K, Serio, C., Masiello, G., Hartfield, Kyle, Gillan, Jeffrey K, Norton,
1051 C.L., Conley, C., van Leeuwen, W.J.D., 2022. A Novel Spectral Index to Identify Cacti
1052 in the Sonoran Desert at Multiple Scales Using Multi-Sensor Hyperspectral Data
1053 Acquisitions. *Land* 11, 786. <https://doi.org/10.3390/LAND11060786>

1054 Hartzell, S., Bartlett, M.S., Porporato, A., 2018. Unified representation of the C3, C4, and
1055 CAM photosynthetic pathways with the Photo3 model. *Ecol. Modell.* 384, 173–187.
1056 <https://doi.org/10.1016/J.ECOLMODEL.2018.06.012>

1057 Hassan, S., Liguori, G., Inglese, P., Louhaichi, M., Sortino, G., 2020. The Effect of Soil
1058 Volume Availability on *Opuntia ficus-indica* Canopy and Root Growth. *Agronomy* 10,
1059 635. <https://doi.org/10.3390/AGRONOMY10050635>

1060 Heilman, J.L., Brittin, C.L., Neale, C.M.U., 1989. Fetch requirements for bowen ratio
1061 measurements of latent and sensible heat fluxes. *Agric. For. Meteorol.* 44, 261–273.
1062 [https://doi.org/10.1016/0168-1923\(89\)90021-X](https://doi.org/10.1016/0168-1923(89)90021-X)

1063 Heyduk, K., 2022. Evolution of Crassulacean acid metabolism in response to the
1064 environment: past, present, and future. *Plant Physiol.* 190, 19–30.
1065 <https://doi.org/10.1093/PLPHYS/KIAC303>

1066 Ho, C.L., Chiang, J.M., Lin, T.C., Martin, C.E., 2019. First report of C4/CAM-cycling
1067 photosynthetic pathway in a succulent grass, *Spinifex littoreus* (Brum. f.) Merr., in

1068 coastal regions of Taiwan. *Flora* 254, 194–202.
1069 <https://doi.org/10.1016/J.FLORA.2018.08.005>

1070 Horibe, T., Iwagawa, Y., Kondo, H., Yamada, K., 2016. Hydroponics Culture of Edible
1071 *Opuntia* ‘Maya’: Effect of Constant Red and Blue Lights on Daughter Cladodes Growth
1072 and Spine Development. *Environ. Control Biol.* 54, 165–169.
1073 <https://doi.org/10.2525/ECB.54.165>

1074 Hu, S., Zhao, C., Li, J., Wang, F., Chen, Y., 2014. Discussion and reassessment of the method
1075 used for accepting or rejecting data observed by a Bowen ratio system. *Hydrol. Process.*
1076 28, 4506–4510. <https://doi.org/10.1002/HYP.9962>

1077 Hurni, K., Van Den Hoek, J., Fox, J., 2019. Assessing the spatial, spectral, and temporal
1078 consistency of topographically corrected Landsat time series composites across the
1079 mountainous forests of Nepal. *Remote Sens. Environ.* 231, 111225.
1080 <https://doi.org/10.1016/J.RSE.2019.111225>

1081 Irmak, S., Kukul, M.S., 2022. Alteration in surface energy balance fluxes induced from long-
1082 term disk-tilled versus no-till management in maize production. *Soil Tillage Res.* 221,
1083 105383. <https://doi.org/10.1016/J.STILL.2022.105383>

1084 Izaguirre-Mayoral, M.L., Marys, E., 1996. Interactions between irradiance levels and cactus
1085 X virus infection on the crassulacean acid metabolism in *Nopalea cochenillifera* and
1086 *Acanthocereus tetragonus* plants. *J. Plant Physiol.* 149, 35–42.
1087 [https://doi.org/10.1016/S0176-1617\(96\)80170-2](https://doi.org/10.1016/S0176-1617(96)80170-2)

1088 Jardim, A.M. da R.F., Santos, H.R.B., Alves, H.K.M.N., Ferreira-Silva, S.L., Souza, L.S.B.
1089 de, Araújo Júnior, G. do N., Souza, M. de S., Araújo, G.G.L. de, Souza, C.A.A. de,
1090 Silva, T.G.F. da, 2021a. Genotypic differences relative photochemical activity,
1091 inorganic and organic solutes and yield performance in clones of the forage cactus under
1092 semi-arid environment. *Plant Physiol. Biochem.* 162, 421–430.
1093 <https://doi.org/10.1016/J.PLAPHY.2021.03.011>

1094 Jardim, A.M. da R.F., Souza, L.S.B. de, Alves, C.P., Araújo, J.F.N. de, Souza, C.A.A. de,
1095 Pinheiro, A.G., Araújo, G.G.L. de, Campos, F.S., Tabosa, J.N., Silva, T.G.F. da, 2021b.
1096 Intercropping forage cactus with sorghum affects the morphophysiology and phenology
1097 of forage cactus. *African J. Range Forage Sci.* 1–12.
1098 <https://doi.org/10.2989/10220119.2021.1949749>

1099 Jardim, A.M.R.F., Araújo Júnior, G.N., Silva, M.V., Santos, A., Silva, J.L.B., Pandorfi, H.,
1100 Oliveira-Júnior, J.F., Teixeira, A.H.C., Teodoro, P.E., de Lima, J.L.M.P., Silva Junior,
1101 C.A., Souza, L.S.B., Silva, E.A., Silva, T.G.F., 2022. Using Remote Sensing to Quantify
1102 the Joint Effects of Climate and Land Use/Land Cover Changes on the Caatinga Biome
1103 of Northeast Brazilian. *Remote Sens.* 14, 1911. <https://doi.org/10.3390/RS14081911>
1104 Jung, M., Koirala, S., Weber, U., Ichii, K., Gans, F., Camps-Valls, G., Papale, D., Schwalm,
1105 C., Tramontana, G., Reichstein, M., 2019. The FLUXCOM ensemble of global land-
1106 atmosphere energy fluxes. *Sci. Data* 6, 1–14. [https://doi.org/10.1038/s41597-019-0076-](https://doi.org/10.1038/s41597-019-0076-8)
1107 8
1108 Kaiser, H.F., 1960. The application of electronic computers to factor analysis. *Educ. Psychol.*
1109 *Meas.* 20, 141–151. <https://doi.org/10.1177/001316446002000116>
1110 Khapte, P.S., Kumar, P., Wakchaure, G.C., Jangid, K.K., Colla, G., Cardarelli, M., Rane, J.,
1111 2022. Application of Phenomics to Elucidate the Influence of Rootstocks on Drought
1112 Response of Tomato. *Agronomy* 12, 1529.
1113 <https://doi.org/10.3390/AGRONOMY12071529>
1114 Kumar, S., Louhaichi, M., Dana Ram, P., Tirumala, K.K., Ahmad, S., Rai, A.K., Sarker, A.,
1115 Hassan, S., Liguori, G., Probir Kumar, G., Govindasamy, P., Prasad, M., Mahawer,
1116 S.K., Appaswamygowda, B.H., 2021. Cactus Pear (*Opuntia ficus-indica*) Productivity,
1117 Proximal Composition and Soil Parameters as Affected by Planting Time and
1118 Agronomic Management in a Semi-Arid Region of India. *Agronomy* 11, 1647.
1119 <https://doi.org/10.3390/AGRONOMY11081647>
1120 Kumar, S., Palsaniya, D.R., Kumar, T.K., Misra, A.K., Ahmad, S., Rai, A.K., Sarker, A.,
1121 Louhaichi, M., Hassan, S., Liguori, G., Ghosh, P.K., Govindasamy, P., Mahawer, S.K.,
1122 Bhargavi, H.A., 2022. Survival, morphological variability, and performance of *Opuntia*
1123 *ficus-indica* in a semi-arid region of India. *Arch. Agron. Soil Sci.* 1–18.
1124 <https://doi.org/10.1080/03650340.2022.2031998>
1125 Lamichhane, S., Eğılmez, G., Gedik, R., Bhutta, M.K.S., Erenay, B., 2021. Benchmarking
1126 OECD countries' sustainable development performance: A goal-specific principal
1127 component analysis approach. *J. Clean. Prod.* 287, 125040.
1128 <https://doi.org/10.1016/J.JCLEPRO.2020.125040>
1129 Leite-Filho, A.T., de Sousa Pontes, V.Y., Costa, M.H., 2019. Effects of Deforestation on the

1130 Onset of the Rainy Season and the Duration of Dry Spells in Southern Amazonia. *J.*
1131 *Geophys. Res. Atmos.* 124, 5268–5281. <https://doi.org/10.1029/2018JD029537>

1132 Lewis, D.A., Nobel, P.S., Boyd, P.L., 1977. Thermal Energy Exchange Model and Water
1133 Loss of a Barrel Cactus, *Ferocactus acanthodes*. *Plant Physiol.* 60, 609–616.
1134 <https://doi.org/10.1104/PP.60.4.609>

1135 Lima, L.R., Silva, T.G.F., Jardim, A.M.R.F., Souza, C.A.A., Queiroz, M.G., Tabosa, J.N.,
1136 2018. Growth, water use and efficiency of forage cactus sorghum intercropping under
1137 different water depths. *Rev. Bras. Eng. Agrícola e Ambient.* 22, 113–118.
1138 <https://doi.org/10.1590/1807-1929/AGRIAMBI.V22N2P113-118>

1139 Luo, Y., Nobel, P.S., 1993. Growth characteristics of newly initiated cladodes of *Opuntia*
1140 *ficus-indica* as affected by shading, drought and elevated CO₂. *Physiol. Plant.* 87, 467–
1141 474. <https://doi.org/10.1111/J.1399-3054.1993.TB02495.X>

1142 Ma, J., Wen, X., Li, M., Luo, S., Zhu, X., Yang, X., Chen, M., 2022. Analysis of Surface
1143 Energy Changes over Different Underlying Surfaces Based on MODIS Land-Use Data
1144 and Green Vegetation Fraction over the Tibetan Plateau. *Remote Sens.* 14, 2751.
1145 <https://doi.org/10.3390/RS14122751>

1146 Malhi, Y., Pegoraro, E., Nobre, A.D., Pereira, M.G.P., Grace, J., Culf, A.D., Clement, R.,
1147 2002. Energy and water dynamics of a central Amazonian rain forest. *J. Geophys. Res.*
1148 *Atmos.* 107, LBA 45-1. <https://doi.org/10.1029/2001JD000623>

1149 Martínez-Berdeja, A., Valverde, T., 2008. Growth response of three globose cacti to radiation
1150 and soil moisture: An experimental test of the mechanism behind the nurse effect. *J.*
1151 *Arid Environ.* 72, 1766–1774. <https://doi.org/10.1016/J.JARIDENV.2008.04.010>

1152 Melero-Meraz, V., Zegbe, J.A., Herrera, M.D., Guzmán-Maldonado, S.H., Medina-García,
1153 G., Sánchez-Toledano, B.I., Cruz-Bravo, R.K., Servín-Palestina, M., 2022. On-Farm
1154 Supplemental Irrigation of “Roja Lisa” Cactus Pear: Pre- and Postharvest Effects.
1155 *Horticulturae* 8, 483. <https://doi.org/10.3390/HORTICULTURAE8060483>

1156 Mendes, K.R., Campos, S., Mutti, P.R., Ferreira, R.R., Ramos, T.M., Marques, T. V., Dos
1157 Reis, J.S., de Lima Vieira, M.M., Silva, A.C.N., Marques, A.M.S., da Silva, D.T.C., da
1158 Silva, D.F., Oliveira, C.P., Gonçalves, W.A., Costa, G.B., Pompelli, M.F., Marenco,
1159 R.A., Antonino, A.C.D., Menezes, R.S.C., Bezerra, B.G., Santos E Silva, C.M., 2021.
1160 Assessment of SITE for CO₂ and Energy Fluxes Simulations in a Seasonally Dry

1161 Tropical Forest (Caatinga Ecosystem). *Forests* 12, 86.
1162 <https://doi.org/10.3390/F12010086>

1163 Mulovhedzi, N.E., Araya, N.A., Mengistu, M.G., Fessehazion, M.K., du Plooy, C.P., Araya,
1164 H.T., van der Laan, M., 2020. Estimating evapotranspiration and determining crop
1165 coefficients of irrigated sweet potato (*Ipomoea batatas*) grown in a semi-arid climate.
1166 *Agric. Water Manag.* 233, 106099. <https://doi.org/10.1016/J.AGWAT.2020.106099>

1167 Neupane, D., Mayer, J.A., Niechayev, N.A., Bishop, C.D., Cushman, J.C., 2021. Five-year
1168 field trial of the biomass productivity and water input response of cactus pear (*Opuntia*
1169 spp.) as a bioenergy feedstock for arid lands. *GCB Bioenergy* 13, 719–741.
1170 <https://doi.org/10.1111/GCBB.12805>

1171 Nobel, P.S., 1991. Achievable productivities of certain CAM plants: basis for high values
1172 compared with C3 and C4 plants. *New Phytol.* 119, 183–205.
1173 <https://doi.org/10.1111/J.1469-8137.1991.TB01022.X>

1174 Nobel, P.S., Cavelier, J., Andrade, J.L., 1992. Mucilage in cacti: Its apoplastic capacitance
1175 associated solutes, and influence on tissue water relations. *J. Exp. Bot.* 43, 641–648.
1176 <https://doi.org/10.1093/JXB/43.5.641>

1177 Nobel, P.S., De La Barrera, E., 2003. Tolerances and acclimation to low and high
1178 temperatures for cladodes, fruits and roots of a widely cultivated cactus, *Opuntia ficus-*
1179 *indica*. *New Phytol.* 157, 271–279. <https://doi.org/10.1046/J.1469-8137.2003.00675.X>

1180 Nobel, P.S., Zutta, B.R., 2008. Temperature tolerances for stems and roots of two cultivated
1181 cacti, *Nopalea cochenillifera* and *Opuntia robusta*: Acclimation, light, and drought. *J.*
1182 *Arid Environ.* 72, 633–642. <https://doi.org/10.1016/J.JARIDENV.2007.08.005>

1183 Norton, C.L., Hartfield, K., Holifield Collins, C.D., Van Leeuwen, W.J.D., Metz, L.J., 2022.
1184 Multi-Temporal LiDAR and Hyperspectral Data Fusion for Classification of Semi-Arid
1185 Woody Cover Species. *Remote Sens.* 14, 2896. <https://doi.org/10.3390/RS14122896>

1186 Ojeda-Pérez, Z.Z., Jiménez-Bremont, J.F., Delgado-Sánchez, P., 2017. Continuous high and
1187 low temperature induced a decrease of photosynthetic activity and changes in the diurnal
1188 fluctuations of organic acids in *Opuntia streptacantha*. *PLoS One* 12, e0186540.
1189 <https://doi.org/10.1371/JOURNAL.PONE.0186540>

1190 Ortega-Farias, S.O., Cuenca, R.H., Ek, M., 1996. Daytime variation of sensible heat flux
1191 estimated by the bulk aerodynamic method over a grass canopy. *Agric. For. Meteorol.*

1192 81, 131–143. [https://doi.org/10.1016/0168-1923\(95\)02278-3](https://doi.org/10.1016/0168-1923(95)02278-3)

1193 Ouko, E., Omondi, S., Mugo, R., Wahome, A., Kasera, K., Nkurunziza, E., Kiema, J., Flores,
1194 A., Adams, E.C., Kuraru, S., Wambua, M., 2020. Modeling Invasive Plant Species in
1195 Kenya's Northern Rangelands. *Front. Environ. Sci.* 8, 69.
1196 <https://doi.org/10.3389/FENVS.2020.00069/BIBTEX>

1197 Panigada, C., Rossini, M., Meroni, M., Cilia, C., Busetto, L., Amaducci, S., Boschetti, M.,
1198 Cogliati, S., Picchi, V., Pinto, F., Marchesi, A., Colombo, R., 2014. Fluorescence, PRI
1199 and canopy temperature for water stress detection in cereal crops. *Int. J. Appl. Earth*
1200 *Obs. Geoinf.* 30, 167–178. <https://doi.org/10.1016/J.JAG.2014.02.002>

1201 Perez-Priego, O., Guan, J., Rossini, M., Fava, F., Wutzler, T., Moreno, G., Carvalhais, N.,
1202 Carrara, A., Kolle, O., Julitta, T., Schrumpp, M., Reichstein, M., Migliavacca, M., 2015.
1203 Sun-induced chlorophyll fluorescence and photochemical reflectance index improve
1204 remote-sensing gross primary production estimates under varying nutrient availability
1205 in a typical Mediterranean savanna ecosystem. *Biogeosciences* 12, 6351–6367.
1206 <https://doi.org/10.5194/BG-12-6351-2015>

1207 Perez, P.J., Castellvi, F., Ibañez, M., Rosell, J.I., 1999. Assessment of reliability of Bowen
1208 ratio method for partitioning fluxes. *Agric. For. Meteorol.* 97, 141–150.
1209 [https://doi.org/10.1016/S0168-1923\(99\)00080-5](https://doi.org/10.1016/S0168-1923(99)00080-5)

1210 Pierini, N.A., Vivoni, E.R., Robles-Morua, A., Scott, R.L., Nearing, M.A., 2014. Using
1211 observations and a distributed hydrologic model to explore runoff thresholds linked with
1212 mesquite encroachment in the Sonoran Desert. *Water Resour. Res.* 50, 8191–8215.
1213 <https://doi.org/10.1002/2014WR015781>

1214 Pinheiro, K.M., Silva, T.G.F., Carvalho, H.F. de S., Santos, J.E.O., Morais, J.E.F., Zolnier,
1215 S., Santos, D.C. dos, 2014. Correlações do índice de área do cladódio com
1216 características morfogênicas e produtivas da palma forrageira. *Pesqui. Agropecuária*
1217 *Bras.* 49, 939–947. <https://doi.org/10.1590/S0100-204X2014001200004>

1218 Pokhariyal, S., Patel, N., 2021. Evaluation of variation in radiative and turbulent fluxes over
1219 winter wheat ecosystem along Indo-Gangetic region. *Arab. J. Geosci.* 14, 1–11.
1220 <https://doi.org/10.1007/S12517-021-08320-8/FIGURES/7>

1221 R Core Team, 2022. R: The R Project for Statistical Computing.

1222 Rahman, M.M., Zhang, W., Wang, K., 2019. Assessment on surface energy imbalance and

1223 energy partitioning using ground and satellite data over a semi-arid agricultural region
1224 in north China. *Agric. Water Manag.* 213, 245–259.
1225 <https://doi.org/10.1016/J.AGWAT.2018.10.032>

1226 Salack, S., Klein, C., Giannini, A., Sarr, B., Worou, O.N., Belko, N., Bliedernicht, J.,
1227 Kunstman, H., 2016. Global warming induced hybrid rainy seasons in the Sahel.
1228 *Environ. Res. Lett.* 11, 104008. <https://doi.org/10.1088/1748-9326/11/10/104008>

1229 Sanchez, F., Bassil, E., Crane, J.H., Shahid, M.A., Vincent, C.I., Schaffer, B., 2022. Spectral
1230 light distribution affects photosynthesis, leaf reflective indices, antioxidant activity and
1231 growth of *Vanilla planifolia*. *Plant Physiol. Biochem.* 182, 145–153.
1232 <https://doi.org/10.1016/J.PLAPHY.2022.04.020>

1233 Santos-Díaz, M. del S., Camarena-Rangel, N.G., 2019. Cacti for production of metabolites:
1234 current state and perspectives. *Appl. Microbiol. Biotechnol.* 103, 8657–8667.
1235 <https://doi.org/10.1007/S00253-019-10125-5/TABLES/1>

1236 Scalisi, A., Morandi, B., Inglese, P., Lo Bianco, R., 2016. Cladode growth dynamics in
1237 *Opuntia ficus-indica* under drought. *Environ. Exp. Bot.* 122, 158–167.
1238 <https://doi.org/10.1016/J.ENVEXPBOT.2015.10.003>

1239 Silva, M.V. da, Pandorfi, H., Almeida, G.L.P. de, Lima, R.P. de, Santos, A. dos, Jardim,
1240 A.M. da R.F., Rolim, M.M., Silva, J.L.B. da, Batista, P.H.D., Silva, R.A.B. da, Lopes,
1241 P.M.O., Silva, D.C. da, 2021. Spatio-temporal monitoring of soil and plant indicators
1242 under forage cactus cultivation by geoprocessing in Brazilian semi-arid region. *J. South*
1243 *Am. Earth Sci.* 107, 103155. <https://doi.org/10.1016/J.JSAMES.2021.103155>

1244 Silva, T.G.F., Miranda, K.R., Santos, D.C., Queiroz, M.G., Silva, M.C., Cruz Neto, J.F.,
1245 Araújo, J.E.M., 2014. Área do cladódio de clones de palma forrageira: modelagem,
1246 análise e aplicabilidade. *Rev. Bras. Ciências Agrárias* 9, 626–632.
1247 <https://doi.org/10.5039/AGRARIA.V9I4A4553>

1248 Snyman, H.A., 2013. Growth Rate and Water-Use Efficiency of Cactus Pears *Opuntia ficus-*
1249 *indica* and *O. robusta*. *Arid L. Res. Manag.* 27, 337–348.
1250 <https://doi.org/10.1080/15324982.2013.771232>

1251 Soares, W.D.A., 2018. Impact of spineless cactus cultivation (*O. Ficus-indica*) on the thermal
1252 characteristics of soil. *Rev. Ambient. Água* 13, e2148. <https://doi.org/10.4136/AMBI->
1253 [AGUA.2148](https://doi.org/10.4136/AMBI-AGUA.2148)

- 1254 Souza, A.M., Silva, C.M.S.E., Bezerra, B.G., 2021. Caatinga Albedo Preserved and Replaced
1255 by Pasture in Northeast Brazil. *Atmosphere* (Basel). 12, 1622.
1256 <https://doi.org/10.3390/ATMOS12121622>
- 1257 Souza, M. de S., Silva, T.G.F. da, Souza, L.S.B. de, Alves, H.K.M.N., Leite, R.M.C., Souza,
1258 C.A.A. de, Araújo, G.G.L.D., Campos, F.S., Silva, M.J.D., Souza, P.J.D.O.P., 2022.
1259 Growth, phenology and harvesting time of cactus-millet intercropping system under
1260 biotic mulching. *Arch. Agron. Soil Sci.* 68, 764–778.
1261 <https://doi.org/10.1080/03650340.2020.1852553>
- 1262 Tai, X., Epstein, H.E., Li, B., 2021. Effects of grazing exclusion on spring and autumn
1263 pastures in arid regions of China: Insights from field surveys and landsat images. *Agric.*
1264 *Ecosyst. Environ.* 310, 107302. <https://doi.org/10.1016/J.AGEE.2021.107302>
- 1265 Tapia, P.I., Negoita, L., Gibbs, J.P., Jaramillo, P., 2019. Effectiveness of water-saving
1266 technologies during early stages of restoration of endemic *Opuntia* cacti in the
1267 Galápagos Islands, Ecuador. *PeerJ* 3, e8156.
1268 <https://doi.org/10.7717/PEERJ.8156/SUPP-3>
- 1269 Tenorio-Escandón, P., Ramírez-Hernández, A., Flores, J., Juan-Vicedo, J., Martínez-Falcón,
1270 A.P., 2022. A Systematic Review on *Opuntia* (Cactaceae; Opuntioideae) Flower-
1271 Visiting Insects in the World with Emphasis on Mexico: Implications for Biodiversity
1272 Conservation. *Plants* 11, 131. <https://doi.org/10.3390/PLANTS11010131/S1>
- 1273 Unland, H.E., Houser, P.R., Shuttleworth, W.J., Yang, Z.L., 1996. Surface flux measurement
1274 and modeling at a semi-arid Sonoran Desert site. *Agric. For. Meteorol.* 82, 119–153.
1275 [https://doi.org/10.1016/0168-1923\(96\)02330-1](https://doi.org/10.1016/0168-1923(96)02330-1)
- 1276 Winter, K., Smith, J.A.C., 2022. CAM photosynthesis: the acid test. *New Phytol.* 233, 599–
1277 609. <https://doi.org/10.1111/NPH.17790>
- 1278 Yang, J., Yao, Y., Shao, C., Li, Y., Fisher, J.B., Cheng, J., Chen, J., Jia, K., Zhang, X., Shang,
1279 K., Yu, R., Guo, X., Xie, Z., Liu, L., Ning, J., Zhang, L., 2022. A novel TIR-derived
1280 three-source energy balance model for estimating daily latent heat flux in mainland
1281 China using an all-weather land surface temperature product. *Agric. For. Meteorol.* 323,
1282 109066. <https://doi.org/10.1016/J.AGRFORMET.2022.109066>
- 1283 Yao, J., Liu, H., Huang, J., Gao, Z., Wang, G., Li, D., Yu, H., Chen, X., 2020. Accelerated
1284 dryland expansion regulates future variability in dryland gross primary production. *Nat.*

1285 Commun. 11, 1–10. <https://doi.org/10.1038/s41467-020-15515-2>

1286 Yue, P., Zhang, Q., Yang, Y., Liang, Z., Hongli, Z., Hao, X., Sun, X., 2018. Seasonal and
1287 inter-annual variability of the Bowen smith ratio over a semi-arid grassland in the
1288 Chinese Loess Plateau. *Agric. For. Meteorol.* 252, 99–108.
1289 <https://doi.org/10.1016/J.AGRFORMET.2018.01.006>

1290 Yue, P., Zhang, Q., Zhang, L., Li, H., Yang, Y., Zeng, J., Wang, S., 2019. Long-term
1291 variations in energy partitioning and evapotranspiration in a semiarid grassland in the
1292 Loess Plateau of China. *Agric. For. Meteorol.* 278, 107671.
1293 <https://doi.org/10.1016/J.AGRFORMET.2019.107671>

1294 Zhang, Kuiyue, Liu, D., Liu, H., Lei, H., Guo, F., Xie, S., Meng, X., Huang, Q., 2022. Energy
1295 flux observation in a shrub ecosystem of a gully region of the Chinese Loess Plateau.
1296 *Ecohydrol. Hydrobiol.* 22, 323–336. <https://doi.org/10.1016/J.ECOHYD.2021.10.001>

1297 Zhang, Kai, Wang, X., Li, Y., Zhao, J., Yang, Y., Zang, H., Zeng, Z., 2022. Peanut residue
1298 incorporation benefits crop yield, nitrogen yield, and water use efficiency of summer
1299 peanut – winter wheat systems. *F. Crop. Res.* 279, 108463.
1300 <https://doi.org/10.1016/J.FCR.2022.108463>

1301 Zutta, B.R., Nobel, P.S., Aramians, A.M., Sahaghian, A., 2011. Low- and High-Temperature
1302 Tolerance and Acclimation for Chlorenchyma versus Meristem of the Cultivated Cacti
1303 *Nopalea cochenillifera*, *Opuntia robusta*, and *Selenicereus megalanthus*. *J. Bot.* 2011,
1304 1–6. <https://doi.org/10.1155/2011/347168>

1305

CHAPTER 8

Sink or carbon source? How the *Opuntia* cactus interacts in the use of carbon, nutrients and radiation in a semi-arid environment

Abstract

Anthropogenic disturbances directly influence environmental processes and increase the concentration of carbon (C) in the atmosphere. Here, we compare the differences in the seasonality of the balance of carbon, energy, and radiation, as well as seek to identify the interrelationships between these environmental variables and their impact on the growth of *Opuntia* cactus. Data were acquired from an eddy covariance flux tower over a cactus crop (2019–2021) in the Brazilian semi-arid region. In addition, we use plant growth rates, nutrient stocks, carbon and water use efficiency (WUE), and radiation (RUE). We show that the closure of the surface energy balance was 71%, although there are minimal fluxes of available energy lost (29%) by unquantified processes. At all seasons, the highest net ecosystem CO₂ exchange (NEE) rate was between 11:00–13:00 ($-16.36 \mu\text{mol m}^{-2} \text{s}^{-1}$). During the wet-dry transition season, there was the lowest daily gross primary productivity (GPP) ($9.96 \mu\text{mol m}^{-2} \text{s}^{-1}$) and net radiation— R_n (217.97 W m^{-2}). Ecosystem respiration was more expressive during the wet season ($3.73 \mu\text{mol m}^{-2} \text{s}^{-1}$), and maximum diurnal value of $4.46 \mu\text{mol m}^{-2} \text{s}^{-1}$. Furthermore, the latent heat flux was higher during the wet season (114.68 W m^{-2}) and lowered in the dry season (9.39 W m^{-2}). The net assimilation rate showed higher values during the dry-wet transition. The dry and wet seasons presented, respectively, higher and lower efficiency in the use of nutrients and WUE. The RUE of the wet season was 81.48% higher than in the dry season. Overall, the cactus is a potential year-round C sink (NEE: $-4,517 \text{ g C m}^{-2}$; GPP: $2,352 \text{ g C m}^{-2}$). The results help us to understand that most of the R_n energy is used in the sensible heat flux (58% ratio).

Keywords: Eddy covariance; Rainfed cactus; Net ecosystem CO₂ exchange; Carbon budget; CAM plant

31 **1. Introduction**

32 Anthropogenic activities are one of the main contributors to the increase in the
33 concentration of carbon (C) in the atmosphere, and this has been causing damage and threats
34 to the survival of various species worldwide. Terrestrial ecosystems, in general, are
35 responsible for exchanging carbon and energy with the atmosphere, which provides annual
36 sequestration of 3.2 ± 0.6 Pg C, with great spatial and temporal variability between regions
37 of the globe (Del Grosso et al., 2018; Rodda et al., 2021; Yao et al., 2018; Zeng et al., 2020).
38 In agricultural land, since 44% of them are inserted in arid lands (Kumar et al., 2021), soil
39 management, type of cultivation, and species used can alter the carbon dioxide (CO₂) balance
40 of landscapes (Bilderback et al., 2021; Camelo et al., 2021; Wilson et al., 2002; Zeng et al.,
41 2020).

42 In pastures composed of grasses and legumes with C₃ and C₄ photosynthetic
43 metabolism, the ability to sequester carbon is similar or greater compared to forest
44 ecosystems (Saliendra et al., 2018). Plants that have crassulacean acid metabolism (CAM)
45 photosynthesis, for example, cacti, have reduced water loss and high efficiency in the use of
46 water and carbon (i.e., more efficient than C₃ and C₄ photosynthesis plants), helping to
47 survive even in places with high-stress conditions, mainly abiotic (Cortázar and Nobel, 1986;
48 Dubeux Jr. et al., 2006; Jardim et al., 2021a; Nobel and Bobich, 2002; Owen et al., 2016).
49 Although cacti are promising in carbon and water use (Nobel and Bobich, 2002; Scalisi et
50 al., 2016; Snyman, 2006), to our knowledge, this is the first study quantifying carbon-energy
51 fluxes with the eddy covariance technique in exclusive cultivation of cactus (*Opuntia stricta*)
52 in the Brazilian semi-arid region and South America. In the Sonoran Desert region of the
53 United States, studies such as those by Flanagan and Flanagan (2018) and Bilderback et al.
54 (2021) evaluated CO₂ fluxes in ecosystems composed of species of the genus *Opuntia*,
55 demonstrating the deposition of carbon in the soil (Bilderback et al., 2021), and that the
56 photosynthetic activity of the cactus exceeds respiration (Flanagan and Flanagan, 2018).

57 For many decades, monitoring of environmental conditions has been carried out by
58 flux towers in various biomes and surfaces (Baldocchi et al., 2000; Costa et al., 2022;
59 Cunliffe et al., 2022; McGloin et al., 2018). Among the applied techniques, the eddy
60 covariance method is well established in several parts of the world, measuring latent heat
61 (*LE*) fluxes and the net ecosystem CO₂ exchange (NEE) (Cunliffe et al., 2022; Flores-

62 Rentería et al., 2023). In this method, the *LE* and NEE results are measured by the transport
63 of turbulent fluxes in the boundary layer of the vegetation canopy and atmosphere (Anapalli
64 et al., 2019). In turn, the high-frequency data—generally measured at 10 to 20 Hz by the
65 eddy covariance system such as the *LE*, can be used to determine the evapotranspiration (ET)
66 of the crop, and the NEE carbon flux can be partitioned in gross primary production (GPP)
67 and ecosystem respiration (*R_{eco}*), aiding in the understanding of crop water and the local
68 carbon budget (Anapalli et al., 2019; Cunliffe et al., 2022; Flores-Rentería et al., 2023;
69 Guevara-Escobar et al., 2021).

70 In places with average annual precipitation of 200–700 mm, as is the case in a semi-
71 arid environment (Kumar et al., 2021), understanding the carbon balance, and the specific
72 responses of the net ecosystem exchange of CO₂, gross primary production and ecosystem
73 respiration at different times of the year help to understand how vegetation behaves as a
74 carbon sink and source. According to Mendes et al. (2020), evaluating the Caatinga biome,
75 a typical dry ecosystem with the presence of cacti, grasses, and tree-shrub species, found
76 NEE results ranging from -169.0 to -145.0 g C m⁻² year⁻¹, with a strong influence of the
77 GPP in the wet and dry seasons. Flores-Rentería et al. (2023) evaluated xerophilous
78 shrubland in the Chihuahuan Desert of Northeast Mexico, with species of *Opuntia* spp. and
79 other CAM plants (e.g., *Agave asperrima*, *Cylindropuntia leptocaulis*) found annual NEE of
80 -303.5 g C m⁻², GPP of 841.3 g C m⁻², and cumulative *R_{eco}* of 537.7 g C m⁻². These authors
81 concluded that the ecosystem was a sink during most of the year because the vegetation is
82 adapted to grow and absorb carbon under arid conditions. Notably, information on cactus
83 ecosystems is lacking, with some of these processes of carbon fluxes and stocks being
84 difficult to quantify.

85 Thus, the hypothesis that motivated this research was—do cactus crops have a high
86 CO₂ absorption capacity for long periods, and can they be efficient even in dry seasons?
87 Based on the rationale for this hypothesis, the objectives of this study were (1) to compare
88 the differences in the seasonality of the balance of carbon, energy, and radiation and (2) to
89 identify the interrelationships between fluxes of carbon, energy and radiation, meteorological
90 variables and its impacts on the growth of cactus plants (*Opuntia stricta*) cultivated in a semi-
91 arid environment. The findings and details of the dynamics of CO₂ and energy fluxes during

92 the seasons can inform agricultural management decisions and provide a baseline for future
93 work aimed at carbon sequestration in cactus agroecosystems.

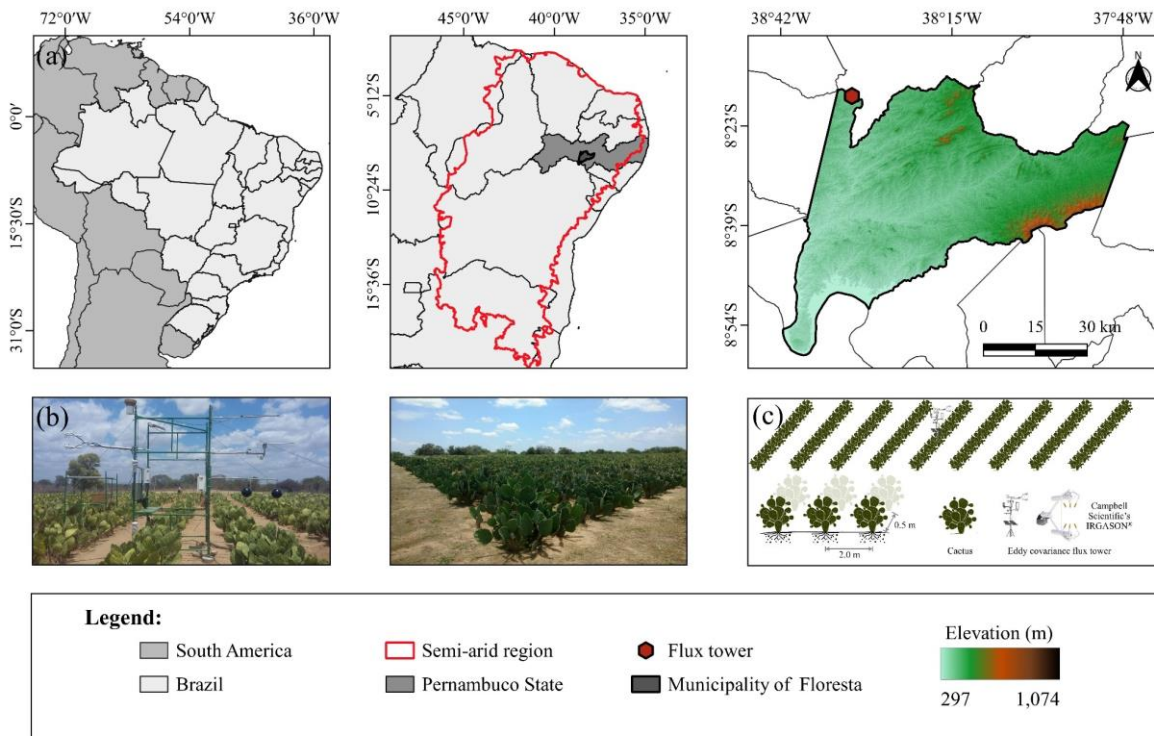
94

95 **2. Materials and methods**

96 *2.1. Study site description*

97 The study was conducted in a crop field located in the municipality of Floresta, State
98 of Pernambuco, Brazil (8°18' S, 38°30' W, and 367 m above mean sea level) (Figure 1a).
99 The climate is characterized by irregular rainfall from December to April, classified as hot
100 semi-arid (BSh), according to Köppen-Geiger (Beck et al., 2018). The annual average
101 rainfall, relative humidity, and air temperature are 489 mm, 61% and 26.1 °C, respectively,
102 and 2023 mm year⁻¹ of reference evapotranspiration. The dominant wind direction is
103 Southeast, with an average annual speed of 1.8 m s⁻¹. The soil has a sandy loam texture (56%
104 sand, 41% silt, and 3% clay) of the Chromic Luvisols type, with a bulk density of 1.33 g cm⁻³,
105 total porosity of 48.05%, pH of 5.35, the electrical conductivity of 0.28 dS m⁻¹, cation
106 exchange capacity of 8.08 cmol_c dm⁻³ and base saturation of 78.60%. All soil samples were
107 collected from the 0–0.40 m depth layer. Soil pH and electrical conductivity were determined
108 in a 1:2.5 soil/distilled water suspension. The average slope at the site is less than 1%.

109



110

111 Figure 1. Description and geographical location of the study area (a). Photo of the flux tower
 112 with eddy covariance system, cultivation of *Opuntia stricta* cactus (b), and schematic layout
 113 of the experimental field (c).

114

115 Data were collected between January 2019 and December 2021 at a site cultivated
 116 with cactus [*Opuntia stricta* (Haw.) Haw.] (henceforth called *Opuntia*), species resistant to
 117 *Dactylopius opuntiae* Cockerell (Hemiptera: Dactylopiidae). In August 2014, cactus planting
 118 and conventional soil preparation were carried out, i.e., plowing, harrowing, and furrowing.
 119 We used single crop rows spaced 2.0×0.5 m, totaling a plant density of $10,000 \text{ plants ha}^{-1}$
 120 (Figure 1b–c). After soil preparation, the cladodes were planted, keeping the lower base
 121 inserted at 50% of the soil surface. To maintain ideal growth conditions, cultural treatments
 122 (i.e., manual weeding, herbicide, and insecticide application) were carried out when
 123 necessary, thus reducing competition with weeds and the presence of phytopathogens. In
 124 addition, the cactus plants were grown in rainfed conditions throughout the experimental
 125 period, and no fertilization was applied.

126 Based on the climatic conditions, we differentiated the wet and dry seasons from 2019
 127 to 2021 into four seasons: wet, dry, transitional dry-wet and wet-dry (Table 1). For example,
 128 the wet season is when the accumulated rainfall in five or more consecutive days is at least
 129 20 mm, without any dry period exceeding seven days during the following 30 days. If in 30
 130 days the accumulated rainfall is less than 20 mm with less than five days of rainfall, the dry
 131 season occurs. On the other hand, if none of these criteria are met, the dry-wet or wet-dry
 132 transition season occurs, the first being after the dry season and the second after the
 133 occurrence of the wet season. This delimitation was to explore the role of seasonal
 134 hydrological components as a function of the onset and end of rainfall (Leite-Filho et al.,
 135 2019; Salack et al., 2016).

136

137 Table 1. Delimitation of the beginning and end of seasons during the experimental period
 138 from January 2019 to December 2021 in *Opuntia* cactus cultivation in the Brazilian semi-
 139 arid region.

Season	Start date	End date	Length (days)	Rainfall totals (mm)
Dry-wet transition	1 January 2019	20 January 2019	20	24
Wet season	21 January 2019	6 April 2019	76	834
Wet-dry transition	7 April 2019	8 September 2019	155	166
Dry season	9 September 2019	27 October 2019	49	7
Dry-wet transition	28 October 2019	5 December 2019	39	76
Wet season	6 December 2019	1 June 2020	179	928
Wet-dry transition	2 June 2020	22 July 2020	51	31
Dry season	23 July 2020	4 October 2020	74	17
Dry-wet transition	5 October 2020	19 February 2021	138	146
Wet season	20 February 2021	18 April 2021	58	381
Wet-dry transition	19 April 2021	29 July 2021	102	37
Dry season	30 July 2021	27 October 2021	90	6
Dry-wet transition	28 October 2021	27 November 2021	31	46
Wet season	28 November 2021	31 December 2021	34	58

140

141 2.2. Measurements of environmental variables

142 Micrometeorological measurements were performed using a 3 m high tower installed
 143 above the cactus canopy near the center of the experimental area. To measure the net radiation
 144 (R_n) components, we used closed-cell thermopile-style sensors (NR-Lite, Kipp & Zonen,
 145 Delft, Netherlands) in addition to net radiometers (SP-230, Apogee Instruments, Logan,
 146 Utah, USA) that measure upward and downward shortwave and longwave radiation. Each

147 radiometer sensor was installed 2.8 m above the canopy to quantify the incident radiation and
148 another one for the radiation reflected by the canopy, i.e., sensors positioned up- and down-
149 looking. Photosynthetically active radiation (PAR) was measured with a quantum sensor (LI-
150 190SB, LI-COR, Inc., Lincoln, Nebraska, USA) mounted at the top and bottom of the
151 canopy. Soil heat flux (G) was measured using a heat flux plate (HFT3, REBS, Hukseflux,
152 Delft, Netherlands) installed at a depth of 0.05 m close to the cactus crop line. Air temperature
153 and relative humidity were measured by two thermo-hygrometers (HMP45C, Campbell
154 Scientific, Logan, Utah, USA), creating a vertical profile 0.5 and 1.5 m above the soil surface.
155 Rainfall was measured using an automatic rain gauge (CS700-L, Hydrological Services Rain
156 Gauge, Liverpool, Australia) positioned 3 m above the canopy. Soil moisture ($m^3 m^{-3}$) was
157 quantified at a depth of 0.30 m using a time domain reflectometry (TDR) sensor (Campbell
158 Scientific CS616, Logan, UT, USA) buried vertically in the soil next to the eddy covariance
159 tower. Data from the micrometeorological sensors were recorded by a CR3000 data logger
160 (Campbell Scientific Inc., Logan, Utah, USA) every 60 seconds, with a storage interval of
161 10 minutes. Measurements were collected continuously during the daytime and nighttime.

162

163 2.3. Flux measurements and data processing

164 Flux measurements with the eddy covariance system were performed using an open-
165 path CO_2/H_2O gas analyzer and a sonic anemometer (IRGASON; Campbell Scientific Inc.,
166 Logan, Utah, USA), with data stored in averages of 30 minutes on a CR3000 data logger
167 (Campbell Scientific Inc., Logan, Utah, USA). The IRGASON is a system that combines an
168 open-path infrared gas analyzer (IRGA) together with a three-dimensional sonic anemometer
169 (Figure 1b–c). The sensor was fixed during the entire experimental period at 2.0 m above
170 ground level, oriented towards the Southeast (135°) in favor of the predominance of the wind,
171 to ensure that the measurements were contained in the appropriate coverage area of the flux
172 system. In this way, the average value of the fetch/height ratio in almost stable conditions
173 was 65:1. For calculations of latent heat flux (LE), sensible heat flux (H), and CO_2 flux, we
174 used EasyFlux PC software (Campbell Scientific Inc.) which performs high frequency (10
175 Hz) raw data corrections, generating averages every 30 minutes. During the post-processing
176 step in EasyFlux all necessary corrections were applied, including outlier removal (Vickers
177 and Mahrt, 1974), bias correction (Rannik and Vesala, 1999), rotation of two-dimensional

178 coordinates (Wilczak et al., 2001), sonic temperature correction (Schotanus et al., 1983), and
179 frequency response (Moore, 1986) and Webb-Pearman-Leuning density corrections (Webb
180 et al., 1980). In addition, flux measurements were classified according to three quality
181 criteria: high, moderate, or low-quality data (Yang et al., 2022). In this step, only high- and
182 moderate-quality flux measurements were used. Finally, after the post-processing step and
183 quality filtering, 94% of the CO₂ flux data were suitable for analysis.

184 We used the online platform developed by the Max Planck Institute for
185 Biogeochemistry in Jena, Germany (<http://www.bgc-jena.mpg.de/~MDIwork/eddyproc/>) to
186 perform the partitioning of the net ecosystem CO₂ exchange (NEE) (Wutzler et al., 2018).
187 NEE was monitored using the eddy covariance technique and refers to the net exchange of
188 CO₂ between the ecosystem and the atmosphere, basically composed of gross primary
189 productivity (GPP) and ecosystem respiration (R_{eco}), the latter being equivalent to the sum of
190 autotrophic and heterotrophic respiration (Silva et al., 2022). In the present study, we used
191 the meteorological convention, i.e., negative NEE values indicate CO₂ absorption in the
192 ecosystem, while positive values indicate net CO₂ loss to the atmosphere (Silva et al., 2022).
193 With the adjusted LE data measured by the eddy covariance system, we converted it to
194 evapotranspiration—ET in millimeters (mm) through the latent heat of water vaporization
195 (2.45 MJ kg^{-1}) (Salazar-Martínez et al., 2022).

196

197 2.4. Surface energy budget

198 The estimate of Earth's surface radiation was made through the energy balance
199 between short and longwave radiation described as follows:

$$200 \quad SR_n = SR_d - SR_u \quad (1)$$

$$201 \quad LR_n = LR_d - LR_u \quad (2)$$

$$202 \quad R_n = SR_n + LR_n \quad (3)$$

203 where SR_n is the net shortwave radiation, SR_d is the downward shortwave radiation, SR_u is
204 the upward shortwave radiation (i.e., reflected outgoing shortwave radiation), LR_n is the net
205 longwave radiation, LR_d is the downward longwave radiation, LR_u is the upward longwave
206 radiation, and R_n is the net radiation. All radiation variables were measured in W m^{-2} . Still
207 using ascending and descending shortwave radiation, we calculated the albedo (α) of the
208 cultivated surface with cactus:

209
$$\alpha = \frac{SR_u}{SR_d} \quad (4)$$

210

211 *2.5. Energy budget partitioning*

212 In this paper, we use the simplified version of the surface energy balance method
 213 (Equation 5). This method is based on the principle of conservation of energy:

214
$$R_n = LE + H + G \quad (5)$$

215 where LE is the latent heat flux (W m^{-2}), H is the sensible heat flux (W m^{-2}), and G is the
 216 soil heat flux (W m^{-2}).

217

218 All data sets are presented in local time (i.e., 3 h behind Greenwich Mean Time).
 219 Furthermore, energy from metabolic activities, heat storage in plant tissue and canopy, and
 220 horizontal advection were omitted and considered insignificant (Papale et al., 2006). Thus,
 221 these energy components were not included in our energy balance algorithm. The
 222 components described in Equation 5 are normally positive during the daytime, with net
 223 radiation and soil heat flux positive downwards and latent and sensible heat fluxes positive
 224 upwards.

225

226 *2.5.1. Energy balance closure*

227 A common feature when using measurements with eddy covariance is the lack of
 228 closure of the surface energy budget. Thus, the sum of latent and sensible heat fluxes ($LE +$
 229 H) is commonly smaller than the measured available energy ($R_n - G$), which causes an energy
 230 imbalance in the system (Dhungel et al., 2021; Widmoser and Wohlfahrt, 2018). To analyze
 231 the energy balance closure (EBC), we fitted an origin-forced linear regression model to the
 232 half-hour data, establishing a relationship between the turbulent fluxes as the dependent
 233 variable and the available energy as the independent variable (McGloin et al., 2018). This
 234 type of linear regression approach provides a stable and robust estimate of energy balance
 235 closure, even when available energy is close to zero. Furthermore, we do not use any
 236 technique for forcing the closure of the energy balance. Here, the quotient of latent and
 237 sensible heat fluxes and available energy expresses the EBC:

238
$$\text{EBC} = \frac{(LE + H)}{(R_n - G)} \quad (6)$$

239

240 2.6. Biomass yield and growth allometry

241 We determined the biomass yield produced each year and season, considering the
242 weight of four representative random plants. The aboveground plant biomass was harvested
243 entirely and weighed on an electronic balance to quantify the fresh matter (g FM plant⁻¹) and
244 subsequently dried in a forced air circulation oven at 55 °C until reaching a constant weight.
245 Here, we determined the weight of dry matter per plant (g DM plant⁻¹); thus, the productivity
246 of cacti was estimated in grams per square meter per season or year (g m⁻² season⁻¹ and g
247 m⁻² year⁻¹, respectively). In addition, morphometric data and plant biomass were collected
248 monthly, with five plants being measured to compose the morphometric data and another
249 four plants collected for biomass analysis over time. For each plant, we quantified the cladode
250 and plant morphometric variables. In cladode structures, the length and width were measured,
251 as well as the number of cladodes (units), by counting cladodes in order of appearance in the
252 plant (i.e., first order, second order, third order and so on) and the total number of cladodes,
253 i.e., through the sum of cladodes by order. For plant height measurements, we considered the
254 vertical distance from the ground to the canopy apex, and the plant width was across two
255 widths from the canopy edge. Then, the collected samples were used to quantify the
256 morphophysiological indices of the cacti.

257 In our study, Equations 7 and 8 were used to determine the cladode area—CA and the
258 cladode area index—CAI (Pinheiro et al., 2014; Silva et al., 2014). Furthermore, with data
259 on dry mass yield and cladode parameters, we calculated the morphophysiological indices of
260 *Opuntia* using a sigmoidal model with three parameters (Equation 9) (Jardim et al., 2021b).

$$261 \quad CA = 0.7086 \times \left[\frac{1 - e^{(-0.000045765 \times CL \times CW)}}{0.000045765} \right] \quad (7)$$

$$262 \quad CAI = \left[\frac{\sum_{n=1}^{i=1} (CA)}{n} / \frac{10,000}{(S1 \times S2)} \right] \quad (8)$$

$$263 \quad y = \frac{a}{1 + e^{\left(-\frac{x-x_0}{b}\right)}} \quad (9)$$

264 where CL is the cladode length (cm), CW is the cladode width (cm), *i* is the observation
265 number, *n* is the total number of observations, 10,000 is the conversion factor from cm² to
266 m², and S1 × S2 is the spacing between the rows and plants of each cactus (i.e., 2.0 × 0.5 m),

267 respectively. Here, the parameters for the morphophysiological analysis were: y is the
268 response variable (e.g., cladodes dry matter, cladode area index, and the number of
269 cladodes), a is the maximum value for the rate (i.e., the distance between the two
270 asymptotes), x is the accumulated days, x_0 is the number of days necessary for the plant to
271 express 50% of the maximum rate (i.e., the inflection point of the curve), and b is the number
272 of days necessary for the start of the rate.

273

274 Next, we quantified the relative growth rate—RGR ($\text{g g}^{-1} \text{day}^{-1}$), net assimilation
275 rate—NAR ($\text{g m}^{-2} \text{day}^{-1}$), and specific cladode area—SCA ($\text{m}^2 \text{g}^{-1}$) (Jardim et al., 2021b;
276 Khapte et al., 2022). The RGR is determined by fitting the increase in dry biomass with the
277 accumulated biomass over time. NAR represents the dry mass produced by cladode area per
278 unit of time, and this variable is commonly used to represent the net photosynthesis rate of
279 plants. The SCA refers to the cladode area useful for photosynthesis (Jardim et al., 2021b).
280 All growth rates were calculated during the experimental period of the plants, from 2015 to
281 2021.

282

283 2.7. Resource use efficiencies

284 2.7.1. Water use efficiency

285 The water use efficiency (WUE, $\text{g m}^{-2} \text{mm}^{-1}$) was calculated by dividing the crop
286 biomass yield and its evapotranspiration (Kai Zhang et al., 2022):

$$287 \quad \text{WUE} = \frac{\text{DMY}}{\text{ET}} \quad (10)$$

288 where DMY is the dry matter yield (g m^{-2}), and ET is the evapotranspiration (mm).

289

290 2.7.2. Radiation use efficiency and interception photosynthetically active radiation

291 The radiation use efficiency (RUE, g MJ^{-1}) over the entire experimental period was
292 calculated using the following equation (Raza et al., 2019):

$$293 \quad \text{RUE} = \frac{\text{DMY}}{I_0 \times f\text{IPAR}} \quad (11)$$

294 where I_0 is the amount of daily-incident photosynthetically active radiation (PAR) above the
295 canopy (MJ m^{-2}), and $f\text{IPAR}$ is the fraction of PAR intercepted (400–700 nm). Therefore,
296 we can calculate $f\text{IPAR}$ using Equations 12 and 13 as follows:

297
$$f\text{IPAR} = \left(1 - \frac{\text{PAR}_b}{I_0}\right)$$
 (12)

298
$$f\text{IPAR} = 1 - e^{(-k \times \text{CAD})}$$
 (13)

299 where PAR_b is the PAR measured below the plant canopy, and k is the light extinction
 300 coefficient based on the Beer-Lambert law.

301

302 *2.7.3. Nutrient stocks and use efficiency*

303 Above-ground dry biomass was ground to powder using a Wiley-type mill (Model 4,
 304 Thomas-Wiley Laboratory Mill, Thomas Scientific) with a 1 mm sieve. The nutrients
 305 presented here were chosen because they are essential and indispensable for the growth and
 306 development of cactus plants. Then, we carried out an analysis of the concentration of
 307 mineral elements in the plant tissue of the plants. The micro-Kjeldahl method determined the
 308 cladode's total nitrogen content (N, mg kg⁻¹) (Santos et al., 2020). Phosphorus (P, mg kg⁻¹)
 309 was measured by the vanado-molybdate method with UV-visible spectrophotometry reading
 310 at 430 nm (Du Toit et al., 2018). Meanwhile, the potassium (K⁺, mg kg⁻¹) was determined
 311 by a flame photometer (Rodrigues et al., 2013). To determine calcium (Ca²⁺, mg kg⁻¹) and
 312 magnesium (Mg²⁺, mg kg⁻¹), we used an atomic absorption spectrophotometer (Loupassaki
 313 et al., 2007). The dry biomass's carbon content (C, mg kg⁻¹) was determined by the Dumas
 314 method via dry combustion (Adamič and Leskovšek, 2021). Finally, the nutrient use
 315 efficiency (NUE, mg m⁻² mm⁻¹) was calculated according to Equation 14. The nutrient stock
 316 (g m⁻²) was obtained by multiplying the dry biomass per square meter by the nutrient
 317 concentration.

318
$$\text{NUE} = \frac{\text{DMY} \times Nu}{\text{ET}}$$
 (14)

319 where Nu is the concentration of the nutrient in the analyzed sample of plant tissue. Equation
 320 14 was adapted (Zhang et al., 2020), making it a function of crop evapotranspiration. This
 321 adaptation provides more clarity in understanding the nutrient uptake capacity of the plant
 322 from the soil solution, together with the consumption of water lost through
 323 evapotranspiration.

324

325 2.7.4. *Carbon stock and efficiency*

326 Using the carbon that was quantified in the plants' dry biomass (without the root
327 biomass), we quantified the carbon use efficiency—CUE ($\mu\text{g m}^{-2} \text{mm}^{-1}$). Thus, based on
328 Equation 14, the efficiency in the use of carbon was realized. Furthermore, the carbon stock
329 (g m^{-2}) was calculated by multiplying the elemental carbon concentration by the dry biomass
330 produced per square meter (Siddiq et al., 2021).

331

332 2.8. *Statistical analysis*

333 In this study, we use the linear regression method to quantify the energy balance
334 closure of the eddy covariance system through the ratio between available energy ($R_n - G$)
335 and turbulent heat fluxes ($LE + H$) during the experimental period. We fitted non-linear
336 regression models (sigmoidal model) for plant growth rates. The components of carbon,
337 energy, and radiation balances during the four seasons (i.e., wet season, dry season, wet-dry
338 and dry-wet transitions) were presented in curves and boxplots over time (i.e., hour, month,
339 year and station). All boxplots include median, whiskers, and 1.5 times the upper and lower
340 interquartile ranges. Subsequently, we applied principal component analysis (PCA) to
341 examine the interrelationships between seasons and environmental and cactus plant
342 parameters. PCA is a type of multivariate analysis that reduces large data sets through
343 orthogonal transformation, generating linearly uncorrelated variables called principal
344 components (Lamichhane et al., 2021). In this way, the new set of data generated by the PCA
345 provides new values, called scores and loadings, and are visualized in biplots in multivariate
346 space. Furthermore, before performing the PCA, all variables were standardized using the z-
347 transformation, with zero mean and unit standard deviation. Finally, the significant principal
348 components were selected according to the Kaiser criterion, considering only eigenvalues
349 greater than 1.0 (Jardim et al., 2021a; Kaiser, 1960; Lamichhane et al., 2021). All data
350 processing and analysis were performed using the R program version 4.1.3 (R Core Team,
351 2022).

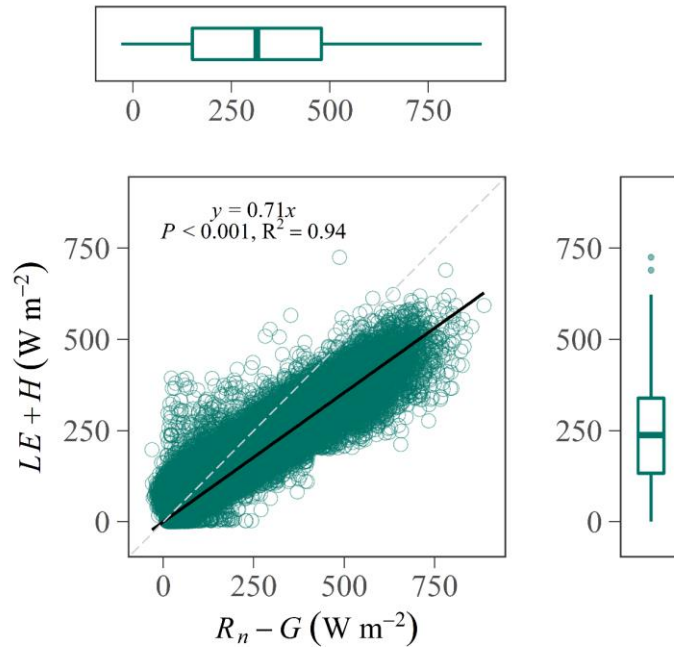
352

353 **3. Results**

354 *3.1. Energy balance closing overview*

355 Figure 2 shows the relationship between available and turbulent energy fluxes with
356 half-hour data from eddy covariance measurements. The result of the energy balance closure
357 (EBC) during the period from 2019 to 2021 was 0.71 (corresponding to the slope of the
358 estimated line), and the coefficient of determination (R^2) of 0.94 ($P < 0.001$). The closer the
359 EBC result is to 1.0, the better the energy closure response status. In this analysis, we chose
360 to force the intercept to zero, helping to visualize the slope of the regression line in relation
361 to the 1:1 line. The regression and determination coefficients show adequate data fit.
362 Furthermore, the horizontal (i.e., $R_n - G$) and vertical (i.e., $LE + H$) coordinate boxplots show
363 that the fluxes are concentrated at 316.83 W m^{-2} (median 314, interquartile range 150–478
364 W m^{-2}) and 236.69 W m^{-2} (median 238, interquartile range 133–339 W m^{-2}), respectively,
365 and the rest of the scattered data above the mean are causing a slope of the line for available
366 energy (i.e., indicating greater expressiveness of this flux). Although there is a high EBC
367 value, minimal fluxes of available energy are being lost (29%) by unquantified processes,
368 e.g., heat storage in the canopy. In addition, we did not use a technique to force the EBC,
369 such as for example, the Bowen ratio and the residual technique.

370



371

372 Figure 2. Relationships between available energy ($R_n - G$) and turbulent fluxes ($LE + H$) for
 373 half-hour measurements from 2019 to 2021 in cactus cultivation in the Brazilian semi-arid
 374 region. The white dashed line is the 1:1 line, and the black line is the fitted line determined
 375 by linear regression. The boxes represent the 25th, 50th (median) and 75th percentiles of the
 376 data; the whiskers represent the lowest (or highest) datum within the $1.5\times$ interquartile range.
 377 Dots above the boxplots indicate outliers.

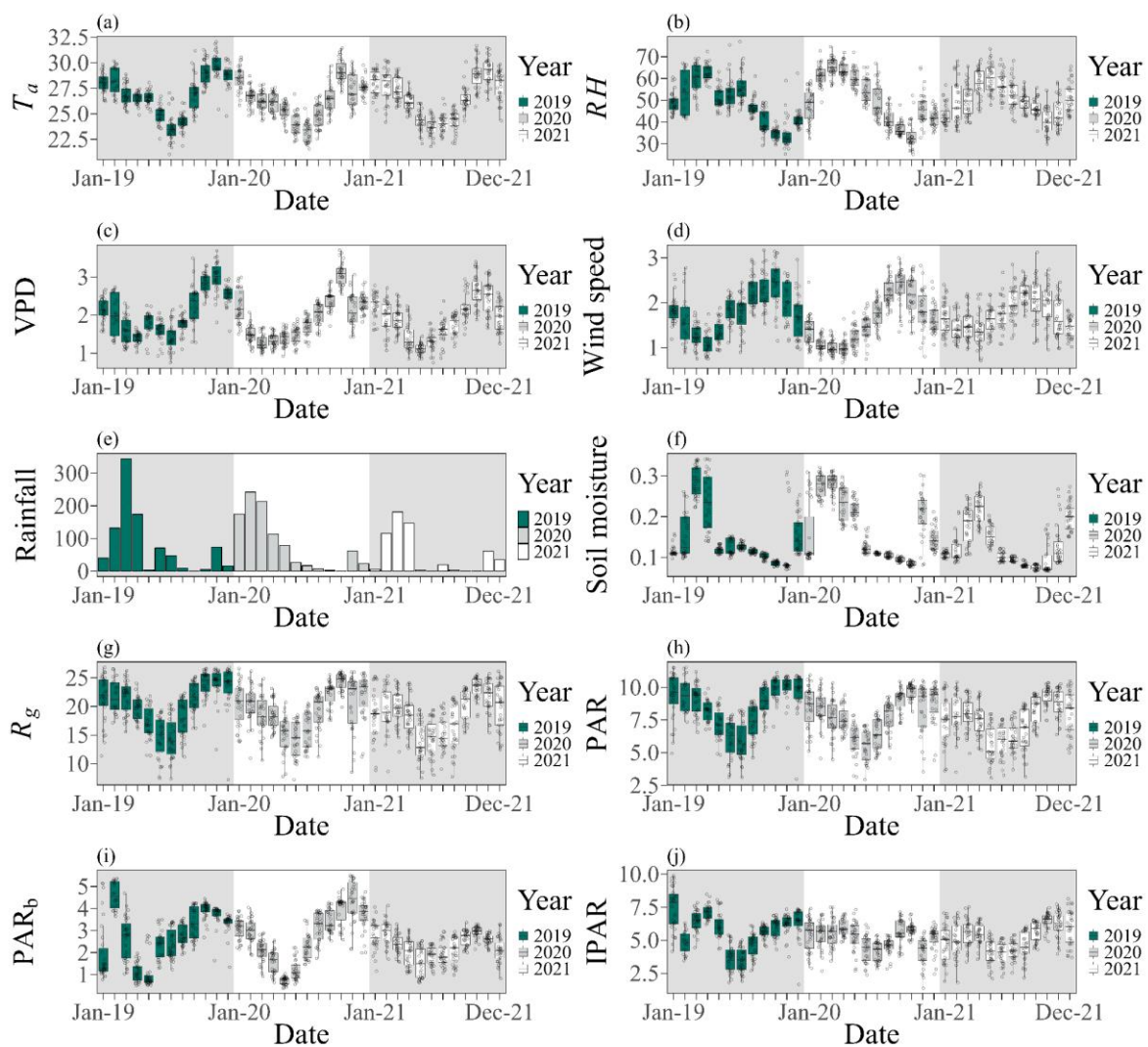
378

379 3.2. Environmental conditions during the experimental period

380 Our timescale results for environmental conditions are shown in Figure 3. During the
 381 study period, the average air temperature was 26.58 °C, with minimum (July 2020) and
 382 maximum (November 2019) values of 23.25 and 29.77 °C, respectively. On average, the
 383 lowest records occurred from June to August (24.09 °C), being 12.13% lower in relation to
 384 the other months (Figure 3a). The results for relative humidity (RH) and vapor pressure
 385 deficit (VPD) showed consistent trends over the years (Figure 3b–c) with air temperature and
 386 rainfall. The RH average was 49.57%, with the wettest months from February to May being
 387 16.78% higher than the annual average. The VPD showed a similar variation with air
 388 temperature, an average of 1.94 kPa, with the most deficit period from April to July, and
 389 2021 with the lowest average (1.88 kPa). The mean annual rainfall was 820.32 mm, 67.76%
 390 above the climatological normal for the municipality (489 mm year⁻¹). The highest rainfall

391 was in 2020 (964.34 mm), followed by 2019 and 2021 with 924.14 and 572.48 mm,
 392 respectively. March 2019 reached the highest accumulated rainfall (343.55 mm), and the
 393 lowest (0.6 mm) occurred in September 2019. In addition, the rainiest months had the lowest
 394 average wind speed (1.35 m s^{-1}), 20.62% lower than the average (Figure 3d–e). The variation
 395 in soil moisture ranged from 0.08 to $0.29 \text{ m}^3 \text{ m}^{-3}$, and the months from February to May
 396 showed the highest results (Figure 3f). Particularly, in March 2019, we observed the highest
 397 soil moisture, with $0.29 \text{ m}^3 \text{ m}^{-3}$ (median 0.29, interquartile range $0.25\text{--}0.32 \text{ m}^3 \text{ m}^{-3}$), and in
 398 2021 there was the highest moisture deficit (mean of $0.13 \text{ m}^3 \text{ m}^{-3}$).

399
 400



401

402 Figure 3. Monthly environmental conditions during the study period (2019–2021) in cactus
 403 cultivation in the Brazilian semi-arid region. The plots show the local conditions of (a) air

404 temperature— T_a (°C), (b) relative air humidity— RH (%), (c) vapor pressure deficit—VPD
405 (kPa), (d) wind speed (m s^{-1}), (e) rainfall (mm), (f) soil moisture ($\text{m}^3 \text{m}^{-3}$), (g) global solar
406 radiation— R_g ($\text{MJ m}^{-2} \text{day}^{-1}$), (h) photosynthetically active radiation—PAR ($\text{MJ m}^{-2} \text{day}^{-1}$),
407 (i) PAR measured below the cactus canopy— PAR_b ($\text{MJ m}^{-2} \text{day}^{-1}$), and (j) intercepted
408 photosynthetically active radiation—IPAR ($\text{MJ m}^{-2} \text{day}^{-1}$). The shaded areas indicate the
409 boundaries of the years.

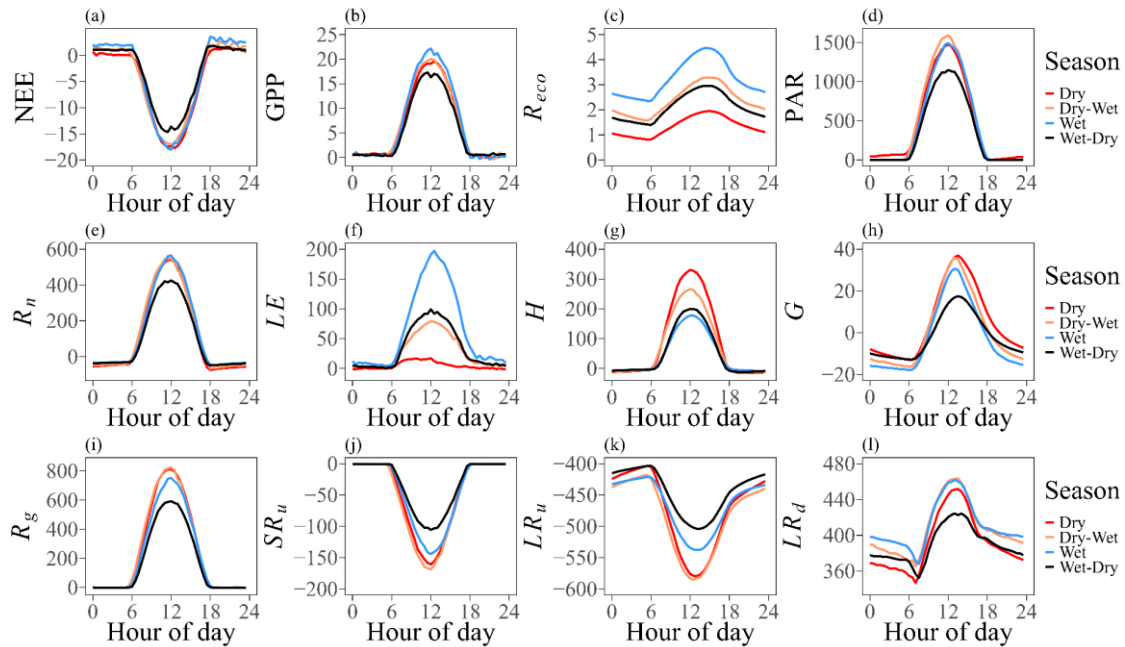
410

411 For each year studied, there was a very similar intra-annual cyclic variation in global
412 solar radiation— R_g (Figure 3g). In the middle of each year (i.e., between May and July), we
413 observed the lowest average values of R_g ($14.99 \text{ MJ m}^{-2} \text{day}^{-1}$), and the highest values
414 occurred between October and December ($22.62 \text{ MJ m}^{-2} \text{day}^{-1}$). However, the three-year
415 average R_g was $19.31 \text{ MJ m}^{-2} \text{day}^{-1}$. During the warmer months and with high R_g ,
416 photosynthetically active radiation (PAR) results were more expressive each year (Figure
417 3h). In this study, the lowest PAR value occurred in June 2020, being $5.55 \text{ MJ m}^{-2} \text{day}^{-1}$
418 (median 5.69 , interquartile range 4.44 – $6.62 \text{ MJ m}^{-2} \text{day}^{-1}$), and the highest in November
419 2019, with $9.94 \text{ MJ m}^{-2} \text{day}^{-1}$ (median 10.18 , interquartile range 9.76 – $10.57 \text{ MJ m}^{-2} \text{day}^{-1}$),
420 while the average value for 2019–2021 was $7.91 \text{ MJ m}^{-2} \text{day}^{-1}$. The temporal variation of
421 PAR below the canopy (PAR_b) and PAR intercepted by the cactus canopy (IPAR) was due
422 to environmental conditions and canopy density (Figure 3i–j). On average, the months with
423 the lowest PAR_b results annually occur from April to June ($1.48 \text{ MJ m}^{-2} \text{day}^{-1}$). Interestingly,
424 there was a high dispersion and response in January and February 2019 (average of 3.27 MJ
425 $\text{m}^{-2} \text{day}^{-1}$) and September to November 2020 ($3.90 \text{ MJ m}^{-2} \text{day}^{-1}$) due to two harvests carried
426 out on cactus during these periods (i.e., January 2019 and September 2020), leaving the soil
427 partially uncovered by vegetation. Furthermore, these variations are also visible in the canopy
428 radiation interception response. We observed significant inter-annual and intra-annual IPAR
429 variations, with the years 2019 and 2021 having the highest values, with mean of 5.66 and
430 $5.16 \text{ MJ m}^{-2} \text{day}^{-1}$, respectively, both averaging 5.91% higher than the 2020 IPAR (Figure
431 3j).

432

433 3.3. Seasonal and temporal variation in the balance of carbon, energy and radiation

434 Figure 4 shows the half-hourly averages of carbon, energy, and radiation exchanges
435 in *Opuntia* cactus cultivation during the four seasons (dry season, dry-wet transition, wet
436 season, and wet-dry transition). Diurnal dynamics of carbon exchange exhibited similar
437 patterns of variation across seasons. Clearly, during the night, the net ecosystem CO₂
438 exchange (NEE) was positive—release, and at dawn, it became more negative, increasing its
439 absorption of CO₂ (Figure 4a). The highest daytime absorption rate of all seasons occurred
440 between 11:00–13:00, averaging $-16.36 \mu\text{mol m}^{-2} \text{s}^{-1}$. At the same time, the dry, wet, and
441 dry-wet transition seasons showed similarity and the highest average (more negative) -17.10
442 $\mu\text{mol m}^{-2} \text{s}^{-1}$, with 20.70% higher than the wet-dry transition season that had the lowest CO₂
443 absorption (less negative). Gross primary productivity (GPP) exhibited marked variations
444 across the seasons, and the wet season had a daytime average of $12.94 \mu\text{mol m}^{-2} \text{s}^{-1}$ ranging
445 from 0.02 to $22.16 \mu\text{mol m}^{-2} \text{s}^{-1}$ over 6:00–18:00 (Figure 4b). There was a minimal difference
446 in mean cactus GPP during the dry and wet-dry transition seasons ($0.76 \mu\text{mol m}^{-2} \text{s}^{-1}$), both
447 of which were, on average, 9.27% lower than during the wet season. We observed a lower
448 diurnal GPP of $9.96 \mu\text{mol m}^{-2} \text{s}^{-1}$ during the wet-dry transition season, with both the seasonal
449 trend of GPP and NEE limited by PAR. Consistent with previous results, ecosystem
450 respiration— R_{eco} was more expressive during the wet season (mean of $3.73 \mu\text{mol m}^{-2} \text{s}^{-1}$),
451 and maximum daytime value of $4.46 \mu\text{mol m}^{-2} \text{s}^{-1}$. In addition, the dry-wet, wet-dry and dry
452 seasons were respectively 27.13, 34.27, and 58.17% lower than the wet season (Figure 4c).
453 After 15:00 in all seasons, there was a clear decline in the respiration rate in cactus
454 cultivation. On average, the PAR during the dry-wet transition season was higher, with a
455 peak of $1590.4 \mu\text{mol m}^{-2} \text{s}^{-1}$ and a mean value of $915.05 \mu\text{mol m}^{-2} \text{s}^{-1}$, while between the
456 dry and wet seasons, there was no difference (mean of $838.17 \mu\text{mol m}^{-2} \text{s}^{-1}$). During the wet-
457 dry transition, we observed the lowest PAR value, a mean of $656.38 \mu\text{mol m}^{-2} \text{s}^{-1}$ (Figure
458 4d), and a peak around noon.
459



460

461 Figure 4. Diurnal cycle of carbon exchange, energy budget, and hourly radiation during dry
 462 and wet seasons (i.e., dry season, dry-wet transition, wet season, and wet-dry transition) in
 463 cactus cultivation in the Brazilian semi-arid region. (a) Net ecosystem CO₂ exchange—NEE,
 464 (b) gross primary productivity—GPP, (c) ecosystem respiration— R_{eco} , (d) photosynthetic
 465 active radiation—PAR, are expressed in $\mu\text{mol m}^{-2} \text{s}^{-1}$. (e) Net radiation— R_n , (f) latent heat
 466 flux— LE , (g) sensible heat flux— H , (h) soil heat flux— G , (i) global solar radiation— R_g , (j)
 467 upward shortwave radiation— SR_u , (k) upward longwave radiation— LR_u , and (l) downward
 468 longwave radiation— LR_d , all expressed in W m^{-2} . Negative values in panel (a) indicate
 469 carbon uptake while positive values in panels (b) and (c) indicate carbon release by the
 470 ecosystem.

471

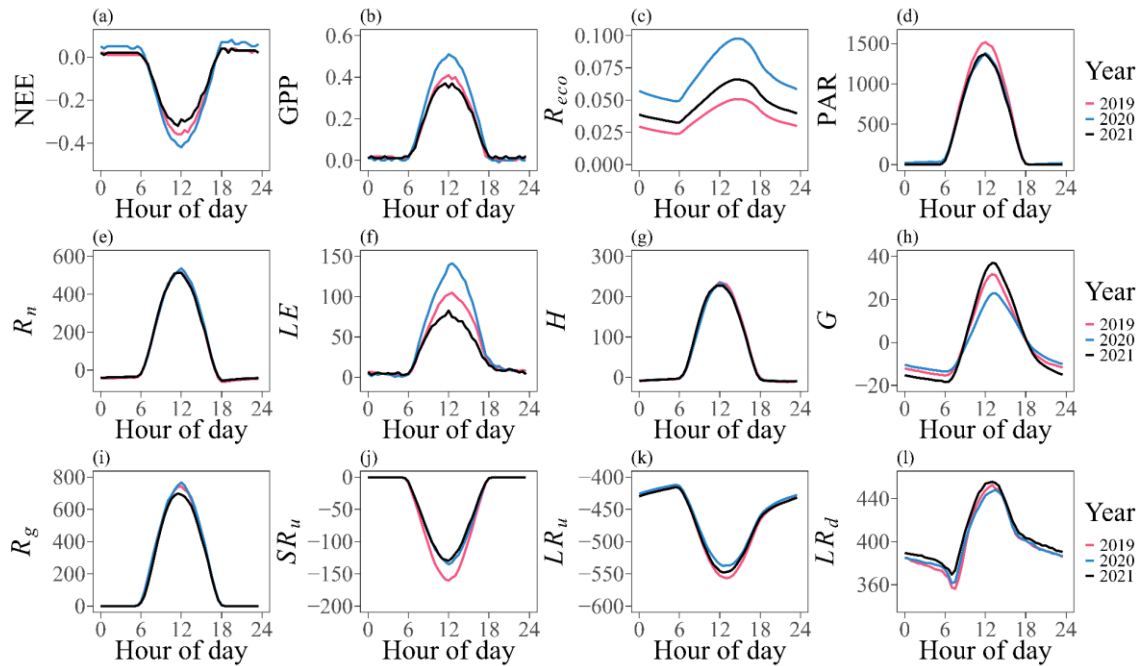
472 Net radiation (R_n) exhibited smaller flux patterns during the wet-dry transition season,
 473 with a daytime average of 217.97 W m^{-2} and a peak occurring at noon (Figure 4e). On the
 474 other hand, we did not observe the difference between the dry season, dry-wet transition, and
 475 wet season, with an average value of 283.11 W m^{-2} and a gradual decline for all stations after
 476 solar noon. The latent heat flux (LE) was higher during the wet season (114.68 W m^{-2}) and
 477 lowered in the dry season (mean of 9.39 W m^{-2}). In addition, the transition stations (i.e., dry-
 478 wet and wet-dry) presented intermediate LE fluxes, with the wet-dry season averaging 60.05
 479 W m^{-2} and the dry-wet transition slightly lower (17.57%) (Figure 4f). The dry and wet

480 seasons had the highest (183.33 W m^{-2}) and lowest (93.82 W m^{-2}) sensible heat flux— H
481 values, respectively. In contrast, H decreased in the dry-wet (19.07%) and wet-dry (43.08%)
482 transitions compared to the dry season. Soil heat flux (G) was highest during dry season >
483 dry-wet transition > wet season > wet-dry transition and peaked between 13:00 and 14:00,
484 ranging from 36.90 to 17.42 W m^{-2} between the dry season and the wet-dry transition season,
485 respectively.

486 In general, the radiation balance was lowest during the wet-dry transition season. For
487 example, global solar radiation (R_g) in the wet-dry transition was on average 21.02% lower
488 than the wet season, 27.98% lower than the dry season, and 29.88% lower than the dry-wet
489 transition (Figure 4i). We also observed the same tendency for shortwave— SR_u and
490 longwave— LR_u radiation for cactus cultivation (Figure 4j–k). However, there was a greater
491 distance after noon from the LR_u during the dry and dry-wet transition seasons than during
492 the wet season. Our results show no difference between the wet season and the dry-wet
493 transition, with an average of 422.99 W m^{-2} for descending longwave radiation (LR_d). As for
494 the dry season, the average was 408.93 W m^{-2} with a peak of 451.47 W m^{-2} , followed by the
495 wet-dry transition (average of 398.03 W m^{-2}), reaching a peak of 424.41 W m^{-2} .

496 Figure 5 shows the cactus agroecosystem response to carbon, energy and radiation
497 exchanges on an annual scale (2019–2021). In 2021, there was an apparent decrease in NEE
498 on a diurnal scale, while 2019 and 2020 were more expressive sinks, with the NEE being
499 14.36 and 28.36% higher, respectively (Figure 5a). The GPP showed the same trend as the
500 NEE, with a peak occurring at noon and a daytime average of 0.22 g C m^{-2} during 2021, 0.23
501 g C m^{-2} (2019), and 0.30 g C m^{-2} (2020). Here, we reveal that the cactus agroecosystem
502 becomes a carbon sink as global solar radiation increases. We observed variation with a mean
503 GPP value of 0.01 to 0.51 g C m^{-2} (Figure 5b). In this study, during 2020, which was
504 particularly wet, R_{eco} was higher than in 2021 and 2019, and the highest values occurred
505 between 13:30 and 16:30 (Figure 5c). Overall, the ecosystem respiration rate in 2020 is
506 approximately 49% higher than in 2021 and 94% higher than in 2019. The carbon budget
507 was also boosted by the increase in PAR, although there were no differences between 2020
508 and 2021 (Figure 5d).

509



510

511 Figure 5. Variation of carbon exchange, energy budget and radiation on an hourly scale
 512 during 2019–2021 in cactus cultivation in the Brazilian semi-arid region. (a) Net ecosystem
 513 CO₂ exchange—NEE, (b) gross primary productivity—GPP, (c) ecosystem respiration—
 514 R_{eco} , are expressed in g C m^{-2} , and (d) photosynthetic active radiation—PAR, is expressed in
 515 $\mu\text{mol m}^{-2} \text{s}^{-1}$. (e) Net radiation— R_n , (f) latent heat flux— LE , (g) sensible heat flux— H , (h)
 516 soil heat flux— G , (i) global solar radiation— R_g , (j) upward shortwave radiation— SR_u , (k)
 517 upward longwave radiation— LR_u , and (l) downward longwave radiation— LR_d , all expressed
 518 in W m^{-2} . Negative values in panel (a) indicate carbon uptake while positive values in panels
 519 (b) and (c) indicate carbon release by the ecosystem.

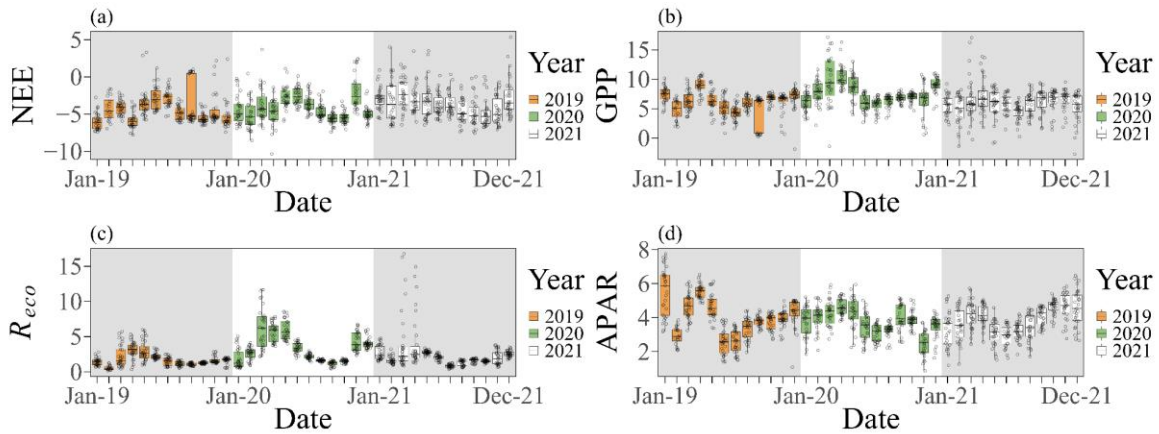
520

521 Despite the high values of net radiation and sensible heat fluxes, with an average peak
 522 of 522.36 and 232.10 W m^{-2} , respectively, our results show no significant changes between
 523 2019–2021 (Figures 5e and 5g). In contrast, the LE began to differ between years after 7:30
 524 and reached a maximum value around noon (12:00–13:00). Indeed, the latent heat flux
 525 averaged 82.78 W m^{-2} in 2020 and had lower diurnal responses during 2021 and 2019,
 526 averaging 49.57 and 63.52 W m^{-2} , respectively (Figure 5f). We observed substantial
 527 variations in the soil heat flux, with 2021 having the highest result, an average of 12.79 W
 528 m^{-2} . In all years, the sharpest decline in G occurs after 14:00 (Figure 5h). Throughout the
 529 daytime, we observed a slight difference between the peaks of global solar radiation during

530 2019–2021, in addition to greater losses (more negative) of short and long radiation by the
531 surface of cacti (Figure 5i–k). Likewise, the LR_d was slightly higher in 2021, averaging
532 419.96 W m^{-2} and diurnal variation from 369.49 to 455.70 W m^{-2} . On the other hand, the
533 LR_d of 2019 and 2020 showed no difference, an average of 412.57 W m^{-2} with its peaks at
534 $13:00$ (2019) and $13:30$ (2020) and a less significant decrease after $16:30$ (Figure 5l).

535 Figure 6 shows the monthly scale variability of the carbon balance and
536 photosynthetically active radiation absorbed by growing *Opuntia* during 2019–2021.
537 Throughout all the years, we can observe that in each month, the cactus mainly was a carbon
538 sink on average (Figure 6a). On a monthly scale, the maximum (most negative) mean NEE
539 values were $-6.02 \text{ g C m}^{-2} \text{ day}^{-1}$ and $-5.83 \text{ g C m}^{-2} \text{ day}^{-1}$ in January and April 2019,
540 respectively. In 2020, the highest NEE values were in September ($-5.61 \text{ g C m}^{-2} \text{ day}^{-1}$) and
541 October ($-5.41 \text{ g C m}^{-2} \text{ day}^{-1}$), and in 2021 it also occurred in September and October, with
542 an average of -4.73 and $-4.91 \text{ g C m}^{-2} \text{ day}^{-1}$, respectively. The *Opuntia* cactus presented
543 GPP ranging from 4.32 to $10.38 \text{ g C m}^{-2} \text{ day}^{-1}$ and an average for the entire period of 6.51 g
544 $\text{C m}^{-2} \text{ day}^{-1}$ (Figure 6b). In addition, R_{eco} presented very similar variations between the years,
545 with higher respiration between March and May, and we also observed more expressive
546 peaks occurring in 2020 (Figure 6c). Contrary to what was seen in 2020, our results show
547 lower R_{eco} in 2019 (mean of $1.73 \text{ g C m}^{-2} \text{ day}^{-1}$), which coincides with high NEE and PAR
548 values absorbed by the cactus. In 2019, substantial variations were found in the absorbed
549 photosynthetically active radiation (APAR) by the cactus (Figure 6d), with a minimum value
550 ($2.46 \text{ MJ m}^{-2} \text{ day}^{-1}$) and a maximum value ($5.55 \text{ MJ m}^{-2} \text{ day}^{-1}$) in November 2020 and April
551 2019, respectively.

552



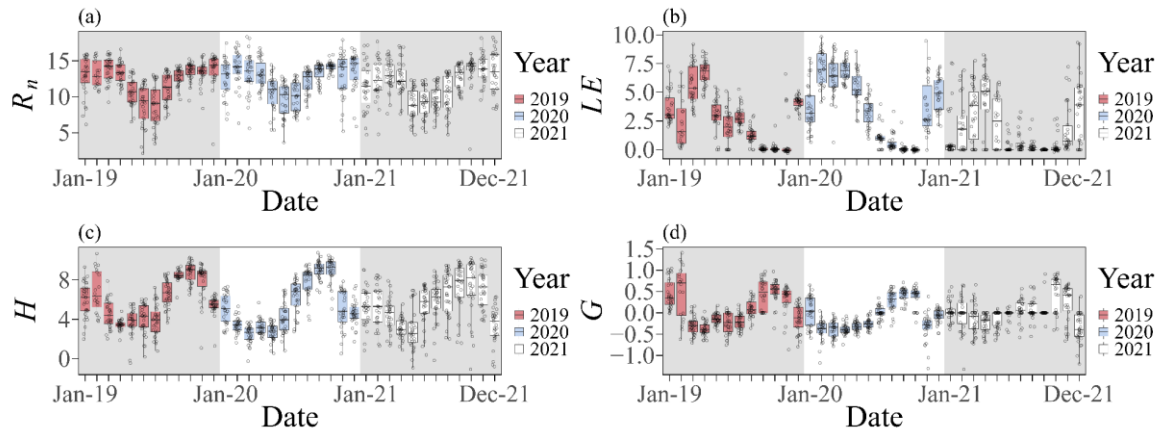
553

554 Figure 6. Monthly variation of carbon balance (i.e., net ecosystem CO₂ exchange—NEE,
 555 gross primary productivity—GPP, and ecosystem respiration—*R_{eco}*) and absorbed
 556 photosynthetically active radiation (APAR) in *Opuntia* cactus cultivation during 2019–2021
 557 in the Brazilian semi-arid region. The shaded areas indicate the boundaries of the years. Note:
 558 NEE, GPP, *R_{eco}* in g C m⁻² day⁻¹, and APAR in MJ m⁻² day⁻¹.

559

560 There were significant variations in the energy balance between months and years in
 561 cactus cultivation (Figure 7). The lowest mean value of *R_n* was found in May–July (9.61 MJ
 562 m⁻² day⁻¹); by contrast, fluxes were higher at the beginning and end of the year (Figure 7a).
 563 In 2019, the months with the lowest *LE* results were September–November; in 2020, they
 564 were August–October, followed by 2021 with the lowest *LE* responses in June–October.
 565 Furthermore, *H* reached its minimum value in March (2.48 MJ m⁻² day⁻¹) and its maximum
 566 value in September (9.05 MJ m⁻² day⁻¹), both in 2020. Clearly, when the *H* was high, there
 567 was a lower energetic contribution to *LE* (Figure 7b–c). For *G*, curiously there was a flux
 568 variation very similar to the trend of *H* (Figure 7d). For example, we found higher soil heat
 569 fluxes at the beginning and end of the year, and the maximum flux occurred in October 2019,
 570 averaging 0.51 MJ m⁻² day⁻¹. On the other hand, the lowest soil heat flux was observed in
 571 February 2020 (mean -0.40 MJ m⁻² day⁻¹) due to rainfall (see Figure 3e).

572



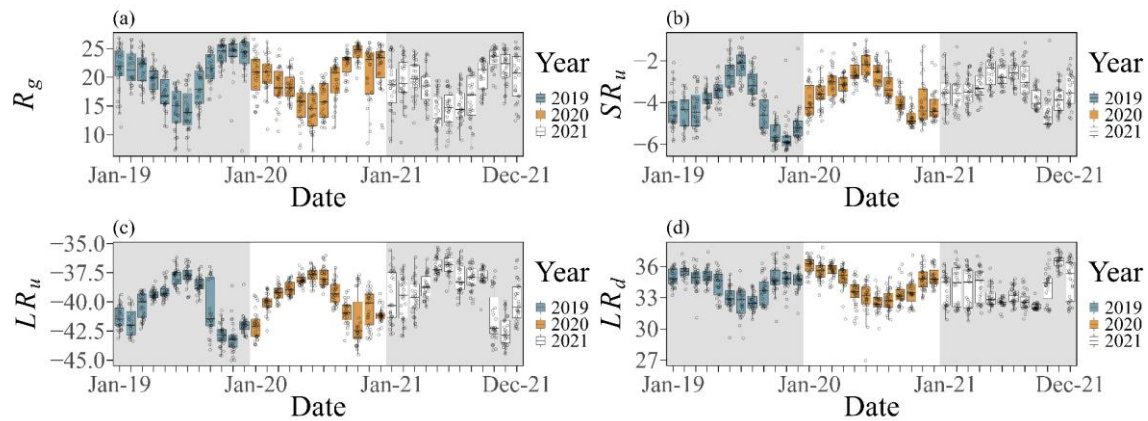
573

574 Figure 7. Diurnal variation of (a) net radiation— R_n , (b) latent heat flux— LE , (c) sensible heat
 575 flux— H , and (d) soil heat flux— G during the period 2019–2021 in *Opuntia* cactus cultivation
 576 in the Brazilian semi-arid region. All the variables were measured in $\text{MJ m}^{-2} \text{day}^{-1}$. The
 577 shaded areas indicate the boundaries of the years.

578

579 On average, the R_g varied between 13.86 and $24.31 \text{ MJ m}^{-2} \text{day}^{-1}$, with the minimum
 580 and maximum values occurring in May 2021 and October 2020, respectively (Figure 8).
 581 Although a similar variation is observed over the years, in 2021 the lowest R_g balance
 582 occurred on average ($18.44 \text{ MJ m}^{-2} \text{day}^{-1}$) (Figure 8a). At the beginning of the year, SR_u is
 583 higher (more negative), and at the end, it is more pronounced. The months of June–August
 584 had the lowest values of SR_u (mean $-2.69 \text{ MJ m}^{-2} \text{day}^{-1}$), while October–December was on
 585 average 68.73% higher than June–August (Figure 8b). Likewise, LR_u was similar to SR_u , but
 586 with different magnitudes, with longwave radiation lost more significantly (Figure 8c).
 587 Consequently, after January and February of each year, there was a gradual decrease in the
 588 LR_u until mid-year, ranging from -36.87 to $-43.15 \text{ MJ m}^{-2} \text{day}^{-1}$, and we observed
 589 significant variations in the LR_d from 32.16 to $36.49 \text{ MJ m}^{-2} \text{day}^{-1}$ (Figure 8d).

590



591

592 Figure 8. Temporal variation of radiation balance in *Opuntia* cactus cultivation in the
 593 Brazilian semi-arid region. (a) R_g is the global solar radiation, (b) SR_u is the upward
 594 shortwave radiation, (c) LR_u is the upward longwave radiation, and (d) LR_d is the downward
 595 longwave radiation. All the variables were measured in $\text{MJ m}^{-2} \text{ day}^{-1}$. The shaded areas
 596 indicate the boundaries of the years.

597

598 3.4. Characteristics of seasonal changes in radiation, energy, carbon and water fluxes

599 The wet-dry transition season showed the lowest values of the radiation balance
 600 components (Table 2). On average, the R_g of the wet-dry transition season was 26.74% lower
 601 than all stations (e.g., dry-wet, wet, and dry) that had solar radiation greater than 20 MJ m^{-2}
 602 day^{-1} . Consequently, in this same wet-dry transition season, the lowest results of short and
 603 long radiation (i.e., SR_u , LR_u , and LR_d) and net radiation for the cactus surface occurred on
 604 average. During the dry season, LE was lower than in all seasons and caused an excessive
 605 increase in H ($7.9 \text{ MJ m}^{-2} \text{ day}^{-1}$), followed by $6.4 \text{ MJ m}^{-2} \text{ day}^{-1}$, referring to the dry-wet
 606 transition season. In wet seasons the energy for soil heat flux was more negative, while the
 607 results of dry seasons were positive, i.e., higher energy for soil heating. Overall, there was
 608 stability in the carbon balance for cactus cultivation. Our results show that the cactus was a
 609 carbon sink in all seasons and years, with more expressive values during the dry-wet (-4.3 g
 610 $\text{C m}^{-2} \text{ day}^{-1}$) and dry ($-5 \text{ g C m}^{-2} \text{ day}^{-1}$) seasons. Furthermore, during the wet season, the
 611 NEE of the cactus was 23.67% lower than in the dry season. NEE presented very similar
 612 results annually, although in 2021 it was 11.56% lower than the annual average (Table 2).

613

614 Table 2. Diurnal variation of radiation and energy balance, carbon budget, evapotranspiration (ET) and rainfall for three
 615 years of cactus cultivation in the Brazilian semi-arid region. Net ecosystem CO_2 exchange (NEE), gross primary productivity

616 (GPP), and ecosystem respiration (R_{eco}) with negative values indicate carbon input into the ecosystem (absorption), while
 617 positive values indicate carbon loss (release).

Season / Year	R_g	SR_u	LR_u	LR_d	R_n	LE	H	G	NEE	GPP	R_{eco}	ET	Rainfall
	MJ m ⁻² day ⁻¹								g C m ⁻² day ⁻¹			mm	
Dry-wet/2019	23.2	5.1	42.4	34.8	13.2	2.0	7.0	0.2	-5.0	6.6	1.6	48	100
Wet/2019	22.2	4.6	41.2	35.0	13.7	4.4	5.5	0.1	-5.0	6.5	1.6	169	849
Wet-dry/2019	16.7	3.1	38.4	33.4	10.5	2.8	4.2	-0.2	-3.6	5.8	2.1	178	166
Dry/2019	23.1	5.1	42.3	34.6	13.2	0.1	8.2	0.6	-5.2	6.4	1.1	3	7
Dry-wet/2020	22.2	4.3	41.1	34.5	13.6	3.0	6.1	-0.03	-4.1	7.4	3.3	108	85
Wet/2020	18.6	3.3	39.7	35.1	12.7	5.8	3.4	-0.3	-4.1	8.6	4.5	365	913
Wet-dry/2020	14.7	2.4	37.7	32.8	9.6	2.3	4.9	-0.2	-2.8	5.8	2.9	47	31
Dry/2020	20.6	3.6	39.9	33.0	12.6	0.5	8.3	0.3	-5.1	6.5	1.5	14	17
Dry-wet/2021	20.2	3.7	40.6	34.6	12.6	1.2	6.2	0.1	-4.0	6.1	2.1	41	107
Wet/2021	19.5	3.4	39.8	34.6	13.2	3.9	3.9	-0.2	-2.4	6.0	3.6	148	439
Wet-dry/2021	14.8	2.6	37.3	33.0	9.5	1.0	4.4	-0.1	-3.5	5.4	1.9	41	37
Dry/2021	19.8	3.7	39.0	33.0	12.2	0.1	7.1	0.2	-4.7	6.2	1.5	5	6
Season													
Dry-wet	21.9	4.4	41.4	34.6	13.2	2.1	6.4	0.1	-4.3	6.7	2.4	65	97
Wet	20.1	3.7	40.2	34.9	13.2	4.7	4.3	-0.2	-3.8	7.0	3.2	227	733
Wet-dry	15.4	2.7	37.8	33.0	9.9	2.0	4.5	-0.1	-3.3	5.6	2.3	88	78
Dry	21.2	4.1	40.4	33.5	12.7	0.2	7.9	0.4	-5.0	6.4	1.4	7	10
Crop cycle													
1	19.1	3.7	39.8	34.3	12.1	3.4	5.0	-0.04	-4.2	6.8	2.6	819	2075
2	19.5	3.6	39.6	33.8	12.3	1.7	5.8	0.04	-3.9	6.3	2.4	347	680
Year													
2019	21.3	4.5	41.1	34.5	12.7	2.3	6.2	0.2	-4.7	6.3	1.6	398	1122
2020	19.0	3.4	39.6	33.8	12.1	2.9	5.7	-0.04	-4.0	7.1	3.1	534	1045
2021	18.6	3.4	39.2	33.8	11.9	1.6	5.4	0.002	-3.6	5.9	2.3	235	589
Annual mean	19.6	3.7	40.0	34.0	12.2	2.3	5.8	0.05	-4.1	6.4	2.3	388.7	918.5

R_g is the global solar radiation, SR_u is the upward shortwave radiation, LR_u is the upward longwave radiation, LR_d is the downward longwave radiation, R_n is the net radiation, LE is the latent heat flux, H is the sensible heat flux, G is the soil heat flux, NEE is the net ecosystem CO₂ exchange, GPP is the gross primary productivity, R_{eco} is the ecosystem respiration, and ET is the evapotranspiration.

618

619 Our results also show an expressive contribution of GPP during the experimental
 620 period (Table 2). GPP during the wet-dry transition season showed the lowest results,
 621 averaging 5.6 g C m⁻² day⁻¹. When examining only the dry season, we observed a lower
 622 carbon efflux due to low ecosystem respiration and, consequently, a high NEE response.
 623 Also, in this season, there were the lowest average records of evapotranspiration and rainfall
 624 (7 mm and 10 mm, respectively), while the season with the greatest influence of rainfall, for
 625 example, the wet season (average of 733 mm of rainfall) had a R_{eco} of 136.74% higher than
 626 the dry season. On an annual scale, as well as for each crop cycle, the radiation and energy

627 balances were very similar. As for the carbon balance, the first cactus cycle was more
 628 expressive, with greater carbon accumulation and high productivity. In addition, the total flux
 629 of CO₂ released from the ecosystem between the two cycles showed a difference of 8.23%,
 630 with the first cactus cycle being larger. Evapotranspiration (ET) in the first cactus cycle was
 631 more expressive (accumulated 819 mm) but decreased by more than half in the second cycle,
 632 which reveals the influence of rainfall in this agroecosystem and ET responses.

633

634 3.5. Flux partitioning

635 Table 3 shows our results of partitioning the radiation and energy fluxes, as well as
 636 the PAR fraction intercepted in cactus cultivation. The SR_u/R_g ratio ranged from 0.16 to 0.22
 637 during the seasons and years, with the wet-dry transition season having the lowest response
 638 (mean of 0.17). R_n was responsible for 64% and 60% of global radiation during the wet season
 639 and wet-dry transition, respectively. Interestingly, the PAR/R_g ratio averaged 0.41 in all
 640 seasons and showed slight variation over time. Furthermore, our results show a greater
 641 fraction of PAR intercepted ($fPAR$) during the wet season and wet-dry transition and a
 642 greater increase in the LE/R_n ratio during these previously mentioned seasons. The dry and
 643 dry-wet transition seasons represented 3% and 19%, respectively, of the LE/R_n , thus
 644 configuring the lowest ratios of this partition. Consequently, the highest response of the H/R_n
 645 ratio was during the dry season (mean of 0.78), being 107.13%, 38.69%, and 30.27% higher
 646 than the wet season and wet-dry and dry-wet transitions, respectively. The partitioning of R_n
 647 into LE and H differed between the wettest and driest seasons and years during the
 648 experimental period. There was a smaller contribution to the partition of the G in relation to
 649 net radiation. The G/R_n ratio during the dry season was the most expressive, with an average
 650 of 4%, while the other seasons were equal to or less than 2%. For each evaluated year and
 651 cactus cycle, the flux partitions were slightly similar, except for the LE/R_n of the first cycle,
 652 which was 122.13% higher than the LE/R_n of the second cycle.

653

654 Table 3. Partitions of radiation, energy and photosynthetic active radiation (PAR) during seasons (dry-wet transition, wet
 655 season, wet-dry transition, and dry season) and years (2019–2021) in cactus cultivation in the Brazilian semi-arid region.

Season / Year	SR_u/R_g	R_n/R_g	PAR/R_g	$fPAR$	LE/R_n	H/R_n	G/R_n
Dry-wet/2019	0.22	0.56	0.42	0.71	0.19	0.66	0.03
Wet/2019	0.20	0.61	0.42	0.66	0.39	0.48	0.02
Wet-dry/2019	0.18	0.60	0.42	0.70	0.36	0.51	0.003

Dry/2019	0.22	0.56	0.42	0.61	0.01	0.79	0.05
Dry-wet/2020	0.19	0.60	0.40	0.55	0.26	0.54	0.01
Wet/2020	0.17	0.67	0.41	0.74	0.52	0.31	0.003
Wet-dry/2020	0.16	0.62	0.39	0.73	0.31	0.63	0.001
Dry/2020	0.17	0.60	0.40	0.61	0.06	0.82	0.03
Dry-wet/2021	0.18	0.59	0.40	0.66	0.11	0.61	0.02
Wet/2021	0.17	0.65	0.41	0.71	0.34	0.35	0.003
Wet-dry/2021	0.18	0.58	0.40	0.71	0.13	0.56	0.004
Dry/2021	0.18	0.56	0.41	0.68	0.02	0.74	0.02
Season							
Dry-wet	0.20	0.58	0.41	0.64	0.19	0.60	0.02
Wet	0.18	0.64	0.41	0.70	0.42	0.38	0.01
Wet-dry	0.17	0.60	0.41	0.71	0.27	0.56	0.003
Dry	0.19	0.57	0.41	0.63	0.03	0.78	0.04
Crop cycle							
1	0.19	0.61	0.41	0.70	0.35	0.51	0.01
2	0.18	0.59	0.40	0.66	0.16	0.58	0.01
Year							
2019	0.20	0.58	0.42	0.67	0.24	0.61	0.03
2020	0.17	0.62	0.40	0.66	0.29	0.57	0.01
2021	0.18	0.59	0.41	0.69	0.15	0.56	0.01
Annual mean	0.19	0.60	0.41	0.67	0.22	0.58	0.02

SR_u is the upward shortwave radiation, R_g is the global solar radiation, R_n is the net radiation, PAR is the photosynthetic active radiation, $fPAR$ is the fraction of PAR intercepted, LE is the latent heat flux, H is the sensible heat flux, and G is the soil heat flux.

656

657 3.6. Yield and efficiency responses in the use of biophysical resources

658 The average contribution of biomass, changes in morphophysiological rates, nutrient
659 and carbon stocks, and efficiency in the use of biophysical resources was calculated for each
660 season, cycle and year during the experimental period in *Opuntia* cactus cultivation (Table
661 4). We found higher values of dry biomass during wet seasons (i.e., wet and wet-dry
662 transition) reaching 356–361 g m⁻². The cactus clearly increased its CAI during the wet-dry
663 transition season, with an average growth of 1.14 m² m⁻² and average values reaching 0.88
664 to 1.37 m² m⁻². Although the cactus maintained a high CAI during the dry season, it was
665 13.31% lower in relation to the wet-dry transition. The net assimilation rate (NAR) showed
666 higher values during the dry-wet transition, and 2019 was the most expressive year for net
667 photosynthesis; consequently, the relative growth rate (RGR) was higher during this period.
668 On the other hand, the specific cladode area (SCA) was higher during the wet-dry transition
669 (0.001 m² g⁻¹) and dry season (0.001 m² g⁻¹), with the dry-wet transition having the lowest

670 cactus response to SCA (mean 0.0003 m² g⁻¹). For the first cycle, the cactus was more
 671 productive and slightly similar in terms of cladode and morphophysiological characteristics.

672

673 Table 4. Biomass, morphophysiological index and growth rate, stocks and efficiencies of nutrients, water and radiation in
 674 cacti cultivation in the Brazilian semi-arid region.

Season / Year	Stock											NUE						WUE	RUE	
	biomass	CAI	NAR	RGR	SCA	N	P	K ⁺	Ca ²⁺	Mg ²⁺	C	N	P	K ⁺	Ca ²⁺	Mg ²⁺	C			
	g m ⁻²	m ²	g m ⁻² day ⁻¹	g g ⁻¹ day ⁻¹	m ² g ⁻¹	g m ⁻²						mg m ⁻² mm ⁻¹								μg m ⁻² mm ⁻¹
Dry-wet/2019	245	0.79	91	0.004	0.0003	2.9	0.8	4.8	12.7	10.2	84	60	18	100	264	211	1738	5.09	0.89	
Wet/2019	895	0.37	120	0.006	0.0001	10.6	3.1	17.6	46.3	37.1	306	62	18	104	274	220	1809	5.30	2.24	
Wet-dry/2019	978	0.88	11	0.003	0.0003	11.5	3.4	19.2	50.7	40.6	334	65	19	108	285	229	1881	5.51	1.71	
Dry/2019	84	1.17	1	0.001	0.0004	1.0	0.3	1.7	4.4	3.5	29	359	105	597	1576	1263	10393	30.43	0.47	
Dry-wet/2020	450	0.07	80	0.007	0.0001	5.3	1.6	8.8	23.3	18.7	154	49	14	82	217	174	1428	4.18	1.57	
Wet/2020	28	1.17	0.2	0.0001	0.0004	0.3	0.1	0.6	1.5	1.2	10	1	0.3	2	4	3	27	0.08	0.04	
Wet-dry/2020	2	1.17	0.03	0.00001	0.0004	0.0	0.0	0.0	0.1	0.1	1	0.4	0.1	1	2	2	13	0.04	0.01	
Dry/2020	221	0.42	59	0.007	0.0002	2.6	0.8	4.3	11.5	9.2	76	181	53	300	793	635	5229	15.31	0.83	
Dry-wet/2021	200	0.75	9	0.002	0.0006	2.4	0.7	3.9	10.4	8.3	68	58	17	97	256	205	1688	4.94	0.63	
Wet/2021	145	1.20	2	0.001	0.0009	1.7	0.5	2.8	7.5	6.0	49	12	3	19	51	41	334	0.98	0.37	
Wet-dry/2021	102	1.37	1	0.001	0.0010	1.2	0.4	2.0	5.3	4.2	35	29	9	49	129	104	853	2.50	0.32	
Dry/2021	25	1.38	0.2	0.0002	0.0009	0.3	0.1	0.5	1.3	1.0	8	57	17	95	249	200	1645	4.82	0.07	
Season																				
Dry-wet	299	0.54	60	0.004	0.0003	3.5	1.0	5.9	15.5	12.4	102	54	16	90	236	189	1558	4.56	1.02	
Wet	356	0.91	41	0.002	0.0005	4.2	1.2	7.0	18.4	14.8	122	18	5	31	81	65	535	1.57	0.74	
Wet-dry	361	1.14	4	0.001	0.001	4.3	1.2	7.1	18.7	15.0	123	48	14	80	211	169	1392	4.08	1.02	
Dry	110	0.99	20	0.002	0.001	1.3	0.4	2.2	5.7	4.6	38	174	51	290	765	613	5046	14.77	0.41	
Crop cycle																				
1	2233	0.92	33	0.0020	0.0003	26.3	7.7	43.8	115.7	92.7	763	32	9	53	141	113	931	2.73	0.96	
2	1143	0.88	24	0.0029	0.0006	13.5	3.9	22.4	59.2	47.5	391	39	11	65	171	137	1126	3.30	0.61	
Year																				
2019	2203	0.80	56	0.003	0.0003	6.5	1.9	10.8	28.5	22.9	752	16	5	27	72	57	1892	5.54	6.17	
2020	702	0.71	35	0.003	0.0003	2.1	0.6	3.4	9.1	7.3	240	4	1	6	17	14	449	1.31	2.06	
2021	472	1.18	3	0.001	0.001	1.4	0.4	2.3	6.1	4.9	161	6	2	10	26	21	687	2.01	1.36	
Annual mean	1126	0.90	31	0.003	0.0005	3.3	1.0	5.5	14.6	11.7	384	8.7	2.6	14.5	38.3	30.7	1010	2.96	3.19	

NUE is the nutrient use efficiency (mg m⁻² mm⁻¹), CAI is the cladode area index (m² m⁻²), NAR is the net assimilation rate (g m⁻² day⁻¹), RGR is the relative growth rate (g g⁻¹ day⁻¹), SCA is the specific cladode area (m² g⁻¹), WUE is the water use efficiency (g m⁻² mm⁻¹), and RUE is the radiation use efficiency (g m⁻²).

675

676 The cactus had higher nutrient and carbon stocks during the wet season and wet-dry
 677 transition (Table 4). The dry-wet transition season was generally the third season with the
 678 best performance of nutrient and carbon stocks, making it clear that the lowest stock
 679 performances occurred in the dry season. Our results highlighted a lower efficiency of
 680 nutrients, carbon, and water and radiation use when cacti were exposed to more wet periods,
 681 i.e., during the dry-wet, wet-dry, and wet season transitions smaller ones (ranked by
 682 decreasing order). In contrast, the dry and wet seasons showed higher and lower efficiency
 683 in the use of nutrients and water, respectively. However, the wet season was 81.48% higher
 684 than the dry season for radiation use efficiency (RUE) data. Furthermore, the RUE of the

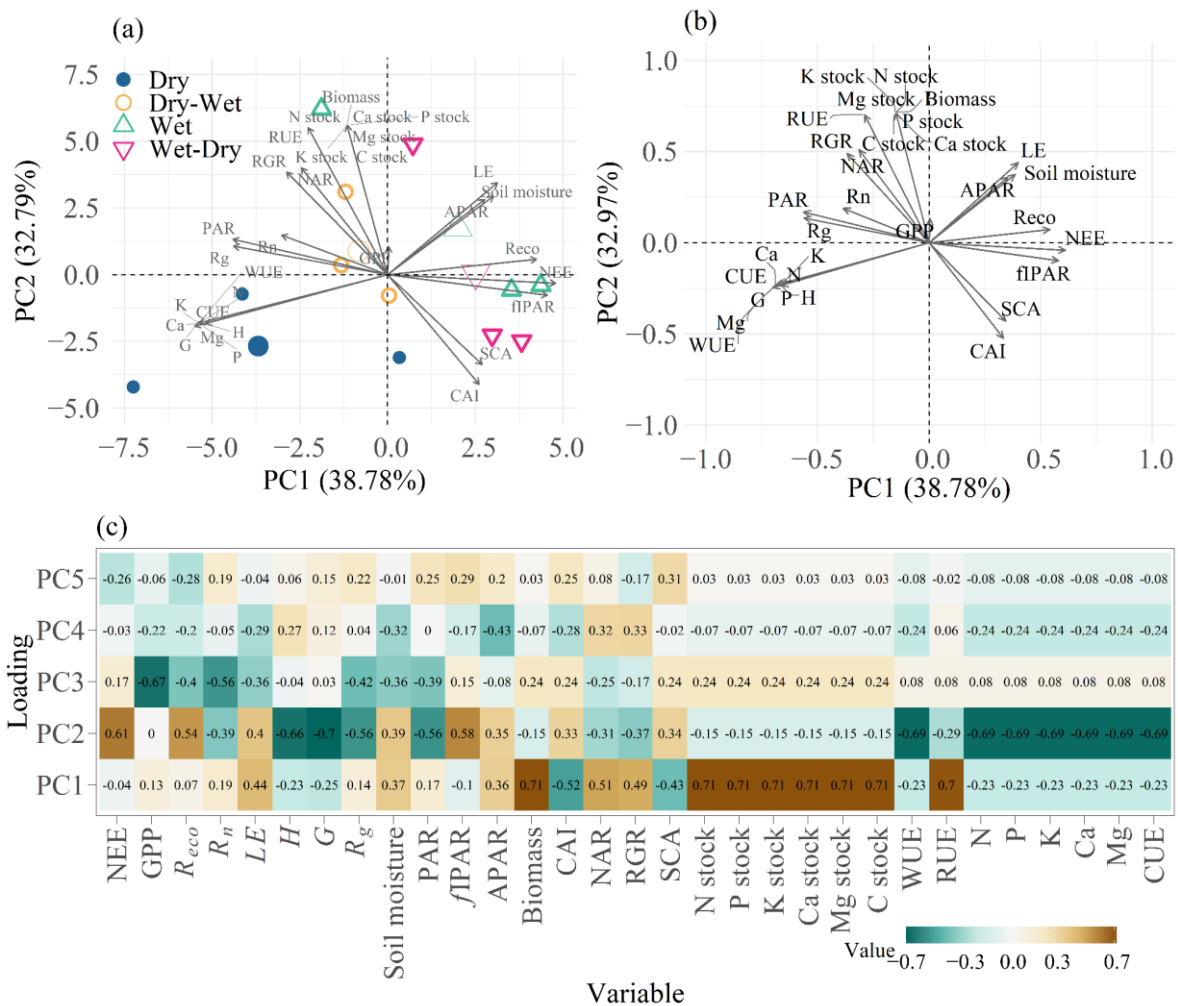
685 dry-wet and wet-dry transition seasons was the same, averaging 1.02 g MJ^{-1} . We found that
686 in cactus plants with high dry biomass and values of nitrogen and carbon stocks, their
687 efficiency in the use of radiation is maximized, and the inverse condition is true as seen in
688 the first (higher) and second (lower) crop cycles.

689

690 3.7. *Principal component analysis*

691 Figure 9 shows the principal component analysis (PCA) of the measured environment
692 and cactus variables to examine their interactions within a multivariate space. For
693 visualization purposes, the biplots generated in the PCA focus on the first two components
694 (Figure 9a–b), although five principal components have presented eigenvalues greater than
695 1.0 when we use the Kaiser criterion (Kaiser, 1960) (Figure 9c). Principal component score
696 plots depict the characteristics of stations and help you understand their dispersion pattern
697 for variables. The variance explained by the first two components was 71.57%, with 38.78%
698 explained by principal component 1 (PC1), while 32.79% was explained by principal
699 component 2 (PC2). In the season score plot (Figure 9a), our results show a clear dispersion
700 between the dry seasons (i.e., dry and dry-wet) presented on the left side of the biplot and
701 wet seasons (i.e., wet and wet-dry) projected on the right side. Here, the loading plots display
702 the relationships between the analyzed variables, with loadings ranging between principal
703 components from -0.70 to 0.71 (Figure 9b–c).

704



705

706 Figure 9. Principal component analysis (PCA) shows the relationship between environmental
 707 and cactus plant variables. The panels show (a) season score variation along the first (PC1)
 708 and second (PC2) principal components, (b) variable loadings on the first two axes, and (c)
 709 component matrix with loading factors for each variable in the first five principal components
 710 with an eigenvalue greater than 1.0. For full variable names, see the Material and Methods
 711 section. The variables N, P, K, Ca and Mg mentioned represent the efficiency in the use of
 712 these nutrients. The symbols denote the four seasons (dry season, dry-wet transition, wet
 713 season and wet-dry transition) evaluated.

714

715 Figure 9b illustrates the variables that represent the nutrient-use efficiency (e.g., N,
 716 P, K, Ca, and Mg), water (WUE), and carbon (CUE) indicate that low loadings are found in
 717 PC1 (0.23), and high loadings are found in PC2 (0.69), with a high correlation with the dry
 718 season (see Figure 9c). Dry biomass, CAI, NAR, nutrient stocks, and RUE were the main

719 contributors to PC1 (presence of positive and negative loadings greater than 0.5). In contrast,
720 NEE, R_{eco} , H , G , R_g , PAR, $fIPAR$, WUE, and nutrient and carbon use efficiency mainly
721 contributed to the PC2 (positive and negative charge value ≥ 0.5). When presenting highly
722 correlated components, the environmental and plant variables pointed approximately in the
723 same direction. Furthermore, we observed that during the dry season, there was greater
724 expressiveness of the variables G and H (with loadings of -0.7 and -0.66 , respectively), with
725 both inserted in CP2. During the dry-wet transition season, the highest negative loadings
726 were grouped between the variables R_n (-0.39), R_g (-0.56), and PAR (-0.56) for PC2, and
727 positively in PC1 at variables RGR, NAR, and RUE with loadings of 0.49, 0.51 and 0.7,
728 respectively (Figure 9b–c). An interesting finding was the similarity between the GPP of all
729 four seasons, explained by the proximity of the vector (variable) to the biplot's central axis.
730 In the wet and wet-dry transition seasons, we observed greater correlations (i.e., narrow
731 angles between vectors) between plant nutrient and carbon stocks, biomass, soil moisture,
732 LE , APAR, R_{eco} , NEE, $fIPAR$, SCA and CAI. The higher the soil moisture, the higher the
733 LE , APAR and R_{eco} during the wet season. Clearly, when the cactus had a high WUE (loading
734 of -0.69) in the dry season (entered in PC2), the R_{eco} was lower, and consequently the NEE
735 increased. The CAI and SCA variables were more expressive in the wet-dry transition season
736 since, in this same season, when CAI and SCA increased, there was a decrease in NAR and
737 RGR. This is because CAI and SCA have opposite relationships with NAR and RGR
738 promoting proportional positive and negative loadings on principal components.

739

740 **4. Discussion**

741 *4.1. Energy balance closure and overview of site environmental conditions*

742 One way to evaluate the performance of the data collected by the eddy covariance
743 system is through the degree of energy balance closure using linear regression (Baldochi et
744 al., 2000; Wilson et al., 2002). When the result of the ratio between turbulent fluxes and
745 available energy is equal to 1, the balance closure is perfect. However, several studies report
746 a classic lack of energy balance closure (EBC) on different vegetated surfaces (e.g., dry and
747 humid forests, cacti, and agricultural crops) when using the eddy covariance system (Campos
748 et al., 2019; Eshonkulov et al., 2019; Flanagan and Flanagan, 2018). This study found that
749 cactus vegetation under semi-arid conditions displayed an EBC of 0.71; therefore, sensible

750 and latent heat flux underestimated the available energy by up to 29%. A 29% imbalance in
751 the vegetated surface may be a high value; however, it is not inconsistent (Grachev et al.,
752 2020) and may still be satisfactory (Wilson et al., 2002). Our EBC results are in line with the
753 findings of Campos et al. (2019) in Caatinga (mean of 0.7), in the Brazilian semi-arid region,
754 and lower than those reported by Owen et al. (2016) in *Agave* and *Opuntia* cultivation, in
755 Jalisco, semi-arid region of Mexico, with an average closure of 0.9. For example, San-José
756 et al. (2007) reported an energy imbalance of 0.9 for growing pineapple [*Ananas comosus*
757 (L.) Merr.] in Santa Barbara, Venezuela. Still, according to the cited authors, factors such as
758 short and homogeneous cultivation growing in a flat area and the absence of advection help
759 close the balance.

760 In some cases, incorporating variables such as the energy stored in the canopy and
761 energy from photosynthesis favors the improvement of the closure of the surface energy
762 balance (Eshonkulov et al., 2019; Kutikoff et al., 2019). This adjustment can benefit the
763 accuracy of the method, increasing the slope of the line and leaving the intercept close to
764 zero (Campos et al., 2019; Kutikoff et al., 2019) when it is not forced to such a value. We
765 believe that variations in seasons (dry season, dry-wet transition, wet season, and wet-dry
766 transition), such as periods of greater and lesser rainfall events, may have caused an
767 imbalance in the EBC (Chatterjee et al., 2021). Furthermore, we assume that the architecture
768 of the cactus canopy, which does not completely cover the ground due to the cladodes'
769 position and the two harvests carried out, may have caused changes in the turbulent energy
770 exchange.

771 The effects of weather conditions on *Opuntia* cactus cultivation were explored in this
772 study (Figure 3). Our results indicate high air temperature, high VPD, and low relative
773 humidity over the years. Classically, this type of evidence is common in places with a semi-
774 arid climate due to poor environmental conditions (Flanagan and Flanagan, 2018). Although
775 these conditions can cause problems with some species' performance, cacti develop well in
776 hostile and high-temperature conditions (Nobel and De La Barrera, 2003; Ojeda-Pérez et al.,
777 2017; Zutta et al., 2011). During the months with higher rainfall events, there was a
778 significant decrease in wind speed and VPD due to the thermal cooling of the environment
779 caused by the entry of water into the system, consequently contributing to higher soil
780 moisture. Decreased wind speed may cause instability of turbulent fluxes, and thus, this could

781 be a hypothesis for lower energy balance closure (Flanagan and Flanagan, 2018; Teng et al.,
782 2021). Plants can help cool the environment through transpiration and the soil through
783 evaporation when there is high soil moisture and favorable air temperature. Furthermore,
784 Pimienta-Barrios et al. (2000) stated that decreasing air temperature ($< 29\text{ }^{\circ}\text{C}$) and increasing
785 soil moisture provide improvements in CO_2 uptake for the *Opuntia ficus-indica* cactus. On
786 the other hand, when temperatures are very low, photosynthesis is inhibited in *Opuntia stricta*
787 (Barker et al., 1998; Ojeda-Pérez et al., 2017).

788 The highest input of R_g in the crop was followed by a high PAR over the months, and
789 the reduction in R_g automatically caused a decrease in PAR (Figure 3 and Figure 4). The
790 photosynthetically active radiation intercepted by the canopy helps to understand the
791 photosynthetic processes of plants, although meteorological conditions and the phenological
792 phase of the species can influence this characteristic (Cortázar and Nobel, 1986; Hartzell et
793 al., 2021; Ma et al., 2021). Cortázar and Nobel (1986) reported that PAR limitations can
794 significantly compromise the performance of *Opuntia ficus-indica*. This is because
795 cloudiness decreases the intensity of PAR and causes a reduction in the photosynthetic
796 efficiency of *Opuntia* (Geller and Nobel, 1987; Pimienta-Barrios et al., 2000). In addition,
797 several species of *Opuntia* cacti may undergo changes in morphology due to the anisotropic
798 characteristics of PAR (Drezner, 2020; Geller and Nobel, 1987). In the present study, periods
799 with high R_g and PAR also presented significant rainfall events, which favored the
800 photosynthetic activity of the cactus and light interception. Even with water restriction, cacti
801 maintain their cells turgid because the cladodes compensate for a prolonged period of low
802 water availability in the environment (Pimienta-Barrios et al., 2000; Scalisi et al., 2016).

803

804 4.2. Changes in the balance of carbon, energy, and radiation

805 Our results revealed that the climatic conditions of the wet-dry transition season alter
806 the biophysical factors and result in more abrupt changes in the carbon balance (Figure 4 and
807 Figure 6). Due to the lower PAR magnitude during the wet-dry transition season, carbon
808 uptake by plants was lower, limiting CO_2 sequestration (Nobel and Bobich, 2002). Still,
809 cactus cultivation showed strong potential for carbon sequestration, a crucial component of
810 the carbon cycle in arid environments (Figure 5 and Figure 6). These results lead us to believe
811 that PAR is an important modulating indicator of carbon uptake by cacti. Guevara-Escobar

812 et al. (2021) also observed positive results for NEE at night, despite the ecosystem being
813 composed of cacti. Our results are slightly similar to those found by Guevara-Escobar et al.
814 (2021), although we found higher magnitudes (NEE greater than $-10 \mu\text{mol m}^{-2} \text{s}^{-1}$) around
815 noon. Furthermore, cacti do not shed their leaves (cladodes) like some forest species, and
816 thus the NEE is maintained higher (more negative) for longer periods (Guevara-Escobar et
817 al., 2021).

818 The release of carbon from R_{eco} was not as high (Figure 4 and Figure 5), with NEE
819 much higher. This carbon loss may be linked to the growth and maintenance of roots, as well
820 as respiration by organisms in the soil (Bilderback et al., 2021; De León-González et al.,
821 2018; Nobel and Bobich, 2002). On the other hand, we found significant R_{eco} during the wet
822 season (Figure 4), which supports that rainfall stimulates the rate of heterotrophic respiration
823 and can often equal or exceed photosynthesis daily or even seasonally (Del Grosso et al.,
824 2018; Flores-Rentería et al., 2023). The cactus has small caliber roots—called “rain roots”
825 that are fast growing and specialized in water absorption (Camelo et al., 2021; Hassan et al.,
826 2019); we believe that they may have caused greater respiration during the period with higher
827 soil moisture. Snyman (2006) reported that cactus rain roots are short-lived in plants, and
828 their decomposition contributes to microbial activity and increased soil respiration. Studying
829 cacti of the genus *Opuntia*, Dubeux Junior et al. (2013) found that at a density of 20,000
830 plants per ha, a cactus plant produces 136 g of root biomass, which contributes to the
831 heterotrophic respiration fraction and increases ecosystem respiration. Clearly, on days
832 without rainfall, seasonal daytime carbon uptake exceeds respiration (Del Grosso et al., 2018;
833 Flores-Rentería et al., 2023), and even with low rainfall events (~ 2 mm), microbial
834 respiration in a semi-arid environment responds quickly (Huxman et al., 2004). GPP may
835 decrease during the dry season (Flores-Rentería et al., 2023); however, in the present study,
836 R_{eco} was more sensitive than GPP at the same time (Figure 4 and Figure 6). The expressive
837 behavior of the cactus sink can be explained because it is a perennial plant, and, together with
838 the CAM pathway and the presence of humidity in the environment, its carbon absorption is
839 maximized during the seasons, whether in dry or wet periods.

840 Solar radiation makes an important contribution to stimulating photosynthesis for
841 plants, and by carrying out photosynthesis, ecosystems' carbon and water exchange processes
842 are driven (Flanagan and Flanagan, 2018; Nobel, 1980). On the other hand, inadequate water

843 and solar radiation availability can negatively influence plants' photosynthetic efficiency and
844 cause photochemical damage (Han et al., 2020; Jardim et al., 2021a). In this study, energy
845 and radiation balances were affected by environmental conditions and the time of year.
846 According to Gao et al. (2022), the short upward radiation is mainly controlled by the short
847 downward radiation and is influenced by ground cover. Factors such as surface temperatures
848 control the daily and seasonal variations of the long descending and ascending radiation,
849 influenced mainly by air temperature and humidity. Here, we found that lower availability of
850 R_g and R_n influenced the carbon balance and decreased G , SR_u , LR_u and LR_d . Wettest seasons
851 promoted higher LE and lower H , while transition seasons, as expected, presented
852 intermediate fluxes to extremely dry and wet seasons. In the rainy period, LE increases
853 rapidly due to the availability of water and energy, which increases ET and water vapor
854 exchange (J. Ma et al., 2022; Kuiyue Zhang et al., 2022). Although high LE values can be
855 reached in rainy periods, the cactus still uses a substantial part of the net radiation for sensible
856 heat flux (Unland et al., 1996).

857 During the two evaluated cycles, the cactus vegetation showed little variation in the
858 radiation and energy budgets. In the energy balance, the variables most responsive to rainfall,
859 such as latent and soil heat fluxes, showed greater discrepancies (Table 2). In terms of
860 sensible heat flux, despite the expressive cumulative difference in rainfall, the mean
861 difference in sensible heat flux ($0.8 \text{ MJ m}^{-2} \text{ day}^{-1}$) for the two cropping cycles (Table 2) may
862 be due to the greater use of net radiation in H (Unland et al., 1996). Regarding the temporal
863 variability of the carbon balance, we found greater carbon accumulations during the cactus's
864 first cycle because the plants had higher productivity. Even in the first cycle, ET was higher
865 due to higher rainfall (2,075 mm) and higher GPP ($6.8 \text{ g C m}^{-2} \text{ day}^{-1}$). Although biological
866 and abiotic factors may influence plant performance (Jardim et al., 2021a; Roeber et al.,
867 2021), our findings clarify that the *Opuntia* cactus had a high carbon sink capacity throughout
868 the experimental period. This clearly agrees with the capacity for efficient use of water and
869 carbon that CAM plants possess (H. Ma et al., 2022; Pikart et al., 2018).

870

871 4.3. Flux partitioning and efficiency in the use of biophysical resources in cactus cultivation

872 In the present study, we show that the components of radiation, energy balances, and
873 PAR can be affected by environmental conditions and plant characteristics (Table 3). This

874 occurs due to the interaction of the balance components and the surface. We believe that the
875 lower responses of the SR_u/R_g ratio during the wet-dry transition season may be related to the
876 higher CAI and SCA (Table 4) since the short upward radiation is influenced by the land
877 cover (Gao et al., 2022) due to greater absorption of radiation by the canopy (Braghiere et
878 al., 2020). In our cactus plants, no phenological phase changes were observed, with only the
879 vegetative phase nor cladode senescence, which justifies the high similarity of the PAR/R_g
880 ratio results (Baldocchi et al., 1984). In addition, PAR/R_g measurements were always
881 performed at the same depth of the canopy (i.e., at the top of the canopy) since, as one
882 approaches the ground, the PAR/R_g ratio may decrease (Baldocchi et al., 1984). Due to the
883 plants being more developed during the wet season and wet-dry transition, as a result of the
884 higher CAI and SCA, this development was crucial for better intercepted PAR fraction
885 ($fIPAR$) responses. In the same period, the plants had a higher dry biomass yield, which
886 shows the close relationship of $fIPAR$ with the photosynthetic activity of plants (Li et al.,
887 2021; Nobel, 1980).

888 When the environmental deficit is high, plants can decrease the LE/R_n ratio through
889 physiological controls, reducing water loss to the atmosphere (Yue et al., 2019). On the other
890 hand, the LE reduction caused an increase in H , with 78% of the R_n being converted into H
891 during the dry season. According to Campos et al. (2019) and Costa et al. (2022), in the dry
892 forest (Caatinga) in the Brazilian semi-arid region, approximately 70% of R_n was converted
893 into H , and less than 5% was converted into LE during the dry season, and these results are
894 consistent with our study. Similar to dry forests, environments with cacti are marked by high
895 fluxes of sensible heat in relation to latent heat fluxes; this was also observed by Pierini et al.
896 (2014) in a landscape of cacti (*Opuntia spinisior* and *Opuntia engelmannii*) in the semi-arid
897 region of Tucson, Arizona. Despite being influenced by the H , the G/R_n ratio was equal to or
898 less than 4%, and this ratio may change due to rainfall events and radiation incidence in
899 cactus cultivation (Consoli et al., 2013; Flanagan and Flanagan, 2018). Flanagan and
900 Flanagan (2018) found a mean of $2.0 \text{ MJ m}^{-2} \text{ day}^{-1}$ for G , explaining the low flux values of
901 this variable.

902 Our results indicate a strong relationship between environmental conditions in
903 response to growth, nutrient, and carbon stocks in *Opuntia* cactus plants (Table 4). Despite
904 the expressive adaptability of *Opuntia* cactus, it has a slow relative growth rate (Luo and

905 Nobel, 1993; Martínez-Berdeja and Valverde, 2008). Although slow but not low, the rates
906 that express plant growth and net carbon assimilation have greater relevance in periods with
907 lower humidity. A likely explanation is that because these plants are adapted to conditions
908 with less rainfall, their response is less expressive in high rainfall (Jardim et al., 2021b).
909 Regarding stored nutrients and carbon in the cladodes, cacti have a significant accumulation
910 of calcium, potassium, and magnesium, being important forage foods (Garcia et al., 2021;
911 Mayer and Cushman, 2019). Potassium, for example, helps regulate the osmotic potential of
912 cells, decreasing water loss and consequently increasing WUE and photochemistry (Mostofa
913 et al., 2022). This supports our satisfactory WUE and RUE results, with the RUE being more
914 sensitive to conditions with lower water availability. In addition, cacti can store carbon very
915 similar to forest ecosystems (De León-González et al., 2018), which maximizes their
916 exploitation potential in areas with low resource availability.

917

918 *4.4. Relations between variables and environment*

919 The results presented in Figure 9 highlighted the distinct associations between
920 environmental and plant variables under the four seasons. Clearly, the factor loadings in the
921 PCA revealed the most important variables and their grouping in relation to environmental
922 water availability (Mounir et al., 2020). Although the five principal components were
923 significant, the first two principal components were fundamental for the best visualization of
924 the biplot and explained 71.57% of the data variation. Using PCA, Juhász et al. (2020) and
925 Mounir et al. (2020) reported dispersions between seasons and the analyzed plant variables.
926 There is a correlation between the efficiency of the use of water, nutrients, and carbon during
927 the dry season due to the CAM pathway the plants have. In addition to their high WUE and
928 CUE values, the nutrients boost the osmotic effect of their cells, making the best use even
929 easier of these resources and, therefore, the best use of carbon as well (H. Ma et al., 2022;
930 Nobel and Bobich, 2002). The cladode and plant biomass variables were included in PC1, in
931 agreement with the findings of Jardim et al. (2020) and Jardim et al. (2021a), using cactus
932 species of the genus *Opuntia* and *Nopalea*. A high CAI value in cactus plants is an important
933 indicator of the high biomass yield of the crop (Dubeux Jr. et al., 2006; Jardim et al., 2021a,
934 2020). In the wet seasons, the variables (biplot vectors) R_{eco} and NEE point in the same
935 direction and with parallel vectors (Figure 9); this shows that in the wet period, there was

936 greater ecosystem respiration (positive) and lower (less negative) NEE. In this way, the
937 cultivation of *Opuntia* cactus proved to be an important atmospheric CO₂ sink during the dry
938 season, with higher (more negative) NEE results, a behavior also observed by Mendes et al.
939 (2020) in dry forests (Caatinga). Bilderback et al. (2021) also reported higher carbon losses
940 in an environment with cacti (e.g., *Opuntia chlorotica* and *Cylindropuntia acanthocarpa*) in
941 the rainy season in the Sonoran Desert of Arizona. In addition, research shows that moisture
942 and radiation conditions can change the behavior of the energy balance and carbon flux in a
943 cactus ecosystem (Camelo et al., 2021; Flanagan and Flanagan, 2018; Guevara-Escobar et
944 al., 2021; Jardim et al., 2022).

945

946 **5. Conclusions**

947 We analyzed eddy flux covariance data over three years (2019–2021) in a cactus crop,
948 observing the behavior of carbon, energy, and radiation balance. This work shows that on a
949 surface cultivated with the cactus *Opuntia stricta*, the energy balance closure using data from
950 the eddy covariance system reached satisfactory results (71%). We found that the cactus is a
951 potential carbon sink throughout the year, with net ecosystem CO₂ exchange cumulative in
952 three years of $-4,517 \text{ g C m}^{-2}$; thus, it can be an important alternative for revitalizing
953 degraded areas of the semi-arid region. Regardless of the season and adverse weather
954 conditions, the cactus persisted with net CO₂ sequestration, being an important carbon sink.
955 The cumulative (2019–2021) gross primary production and ecosystem respiration averaged
956 2352 g C m^{-2} and 846 g C m^{-2} , respectively. In addition, the rainfall, despite having increased
957 the release of CO₂ from the environment, did not transform the semi-arid ecosystem of cacti
958 into a source of carbon. Meteorological conditions act as the main drivers of physiological
959 adjustments and plant growth. Our analyses revealed that the latent and sensible heat fluxes
960 had marked seasonality, with most of the net radiation energy used in the sensible heat flux
961 (58% ratio), with an annual average of $5.8 \text{ MJ m}^{-2} \text{ day}^{-1}$. We found a substantial amount of
962 nutrients in the cactus biomass and high efficiency in the use of water and nutrients during
963 the dry seasons. Particularly, the findings presented here bring news in studies with CAM
964 plants and can help in the better use of agricultural land or places where agricultural and
965 forest species may have a low capacity to develop and obtain a better balance of terrestrial
966 carbon.

967

968 **Acknowledgments**

969 We thank the Research Support Foundation of the State of Pernambuco (FACEPE -
970 APQ-0300-5.03/17, APQ-0215-5.01/10 and APQ-1159-1.07/14) and the National Council
971 for Scientific and Technological Development (CNPq - 152251/2018-9) for their financial
972 support. This study had also the support of Portuguese funds through Fundação para a Ciência
973 e Tecnologia, I. P (FCT), under the projects UIDB/04292/2020, UIDP/04292/2020, granted
974 to MARE, and LA/P/0069/2020, granted to the Associate Laboratory ARNET. We also are
975 grateful to the São Paulo Research Foundation (FAPESP, 2017/22269-2), FACEPE and
976 Coordination for the Improvement of Higher Education Personnel (CAPES - Finance Code
977 001) for the research and study grants.

978

979 **References**

- 980 Adamič, S., Leskovšek, R., 2021. Soybean (*Glycine max* (L.) Merr.) Growth, Yield, and
981 Nodulation in the Early Transition Period from Conventional Tillage to Conservation
982 and No-Tillage Systems. *Agronomy* 11, 2477.
983 <https://doi.org/10.3390/AGRONOMY11122477>
- 984 Anapalli, S.S., Fisher, D.K., Reddy, K.N., Krutz, J.L., Pinnamaneni, S.R., Sui, R., 2019.
985 Quantifying water and CO₂ fluxes and water use efficiencies across irrigated C₃ and C₄
986 crops in a humid climate. *Sci. Total Environ.* 663, 338–350.
987 <https://doi.org/10.1016/J.SCITOTENV.2018.12.471>
- 988 Baldocchi, D., Hutchison, B., Matt, D., McMillen, R., 1984. Seasonal variations in the
989 radiation regime within an oak-hickory forest. *Agric. For. Meteorol.* 33, 177–191.
990 [https://doi.org/10.1016/0168-1923\(84\)90069-8](https://doi.org/10.1016/0168-1923(84)90069-8)
- 991 Baldocchi, D.D., Law, B.E., Anthoni, P.M., 2000. On measuring and modeling energy fluxes
992 above the floor of a homogeneous and heterogeneous conifer forest. *Agric. For.*
993 *Meteorol.* 102, 187–206. [https://doi.org/10.1016/S0168-1923\(00\)00098-8](https://doi.org/10.1016/S0168-1923(00)00098-8)
- 994 Barker, D.H., Logan, B.A., Adams, W.W., Demmig-Adams, B., 1998. Photochemistry and
995 xanthophyll cycle-dependent energy dissipation in differently oriented cladodes of
996 *Opuntia stricta* during the winter. *Funct. Plant Biol.* 25, 95–104.
997 <https://doi.org/10.1071/PP97106>

998 Beck, H.E., Zimmermann, N.E., McVicar, T.R., Vergopolan, N., Berg, A., Wood, E.F., 2018.
999 Present and future Köppen-Geiger climate classification maps at 1-km resolution. *Sci.*
1000 *Data* 5, 180214. <https://doi.org/10.1038/sdata.2018.214>

1001 Bilderback, A.H., Torres, A.J., Vega, M., Ball, B.A., 2021. The structural and nutrient
1002 chemistry during early-stage decomposition and desiccation of cacti in the Sonoran
1003 Desert. *J. Arid Environ.* 195, 104636.
1004 <https://doi.org/10.1016/J.JARIDENV.2021.104636>

1005 Braghieri, R.K., Quaife, T., Black, E., Ryu, Y., Chen, Q., De Kauwe, M.G., Baldocchi, D.,
1006 2020. Influence of sun zenith angle on canopy clumping and the resulting impacts on
1007 photosynthesis. *Agric. For. Meteorol.* 291, 108065.
1008 <https://doi.org/10.1016/J.AGRFORMET.2020.108065>

1009 Camelo, D., Dubeux Jr, J.C.B., Santos, M.V.F. dos, Lira, M.A., Fracetto, G.G.M., Fracetto,
1010 F.J.C., Cunha, M.V. da, Freitas, E.V. de, 2021. Soil Microbial Activity and Biomass in
1011 Semiarid Agroforestry Systems Integrating Forage Cactus and Tree Legumes.
1012 *Agronomy* 11, 1558. <https://doi.org/10.3390/AGRONOMY11081558>

1013 Campos, S., Mendes, K.R., da Silva, L.L., Mutti, P.R., Medeiros, S.S., Amorim, L.B., dos
1014 Santos, C.A.C., Perez-Marin, A.M., Ramos, T.M., Marques, T. V., Lucio, P.S., Costa,
1015 G.B., Santos e Silva, C.M., Bezerra, B.G., 2019. Closure and partitioning of the energy
1016 balance in a preserved area of a Brazilian seasonally dry tropical forest. *Agric. For.*
1017 *Meteorol.* 271, 398–412. <https://doi.org/10.1016/J.AGRFORMET.2019.03.018>

1018 Chatterjee, D., Kumar Swain, C., Chatterjee, S., Bhattacharyya, P., Tripathi, R., Lal, B.,
1019 Gautam, P., Shahid, M., Kumar Dash, P., Dhal, B., Kumar Nayak, A., Chatterjee, D.,
1020 Kumar Swain, C., Chatterjee, S., Bhattacharyya, P., Tripathi, R., Lal, B., Gautam, P.,
1021 Shahid, M., Kumar Dash, P., Dhal, B., Kumar Nayak, A., 2021. Is the energy balance
1022 in a tropical lowland rice paddy perfectly closed? *Atmósfera* 34, 59–78.
1023 <https://doi.org/10.20937/ATM.52734>

1024 Consoli, S., Inglese, G., Inglese, P., 2013. Determination of Evapotranspiration and Annual
1025 Biomass Productivity of a Cactus Pear [*Opuntia ficus-indica* L. (Mill.)] Orchard in a
1026 Semiarid Environment. *J. Irrig. Drain. Eng.* 139, 680–690.
1027 [https://doi.org/10.1061/\(ASCE\)IR.1943-4774.0000589](https://doi.org/10.1061/(ASCE)IR.1943-4774.0000589)

1028 Cortázar, V.G. de, Nobel, P.S., 1986. Modeling of PAR Interception and Productivity of a

1029 Prickly Pear Cactus, *Opuntia ficus-indica* L., at Various Spacings1. *Agron. J.* 78, 80–
1030 85. <https://doi.org/10.2134/AGRONJ1986.00021962007800010018X>

1031 Costa, G.B., Mendes, K.R., Viana, L.B., Almeida, G.V., Mutti, P.R., Silva, C.M.S., Bezerra,
1032 B.G., Marques, T.V., Ferreira, R.R., Oliveira, C.P., Gonçalves, W.A., Oliveira, P.E.,
1033 Campos, S., Andrade, M.U.G., Antonino, A.C.D., Menezes, R.S.C., 2022. Seasonal
1034 Ecosystem Productivity in a Seasonally Dry Tropical Forest (Caatinga) Using Flux
1035 Tower Measurements and Remote Sensing Data. *Remote Sens.* 14, 3955.
1036 <https://doi.org/10.3390/RS14163955>

1037 Cunliffe, A.M., Boschetti, F., Clement, R., Sitch, S., Anderson, K., Duman, T., Zhu, S.,
1038 Schlumpf, M., Litvak, M.E., Brazier, R.E., Hill, T.C., 2022. Strong Correspondence in
1039 Evapotranspiration and Carbon Dioxide Fluxes Between Different Eddy Covariance
1040 Systems Enables Quantification of Landscape Heterogeneity in Dryland Fluxes. *J.*
1041 *Geophys. Res. Biogeosciences* 127, e2021JG006240.
1042 <https://doi.org/10.1029/2021JG006240>

1043 De León-González, F., Fuentes-Ponce, M.H., Bautista-Cruz, A., Leyva-Pablo, T., Castillo-
1044 Juárez, H., Rodríguez-Sánchez, L.M., 2018. Cactus crop as an option to reduce soil C–
1045 CO₂ emissions in soils with declining fertility. *Agron. Sustain. Dev.* 38, 1–10.
1046 <https://doi.org/10.1007/S13593-017-0481-3/TABLES/1>

1047 Del Grosso, S.J., Parton, W.J., Derner, J.D., Chen, M., Tucker, C.J., 2018. Simple models to
1048 predict grassland ecosystem C exchange and actual evapotranspiration using NDVI and
1049 environmental variables. *Agric. For. Meteorol.* 249, 1–10.
1050 <https://doi.org/10.1016/J.AGRFORMET.2017.11.007>

1051 Dhungel, R., Aiken, R., Evett, S.R., Colaizzi, P.D., Marek, G., Moorhead, J.E., Baumhardt,
1052 R.L., Brauer, D., Kutikoff, S., Lin, X., 2021. Energy Imbalance and Evapotranspiration
1053 Hysteresis Under an Advective Environment: Evidence From Lysimeter, Eddy
1054 Covariance, and Energy Balance Modeling. *Geophys. Res. Lett.* 48, e2020GL091203.
1055 <https://doi.org/10.1029/2020GL091203>

1056 Drezner, T.D., 2020. The importance of microenvironment: *Opuntia* plant growth, form and
1057 the response to sunlight. *J. Arid Environ.* 178, 104144.
1058 <https://doi.org/10.1016/J.JARIDENV.2020.104144>

1059 Du Toit, A., De Wit, M., Hugo, A., 2018. Cultivar and Harvest Month Influence the Nutrient

1060 Content of *Opuntia* spp. Cactus Pear Cladode Mucilage Extracts. *Molecules* 23, 916.
1061 <https://doi.org/10.3390/MOLECULES23040916>

1062 Dubeux Jr., J.C.B., dos Santos, M.V.F., Lira, M.A., dos Santos, D.C., Farias, I., Lima, L.E.,
1063 Ferreira, R.L.C., 2006. Productivity of *Opuntia ficus-indica* (L.) Miller under different
1064 N and P fertilization and plant population in north-east Brazil. *J. Arid Environ.* 67, 357–
1065 372. <https://doi.org/10.1016/J.JARIDENV.2006.02.015>

1066 Dubeux Junior, J.C.B., Silva, N.G.M., Santos, M.V.F., Cunha, M.V., Santos, D.C., Lira,
1067 M.A., Mello, A.C.L., Pinto, M.S.C., 2013. Organic fertilization and plant population
1068 affect shoot and root biomass of forage cactus pear (*Opuntia ficus-indica* Mill.). *Acta*
1069 *Hortic.* 995, 221–224. <https://doi.org/10.17660/ACTAHORTIC.2013.995.25>

1070 Eshonkulov, R., Poyda, A., Ingwersen, J., Pulatov, A., Streck, T., 2019. Improving the energy
1071 balance closure over a winter wheat field by accounting for minor storage terms. *Agric.*
1072 *For. Meteorol.* 264, 283–296. <https://doi.org/10.1016/J.AGRFORMET.2018.10.012>

1073 Flanagan, L.B., Flanagan, J.E.M., 2018. Seasonal controls on ecosystem-scale CO₂ and
1074 energy exchange in a Sonoran Desert characterized by the saguaro cactus (*Carnegiea*
1075 *gigantea*). *Oecologia* 187, 977–994. [https://doi.org/10.1007/S00442-018-4187-](https://doi.org/10.1007/S00442-018-4187-2)
1076 [2/FIGURES/10](https://doi.org/10.1007/S00442-018-4187-2)

1077 Flores-Rentería, D., Delgado-Balbuena, J., Campuzano, E.F., Curiel Yuste, J., 2023.
1078 Seasonal controlling factors of CO₂ exchange in a semiarid shrubland in the Chihuahuan
1079 Desert, Mexico. *Sci. Total Environ.* 858, 159918.
1080 <https://doi.org/10.1016/J.SCITOTENV.2022.159918>

1081 Gao, X., Du, Z., Yang, Q., Zhang, J., Li, Y., Wang, X., Gu, F., Hao, W., Yang, Z., Liu, D.,
1082 Chu, J., 2022. Energy partitioning and evapotranspiration in a black locust plantation
1083 on the Yellow River Delta, China. *J. For. Res.* 33, 1219–1232.
1084 <https://doi.org/10.1007/S11676-021-01376-Y>/FIGURES/7

1085 Garcia, C.V., Mello, A.C.L., Cunha, M.V. da, Silva, M. da C., Santos, D.C. dos, Santos,
1086 M.V.F., Dubeux Jr., J.C.B., Homem, B.G.C., 2021. Agronomic characteristics and
1087 nutritional value of cactus pear progenies. *Agron. J.* 113, 4721–4735.
1088 <https://doi.org/10.1002/AGJ2.20868>

1089 Geller, G.N., Nobel, P.S., 1987. Comparative Cactus Architecture and PAR Interception.
1090 *Am. J. Bot.* 74, 998–1005. <https://doi.org/10.1002/J.1537-2197.1987.TB08709.X>

1091 Grachev, A.A., Fairall, C.W., Blomquist, B.W., Fernando, H.J.S., Leo, L.S., Otárola-Bustos,
1092 S.F., Wilczak, J.M., McCaffrey, K.L., 2020. On the surface energy balance closure at
1093 different temporal scales. *Agric. For. Meteorol.* 281, 107823.
1094 <https://doi.org/10.1016/J.AGRFORMET.2019.107823>

1095 Guevara-Escobar, A., González-Sosa, E., Cervantes-Jimenez, M., Suzán-Azpiri, H.,
1096 Queijeiro-Bolanos, M.E., Carrillo-Ángeles, I., Cambron-Sandoval, V.H., 2021.
1097 Machine learning estimates of eddy covariance carbon flux in a scrub in the Mexican
1098 highland. *Biogeosciences* 18, 367–392. <https://doi.org/10.5194/BG-18-367-2021>

1099 Han, J., Guo, C., Ye, S., Zhang, L., Li, S., Wang, H., Yu, G., 2020. Effects of diffuse
1100 photosynthetically active radiation on gross primary productivity in a subtropical
1101 coniferous plantation vary in different timescales. *Ecol. Indic.* 115, 106403.
1102 <https://doi.org/10.1016/J.ECOLIND.2020.106403>

1103 Hartzell, S., Bartlett, M.S., Inglese, P., Consoli, S., Yin, J., Porporato, A., 2021. Modelling
1104 nonlinear dynamics of Crassulacean acid metabolism productivity and water use for
1105 global predictions. *Plant. Cell Environ.* 44, 34–48. <https://doi.org/10.1111/PCE.13918>

1106 Hassan, S., Inglese, P., Gristina, L., Liguori, G., Novara, A., Louhaichi, M., Sortino, G.,
1107 2019. Root growth and soil carbon turnover in *Opuntia ficus-indica* as affected by soil
1108 volume availability. *Eur. J. Agron.* 105, 104–110.
1109 <https://doi.org/10.1016/J.EJA.2019.02.012>

1110 Huxman, T.E., Snyder, K.A., Tissue, D., Leffler, A.J., Ogle, K., Pockman, W.T., Sandquist,
1111 D.R., Potts, D.L., Schwinning, S., 2004. Precipitation pulses and carbon fluxes in
1112 semiarid and arid ecosystems. *Oecologia* 141, 254–268.
1113 <https://doi.org/10.1007/S00442-004-1682-4/FIGURES/6>

1114 Jardim, A.M. da R.F., Santos, H.R.B., Alves, H.K.M.N., Ferreira-Silva, S.L., Souza, L.S.B.
1115 de, Araújo Júnior, G. do N., Souza, M. de S., Araújo, G.G.L. de, Souza, C.A.A. de,
1116 Silva, T.G.F. da, 2021a. Genotypic differences relative photochemical activity,
1117 inorganic and organic solutes and yield performance in clones of the forage cactus under
1118 semi-arid environment. *Plant Physiol. Biochem.* 162, 421–430.
1119 <https://doi.org/10.1016/J.PLAPHY.2021.03.011>

1120 Jardim, A.M. da R.F., Souza, L.S.B. de, Alves, C.P., Araújo, J.F.N. de, Souza, C.A.A. de,
1121 Pinheiro, A.G., Araújo, G.G.L. de, Campos, F.S., Tabosa, J.N., Silva, T.G.F. da, 2021b.

1122 Intercropping forage cactus with sorghum affects the morphophysiology and phenology
1123 of forage cactus. *African J. Range Forage Sci.* 1–12.
1124 <https://doi.org/10.2989/10220119.2021.1949749>

1125 Jardim, A.M.R.F., Morais, J.E.F., Souza, L.S.B., Silva, T.G.F., 2022. Understanding
1126 interactive processes: a review of CO₂ flux, evapotranspiration, and energy partitioning
1127 under stressful conditions in dry forest and agricultural environments. *Environ. Monit.*
1128 *Assess.* 194, 1–22. <https://doi.org/10.1007/S10661-022-10339-7>

1129 Jardim, A.M.R.F., Silva, T.G.F., Souza, L.S.B., Souza, M.S., Morais, J.E.F., Araújo Júnior,
1130 G.N., 2020. Multivariate analysis in the morpho-yield evaluation of forage cactus
1131 intercropped with sorghum. *Rev. Bras. Eng. Agrícola e Ambient.* 24, 756–761.
1132 <https://doi.org/10.1590/1807-1929/AGRIAMBI.V24N11P756-761>

1133 Juhász, C., Gálya, B., Kovács, E., Nagy, A., Tamás, J., Huzsvai, L., 2020. Seasonal
1134 predictability of weather and crop yield in regions of Central European continental
1135 climate. *Comput. Electron. Agric.* 173, 105400.
1136 <https://doi.org/10.1016/J.COMPAG.2020.105400>

1137 Kaiser, H.F., 1960. The application of electronic computers to factor analysis. *Educ. Psychol.*
1138 *Meas.* 20, 141–151. <https://doi.org/10.1177/001316446002000116>

1139 Khapte, P.S., Kumar, P., Wakchaure, G.C., Jangid, K.K., Colla, G., Cardarelli, M., Rane, J.,
1140 2022. Application of Phenomics to Elucidate the Influence of Rootstocks on Drought
1141 Response of Tomato. *Agronomy* 12, 1529.
1142 <https://doi.org/10.3390/AGRONOMY12071529>

1143 Kumar, S., Louhaichi, M., Dana Ram, P., Tirumala, K.K., Ahmad, S., Rai, A.K., Sarker, A.,
1144 Hassan, S., Liguori, G., Probir Kumar, G., Govindasamy, P., Prasad, M., Mahawer,
1145 S.K., Appaswamygowda, B.H., 2021. Cactus Pear (*Opuntia ficus-indica*) Productivity,
1146 Proximal Composition and Soil Parameters as Affected by Planting Time and
1147 Agronomic Management in a Semi-Arid Region of India. *Agronomy* 11, 1647.
1148 <https://doi.org/10.3390/AGRONOMY11081647>

1149 Kutikoff, S., Lin, X., Evett, S., Gowda, P., Moorhead, J., Marek, G., Colaizzi, P., Aiken, R.,
1150 Brauer, D., 2019. Heat storage and its effect on the surface energy balance closure under
1151 advective conditions. *Agric. For. Meteorol.* 265, 56–69.
1152 <https://doi.org/10.1016/J.AGRFORMET.2018.10.018>

- 1153 Lamichhane, S., Eğılmez, G., Gedik, R., Bhutta, M.K.S., Erenay, B., 2021. Benchmarking
1154 OECD countries' sustainable development performance: A goal-specific principal
1155 component analysis approach. *J. Clean. Prod.* 287, 125040.
1156 <https://doi.org/10.1016/J.JCLEPRO.2020.125040>
- 1157 Leite-Filho, A.T., de Sousa Pontes, V.Y., Costa, M.H., 2019. Effects of Deforestation on the
1158 Onset of the Rainy Season and the Duration of Dry Spells in Southern Amazonia. *J.*
1159 *Geophys. Res. Atmos.* 124, 5268–5281. <https://doi.org/10.1029/2018JD029537>
- 1160 Li, W., Fang, H., Wei, S., Weiss, M., Baret, F., 2021. Critical analysis of methods to estimate
1161 the fraction of absorbed or intercepted photosynthetically active radiation from ground
1162 measurements: Application to rice crops. *Agric. For. Meteorol.* 297, 108273.
1163 <https://doi.org/10.1016/J.AGRFORMET.2020.108273>
- 1164 Loupassaki, M.H., Chartzoulakis, K.S., Digalaki, N.B., Androulakis, I.I., 2007. Effects of
1165 salt stress on concentration of nitrogen, phosphorus, potassium, calcium, magnesium,
1166 and sodium in leaves, shoots, and roots of six olive cultivars. *J. Plant Nutr.* 25, 2457–
1167 2482. <https://doi.org/10.1081/PLN-120014707>
- 1168 Luo, Y., Nobel, P.S., 1993. Growth characteristics of newly initiated cladodes of *Opuntia*
1169 *ficus-indica* as affected by shading, drought and elevated CO₂. *Physiol. Plant.* 87, 467–
1170 474. <https://doi.org/10.1111/J.1399-3054.1993.TB02495.X>
- 1171 Ma, H., Li, L., Liu, S., Shi, W., Wang, C., Zhao, Q., Cui, N., Wang, Y., 2022. Physiological
1172 response, phytohormone signaling, biomass production and water use efficiency of the
1173 CAM plant *Ananas comosus* under different water and nitrogen regimes. *Agric. Water*
1174 *Manag.* 266, 107563. <https://doi.org/10.1016/J.AGWAT.2022.107563>
- 1175 Ma, J., Wen, X., Li, M., Luo, S., Zhu, X., Yang, X., Chen, M., 2022. Analysis of Surface
1176 Energy Changes over Different Underlying Surfaces Based on MODIS Land-Use Data
1177 and Green Vegetation Fraction over the Tibetan Plateau. *Remote Sens.* 14, 2751.
1178 <https://doi.org/10.3390/RS14122751>
- 1179 Ma, L., Zheng, G., Ying, Q., Hancock, S., Ju, W., Yu, D., 2021. Characterizing the three-
1180 dimensional spatiotemporal variation of forest photosynthetically active radiation using
1181 terrestrial laser scanning data. *Agric. For. Meteorol.* 301–302, 108346.
1182 <https://doi.org/10.1016/J.AGRFORMET.2021.108346>
- 1183 Martínez-Berdeja, A., Valverde, T., 2008. Growth response of three globose cacti to radiation

1184 and soil moisture: An experimental test of the mechanism behind the nurse effect. J.
1185 Arid Environ. 72, 1766–1774. <https://doi.org/10.1016/J.JARIDENV.2008.04.010>

1186 Mayer, J.A., Cushman, J.C., 2019. Nutritional and mineral content of prickly pear cactus: A
1187 highly water-use efficient forage, fodder and food species. J. Agron. Crop Sci. 205, 625–
1188 634. <https://doi.org/10.1111/JAC.12353>

1189 McGloin, R., Šigut, L., Havránková, K., Dušek, J., Pavelka, M., Sedlák, P., 2018. Energy
1190 balance closure at a variety of ecosystems in Central Europe with contrasting
1191 topographies. Agric. For. Meteorol. 248, 418–431.
1192 <https://doi.org/10.1016/J.AGRFORMET.2017.10.003>

1193 Mendes, K.R., Campos, S., da Silva, L.L., Mutti, P.R., Ferreira, R.R., Medeiros, S.S., Perez-
1194 Marin, A.M., Marques, T. V., Ramos, T.M., Vieira, M.M. de L., Oliveira, C.P.,
1195 Gonçalves, W.A., Costa, G.B., Antonino, A.C.D., Menezes, R.S.C., Bezerra, B.G.,
1196 Santos e Silva, C.M., 2020. Seasonal variation in net ecosystem CO₂ exchange of a
1197 Brazilian seasonally dry tropical forest. Sci. Rep. 10, 1–16.
1198 <https://doi.org/10.1038/s41598-020-66415-w>

1199 Moore, C.J., 1986. Frequency response corrections for eddy correlation systems. Boundary-
1200 Layer Meteorol. 37, 17–35. <https://doi.org/10.1007/BF00122754>

1201 Mostofa, M.G., Rahman, M.M., Ghosh, T.K., Kabir, A.H., Abdelrahman, M., Rahman Khan,
1202 M.A., Mochida, K., Tran, L.S.P., 2022. Potassium in plant physiological adaptation to
1203 abiotic stresses. Plant Physiol. Biochem. 186, 279–289.
1204 <https://doi.org/10.1016/J.PLAPHY.2022.07.011>

1205 Mounir, B., Younes, E.G., Asmaa, M., Abdeljalil, Z., Abdellah, A., 2020. Physico-chemical
1206 changes in cladodes of *Opuntia ficus-indica* as a function of the growth stage and
1207 harvesting areas. J. Plant Physiol. 251, 153196.
1208 <https://doi.org/10.1016/J.JPLPH.2020.153196>

1209 Nobel, P.S., 1980. Interception of photosynthetically active radiation by cacti of different
1210 morphology. Oecologia 45, 160–166. <https://doi.org/10.1007/BF00346455>

1211 Nobel, P.S., Bobich, E.G., 2002. Initial Net CO₂ Uptake Responses and Root Growth for a
1212 CAM Community Placed in a Closed Environment. Ann. Bot. 90, 593–598.
1213 <https://doi.org/10.1093/AOB/MCF229>

1214 Nobel, P.S., De La Barrera, E., 2003. Tolerances and acclimation to low and high

1215 temperatures for cladodes, fruits and roots of a widely cultivated cactus, *Opuntia ficus-*
1216 *indica*. *New Phytol.* 157, 271–279. <https://doi.org/10.1046/J.1469-8137.2003.00675.X>

1217 Ojeda-Pérez, Z.Z., Jiménez-Bremont, J.F., Delgado-Sánchez, P., 2017. Continuous high and
1218 low temperature induced a decrease of photosynthetic activity and changes in the diurnal
1219 fluctuations of organic acids in *Opuntia streptacantha*. *PLoS One* 12, e0186540.
1220 <https://doi.org/10.1371/JOURNAL.PONE.0186540>

1221 Owen, N.A., Choncubhair, Ó.N., Males, J., del Real Laborde, J.I., Rubio-Cortés, R.,
1222 Griffiths, H., Lanigan, G., 2016. Eddy covariance captures four-phase crassulacean acid
1223 metabolism (CAM) gas exchange signature in *Agave*. *Plant. Cell Environ.* 39, 295–309.
1224 <https://doi.org/10.1111/PCE.12610>

1225 Papale, D., Reichstein, M., Aubinet, M., Canfora, E., Bernhofer, C., Kutsch, W., Longdoz,
1226 B., Rambal, S., Valentini, R., Vesala, T., Yakir, D., 2006. Towards a standardized
1227 processing of Net Ecosystem Exchange measured with eddy covariance technique:
1228 Algorithms and uncertainty estimation. *Biogeosciences* 3, 571–583.
1229 <https://doi.org/10.5194/BG-3-571-2006>

1230 Pierini, N.A., Vivoni, E.R., Robles-Morua, A., Scott, R.L., Nearing, M.A., 2014. Using
1231 observations and a distributed hydrologic model to explore runoff thresholds linked with
1232 mesquite encroachment in the Sonoran Desert. *Water Resour. Res.* 50, 8191–8215.
1233 <https://doi.org/10.1002/2014WR015781>

1234 Pikart, F.C., Marabesi, M.A., Miotto, P.T., Gonçalves, A.Z., Matiz, A., Alves, F.R.R.,
1235 Mercier, H., Aidar, M.P.M., 2018. The contribution of weak CAM to the photosynthetic
1236 metabolic activities of a bromeliad species under water deficit. *Plant Physiol. Biochem.*
1237 123, 297–303. <https://doi.org/10.1016/J.PLAPHY.2017.12.030>

1238 Pimienta-Barrios, Eulogio, Zañudo, J., Yopez, E., Pimienta-Barrios, Enrique, Nobel, P.S.,
1239 2000. Seasonal variation of net CO₂ uptake for cactus pear (*Opuntia ficus-indica*) and
1240 pitayo (*Stenocereus queretaroensis*) in a semi-arid environment. *J. Arid Environ.* 44,
1241 73–83. <https://doi.org/10.1006/JARE.1999.0570>

1242 Pinheiro, K.M., Silva, T.G.F., Carvalho, H.F. de S., Santos, J.E.O., Morais, J.E.F., Zolnier,
1243 S., Santos, D.C. dos, 2014. Correlações do índice de área do cladódio com
1244 características morfogênicas e produtivas da palma forrageira. *Pesqui. Agropecuária*
1245 *Bras.* 49, 939–947. <https://doi.org/10.1590/S0100-204X2014001200004>

1246 R Core Team, 2022. R: The R Project for Statistical Computing.

1247 Rannik, Ü., Vesala, T., 1999. Autoregressive filtering versus linear detrending in estimation
1248 of fluxes by the eddy covariance method. *Boundary-Layer Meteorol.* 91, 259–280.
1249 <https://doi.org/10.1023/A:1001840416858>

1250 Raza, M.A., Feng, L.Y., van der Werf, W., Cai, G.R., Khalid, M.H. Bin, Iqbal, N., Hassan,
1251 M.J., Meraj, T.A., Naeem, M., Khan, I., Rehman, S. ur, Ansar, M., Ahmed, M., Yang,
1252 F., Yang, W., 2019. Narrow-wide-row planting pattern increases the radiation use
1253 efficiency and seed yield of intercrop species in relay-intercropping system. *Food*
1254 *Energy Secur.* 8, e170. <https://doi.org/10.1002/FES3.170>

1255 Rodda, S.R., Thumaty, K.C., Praveen, M.S.S., Jha, C.S., Dadhwal, V.K., 2021. Multi-year
1256 eddy covariance measurements of net ecosystem exchange in tropical dry deciduous
1257 forest of India. *Agric. For. Meteorol.* 301–302, 108351.
1258 <https://doi.org/10.1016/J.AGRFORMET.2021.108351>

1259 Rodrigues, C.R.F., Silva, E.N., Ferreira-Silva, S.L., Voigt, E.L., Viégas, R.A., Silveira,
1260 J.A.G., 2013. High K⁺ supply avoids Na⁺ toxicity and improves photosynthesis by
1261 allowing favorable K⁺ : Na⁺ ratios through the inhibition of Na⁺ uptake and transport to
1262 the shoots of *Jatropha curcas* plants. *J. Plant Nutr. Soil Sci.* 176, 157–164.
1263 <https://doi.org/10.1002/JPLN.201200230>

1264 Roeber, V.M., Bajaj, I., Rohde, M., Schmülling, T., Cortleven, A., 2021. Light acts as a
1265 stressor and influences abiotic and biotic stress responses in plants. *Plant. Cell Environ.*
1266 44, 645–664. <https://doi.org/10.1111/PCE.13948>

1267 Salack, S., Klein, C., Giannini, A., Sarr, B., Worou, O.N., Belko, N., Bliefernicht, J.,
1268 Kunstman, H., 2016. Global warming induced hybrid rainy seasons in the Sahel.
1269 *Environ. Res. Lett.* 11, 104008. <https://doi.org/10.1088/1748-9326/11/10/104008>

1270 Salazar-Martínez, D., Holwerda, F., Holmes, T.R.H., Yépez, E.A., Hain, C.R., Alvarado-
1271 Barrientos, S., Ángeles-Pérez, G., Arredondo-Moreno, T., Delgado-Balbuena, J.,
1272 Figueroa-Espinoza, B., Garatuza-Payán, J., González del Castillo, E., Rodríguez, J.C.,
1273 Rojas-Robles, N.E., Uuh-Sonda, J.M., Vivoni, E.R., 2022. Evaluation of remote
1274 sensing-based evapotranspiration products at low-latitude eddy covariance sites. *J.*
1275 *Hydrol.* 610, 127786. <https://doi.org/10.1016/J.JHYDROL.2022.127786>

1276 Saliendra, N.Z., Liebig, M.A., Kronberg, S.L., 2018. Carbon use efficiency of hayed alfalfa

1277 and grass pastures in a semiarid environment. *Ecosphere* 9, e02147.
1278 <https://doi.org/10.1002/ECS2.2147>

1279 San-José, J., Montes, R., Nikonova, N., 2007. Diurnal patterns of carbon dioxide, water
1280 vapour, and energy fluxes in pineapple [*Ananas comosus* (L.) Merr. cv. Red Spanish]
1281 field using eddy covariance. *Photosynthetica* 45, 370–384.
1282 <https://doi.org/10.1007/S11099-007-0064-7>

1283 Santos, F.N.S., Santos, E.M., Oliveira, J.S., Medeiros, G.R., Zanine, A.M., Araújo, G.G.L.,
1284 Perazzo, A.F., Lemos, M.L.P., Pereira, D.M., Cruz, G.F.L., Paulino, R.S., Oliveira,
1285 C.J.B., 2020. Fermentation profile, microbial populations, taxonomic diversity and
1286 aerobic stability of total mixed ration silages based on Cactus and *Gliricidia*. *J. Agric.*
1287 *Sci.* 158, 396–405. <https://doi.org/10.1017/S0021859620000805>

1288 Scalisi, A., Morandi, B., Inglese, P., Lo Bianco, R., 2016. Cladode growth dynamics in
1289 *Opuntia ficus-indica* under drought. *Environ. Exp. Bot.* 122, 158–167.
1290 <https://doi.org/10.1016/J.ENVEXPBOT.2015.10.003>

1291 Schotanus, P., Nieuwstadt, F.T.M., De Bruin, H.A.R., 1983. Temperature measurement with
1292 a sonic anemometer and its application to heat and moisture fluxes. *Boundary-Layer*
1293 *Meteorol.* 26, 81–93. <https://doi.org/10.1007/BF00164332>

1294 Siddiq, Z., Hayyat, M.U., Khan, A.U., Mahmood, R., Shahzad, L., Ghaffar, R., Cao, K.F.,
1295 2021. Models to estimate the above and below ground carbon stocks from a subtropical
1296 scrub forest of Pakistan. *Glob. Ecol. Conserv.* 27, e01539.
1297 <https://doi.org/10.1016/J.GECCO.2021.E01539>

1298 Silva, M.R.F., McHugh, I., Peixoto Neto, A.M.L., Pauwels, V.R.N., Cartwright, I., Daly, E.,
1299 2022. Trading a little water for substantial carbon gains during the first years of a
1300 *Eucalyptus globulus* plantation. *Agric. For. Meteorol.* 318, 108910.
1301 <https://doi.org/10.1016/J.AGRFORMET.2022.108910>

1302 Silva, T.G.F., Miranda, K.R., Santos, D.C., Queiroz, M.G., Silva, M.C., Cruz Neto, J.F.,
1303 Araújo, J.E.M., 2014. Área do cladódio de clones de palma forrageira: modelagem,
1304 análise e aplicabilidade. *Rev. Bras. Ciências Agrárias* 9, 626–632.
1305 <https://doi.org/10.5039/AGRARIA.V9I4A4553>

1306 Snyman, H.A., 2006. A greenhouse study on root dynamics of cactus pears, *Opuntia ficus-*
1307 *indica* and *O. robusta*. *J. Arid Environ.* 65, 529–542.

1308 <https://doi.org/10.1016/J.JARIDENV.2005.10.004>

1309 Teng, D., He, X., Qin, L., Lv, G., 2021. Energy Balance Closure in the Tugai Forest in Ebinur
1310 Lake Basin, Northwest China. *Forests* 12, 243. <https://doi.org/10.3390/F12020243>

1311 Unland, H.E., Houser, P.R., Shuttleworth, W.J., Yang, Z.L., 1996. Surface flux measurement
1312 and modeling at a semi-arid Sonoran Desert site. *Agric. For. Meteorol.* 82, 119–153.
1313 [https://doi.org/10.1016/0168-1923\(96\)02330-1](https://doi.org/10.1016/0168-1923(96)02330-1)

1314 Vickers, D., Mahrt, L., 1974. Quality Control and Flux Sampling Problems for Tower and
1315 Aircraft Data. *J. Atmos. Ocean. Technol.* 7, 363–372.
1316 <https://doi.org/10.1007/BF00240838>

1317 Webb, E.K., Pearman, G.I., Leuning, R., 1980. Correction of flux measurements for density
1318 effects due to heat and water vapour transfer. *Q. J. R. Meteorol. Soc.* 106, 85–100.
1319 <https://doi.org/10.1002/QJ.49710644707>

1320 Widmoser, P., Wohlfahrt, G., 2018. Attributing the energy imbalance by concurrent
1321 lysimeter and eddy covariance evapotranspiration measurements. *Agric. For. Meteorol.*
1322 263, 287–291. <https://doi.org/10.1016/J.AGRFORMET.2018.09.003>

1323 Wilczak, J.M., Oncley, S.P., Stage, S.A., 2001. Sonic Anemometer Tilt Correction
1324 Algorithms. *Boundary-Layer Meteorol.* 99, 127–150.
1325 <https://doi.org/10.1023/A:1018966204465>

1326 Wilson, K., Goldstein, A., Falge, E., Aubinet, M., Baldocchi, D., Berbigier, P., Bernhofer,
1327 C., Ceulemans, R., Dolman, H., Field, C., Grelle, A., Ibrom, A., Law, B.E., Kowalski,
1328 A., Meyers, T., Moncrieff, J., Monson, R., Oechel, W., Tenhunen, J., Valentini, R.,
1329 Verma, S., 2002. Energy balance closure at FLUXNET sites. *Agric. For. Meteorol.* 113,
1330 223–243. [https://doi.org/10.1016/S0168-1923\(02\)00109-0](https://doi.org/10.1016/S0168-1923(02)00109-0)

1331 Wutzler, T., Lucas-Moffat, A., Migliavacca, M., Knauer, J., Sickel, K., Šigut, L., Menzer,
1332 O., Reichstein, M., 2018. Basic and extensible post-processing of eddy covariance flux
1333 data with REddyProc. *Biogeosciences* 15, 5015–5030. [https://doi.org/10.5194/BG-15-](https://doi.org/10.5194/BG-15-5015-2018)
1334 [5015-2018](https://doi.org/10.5194/BG-15-5015-2018)

1335 Yang, F., Huang, J., Zheng, X., Huo, W., Zhou, C., Wang, Y., Han, D., Gao, J., Mamtimin,
1336 A., Yang, X., Sun, Y., 2022. Evaluation of carbon sink in the Taklimakan Desert based
1337 on correction of abnormal negative CO₂ flux of IRGASON. *Sci. Total Environ.* 838,
1338 155988. <https://doi.org/10.1016/J.SCITOTENV.2022.155988>

1339 Yao, Y., Li, Z., Wang, T., Chen, A., Wang, X., Du, M., Jia, G., Li, Y., Li, H., Luo, W., Ma,
1340 Y., Tang, Y., Wang, H., Wu, Z., Yan, J., Zhang, X., Zhang, Yiping, Zhang, Yu, Zhou,
1341 G., Piao, S., 2018. A new estimation of China's net ecosystem productivity based on
1342 eddy covariance measurements and a model tree ensemble approach. *Agric. For.
1343 Meteorol.* 253–254, 84–93. <https://doi.org/10.1016/J.AGRFORMET.2018.02.007>

1344 Yue, P., Zhang, Q., Zhang, L., Li, H., Yang, Y., Zeng, J., Wang, S., 2019. Long-term
1345 variations in energy partitioning and evapotranspiration in a semiarid grassland in the
1346 Loess Plateau of China. *Agric. For. Meteorol.* 278, 107671.
1347 <https://doi.org/10.1016/J.AGRFORMET.2019.107671>

1348 Zeng, J., Matsunaga, T., Tan, Z.H., Saigusa, N., Shirai, T., Tang, Y., Peng, S., Fukuda, Y.,
1349 2020. Global terrestrial carbon fluxes of 1999–2019 estimated by upscaling eddy
1350 covariance data with a random forest. *Sci. Data* 7, 1–11. [https://doi.org/10.1038/s41597-](https://doi.org/10.1038/s41597-020-00653-5)
1351 [020-00653-5](https://doi.org/10.1038/s41597-020-00653-5)

1352 Zhang, Kuiyue, Liu, D., Liu, H., Lei, H., Guo, F., Xie, S., Meng, X., Huang, Q., 2022. Energy
1353 flux observation in a shrub ecosystem of a gully region of the Chinese Loess Plateau.
1354 *Ecohydrol. Hydrobiol.* 22, 323–336. <https://doi.org/10.1016/J.ECOHYD.2021.10.001>

1355 Zhang, Kai, Wang, X., Li, Y., Zhao, J., Yang, Y., Zang, H., Zeng, Z., 2022. Peanut residue
1356 incorporation benefits crop yield, nitrogen yield, and water use efficiency of summer
1357 peanut – winter wheat systems. *F. Crop. Res.* 279, 108463.
1358 <https://doi.org/10.1016/J.FCR.2022.108463>

1359 Zhang, Q., Song, Y., Wu, Z., Yan, X., Gunina, A., Kuzyakov, Y., Xiong, Z., 2020. Effects
1360 of six-year biochar amendment on soil aggregation, crop growth, and nitrogen and
1361 phosphorus use efficiencies in a rice-wheat rotation. *J. Clean. Prod.* 242, 118435.
1362 <https://doi.org/10.1016/J.JCLEPRO.2019.118435>

1363 Zutta, B.R., Nobel, P.S., Aramians, A.M., Sahaghian, A., 2011. Low- and High-Temperature
1364 Tolerance and Acclimation for Chlorenchyma versus Meristem of the Cultivated Cacti
1365 *Nopalea cochenillifera*, *Opuntia robusta*, and *Selenicereus megalanthus*. *J. Bot.* 2011,
1366 1–6. <https://doi.org/10.1155/2011/347168>

1367